ITB
Graduate School
Conference

THE 3RD ITB GRADUATE SCHOOL CONFERENCE (IGSC) 2022

"Enhancing Creativity in Research Through Developing Innovative Capabilities"

Bandung, Indonesia 21 Desember 2022

Sekolah Pascasarjana
Institut Teknologi Bandung

LEMBAGA PENELITIAN
DAN PENGABDIAN
KEPADA MASYARAKAT
INSTITUT TEKNOLOGI BANDUNG

Proceedings of the 3rd ITB Graduate School Conference ISSN: 2963-718X
Enhancing Creativity in Research Through Developing Innovative Capabilities
December 21, 2022

PREFACE

It is a great privilege for us to present the proceedings of the 3rd ITB Graduate School Conference to the authors and delegates of the event. The postgraduate education in ITB is a locomotive for achieving academic excellence through research, innovation, and scientific publications. The ITB's Graduate School Conference (i-GSC) is held by ITB's Graduate School and Institute for Research and Community Service (LPPM) as a platform for scientific publications of ITB postgraduate students whose basis is the results of their thesis and dissertation research. The conference is also open to academia and researchers from outside the university.

The responses to the call-for-papers had been overwhelming both from ITB and from other universities. This conference invited 3 keynote speakers from ITB (Prof. Dr. Yudi Darma, S.Si., M.Si.), BRIN (Dr. Deni Shidqi Khaerudini, S.Si., M.Eng.), and Monash University (Dr. Ella Whateley). The organizing committee of the 3rd IGSC also collaborated with eight (8) ITB reputable Scientific Journals with various scopes of research. The submitted manuscripts were peer-reviewed and parts of them were accepted for publication in the journal. We are truly appreciating all the participants.

In the end, we would like to express our gratitude and appreciation for all the reviewers who helped us maintain the high quality of the manuscripts. We would also like to extend our thanks to the organising team members for their hard work. Last but not least, we thank all participants and wish to see you on the next occasion.

We do hope that this conference activity can continue and support the advancement of science, art, and technology in Indonesia.

Conference Chair

Dr. Kiki Adi Kurnia
On behalf of the 3rd IGSC Committees
21st December 2022
Bandung, Indonesia

Proceedings of the 3rd ITB Graduate School Conference ISSN: 2963-718X
Enhancing Creativity in Research Through Developing Innovative Capabilities
December 21, 2022

Proceeding Book
ITB GRADUATE SCHOOL CONFERENCE (IGSC)
Volume 3, 2022

Editors:

Prof. Dr. Eng. Suprijadi, M.Eng.
Dr. Yuli Setyo Indartono
Prof. Dr-mont. Zaki Mubarok

Reviewers:

Dr. rer.nat. apt Sophi Damayanti
Deny Willy Junaidy, S.Sn., MT., Ph.D.
Dr.rer.nat. Rino Rakhmata Mukti, S.Si., M.Si.
Mohammad Farid, S.T, M.T, Ph.D.
Prof. Dr. Eng. Nining Sari Ningsih, MS
Prof. Intan Ahmad Musmeinan, Ph.D.
Prof. Dr. Ir. Bambang Kismono Hadi
Prof. Dr. Umar Fauzi
Prof. Dr. Yasraf Amir Piliang
Prof. Dr. Dwi Hendratmo Widyantoro
Prof. Asep Kurnia Permadi, Ph.D.
Prof. Dr. Daryono Hadi Tj.
Prof. Dr. Barti Setiani Muntalif
Prof. Dr. Ir. Dermawan Wibisono, M.Eng.
Prof. Dr. Eng. Pradono
Prof. Ir. Johnner Sitompul, M.Sc., Ph.D.

Committee

Steering Committee :
Prof. Dr. Eng. Suprijadi, M.Eng. (FMIPA, ITB)
Dr. Yuli Setyo Indartono (FTMD, ITB)
Prof. Dr-mont. Zaki Mubarok (FTTM, ITB)
Dr. rer.nat. apt Sophi Damayanti (SF, ITB)
Deny Willy Junaidy, S.Sn., MT., Ph.D. (FSRD, ITB)
Dr.rer.nat. Rino Rakhmata Mukti, S.Si., M.Si. (FMIPA, ITB)
Mohammad Farid, S.T, M.T, Ph.D. (FTSL, ITB)
Prof. Dr. Eng. Nining Sari Ningsih, MS (FITB, ITB)
Prof. Intan Ahmad Musmeinan, Ph.D (SITH, ITB)
Prof. Dr. Ir. Bambang Kismono Hadi (FTMD, ITB)
Prof. Dr. Umar Fauzi (FMIPA, ITB)
Prof. Dr. Yasraf Amir Piliang (FSRD, ITB)
Prof. Dr. Dwi Hendratmo Widyantoro (STEI, ITB)
Prof. Asep Kurnia Permadi, Ph.D. (FTTM, ITB)
Prof. Dr. Daryono Hadi Tj. (SF, ITB)
Prof. Dr. Barti Setiani Muntalif (FTSL, ITB)
Prof. Dr. Ir. Dermawan Wibisono, M.Eng (SBM, ITB)
Prof. Dr. Eng. Pradono (SAPPK, ITB)
Prof. Ir. Johnner Sitompul, M.Sc., Ph.D. (FTI, ITB)

Keynote Speaker :
Prof. Dr. Yudi Darma, S.Si., M.Si. (FMIPA, ITB)
Dr. Deni Shidqi Khaerudini, S.Si., M.Eng. (BRIN)
Dr. Ella Whateley (Monash University)

Chief Executive	:	Dr. Kiki Adi Kurnia, Ph.D. (FTI, ITB)
Secretariat Coordinators	:	Dr. Windy Iriana (FTSL, ITB)
		Housny Mubarok, ST.
		Ani Hamidah Nurhayati, MAB
		Diki Rustandi
Scientific Coordinators	:	Dr. Nur Ahmadi (STEI, ITB)
Event Coordinators	:	Maya Fitriyanti, Ph.D. (SITH, ITB)
		Roslina Sawitri, M.Pd.
Treasury Coordinators	:	Nia Nuraeni S.Pd.
		Santi, A.Md.
		Budiman, A.Md.
Moderators of Program	:	Dr. Shofarul Wustoni (FMIPA, ITB)
		Rizal Dwi Prayogo (STEI, ITB)
		Dr. Jihad Furqani (STEI, ITB)
		Dr. Agung Budiyono (FTI, ITB)
		Dr.Pipit Fitriani (FMIPA, ITB)
		Dr. Aqsha (FTI, ITB)
		Dr. Mahesa Akbar (FTMD, ITB)
		Dr. Faizal Rohmat (FTSL, ITB)
		Dr. Alfredo Kono (FMIPA, ITB)
Program Support Division	:	Moch. Saifur Rijal (28720304)
		Muhammad Nauval Farras R (28721304)
Informations Division	:	Mandhalika Ayu Shania, S.T.
		Irma Siti Rohimah, S.E.
		Ali Hasan Asyari
		Suyanto
		Irvan Sidik
		Rama Anugrah
Logistics Division	:	Suwitno
		Iin Gumilar

Table of Contents

1. Simulation of the Properties of the Coprime Graph of the Dihedral Group with Prime Order 1
Verrel Rievaldo Wijaya & Abdul Gazir Syarifudin

2. Design of Hydrogen on Demand Production Generator Based on Aluminum Waste and Water Hydrolysis using VDI 2221 Method 12
Aditya Putra Widodo & Deni Shidqi Khaerudini

3 Open-system Magmatic Process at Agung Volcano, Bali, Indonesia: Evidence from Phenocryst Compositions and Textures 27
Adzkia Noerma Arifa, I Gusti Bagus Eddy Sucipta & Idham Andri Kurniawan

4 The Effect of Element (Sr, Ti, B, and Mg) Modification on Microstructure to Increase Micro-Hardness of A356 Aluminum Alloy 40
Afghany Mostavan, Asep Ridwan, Arif Basuki & Husaini Ardy

5 Analysis of The Subsurface Structure of the Geothermal Potential Area Based on Magnetic Data (Case Study in Blue Mountain-North Nevada) 50
Agnes Br. Manurung & Alamta Singarimbun

6 Limestone Resources Estimation using Standard Facies Belt as Domain Constraint, Banten, Indonesia 63
Ahmad Nur Taufiqurrahman, Antoni Sahar, Asep Heri Patria Kesumajana, & Dwiharso Nugroho

7 Analysis of Community-based Enterprise Development Process in Indonesian Return Migrant Workers Community 75
Annida Mardhotillah & Tubagus Furqon Sofhani

8 Optimization of Local Revenue: Indragiri Hulu Regency 87
Baiq Rizky Fatmasari, Septian Asriadi Putra, & Wiwik Dwi Pratiwi
9 Merchants' Acceptability of Mobile Payment: A Systematic Literature Review 103
Chairil Zidane & Tengku Munawar Chalil
10 Analysis of Factors Influencing the Decision to Adopt 3D Printing Technology in a Case Study of Residential Housing Development 118
Dhania Salsabila & Rani G. K. Pradoto
11 Comparison of Dissolved Gas Analysis Interpretation Methods for Power Transformer 132
Dhiastara Rahmanda & Suwarno
12 Synthesis of Silica Nanoparticle and Cd-Based Carboxyl Quantum Dots (SiNP@QDs) Conjugates as Biosensing Platform: A Pleriminary Study 144
Diaz Ayu Widyasari, Fauzan Aulia, Agustina Sus Andreani, Rizna Triana Dewi, Ni Luh Wulan Septiani, Brian Yuliarto, & Siti Nurul Aisyiyah Jenie
13 Analysis of Achievements of Irrigators on Pillar Three of Irrigation Modernization in the Rentang Irrigation Area 153
Ernawati, Indratmo Soekarno, Joko Siswanto, & Yadi Suryadi
14 Study of Pipe Selection Methods to Be Rehabilitated: A Case Study of Jakarta City 161
Ervin J. Mansyur, Biemo W. Soemardi, & Reini D. Wirahadikusumah
15 The Role of Agrotourism in Environmental Sustainability (Case Study: Batu City, East Java) 175
Fardiah Qonita Ummi Naila & Djoko Santoso Abi Suroso

16 Cost-benefit Analysis Elements for Green Building Concepts in Architectural Projects 186
Furry Andini Wilis & Dewi Larasati
17 Analysis of Resonance in Sumatra 500 kV Extra High Voltage Transmission Line Energization Schemes 198
Ika Mayla Sari & Nanang Hariyanto
18 Branding Identity in Brochure as Media Branding of Destination On Purwakarta Tourism 210
Intan Kusuma Ayu & Agung Eko Budiwaspada
19 Even Mass Plutonium Effect On Plutonium Proliferation Evaluation For Delta Phase 223
Ismail Humolango, Muhamad Irfan, Imam Ghazali Yasmint, Sidik Permana, Sparisoma Viridi, Dwi Irwanto, & Abdul Waris
20 Sustainable Fashion: A Content Analysis of Indonesian Sustainable Lifestyle Instagram Influencer (Case Study: @dkwardhani) 234
Jennifer A Angwyn & Hafiz Aziz Ahmad
21 Design and Analysis of 5 MW Kaplan Runner Wheel for Small Hydro Powerplant 245
Muhammad Febrilian Syah, Priyono Soetikno & Isnain 'Aliman
22 On the Field Localization in a Thick Braneworld 260
Muhammad Taufiqur Rohman, Triyanta, & Agus Suroso
23 Development of Application Design to Support Mathematics Learning in the Subject of Three-Dimensional Geometry for Class XII High School Students 272
Nidya Putri & Banung Grahita
24 Deformation Monitoring of Lava Dome Growth derived by Sentinel-1A images at Mt. Ibu, North Maluku, Indonesia 289
Nur Ayu Anas & Asep Saepuloh

25 The Effect of Salt and Sulfuric Acid on the Resistivity Value of Bentonite Mixed with Calcium Carbonate Soil under DC Voltage 304
Pequinta Alnajua Wisyah, Bambang Anggoro Soedjarno P., & Pradita Octoviandiningrum Hadi

26 Effect of Water Level Elevation in Madiun River on Flooding in Jeroan River 318
Rif'atul Ummah, Arno Adi Kuntoro & Hendrianto Alamsyah

27 The Color Map of Death in the Scene of the Bridge Connecting the Land of the Living and the Land of the Dead in Coco Film 332
Satria Budiana Tresna, Chandra Tresnadi, & Pindi Setiawan

28 The Associations of Children Characteristics, Sociodemographic, and Sanitation Factors and The Risk of Stunting in Bandung Regency (Case Study: Rancaekek and Majalaya District) 344
Sharnella Janet Yapfrine, Katharina Oginawati, Nurul Fahimah, Indah Rachmatiah Siti Salami, & Septian Hadi Suseno

29 Flood Hazard Assessment in Kalinyamatan District Generated by Dam Break of Bakalan Dam in Jepara Regency 353
Tania Sinayangsih, Eka Oktariyanto Nugroho, & Agung Wiyono Hadi Soeharno

30 Identifying Collapse of Topography Using Temporal Pansharpened Optical Images at Active Volcano: Case Study of Mt. Semeru Eruptions in 2021 368
Vismaia Isanjarini & Asep Saepuloh

31 The Potential of Clay Material as CO2 Capture Sorbent in the Pressure Temperature Swing Adsorption (PTSA) Process 383
Wahid Ahmadi & Deni Shidqi Khaerudini

Proceedings of the 3rd ITB Graduate School Conference ISSN: 2963-718X
Enhancing Creativity in Research Through Developing Innovative Capabilities
December 21, 2022

Simulation of the Properties of the Coprime Graph of the Dihedral Group with Prime Order

Verrel Rievaldo Wijaya* & Abdul Gazir Syarifudin

Institut Teknologi Bandung, Jalan Ganesa No. 10 Bandung 40132, Indonesia
*Email: arywijaya86@gmail.com

Abstract. The dihedral group of order $2n$ denoted by D_{2n} is the symmetry group of a regular n-polygon consisting of rotation and reflection elements and the composition of both elements. We then construct a coprime graph of the dihedral group with prime order. Many properties can be studied from this coprime graph including the shape, spectrum, tree numbers, chromatic numbers, etc. By utilizing the Python programming language, we can draw this graph and simulate the properties concerning this graph to get more insight on it.

Keywords: *coprime graph; dihedral group; spanning tree; python; network.*

1 Introduction

Since the first coprime graph of a group was defined by Ma et al in 2014 [1], research on these topics has continued to grow. Starting from looking at the properties of coprime graphs from finite groups to special groups such as integer groups modulo n, dihedral groups to generalized quaternion groups. In 2020, Rina et al [2] examined the form of coprime graphs in the integer group modulo n. In the same year Syarifudin et al examined the shape of the coprime graph in the dihedral group, then continued to look at other properties such as the degree of vertex, radius, diameter, girth, clique number and chromatic number [3, 4, 5]. In 2021, Nurhabibah et al examined some properties of the coprime graph of the generalized quaternion group [6]. In addition, the parameters of the coprime graph in an infinite group were discussed, likes the so-called freedoms number.

Based on a lot of interest in obtaining properties on coprime graphs, for this reason in this study a program will be made to simulate the properties on coprime graphs. To be more specific to dihedral graphs with prime order, some of the properties simulated in this study are graph shape, adjacency matrix, graph spectrum, tree number and chromatic number.

Copyright © 2023 Published by ITB, ISSN: 2963-718X

2 Main Theory and Results

First, we give some definition and known results regarding coprime graph of dihedral group. Here and next, we will concern ourselves especially with dihedral group of prime order.

Definition 2.1 (Dihedral Group) [3] Group G is called a dihedral group of order $2n,\ n \geq 3$ and $n \in \mathbb{N}$, if it is being generated by two elements $a, b \in G$ with the properties

$$G = \langle a, b | a^n = e, b^2 = e, bab^{-1} = a^{-1} \rangle$$

Dihedrap group with order $2n$ will be denoted by D_{2n}.

From the definition it is easy to see that $|D_{2n}| = 2n$ and D_{2n}can be written as the set $D_{2n} = \{e, a, a^2, a^3, \dots, a^{n-1}, b, ab, a^2b, a^3b, \dots, a^{n-1}b\}$.

Definition 2.2 (Order) [7] Let G is a group with identity e and $x \in G$, the order of x is the smallest natural number k such that $x^k = e$ and denoted $|x| = k$.

Theorem 2.1 (Order of Element in D_{2n}) Let D_{2n} be a dihedral group. Then the order of its element is showed as follows

$$\left|a^i b^j\right| = \begin{cases} \dfrac{n}{\gcd\,(i,n)}, & j = 0 \\ 2\quad, & j = 1 \end{cases}$$

where $a^i b^j \neq e$ dan $0 \leq i < n$

Next, we give definition of some properties concerning the algebraic graph theory that will be shown in the simulation.

Definition 2.3 (Coprime Graph) [1] The coprime graph of a group G, denoted by Γ_G is a graph whose vertices are elements of G and two distinct vertices u and v are adjacent if and only if $(|a|, |b|) = 1$.

Definition 2.4 (Adjacency Matrix) [8] The adjacency matrix of Γ is the $n \times n$ matriks $A = A(\Gamma)$ whose entries a_{ij} are given by

$$a_{ij} = \begin{cases} 1, & if\ v_i\ is\ adjacent\ to\ v_j \\ 0, & otherwise \end{cases}$$

Definition 2.5 (Incidence Matrix) [8] The incidence matrix D of Γ, with respect to a given orientation, is the $n \times m$ matrix d_{ij} whose entries are

$$d_{ij} = f(x) = \begin{cases} +1, & if\ v_i\ the\ positif\ end\ of\ e_j \\ -1, & if\ v_i\ is\ the\ negatif\ end\ of\ e_j \\ 0, & otherwise \end{cases}$$

Definition 2.6 (Spectrum) [8] The spectrum of a graph Γ is the set of numbers which are eigenvalues of $A(\Gamma)$, together with their multiplicities. If the distinct eigenvalues of $A(\Gamma)$ are $\lambda_0 > \lambda_1 > \cdots > \lambda_{s-1}$, and their multiplicities are $m(\lambda_0), m(\lambda_1)$, then we shall write

$$Spec\ \Gamma = \begin{pmatrix} \lambda_0 & \lambda_1 & \dots & \lambda_{s-1} \\ m(\lambda_0) & m(\lambda_1) & \dots & m(\lambda_{s-1}) \end{pmatrix}$$

Definition 2.7 (Spanning Tree) [8] A spanning tree in Γ is a subgraph which has $n - 1$ edges and contains no cycles.

Definition 2.8 (**Tree Number**) [8] The number of spanning trees of a graph Γ is called a tree-number, denoted by $\kappa(\Gamma)$.

Theorem 2.2 [8] Every cofactor of Q is equal to the tree-number of Γ, that is

$$adj\ Q = \kappa(\Gamma)\ \mathbf{J}$$

with **Q** is a Laplacian matrix of Γ and **J** is a matrix with all its entry 1.

Theorem 2.3 [8] Let the complete multipartite graph $K_{a_1,a_2,\dots,a_m}$, where $a_1 + a_2 + \cdots + a_m = n$, then $\kappa\left(K_{a_1,a_2,\dots,a_m}\right) = n^{m-2}(n-a_1)^{a_1-1} \dots (n-a_m)^{a_m-1}$

Theorem 2.4 Coprime graph of dihedral group D_{2n}, n a prime number is a complete tripartite graph $K_{1,n-1,n}$. Furthermore, the tree number of this graph is

$$\kappa\left(K_{1,n-1,n}\right) = 2(n+1)^{n-2}n^n$$

Proof.

The dihedral group with n a prime number can be partitioned into three partition that is $\{e\}$, $\{a, a^2, \dots, a^{n-1}\}$, and $\{b, ab, \dots, a^{n-1}b\}$. These three partitions can easily be seen to be coprime with each other. So, the coprime graph is a complete tripartite graph $K_{1,n-1,n}$. Furthermore, using formula from Theorem 2.3 we get the tree number of this graph is

$$\begin{aligned} \kappa\left(K_{1,n-1,n}\right) &= (2n)^{3-2}(2n-1)^{1-1}\left(2n-(n-1)\right)^{n-1-1}(2n-n)^{n-1} \\ &= 2n(n+1)^{n-2}n^{n-1} \end{aligned}$$

Definition 2.8 (Chromatic Numbers) [8] A proper coloring of a graph G is a coloring of the vertices of G so that no two adjacent vertices receive the same color. The chromatic number $\chi(G)$ is the least integer k such that there is a proper coloring of G using k colors.

Theorem 2.5 (Chromatic Numbers of D_{2n} Graph) [5] Let D_{2n} dihedral group. If $n = p_1^{k_1} p_2^{k_2} \dots p_m^{k_m}$, where p_i are distinct odd prime number then the chromatic numbers of coprime graph of dihedral group is $(m + 2)$-partite.

3 Program Simulation

3.1 Python and Packages

In this paper, we will use programming language called Python to help simulating some properties of graph. Python is one of the most popular object-oriented high-level programming languages today and is widely used as a tool for mathematical computing and data analysis [9]. Previously, Python has been used to generate all subgroups of a particular group, for example Z_n [10].

Python contains package that can help us to work with studying graph and its properties. Some of the packages that will be used in our program are the following.

- **numPy**: fundamental package for scientific computing in Python
- **math**: provides access to many mathematical functions
- **matplotlib**: comprehensive library for creating static, animated, and interactive visualizations in Python.
- **tabulate**: creating table from another data
- **networkx**: library for studying graphs and networks

We are running our simulation in computer with processor AMD Ryzen 5 3500U with Radeon Vega Mobile Gfx, 2100 Mhz, 4 Core(s), 8 Logical Processor(s).

```
In [1]: import numpy as np
        import networkx as nx
        import matplotlib.pyplot as plt
        from math import *
        from tabulate import tabulate
```

3.2 Group D_{2n} and the Order of each Element

First, we simulate the code to generate the group D_{2n} and the order of each element as follows.

```
In [2]: # Initialization
        print("============================================")
        print("Generating all the proper subgroups of D_2n")
        print("============================================")
        n = int(input("Input n: "))
        print("D_%d = " %(2*n), end="")

        # Group D_2n
        keys = []
        for i in range(2*n):
            if i==0:
                keys.append('e')
            elif i<n:
                keys.append("a^" + str(i))
            else: keys.append("a^" + str(i-n) +"b")
        print(keys, "\n")

        list_orde = {}
        print('Order of each element')
        for index, i in enumerate(keys):
            if index == 0:
                orde = 1
            elif index < n:
                orde = int(n / gcd(index, n))
            else:
                orde = 2
            list_orde[i] = orde
            print('| {} | = {}'.format(i, orde))
```

Simulations with an example $n = 11$ will obtained the following results.

```
============================================
Generating all the proper subgroups of D_2n
============================================
Input n: 11
D_22 = ['e', 'a^1', 'a^2', 'a^3', 'a^4', 'a^5', 'a^6', 'a^7', 'a^8', 'a^9', 'a^10', 'a^0b', 'a^1b', 'a^2b', 'a^3b', 'a^4b', 'a^
5b', 'a^6b', 'a^7b', 'a^8b', 'a^9b', 'a^10b']

Order of each element
| e | = 1
| a^1 | = 11
| a^2 | = 11
| a^3 | = 11
| a^4 | = 11
| a^5 | = 11
| a^6 | = 11
| a^7 | = 11
| a^8 | = 11
| a^9 | = 11
| a^10 | = 11
| a^0b | = 2
| a^1b | = 2
| a^2b | = 2
| a^3b | = 2
| a^4b | = 2
| a^5b | = 2
| a^6b | = 2
| a^7b | = 2
| a^8b | = 2
| a^9b | = 2
| a^10b | = 2
```

3.3 Drawing the Coprime Graph

First, we check whether the orders of the two elements in D_{2n} are coprime or not. If yes, then the two elements are connected by an edge in the graph. The following code checks and generates the edges of the coprime graph.

```
In [3]: all_edge = []

        for i in list_orde.keys():
            for j in list_orde.keys():
                if i != j:
                    if gcd(list_orde[i], list_orde[j]) == 1:
                        all_edge.append((i,j))
```

From the edge that has been obtained, the coprime graph can be drawn.

```
In [4]: G = nx.Graph()
        G.add_edges_from(all_edge)

        plt.figure(1,figsize=(10,10))
        nx.draw_circular(G, node_color = 'aqua',
                         with_labels=True, node_size=500, font_size=10)
        plt.show()
```

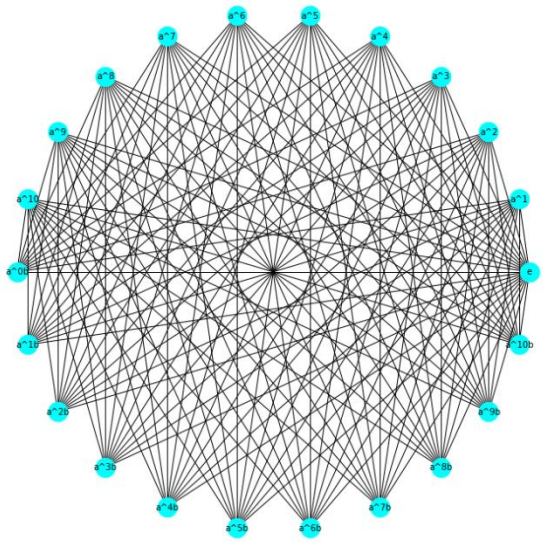

Figure 1 Coprime graph of Dihedral Group D_{22}

3.4 Adjacency Matrix, Incidence Matrix, and Spectrum

Determining the adjacency matrix and incidence matrix of a graph can be done by utilizing the methods already available in the *networkx* package, namely *adjacency_matrix* and *incidence_matrix*.

```
In [5]: print('Adjacency matrix of G is ')
        print(nx.adjacency_matrix(G).toarray(), '\n')

        print('Incidence matrix of G is ')
        print(nx.incidence_matrix(G).toarray())
```

```
Adjacency matrix of G is
[[0 1 1 1 1 1 1 1 1 1 1 1 1 1 1 1 1 1 1 1 1]
 [1 0 0 0 0 0 0 0 0 0 0 1 1 1 1 1 1 1 1 1 1]
 [1 0 0 0 0 0 0 0 0 0 0 1 1 1 1 1 1 1 1 1 1]
 [1 0 0 0 0 0 0 0 0 0 0 1 1 1 1 1 1 1 1 1 1]
 [1 0 0 0 0 0 0 0 0 0 0 1 1 1 1 1 1 1 1 1 1]
 [1 0 0 0 0 0 0 0 0 0 0 1 1 1 1 1 1 1 1 1 1]
 [1 0 0 0 0 0 0 0 0 0 0 1 1 1 1 1 1 1 1 1 1]
 [1 0 0 0 0 0 0 0 0 0 0 1 1 1 1 1 1 1 1 1 1]
 [1 0 0 0 0 0 0 0 0 0 0 1 1 1 1 1 1 1 1 1 1]
 [1 0 0 0 0 0 0 0 0 0 0 1 1 1 1 1 1 1 1 1 1]
 [1 0 0 0 0 0 0 0 0 0 0 1 1 1 1 1 1 1 1 1 1]
 [1 1 1 1 1 1 1 1 1 1 1 0 0 0 0 0 0 0 0 0 0]
 [1 1 1 1 1 1 1 1 1 1 1 0 0 0 0 0 0 0 0 0 0]
 [1 1 1 1 1 1 1 1 1 1 1 0 0 0 0 0 0 0 0 0 0]
 [1 1 1 1 1 1 1 1 1 1 1 0 0 0 0 0 0 0 0 0 0]
 [1 1 1 1 1 1 1 1 1 1 1 0 0 0 0 0 0 0 0 0 0]
 [1 1 1 1 1 1 1 1 1 1 1 0 0 0 0 0 0 0 0 0 0]
 [1 1 1 1 1 1 1 1 1 1 1 0 0 0 0 0 0 0 0 0 0]
 [1 1 1 1 1 1 1 1 1 1 1 0 0 0 0 0 0 0 0 0 0]
 [1 1 1 1 1 1 1 1 1 1 1 0 0 0 0 0 0 0 0 0 0]
 [1 1 1 1 1 1 1 1 1 1 1 0 0 0 0 0 0 0 0 0 0]
 [1 1 1 1 1 1 1 1 1 1 1 0 0 0 0 0 0 0 0 0 0]]

Incidence matrix of G is
[[1. 1. 1. ... 0. 0. 0.]
 [1. 0. 0. ... 0. 0. 0.]
 [0. 1. 0. ... 0. 0. 0.]
 ...
 [0. 0. 0. ... 1. 0. 0.]
 [0. 0. 0. ... 0. 1. 0.]
 [0. 0. 0. ... 0. 0. 1.]]
```

The adjacency matrix of a graph is symmetric and real, so its eigenvalues are always real. The spectrum of this graph is as the following.

```
In [6]: print('Spectrum of G is ')

        unique_lambda = [np.real(i) for i in set(nx.adjacency_spectrum(G))]
        unique_lambda.sort(reverse=True)

        head = [['Lambda'], ['Count']]

        for index,i in enumerate(unique_lambda):
            head[0].append('{:.2e}'.format(np.real(i)))
            head[1].append(list(nx.adjacency_spectrum(G)).count(i))

        print(tabulate(head))
```

```
Spectrum of G is
------  ----  --------  --------  --------  --------  --------  -  ----------  --------  ---------  ---------  ---------  -----
-----
Lambda  12.2  1.94e-15  4.11e-30  3.59e-67  4.74e-81  3.01e-85  0  -5.71e-101  -1.9e-65  -6.79e-50  -7.25e-37  -1.52e-31  -1.72
-10.5
Count    1    1         1         1         1         1         9   1           1         1          1          1          1
1
------  ----  --------  --------  --------  --------  --------  -  ----------  --------  ---------  ---------  ---------  -----
```

3.5 Spanning Tree and Tree Number

Here we show one example of a spanning tree by utilizing the *minimum_spanning_tree* method in the *networkx* package as follows.

```
In [7]: T = nx.minimum_spanning_tree(G)
        plt.figure(1, figsize=(10,10))
        nx.draw(T, node_color = 'aqua', with_labels=True,
                node_size=500, font_size=10)
        plt.show()
```

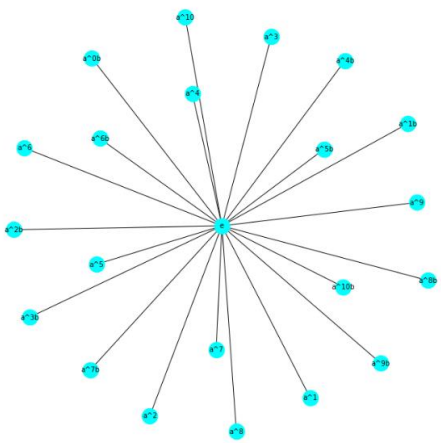

Figure 2 Spanning tree of Coprime graph

To find the number of all spanning tree of this graph we can use Theorem and Theorem from section 2. Using Theorem 2.2, we must find the determinant of cofactor of Laplacian matrix of the graph as follows.

```
In [8]: # Finding the degree matrix
        degree_m = np.zeros(shape=(2*n,2*n))

        index = 0
        for i in G.degree:
            degree_m[index, index] = i[1]
            index = index + 1
```

```
In [9]: laplacian_m = degree_m - nx.adjacency_matrix(G)
        laplacian_m_temp = laplacian_m[:, :2*n-1]
        laplacian_m_temp = laplacian_m_temp[:2*n-1,:]

        kappa1_G = int(np.linalg.det(laplacian_m_temp))
        kappa1_G

Out[9]: 2944291104429866221568
```

On the other hand, using the formula from Theorem 2.4 we get the results

```
In [10]: kappa2_G = 2* (n+1)**(n-2) * n**n
         kappa2_G

Out[10]: 2944291104429867270144
```

We also try to calculate this tree number for various value of prime n and we get the following result.

Tabel 1 The tree number of the Coprime graph

n	$\kappa_1(G)$	$\kappa_2(G)$
3	216	216
5	1350000	1350000
7	53971714048	53971714048
11	2944291104429866221568	2944291104429867270144
13	2453024964828541355485560832	2453024964828518209626025984

The actual real value of the tree number is the $\kappa_2(G)$. The results we get for $\kappa_1(G)$ is different because of the error in Python when calculating the determinant of big matrix. From this table, we can see that the tree number of coprime graph is increasing very fast.

3.6 Chromatic Number

The chromatic number of a graph can be determined with the following code.

```
In [11]: H = nx.greedy_color(G)
         color = list(H.values())
         unique_color = set(color)
         print('The chromatic number of graph is', len(unique_color))

         The chromatic number of graph is 3
```

Based on the chromatic number, the code for coloring the graph so that the two neighboring vertex have different colors is as follows.

```
In [12]: def get_cmap(n, name='prism'):
             '''Returns a function that maps each index in 0, 1, ..., n-1 to a distinct
             RGB color; the keyword argument name must be a standard mpl colormap name.
             return plt.cm.get_cmap(name, n)

         cmap = get_cmap(len(unique_color))

         new_color = []
         for i in color:
             new_color.append(cmap(i))

         plt.figure(1, figsize=(10,10))
         nx.draw_circular(G, node_color = new_color, with_labels=True)
```

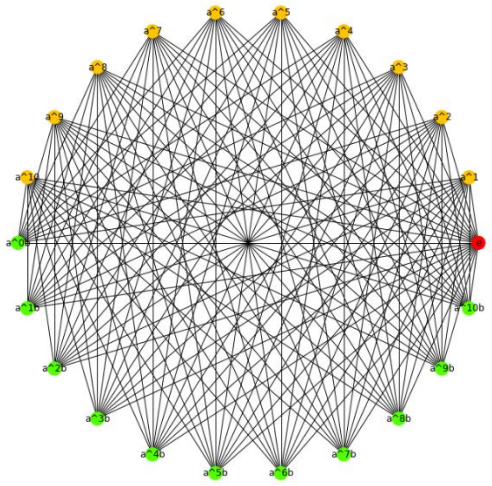

Figure 3 Minimal coloring of the Coprime graph

4 Conclusion

Using the Python program, several properties of the coprime graph of the dihedral group can be seen, including the adjacency matrix, spectrum, tree number and

chromatic number. Simulation using python helps in illustrating the graph image and minimal coloring of the graph. The tree number is also calculated with various prime n by two different formulas to compare its results. As seen in the table, the calculation of the tree number based on the determinant of the Laplacian cofactor matrix is still not accurate due to computational errors in Python.

References

[1] X. Ma, H. Wei and L. Yang, "The Coprime graph of a Group," *International Journal of Group Theory,* vol. 3, no. 3, pp. 13-23, 2014.

[2] R. Juliani, M. Masriani, I. G. A. W. Wardhana, N. W. Switrayni and I. Irwansyah, "Coprime Graph Of Integers Modulo N Group And Its Subgroups," *Journal of Fundamental Mathematics and Applications (JFMA),* vol. 3, no. 1, pp. 15-18, 2020.

[3] A. G. Syarifudin, N. Nurhabibah, D. P. Malik and I. G. A. W. Wardhana, "Some characterizatsion of coprime graph of dihedral group D2n," *Journal of Physics: Conference Series,* vol. 1722, no. 1, 2021.

[4] A. G. Syarifudin, I. G. A. W. Wardhana, N. W. Switrayni and Q. Aini, "Some Properties of Coprime Graph of Dihedral Group D2n When n is prime power," *Journal of Physics: Conference Series,* vol. 1722, no. 1, 2021.

[5] A. G. Syarifudin, I. G. A. W. Wardhana, N. W. Switrayni and Q. Aini, "The Clique Numbers and Chromatic Numbers of The Coprime Graph of a Dihedral Group," *IOP Conference Series: Materials Science and Engineering,* vol. 1115, no. 1, 2021.

[6] N. Nurhabibah, A. G. Syarifudin and I. G. A. W. Wardhana, "Some Results of The Coprime Graph of a Generalized Quaternion Group Q_4n," *InPrime: Indonesian Journal of Pure and Applied Mathematics,* vol. 3, no. 1, pp. 29-33, 2021.

[7] J. A. Gallian, Contemporary Abstract Algebra 7th Edition, Belmont: Cengage Learning, 2009.

[8] N. Biggs, Algebraic Graph Theory, New York: Cambridge University Press, 1996.

[9] H. P. Langtangen, A Primer on Scientific Programming with Python 5th Edition, Springer Nature, 2016.

[10] I. B. Muktyas and S. Arifin, "Semua Subgrup Siklik dari Grup (Zn,+)," *Jurnal Teorema: Teori dan Riset Matematika,* pp. 177-186, 2018.

[11] J. Hamm and A. Way, "Parameters of the Coprime Graph of a Group," *International Journal of Group Theory,* vol. 10, no. 3, 2021.

Proceedings of the 3rd ITB Graduate School Conference ISSN: 2963-718X
Enhancing Creativity in Research Through Developing Innovative Capabilities
December 21, 2022

Design of Hydrogen on Demand Production Generator Based on Aluminum Waste and Water Hydrolysis using VDI 2221 Method

Aditya Putra Widodo[1,*] & Deni Shidqi Khaerudini[2]

[1]Postgraduate Master of Mechanical Engineering, Mercu Buana University, Jl. Meruya Selatan No. 1 Kembangan West Jakarta 11650
[2]Research Center for Advanced Materials, National Research and Innovation Agency (BRIN), Puspiptek, South Tangerang, 15314, Banten, Indonesia
[*]Email: adityaputrawidodo@yahoo.co.id

Abstract. Hydrogen is one of the transition energy sources and has an important role in the decarbonization of the global energy system. There are several methods of generating hydrogen such as reforming hydrocarbon, electrolysis of water as well as chemical reactions between active metals such as aluminum or primary hybrid solution. Hydrogen production from aluminum can provide an alternative way to produce hydrogen on demand. Hydrogen generator on demand is a generator that can produce hydrogen as needed, in other words the generator will only produce hydrogen when there is a demand. This research aims to design a hydrogen on demand generator with a more minimalist dropping mechanism to reduce blockage of aluminum powder so that it can overcome the weaknesses of the previous system. The method used in this research is the VDI 2221, which is a method with a systematic approach to solving problems and optimizing the use of materials and technology which is expected to facilitate a design. The result of this research is the design of a hydrogen on demand generator with a minimalistic dropping mechanism. From the results, it can be concluded that the VDI 2221 method is very helpful and facilitates of the design process and the realization of a hydrogen on demand generator design with minimalistic dropping mechanism, namely an automatic opening system supported by spring.

Keywords: *Hydrogen on Demand; Aluminum Waste; Hydrolysis; Generator Design; VDI 2221.*

1 Introduction

Hydrogen is one of the transition energy sources and has an important role in the decarbonization of the global energy system in [1]. Hydrogen is also the best fuel to get high performance from fuel cells in [2]. There are several methods of generating hydrogen such as reforming hydrocarbon, electrolysis of water as well as chemical reactions between active metals such as aluminum or primary hybrid solution in [3]. Hydrogen production from aluminum can provide an alternative

way to produce hydrogen on demand. Hydrogen generator on demand is a generator that can produce hydrogen as needed, in other words the generator will only produce hydrogen when there is demand. However, to date no sustainable generator solutions have been adopted by industry or consumers as an economically viable, financially attractive, and beneficial solution to society in [4]. However, Avrahami et al in [3] argue that the method of dropping aluminum powder continuously and controlled from time to time in two closed spaces has the potential to produce hydrogen on demand. In his research, it was stated that of the 5 design variations, the mechanism of dropping aluminum powder through a rotating disc was the best mechanism with an average H_2 flow rate of 420 ml/minute, but had a weakness, namely the blockage of aluminum powder between the discs, which interfered with the release of aluminum powder into the water container (cartridge reactor).

The design in this research aims to make a new generator that is better at refining previous research. Therefore the design of the generator must have more value than the previous generator, such as in terms of the mechanism and effectiveness of the generator. In designing a generator, a method can be used is the VDI 2221 method. The VDI 2221 method is a method used to design a product, including for designing hydrogen generators on demand because the VDI 2221 method can be used to overcome problems in a design by optimizing the material using and technology used in a design.Therefore, in this research designed a hydrogen on demand production generator with an update on the dropping mechanism with the aim of reducing the blockage of aluminum powder so that the expected hydrogen production will be more optimal.

2 Method

2.1 Flow chart Research

The research flowchart explains the outline of the research implementation methodology. The research sequence starts from; study literature, conclusions. The research sequence can be seen more clearly in Figure 1.

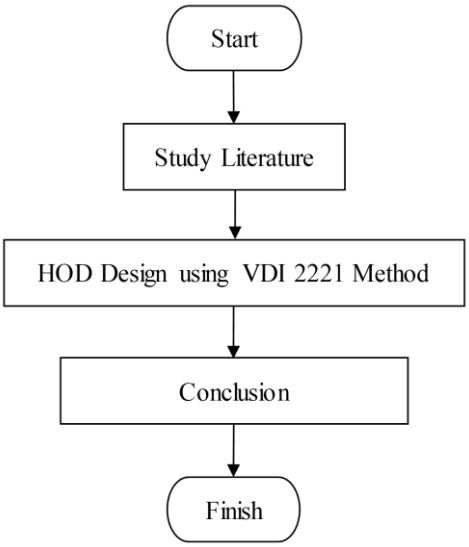

Figure 1 Flow chart research of design generator hydrogen on demand.

2.2 VDI 2221 Method

The design method in the Design of Hydrogen on Demand Production Generator Based on Aluminum Waste and Water Hydrolysis using VDI 2221 Method must be systematic so that it can fulfill several aspects such as tool safety, ease of use, ease of maintenance, and ease of repair. The VDI 2221 method (Verein Deutcher Ingenieure) written in a book by Gerhard Pahl and Wolfgang Beitz entitled Engineering Design: A Systematic Approach is a Systematic Method for Solving Problems. In the VDI 2221 method there are several phases, namely:

- Phase 1 : Classification of the Task (Clarification of the Task)
- Phase 2 : Conceptual Design
- Phase 3 : Form Design (Embodiment Concept)
- Phase 4 : Detailed Design (Detail Design)

The phases in the VDI 2221 method can be illustrated through the following flowchart, see figure 2:

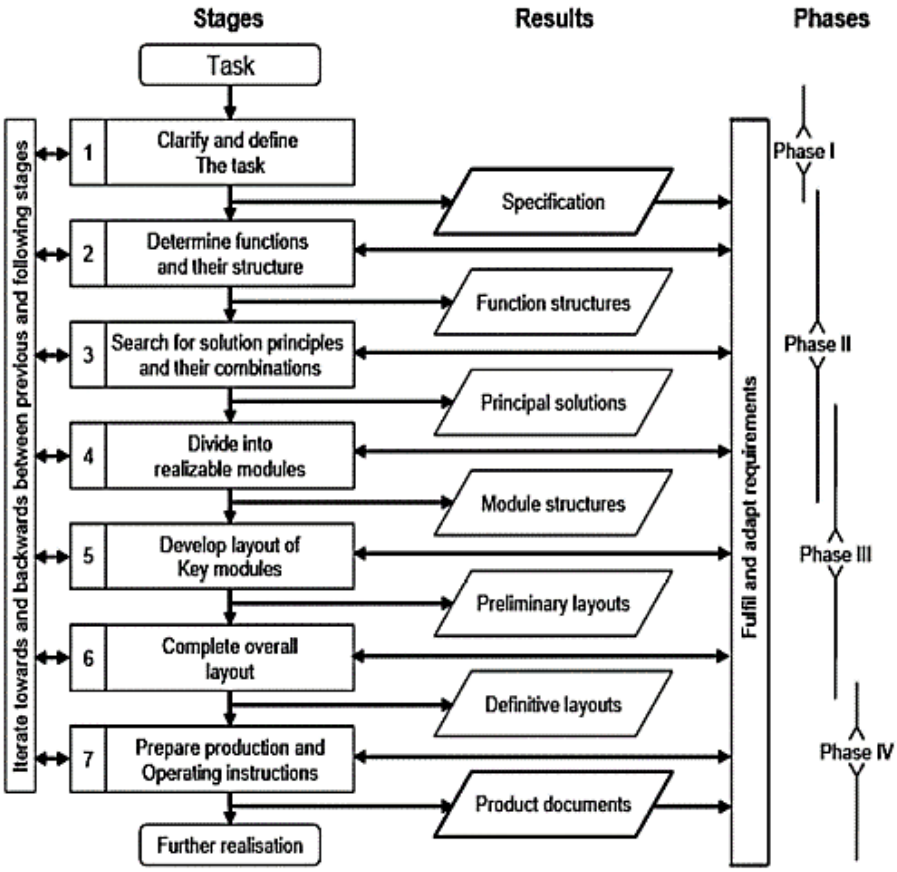

Figure 2 Flow chart of VDI 2221 method

3 Results and Discussion

3.1 Wish List

At this stage, an idea or wishes is carried out to realize a hydrogen generator that meets the specifications. The list of inclinations is arranged systematically into a list called a Wish List. Each specification is divided into 2 categories: D (Demands) dan W (Wishes), See Table 1.

Table 1 Wish list.

PARAMETER	SPESIFICATION	DEMAND (D) / WISHES (W)
GEOMETRY	Powder chamber height 163 mm	D
	Water chamber height 296 mm	D
	Diameter 150 mm	D
KINEMATIC	Can produce hydrogen 300 liter/minute	W
	Mixer blade upper dan mixer blade lower can operate together	D
	Driver motor DC 30 RPM	D
	Ball Bearing	D
MATERIAL	Tank stainless steel	D
	Elbow Plate	D
	Steel	D
	Wire springs	D
	Hex and SHCS Bolt	D
	Tank Acrylic	W
ASSEMBLY	Assembly system is easy to understand	D
	Easy to assembly - disassembly	D
MANUFACTURE	Manufacture in workshop (subcontract)	D
	Using standart part	D
	Easy to manufacture	D
	Manufacture in college	W
OPERATION	Easy to operate	D
	No special skills require	D
	Safe to use	D
	Full automatic	W
MAINTENANCE	Easy to refill	D
	Easy to clean	D
PRICE	Affordable for students	D

3.2 Abstraction

Abstraction is the formulation of the problem and analysis of the wish list. In the abstraction there are 5 steps, namely:

1. Eliminate all wishes (w) statement, see Table 2.

Table 2 Abstraction 1.

PARAMETER	SPESIFICATION	DEMAND (D) / WISHES (W)
GEOMETRY	Powder chamber height 163 mm	D
	Water chamber height 296 mm	D
	Diameter 150 mm	D
KINEMATIC	Mixer blade upper dan mixer blade lower can operate together	D
	Driver motor DC 30 RPM	D
MATERIAL	Ball Bearing	D
	Tank stainless steel	D
	Elbow Plate	D
	Steel	D
	Wire springs	D
	Hex and SHCS Bolt	D
ASSEMBLY	Assembly system is easy to understand	D
	Easy to assembly - disassembly	D
MANUFACTURE	Manufacture in workshop (subcontract)	D
	Using standart part	D
	Easy to manufacture	D
OPERATION	Easy to operate	D
	No special skills require	D
	Safe to use	D
MAINTENANCE	Easy to refill	D
	Easy to clean	D
PRICE	Affordable for students	D

2. Ignore wishes that have no direct impact to the main functions and constraints, see Table 3.

Table 3 Abstraction 2.

PARAMETER	SPESIFICATION	DEMAND (D) / WISHES (W)
GEOMETRY	Powder chamber height 163 mm	D
	Water chamber height 296 mm	D
	Diameter 150 mm	D

KINEMATIC	Mixer blade upper and mixer blade lower can operate together	D
MATERIAL	Driver motor DC 30 RPM	D
ASSEMBLY	Easy to assembly - disassembly	D
MANUFACTURE	Using standart part	D
OPERATION	Easy to operate	D
MAINTENANCE	Easy to refill	D
	Easy to clean	D

3. Change data quantitative into qualitative and make it a statement that is basic and of high quality, see Table 4.

Table 4 Abstraction 3.

PARAMETER	SPESIFICATION	DEMAND (D) / WISHES (W)
FUNCTION	Generator can generate hydrogen on demand	D
ASSEMBLY	Easy to assembly - disassembly	D
MANUFACTURE	Using standart part	D
OPERATION	Easy to operate	D
MAINTENANCE	Easy to refill	D
	Easy to clean	D

4. The results of step 3 above are then made more general, namely:
   - Generator can produce hydrogen on demand.
   - Generator uses standard parts so it is easy to assemble and disassemble.
   - Generator easy to maintain and operate.
5. Solve the problem in step 4 to be more neutral, namely the generator can produce hydrogen on demand more optimal.

3.3 Conceptual Design

3.3.1 Create generator function structure

Function structure is the general relationship between the input and output of a system that will carry out certain tasks. The function structure of the hydrogen generator is described in the form of a block diagram showing the input and output relationships as shown in Figure 2.

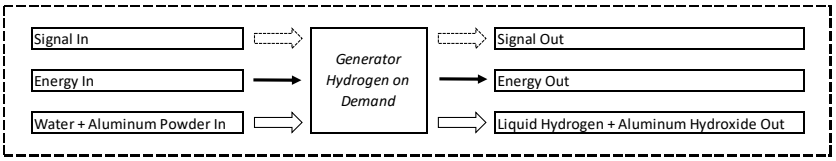

Figure 3 Function structure generator hydrogen on demand

3.3.2 Make the overall function of the generator

In this stage, a diagram of the overall function of the generator is described which can be provide into sub-functions, which can be seen in Figure 3.

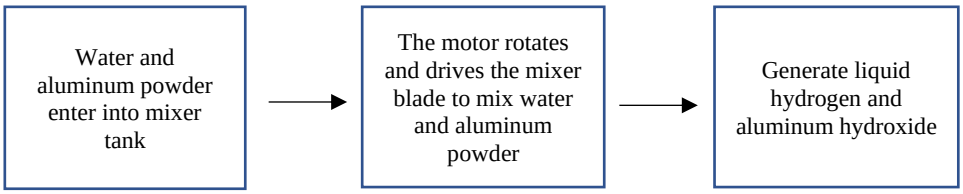

Figure 4 Sub function diagram of generator hydrogen on demand

3.3.3 Selection principle of generator function solutions

At this stage, we are looking for a principle solution to fulfill the sub-function of the hydrogen on demand generator that was made before, which can be seen in Table 5.

Table 5 Principles of sub function solutions.

No	Sub Function	Tool Part Functions	Principles Solutions		
			I	II	III
1	Dropping Mechanism	For dropping aluminum powder into water chamber	Automatic opening system (A)		
2	Chamber	Container to hold water and aluminum powder	Mild steel (A)	Acrylic (B)	Stainless steel (C)
3	Locking System	Components to bond the mixer tank and powder tank when assembled	Quick Release System (A)		

4	Motor	Mixer blade drive	High torque motor DC worm gear 12V 30RPM with encoder (A)	Motor DC – kipas angina (B)	Motor stepper (C)
5	Holder generator	Used to support a hydrogen generator	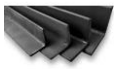 Elbow (A)	Hollow (B)	Pipe (C)

From Table 5 several solution principles have been compiled, so that alternative combination variants are obtained. Then it is selected again to be realized in the right choice. Combination variants can be seen in Table 6.

Table 6 Principles solutions combination chart.

No	Sub Function	Variant I (A)	Variant II (B)	Variant III (C)
1	*Dropping Mechanism*	1A		
2	*Powder Tank*	2A	2B	2C
3	Pengikat antar tangki	3A		
4	*Motor*	4A	4B	4C
5	*Holder generator*	5A	5B	5C

From Table 6 the combination principal chart of the solution obtained the following concept combination variants:

Variant I = 1A + 2A + 3A + 4B + 5B
Variant II = 1A + 2B + 3A + 4C + 5C
Variant III = 1A + 2C + 3A + 4A + 5A

Description of the variant combination of concepts I, II, and III can be seen in Table 7 below.

Table 7 Solution principle combination diagram.

Variant	Description
I	The mixer and powder tank uses mild steel material, uses a quick release, uses a stepper motor and uses an iron pipe generator support and a dropping mechanism uses a spring.
II	The mixer and powder tank uses acrylic material, uses a quick release, uses a fan motor and uses a hollow iron generator support and a dropping mechanism uses a spring.
III	The mixer and powder tank uses stainless steel material, uses a quick release, uses a DC worm gear motor with encoder and uses an angle iron generator support and a dropping mechanism uses a spring.

3.3.4 Choice of variant combinations

Combination selection is assessing variations with existing requirements in order to get the best design concept, see Figure 4.

TABLE OF SELECTION OF CONCEPTS FOR VARIATIONS HYDROGEN GENERATOR

MERCU BUANA

Decition Criteria :
(Y) Yes
(N) No
(?) Less Information
(!) Check Specification

Variations Design Concept

Variations	A	B	C	D	E	F	G	Remark	Result
	According to Overall of Function	According to Wish List	Production Cost	Easy to Assembly	Easy to Operate	Easy to Cleaning	Chamber Material Not Easy to Break		Decition
V1	Y	Y	Y	Y	Y	N	N	Input water & powder in 1 hole	N
V2	Y	Y	N	Y	Y	N	N	Input water & powder in 1 hole, Cost is more expensive because it uses pulleys & belts	N
V3	Y	Y	Y	Y	Y	Y	Y	OK	Y

Date : Nov 30, 2022 | Name : Aditya Putra Widodo | Postgraduate Master of Mechanical Engineering Mercu Buana University

Figure 5 Selection of the design concept variations

3.4 Embodiment Design

From the results of the table selection of the concept design variation and considering several factors to realize the design, it can be concluded that the best variation for design hydrogen on demand generator is variation 3. Then the next

step is to design sketch. The schematic design of hydrogen generator on demand can be see in Figure 5.

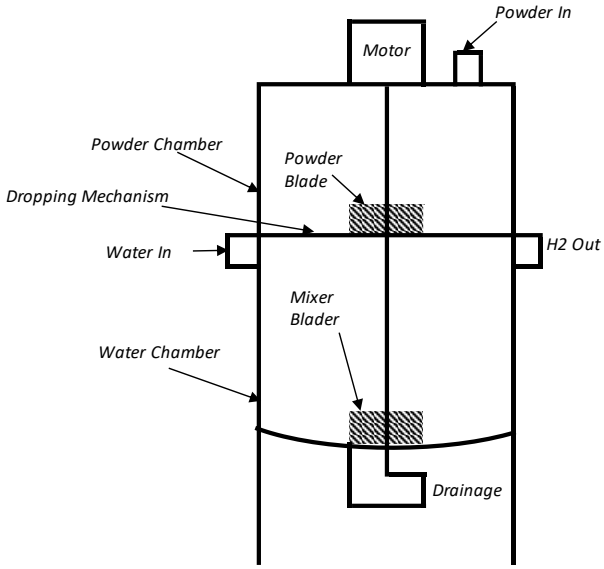

Figure 6 Design sketch of generator hydrogen on demand

3.5 Detail Design

Detail design is the final stage in a design namely in a documents that including such as tool drawings, detailed tool drawings, part lists, material specifications, operating systems, tolerances and other documents. The design generator made using the Siemens NX 7.5 software application. The main components of this tool can be see in Table 7.

Table 7 Main component of generator hydrogen on demand.

No	Part Name	Function
1	Mixer Tank	To hold water and aluminum powder when stireed
2	Mixer Blade	To stirring water
3	Powder Tank	To hold aluminum powder when stopped
4	Spring Holder	Part of powder valve so it can be open/close as automatically
5	Powder Valve	To open-close aluminum powder hole
6	Cover	Motor's cover guard or safety guard
7	Motor Holder	To hold motor
8	Mixer Upper Blade	To sweep aluminum powder so that it falls into the mixer tank area

3.5.1 Shop Drawing

Shop drawing of generator hydrogen on demand can be see in Figure 7 and Figure 8 as follows:

Figure 7 Detail 3D of generator hydrogend on demand

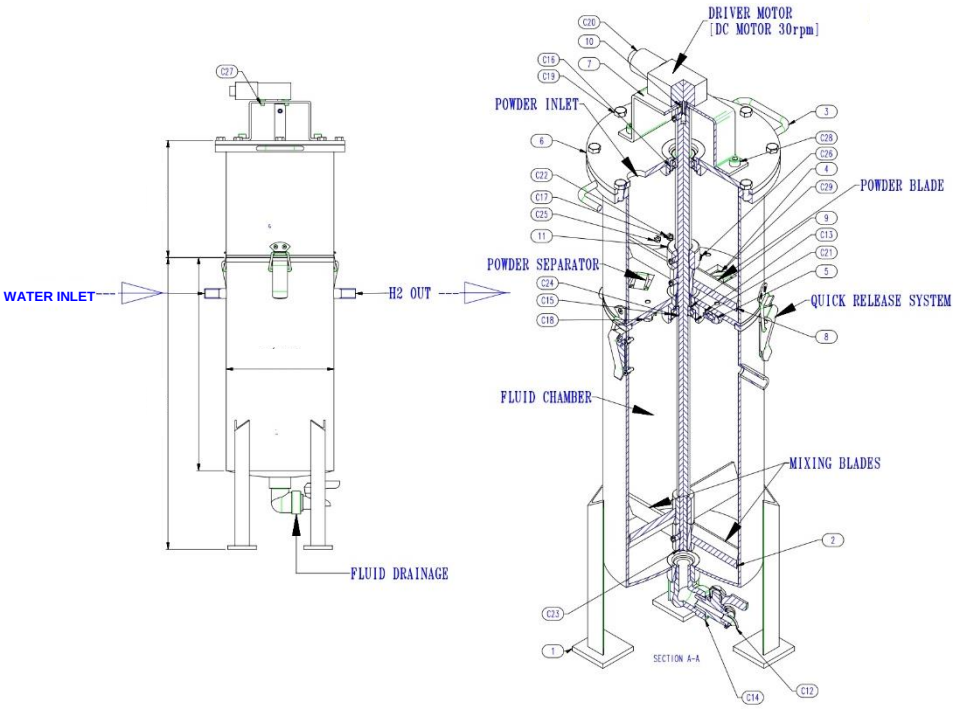

Figure 8 Detail assembly drawing of generator hydrogen on demand

3.5.2 Part List

Part List of generator hydrogen on demand can be seen in Table 8 as follows:

Table 8 Part list of generator hydrogen on demand.

No. Part	Name Of Part	Qty	Remark
1	00-Mix-01 [Mixer Tank]	1	Manufactur
2	00-Mix-02 [Mixer Blade]	2	Manufactur
3	00-Mix-03 [Powder Tank]	1	Manufactur
4	00-Mix-04 [Spring Holder]	3	Manufactur
5	00-Mix-05 [Powder Valve]	3	Manufactur
6	00-Mix-06 [Cover]	1	Manufactur
7	00-Mix-07 [Motor Holder]	1	Manufactur
8	00-Mix-08 [Mixer Blade Upper]	1	Manufactur
9	00-Mix-09 [Spacer]	1	Manufactur
10	00-Mix-10 [Shaft]	1	Manufactur
11	00-Mix-11 [Collar]	1	Manufactur
C12	Ball Valve 1_2 Bbpl2	1	Commercial Part
C13	Clgn5-40.0	3	Commercial Part
C14	Elbow 90 Deg-Sgpelh15a	1	Commercial Part
C15	Fag Bearing, 6201.27r	1	Commercial Part
C16	Fag Bearing, 6202.2zr	1	Commercial Part
C17	Fhcs Screw, Mjx10	12	Commercial Part
C18	Hex Bolt,M5x15	6	Commercial Part
C19	Hex Bolt,M6x15	8	Commercial Part
C20	High Torque Motor Dc Worm Gear 12v 30 Rpm With Encoder	1	Commercial Part
C21	Inner Snap Ring, M32x1.2	2	Commercial Part
C22	Nut M 3	12	Commercial Part
C23	Outer Snap Ring, S 10x0,6	1	Commercial Part
C24	Outer Snap Ring, S 12x1	1	Commercial Part
C25	Pkws4	3	Commercial Part
C26	Set Screw, M6x10	7	Commercial Part
C27	Shos Screw, M3x10	4	Commercial Part
C28	Shcs Screw, M6x10	4	Commercial Part
C29	Wire Spring Wm8-10	6	Commercial Part

4 Conclusion

Based on the results and discussion described above, it can be concluded that the VDI 2221 method is very helpful and facilitates the design process and the realization of a hydrogen on demand generator design with a minimalist dropping mechanism, namely an automatic opening system supported by spring system. In this research the method used is VDI 2221, so it is necessary to carry out further validation using the taguchi method to prove that the design is fit for purpose and is feasible for making a prototype. In addition, further research is needed to determine fluid dynamics or reactions that occur inside generator using computational fluid dynamic (CFD).

5 References

[1] Tasrif, A. *Hidrogen Didorong Jadi Kontributor Transisi Energi Indonesia. Direktorat Jendral EBTKE*. https://ebtke.esdm.go.id. (23 Februari 2022). (https://ebtke.esdm.go.id/post/2022/02/23/3094/hidrogen.didorong.jadi.kontributor.transisi.energi.indonesia).

[2] Jung, C.R., et al, *Hydrogen from aluminium in a flow reactor for fuel cell applications.* Journal of Power Source, 175, pp. 490-494, Sep. 2007.

[3] Avrahami, I. et al, *Hydrogen Production On-Demand By Hydride Salt And Water Two-Phase Generator,* International Journal of Hydrogen Energy, 45, pp. 15270-15282, Mei. 2020.

[4] Demirci, U.B., et al, *Ten-Year Efforts And A No-Go Recommendation For Sodium Borohydride For On-Board Automotive Hydrogen Storage,* International Journal of Hydrogen Energy, 34(6), pp. 2638-2645, Mar. 2009.

[5] Nurdin, H., Ambiyar, and Waskito, *Peracangan Elemen Mesin*, UNP Press. 2020.

[6] Panjaitan, U., *Perancangan Mesin Pencacah Rumput Multifungsi Dengan Metode VDI 2221*, Presisi Jurnal Teknik Mesin, 22(1), pp. 65–78, Jan. 2020.

[7] Pratama, A. and Fitri, M., *Rancang Bangun Alat Uji Konstanta Pegas Ulir Tekan Untuk Kapasitas 50 N/Mm Menggunakan Metode VDI 2221,* Jurnal Ilmiah Teknik Mesin, 6(1), pp. 41-49, Sep. 2020.

[8] Dermawan, R. and Hadi, V., *Pengembangan Mesin Pengupas Kulit Kopi Menggunakan Metode Vdi 2221,* Presisi, 24(2), Jul. 2022.

[9] Shkolnikov, E.L., et al, *Aluminum as Energy Carrier: Feasibility Analysis And Current Technologies Overview.* Renewable and Sustainable Energy Reviews, 15, pp. 4611-4623, Okt. 2011.

[10] Zhong, H. et al, *An One-Step Approach Towards Hydrogen Production And Storage Through Regeneration of* $NaBH_4$, Energy Storage Material, 7, pp. 222-228, Apr. 2017.

[11] Garin, G. F. N. A., and Nugroho, Y. A., *Perancangan Alat Penggulung Benang Menggunakan Metode VDI 2221 Pada Ukm Kf Kayra*. Jurnal Ilmiah Teknik Mesin, Elektro dan Komputer, 2(3), pp. 130-135, Nov. 2022.

[12] Leu, M. C., Joshi, A., and Kolan, K. C. R., NX7 For Engineering Design, 2007.

[13] Harfi, R., Gunawan, F., Hadi, V., and Supriyadi, E., *Perancangan Mesin Pemotong Karet Alam Dengan Menggunakan Metode VDI 2221*, Jurnal Terapan Teknik Mesin, 3(2), pp. 57-68, Okt. 2022.

[14] Setiawan, A. B., and Nugroho, Y. A., *Rancang Bangun Alat Cetak Kue Nastar Keranjang Menggunakan Metode VDI 2221*, Jurnal Cakrawala Ilmiah, 1(11), pp. 2713-2722, Jul. 2022.

[15] Kosasih, W., et al., *Modification of Chocolate Stirring Machine Using Reverse Engineering and VDI 2221 Methods*, Proceedings of the Second Asia Pacific International Conference on Industrial Engineering and Operations ManagemeSurakarta, Indonesia, pp. 1524-1536, 2021.

[16] Andreas, W., Daywin, F. J., Laricha, L., Gozali, L., and Purnairawan, A., *Modification of Group Head Coffee Machine Using Reverse Engineering and VDI 2221 Methods*, Proceedings of the Second Asia Pacific International Conference on Industrial Engineering and Operations Management, pp. 14-16, 2021.

Proceedings of the 3rd ITB Graduate School Conference ISSN: 2963-718X
Enhancing Creativity in Research Through Developing Innovative Capabilities
December 21, 2022

Open-system Magmatic Process at Agung Volcano, Bali, Indonesia: Evidence from Phenocryst Compositions and Textures

Adzkia Noerma Arifa[1, *], I Gusti Bagus Eddy Sucipta[2], & Idham Andri Kurniawan[2]

[1]Geological Engineering Master Program, Faculty of Earth Sciences and Technology, Institut Teknologi Bandung
[2]Petrology, Volcanology and Geochemistry Research Group, Geological Engineering, Faculty of Earth Sciences and Technology, Institut Teknologi Bandung
*Email: adzkiaarifa@gmail.com

Abstract. Agung volcano is an active stratovolcano located in Bali, Indonesia. It is the highest volcano on Bali at 3142 m a.s.l. Samples are collected along the flanks and represent each lava unit. In term of petrology, samples are porphyritic high alumina basalt, basaltic andesite and andesite with inhomogeneous phenocrysts of plagioclase, clinopyroxene, orthopyroxene, olivine, amphibole and titano-magnetite. Plagioclase phenocrysts frequently show fine sieve, resorption surface, coarse sieve and oscillatory zoning texture. Augite and enstatite phenocrysts display texture less zone and monotonous crystal zoning. Olivine phenocrysts are less abundant and present reaction rims of Mg-rich of orthopyroxene and titano-magnetite or Ca-poor clinopyroxene. Hornblende micro-phenocrysts just found in AD 1963 andesitic lava. They have reaction rims composed of augite, feldspar and symplectitic intergrowth of titanomagnetite. Plagioclase, pyroxene and olivine phenocrysts frequently display increases in Mg or Ca contents within mid-crystals. Dissolution, resorption and reverse zoning suggest open system magmatic behavior of repeated mafic magma recharge and also mineral-magma disequilibrium.

Keywords: *Agung volcano; disequilibrium; magma recharge; open system.*

1 Introduction

Indonesia is one of the most densely inhabited nations and home to hundreds of volcanoes. Most volcanoes belong to the Sunda volcanic arc, stretching from Sumatera to Banda Island as the result of subducted the Indo-Australia plate beneath the Eurasia plate. One of the active volcanoes is the Agung volcano on Bali Island. It had recorded effusive and explosive eruptions with the average eruptive frequency of one VEI >= 2-3 eruptions per century [1]. The biggest eruption was in 1963, following 120 years of dormancy, which caused a thousand fatalities [2]. Here we employ petrological and geochemical studies on lavas from the AD 1963 eruption to before the AD 1040 eruption of the Agung volcano

(Table 1). The data is used to understand the magmatic process beneath the Agung volcano as the minerals respond texturally and compositionally to changing magmatic environments.

Table 1 Lava units of Agung volcano [3] and the samples position.

Age	Stratigraphic Unit			Eruption Activity	Lava Flow	Sample Position
Relative	Absolute	Khuluk	Gumuk			
Quarternary	AD 1963	Agung			Al 14	BEL-1 & BEL-4
					Al 13	
	AD 1830 ± 40				Al 12	GA-TU 1
					Al 11	MTG-3
					Al 10	GA-180805 MT
					Al 9	GA-DA 1
	AD 1040 ± 40				Al 8	
			Pawon	Flank	Pl	BPW-2
					Al 7	DTH-1
					Al 6	
					Al 5	
					Al 4	GA-TD 1
					Al 3	
					Al 2	
					Al 1	

2 Geological Setting

The Agung volcano situated at latitude 08°20’20” S and longitude 115°30’30” E dominated the eastern part of Bali (Figure 1). It is one of the volcanoes in the western area of the Lesser Sunda in the central part of the Sunda volcanic arc. The oceanic crust that subducts beneath Agung volcano is some of the oldest in the Indian Ocean. It lies approximately 300 km north of the Java Trench and is situated about 162 km above the Benioff Zone [4].

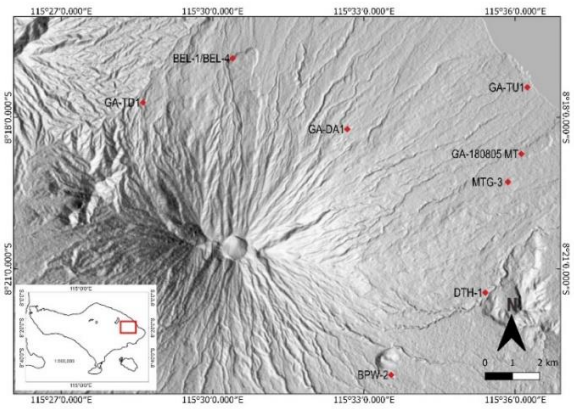

Figure 1 Sampling points map overlain onto a DEM. The inset map shows the location of Agung volcano (red) on the Bali Island.

Based on the geochemistry data, the affinity magma of Agung volcano is calc-alkaline series which are typical of those many Sunda volcanic arc. Based on discriminant diagrams (immobile trace element; La, Ce, Sm, Nb, Th, Y, Zr, Yb) for intermediate volcanic rocks, the tectonic environment of the Agung volcano is an island arc (Figure 2). The Quaternary eruptions of the Agung volcano generated basaltic to andesitic lava in composition and pyroclastic fall or flow deposits around the flanks.

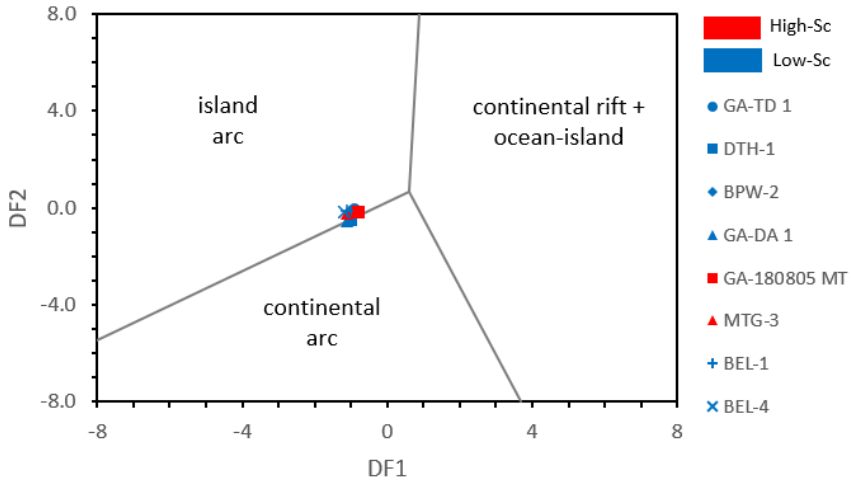

Figure 2 Discriminant diagram [5] to identify tectonic environment.

3 Methodology

Lava samples were prepared for petrology and mineralogy analyses. The optical microscope was used to obtain important information on mineral texture, abundance, and distribution. Polished sections, which were carbon coated, were used to examine mineral chemistry. The analytical instrument used to obtain mineral chemical composition was scanning electron microscope-energy dispersive X-ray spectroscopy (SEM-EDS) JEOL JSM-IT-300. We used back-scattered electron images to identify the compositional changes. Point and line analyses on olivine, pyroxene, plagioclase and titanomagnetite were acquired using 15kV accelerating voltage in high vacuum mode and ZAF correction procedure.

The samples were cut to remove the weathered surface before whole-rock composition analysis. Major element compositions of whole-rock were analyzed using an X-ray fluorescence spectrometer (XRF) and trace element compositions of whole rock were analyzed using ICP-MS/OES. Eight samples have LOI values <0.01 wt.% and one sample has LOI of 0.28 wt.% (Table 2).

Table 2 Major and trace elements data for lava of Agung volcano.

Sample	GA-TD 1	DTH-1	BPW-2	GA-DA 1	GA-180805 MT	MTG-3	GA-TU 1	BEL-1	BEL-4
Lava Unit [3]	Al4	Al7	Pl	Al9	Al10	Al11	Al12	Al14	Al14
Major elements (wt.%) recalculate dry									
SiO_2	57.69	54.59	54.43	60.09	53.59	52.41	51.43	58.53	57.61
TiO_2	0.80	0.85	0.86	0.68	0.97	1.03	1.20	0.73	0.79
Al_2O_3	17.40	20.58	20.76	17.35	18.13	19.64	17.78	17.39	17.27
Fe_2O_3t	8.31	7.75	7.61	7.31	10.11	9.67	11.57	7.68	8.22
MnO	0.19	0.17	0.17	0.18	0.19	0.19	0.21	0.17	0.18
MgO	3.29	2.47	2.52	2.31	4.25	3.72	4.98	3.17	3.50
CaO	6.99	8.71	8.76	6.63	8.26	8.88	8.56	7.12	7.35
Na_2O	3.43	3.32	3.44	3.33	2.99	3.14	2.92	3.25	3.21
K_2O	1.60	1.29	1.18	1.86	1.24	1.09	1.11	1.71	1.61
P_2O_5	0.29	0.27	0.27	0.28	0.27	0.23	0.24	0.26	0.27
LOI (wt.%)	*<0.01*	0.28	*<0.01*	*<0.01*	*<0.01*	*<0.01*	*<0.01*	*<0.01*	*<0.01*
Trace elements (ppm)									
La	15.00	12.30	12.40	20.00	11.20	10.50	11.30	15.70	15.50
Ce	31.60	26.80	26.20	42.50	24.80	22.60	24.80	34.30	34.00
Sm	4.50	3.60	4.10	5.10	3.70	3.70	4.20	4.30	4.70
Nb	5.10	3.30	3.70	4.60	3.80	3.30	2.90	5.10	4.90
Th	3.57	2.29	2.69	4.51	2.31	1.98	1.89	4.06	3.98
Y	23.60	21.90	21.50	28.10	20.70	21.30	22.30	23.10	24.10
Zr	118.00	89.50	87.90	163.00	85.90	80.10	83.40	126.00	125.00
Yb	2.90	2.30	2.50	3.10	2.30	2.50	2.70	2.90	3.10

4 Result

The lavas of Agung and its flank eruption fall into three main groups; (1) high alumina basalts, (2) medium-K basaltic andesite, (3) medium-K andesite. They are distinguished based on SiO_2, Na_2O and K_2O variation diagrams. In addition, two magma types are identified based on scandium (Sc) content, i.e. high-Sc (>20 ppm) and low-Sc (≤20 ppm) (Figure 3).

High alumina basalt (Figure 4). The high-Al basalt is inferred to be A12 lava unit. It dated to AD 1843+-40 [3]. This lava is designated based on SiO_2 content of 51.43 wt.%, more than 17 wt.% of Al_2O_3 and high-Sc (>20 ppm). It has porphyritic texture consisting of olivine (Fo65-76), plagioclase (An38-86), a small amount of augite (Mg#67-81) and enstatite (Mg#67-72). Olivine phenocrysts have zoning and frequently with thick reaction rims of pigeonite. Plagioclase phenocrysts are normal zoning from core to rim-crystal but compositional inversion in mid-crystal. Moreover, they dominantly display fine sieve texture, coarse sieve texture and glomerocrysts. The characteristic of Al-enrichment is due to the more prolonged episode of clinopyroxene or olivine crystallization before the appearance of plagioclase [6].

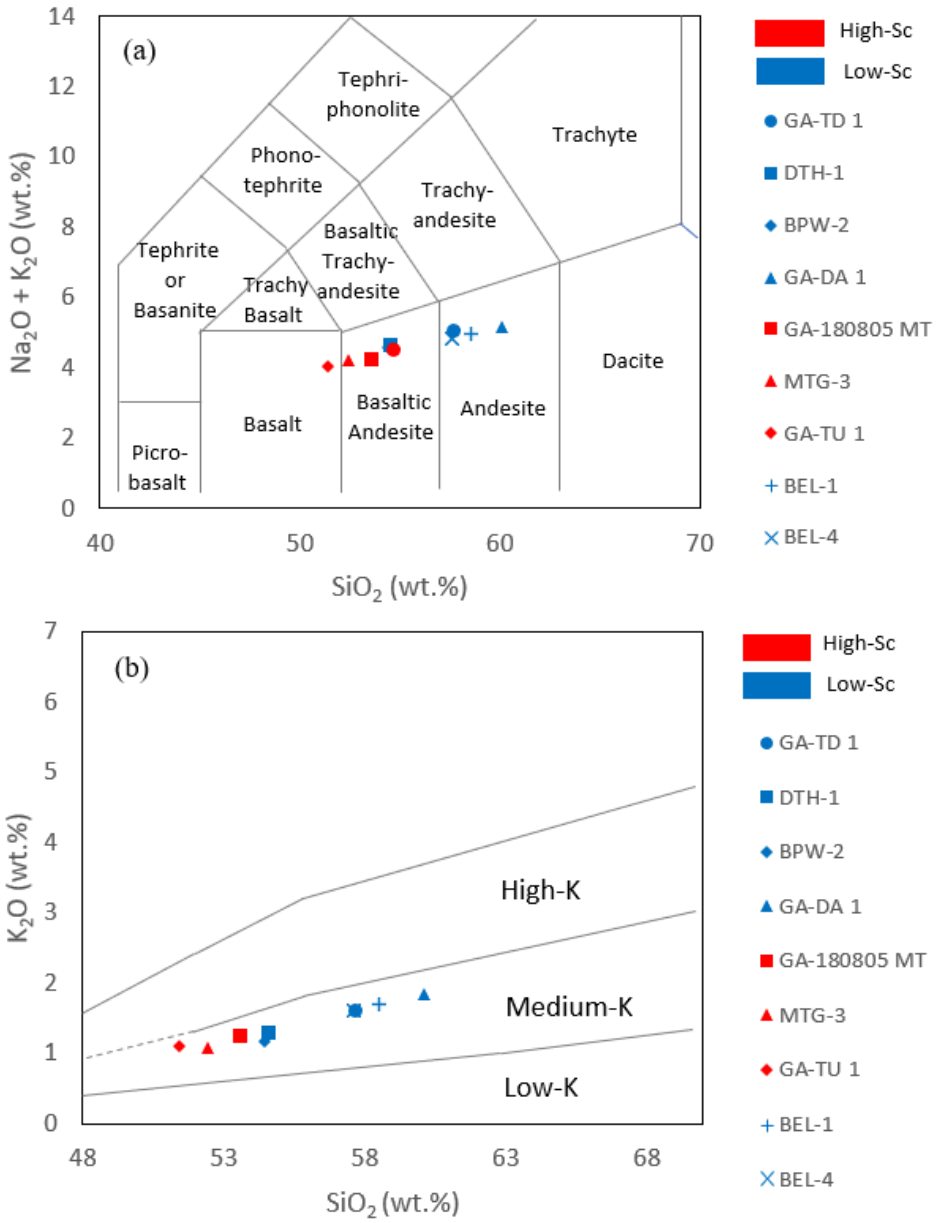

Figure 3 **(a)** Total alkali (TAS) [7] and **(b)** K_2O versus silica [8] classification diagram for lava of Agung volcano.

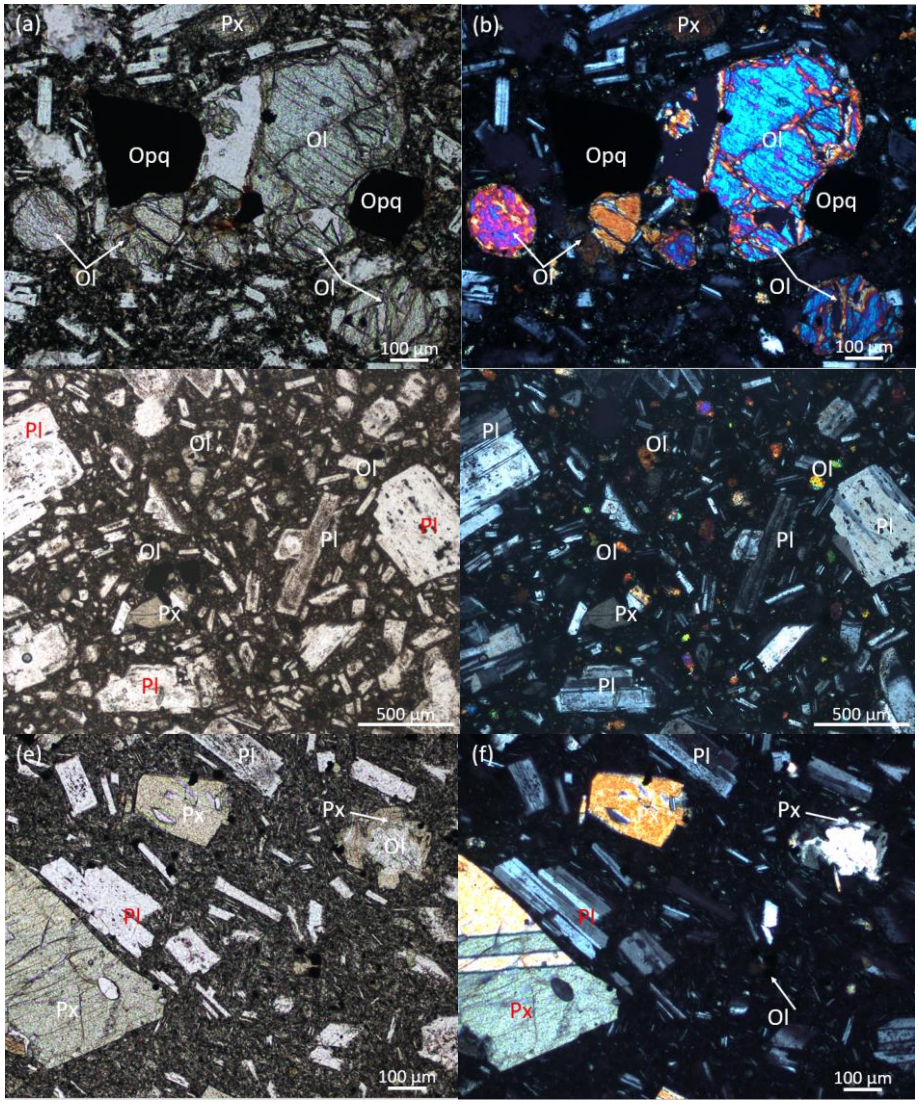

Figure 4 **(a)** and **(b)** Photomicrographs of basalt (GA-TU 1). **(c)** and **(d)** Photomicrographs of basaltic andesite (MTG-3). **(e)** and **(f)** Photomicrographs of andesite (BEL-4). Ol, olivine; Pl, plagioclase; Px, pyroxene; Opq, opaque mineral.

Medium-K basaltic andesite (Figure 4). The samples of medium-K basaltic andesite consist of Al7, Pl, Al10 and Al11 lava units. The group ranges from 52.41-54.59 wt.% SiO_2 and identified as low/high-Sc type. All rocks of this group are aluminous rich. Phenocrysts of this group are composed of olivine (Fo59-79), plagioclase (An43-85), a small amount of augite (Mg#70-77) and enstatite (65-

76). Olivine is zoned, often with reaction rims of clinoenstatite and symplectitic intergrowth of Fe-Ti oxide or pigeonite. Plagioclase phenocrysts are normal zoning from core to rim-crystal but compositional inversion in mid-crystal. They frequently display coarse sieve texture and glomerocrysts in all samples and fine sieve texture, resorption surface and rounded zone corner in several samples. Compared with the pyroxenes of high-Al basalts, the pyroxenes from basaltic andesitic are less Al-rich and slightly less Ti-rich. Moreover, they show a slightly increasing in Mg content in the mid-crystal.

Andesite (Figure 4). Al4, Al9 and Al14 lava units have andesitic composition with 57.61-60.09 wt.% SiO_2. The andesites are phenocryst-rich (28-43% volume) and dominated by plagioclase. The plagioclase phenocrysts (An30-86) are highly sieved (dominantly by fine sieve texture), oscillatory zoning and compositional inversion of Ca within mid-crystal. Rarely olivine is present (<2% volume) with reaction rims of clinoenstatite and pigeonite. Augite, enstatite and titanomagnetite phenocrysts are found in all the samples. Only in Al14 samples (lava of 1963 eruption), amphibole and xenolith are present. In general, the amphibole phenocrysts are hornblendes. They occur as micro-phenocrysts and appear to be the product of late-stage crystallization in H_2O-saturated condition. They have reaction rims composed of augite, feldspar and symplectitic intergrowth of titanomagnetite. Moreover, olivine xenocrysts with the highest forsterite content (Fo95) are found in the andesite xenolith in Al14 samples. These olivine xenocrysts are more magnesian than the other olivine phenocrysts. The high forsterite content of olivine may have crystallized from ultramafic rocks of presumed mantle origin [9].

Based on its stratigraphic position [3] the samples likely correspond to Al4, Al7, Pl, Al9, Al10, Al11, Al12, and Al14 lava units (Table 1). Lavas of Agung changed in composition throughout the eruption from andesite to basaltic-andesite and basalt i.e. the basaltic magma of the AD 1843 eruption differentiated into andesitic composition of the AD 1963 eruption. This open system behavior of Agung volcano includes magmatic recharge (mixing) recorded in minerals composition and micro-textures.

Crystal zoning reflects compositional changes in the mineral from core to rim-crystal [10]. Plagioclase, olivine, and pyroxene phenocryst of Agung's lava record normal zoning from core to rim-crystal but there are compositional inversions within mid-crystals. This condition suggests a more calcic magma injection, often considered to be synonymous with the recharge of more mafic magma, during the solidification process. It can be interpreted as open system process.

Plagioclase phenocrysts display a wide range of textures for investigating magma dynamics (Figure 5). Dissolution surfaces are found in most plagioclase phenocrysts and are described as coarse sieve and fine sieve textures. Coarse sieve interprets as a result of dissolution by the varying rate of adiabatic decompression during magma ascending into the shallower magma storage.

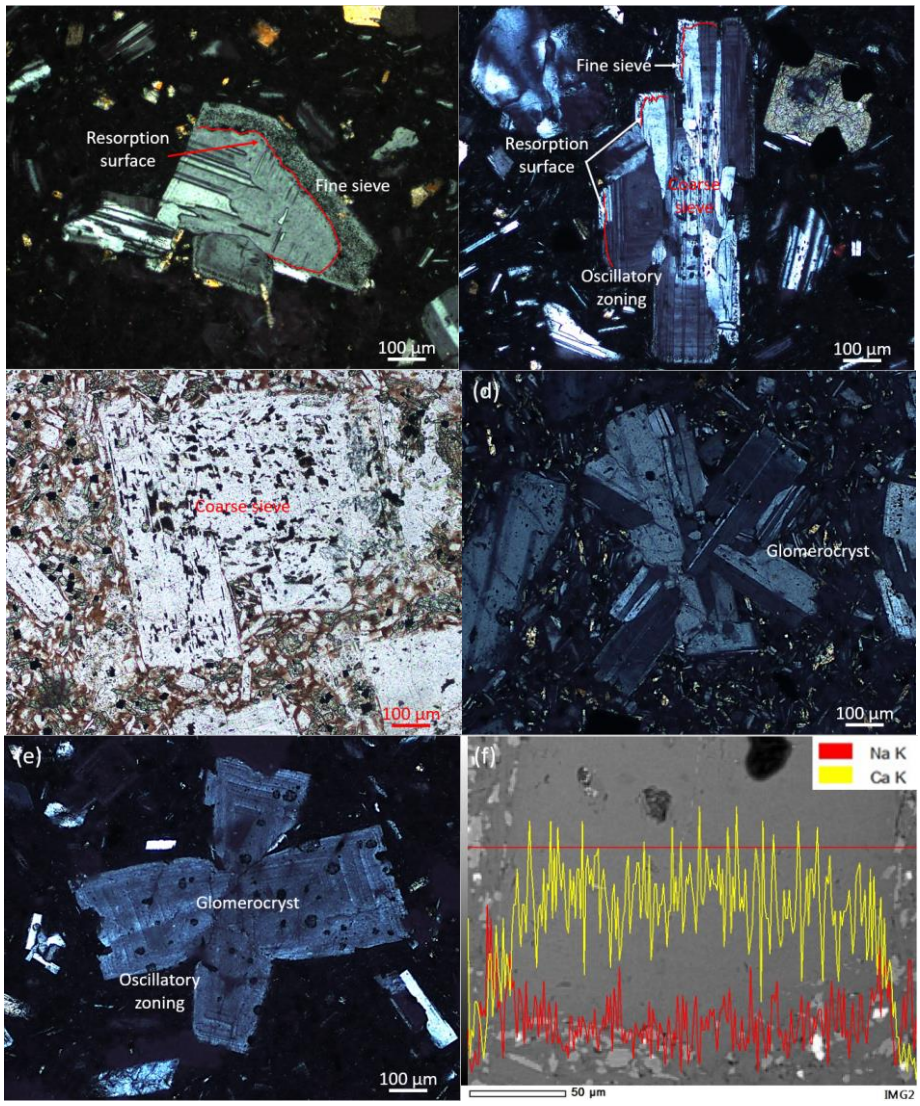

Figure 5 **(a)-(e)** Photomicrographs of various micro-textures in plagioclase phenocrysts. **(f)** Line analysis of plagioclase phenocryst show increases of Ca content in the mid mineral.

However, fine sieve interprets as a result of dissolution due to reaction with more calcic magma [11]. These sieve textures are frequently found at the core, mid or rim of plagioclase phenocrysts. The resorption surface is frequently found as the irregular surface at the outer edge of the fine sieve domain and the fine oscillatory zoning. Moreover, the fine oscillatory zoning is developed from the dynamic process such as crystallization from melt that was undergoing rhythmic changes in temperature or $P(H_2O)$ or composition and kinetic process such as local incremental diffusion-controlled kinetic growth at the crystal-melt interface in response to near equilibrium condition [11]. The presence of fine sieve texture and resorption surface are evidence for the recharge of more mafic magma into the shallower magma storage.

Olivine crystals can respond to diffusional re-equilibration, forming reaction rims or dissolution. These processes indicate open system behaviour [10]. Many olivine phenocrysts of Agung's lava have reaction rims of clinoenstatite or pigeonite, some texture less (Figure 6 and 7). Olivine phenocrysts in the basaltic andesitic lava also show symplectitic intergrowth of titanomagnetite within reaction rims of clinoenstatite or pigeonite (Figure 7). It serves as evidence for disequilibrium and indicates a different state of oxygen fugacity during crystallization from core to rim [12].

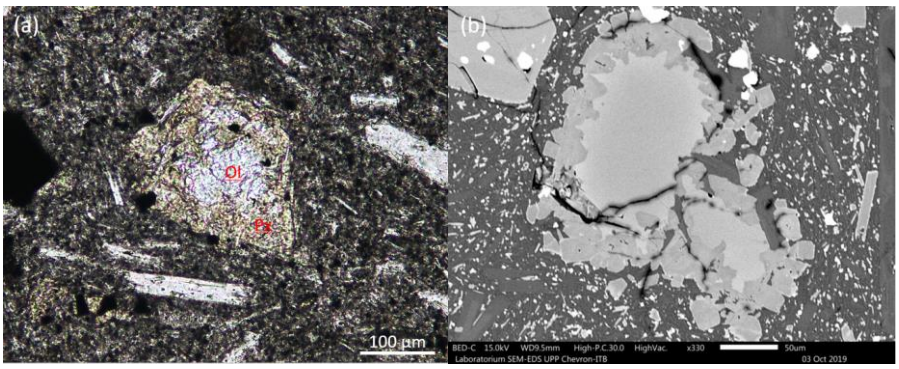

Figure 6 Reaction rims of olivine phenocrysts. **(a)** Photomicrograph of olivine phenocryst with thick reaction rim of pyroxene. **(b)** BED image of olivine phenocryst with thick reaction rim of clinoenstatite.

Orthopyroxene rim of olivine phenocrysts in basaltic andesitic or andesitic lava suggests mixing between basaltic and more silicic magma. Moreover, many olivine phenocrysts show a slightly increasing in Mg content in the mid-crystal that indicate recharge of more mafic magma during crystal growth. The presence of olivine crystals in intermediate to silicic magma is often taken as evidence for influx of more mafic magma [10].

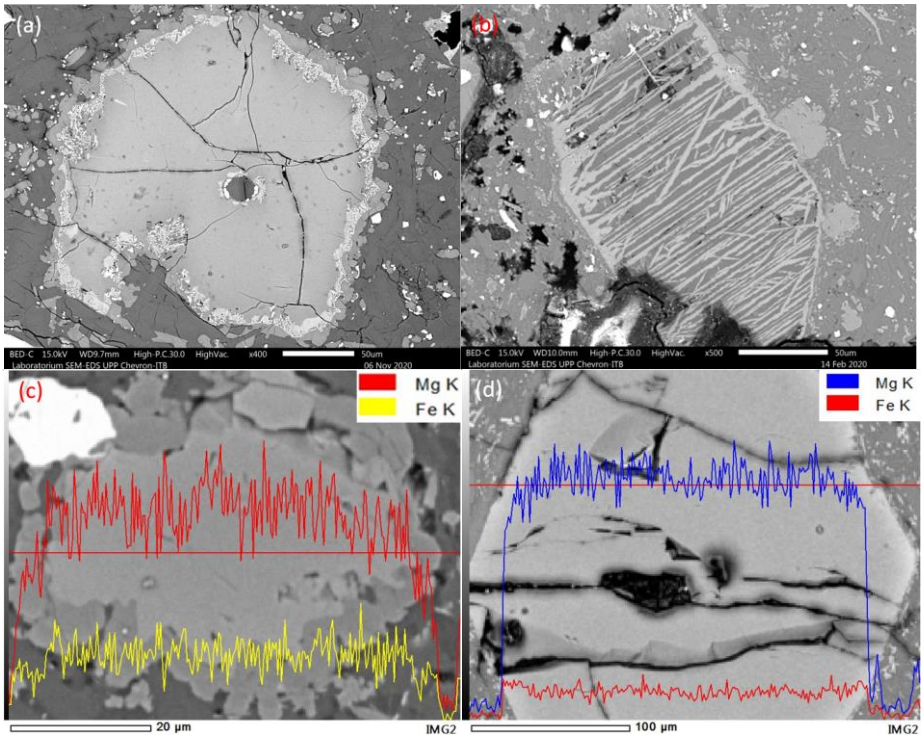

Figure 7 **(a)** BED image of of olivine phenocryst with reaction rim of clinoenstatite.and symplectitic intergrowth of titanomagnetite. **(b)** BED image of xenocryst olivine (Fo95) with lamella of lower forsterite content in the AD 1963 andesitic lava. **(c)** and **(d)** Line analyses of olivine phenocryst show slightly increasing in Mg content in the mid mineral.

Volatile-bearing minerals such as hornblende are particularly useful tools to constrain the syn-eruptive magma ascent rate because they become unstable as the concentration of dissolved water in the melt decreases during decompression. If magma ascends at a sufficiently slow rate, reaction rims of pyroxene, plagioclase and Fe-Ti oxides may develop around a hornblende crystal where it is in contact with melt [13] [14]. Hornblende with thinner reaction rims was interpreted to have originated from the main pulse of ascending magma, whereas the population of hornblende characterized by thicker rims was interpreted to have originated from batches of leftover or stalled magma in conduit [14].

Hornblende phenocrysts are only present in andesitic lava of the AD 1963 eruption. There are two types of hornblende phenocrysts, i.e. with thick opacitic rim and thick reaction rim of augite, plagioclase and symplectitic intergrowth of

titanomagnetite (Figure 8). First, the opacitic rim is described by the appearance of fine-grained magnetite [13]. This condition suggests a prolonged disequilibrium state when the magma ascended into storage depth outside amphibole stability. Second, thick reaction rims of augite, plagioclase and symplectitic intergrowth of titanomagnetite interpret to result from a heating event of leftover magma. Reaction rims are composed of orthopyroxene and plagioclase, with lesser amounts of Fe-Ti oxides produced during decompression [15].

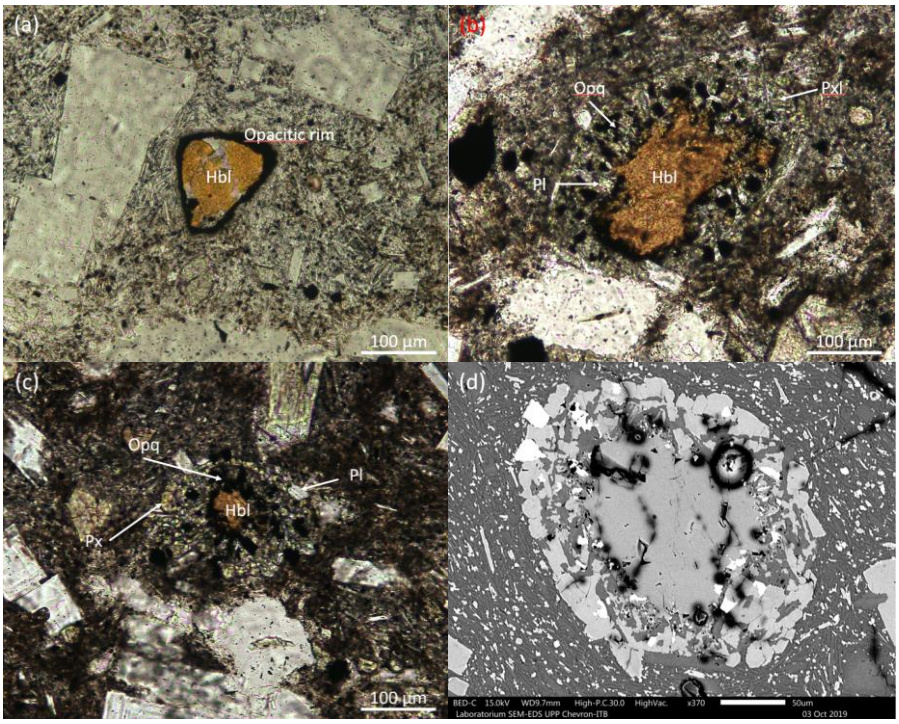

Figure 8 **(a)** Opacitic rim in hornblede. **(b)-(d)** Photomicrographs and BED image of thick reaction rim that composed of augite, plagioclase and titanomagnetite.

5 Conclusion

Agung volcano has three group of magma composition, i.e., andesite, basaltic-andesite and basalt. During the eruption before AD 1040 and AD 1963 there were changing magmatic composition from andesite to basaltic andesite, then basalt and andesite. The combined results between petrological and geochemical analyses show strong evidence for open system characteristics and disequilibrium condition between mineral and injected magma or leftover melt.

Plagioclase phenocrysts record wide range of textures and composition. There are many various micro-textures in plagioclase that can be described. Many plagioclase and olivine phenocrysts in all three groups are zoned from core to rim with compositional inversion in mid. Plagioclase phenocrysts dominantly display sieve texture and resorption surface due to dissolution and fine oscillatory zoning or glomerocrysts due to convective flow in the shallower magma chamber. Olivine phenocrysts display three types of reaction rims. i.e. pigeonite reaction rims, clinoenstatite with or without symplectitic intergrowth of titanomagnetite and texture less crystal. These textures may support the open system behavior and disequilibrium between olivine and the leftover magma in the magma chamber. Hornblende phenocrysts are only found in the AD 1963 andesitic lava. It strongly indicated that the AD 1963 andesitic magma was differentiated from leftover more mafic magma. Other evidence that supports this interpretation is thick reaction rims of augite, plagioclase and titanomagnetite in hornblende due to the heating event of leftover magma. However, thick opacitic rims suggest mineral-melt disequilibrium during magma ascending.

References

[1] Fontijn, K., Costa, F., Sutawidjaja, I., Newhall, C. G., & Herrin, J. S., *A 5000-year record of multiple highly explosive mafic eruptions from Gunung Agung (Bali, Indonesia): implication for eruption frequency and volcanic hazard*, Bulletin of Volcanology, **77**(59), Jun. 2015.

[2] Geiger, H., Troll, V. R., Jolis, E. M., Deegan, F. M., Harris, C., Hilton, D. R. & Freda, C., *Multi-level magma plumbing at Agung and Batur volcanoes increases risk of hazardous eruptions*, Scientific Report, **8**, pp. 1-14, Jul. 2018.

[3] Nasution, A., Haerani, N., Mulyadi, D., & Hendrasto, M., *Geological map of Agung volcano, Bali*, Directorate of Volcanology and Geological Hazard Mitigation, Bandung, 2004.

[4] Syracuse, E. M. & Goeffrey, A. A., *Global compilation of variations in slab depth beneath arc volcanoes and implications*, Geochemistry, Geophysics, Geosystems, **7**(5), pp. 1-18, May 2006.

[5] Verma, S. P. & Verma S. K., *First 15 probability-based multidimensional tectonic discrimination diagrams for intermediate magmas and their robustness against post emplacement compositional changes and petrogenetic processes*, Turkish Journal of Earth Sciences, **22**, pp. 931-995, Oct 2013.

[6] Foden, J. D., *The Petrology of The Calcalkaline Lavas of Rindjani Volcano, East Sunda Arc: A model for Island Arc Petrogenesis*, Journal of Petrology, **24**(1), pp. 98-130, 1983.

[7] Le Bas, M. J., Le Maitre, R. W. & Streckeisen, A., *A chemical classification of volcanic rocks based on the Total Alkali-Silica diagram*, Journal of Petrology, **27**, pp. 745-750, 1984.

[8] Peccerillo, A. & Taylor, S. R., *Geochemistry of Eocene calc-alkaline volcanic rocks from the Kastamonu area, northern Turkey*. Contributions to Mineralogy and Petrology, **58**, 63-81, 1976.

[9] Deer, W. A., Howie, R. A. & Zussman, J. *An introduction to the rock forming mineral*, ed.3, Mineralogical Society of Great Britain and Ireland, 2013.

[10] Streck, M. J., *Mineral textures and zoning as evidence for open system processes*, Minerals, inclusions and volcanic processes, Putirka, K. D. & Tepley III, F. J., eds., Walter de Gruyter GmbH & Co KG, pp. 595-622, 2018.

[11] Renjith, M.L., *Micro-texture in plagioclase from 1994-1995 eruption, barren island volcano: evidence of dynamic magma plumbing system in the Andaman subduction zone*, Geoscience Frontier, **5**, pp. 113-126, 2014.

[12] Perugini, D. Busa, T., Poli, G. & Nazzareni S., *The role of chaotic dynamics and flow fields in the development of disequilibrium textures in volcanic rocks*, Journal of Petrology, **44**(4), p. 733-756, Apr. 2003.

[13] Rutherford, M. J. & Devine, J. D., *The role of chaotic dynamics and flow fields in the development of disequilibrium textures in volcanic rocks*, Journal of Petrology, **44**(8), pp. 1433-1454, 2003.

[14] Szramek, L. & Browne, B., *Rates of magma ascent and storage*, The Encyclopedia of Volcanoes (Second Edition), Sigurdsson, H., ed., Academic Press, pp. 2013-214, 2015.

[15] Browne, B., Gardner, J. E. & Larsen, J. F. *Amphibole reaction rims in response to decompression compared to heating: an experimental approach*, AGU Fall meeting, 2003.

Proceedings of the 3rd ITB Graduate School Conference ISSN: 2963-718X
Enhancing Creativity in Research Through Developing Innovative Capabilities
December 21, 2022

The Effect of Element (Sr, Ti, B, and Mg) Modification on Microstructure to Increase Micro-Hardness of A356 Aluminum Alloy

Afghany Mostavan[1,*], Asep Ridwan[2], Arif Basuki[2] & Husaini Ardy[2]

[1]Doctoral Program of Materials Science and Engineering, Faculty of Mechanical and Aerospace Engineering, Institut Teknologi Bandung, Jl. Ganesha 10, Bandung, 40132, Jawa Barat, Indonesia
[2]Department of Materials Science and Engineering, Faculty of Mechanical and Aerospace Engineering, Institut Teknologi Bandung, Jl. Ganesha 10, Bandung, 40132, Jawa Barat, Indonesia
[*]E-mail: 33720001@mahasiswa.itb.ac.id

Abstract. It is known that Sr, Ti, B, and Mg can modify the microstructure of the A356 aluminum alloy, and the heat treatment process causes spheroidization of eutectic silicon. This experiment presents the effect of modifier elements and heat treatment on microstructure and microhardness. The A356 aluminum alloy is modified with a combination of elements containing Sr, Ti, B, and Mg. The microstructure analysis of the modified A356 aluminum alloy revealed that the size distribution of the α-phase and eutectic silicon particles that form spheroid Si particles varies depending on the combination composition. Comparisons between unmodified and modified alloys show that the aspect ratios of the α phase and the eutectic silicon particles are different. The modified A356 aluminum alloy's microhardness can be improved. This could be related to the aspect ratio of the α phase and eutectic silicon phases, spheroidization of fine eutectic silicon, and precipitation hardening.

Keywords: *A356 alloy; microstructure modification; micro hardness.*

1 Introduction

Al–Si casting alloys have an important role in the field of cast aluminium alloys. One of them is the A356 aluminium alloy, which has been widely used in the automobile, aerospace, and engineering industries because of its excellent cast ability, weld ability, high corrosion resistance, and various other desirable properties. Currently, the hypoeutectic alloy A356 (Al–7% Si–0.3% Mg) is used as a casting wheel product that is commonly used in the automotive. However, as-cast A356 aluminium alloy consists of coarse primary α-Al dendrites and acicular-shaped eutectic silicon, which degrades the mechanical properties and limits its industrial applications. The mechanical properties are determined by controlling the microstructure of the alloy. [1].

[1]Current address: R&D Laboratory for Metallurgy, PT. Chemco Harapan Nusantara Kawasan Industri Mitra Karawang, 413632, Jawa Barat, Indonesia.

Currently, casting wheel A356 aluminium alloy is processed through gravity die casting (GDC) and low-pressure die casting (LPDC) techniques. The composition of the metal alloy, casting process technique, cooling rate, and heat treatment will influence the high-quality of casting wheel. The high requirements of casting wheels specification standard are Ultimate Tensile Strength: min. 277 MPa, Yield Strength: min. 200 MPa, Elongation: min. 7-12 %, and Hardness: 80 – 95 HB [2][3]. According to ASTM B108 standard, A356 aluminium alloy material after the heat treatment process T6 has mechanical properties for Ultimate Tensile Strength min. 260 MPa, Yield Strength min. 150 MPa, and elongation min. 3% [4]. It demonstrates that increasing the strength through heat treatment is achievable, nonetheless the ductility of the A356 aluminium alloy is still poor, this needs to be accomplished.

The parameters affecting the microstructure, strength, and ductility of as-cast alloys are complex from a metallurgical perspective. The resulting microstructure, depending on solidification processing variables, heat treatment, and the addition of alloying elements. Strength will increase with a reduction in grain size only if the production of small grains does not increase the amount of micro porosity and the percentage of second phase. In order to improve the quality of cast Al alloys, grain refinement has generally been employed to decrease grain size and modify grain morphology from columnar to equiaxed, for example, by adding Ti and B. Some researchers observed that adding relatively small amounts of Sr can also modify the eutectic structure [5][6]. In order to create Mg-Si precipitates, Mg is a key alloying element added to Al-Si alloys. [7]. Therefore, the modifier is expected to result in a finer equiaxed structure, which improves secondary phase dispersion, castability, and mechanical characteristics. It also increases feed during solidification and lowers shrinkage porosity [8].

Adding grain refiners to casting processes for aluminium alloys is a common way to achieve grain refinement. According to some published research, grain refiners with particles of TiAl3, TiB2, and AlB2 refine aluminium alloys more effectively than those with only a single particle [9][10]. The effective on grain refinement of aluminium alloys have been observed through the addition of Al–Ti–B refiner. By addition of Sr will modify the eutectic silicon microstructure which can improve the mechanical properties of the Al-Si alloy. Sr has been observed to change the morphology of the eutectic Si phase from a coarse plate to a fine fibre-like network [6][11]. Furthermore, through T6 heat treatment on A356 aluminium alloy, the morphology of the eutectic silicon particles can alter from plate shape to spherical. Thus, this morphology significantly affects the mechanical properties of aluminium alloy, particularly its ductility [12][13]. However, prior research concentrated on the modification mechanism and/or altering the heat treatment process in order to increase the tensile strength and ductility. In this article, it is our aim to study the influence of element Sr by adding AlSr15, after that the effect of grain refiner by addition of ALTAB Ti80 and AlTi5B1 to form Ti and B which influence on grain refinement, and Mg by adding Mg 99% Ingot

to form precipitate on matrix α phases. Heat treatment T6 from solution treatment and aging treatment have been performed to modify the microstructure of A356 alloys and to improve the microhardness.

2 Experimental Method

2.1 Preparation

In this experiment, the A356 aluminium alloy ingot was melted in a 200 kg electric resistance furnace at 720 ± 10 °C. The molten metal was treated with the flux to remove impurities that cause slag to form at the melt's surface, and nitrogen gas was used for a degassing process. Then, the liquid metal was poured into a 1.25-kilogram capacity tiny crucible. The A_0 (A356 aluminium alloy ingot melt) melt is designed to be used as a baseline for comparison with additional elements. The A356 aluminium alloy will then be changed by adding AlSr15 (0,75 gr.) for A_1, ALTAB Ti80 (1,25 gr.) and AlSr15 (0,75 gr.) for A_2, ALTAB Ti80 (1,25 gr.), AlTi5B1 (1,5 gr.), and AlSr15 (0,75 gr.) for A_3, and ALTAB Ti80 (1,25 gr.), AlTi5B1 (1,5 gr), Mg (1,5 gr), and AlSr15 (0,75 gr) for A_4. Optical Emission Spectroscopy (OES) Shimadzu was used to determine the chemical compositions of the alloys, and the results are shown in Table 1/

Table 1 Chemical composition of experimental alloys analysed by OES (wt.%).

ITEM	CHEMICAL INGREDIENT (%)							
	Si	Mg	Fe	Mn	Cu	Zn	Ti	Sr
A0 (A356, base alloy)	7,05	0,43	0,09	0,002	0,002	0,02	0,14	0,010
A1 (A356 + AlSr15)	7,03	0,29	0,09	0,003	0,002	0,02	0,14	0,010
A2 (A356 + ALTAB Ti80 + AlSr15)	7,02	0,37	0,08	0,003	0,002	0,02	0,14	0,008
A3 (A356 + ALTAB Ti80 + AlTi5B1+ AlSr15)	7,04	0,38	0,09	0,003	0,002	0,02	0,14	0,008
A4 (A356 + ALTAB Ti80 + AlTi5B1+ AlSr15 + Mg)	6,96	0,48	0,09	0,003	0,002	0,02	0,14	0,010

2.2 Casting Process and Heat Treatment

According to ASTM B-108, the specimen test was carried out by pouring an aluminium melt into a permanent mould. Two sample bars were generated from each casting, as illustrated in Fig. 1. (a). The molten alloys are shown in Fig 1(b) being brought into the crucible before being poured into the permanent mould using the gravity casting technique. Before casting, the mould was heated to 300°C. For each of the A0, A1, A2, A3, and A4 conditions in Fig. 1(c), five castings were made one after the other in 15 minutes. The T6 heat treatment, which includes temperature of solution treatment and artificial aging, was applied to the cast specimen test after it had been maintained at ambient conditions for at least 24 hours. The first stage involved solution treatment for the solution condition (530°C ± 20°C), which was immediately followed by an immediate

water quench to room temperature. The aging treatment (160°C ± 20°C) was then carried out, and it was followed by air cooling.

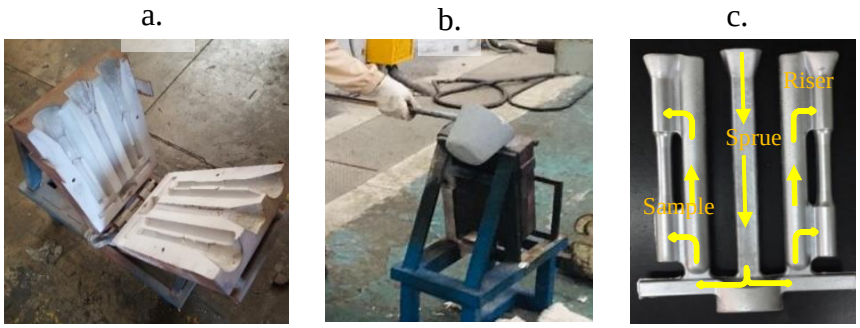

Figure 1. (a) The Permanent Mould is made according to ASTM B-108, (b) Manual gravity casting (c) Sample Test

2.3 Characterization

Specimen ϕ9 mm round test rod that has been split in half for microstructural analysis. Using a Keyence optical microscope (OM), a. The specimens were examined using OM after being ground using standard methods. After polishing without employing an etching solution, OM observations were made, and the results of metallography using OM were measured using the image J software program. According to ASTMN E384 standard, the ratio of the long diagonal to the short diagonal in the micro-Vickers hardness test is 7:1. This test is performed using a Knoop Indenter in the shape of a pyramid to identify the two separate diagonals, long and short. The properties obtained from 3 to 5 samples are the basis for each data point presented with a standard deviation.

3 Results and Discussion

3.1 Microstructure

Figure 2 illustrates how the addition of Sr, Ti, B, and Mg affected the microstructure of the as-cast A356 alloy. Due to the high solute content of the alloys with an amount of Si of ~7 wt%, it was discovered that Al Phases were dominating. As-cast A356 aluminum alloys modified with AlSr15, ALTAB Ti80, AlTi5B1, and Mg are each shown in Fig. 2 with their different OM morphologies. While the α–Al phase in the heat-treated condition exhibits dendritic development into an equiaxed structure, the α–Al phase in the cast condition exhibits coarse dendrite morphology. Primary α-Al phases and eutectic silicon phases respond differently to heat treatment following solution treatment and aging treatment than when mixed with as-cast A356 aluminum alloys. After solution treatment, it was demonstrated that the eutectic silicon microstructure may transform from fine fibrous to fine spherical structures. In comparison to

other samples, the aging treatment can significantly affect microstructure.

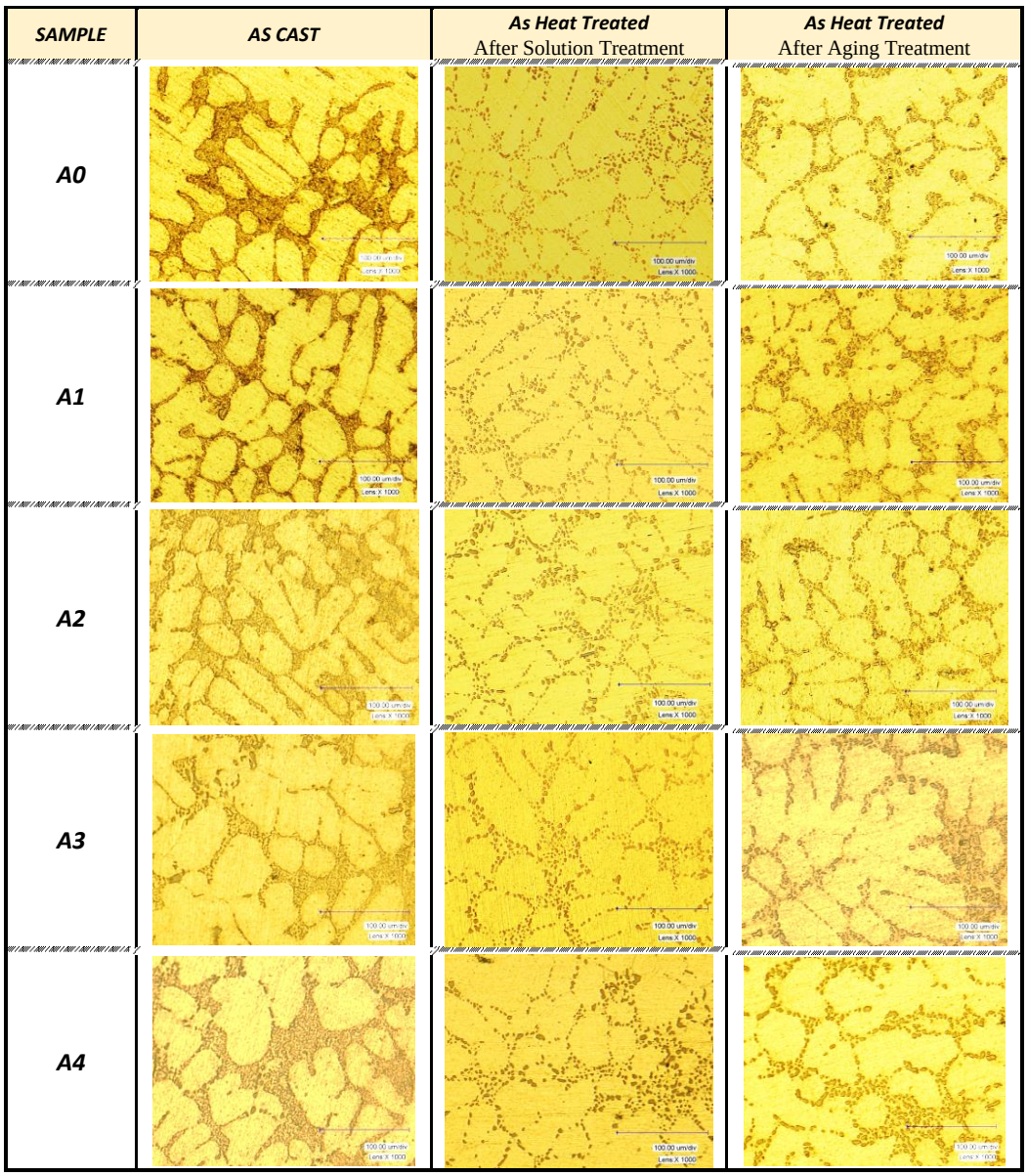

Figure 2. shows the microstructures of the materials A0, A1, A2, A3, and A4 before (as cast), after solution treatment, and after aging treatment (as heat treated), 1000x magnification.

In the A356 alloys with various combinations of Sr, Ti, B, and Mg, the optical micrograph analysis in Fig. 3 illustrates the size area of the primary α–Al phase and the Si eutectic phases, respectively. In the as-cast A356 alloy, the primary α–Al phase exhibits coarse dendritic morphology, and the statistical distribution of α–Al phase size area and Si eutectic phase size area were calculated using the Image J program. Figure 3 demonstrates that the size of the α–Al phase area has a comparatively small size in the as cast state compared to the combined aluminium alloy, but the size of the Si eutectic phases area has a relatively big size in the as cast state. In comparison to the AlTi5B1 or ALTAB Ti combination, the distribution size area of the primary α-Al phase is slightly altered.

The distribution size area of the α -Al phase is unaffected by ALTAB Ti80 and AlTi5B, which is in accordance with expectations that the A356 alloy will have grain refinement. According to the majority of research, Al3Ti precipitates will be created when Ti atoms in the A356 alloy react with Al atoms in the melt. Al3Ti particle size increased with an increase in Ti content [14][15]. The initial α–Al phase should therefore be able to be decreased by it. The size area distribution after solution treatment and after aging treatment (as heat treat), the size area distribution of α–Al phase on Fig 3 has increased compared to as cast and the size area distribution of Si eutectic phase has decreased compared to as cast. Therefore, the mechanical properties of cast aluminium alloys are depended on grain size, phase distribution, secondary phase grain, and precipitation hardening.

Item	α – Aluminium Phase Distribution	Eutectic silicon Phases Distribution
As - Cast	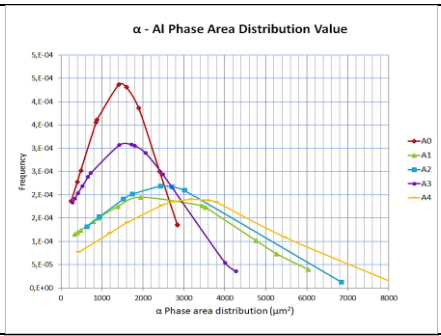	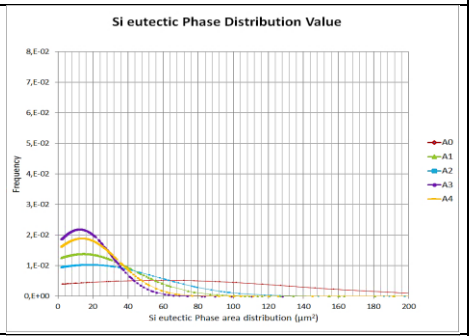
As Heat Treated ***After Solution Treatment***	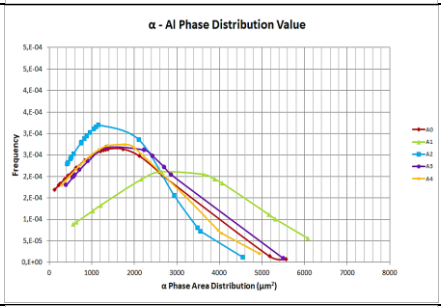	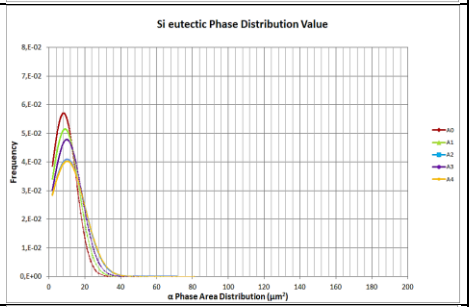
As Heat Treated ***After Aging Treatment***	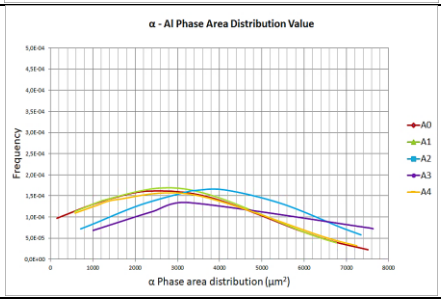	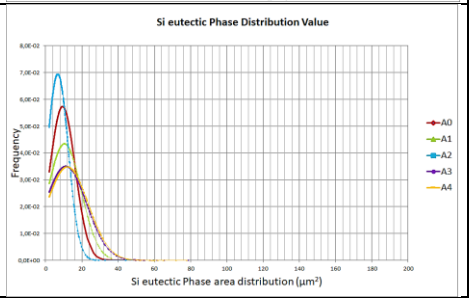

Figure 3. The curve in the α phase size area distribution and the Si eutectic phase size area distribution (as cast and as heat treated: After Solution Treatment and After Aging Treatment)

The microhardness between α–Al phase and Si eutectic phase in figure 4 shows that in the as cast condition, the eutectic phase has a higher hardness than the α – Al phase. After heat treatment, the microhardness increases in both phases and the α – aluminium phase showed a higher hardness than the eutectic phase. This is consistent with the several research that the effect of heat treatment T6 can increase grain size. As a result of the addition of Mg the Mg2Si intermetallic compound is formed which causes increased hardness.

According to Figure 4, which compares the microhardness of the Si eutectic phase and the α - Al phase under as-cast conditions, the eutectic phase is harder than the -aluminium phase. Figure 4 demonstrates that, under as-cast conditions, the eutectic phase has a higher hardness than the α - Al phase after the addition of the components Sr, Ti, B, and Mg via the material of AlTi5B1, ALTAB Ti80, AlSr15, and Mg. The size area distribution of the α - Al phase on Fig. 4 has grown

compared to as cast, and the size area distribution of the Si eutectic phase has decreased compared to as cast following heat treatment (as heat treat). As a result, grain size, phase distribution, secondary phase grain, and precipitation hardening all affect the mechanical properties of cast aluminium alloys.

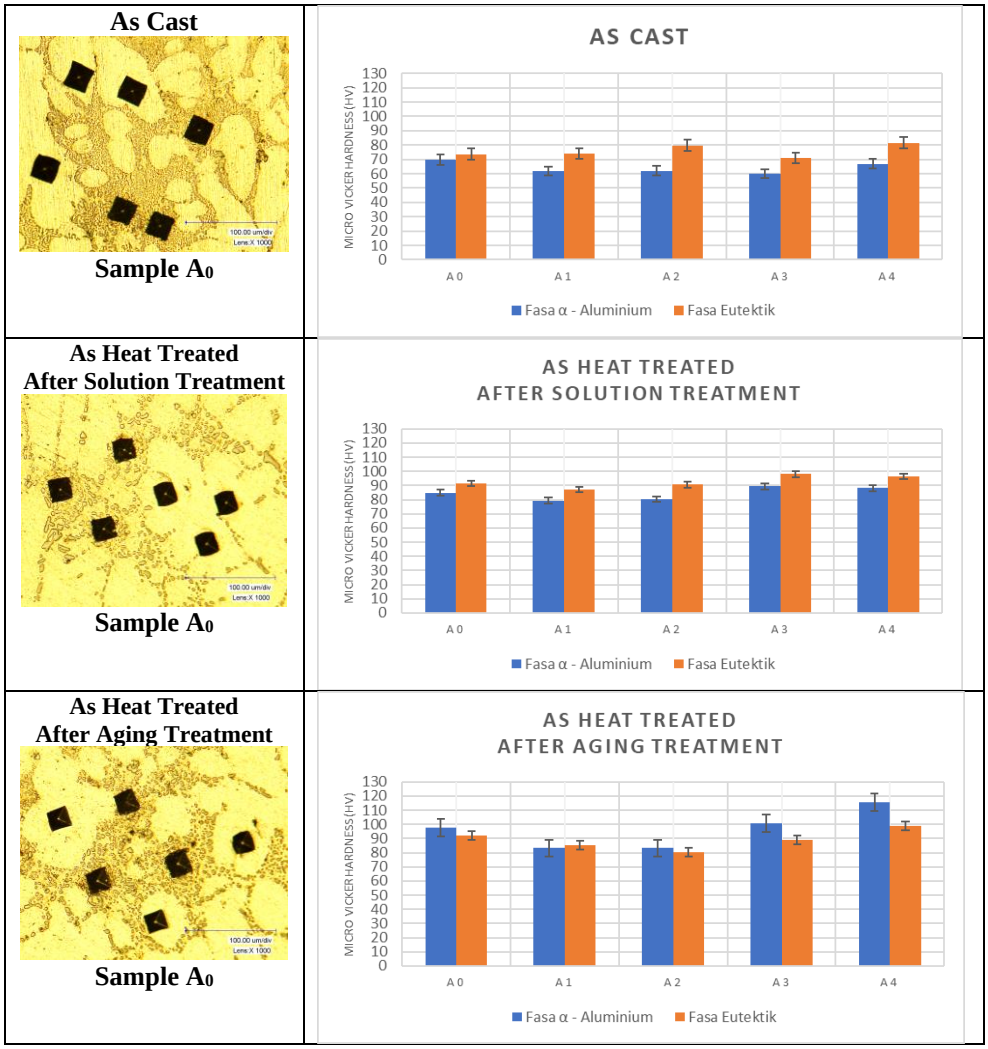

Figure 4. Results of Micro Vickers Hardness
(as cast and as heat treated: After Solution Treatment and After Aging Treatment)

4 Conclusions

The chemical composition of the A356 aluminum alloy did not alter significantly with the addition of a mixture of components, including AlTi5B1, ALTAB Ti80, AlSr15, and 99% Mg Ingot.

The results of the structural study demonstrated the impact of changing Sr to produce Si precipitates with a fine fibrous morphology under as-cast circumstances. The morphology of the precipitates changed to spheroidized Si after the heat treatment (solution treatment and aging treatment).

Results from the Micro Vickers Hardness test reveal that the eutectic phase is harder than the α-aluminum phase. The two phases' hardness increased after the T6 heat treatment process, with the hardness of the α-aluminum phase increasing significantly and exceeding the eutectic phase in hardness.

Acknowledgement

This study is a part of a dissertation for a PhD program at ITB supported by the Mayasari Bakti Utama Foundation. The authors further acknowledge PT. Chemco Harapan Nusantara for providing sample and experiment facilities.

References

[1] S. P. Dwivedi, S. Sharma, & K. R. Mishra, *A356 Aluminum Alloy and applications- A Review*, Int. J. Adv. Mater. Manuf. Charact.,**4**(2), pp. 81–86, 2014, doi: 10.11127/ijammc.2014.08.01.

[2] M. Kaba, A. Donmez, A. Cukur, A. F. Kurban, H. E. Cubuklusu, & Y. Birol, *AlSi5Mg0.3 Alloy for the Manufacture of Automotive Wheels*, Int. J. Met., **12**(3), pp. 614–624, 2018, doi: 10.1007/s40962-017-0191-2.

[3] European Aluminium Association, *Applications - Chassis & Suspension - Wheels*, The Aluminium Automotive Manual, 2011. https://european-aluminium.eu/wp-content/uploads/2022/11/aam-applications-chassis-suspension-3-wheels.pdf.

[4] ASTM Standard B 108/B108M - 08, *Standard Specification for Aluminum-Alloy Permanent Mold Castings*. ASTM International, 2009.

[5] D. G. Mallapur, S. A. Kori, & K. R. Udupa, *Influence of Ti, B and Sr on the microstructure and mechanical properties of A356 alloy*, J. Mater. Sci., **46**(6), pp. 1622–1627, 2011, doi: 10.1007/s10853-010-4977-3.

[6] M. R. S. Ganesh, N. Reghunath, M. J.Levin, A. Prasad, S. Doondi, and K. V. Shankar, Strontium in Al–Si–Mg Alloy: A Review, **28**(1). The Korean Institute of Metals and Materials, 2022.

[7] R. Chen, Q. Xu, H. Guo, Z. Xia, Q. Wu, & B. Liu, *Correlation of solidification microstructure refining scale, Mg composition and heat treatment conditions with mechanical properties in Al-7Si-Mg cast aluminum alloys*, Mater. Sci. Eng. A, **685**, no. October 2016, pp. 391–402, 2017, doi: 10.1016/j.msea.2016.12.051.

[8] B. T. Sofyan, D. J. Kharistal, L. Trijati, K. Purba, & R. E. Susanto, *Grain refinement of AA333 aluminium cast alloy by Al-Ti granulated flux*, Mater. Des., **31**, no. SUPPL. 1, pp. S36–S43, 2010, doi: 10.1016/j.matdes.2010.02.007.

[9] R. G. Guan & D. Tie, *A review on grain refinement of aluminum alloys: Progresses, challenges and prospects*, Acta Metall. Sin. (English Lett., **30**(5), pp. 409–432, 2017, doi: 10.1007/s40195-017-0565-8.

[10] Y. Cui, D. J. M. King, A. P. Horsfield, & C. M. Gourlay, *Solidification orientation relationships between Al3Ti and TiB2*, Acta Mater.,**186**, pp. 149–161, 2020, doi: 10.1016/j.actamat.2019.12.013.

[11] L. M. Chart, *Effect of Alloying Elements on the Sr Modification of Al-Si Cast Alloys*, pp. 8–9, 2019.

[12] M. Emamy, M. Malekan, A. H. Pourmonshi, & K. Tavighi, *the influence of heat treatment on the structure and tensile properties of thin-section A356 aluminum alloy casts refined by Ti, B and Zr*," J. Mater. Res., **32**(18), pp. 3540–3547, 2017, doi: 10.1557/jmr.2017.193.

[13] J. H. Peng, X. L. Tang, J. T. He & D. Y. Xu, *Effect of heat treatment on microstructure and tensile properties of A356 alloys*, Trans. Nonferrous Met. Soc. China (English Ed., **21**(9), pp. 1950–1956, 2011, doi: 10.1016/S1003-6326(11)60955-2.

[14] X. Dong, Y. Zhang, S. Amirkhanlou, & S. Ji, *High performance gravity cast Al9Si0.45Mg0.4Cu alloy inoculated with AlB2 and TiB2*, J. Mater. Process. Technol., **252**, no. August 2017, pp. 604–611, 2018, doi: 10.1016/j.jmatprotec.2017.10.028.

[15] Y. Birol, *Effect of silicon content in grain refining hypoeutectic Al-Si foundry alloys with boron and titanium additions*, Mater. Sci. Technol., **28**(4), pp. 385–389, 2012, doi: 10.1179/1743284711Y.0000000049.

Proceedings of the 3rd ITB Graduate School Conference ISSN: 2963-718X
Enhancing Creativity in Research Through Developing Innovative Capabilities
December 21, 2022

Analysis of The Subsurface Structure of the Geothermal Potential Area Based on Magnetic Data (Case Study in Blue Mountain-North Nevada)

Agnes Br. Manurung* & Alamta Singarimbun

Physics of Earth and Complex System, Faculty Mathematics and Natural Sciences, Institut Teknologi Bandung
*Email: agnesmanurung27@gmail.com

Abstract. Energy is an absolute necessity in human life and its availability has a significant influence on the progress of development. One of renewable energy sources exist all the time is geothermal. The magnetic method is one of the advanced exploration techniques in geothermal observations. Magnetic methods are used to determine the magnetic properties of rocks and subsurface geological structures based on magnetic field anomalies. Knowing the subsurface geological structure will be very helpful in interpreting the basic system and faults that may be used as a path for geothermal fluids to escape. This study is an analysis of the magnetization of the earth's surface from the acquisition of magnetic susceptibility values. Geothermal causes the value of the magnetic anomaly to be low because a demagnetization process removes the rock's magnetic properties. Mag2dc software is used to determine the earth's subsurface structure in 2 dimensions. In the modeling obtained, there is magnetic susceptibility contrast which is negative and that is at a depth close to the earth's core. This area indicates the existence of a geothermal source. In the modelling there are three types of rocks that make up the subsurface structure: granitic, volcanic, and sedimentary rocks.

Keywords: *geothermal; magnetic method; modeling; susceptibility.*

1 Introduction

Energy is an absolute necessity in human life, and its availability significantly influences the progress of development. Indonesia's energy needs have so far been supplied from fossil energy sources such as oil, gas and coal. This fossil energy source is not environmentally friendly because it produces pollution that increases global warming. Apart from being less friendly to the environment, the availability of fossil fuels will also gradually run out if they are continuously used. Therefore, geothermal energy is a renewable energy source that is widely available in Indonesia that can provide energy for all time. One of the most extensive renewable energies in Indonesia is geothermal. Geothermal is 40% of the contributors to geothermal potential worldwide, spread over 299 locations in Indonesia [1], (Sugiharta, et al. 2013). According to UU No. 27 of 2003

concerning geothermal energy, geothermal resources are thermal energy source contained in hot water, steam, and rocks along with other minerals and gases, all of which cannot be separated in a geothermal system.

Geothermal, which is widely spread in the territory of Indonesia, can be identified by several kinds of exploration activities carried out by researchers. Various type sort of method and geophysical surveys can be used in the search for potential geothermal areas, one of them is the magnetic method. Geophysical investigations apply the principles of applied physics to determine the structure and composition of layers within the earth to find potential geothermal sources in an area [2], (Sarkowi, 2010). This investigation is applied by knowing the physical properties of rocks below the surface. Anomalies found in the rocks can predict the potential of geothermal systems. One of the geophysical methods used to investigate the existence of a geothermal system is the magnetic method [3], (Loper, 2007).

The magnetic method is a method that uses the basis of measuring variations in the intensity of the magnetic field on the earth's surface caused by anomalies of magnetic objects (rocks) below the earth's surface. This research uses the magnetic method. The magnetic survey shows the various states of the magnetic field at the location to be measured. The magnetic method is often used in the field because it is cheaper and easier than other geophysical methods [4], (Telford, 1990).

This study uses the magnetic method. The research data processed is the data from a geophysical survey from the United States Geological Survey (USGS) in the Blue Mountain and Pumpernickel Valley north-central Nevada using the geomagnetic method. The field data collection took place in August 2012. The data were processed using the following software: Microsoft Excel, Surfer 20, Magpick, and Mag2dc to obtain anomalous object models.

2 Research Methodology

2.1 Measurement

Magnetic data were taken using two magnetometers (in this case, the Proton Procession Magnetometer) where had mapped one tool to measure the magnetic field at the Base Station (BS) for measuring the daily variations and another tool to measure the magnetic field in the field had been mapped in the form as grids. The frequency of the proton precession is directly proportional to the strength of the magnetic field ([5], Kearey et al. 2002 [6], Lowrie, 2007 [7], John et al. 2011).

Measurements in the field are carried out in several stages. First, the PPM instrument is calibrated. Then, daily magnetic field measurements in the Base Station are carried out every minute interval that is determined and adjusted to the needs of the measurements. Several corrections are made in measuring the magnetic field to determine the daily variation of the magnet, after obtaining the

magnetic field data. In collecting data in the area, the data recorded is the magnetic field data listed on the tool, the position of the measurement point using GPS, and the time of measurement.

2.2 Correction

The magnitude of the magnetic field measured at station point is the contribution of the earth's main magnetic field, the external magnetic field, and the anomalous magnetic field. To obtain the strength of the anomalous magnetic field generated by the rock under each surface measurement point, it is necessary to make corrections to the main magnetic field and the external magnetic field, which is also measured through PPM. The corrections made include the following;

1) Daily correction (diurnal correction) is a correction to remove the influence of the external magnetic field, especially from solar activity. The daily correction is obtained from the variation of the magnetic field strength over a spesific time interval at the base point corresponding to the measurement time of each station point. If there is a decrease in the strength of the magnetic field, it must be added for the reduction to the measurement result at the station point, and vice versa.
2) Topographic correction is a correction to eliminate the influence of the magnetic field due to topographic differences. There is no general rule in this correction, but if it is considered that there is no magnetization, the correction made only refers to the difference in elevation.
3) IGRF correction is a correction to eliminate the influence of the main magnetic field. This is necessary because the main magnetic field of the earth changes with time [8], (Broto, 2013).

The final result of the magnetic method is the strength of the magnetic field after correction. With the equation:

$$H_{daily} = \frac{(t_n - t_{in})}{(t_{fi} - t_{in})}\left(H_{fi} - H_{in}\right)$$

Where t represents time, H represents the measured magnetic field, index n represents the nth data, index in represents the initial data at the base station, index fi represents the final data at the base station.

This daily correction (H_{daily}) can be positive or negative. If the value is positive (H_{daily}), subtract the value of the measured magnetic field (H_{tot}) at that time from this daily value. If the value is negative (H_{daily}), then add the measured magnetic field value (H_{tot}) at a certain time to this daily value. The corrected magnetic field (ΔH) can be written by the equation:

$$\Delta H = H_{tot} \pm \Delta H_{daily}$$

Susceptibility is the degree of magnetism of an object by the influence of a magnetic field. To calculate the magnetic susceptibility value at the measurement point, this can be obtained from the equation:

$$K = \frac{\Delta H}{H}$$

with,
K = Magnetic field susceptibility at the measuring point
ΔH = Magnetic field anomaly at the measurement point (nT)
H = Average magnetic field over the measuring area (nT)

The value of susceptibility is significant in looking for objects that have anomalies because of the variation in the characteristics of each type of mineral or mineral rock.

4) Upward continuation aims to eliminate local influences still present in the data and look for the effects of regional anomalies. The higher the data continuity, the more local information is lost, and regional information is more precise. Upward continuation should be manageable because it can reduce the local magnetic anomaly value from the magnetic source.

2.3 Data Interpretation

Data interpretation is carried out in two ways, that are quantitative interpretation and qualitative interpretation. Qualitative interpretation is based on regional anomaly contour map analysis, while quantitative interpretation is performed using Mag2dc software.

Qualitative interpretation aims to predict the presence of anomaly-causing objects and to localize areas that have anomalies. Quantitative interpretation aims to determine the shape and model and depth of anomalous objects or geological structures through mathematical modeling.

On the local contour map that has been obtained, a line is drawn that crosses the lowest anomaly and the highest anomaly (line section) on the contour map. This trajectory can be created using Surfer20 software. The trajectory data obtained is input data for the Mag2dc software as an anomaly cross-section. In Mag2dc, a match is made between the observed curve and the model curve in forming the subsurface layer with a forward modeling approach (matching the model profile with the field data profile) using the trial and error method. Magnetic susceptibility values for rock types are obtained by adding up the magnetic susceptibility contrast values for rock types obtained by adding up the magnetic susceptibility contrast values for rock types to the average magnetic susceptibility value.

2.4 Research Flow Chart

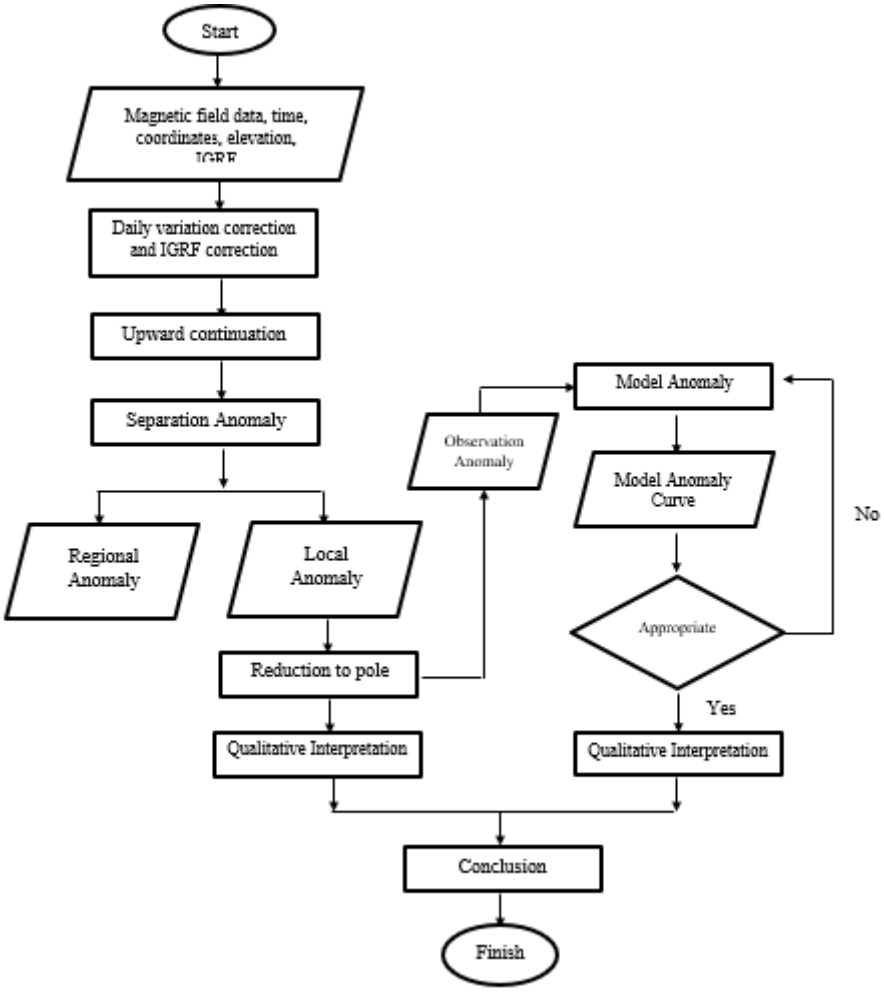

Figure 1. Research Flow Chart

3 Result and Discussion

3.1 Magnetic Anomaly Distribution

The data obtained from the research area are in the form of latitude and longitude coordinates in the decimal degree coordinate system, as well as the total magnetic anomaly value resulting from daily (diurnal) and IGRF corrections. So, before carrying out further data processing, the decimal degree coordinate system is converted to Universal Transfer Mercator (UTM), namely easting and northing coordinates in meters. The aim is to make it easier to read the contour map maker software. In Figure 2, the contours of the total magnetic field show variations of

different magnetic field anomalies based on the color scale. This anomaly value describes the difference in the susceptibility of rock layers beneath the surface of the area. Thus, the contrasting magnetic anomaly on the contour map indicates the possibility of a potential geothermal source below the surface so that it can continue that data processing. Anomaly values are grouped into three groups, namely: high anomaly shown in yellow to red (-6 to 14 nT), moderate anomaly shown in light blue to light green (-26 to -10 nT) and low anomaly depicted in color purple to blue (-46 to -30 nT).

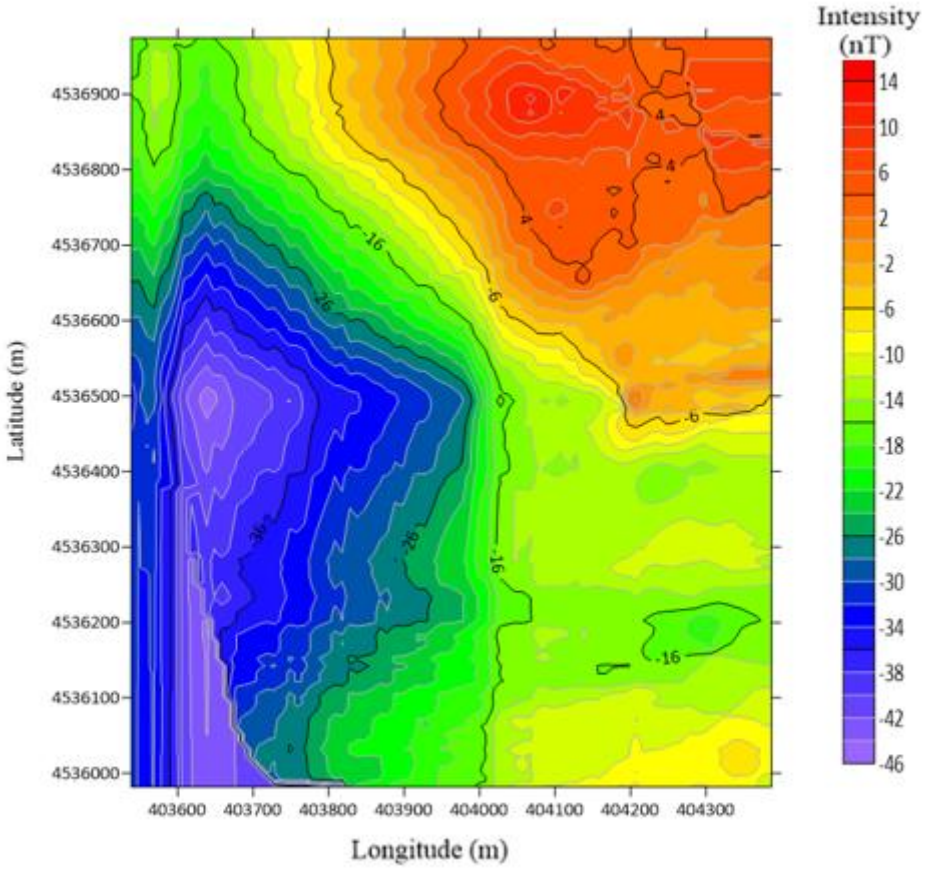

Figure 2. Total anomalous magnetic field.

3.2 Magnetic Data Interpretation

Based on the magnetic anomaly and rock susceptibility obtained, magnetic anomaly modeling is made to interpret the subsurface structure. The initial modeling step is in the form of 7 lines sections in Figure 3, representing all anomaly contours.

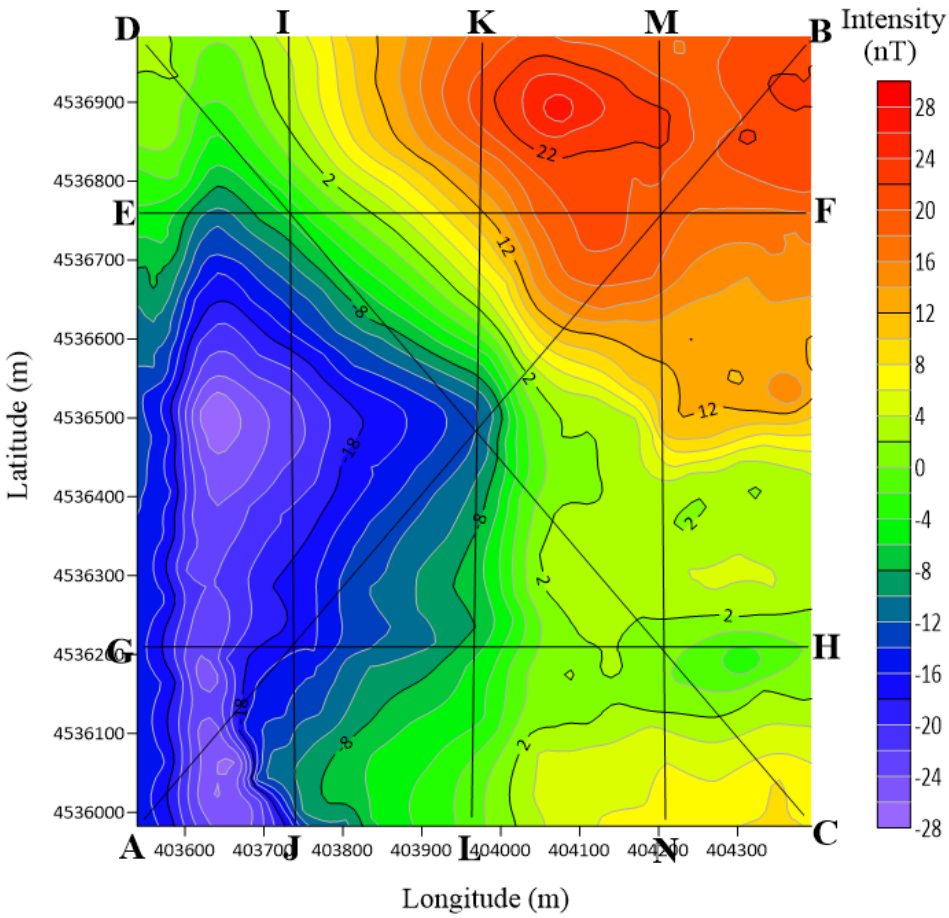

Figure 3. Modeling trajectory on local anomaly contour area

3.2.1 Magnetic Anomaly Modeling

Quantitative interpretation is needed to describe the subsurface structure from the measured data. Quantitative interpretation aims to determine the lithology of the research area. Interpretation is carried out by making a geomagnetic cross-sectional model using Mag2dc software by inputting data in table 4.1 so that Figure 4.4 will be obtained, which has a translation in the form of an image showing the susceptibility and color values based on rock layers. In conducting numerical modeling, several parameters of the earth's magnetic field are required in the study area, which include the IGRF value (51,722 nT), declination angle (64.5°), inclination angle (-14.5°), as well as several modeling parameters. Look at the picture below.

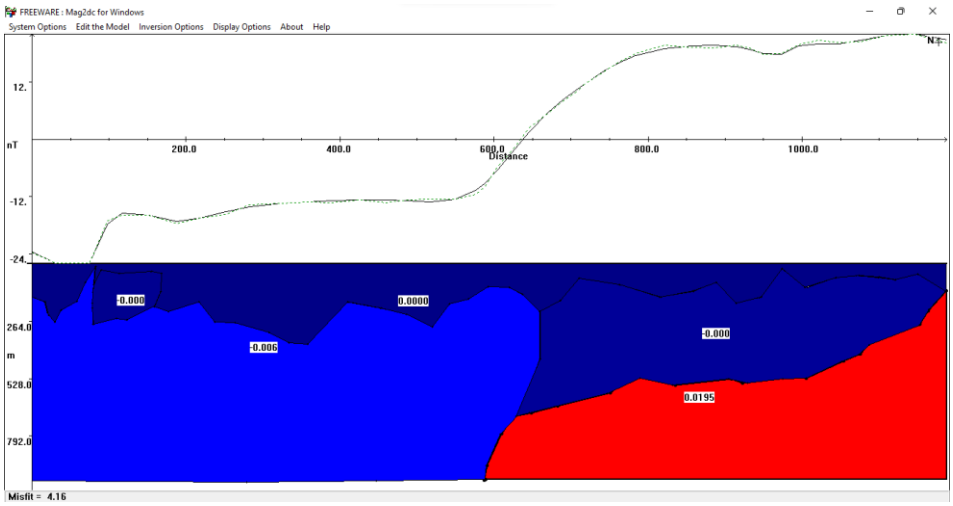

Figure 4. A-B Path Modeling

Based on the results of subsurface geological modeling of A-B slices and actual regional geological information in Figure 4, rocks with a susceptibility range of 0.0000 to 0.000, which are blue, are suspected of sedimentary rocks such as argillite, mudstone, metasediment, and slate types. Rock layers with red susceptibility 0.0195 are considered gabbro or diorite rock types. At a depth of 100 meters down to 1000 meters, the susceptibility values of several layers show negative values of -0.000 and -0.006. It is caused because the rock is demagnetized. Rocks with a negative susceptibility value are suspected as rocks with geothermal potential, which is indicated as a path passed by the hot fluid flow underneath.

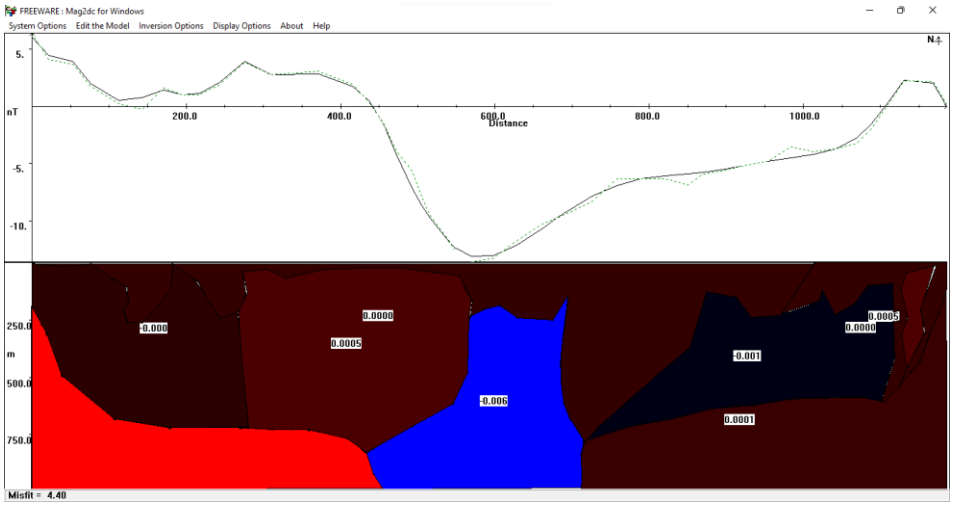

Figure 5. C-D Path Modeling

From the results of the C-D modeling and based on the basic geological information of the area in Figure 5, the red, blue and brown rock layers with a

susceptibility 0.0000, 0.000, 0.0001, and 0.0005 are presumed as sedimentary rocks such as argillite, mudstone, metasediment, and slate rock types. The rock with susceptibility 0.001 is presumed as volcanic rock which is basalt rock types. The rock with susceptibility 0.006 is presumed as granitic rock which is gabbro or diorite rock types. In rock layers with negative susceptibility values, namely -0.000, -0.001 and -0.006, it indicates that the rock is demagnetized. This rock layer is marked as a path of hot fluid under the surface of an area with geothermal potential.

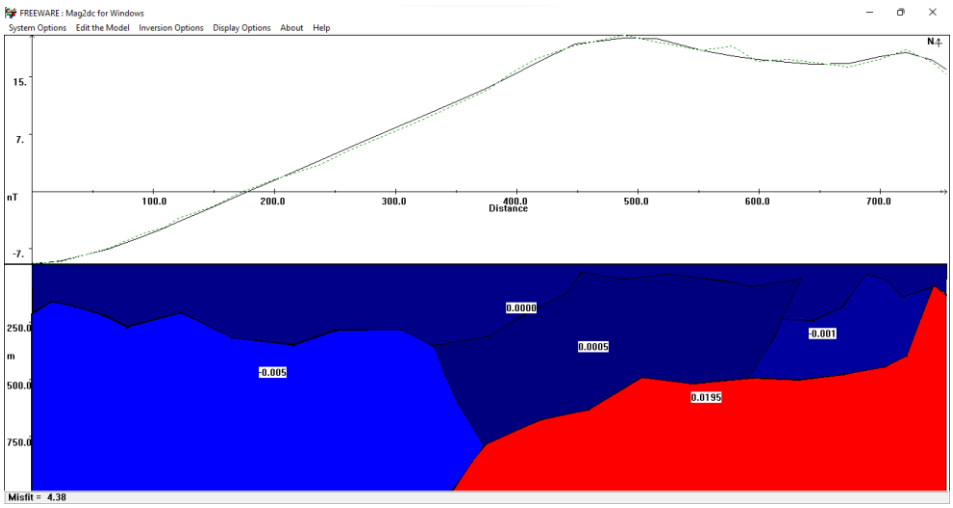

Figure 6. E-F Path Modeling

From the results of the E-F modeling and based on the basic geological information of the area in Figure 6, the red rock layer with a susceptibility of 0.0195 is suspected as a type of gabbro or diorite rock. Blue rock layers with a susceptibility range of 0.0000 and 0.0005 are presumed as sedimentary rocks such as argillite, mudstone, metasediment, and slate rock types. The rock with susceptibility 0.001 is presumed as volcanic rock which is basalt rock types. The rock with susceptibility 0.005 is presumed as granitic rock which is granite rock types. Rock layers with negative susceptibility, namely -0.001 and -0.005 indicate that the rock is demagnetized. This rock layer is marked as a path of hot fluid under the surface of an area with geothermal potential.

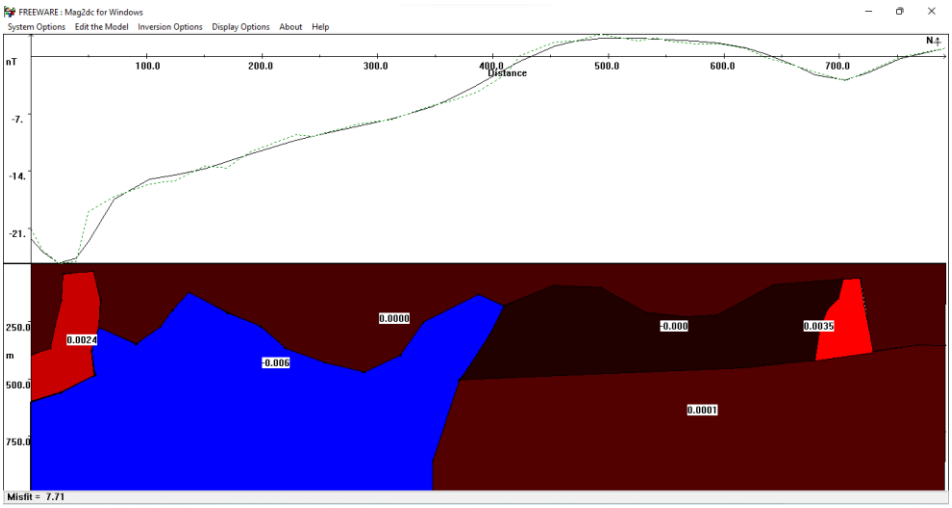

Figure 7. G-H Path Modeling

Based on basic regional geological information, the G-H modeling results in Figure 7 show that rock layers with a susceptibility 0.0000, 0.000, 0.0001 in brown are suspected as sedimentary rocks such as argillite, mudstone, metasediment, and slate rock types. The rock with susceptibility 0.0024 in red is presumed as volcanic rock which is basalt rock types. The rock with susceptibility 0.006 in blue is presumed as granitic rock which is granite rock types. The rock with susceptibility 0.0035 is presumed as granitic rock which is granodiorite rock types. Rock layers with a depth of 100 meters to 1000 meters with a negative susceptibility of -0.000 and -0.006 indicate that the rock is demagnetized. This rock layer is marked as a path of hot fluid under the surface of an area with geothermal potential.

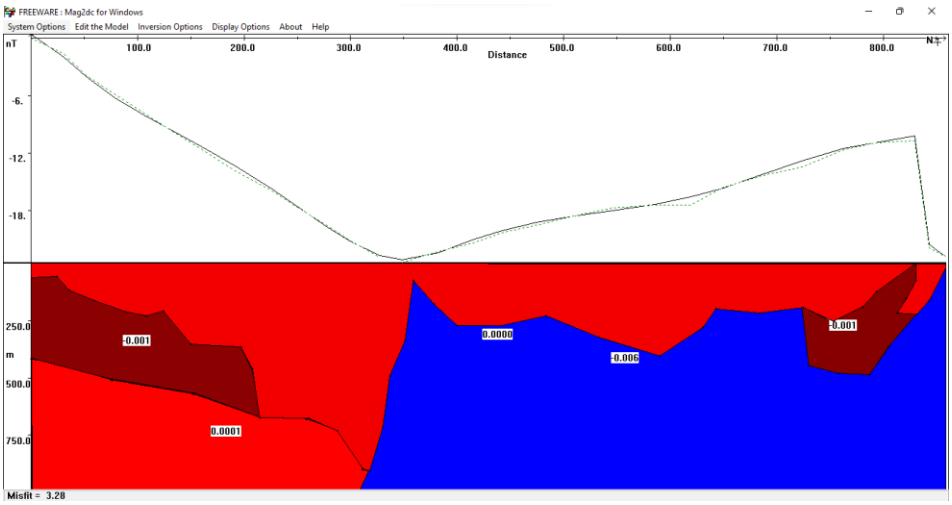

Figure 8. I-J Path Modeling

From Figure 8, the results of the I-J modeling and based on actual regional geological information, the blue layers with a susceptibility 0.0001, 0.00000 are suspected as sedimentary rocks such as argillite, mudstone, metasediment, and slate rock types. The rock with susceptibility 0.001 in red is presumed as volcanic rock which is basalt rock types. The rock with susceptibility 0.006 in blue is presumed as granitic rock which is granite rock types. In rocks with negative susceptibility, namely -0.001 and -0.006, it indicates that the rock is demagnetized and is a path for the geothermal fluid underneath.

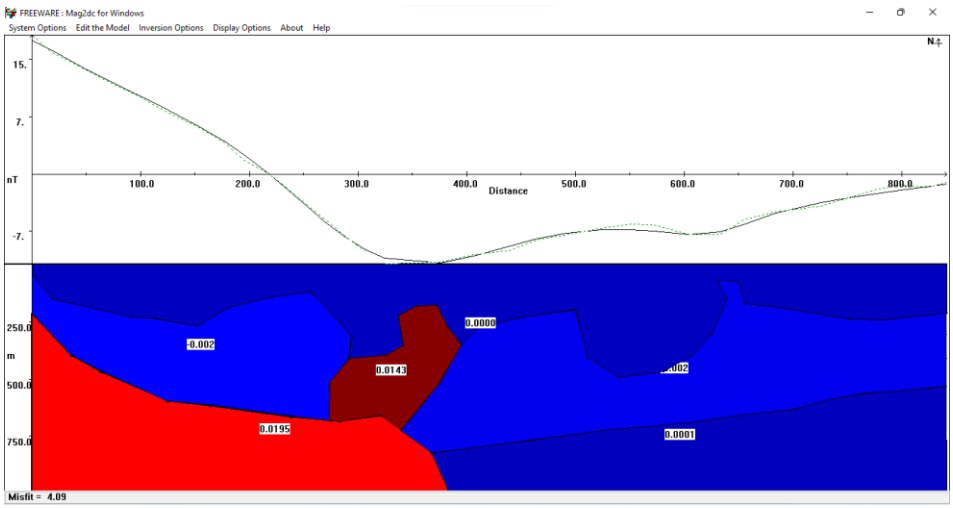

Figure 9. K-L Path Modeling.

From Figure 9, the K-L modeling is the point of intersection of the locations of the sections AB, CD, and KL so that at the end of the meeting of the three tracks, they are in the exact location and show the same rock structure. In the blue rock layers with a susceptibility 0.0000, 0.0001 are suspected as sedimentary rocks such as argillite, mudstone, metasediment, and slate rock types. The rock with susceptibility 0.002 in blue is presumed as volcanic rock which is basalt rock types. The rock layer with a red color with a susceptibility of 0.0195 and 0.0143 is a type of granitic rock which is gabbro or diorite rock types. Rocks with negative exposure is -0.002 demagnetized rock and is indicated as a path for geothermal fluid flow.

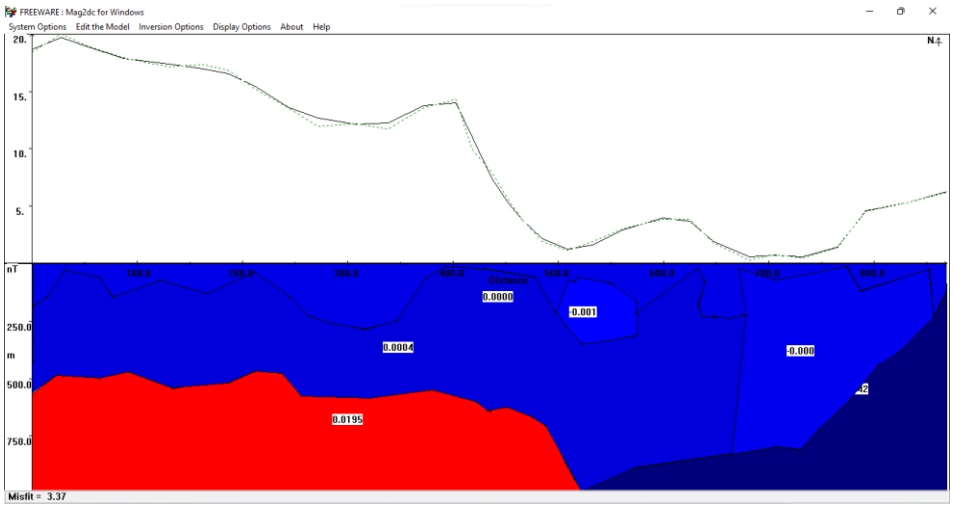

Figure 10. M-N Path Modeling

In Figure 10, based on the M-N modeling results and actual regional geological information, blue rock layers with a susceptibility 0.0000, 0.000, 0.0004 are suspected as sedimentary rocks such as argillite, mudstone, metasediment, and slate rock types. The rock with susceptibility 0.001 is presumed as volcanic rock which is basalt rock types. The rock with susceptibility 0.006 in blue is presumed as granitic rock which is granite rock types. The rock with susceptibility 0.0035 is presumed as granitic rock which is granodiorite rock types.are suspected of argillite, mudstone, and sandstone types. In the red rock layer with a susceptibility of 0.0195, it is supposed that it is a type of gabbro rock. The rock with susceptibility 0.00422 is presumed as granitic rock which is granodiorite rock types. Rocks with negative susceptibility, namely -0.000 and -0.001, are demagnetized rocks and are geothermal fluid flow paths.

4 Conclusion

Based on the results of data processing using the magnetic method of magnetic field anomalies on the surface of the Blue Mountain and Pumpernickel Valley area of north-central Nevada, it can be concluded that there is a magnetic anomaly with a maximum magnetic value (positive value) and a minimum magnetic field value (negative value) indicating there is geothermal potential underneath. Through forward modeling carried out with Surfer 20, Magpick, and Mag2dc software, it can be found that there are rock layers below the surface of the area in the form of argillite, mudstone, sandstone, and gabbro which is the rock which has been altered due to high temperatures resulting in a decrease in the value of the magnetic susceptibility of rocks, and sedimentary rocks of shales or shales.

Acknowledgement

The authors thank the U.S. Geological Survey for providing the magnetic data.

Ponce, D.A., 2012, Geophysical studies in the vicinity of Blue Mountain and Pumpernickel Valley near Winnemucca, north-central Nevada: U.S. Geological Survey

Open-File Report 2012–1207, 14 p.

References

[1] Sugiharta, A., Elny, Sumaedi, Lihu, I. J., Tatang, Aminuddin, A. H., Winarti, S., *Buku Informasi Pemanfaatan Jasa Lingkungan Panas Bumi di Hutan Konservasi, Direktorat Pemanfaatan Jasa Lingkungan Hutan Konservasi*, Bogor, 2016.

[2] Sarkowi, N.M., *Buku Ajar Pengantar Teknik Geofisika*. Lampung: Universitas Lampung, 2010.

[3] Loper, David, *Depth to Curie Temperature. Encyclopedia of Geomagnetism and Paleomagnetism*, 2007.

[4] Telford. W. M., L. P. Geldart dan R. E. Sheriff., *Applied Geophysics, Second Edition. Cambridge University Press*: USA, 1990.

[5] Kearey, P., Brooks, M. & Hill, I., *An Introduction to Geophysical Exploration, Blackwell Science*: UK, 2002.

[6] Lowrie, W., *Fundamental of Geophysics*, Cambridge University Press: Newyork, 2007.

[7] John M. & Asger E, *Field Geophysics, 4th ed*., John Wiley & Sons Ltd, West Sussex, P019 8SQ, United Kingdom, 2011.

[8] Broto, S., T. T, Putranto, *Aplikasi Metode Geomagnet Dalam Eksplorasi Panas Bumi*, UNDIP: Semarang, 2011.

Proceedings of the 3rd ITB Graduate School Conference ISSN: 2963-718X
Enhancing Creativity in Research Through Developing Innovative Capabilities
December 21, 2022

Limestone Resources Estimation using Standard Facies Belt as Domain Constraint, Banten, Indonesia

Ahmad Nur Taufiqurrahman[1,3,*], Antoni Sahar[2], Asep Heri Patria Kesumajana[4] & Dwiharso Nugroho[4]

[1]PT. Geo Stroom Indonesia, Pinus Raya 20, Bandung 40294 Indonesia
[2]PT. Gama Group, Banten Indonesia
[3]Master of Geological Engineering Program, Faculty of Earth Science and Technology, Institut Teknologi Bandung, Ganesha 10, Bandung 40132 Indonesia
[4]Faculty of Earth Science and Technology, Institut Teknologi Bandung, Ganesha 10, Bandung 40132 Indonesia
[*]Email: technical@geostroom.com/ahmad.taufiqurrahman@hotmail.com

Abstract. There was scarce literature discussing the estimation of limestone quarry using carbonate platform components as domain constraints. Many estimation studies heavily focus on geostatistical methods. This study offers a new perspective on raw material resource estimation. Carbonate deposits from Pamubulan area are divided into three carbonate platform elements, namely platform interior, platform margin, and platform slope. Twelve different limestone domains were constructed. These solid model act as constraints in further estimation stages. The bimodal nature of CaO and MgO grade from the entire limestone edifice is successfully separated by the domains. Using inverse distance weighting as an estimator, 220 million tons of limestone suitable for cement raw material can be calculated. Only limestone with more than 40% CaO and less than 5% MgO is included in the calculations. Another notable feature is high-grade limestone bisected by low-grade material. Leaving complex and challenging environment for mining production.

Keywords: *3D solid model; carbonate platform; inverse distance weighting; Pamubulan.*

1 Introduction

Our government led by President Joko Widodo has increased the budget for developing mass infrastructure. This step is believed to be one of the fundamental elements that can raise economic growth. Better infrastructure can speed things up and reduce distribution costs, leading to a better price for the community. Population, in general, will benefit greatly from this situation and finally improve national welfare.

Infrastructure like toll roads, airports, terminals, bridges, and seaports require a large number of materials, one of which is cement. Cement production uses natural resources as raw materials, including limestone, sandstone, and claystone. Comprehensive infrastructure development requires support from high profile cement industry. Detail records of the potential and resources of these raw materials, especially limestone, are very important. This can only be achieved by sound mineral resource estimation.

Mineral resources estimation is a series of activities intended to build a mineral deposits model, whether as an exploration target, base for a feasibility study or optimize mining process in Glacken and Trueman [1]. The core step of estimation is geological modeling, practitioners often limit this activity because of the complexity and significant amount of time required. In addition, mining producers often prefer more express decisions.

Suggestions came from Mackenzie and Wilson in [2], and Cowan in [3], who encourage regarding geological concepts as essentials in geological modeling. Models that comply with geological principles are more appropriate as a basis for domaining and interpretation at the estimation stage. This is good practice and will not change, although various methods of analysis and interpretation continue to evolve.

The research area is located in Pamubulan area, Banten Province. It is part of PT. Gama Group exploration mining license. Area extent from 3.5 km WE to 1.2 km NS in size or around 4.2 km^2.

2 Geological Setting

Physiographically research area can be included in Central Depression Ridge Zone in Van Bemmelen in [4]. According to Sujatmiko and Santosa in [5], research location is part of the Limestone Member of Citarete Formation (Tmtl) consisting of limestone, marl, and sandstone. This formation lies unconformably above the Sandstone Member of Cijengkol Formation (Toj), dominated by sandstone, conglomerate, breccia, tuff, and coal. It overlies by Tuff Member of Citarete Formation (Tmt) that constitutes of tuff breccia, sandstone, conglomerate, limestone, and tuff.

Those formations stretch from WNW to ESE direction with relatively homoclinal structure. Two medium size anticline occurs in the northwest area. Strike-slip fault dissects the study location in a relatively north-south manner. While one large reverse fault limits southern boundary of limestone formation (**Figure 1**).

Cijengkol Formation was recognized to have ranged in age from Early to Late Oligocene and interpreted to have been deposited in deltaic to marine environment, according to Sukarna *et al.* in [6]. An unconformity rest in the upper boundary of this formation, separating it from the later Neogene Formation represented by Citarete Formation, which has Late Oligocene to Early Miocene in age. The eruption of Old Andesite Volcano at this time makes this carbonate deposit has an interfingering relationship with its volcanic counterpart. This formation indicates a shallow marine deposition such as littoral that shows a deeper sequence upward and was derived from southern source area.

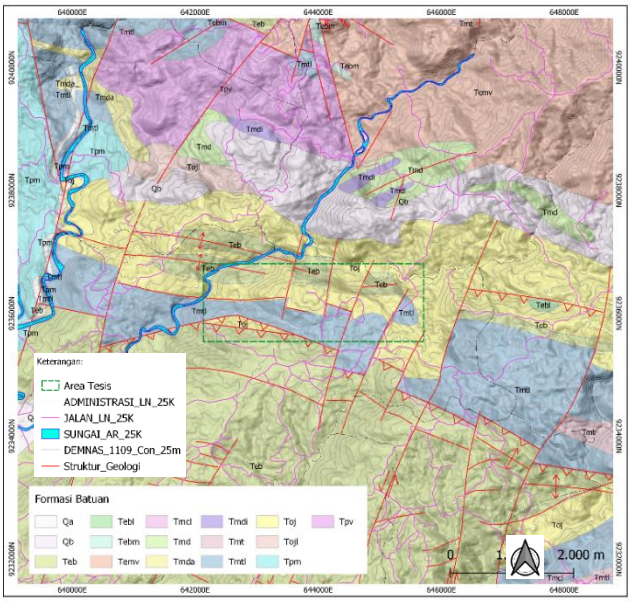

Figure 1 Map showing regional geology from the researched area. Rocks spreading were controlled by the WNW-ESE folds axis and relatively north-south strike-slip faults.

3 Data and Method

Data comes from detailed rocks description originating from 15 drill hole points complemented by 67 surface geological observation locations. Total depth as a whole reached 1697.5 meters. Topographic surveys were carried out throughout the study area accompanied by collar coordinate data from all drill points. There were 538 rock sample intercepts sent to the laboratory. XRF analysis was carried out to determine the levels of CaO and MgO from the samples. The average length of samples was about 2.7 meters with a minimum of 50 cm and a maximum of 4.5 m.

Estimation begins with the development of a conceptual geological model of the site area. This conceptual model is the basis for making solid models (domain). This is an interpretation and correlation between rocks. Philosophically, similar rock sequences with similar geochemical properties with equivalent strike/dip or position, are interpreted as the same unit and will be combined and correlated. In this study, the rock sequences were analyzed, interpreted, and classified according to the standard facies belt from Wilson (1975) in Schlager (2005) [7]. Standard facies belt range from marine to land namely: 1) basin; 2) deep shelf; 3) toe of slope; 4) slope; 5) reef margin; 6) sand shoals; 7) normal platform interior; 8) restricted platform interior, and 9) platform evaporate. To simplify the model created, facies belts are combined to platform margin (belts 5 and 6/PM), platform interior (belts 7 and 8/PI), and platform slope (belts 3 and 4/PS).

In practice, to create a domain is to select several cross-sections between drilled points. These 2-dimensional sections act as canvas to draw the upper, lower, and lateral boundaries of each intercept of the previously interpreted facies belt type. Once they are formed, the lines are connected between sections, thus forming a three-dimensional shape. The next step is to close or triangulate each side of the shapes that have been created and combined. The result is a 3D shape of a limestone body (single facies belt feature) that is closed on each side and so it is called a solid model which has a volume unit.

The next stage is the creation of the blocks model. This model takes the form of many blocks that occupy three-dimensional space, have volume, and their bodies are bound to the x, y, and z-axis. Each unit can be filled with various kinds of data, such as the estimated value of mineral/element grade, density, rocks name, or resource category. The size of the blocks model used is 100 x 60 x 3 meters. The blocks extend west-east following regional rocks spreading. There are 26,516 blocks built into the model.

The result of the main estimation work is a model consisting of a set of blocks whose center point (centroid) has an estimation value. One of the methods that are widely used to process estimation is the inverse distance weighting. IDW method with an exponent of 2 as suggested by Babak and Deutsch in [8] was implemented to estimate the CaO and MgO content of the study area. The minimum number of samples used in the calculation is 3 and can be up to a maximum of 15.

Mineral resources of this area will be divided into several levels, according to their area's proximity to the drill hole points. Corresponding to JORC in [9], resources from highest (nearest) to lowest (farthest) status are divided into measured, indicated, and inferred. The distance of the area of influence will refer to Mucha *et al.* in [10], that probably a development from Snowden in [11], by

looking at the level of continuity of the variable or sill. The relationship between variables is reflected in the sill value of a variogram, beyond this, it can be said that the relationship/continuity is no longer present.

4 Result and Discussion

Field data analysis recognized four rock units with relatively west-east distribution and alluvial deposits. Bayah Formation is dominating the south-southeast region. While Cijengkol Formation is mainly located in the north-northeast area, Citarete Limestone Member is generally found in the central part of the study area. All formations extend relatively northwest to the southeast. Tuff unit (probably Tmt or Tuf Member of the Citarete Formation) intercalates south of Citarete Limestone Member and is bounded by a large reverse fault, before meeting Bayah Formation further to the south (**Figure 2**).

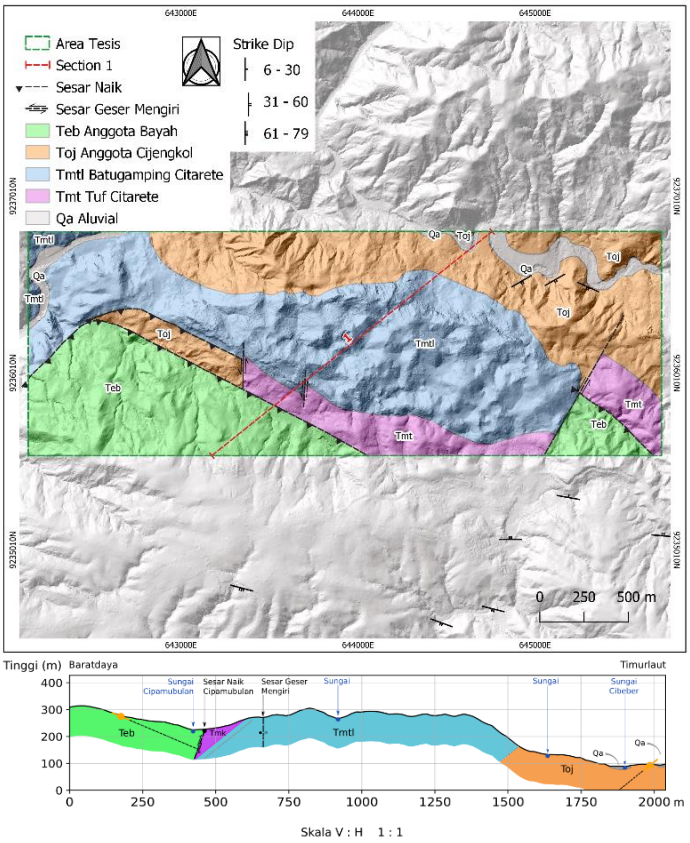

Figure 2 Map showing local geology from the researched area. The section shows that limestone member dive into the southwest with N120°E/35° strike/dip.

Several fold wings were observed in a relatively northwest-southeast elongation, but no fold axis was found specifically in the study area. Cijengkol Formation, followed by Citarete Members form a structurally homoclinal fold with southwest dipping. Average local azimuth or strike/dip angle of formation equal to N120°E/35°. Bayah Formation forms a similar homoclinal fold with north-east dipping flanks. There is a reverse fault that separates Bayah in the south from the Cijengkol and Citarete Members in the north. A sinistral strike-slip fault limits limestone spreading to the east before meeting with Bayah Formation.

4.1 Facies Belt Domain and Geometry

There were 12 limestone solid bodies perceived from the analysis (**Table 1**), each of them having its own geometric, physical, and geochemical characteristics (**Figure 3**). PM has a relatively thin elongated shape which is divided into three cycles/repeating deposits but has variations of up to 10 different features. PI covers the entire PM body and becomes the "background" of all solid bodies. PS is found in the northeast. The lowest PM model, the first cycle, bisected into 1A-1B. The second cycle of the PM model dismembered into five branches with code 2A-2E. The youngest PM cycle is segregated into three splits namely 3A-3B. PM models tend to have a thin, elongated shape like in 1A. Its body stretches up to 1.1 km with a width of 470 m. The thickness of the model reaches 169 meters. Another body has lenses feature with short and thin shapes like 2E. It has only 161 meters long and 86 meters wide with only 71 m thick, the thinnest of all solid bodies. PI model shape is very long and wide, as it spreads by enveloping the PM model. It has more than 2 km long and almost 750 m wide. The model is about 209 meters tall, the thickest of all bodies. PS solid is only found in the northeast. Secluded point location with a relatively low elevation compared to the population of other drill points, causes this model to be correlated thicker and larger than it should be. This model has a fairly high thickness, about 176 m with over 1 km long, and almost 400 m wide.

Table 1 List of facies belt domain and geometry in the Pamubulan area.

No.	Facies Belt	Validated	Status	X min	X max	Y min	Y max	Z min	Z max	X	Y	Z	Surface Area (m2)	Volume (m3)
	Platform Margin													
1	1A	TRUE	Solid	643.856	644.985	9.236.028	9.236.501	108	277	1.128	473	169	556.750	8.298.429
2	1B	TRUE	Solid	644.696	644.985	9.236.028	9.236.258	149	272	288	230	123	95.881	1.476.240
3	2A	TRUE	Solid	643.356	643.923	9.236.267	9.236.469	114	295	567	203	181	192.405	2.224.806
4	2B	TRUE	Solid	643.953	644.327	9.236.044	9.236.357	143	298	374	313	155	143.732	2.433.583
5	2C	TRUE	Solid	643.982	644.198	9.236.071	9.236.227	215	297	215	156	82	47.199	281.747
6	2D	TRUE	Solid	643.259	643.469	9.236.268	9.236.402	114	237	210	134	123	55.382	636.490
7	2E	TRUE	Solid	643.715	643.876	9.236.375	9.236.461	199	270	161	86	71	20.598	104.926
8	3A	TRUE	Solid	643.743	644.705	9.235.752	9.236.219	128	295	962	467	168	374.160	4.460.851
9	3B	TRUE	Solid	643.186	643.496	9.236.138	9.236.273	186	283	310	135	97	70.299	666.496
10	3C	TRUE	Solid	643.359	643.628	9.236.105	9.236.267	174	288	269	162	115	67.528	684.041
	Platform Interior													
11	PI	TRUE	Solid	643.186	645.278	9.235.738	9.236.484	100	309	2.092	746	209	2.536.958	69.461.026
	Platform Slope													
12	PS	TRUE	Solid	643.923	644.968	9.236.155	9.236.544	79	255	1.045	389	176	521.372	13.485.871

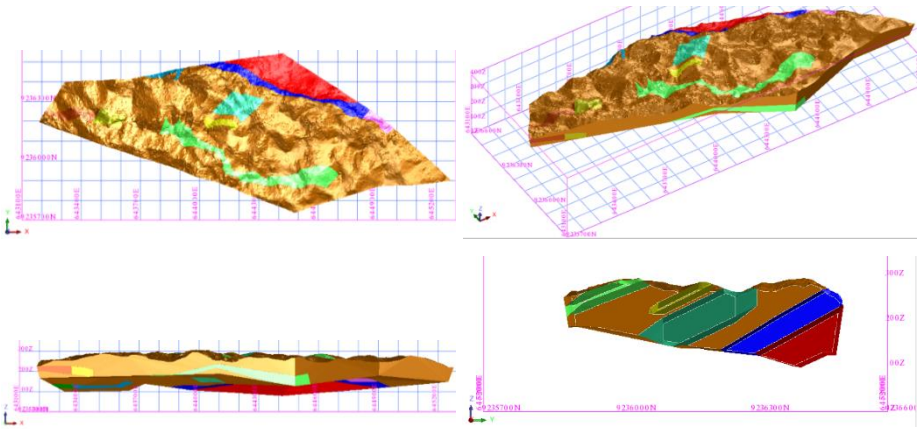

Figure 3 Solid model map from every facies belt. PI envelops other PM bodies, while PS body lies in the northeast part. Map view (upper left), perspective (upper right), W-E section (lower left), S-N section (lower right).

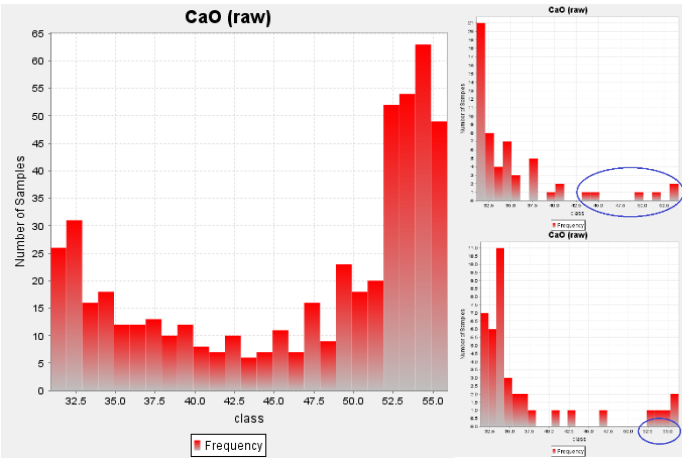

Figure 4 Bimodal CaO grade histogram from all solid models (left). Unimodal histogram from solid model 1A (upper right) and solid model 3A (lower right). Outliers need grade cutting (blue circle).

Every solid model will have their grade constraint. Thus, the bimodal nature of grade data will be refined into unimodal shape (**Figure 4**). This feature is more suitable for input data in the later estimation stage of the block model. Grades that are different from other common grade values (outliers) will be cut. Leaving more homogenous and relatively equal values in every individual solid model.

4.2 Spatial Variability and Resource Categorization

The main objective of variogram fitting in this study is to obtain maximum variation and distance values or sill and range. Range values will be used as references to determine the nature of data continuity in various directions or isotropic/anisotropic. Meanwhile, the sill value will be used to determine the area influence radius for mineral resources categorization.

Data shows horizontal range at 220 meters with azimuth N130°E as the major direction and sill value of 78.65 (**Table 2**). A semi-major range that has a perpendicular direction to the major results in the same value. The ratio between major and semi-major is 1:1, or isotropic. While the minor range that is perpendicular to semi-major is around 57 meters. The ratio between semi-major and minor is 220:57 or 1:3.8. Thus, the study area can be said to have an anisotropic condition. Based on the above-mentioned parameters, the measured resource category area of influence is 1/3 of the sill (78.65) or 25.95 or 50 meters radius (**Figure 5**). Indicated resource category rests on 2/3 of the sill or 51.91, which is equivalent to 105 meters radius. Inferred resource category is based on 0.95 from the sill or 74.72 or 180 meters radius.

Table 2 Sill and range adopted for determining the area of influence in resource categorization in the Pamubulan area.

Variogram Pamubulan		78,65	220 m
Resources Category	**Percentage**	***Sill***	***Range (m)***
Measured	0,33	25,95	50
Indicated	0,66	51,91	105
Inferred	0,95	74,72	180

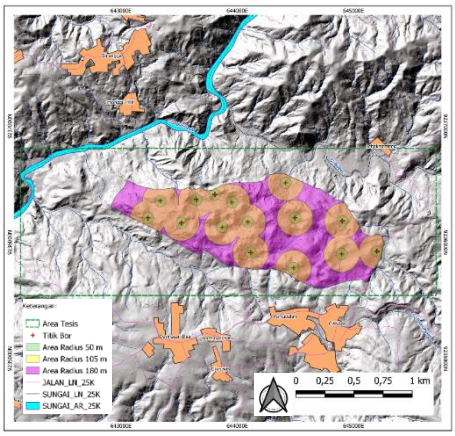

Figure 5 Area of influence map and resource category area.

Blocks model stretched west-east following major formation spreading. Attributes included for estimation are CaO and MgO. No rotational or tilting transformation was applied.

To acquire the tonnage of the deposits, the volume of blocks is multiplied by the density of limestone. Chatterjee [12] studied that the average density of limestone is 2.6 gr/cm^3. Volume and tonnage calculation will only measure blocks with CaO values above 40% and MgO values below 5%. The total volume/tonnage suitable for raw material for cement is around 220 million tonnes or 84 million cubic meters (**Table 3**).

High-grade limestone with a good level of CaO content is concentrated in the east-southeast and northwestern parts of the study area (**Figure 6**). This grade seems to be bisected in the middle by low-grade limestone, stretching from southwest to northeast. A similar aspect is shown in the distribution of MgO (**Figure 7**). High MgO levels tend to gather in the southwestern part extending to the northeast.

Another notable feature is the emergence of high MgO levels in the middle of high-grade limestone in the southeast. Both of these characteristics should handle with care by limestone producers and or company owners. A more sophisticated mining strategy could be needed to achieve desired mining profit. Selective mining operations might be used and concentrated in two different areas.

Table 3 Sill and range adopted for determining the area of influence in resource categorization in the Pamubulan area.

CaO		MgO		Resource	Volume (m^3)	Tonnes	Average	
from	to	from	to	Category			CaO	MgO
40	45	0	5	MEA	720.000	1.872.000	43,32	1,76
				IND	8.370.000	21.762.000	43,22	1,57
				INF	6.048.000	15.724.800	44,09	2,35
45	50	0	5	MEA	1.116.000	2.901.600	47,73	1,29
				IND	15.012.000	39.031.200	46,98	1,66
				INF	6.966.000	18.111.600	47,15	1,45
50	55	0	5	MEA	5.922.000	15.397.200	52,99	0,89
				IND	28.314.000	73.616.400	52,75	0,90
				INF	12.150.000	31.590.000	53,18	0,66
				Grand Total	**84.618.000**	**220.006.800**	**49,64**	**1,23**

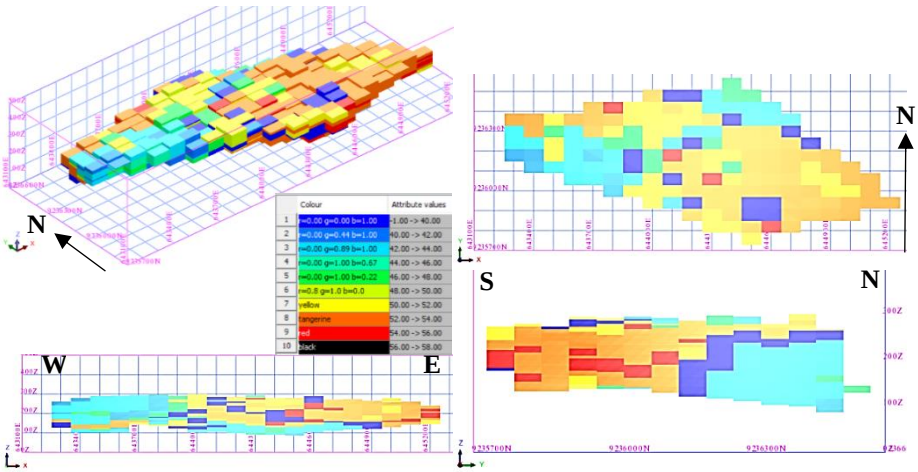

Figure 6 Blocks model representing certain location volume and CaO grade in the researched area. Perspective view (upper left), map view (upper right), W-E section (lower left), S-N section (lower right).

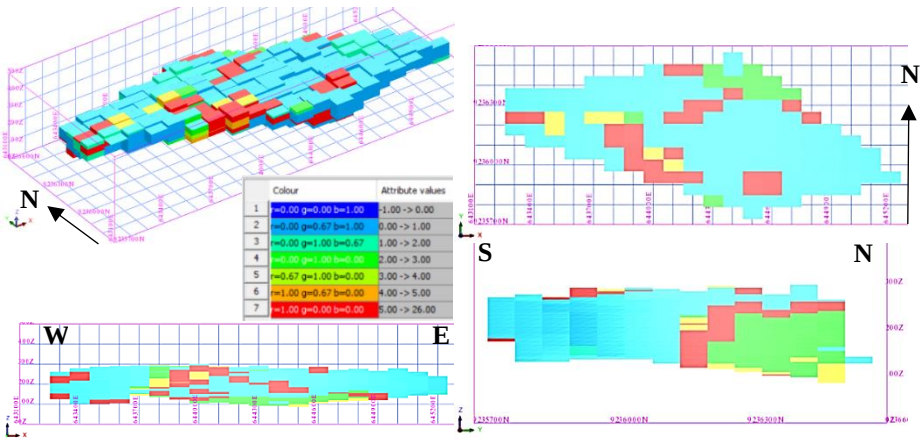

Figure 7 Blocks model representing certain location volume and CaO grade in the researched area. Perspective view (upper left), map view (upper right), W-E section (lower left), S-N section (lower right).

5 Conclusion

Applying estimation directly to the limestone deposits as a whole is common practice in raw material quarries. The entire limestone body is used as an arena for resource estimation without any domains. This is due to the high level of practicality of the geostatistical method and its swift application. Additionally, several methods are claimed to be able to give satisfactory results, even after facing bimodal-grade data. Limestone grade data are generally bimodal although most limestone bodies have a massive, homogenous, uniform edifice.

Limestone estimation using standard facies belt as domain or constraint offers a new perspective in mineral resources evaluation. Estimation should not be carried out directly on the limestone body, as a whole. The nature of limestone grade data, which is generally bimodal, should be separated into domains. Segregation using facies belt as a framework follows the nature of the limestone body.

The author proposes a division of the domain according to the genetics of the limestone deposits, which is based on the architecture of the carbonate platform. This division has been proven to be able to divide the nature of the data into unimodal. Estimation made on a more homogeneous domain will produce better forecasting. Prediction results are more precise. This will reduce uncertainty, and increase efficiency, also possible future loss, which finally leads to company prosperity.

Disclaimer

Resource estimation from this paper is a research product. Results might be different from company products. The distinction is mainly caused by different parameters and levels of completeness of the data used.

Acknowledgments

The author would like to express his gratitude to Dr. Ir. Diky Irawan, S.T., M.T., director of PT. Geo Stroom Indonesia, for permission and grant, to attend Master's school program. The writer is also grateful for the data provided by PT. Gama Group management. Last but not least, the geological team, they have done great work in compiling, recording, and storing the data beautifully.

References

[1] Glacken, I. & Trueman, A., *Overview-Mineral Resource Estimation*, Mineral Resource and Ore Reserve Estimation - The AusIMM Guide to

Good Practice, 2nd Ed., Monograph 30, The Australasian Institute of Mining and Metallurgy, Victoria-Australia, pp. 263-276, 2014.

[2] Mackenzie, D. H. & Wilson, G. I., *Geological Interpretation and Geological Modelling*, Mineral Resource and Ore Reserve Estimation – The AusIMM Guide to Good Practice, Edwards, A.C., ed., The Australasian Institute of Mining and Metallurgy, Melbourne-Australia, pp. 111-118, 2001.

[3] Cowan, E.J., *Overview-Geological Interpretation and Geological Modelling*, Mineral Resource and Ore Reserve Estimation - The AusIMM Guide to Good Practice, 2nd Ed., Monograph 30, The Australasian Institute of Mining and Metallurgy, Victoria-Australia, pp. 137-143, 2014.

[4] Van Bemmelen, R. W., *The Geology of Indonesia Vol. 1A*, Government Printing Office, The Hague, 1949.

[5] Sujatmiko & Santosa, S., *Peta Geologi Lembar Leuwidamar, Jawa*, Pusat Penelitian dan Pengembangan Geologi, 1992.

[6] Sukarna, D., Mangga, A. M., & Brata, K., *Geology of the Bayah Area: Implication for the Cenozoic Evolution of West Java, Indonesia*, Geol. Soc. Malaysia, **33**, pp. 163-180, 1992.

[7] Schlager, W., *Carbonate Sedimentology and Sequence Stratigraphy*, SEPM (Society for Sedimentary Geology), Oklahoma, USA, pp. 200, 2005.

[8] Babak, O. & Deutsch, C.V., *Statistical Approach to Inverse Distance Interpolation*, Stoch. Environ. Res. Risk Assess., **23**, pp. 543–553, 2009.

[9] JORC, *The JORC code: Australasian code for reporting of exploration result, mineral resources and ore reserve*, 2012 Ed., Australasian Institute of Mining and Metallurgy - Australian Institute of Geoscientist - Minerals Council of Australia, Australia, pp. 44, 2012.

[10] Mucha, J., Wasilewska-Blaszczyk, M. & Auguscik, J., *Categorization of Mineral Resources Based upon Geostatistical Estimation of the Continuity of Changes of Resources Parameters*, The 17th Annual Conference of the International Association for Mathematical Geoscience, International Association for Mathematical Geoscience (IAMG), Freiberg-Germany, pp. 1-10, 2015.

[11] Snowden, D.V., *Practical Interpretation of Resource Classification Guidelines*, Proceedings AusIMM Annual Conference 'Diversity, the Key to Prosperity', The Australasian Institute of Mining and Metallurgy, Melbourne, pp. 305–308, 1996.

[12] Chatterjee, A.K., *Cement Production Technology: Principle and Practice*, CRC Press, Taylor and Francis Group, Boca Raton-London-New York, 2018.

Proceedings of the 3rd ITB Graduate School Conference ISSN: 2963-718X
Enhancing Creativity in Research Through Developing Innovative Capabilities
December 21, 2022

Analysis of Community-based Enterprise Development Process in Indonesian Return Migrant Workers Community

Annida Mardhotillah[1, *] & Tubagus Furqon Sofhani[2]

[1]Master's Program of Development Studies, School of Architecture, Planning and Policy Development, Bandung Institute of Technology, Jalan Ganesha No. 10 Bandung, Indonesia
[2] Research Group of Regional and Rural Planning, School of Architecture, Planning and Policy Development, Bandung Institute of Technology, Jalan Ganesha No. 10 Bandung, Indonesia
[*]Email: annida.mardho@gmail.com

Abstract. The purpose of this research is to analysis how a community-based enterprise can be formed in Indonesian return migrant workers community through a series of stages of the development process that has been carried out. This study used a qualitative method with a case study approach. Taking a case study on Sahabat Bersama Cooperative formed by Migrant Workers Family Community or Komunitas Keluarga Buruh Migran (KKBM) Karawang, this research examined how a community can collaborate to create a community-based enterprise. By using the model of the stages of community social enterprise development process from Munoz *et al.* (2014) which has been modified according to research needs, the results show that there were six stages to go through in the creation of the Sahabat Bersama Cooperative. The stages were legitimacy, needs/opportunity recognition, group coalescence, organizational establishment, community enterprise operates, and community enterprise grows. This research shows that the entrepreneurial activities carried out by Komunitas Keluarga Buruh Migran (KKBM) Karawang used a community development approach with the involvement of community members in every stage of the cooperative development process as a community-based enterprise.

Keywords: *return migrant workers community; cooperative; community-based enterprise.*

1 Introduction

As a country with the fourth largest population in the world, Indonesia is often faced with employment problems. The high number of workers demands many jobs, but when domestic conditions cannot meet these demands, looking for work abroad or becoming an Indonesian migrant worker is an alternative [1]. According to the Indonesian Migrant Workers Protection Agency (BP2MI),

463,549 people have gone to work overseas in the last three years (2019-2021) [2]. The five biggest destination countries for migrant workers are Hong Kong, Malaysia, Taiwan, Singapore, and Saudi Arabia [2]. Indonesian migrant workers are called “remittance heroes” because of their contribution to the country's economy through the flow of remittances to their homeland. The number of remittances sent by Indonesian migrant workers is regarded as one of the most important sources of foreign exchange after oil and gas sector [3].

However, the high number of departures of Indonesian migrant workers and their contribution to the country's foreign exchange earnings are accompanied by various problems. The issues are both while working in the placement country and when they return to their homeland. Indonesian migrant workers consider several problems as the primary challenges they face once they arrive in Indonesia [4]. Indonesian migrant workers are generally low-educated workers and return to Indonesia when they are no longer of productive age. They must compete with the current workforce in densely populated areas with high unemployment [4]. Furthermore, limited access to establishing a family economy has encouraged Indonesian return migrant workers back to work abroad [5].

One strategy that can be implemented to prevent Indonesian return migrant workers from returning to work abroad is to provide entrepreneurship training so that they can develop their businesses independently [6]. Most stakeholders in Indonesia, such as the government, NGOs, private institutions, and donor agencies, implement the economic reintegration of Indonesian return migrant workers, focusing on self-employment programs [7]. Entrepreneurship is regarded as one of the solutions and strategies to create a sustainable livelihood for return migrant workers by creating jobs, providing new and better jobs, and to some extent reducing migration [8].

Several previous studies have shown that migrant workers who return to their country of origin tend to engange in entrepreneurial activities as a occupational choice. However, most of this literature only focuses on entrepreneurial activities carried out at the individual level through self-employment, for example, Dustmann & Kirchkamp’s study [9] in Turkey, Black & Costaldo [10] in Ghana and Ivory Coast, Sinatti [11] in Senegal and Åkesson [12] in Cape Verde. Meanwhile, other studies also reveal that not all entrepreneurial activities carried out individually by migrant workers who return to their country of origin can last long. Spitzer's study [13] on the entrepreneurial experiences of migrant workers returning to their countries of origin in the Philippines and Indonesia shows that their businesses or ventures have a low success rate.

Anwar & Chan [14] conducted a comparative study on the entrepreneurial activities of Indonesian return migrant workers in two villages in Yogyakarta

Province. In the first location, the results show that business groups are divided among the community of return migrant workers giving rise to intense competition and socio-economic inequality. Whereas in the second location, the results show that the entrepreneurship of return migrant workers which was carried out cooperatively and initiatives with collective action can survive in the long term [14]. The findings of Anwar and Chan's study [14] show that entrepreneurial activities of Indonesian return migrant workers that are carried out in a community with collective and participatory action are more likely to survive in the long term.

Community-based entrepreneurship is a process of identifying, creating, and utilizing opportunities to collectively produce goods and services that provide economic, social and/or ecological benefits to local communities and/or the larger society [15]. According to Haugh & Pardy [16], the final product of community entrepreneurship is a community business or community enterprise. Until now, most of Indonesian return migrant workers entrepreneurship literature has focused on the business generated and its benefits, while the process of creating an enterprise has not been studied in depth. Wahyono *et al*. [17] and Zid *et al*. [5] about social entrepreneurship run by the female return migrant workers community in Wonosobo and Indramayu shows the positive benefits of community-based entrepreneurship which can solve common problems by creating entrepreneurial opportunities and preventing return migrant workers from returning to work abroad. However, these two studies did not explain the stages of community enterprise development process in Indonesian return migrant workers community. An analysis of a community-based enterprise development process is important to do, to find out how the involvement of community members and the influence of other actors is in every stage of the process. Therefore, this research examined the process of developing a community-based enterprise in Indonesian return migrant workers community by analyzing the stages of development process.

2 Literature Review

2.1 Community-based Entrepreneurship

Pierre *et al*. [18] define community-based entrepreneurship as a locally-based phenomenon that includes for-profit organizations and non-profit organizations, local businesses, individuals, local community-oriented projects, and networks that together or separately seek to create sustainable and thriving communities by engaging the community in efforts to solve problems and increase socio-economic value. According to Haugh & Pardy [16], community-based entrepreneurship is used to describe situations in which a group of individuals from a community works together, initially without a formal organizational

structure, to generate and develop ideas and opportunities with social and economic benefits for the community.

Meanwhile, Hertel [15] defines community-based entrepreneurship as the process of recognizing, creating, and utilizing opportunities to collectively create goods and services that provide economic, social, and/or ecological benefits to local communities and/or the larger society. According to Hertel [15], this definition implies that (1) community-based entrepreneurship is a process; (2) opportunities that can be utilized for community-based entrepreneurship must be created in a co-evolution process which consists of opportunity development, collectivization, and evaluation; and (3) the output of the process is a company that contributes to sustainable development either at the local or community level.

Based on some of the definitions above, it can be concluded that community-based entrepreneurship is an entrepreneurial activity carried out collectively by a community intending to provide social, economic, and/or ecological benefits to its members. As a result of this entrepreneurial process, a community-based enterprise is created [16], an enterprise that is collectively founded, owned and controlled by community members where it appears and aims to make a profit [15].

2.2 Community-based Enterprise

Paredo & Chrisman [19] define a community-based enterprise as a community that acts corporately, both as an entrepreneur and an enterprise, in pursuit of the common good. Communities act as entrepreneurs when their members act as owners, managers, and employees who collaboratively create or identify market opportunities and organize themselves to respond to them [19]. Meanwhile, the community acts as an enterprise if its members work together to produce and exchange goods and/or services by using the existing social structure of society to organize these activities [19].

Meanwhile, Hertel [15] defines a community-based enterprise as a company that is collectively established, owned, and controlled by local community members, where they are bound and aiming to generate economic, social, and/or ecological benefits. Based on this definition, Hertel [15] then reveals five elements that become the characteristics of community-based enterprises: embeddedness; community orientation; self-sustaining business activity; the multiplicity of goals; and collective establishment, ownership, and control.

As an enterprise built with social and economic goals, the process of developing a community-based enterprise is different from conventional business companies in general. According to Haugh [20], building a community-based enterprise is a

creative and collective process requiring various assets provided differently by different actors. In the process of creating a community-based enterprise, the community is considered the primary actor rather than a contextual element, so the community is viewed as part of the enterprise and the entrepreneurial process [19]. The creation process of a community enterprise can vary depending on the nature and time scale between communities [21].

Munoz *et al*. [21] developed a model that represents the process of creating a community social enterprise which consists of five different stages as follows:

1. Stage 1: legitimacy
   At this stage, community members had to be sure of the legitimacy of the community social enterprise. It can be accomplished through a meeting or dialogue with community members and other stakeholders involved in the business establishment to build trust and engagement among community members.
2. Stage 2: needs/opportunity recognition
   At this stage, dialogue or community meetings continue to identify potential opportunities and community needs through social entrepreneurship activities.
3. Stage 3: group coalescence
   At this stage, collective needs and identifying opportunities through social entrepreneurial activities are realized in the joint actions of community members and the emergence of a leader in the community. Examples of activities in the group coalescence stage include skill recognition and skills building through group training or winning start-up finance.
4. Stage 4: organizational establishment
   At this stage, a community social enterprise is established. At the same time, there is an increase in community members' responsibilities related to the emergence of the organization.
5. Stage 5: social enterprise operates
   At this stage, the community social enterprise officially operates in line with its goals and is attentive to the needs of community members. At this stage, community members are also responsible for their organizational needs to provide benefits to the community, provide social value and fulfill the quality and value of the public sector.

3 Methodology

This study used a qualitative method. The qualitative method is based on personal observations of situations, events, individuals, interactions, transactions, document analysis (including quantitative notes), and open-ended interviews that produce in-depth and oral testimonies [22]. The approach in this qualitative research used a case study. The case study is an inquiry design found in many

fields in which the researcher develops an in-depth analysis of a case, for example, a program, event, activity, process, or one or more individuals [23]. This study has taken Sahabat Bersama Cooperative formed by Migrant Workers Family Community or Komunitas Keluarga Buruh Migran (KKBM) Karawang, as a case study to understand how the stages of development process of a community-based enterprise.

Data collection techniques in this study were divided based on the type of data source. For primary data, researchers used observation techniques and semi-structured interviews to collect data directly from informants in the field. The technique to determine the informants used in this study was purposive sampling. Informants selected in this study were those directly involved or had knowledge of the development process of Sahabat Bersama Cooperative. Meanwhile, for secondary data, researchers used a literature study on documents related to the entrepreneurial activities of Komunitas Keluarga Buruh Migran (KKBM) Karawang and Sahabat Bersama Cooperative.

The qualitative data analysis technique used in this study was an interactive model developed by Miles *et al*. [24], which consists of three activities: data condensation, data display, and conclusion drawing/verification. In data condensation activities, researchers carried out the process of selecting, abstracting, and or transforming data that emerged from field notes, interview transcripts, documents, and other empirical materials [24]. The next stage was the presentation of data in the form of narratives and graphics that describe the stages of the development process of Sahabat Bersama Cooperative. The final stage was drawing conclusions and verifying research findings related to the development process of Sahabat Bersama Cooperative.

4 Result and Discussion

In analyzing the process of developing Sahabat Bersama Cooperative as a community-based enterprise in Komunitas Keluarga Buruh Migran (KKBM) Karawang, researchers used the model proposed by Munoz *et al*. [21]. However, based on the analysis results and research findings in the field, it is necessary to add one more stage in addition to the five stages contained in the Munoz *et al*. model; namely, the 'community enterprise grows' stage. Further descriptions of the six stages are explained in the sections below.

4.1 Stage 1: Legitimacy

According to Munoz *et al*. [21], before the organization starts, community members must be convinced of the legitimacy of the community enterprise. This legitimacy must be embedded in the community that will be involved in the

community enterprise, so the community members must 'engage' [21]. In contrast to the theoretical concept put forward by Munoz *et al*., the findings of studies in the field showed that at this first stage, the idea of creating a cooperative as a community enterprise had not yet appeared in Komunitas Keluarga Buruh Migran (KKBM) Karawang. At this stage, the legitimacy process was carried out in relation to the economic empowerment program activities for Indonesian return migrant workers organized by the Indonesian Migrant Worker Protection Service Center (BP3MI) Bandung, which was the main driving factor for the emergence of entrepreneurial activities in Komunitas Keluarga Buruh Migran (KKBM) Karawang.

At this stage, officers of BP3MI Bandung asked for help from the community leader to gather and invite return migrant workers to be willing to become participants in the economic empowerment program. At first, the community leaders faced difficulties in inviting return migrant workers because there was distrust from them who thought that this activity was a form of promotion of the companies that sent Indonesian migrant workers abroad. However, after being given an understanding that economic empowerment activity was an official program from the government, return migrant workers were willing to be involved as participants. In addition, another effort made by community leaders to gain legitimacy was to approach village heads where the economic empowerment program would be held. By getting support from the village heads and assisting community leader in gaining trust of return migrant workers, they were willing to be involved in community entrepreneurship activities in the future.

4.2 Stage 2: Needs/Opportunity Recognition

According to Munoz et al. [21], at this stage, there is a dialogue or community meeting to identify potential opportunities and community needs through social entrepreneurship activities. After obtaining legitimacy from return migrant workers in the first stage, the next step was to identify needs and opportunities related to entrepreneurial activities that would be carried out after the economic empowerment program had been completed. The community leader invited return migrant workers to gather to determine the type of training that community members needed and were interested in for further to be submitted to BP3MI Bandung officers. BP3MI Bandung officers indentified participants in the economic empowerment program proposed by the community based on the interests of the majority of community members and the potential possessed by their area of residence. The process of identifying needs and opportunities was vital because it would determine what type of business the community would run.

4.3 Stage 3: Group Colaescence

According to Munoz et al. [21], at this stage, collective needs and identifying opportunities through social entrepreneurial activities are manifested into joint actions of community members. At this stage, return migrant workers received entrepreneurship training through economic empowerment program organized by BP3MI Bandung. According to BP3MI Bandung officers, the training was given over several days and consisted of entrepreneurship education and financial literacy. After completing the training, the return migrant workers joined and agreed to make plans to form a cooperative as a forum for community businesses. Thus, the initial idea to create a community enterprise in Komunitas Keluarga Buruh Migran (KKBM) Karawang emerged in the third stage.

At this stage, return migrant workers were also willing to collect their personal money as initial capital for funding the cooperative businesses. In addition, to realize the plan to form a cooperative, the community leader consulted with several government agencies such as the Cooperatives and Small and Medium Enterprises Office of the Karawang Regency, the Manpower Office of Karawang Regency, and BP3MI Bandung. Thus, at this stage, there were joint actions of community members, such as completing training, raising initial funds, and coordinating with the public sector to realize the creation of cooperatives as community enterprises.

4.4 Stage 4: Organizational Establishment

According to Munoz *et al.* [21], a community enterprise is established at this stage. At the same time, there is an increase in the responsibilities of community members related to the emergence of the organization. At this stage, the idea to form a cooperative as a forum for community businesses was realized by registering the legality of the cooperative to the Cooperatives and SMEs Office in Karawang Regency. In 2016, Sahabat Bersama Cooperative succeeded in obtaining legality with the existence of a legal entity number for multi-business cooperative groups. The establishment of this cooperative had an impact on the division of roles and tasks among community members, some were involved as cooperative administrators, and some were administrators of Small and Medium Enterprises (UKM). Small and Medium Enterprises (UKM) administrators themselves were divided into several business groups according to the type of entrepreneurship training they had attended.

4.5 Stage 5: Community Enterprise Operates

According to Munoz *et al.* [21], at this stage, the community enterprise operates under its objectives and is attentive to the needs of community members. At this

stage, Sahabat Bersama Cooperative had already performed as a community-based enterprise for return migrant workers who were members of Komunitas Keluarga Buruh Migran (KKBM) Karawang. The types of businesses run by the cooperative include various processed snacks such as breadfruit chips and *rangginang* (traditional rice crackers), as well as souvenirs such as key chains, knitted shoes, and dolls. At this stage, Sahabat Bersama Cooperative products had started to enter the market but with a range that was not so wide. For example, the products were marketed at the nearest shops, sold through family members and relatives, and participated in product exhibition activities organized by government agencies. At this stage, community members began to get various benefits and profits derived from businesses run by the cooperative. The benefits obtained were income, increased knowledge and insight, and social benefits such as more friends.

4.6 Stage 6: Community Enterprise Grows

At this stage, the community enterprise did not only operate but also experienced growth and development. At this stage, Sahabat Bersama Cooperative experienced various developments, including in the aspects of marketing, sales turnover, and assets owned. Sahabat Bersama Cooperative collaborated with minimarket companies so that their products could be marketed in four regencies in West Java province, namely Karawang, Subang, Purwakarta, and Indramayu. The increase in product marketing reach also impacts the sales turnover of the Sahabat Bersama Cooperative every month. Based on interviews with informants, the sales turnover of Sahabat Bersama Cooperative reaches tens to hundreds of millions every month. Along with increasing income, Sahabat Bersama Cooperative can add to the cooperative's assets by purchasing operational vehicles for the delivery of goods. As for future business planning, Sahabat Bersama Cooperative has the desire to expand the marketing of their products to the Jabodetabek area (Jakarta, Bogor, Depok, Tangerang and Bekasi) so that the cooperative's products will increasingly be recognized.

Based on the analysis above, the stages of Sahabat Bersama Cooperative development process as community-based enterprise can be described as follows.

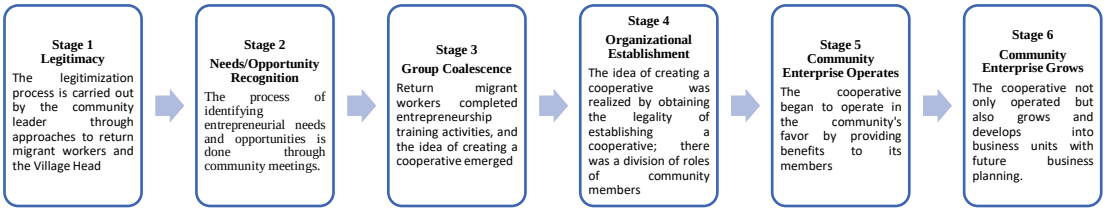

Figure 1 Stages of Sahabat Bersama Cooperative development process

5 Conclusion

Entrepreneurial activities carried out by Komunitas Keluarga Buruh Migran (KKBM) Karawang have resulted in a community-based enterprise through the creation of Sahabat Bersama Cooperative. Based on an analysis using the Munoz model *et al.* [21], which has been modified according to the needs of the study, there are six stages of the development process of Sahabat Bersama Cooperative as a community-based enterprise, namely the stages of legitimacy, need/opportunity recognition, group coalescence, organizational establishment, community enterprise operates and community enterprise grows. In contrast to Munoz's theory, *et al.* [21] state that the initial idea of creating a community enterprise has existed from the first stage. In this case study, the initial idea of creating a community enterprise actually appeared in the third stage, when the community completed economic empowerment activities. In each step of the development process of Sahabat Bersama Cooperative, there is the involvement of community members, so this research strengthens the findings of the Paredo & Chrisman's study [19] that in the process of creating a community-based enterprise, the community is considered as the main actor rather than a contextual element, so the community is viewed as part of the enterprise and entrepreneurial process.

References

[1] Muslihudin, Wulan, T.R., Sugiarto, T., Wardhiana, S., & Wijayanti, S., *Initial Implementation of Productive Migrant Village (PMV) Programs in Banyumas Central Java Indonesia*, Proceeding of The International Conference on Rural Development and Entrepreneurship, pp. 1-6, 2019.

[2] Pusat Data dan Informasi BP2MI, *Data Pekerja Migran Indonesia Periode Tahun 2021*, Badan Pelindungan Pekerja Migran Indonesia, pp. 4-13, 2022.

[3] Dewi, E. & Yazid, S., *Tata Kelola Remitansi Buruh Migran Indonesia oleh Pemangku Kepentingan di Tingkat Nasional dan Akar Rumput: Praktik Baik, Peluang dan Tantangan*, Jurnal Hubungan Internasional, **6**(2), pp. 209-220, 2017.

[4] Maksum, A., *Indonesia post-migrant workers: A challenging problem for human security*, Social Science & Humanities Open, **4**(1), pp. 1-10, 2021.

[5] Zid, M., Alkhudri, A.T., Casmana, A.R., Marini, A., & Wahyudi, A., *Ex Migrant Workers of International Women and Social Entrepreneurship: Study at Kenanga Village in Indramayu Regency West Java Province in Indonesia*, International Journal of Advanced Science and Technology, **29** (6), pp. 1855-1861, 2020.

[6] Hidayat, D.R., *Pencegahan TKI Kembali ke Luar Negeri Melalui Pelatihan untuk dapat Berwirausaha*, Jurnal Sarwahita, **13**(1), pp. 34-39, 2016.

[7] Bachtiar, P.P., & Prasetyo, D.D., *Return Migration and Various Reintegration Programs for Low-Skilled Migrants Workers in Indonesia*, SMERU Research Institute, 2017.

[8] Yuniarto, P.R., *Indonesian Return Migrants Entrepreneurship at Home Village: Knowledge Production and Living Strategy*, Jurnal Kependudukan Indonesia, **13**(2), pp. 89-102, 2018.

[9] Dustmann, C. & Kirchkamp, O., *The Optimal Migration Duration and Activity Choice After Re-Migration*, Journal of Development Economic, **67**, pp. 351 – 372, 2002.

[10] Black, R. & Costaldo, A., *Return Migration and Entrepreneurship in Ghana and Cote D'Ivoire: The Role of Capital Transfer,* Tijdschrift voor Economische en Sociale Geografie **100**(1), pp. 44–58, 2009.

[11] Sinatti, G., *Return Migration, Entrepreneurship and Development: Contrasting the Economic Growth Perspective of Senegal's Diaspora Policy Through a Migrant-centered Approach*, African Studies, **78**(4), pp. 609-623, 2019.

[12] Åkesson, L., *Obstacles and Openings: Returnees and Small-scale Businesses in Cape Verde*, in Åkesson & Eriksson-Baaz (eds), The New Developers? Experiences of African Return Migrants, Zed Books, pp. 152-170, 2015.

[13] Spitzer, D.L., *Return Migrant Entrepreneurship and The Migration and Development Agenda: A Focus on Filipino and Indonesian Migrant Workers*, Migration, Mobility & Displacement, **2**(2), pp. 24-39, 2016.

[14] Anwar, R.P. & Chan, C., *Constrasting Return Migrant Entrepreneurship Experiences in Javanese Villages*, International Migration, International Organization of Migration (IOM), pp. 1-14, 2016.

[15] Hertel, C.J., *Community-based Entrepreneurship – Toward a Legitimate Research Domain*, Doctoral dissertation, TUM School of Management, Technische Universit¨at München, Munchen, 2018.
[16] Haugh, H.M. & Pardy, W., *Community entrepreneurship in north east Scotland*, International Journal of Entrepreneurial Behavior & Research, **5**(4), pp. 163-172, 1999.
[17] Wahyono, E., Kolopaking, L.M., Sumarti, T., & Hubeis, A.V.S., *Jaringan Digital dan Pengembangan Kewirausahaan Sosial Buruh Migran Perempuan*, Jurnal Ilmu Komunikasi, **16**(1), pp. 57-76, 2019.
[18] Pierre, A., von Friedrich, Y. & Wincent, J., *Entrepreneurship in Society: A Review and Definition of Community-Based Entrepreneurship Research*, In: Lundström, A., Zhou, C., von Friedrichs, Y., Sundin, E. (eds) Social Entrepreneurship, International Studies in Entrepreneurship, **29**, pp. 239-257, 2014.
[19] Paredo, A.M. & Chrisman, J.J., *Toward a Theory of Community-Based Enterprise*, Academy of Management Review, **31**(2), pp. 309-328, 2006.
[20] Haugh, H., *Community-Led Social Venture Creation*, Entrepreneurship Theory and Practice, **31**(2), pp. 16-182, 2007.
[21] Munoz, S-A., Steiner, A., & Farmer, J., *Processes of community-led social enterprise development: learning from the rural context*, Community Development Journal, **50**(3), pp. 478-493, 2014.
[22] Dana, L.P., & Dana, T.E., *Expanding the scope of methodologies used in entrepreneurship research*, International Journal Entrepreneurship and Small Business, **2**(1), pp. 79-88, 2005.
[23] Cresswell, J.W., & Cresswell, J.D., *Research Design: Qualitative, Quantitative, and Mixed Methods Approaches*, ed. 5, SAGE Publications, Inc, 2018.
[24] Miles, M., Huberman, A.M., & Saldana, J., *Qualitative Data Analysis – A Methods Sourcebook*, ed. 3, SAGE Publications, Inc, 2014.

Proceedings of the 3rd ITB Graduate School Conference ISSN: 2963-718X
Enhancing Creativity in Research Through Developing Innovative Capabilities
December 21, 2022

Optimization of Local Revenue: Indragiri Hulu Regency

Baiq Rizky Fatmasari *, Septian Asriadi Putra & Wiwik Dwi Pratiwi

Sekolah Arsiterktur, Perencanaan dan Pengembangan Kebijakan,
Institut Teknologi Bandung
*Email: baiqisky@gmail.com

Abstract. In the reform era, the government system in Indonesia underwent a change from a centralized system to a decentralized system. This makes the delegation of authority from the central government to Local governments, including the authority to finance the implementation of government or what is commonly known as Local Revenue. The success of the Local Government in increasing financial capacity is measured using the Local Fiscal Independence Index. One of the things that are considered capable of driving an increase in Local Revenue is also increasing the economy, which is at the district scale by providing economic activities through traditional markets. The services provided also make it possible to withdraw Local Revenue in the form of Local levies. The findings in this article show that the Government of Indragiri Hulu Regency in recent years has also continued to increase Local Revenues through increasing market levies. In the end, the author suggests several things that can be done by the Government of Indragiri Hulu Regency.

Keyword: *Development; Economy; Local Finance; Levies.*

1 Introduction

After the reform, the central government of Indonesia then established a series of policies, including issuing Law Number 22 of 1999 which was later replaced by Law Number 32 of 2004 concerning Local Government to seek Local autonomy policy formats that were able to accelerate Local progress, increase the welfare of the people and at the same time strengthening National Integration. Until the most recent update with the enactment of Law Number 23 of 2014 concerning Local Government. In Article 1 paragraph (6) of Law Number 23 of 2014 concerning Local Government, what is meant by Local Autonomy is the rights, powers, and obligations of an autonomous region to regulate and manage it's Government Affairs and the interests of the local community within the system of the Unitary State of the Republic of Indonesia. Thus, Local autonomy makes every provincial, regency, or city government obtain its autonomous right to advance and develop its region according to its potential.

The implementation of Local autonomy gives authority to Local governments to independently administer their administration. All implementation of the

government is outlined in the form of Concurrent Government Affairs and General Government Affairs. This delegation of authority is accompanied by financial authority in which to be able to carry out these Government Affairs, adequate financial capacity is needed as a resource. Therefore, local governments must be able to develop their full potential in order to run their administration as well as possible.

To support the implementation of Local autonomy through the provision of funding sources based on the authority of the central government, decentralization, deconcentration and co-administration, it is necessary to regulate the financial balance between the central government and Local governments in the form of a financial system that is regulated based on a clear division of authority, tasks and responsibilities among government structure (Yani, 2013). In its implementation in Indonesia, it is regulated in Law 25 of 1999 concerning financial balance between the Central and Local Governments which was later renewed by Law Number 33 of 2004 concerning Financial Balance between the Government and Local Governments, and most recently, with the issuance of Law Number 1 of 2022 on Central Financial Relations and Local Government. This is a form of fiscal decentralization from the central government to local governments.

The enactment of Local autonomy has provided an opportunity for regions to explore local potential and improve their financial performance in order to realize Local independence. This means that the delegation of Local authority is also accompanied by the transfer of financing sources that were previously held by the central government (Mahi et al, 2001). Local autonomy is also expected to be a bridge for local governments to encourage economic efficiency, public service efficiency so as to be able to encourage Local economic growth and improve the welfare of local residents through various multiplier effects of decentralization which are expected to materialize (Khusaini, 2006).

As is well known, various efforts to increase local revenue are carried out in tandem with an increase in the economy in an area, this is in line with research from Fadli (2016), which states that an increase in Local Own-source Revenue is influenced by an increase in added value in the economy by 6%, which means that the performance of economic growth completely affect local original Revenue. Within the Local scope, one form of economic improvement is by providing facilities for economic activity, namely traditional markets. In traditional markets, there is a buying and selling process between communities, and various services and jobs are formed that arise from these activities. In addition, traditional markets are cultural assets and drivers of the national economy which have so far proven to be resilient from the blows of the crisis (Bappelitbangda, 2019). So the local government needs to facilitate these

activities so that the economy will increase. With the facilities provided by the Local government, this can be used as one of the potentials to increase local revenue, through collecting market levies.

Local independence is calculated using the fiscal independence index, from the calculation results of 503 local governments nationally which are attached to the Audit Report on the 2020 Central Government Financial Statements, it is found that the majority of local governments (443 out of 503 local governments or 88.07%) included in the "Not yet Independent" category, apart from that there was also a high gap in fiscal independence between regions. The results of this assessment indicated that the existing policies in general had enabled and encouraged local governments to meet the criteria for reviewing fiscal decentralization. This was then supported by the commitment of local governments which is manifested in various policies to realize transparent and accountable Local financial management.

One of the areas to be analyzed in this case study is Indragiri Hulu Regency, Riau Province.Indragiri Hulu Regency is one of the districts in Riau Province which has Local autonomy authority to implement the affairs of Local government in an effort to improve the welfare of its people. In the era of Local autonomy, financial independence plays an important role for local governments in carrying out government affairs which are their authority in order to create a prosperous society in Indragiri Hulu Regency. Based on the conditions and problems above, the purpose of this research is to find out whether Local autonomy is able to increase fiscal independence in an effort to support the implementation of Local government affairs which are the authority of Indragiri Hulu Regency.

The analysis of fiscal independence studied by Taryono in 2011, shows that during the last 5 (five) years the average Local Revenue of Indragiri Hulu Regency has been able to grow by 7.5% annually with an annual average growth rate of local own-source revenue of 13.55%. However, the role of Local Own-source Revenue in total revenue is still relatively low, as seen from the ratio of Local Own-source Revenue to total government spending, where its role is still around 3%.

Thus, the authors are interested in analyzing the various strategies undertaken to facilitate these market activities, so that they have the potential to improve the economy and have an impact on increasing Local Own-source Revenue through market levies in Indragiri Hulu Regency.

2 Methodology

The research in this article uses secondary data obtained from the Ministry of Finance's DJPK website, Performance Reports of Government Agencies of the Industry and Trade Service Office of Indragiri Hulu Regency, Reports on Audit Results of the 2020 Central Government Financial Statements which released by BPK, and other literature studies. Then, the data that has been collected is processed using a combined qualitative and quantitative descriptive method or it can also be called a mixed method. The descriptive method according to Nazir (2011) is a research method by making descriptions, accurate, systematic, and factual descriptions based on facts in the field and then analyzes the existing problems and describes them in detailed writing regarding observations of certain individuals or groups. Meanwhile, mixed methods is a method for investigating problems using qualitative and quantitative data analysis simultaneously (Creswell, 2010). mixed methods is used by integrating or mixing two research data to generate new insights or understandings rather than what is produced by only quantitative or qualitative data.

3 Discussion

3.1 Indragiri Hulu Regency Fiscal

In 2013 – 2015, Riau Fiscal Independence Index experienced an increase, with the highest score in 2015, namely 0.5031 which was categorized as "Independent". However, from 2016 – 2020, Riau's Fiscal Independence Index value fell again to its lowest point in 2020, namely 0.3866.

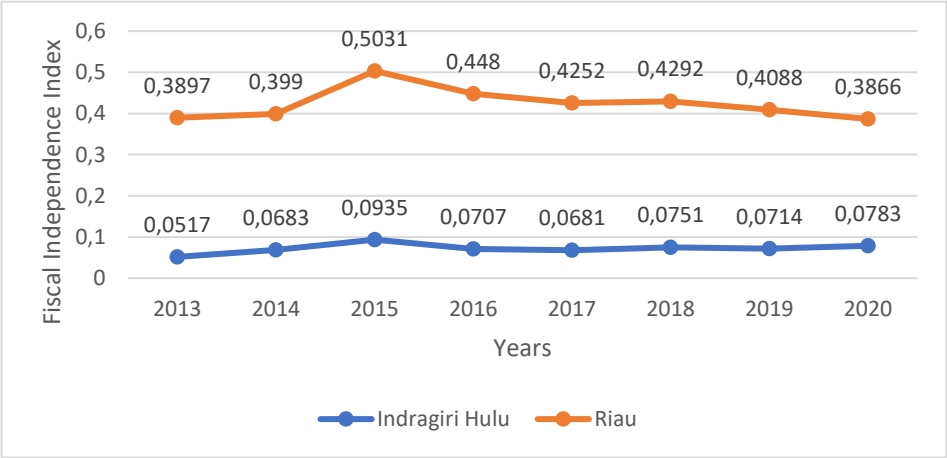

Figure 1. Comparison of Fiscal Independence Index of

Indragiri Hulu Regency to Riau Province
Source: Modfified from Report on Audit Results Central Government Financial Statements, 2020

Meanwhile, referring to figure 1, *the trend* of the Fiscal Independence Index of Indragiri Hulu Regency in 2013 – 2020 tends to be flat and is always below the Fiscal Independence Index of Riau Province, with an average 0.0713, or included in the category "Not yet independent". From 2013 – 2020, the Fiscal Independence Index of Indragiri Hulu Regency only experienced a significant increase in 2015 with a value of 0.0935, after 2014 it was worth 0.0683. Even so, the Fiscal Independence Index score is still in the "Not Independent" category. Therefore, a strategy is needed to increase the fiscal independence of Indragiri Hulu Regency, one of which is through increasing market levies, which is expected to increase Local levies and lead to an increase in Local Own-source Revenue.

Based on Law Number 1 of 2022 concerning Financial Relations between the Central Government and Local Governments, Local Original Revenue is Local revenue consisting of on several components, such as: 1) local taxes; 2) Local levies; 3) results of separated Local wealth management, and 4) other legitimate Local original revenues in accordance with statutory regulations. As shown in Figure 2, the Local Original Revenue of Indragiri Hulu Regency from 2012 to 2015 tended to increase, but began to fluctuate in 2016 – 2018. In 2019, the Local own-sources Revenue of Indragiri Hulu Regency began to increase again, although not significantly. A significant increase occurred in 2012 – 2013, from IDR 5.827.345.000 in 2012—or the lowest during 2012 – 2019, to IDR 52.683.145.618 in 2013. The highest Local own-source Revenue realization was achieved by Indragiri Hulu Regency in 2017 with a value of IDR 164.442.903.083.

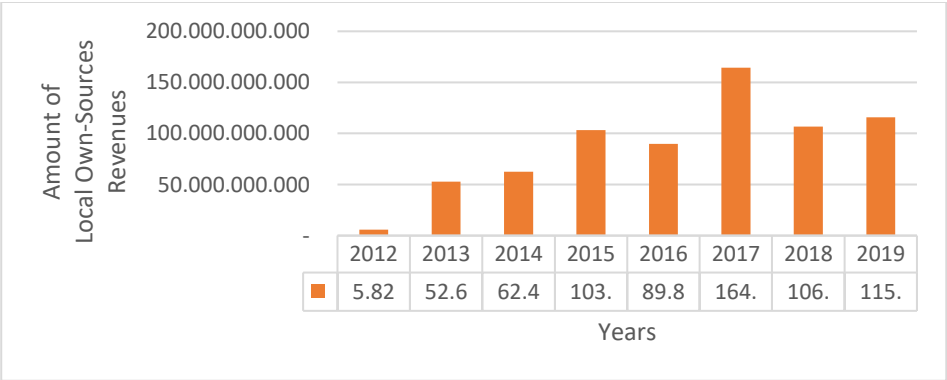

Figure 2. Realization of Local Own Revenue of Indragiri Hulu Regency in 2012 – 2019

Source: Modified from Local Regulation of Indragiri Hulu Regency Regarding Local Expenditure Budget (APBD)/Revision of APBD, 2022

Referring to Law Number 1 of 2022 concerning Financial Relations between the Central Government and Local Governments, Local levies are Local levies as payment for services or granting of certain permits specifically provided and/or granted by the Local Government for the benefit of individuals or entities. Along with the rapid increase in Local own-source revenue, Local levies for Indragiri Hulu Regency in 2012 – 2013 also experienced a significant increase, from IDR 5.457.845.000 in 2012 to IDR 13.477.723.000 in 2013—which is the highest Local levy for Indragiri Hulu Regency in for the period 2012 – 2019 which can be seen in Figure 3. Then, in 2014 – 2019, Local levies for Indragiri Hulu Regency tended to fluctuate, and dropped quite a lot from IDR 10.933.242.800 in 2016 to IDR 4.789.463.658 in 2017. trend ValueThis decline still occurs in 2018 and 2019.

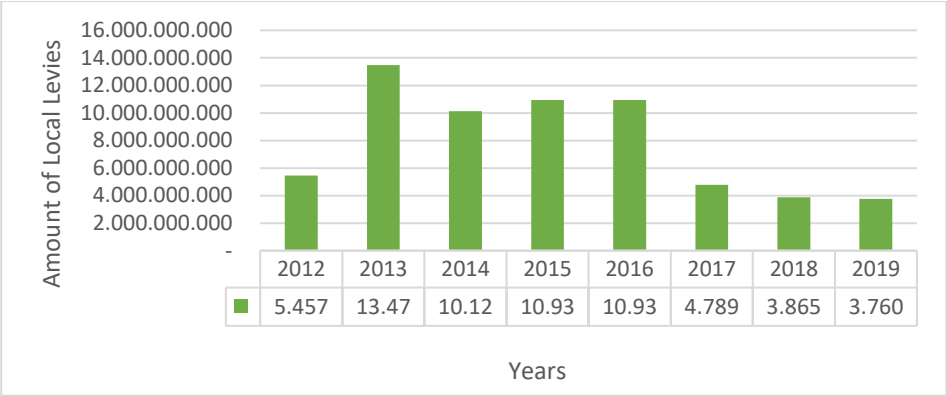

Figure 3. Realization of Local Levies for Indragiri Hulu Regency for 2012 – 2019
Source: Modified from Local Regulation of Indragiri Hulu Regency Regarding Local Expenditure Budget (APBD)/Revisions , 2022

The Indragiri Hulu Regency Government has established a legal basis for collecting Local levies, through the Indragiri Hulu Regency Local Regulation Number 1 of 2012 concerning Public Service Charges, and Indragiri Hulu Regency Local Regulation Number 2 of 2012 concerning Business Service Charges. Its realization by levies type shown in this table below

Table 1
Realization of Levies for Indragiri Hulu Regency
by Type in 2014 – 2016

TYPE OF LEVIES	LEVIES REALIZATION

		2014 (IDR)	2015 (IDR)	2016 (IDR)
1	Health Service Levies	-	76.555.000	-
2	Clean-up Service Levies	174.579.000	211.357.000	192.118.000
3	Reimbursement of Civil Registry Deed Levies	-	-	-
4	Parking Services Levies on Public Roads	158.100.000	160.200.000	180.000.000
5	Motorized Vehicle Testing Levies	606.115.000	650.188.500	665.487.500
6	Liquid Waste Management Levies	-	-	-
7	Telecommunications Tower Control Levies	875.000.000	-	-
8	Local Assets Use Levies	447.596.218	398.682.830	337.828.076
9	Terminal Retribution	136.020.000	143.280.000	138.550.000
10	Animal Housing Levies	75.805.750	67.646.000	71.010.000
11	Local Business Production Levies	31.750.000	33.650.000	74.040.000
12	Building Permit Levies	1.925.398.000	989.269.000	879.469.000
13	Disruption Permit Levies	6.177.492.534	6.913.039.906	6.358.591.678
14	Route Permit Levies	1.740.000	1.890.000	2.040.000
15	Market Service Levies	935.787.500	1.091.714.000	1.058.277.000

Source: Modified from Putra, 2017

Referring to Table 4 above, market levies are one of the highest sources of revenue in Indragiri Hulu Regency, after disturbance permit levies and building permit levies. In addition, the market is the closest place for economic activity to the community, so it is interesting to study further.

Market levies are one source of revenue that contributes to an increase in Local Own-source revenue in Indragiri Hulu Regency. There are 14 markets managed by the Local Government of Indragiri Hulu Regency and are a source of levies collection. The technical implementation of traditional market management in Indragiri Hulu Regency is regulated in Indragiri Hulu Regent Regulation Number 4 of 2016 concerning Traditional Market Management. The regulation also explains the basis for collecting market levies. In Chapter IX Article 40 paragraph (1) Indragiri Hulu Regent Regulation Number 4 of 2016, it is stated that market levies consist of 3 components which include: 1) Market service levies; 2) Cleaning Levies; and 3) Rent of Market Stalls. Furthermore, in paragraph (2) it is explained, the Object for Levies as referred to in paragraph (1) is the provision of public/simple market facilities in the form of courtyards, booths, kiosks, and other facilities in markets managed by the Local Government.

The trend of realization of market levies can be seen in Figure 5 below.

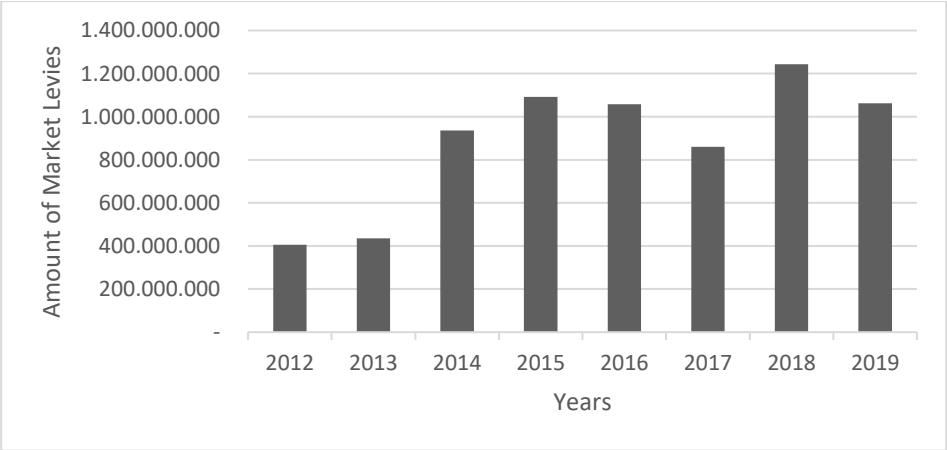

Figure 5. Realization of Market Levies in Indragiri Hulu Regency 2012 – 2019
Source: Modified from Performance Report of Government Agencies Industry and Trade Office of Indragiri Hulu Regency and DJPK Ministry of Finance, 2022

As shown in Figure 5, market levies in Indragiri Hulu Regency in 2012 – 2019 tended to fluctuate, with a significant increase in 2013 – 2014, from IDR 435.229.600 in 2013 to IDR 935.787.500 in 2014. After experiencing a *trend* increased in 2014 – 2015 and decreased slightly in 2016, there was a significant decrease in 2016 – 2017, from IDR 1.058.277.000 in 2016 to IDR 860.288.000 in 2017. The market levy for Indragiri Hulu Regency then increased to IDR 1.242 841.000 in 2018. This figure is the highest levy value in the 2012 – 2019 period. However, in 2019, the levy value has fallen again to Rp. 1.062.592.000.

Based on the Decree of the Minister of Home Affairs Number 690.900-327 of 1994 concerning Criteria for Assessment of Local Performance and Finance as stipulated in Khoiriyah and Ayu (2020), there are 6 classifications of Local financial contribution ratios, namely : very poor (0 - 10%), poor (10.1 - 20%), moderate (20.1 - 30%), quite good (30.1 - 40%), good (40.1 - 50%) , and very good (above 50%). The contribution of market levies to Local levies in Indragiri Hulu Regency in 2012 - 2019 tends to fluctuate as shown in Figure 6, with an average of 14.7%, which is included in the "less" classification. There was a significant increase in 2016 – 2017, from 9.7% to 18%. Then, in 2018 the contribution of market levies to Local levies managed to reach its highest point, namely 32.2% and was included in the fairly good category. However, in 2019 the contribution value fell again to 28.3% (medium category).

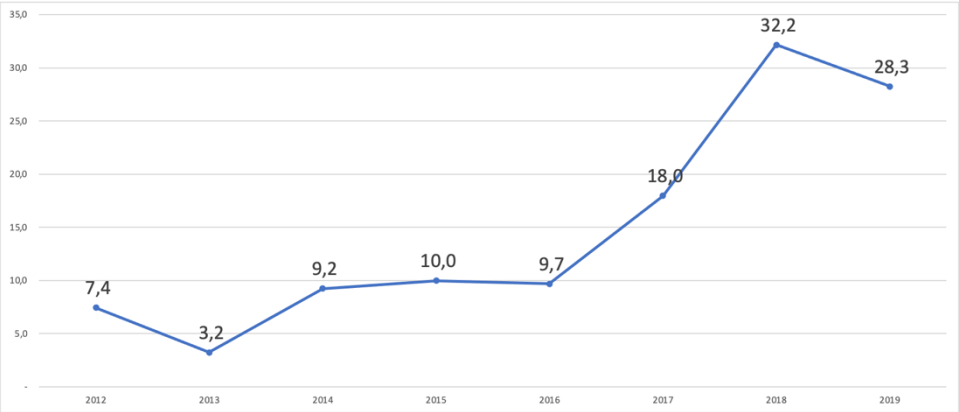

Figure 6. Contribution of Market Levies to Local Levies in Indragiri Hulu Regency 2012 – 2019

Analysis of strategies of optimizing market levies in Indragiri Hulu Regency

Optimization is a series of activities carried out to maximize available resources. In the context of Local revenues, optimization is carried out to strengthen Local financial capacity, by carrying out the following 2 strategies: intensification and extensification. Putra (2017) describes several efforts to increase the contribution of market levies to Local own-sources Revenue in Indragiri Hulu Regency, which in paper, the authors classify into intensification and extensification of market levies.

Intensification is one strategy for optimizing Local revenues by strengthening the mechanism for withdrawing revenues from existing sources (Siregar: 2004), in this case, receipts from market levies. The Indragiri Hulu Regency Government has intensified market levies revenue by taking the following steps, *First*, increased supervision. Supervision is one of the important things to do to control

and control what is not expected. The Department of Industry and Trade of Indragiri Hulu Regency through the Market Management Sector conducts supervision over the implementation of market levies collection in market zones in Indragiri Hulu Regency. Supervision of the market zone is needed to minimize violations and fraud in the field.

Second, apparatus quality improvement. Acceptance of market levies will be achieved if it is supported by professional apparatus and has work discipline. Therefore, by improving the quality of the apparatus, it is hoped that it will become a supporting factor in the successful implementation of tasks and increase in the acceptance of market levies.

Third, increasing the awareness of traders for the facilities provided. In this case the Department of Industry and Trade of Indragiri Hulu Regency routinely holds a Market Cleanliness Contest. Markets that are successfully designated as the cleanest markets will receive awards. Conversely, the market with the lowest level of cleanliness will also receive sanctions. Thus, the traders will compete to improve cleanliness even though winning is not the main goal of the activity, but rather the concern of the traders to be able to continue to maintain the facilities provided by the government which in the end the concern for paying levies also increases with a conducive environment for conducting sales transactions buy.

Fourth, increase outreach to traders and the public as buyers. This is intended so that everyone who conducts transactions in the market can participate in conducting activities in an orderly manner in accordance with regulations. In addition, socialization is also aimed at increasing the awareness of traders to pay levies and for buyers to maintain the conduciveness of buying and selling activities in the community.

Fifth, improve coordination with Local Apparatus Organizations, Village Government, other agencies, and community groups. In this case, coordination was conducted with the Department of Transportation, the Civil Service Police Unit, the Police regarding security and order. Furthermore, coordination with the Local Revenue Agency is related to target reporting and realization of market levies receipts in Indragiri Hulu Regency. Coordination was also conducted with the sub-district head and village head, where it was hoped that the sub-district head and village head would be able to assist in conducting monitoring of market activities and other matters to assist the oversight of the Industry and Trade Office of Indragiri Hulu Regency. Coordination with the community was also conducted intensively to be able to listen to opinions, input and criticisms that were used to be able to improve traditional market services in Indragiri Hulu Regency

In the other side, Extensification is one of the strategies for optimizing Local revenues through increasing production output by adding and/or expanding the production factors used (Alisman, et al: 2018) in this case, revenue from market levies. There have been several implementations of extensification of market levy receipts in the Indragiri Hulu district, including *First*, issuance of a new legal basis. The Indragiri Hulu Regency Government issued Local Regulation Number 3 of 2015 concerning the Management of Traditional markets, Shopping Centers, and Supermarkets. The arrangement in question includes the definition, classification, planning, implementation, control, and evaluation as well as the rights and obligations of traditional market traders. For more technical arrangements, the Regent Regulation Number 4 of 2016 concerning Traditional market Management was also issued as an operational regulation. The regulation in question is more specifically regulated regarding the definition, classification, planning, implementation, control, and evaluation as well as the rights and obligations of traders, empowerment, guidance, supervision, licensing, reporting, levies, buildings, community participation, Standard Operating Procedures, and the determination of sanctions. These two regulations are used as a reference in providing traditional market services in Indragiri Hulu Regency. In terms of local revenue, the two regulations provide the legacy for the government to be able to collect levies related to traditional market services which in general are regulated in Local Regulation Number 1 of 2012 concerning Public Service Charges and Local Regulation Number 2 of 2012 concerning Business Service Charges.

The collection of market levies in Indragiri Hulu Regency is regulated in Indragiri Hulu Regent Regulation Number 4 of 2016 concerning Traditional market Management. In Chapter IX Article 40 of this regulation, it is explained that market levies consisting of market service levies, market cleaning levies, and market stall rentals are levied as payment for the services provided. Furthermore, what is determined as the Object of Levies is the provision of public/simple market facilities in the form of courtyards, stalls, kiosks, and other facilities in markets managed by the Local Government. Several objects that are excluded from the Objects of Levies are market facility services managed by local government owned enterprise (BUMD), State owned enterprise (BUMN) and private parties. Subjects of Levies are individuals or entities that use/enjoy the relevant market services. The stipulation of levies imposed in the regulation is divided into market service levies, market cleaning levies, and market stall rentals. The structure and amount of the Indragiri Hulu Regency market levy is attached in table 2 below:

Table 2

Structure and Amount of Charges for Market Charges
in Indragiri Hulu Regency

	TYPE OF LEVIES	AMOUNT (IDR)
1	**Market Service Charge**	
	· Location/area of plot of land per plot	1000/day
	· Building in the form of Los Perlot	
	a. In the District Capital	2,000/day
	b. Outside the Regency Capital	1,500/day
2	**Market Clean-up Levies**	
	· Los	6,000/month
	· Kiosk	3,000/month
3	**Rent a Market Kiosk**	
	· In the District Capital	60,000/month
	· Outside the Regency Capital	50,000/month

Source: *Modified from Indragiri Hulu Regent Regulation Number 4 of 2016*

This strengthening of the legal basis enables the government to measure the success of the traditional market services provided to the public, in addition to guiding in setting targets and collecting market levies. For the community, they can obtain information about traditional market services. Thus, the implementation of acceptance of levies can run optimally.

Second, the extensification carried out is by adding objects of levies through the establishment carried out was in the form of whole or partial development, renovation, rehabilitation, and rebuild of markets building using Transfer Funds. This activity is based on President Jokowi's 1000 Markets program during the 2014-2019 administration. This is of course very helpful for the Local Government of Indragiri Hulu Regency to provide market establishment facilities. Market establishment in Indragiri Hulu Regency through the Special Allocation Fund (DAK) can be seen in several traditional markets with details in table 3 as follows:

Table 3

Traditional Market Building Data Sourced from
Special Allocation Funds (DAK) in Indragiri Hulu Regency

	Name of Traditional Market	***Year***
1	Construction of Rakit Kulim Traditional Market	2015
2	Construction of Batang Peranap Traditional Market	2016
3	Construction of Japura Traditional Market	2017

4	Construction of Sei Beras-Beras Traditional Market	2017
5	Rehabilitatioin of Rengat Traditional Market	2017
6	Construction of Kuala Cenaku Traditional Market	2018
7	Construction of Pekan Heran Traditional Market	2019

Source: Industry and Trade office of Indragiri Hulu Regency ,2020

Conclusion

Local Finance of Indragiri Hulu Regency is still included in the Not Independent category. The local own-source revenue is still fluctuating. Along with its journey, it can be seen from the Local levies sector has shown an increase by contributing an average of 14.7% which is included in the "less" classification. Several optimization strategies are implemented in the form of intensification and extensification of market levies.

In this article, it is recommended to first increase market levies rates by considering various factors that affect Local revenues, especially economic factors. Second, strengthening collaboration between local governments and the private sector in market procurement. This is by Article 4 letter b of Indragiri Hulu Regent Regulation Number 4 of 2016 concerning Traditional market Management, which states that it is possible to procure traditional markets built by private parties. Third, the government of Indragiri Hulu Regency should draw up laws and regulations that refer to Law Number 1 of 2022 concerning Relations between Central Finance and the Local Government

Reference

[1] Alisman. (2018). Intensifikasi dan ekstensifikasi Penerimaan Pajak Daerah dalam Menunjang Pendapatan Asli Daerah (PAD) di Kabupaten Nagan Raya. Aceh: Jurnal Ekombis: Ekonmi dan Bisnis Universitas Teuku Umar **8**(2)

[2] RI Financial Audit Board. (2021). Report on Audit Results of the 2020 Central Government Financial Statements. Jakarta: BPK RI.

[3] Purwakarta Regency Research and Development Development Planning Agency. (2019). Study on Development of Traditional Market Potential in Purwakarta Regency. Jakarta.

[4] Creswell, John. (2010). Research Design Pendekatan Kualitatif, Kuantitatif, dan Mixed. Yogyakarta: Pustaka Belajar.
[5] Fadly, F. (2016). Adakah Pengaruh Pertumbuhan Ekonomi Terhadap Pendapatan Asli Daerah? JIEP-Vol. 16, No 2, November 2016 ISSN (P) 1412-2200 E-ISSN 2548-1851.
[6] Government of the Republic of Indonesia. (2004). Law No. 32 of 2004 concerning Regional Government. Jakarta: Ministry of State Secretariat.
[7] Government of the Republic of Indonesia. (2014). Law No. 23 of 2014 concerning Regional Government. Jakarta: Ministry of State Secretariat.
[8] Government of the Republic of Indonesia. (2022). Law No. 1 of 2022 concerning Central and Regional Financial Relations. Jakarta: Ministry of State Secretariat.
[9] Indragiri Hulu District Government. (2012). Performance Report of Government Agencies Service of Industry and Trade. Indragiri Hulu: Disperindag.
[10] Indragiri Hulu District Government. (2012). Regional Regulation of Indragiri Hulu Regency Number 5 of 2012 concerning Changes to the Regional Revenue and Expenditure Budget for Fiscal Year 2012. Indragiri Hulu: Regional Secretariat of Indragiri Hulu Regency.
[11] Indragiri Hulu District Government. (2012). Indragiri Hulu Regency Regional Regulation Number 1 of 2012 concerning Public Service Charges. Indragiri Hulu: Regional Secretariat of Indragiri Hulu Regency.
[12] Indragiri Hulu District Government. (2012). Regional Regulation of Indragiri Hulu Regency Number 2 of 2012 concerning Retribution for Business Services. Indragiri Hulu: Regional Secretariat of Indragiri Hulu Regency.
[13] Indragiri Hulu District Government. (2013). Performance Report of Government Agencies Service of Industry and Trade. Indragiri Hulu: Disperindag.
[14] Indragiri Hulu District Government. (2013). Regional Regulation of Indragiri Hulu Regency Number 7 of 2013 concerning Changes to the Regional Revenue and Expenditure Budget for Fiscal Year 2013. Indragiri Hulu: Regional Secretariat of Indragiri Hulu Regency.
[15] Indragiri Hulu District Government. (2014). Performance Report of Government Agencies Service of Industry and Trade. Indragiri Hulu: Disperindag.
[16] Indragiri Hulu District Government. (2014). Regional Regulation of Indragiri Hulu Regency Number 19 of 2014 concerning Amendments to the Regional Revenue and Expenditure Budget for Fiscal Year 2014. Indragiri Hulu: Regional Secretariat of Indragiri Hulu Regency.
[17] Indragiri Hulu District Government. (2015). Performance Report of Government Agencies Service of Industry and Trade. Indragiri Hulu: Disperindag.

[18] Indragiri Hulu District Government. (2015). Indragiri Hulu Regency Regional Regulation Number 1 of 2015 concerning the Revised Regional Revenue and Expenditure Budget for the 2015 Fiscal Year. Indragiri Hulu: Regional Secretariat of Indragiri Hulu Regency.
[19] Indragiri Hulu District Government. (2016). Performance Report of Government Agencies Service of Industry and Trade. Indragiri Hulu: Disperindag.
[20] Indragiri Hulu District Government. (2016). Indragiri Hulu Regency Regional Regulation Number 6 of 2016 concerning the Revised Regional Revenue and Expenditure Budget for the 2016 Fiscal Year. Indragiri Hulu: Regional Secretariat of Indragiri Hulu Regency.
[21] Indragiri Hulu District Government. (2016). Indragiri Hulu Regent Regulation Number 4 of 2016 concerning People's Market Management. Indragiri Hulu: Regional Secretariat of Indragiri Hulu Regency.
[22] Indragiri Hulu District Government. (2017). Indragiri Hulu Regency Regional Regulation Number 8 of 2017 concerning Amendments to the Regional Revenue and Expenditure Budget for the 2017 Fiscal Year. Indragiri Hulu: Regional Secretariat of Indragiri Hulu Regency.
[23] Indragiri Hulu District Government. (2018). Performance Report of Government Agencies Service of Industry and Trade. Indragiri Hulu: Disperindag.
[24] Indragiri Hulu District Government. (2018). Regional Regulation of Indragiri Hulu Regency Number 1 of 2018 concerning Regional Revenue and Expenditure Budget for Fiscal Year 2018. Indragiri Hulu: Regional Secretariat of Indragiri Hulu Regency.
[25] Indragiri Hulu District Government. (2019). Performance Report of Government Agencies Service of Industry and Trade. Indragiri Hulu: Disperindag.
[26] Indragiri Hulu District Government. (2019). Indragiri Hulu Regency Regional Regulation Number 9 of 2019 concerning Amendments to the Regional Revenue and Expenditure Budget for the 2019 Fiscal Year. Indragiri Hulu: Regional Secretariat of Indragiri Hulu Regency.
[27] Indragiri Hulu District Government. (2020). Performance Report of Government Agencies Service of Industry and Trade. Indragiri Hulu: Disperindag.
[28] Kementerian Keuangan RI. (2022). Data Series APBD. *https://djpk.kemenkeu.go.id/?p=5412*
[29] Khoiriyah, N. dan Ayu F. P. (2020). Analisis Efektivitas dan Kontribusi Penerimaan Pajak Kendaraan Bermotor Terhadap Pendapatan Asli Daerah Jawa Timur di Unit Pelaksana Teknis Pengelolaan Pendapatan Daerah Gresik. Jurnal Ilmiah Mahasiswa FEB Universitas Brawijaya, Vol 9

[30] Mahi, Raksaka. (2001). Fiscal Decentalizations : Its Impact on Cities Growth. Jakarta: Jurnal Ekonomi dan Pembangunan Indonesia Vol 2, No. 1, Juli 2001.
[31] Nazir, Moh. (2011). Metode Penelitian. Jakarta: Ghalia Indonesia.
[32] Parks, R. B., Baker, P. C., Kiser, L., Oakerson, R., Ostrom, E., Ostrom, V., Percy, S. L., et al. (1981). Consumers as co-producers of public services. Policy Studies Journal, 9(7), 1001–1011.
[33] Putra, S. A. (2017). Kontribusi Retribusi Pasar dalam Meningkatkan Pendapatan Asli Daerah (PAD) Kabupaten Indragiri Hulu. Jatinangor: Institut Pemerintahan Dalam Negeri.
[34] Shand, W. J. (2014). What are the institutional implications of co-production as a strategy for development?. University of Manchester: School of Environment, Education and Development, Faculty of Humanities.
[35] Siregar (2004). Perpajakan Indonesia. Jakarta: Salemba Empat.
[36] Taryono. (2011). Analisis Kemandirian Fiskal dalam Upaya Mendukung Pelaksanaan Urusan Pemerintahan Daerah di Kabupaten Indragiri Hulu. Riau: Jurnal Sosial Ekonomi Pembangunan, Tahun 1 No. 2 Maret 2011.
[37] Yani, A. (2013). Hubungan Keuangan Antara Pemerintah Pusat dan Daerah di Indonesia. Jakarta: Rajawali Press.

Proceedings of the 3rd ITB Graduate School Conference ISSN: 2963-718X
Enhancing Creativity in Research Through Developing Innovative Capabilities
December 21, 2022

Merchants' Acceptability of Mobile Payment: A Systematic Literature Review

Chairil Zidane[1, *] & Tengku Munawar Chalil[2]

[1]Master Program of Development Studies, School of Architecture, Planning, and Policy Development, Bandung Institute of Technology, Indonesia
[2]Policy Planning and Development Management Research Group, School of Architecture, Planning, and Policy Development, Bandung Institute of Technology, Indonesia
[*]Email: 24021301@mahasiswa.itb.ac.id

Abstract. The form of merchants' acceptability of digital payment technology allows it to vary based on the region or country that is moving towards a cashless society, such as Southeast Asia countries which are included in the developing country group from the lower-middle income group to the upper-middle income group, based on previous survey results. Research using a systematic literature review (SLR) approach needs to be conducted to find the determinants that influence the acceptability of mobile payment technology in the context of the cashless society, especially from the merchants' side based on research results in Southeast Asia countries which are said to be more supportive to the non-cash movement. VOSviewer is used to analyze the literature database and network visualization, the clusters formed from the selected articles are related to user motivation and satisfaction, ease of use, usefulness, demographical factors and behavior, service provider reliability and insight, merchants' perception, innovativeness, perceived risk, and usage effect, and also the complexity of mobile payment service. Based on the clustering analysis, adoption and acceptability of mobile payment technology are more perceived as risk-taking and daring, and also affect merchants by considering consumers' intention in using such financial technology.

Keywords: *cashless society; merchants; mobile payment; SLR; Southeast Asia.*

1 Introduction

The cashless society movement has existed since people started using the barter method and other exchange systems before the production of paper money (cash). However, in the context of digitalization, a cashless society is interpreted as a transformation of the use of cash which is then substituted with electronic money and established as a legal payment tool and digitally recorded. [1]. According to Britannica, the cashless society is defined as a concept in which financial transactions are carried out without going through conventional payment systems, with a focus on digital channels such as internet banking, mobile banking, and

digital wallets. Digital channels are highly recommended and widely used as transaction media throughout the countries globally to reduce the spread of the coronavirus through physical money exchange, during the COVID-19 pandemic. International companies and businesses encourage payments with electronic money during the pandemic as part of the health protocol to prevent coronavirus transmission, and some countries such as India have started to focus on becoming a *cashless society* by using digital transactions. The COVID-19 pandemic has become a driving factor for digital and contactless transactions for merchants and buyers under strict health protocols, which are still being issued until entering a new normal era.

The amount of paper money used in countries from various income class groups has begun to decline, accompanied by the development of alternative forms of electronic money to digital payment applications that are accepted globally. Based on questionnaire data collected by YouGov (docs.cdn.yougov.com) as of 2020 there were 25,823 respondents and income group data from the World Bank, which was then ranked by MoneyTransfers.com according to % that would like a cashless society, as follows as India (79%), Malaysia (65%), UAE (63%), Indonesia (63%), Vietnam (60%), Singapore (56%), Italy (52%), Philippines (52%), Thailand (51%, emerging upper-middle income group), dan Taiwan (48%), where almost half of the countries included in the ranking are developing and Southeast Asia countries. From that data, it can be assumed that the cashless society movement is not only driven in developed countries but in most developing countries in Southeast Asia with various income levels that are more supportive of the use of digital services as a means of payment and national financial circulation. Referring to data on the value of electronic money transactions in countries with the highest percentage towards a cashless society, such as Indonesia, it has started to increase up to 26 times since 2010 (source from Bank Indonesia infographic). The increase of electronic money usage in shopping transactions in various sectors in Indonesia is also due to its benefits, especially from the point of view of financial institutions and most consumers, in terms of efficiency and convenience in transactions, automatic recording, and reduction in the printing of banknotes and the production of coins.

Table 1 Key Events and Policies Related to Digital Transactions Implementation

Year	Key Events	Key Policies
2005	Developing NFC Payment System	Contactless payment experimentation and validation through mobile phones via NFC feature and tags
2014	National Noncash Movement (GNNT) by Bank Indonesia	Bank Indonesia encourages digital payment by using electronic money, as part of the electronification (Local Government transactions, social aid program disbursements, transportation and toll payments)

Year	Key Events	Key Policies
2021	Global Findex Regional by World Bank	Governments investing in digital public infrastructure and technologies for payment and ID systems during the COVID-19 pandemic
2022	G20 Presidency in Bali, Indonesia	"Synergy for Inclusive and Sustainable Economic Growth" seminar to boost payment system digitalization in Indonesia, supported by BSPI Regulatory reform for innovative economy and finance ecosystem through integrated digital payment infrastructure

There are assumptions based on scholars' arguments for merchants' acceptability (especially from the MSME scale business) of electronic payments that have been programmed and supported by the Government. Some of the initial findings in the studies of mobile payment acceptability inhibitors are merchants who belong to marginalized groups of people, demographically poor and elderly, who do not have access to a bank account; the level of financial literacy of merchants towards modern payment systems; and the tradition of buying and selling using cash as a convenient means of payment [1]. Assumptions regarding merchants' acceptability of electronic payment systems are also supported by the results of other studies from Kumari and Khanna in [2], Raya and Vargas in [3], and Heng in [4] with similar arguments, including literacy of payment schemes and merchants; education to understand the functions of supporting devices that are still lacking, large chargeback fees and merchant discount rates (MDR) which are burdensome for merchants, especially if transactions are made in large numbers, complicated bureaucratic and banking procedures for registration and balance withdrawals for merchants, inadequate internet connection for payment processing and connecting to the system server, and also a large population of 'Unbanked People' from informal merchants that tend to be less 'friendly'. The arguments as the initial findings above are the challenges in achieving a cashless society in various countries, because the value of the benefits of the electronification of the buying and selling transaction system must be obtained and seen from both sides, especially from the merchants' side who directly perceive the impact of using digital technology for increasing sales and business success of MSME merchants.

The form of merchants' acceptability of digital payment technology allows it to vary based on the region or country that is moving towards a cashless society, such as Southeast Asia countries which are included in the developing country group from the lower-middle income group to the upper-middle income group, based on previous survey results. Research using a systematic literature review (SLR) approach that has been conducted before is not specific to the subject of MSME actors such as merchants from the market and shopping centers, with the

assumption that digital payments have a more complex level of use and acceptability for merchants (challenges of readiness, exclusivity, and lack of supporting payment technology or tools), other studies conducted by Rahadi, *et al*. in [5] and Patil, *et al.* in [6] only observe at the user side in general (mostly from the consumer or buyer side). Other studies from Abdullah and Khan in [7] focus on enriching information and knowledge on the extent to which determinants of mobile payment adoption affect consumer spending patterns. We also found an SLR study from Diniz, *et al.* in [8] with the same topic on mobile technology as a payment system in developing countries such as Brazil, Colombia, and Peru, but such countries setting is outside of the developing country group based on the results of the survey of % that would like a cashless society and need the latest review of the literature to date (circa 2021-2022) that adapted to the context of policy developments and new technologies in digital payment systems. Therefore, we need to conduct research using a systematic literature review approach to find the determinants that influence the acceptability of mobile payment technology in the context of the cashless society, especially from the merchants' side based on research results in Southeast Asia countries which are said to be more supportive to the non-cash movement.

2 Methods

2.1 Analytic Overview

This study uses a systematic literature review (SLR) approach to analyze various sources of literature on the merchants' acceptability of mobile payment technology in Southeast Asia countries. The SLR method has the advantage of ensuring the quality of the unbiased literature review process which is and can produce a synthesis of the selected literature on a particular scientific field [9] [10], in this case, this scientific research is related to fintech and digital economy. Referring to a study with SLR, the steps we will carry out in this study using the SLR approach are: 1) formulating the research problem and objectives; 2) developing and validating literature review rules; 3) searching for literature in the preferred literature database; 4) filtering the literature based on inclusion or exclusion lists; 5) assessing the quality of the filtered literature; 6) extracting data from selected literature; 7) analyzing and synthesizing data; and 8) reporting the findings from the reviewed literature [11]. Literatures are collected in the form of articles or scientific papers from various journal sources (various studies) in the Scopus database.

2.2 Search Strategy

The database used to search for limited journal articles using Scopus via our institution access, to search for articles from 2005 to 2023. 2005 was the

beginning of the emergence of NFC (experimental stage) as a means of payment in line with the cash movement. While the Scopus database on ScienceDirect was chosen based on considerations of ease of finding international-class publications that have gone through a peer-reviewed process, as well as searching for publications in English (mainly) in various fields of study, especially in the field of social sciences and humanities, related to our SLR research topic.

The initial stage we have to do is formulate the main keywords in the literature search. The main keyword used for cashless payment, namely taking the adjective "cashless" combined with the noun "payment", is structured into the word "cashless payment". Other equivalent words can use the word "non-cash payment", but this word is rarely used in literature outside of publications from Indonesia and other surrounding countries (according to the results of a local journal article search).

There are alternative keywords that are more general and still related in the context of the cashless society and linked to payment systems such as digital payments, so the keyword option uses the adjective "digital" to become "digital payment". Other equivalent words for "digital payment", among others are "electronic payment" and "e-payment". From the keyword "digital payment", we can formulate more specific keywords related to the use of devices and media in digital payments, namely "mobile payment", with equivalent words such as "online payment" and "contactless payment". Equivalent words (added command: OR) are useful for finding documents that may use other terms so the search results will be richer and more varied within the same topic and definition.

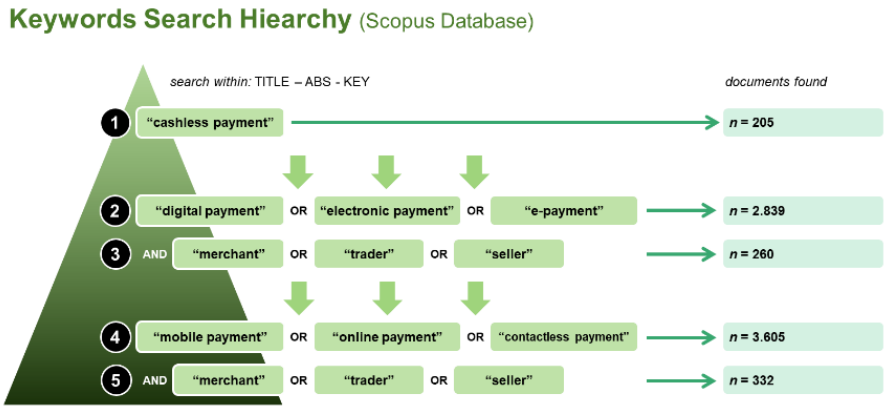

Figure 1 Documents search results based on keywords hierarchy

Based on the keywords search hierarchy (Figure 1), from top to bottom, the main keyword groups have an increasing number of document findings, and fewer when combined with keywords related to the subject or target actors of the research, namely merchants. We discuss that studies using this approach will use the main keyword group, namely "mobile payment" (search: "mobile payment" OR "online payment" OR "contactless payment"), which is combined with the keyword "merchant" (search: ... AND “merchant” OR “trader” or “seller”). The main keywords were chosen because they produce searches with the largest number of documents so the literature which is then analyzed or synthesized will derive various keywords in exploring the determinants that influence merchants' acceptability of mobile payment technology.

2.3 Review Process

Proper documents are used at the review process stage based on inclusion and exclusion criteria (Table 2), which include publication period (year), document type, publication stage, publication country or territory, source type, language, and access type for publication. The inclusion and exclusion criteria are determined based on the refine results feature in the Scopus Database, then each criterion is included and filtered sequentially until the needed articles to review and analyze are found. Our decision to use articles from the publication period 2005-2023 in Southeast Asia countries such as Indonesia, Malaysia, Singapore, Thailand, and Vietnam, based on the context of a background study related to mobile payments, the emergence of digital and contactless payment technology starting from 2005 is associated with the majority of countries that supports and will go towards Cashless Payment. Initially, we decided to focus on countries that are included in the lower-middle income group, but to enrich and deepen the analysis in the literature, Southeast Asia countries are included in the upper-middle income group and the high-income group can be used as benchmarking analysis. These countries could be benchmarked if the merchant groups in there succeed are implementing mobile payment technology in retail transactions.

Table 2 Inclusion and Exclusion Criteria

Inclusion Criteria	Limit Category
Period date/year	2005 – 2023
Document type	Article
Publication stage	Final article paper
Country/territory	Southeast Asia countries Mainly lower-middle income group Upper-middle income group and high-income group for the benchmark study
Source type	Journal
Language	English
Access	All types (full-text access via institution only for descriptive analysis stage for selected articles)

Exclusion Criteria	Exclude Category
Document type	Conference paper
	Review
	Editorial
	Book
	Book chapter
	Note
	Erratum
	Data paper
Publication stage	Article in press
Country/territory	Conference proceeding
	Book series
	Book
	Trade journal
Source type	Journal

The number of published articles about mobile payments in various countries that conducted the research (Figure 2) has increased from year to year with an average growth rate of 13%. Mobile payment research trends (keywords in general) have increased quite high from 2007 to 2008 and 2017 to 2020, and reach the current highest number of publications in 2021 and are projected to attract the attention of researchers and academics in the fields of fintech and digital economy. Internet search results with the keyword "mobile payment" using the Google search engine may give different results, where the highest peak of global search trends is from 2014 to 2015. Overall, from 2,494 literature from various countries, governments and other stakeholders support payments using mobile technology.

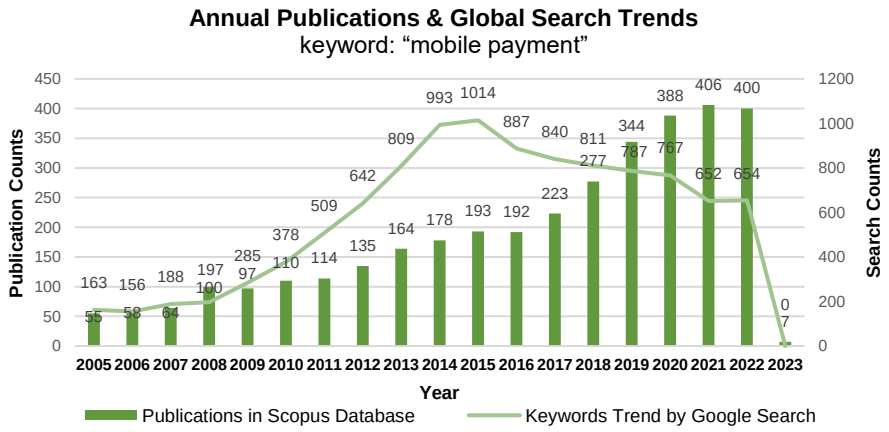

Figure 2 The annual number of documents (all types) using "mobile payment" as a document search keyword (n = 3.505) and tracked by Google search trends

10 Southeast Asia countries are recorded and grouped based on income or GDP according to data from the World Bank (as of 2021), then become inclusion and exclusion requirements in article searches based on country or territory settings (Table 3). Countries with the highest number of publications and the most relevant to the main keywords "mobile payment" and "merchant" (acceptability in mobile payment technology) were found, namely Malaysia, Indonesia, Thailand, Vietnam, Singapore, Philippines, with other countries with minimal (almost none) with articles published using these keywords such as Brunei Darussalam, Cambodia, Laos, and Myanmar.

Table 3 Country Setting as Search Inclusion Criteria (GDP Data per 2021)

Countries	Income Group	*n* Results for "mobile payment" Articles	*n* Results for "mobile payment" AND "merchant" Articles
Brunei Darussalam	High	0	0
Singapore	High	12	1
Malaysia	Upper-middle	77	8
Thailand	Upper-middle	22	1
Cambodia	Lower-middle	0	0
Indonesia	Lower-middle	51	3
Laos	Lower-middle	0	0
Myanmar	Lower-middle	0	0
Philippines	Lower-middle	4	0
Vietnam	Lower-middle	19	2

We can provide an initial conclusion that countries that are included in the upper-middle income group, such as Malaysia and Thailand, have conducted more studies on mobile payment acceptability, followed by Indonesia and Vietnam from the lower-middle income group. The assumption regarding the country setting as search inclusion criteria is that countries with the highest number of publications have a higher concern for the use of mobile payments and there may be issues with it. Meanwhile, countries with the highest income groups, such as Singapore, can be used as a benchmark for study on the successful adoption of digital payment technology.

2.4 Article Extraction

From searching the literature on the Scopus database, the articles were sequentially processed into 4 stages of screening and divided into 2 searches, namely for the keywords ["mobile payment" OR "online payment" OR "contactless payment"] with [("mobile payment" OR "online payment" OR "contactless payment") AND ("merchant" OR "trader" OR "seller")]. The first stage is entering keywords and limiting the publication date between 2005 to 2003; the second stage is to limit the type of final article and the type of

publication source in journals; the third stage is limiting country or territory settings to Southeast Asia countries; and finally, combining search results on articles from the 2 main keywords, as well as separating duplicate articles and articles that are not English. 173 documents were obtained from the screening results, which would then be screened again based on their relevance and information richness of mobile payment acceptability study to be analyzed descriptively-qualitatively, and also to explore all determinants and influences.

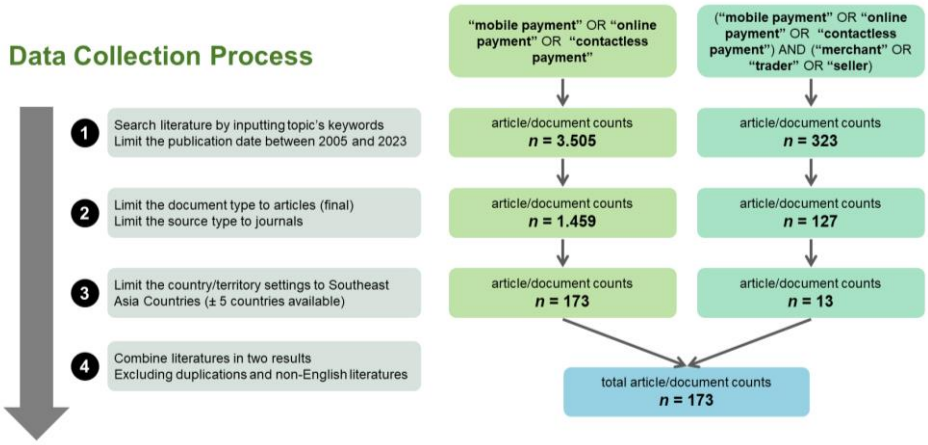

Figure 3 Data collection process for mobile payment studies (n = 173)

2.5 Data Synthesis

The first step in analyzing via VOSviewer is to create a map based on text data from Scopus database files. Then we select the fields in which terms will be extracted, namely title and abstract fields, ignoring structured abstract labels and copyright statements. The calculation method in the analysis uses binary counting, only the presence or the absence of a term in a document matters. The minimum number of occurrences of a term is 3 terms for mobile payments (240 out of 2269 terms) and 2 terms for merchants' acceptability (86 out of 560 terms). Next, we determine a score of 100% (all terms) to select the most relevant keywords. Then a list of terms appears along with the number of occurrences and their relevance value. After that, the network and overlay can be visualized from the clustered terms network, into 6 clusters for mobile payments and 5 clusters for merchants' acceptability. Network visualization results are presented in the following figure (Figure 4) for analysis and a description of how they are grouped, by including some of the terms that appear most dominant in the list of top 5 keywords per cluster for mobile payment and merchants' acceptability articles based on relevance. We determine the list of the top 5 keywords based on the list of terms that appear in each cluster and then we sort them manually, but

those that are relevant to the factor of acceptability by excluding other terms or keywords such as research or analysis methods, similar or other irrelevance words.

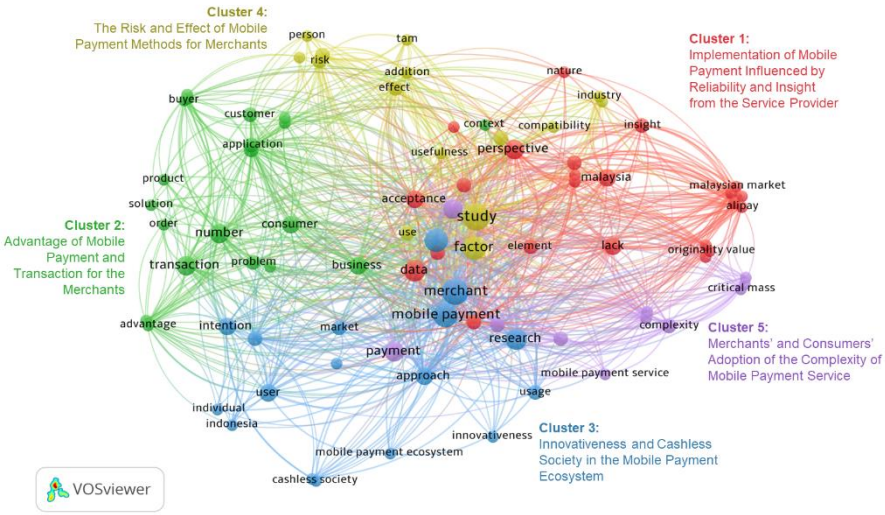

Figure 4 Network visualization and clustering analysis based on text data for merchants' acceptability in mobile payment (via VOSviewer)

Based on text data's network visualization and analysis for merchants' acceptability (Figure 4), clusters can be identified for terms or keywords according to their interrelationships as determinants in technology acceptability, including:

1. Cluster 1: Implementation of mobile payment influenced by reliability and insight from the service provider
   This cluster is composed of dominant keywords related to mobile payment acceptability determinants based on merchants' and service providers' originality and country. Insight is the most relevant keyword in various articles related to mobile payment in the first cluster with 3 times term occurrences and 19,33 average citations, followed by m-payment with 15,50 average citations, nature with 15,00 average citations, reliability with 9,50 average citations, and m-payment service provider with 1,50 average citations. The research method commonly used for this study cluster are case studies in Southeast Asia Countries (mostly from Malaysia), design methodology approach, and study from practical implication.

2. Cluster 2: Advantages of mobile payment and transaction for the merchants
   This cluster is composed of dominant keywords related to sellers' or traders' perceived advantage of mobile payment as a transaction method, also alluding to consumers' intentions. Solution is the most relevant keyword in various articles related to mobile payment in the second cluster with 2 times term occurrences and 8,00 average citations, followed by buyer with 8,00 average citations, transaction with 3,40 average citations, advantage with no average citations, and trust with also no average citations. No research method is commonly used in this cluster.

3. Cluster 3: Innovativeness and cashless society in the mobile payment ecosystem
   This cluster is composed of dominant keywords related to a cashless society, merchants' innovativeness in technology adoption, and mobile payment ecosystem. Cashless society is the most relevant keyword in various articles related to mobile payment in the third cluster with 2 times term occurrences and 16,50 average citations, followed by mobile payment ecosystem with 12,00 average citations, user with 6,00 average citations, innovativeness with 3,00 average citations, and relationship with 0,50 average citations. The research method commonly used for this study cluster are case studies in Southeast Asia Countries (mostly from Indonesia), and other approaches related to technology and innovation studies.

4. Cluster 4: The risk and effect of mobile payment method for merchants
   This cluster is composed of dominant keywords related to merchants' perceived risk and the effect of mobile payment methods in the goods and services industry. Risk is the most relevant keyword in various articles related to mobile payment in the fourth cluster with 3 times term occurrences and 79,00 average citations, followed by effect with 79,00 average citations, payment method with 21,50 average citations, person with 13,50 average citations, and addition with 13,50 average citations. The research method commonly used for this study cluster is Technology Acceptance Model.

5. Cluster 5: Merchants' and consumers' adoption of the complexity of mobile payment service
   This cluster is composed of dominant keywords related to complexity and barrier to merchants' adoption of mobile payment services, also not limited to consumer adoption. Consumer adoption is the most relevant keyword in various articles related to mobile payment in the fifth cluster with 2 times term occurrences and 22,50 average citations, followed by complexity with 18,67 average citations, account with 17,00 average citations, merchant perspective with 16,50 average citations, and mobile payment service with 14,00 average citations. The research method commonly used for this study

cluster is critical mass (sociodynamics) analysis for mobile payment technology adoption from merchants' perspective.

Overlay visualization is used to analyze and explain terms or keywords in the average year of publication (clustering based on publication period). Based on the network terms according to the average year of publication, the terms that affect mobile use in transaction systems, generally, have shifted from 2016 which include the sophistication of modern payment facilities, innovativeness factors, and customer satisfaction. Until the emergence of the COVID-19 pandemic around 2020 and 2022 and as a factor in the increased use of mobile payments as a means of payment, with other factors such as trust, perceived ease of use, and perceived usefulness from the user's side (customer). Whereas in the articles regarding merchants' acceptability of mobile payments, the trend of determinant's terms usage shifted from 2018 on market actors that using mobile payment technology such as consumers, customers, buyers, merchants, markets, and businesses, to the terms of mobile payment ecosystem and mobile payment services and complexity in mobile payment usage from 2018 to 2022.

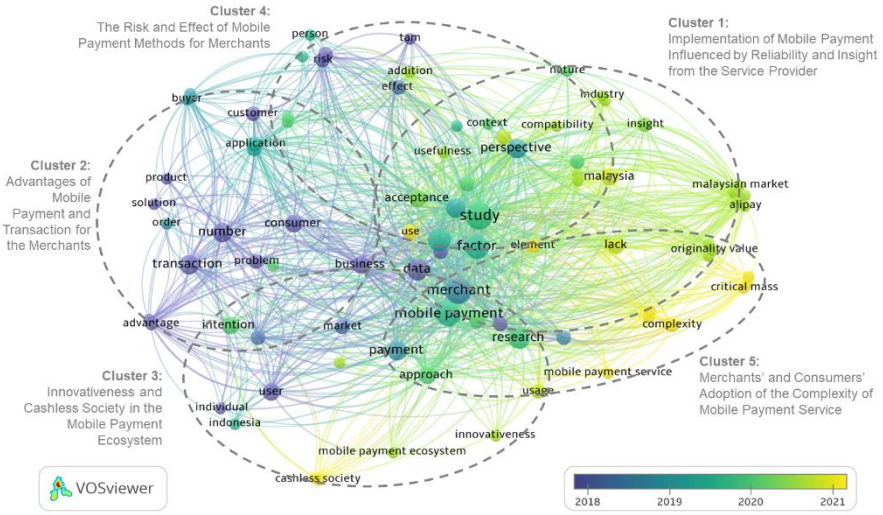

Figure 5 Overlay visualization (average publication year) based on text data for and merchants' acceptability in mobile payment via VOSviewer

3 Results

Final screening results for selected articles related to merchants' acceptability of mobile payment technology were sorted by literature relevance and the number of citations. Each search result ranked by the top 5 articles from the study on the

merchant side to both sides of the market's actors. Note that some documents are not accessible in full text from the Scopus database due to restrictions on the publisher's side, so we searched and accessed the articles through another publication database in case a critical analysis of the literature is required

Table 4 Top 5 Selected Journal Articles (ranked by citations)

No	Title	Authors (Year)	Source Title	Cited by
1	Competition, cooperation, and regulation: Understanding the evolution of the mobile payment's technology ecosystem	Liu et al. (2015)	Electronic Commerce Research and Applications, 14(5), pp. 372–391, 601	98
2	QR code and mobile payment: The disruptive forces in retail	Yan et al. (2021)	Journal of Retailing and Consumer Services, 58, 102300	64
3	Predicting mobile network operator's users m-payment intention	Leong et al. (2021)	European Business Review, 33(1)	29
4	Moving from bricks to clicks: Merchants' acceptance of the mobile payment in Malaysia	Altounjy et al. (2020)	International Journal of eBusiness and eGovernment Studies, 12(2), pp. 126–142	27
5	Intention to use mobile payment system by ethnicity: A partial least squares multi-group approach	Tan et al. (2019)	Asia Journal of Business Research, 9(1), pp. 36–59	13

4 Discussion

Based on the results of literature analysis and network visualization using the SLR approach above, as material for discussion, we obtained five clusters based on the linkage between determinants in mobile payment technology acceptability for merchants, including the following: 1) implementation of mobile payment influenced by reliability and insights from service providers; 2) advantages of mobile payments and transactions for merchants; 3) innovativeness and cashless society in the mobile payment ecosystem; 4) the risk and effect of mobile payment methods for merchants; and 5) merchants' and consumers' adoption of the complexity of mobile payment services. Overall, the keywords "risk" and "effect" had the highest average citations (79 citations) and quite a lot of occurrences (3 times) from the fourth cluster, followed by "consumer adoption" from the fifth cluster. If these keywords are linked to each other, then the adoption and acceptability of mobile payment technology are more perceived as risk-taking and daring, and also affect merchants by considering adoption from consumers as well as in purchase transactions. This initial assumption requires

further investigation in selected articles, especially through empirical study and observation to measure the level of risk in the use of mobile payments technology.

Even though a keyword cluster was formed related to the perceived advantage of mobile payment as a transaction method, the average number of citations for the keywords can be said to be quite low and minimal, and the terms that appear are mostly less relevant to the main theme of the second cluster (except the "solution" keyword). There are other terms, one of which is "consumer intention" in the same cluster, and if it is related to the cluster theme, the actual benefits of using mobile payments are felt more by customers or buyers than by merchants. Besides that, there is a kind of confusion in the second clustering of keywords merchants' acceptability, there are no terms related to research or study methods.

When connected to overlay visualizations, the use of mobile devices in transaction systems experiences a transitional effect in payments that are more modern and innovative to support customer satisfaction when shopping at retail stores, but this is likely to be a problem and an obstacle for merchants who open traditional businesses. Every year, studies on mobile payments are quite interesting, especially when the COVID-19 pandemic occurs in the 2020-2022 range which requires contactless payments. Meanwhile, in context of Southeast Asia countries, mostly Malaysia and Indonesia, are intensively implementing a mobile payment system. The two countries came from different income groups but have almost similar societal and cultural characteristics, especially in the use of financial technology.

5 Conclusion

Our research shows that studies on mobile payment systems' acceptability as a form of the latest financial technology provide quite varied results and nuances. Bibliometric analysis software such as VOS viewer help us analyze and provide network visualization of keywords that are interconnected and form several clusters as the main discussion from each work of literature that studies mobile payment acceptability, especially from the merchants' point of view. Hopefully, our research can contribute as an overview and initial basis for conducting a study related to mobile payments in the context of the cashless society specifically in the cases of Southeast Asia countries. However, further empirical study and observation are required to prove how mobile payment technology influences the acceptability and overall business sustainability of merchants.

References

[1] Fabris, N., *Cashless Society - The Future of Money or a Utopia?*, Journal of Central Banking Theory and Practice, vol. 1, pp. 53-66, 2018. (Journal)

[2] Kumari, N. & Khanna, J. *Cashless Payment: A Behaviourial Change to Economic Growth*, Qualitative and Quantitative Research Review, vol. 2, no. 2, pp. 82-103, 2017. (Journal)

[3] Raya, J.M. & Vargas, C., *How to become a cashless economy and what are the determinants of eliminating cash*, Journal of Applied Economics, vol. 25, no. 1, pp. 543-562, 2022. (Journal)

[4] Heng, S., *E-payments: modern complement to traditional payment systems, Deutsche Bank Research: E-conomics - Digital economy and structural change*, no. 44, pp. 1-8, 2004. (Journal)

[5] Rahadi, R.A., Nainggolan, Y.A., Afgani, K.F., Yusliza, M.Y., Muhammad, Z., Angelina, C., & Farooq, K., *Conceptual Model for Cashless Society: A Literature Synthesis*, European Journal of Business and Management Research, vol. 5, no. 3, pp. 1-7, 2020. (Journal)

[6] Patil, P.P., Dwivedi, Y.K., & Rana, N.P., *Digital Payments Adoption: An Analysis of Literature*, 16th Conference on e-Business, e-Services and e-Society (I3E), Delhi, 2017. (Conference Proceedings)

[7] Abdullah & Khan M.N., *Determining mobile payment adoption: A systematic literature search and bibliometric analysis*, Cogent Business & Management, vol. 8, pp. 1-21, 2021. (Journal)

[8] Diniz, E.H., Albuquerque, J.P.d., & Cernev, A.K., *Mobile Money and Payment: a literature review based on academic and practitioner-oriented publications (2001-2011)*, SSRN Electronic Journal - Proceedings of SIG GlobDev Fourth Annual Workshop, pp. 1-35, 2011. (Conference Proceedings)

[9] Fleming, P., Chan, A.W., & Drucker, A.M., *Research Techniques Made Simple: Assessing Risk of Bias in Systematic Reviews*, Journal of Investigative Dermatology, vol. 136, no. 11, pp. E109-E114, 2016. (Journal)

[10] Fisch, C. & Block, J., *Six tips for your (systematic) literature review in business and management research*, Management Review Quarterly, vol. 68, no. 2, pp. 103-106, 2018. (Journal)

[11] Wimbadi R.W. & Djalante, R., *From decarbonization to low carbon development and transition: a systematic literature review of the conceptualization of moving toward net-zero carbon dioxide emission*, Journal of Cleaner Production, vol. 256, pp. 1-32, 2020. (Journal)

Proceedings of the 3rd ITB Graduate School Conference ISSN: 2963-718X
Enhancing Creativity in Research Through Developing Innovative Capabilities
December 21, 2022

Analysis of Factors Influencing the Decision to Adopt 3D Printing Technology in a Case Study of Residential Housing Development

Dhania Salsabila* & Rani G. K. Pradoto

Faculty of Civil and Environmental Engineering, Bandung Institute of Technology, 10 Ganesha Street, Bandung, Indonesia
*Email: dhaniasalsabila@students.itb.ac.id

Abstract. Construction is the sector that uses the most resources and energy. The amount of waste donated by the construction industry is expected to be 30% of the cost of materials. Furthermore, the construction industry is starting to focus on sustainable development, where technology is one of the enablers to realise it. Technology development is influenced by the level of technology adoption carried out by contractors who have a significant role in the production process. Additive Layer Manufacturing or 3D printing is one of the newest technologies that has developed as a pioneer in pushing the construction industry towards automation. It aims to increase construction productivity. Recently, 3D Printing material construction technology has begun to be applied in Indonesia in a residential project. This step has become a steppingstone for developing construction technology in Indonesia. The adoption of construction technology in a company is caused by many factors, both inhibiting and supporting. The factors influencing the adoption can be used to formulate strategies for subsequent technology development. The Technology Acceptance Model (TAM) and the Technology-Organization-Environment-Cost (TOEC) Framework are used in identifying these factors.

Keywords: *Technology; 3D Printing; Construction; Adoption Factors; Indonesian Company.*

1 Introduction

Construction is the sector that uses the most resources and energy. In the Global Status Renewable Report, the construction sector uses approximately 33% of total final energy consumption and shares 37% of the global greenhouse gas emissions in 2020 [1]. Furthermore, the total cost of waste is expected to be 30% of the cost of materials [2]. Other than that, the construction industry around the world has started to focus its activities on sustainable development, which focuses on three dimensions, namely economic, social, environmental, and technical dimension which means that this sustainable concept is also reviewed from a systematic and technical perspective carried out in the field [3]. The goal of sustainable construction has two functions, to increase efficiency and reduce

waste. In implementing the concept of sustainable construction, technology is the one that can encourage the implementation of this, especially material construction technology. The development of materials construction technology aims to save resources and energy requirements, save construction costs, simplify work by developing materials that are easy to obtain [4], extend the life span of buildings, and improve building quality and safety. The construction industry in Indonesia today has many challenges, such as low work productivity and high amounts of waste. These things occur due to the lack of utilisation of construction technology in construction projects. The construction sector in Indonesia has been slow to adopt new technologies [4]. On the other hand, unique construction projects challenge adapting technology in other industries.

The factor which affects the development of construction technology is the technology adoption by the contractor, whose role in the construction production process is significant [4]. The construction technology advancement that has been developed in many countries today should help contractors improve their quality and efficiency and reduce costs, which are expected to affect the development of the construction industry in Indonesia [4]. Additive Layer Manufacturing, more commonly known as 3D printing, has developed as a pioneer in the construction field, pushing the construction industry towards systems with automated methods [5]. The automated system aims to increase construction productivity by optimising time, minimising production costs, and minimising the use of resources and energy. Recently, 3D Printing material construction technology has begun to be applied in Indonesia in a residential project. The existence of a new step in adopting this technology can be a steppingstone in the development of construction technology in Indonesia. Therefore, knowledge and understanding of contractor mechanisms are needed in utilising construction technology to determine the focus of the steps needed to improve the construction sector environment and improve the construction industry's performance in Indonesia.

1.1 Research Objectives

This study intends to identify the factors that influence the adoption of construction technology in a company to produce an overview of construction technology adoption patterns and to evaluate the implementation of the technology to find out how the company intends to apply this technology for future projects.

2 Literature Review

2.1 Construction Project and Management

Construction work is commonly referred to as a project because of its temporary and unique nature [6]. Construction projects have a relatively high complexity where complexity consists of many interrelated parts, which can be characterised

by differentiation and interdependence [7], [8]. Consequently, a highly complex construction project must be managed. Project management can be defined as planning, organising, directing, and controlling all resources in each period to achieve a specific goal or various targets [9]. Project management is generally required by managing resources according to the 5M frameworks (Manpower, Method, Machine, Material, Money), which are based on the traditional view of the change management process as a technical control strategy for planning, implementation, and evaluation [10].

2.2 Construction Technology in Indonesia

In construction, technological developments aim to create a more productive construction process. Technology is a derivative of the Greek, *techne*, and *logos*. Egmond (2012) defined *techne* as the 'know-how' needed to create something [11]. Meanwhile, *logos* is defined as logic or a logical and structured procedure. Thus, technology is defined as a logical, structured, and applicable way to create something that answers human needs. The term technology in construction is often associated with things that are advanced, sophisticated, or something whose elements of renewal support increased efficiency and productivity to competitiveness both in production and during the implementation process [11]. Construction technology divides into several types depending on its function: product/material technology and process/management technology. For material technology, the history of the application of this technology in Indonesia can see in the following illustration [12].

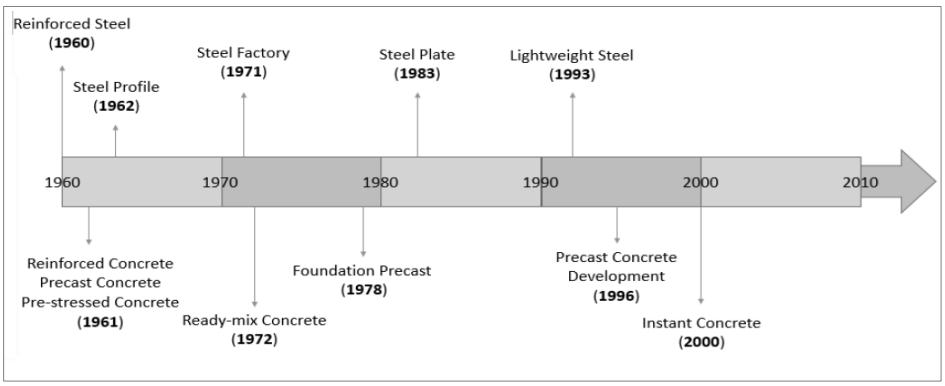

Figure 1 Timeline of Construction Material Technology in Indonesia [12]

Furthermore, in Indonesia, the construction process/management technology that has also begun to develop is BIM technology. Where most projects have used BIM technology, although, from research conduct, 54% only used BIM to make 3D models, 14% reached the scheduling stage (4D), 32% reached the cost estimation and parts list (5D) stages, and none used BIM until 6D and 7D [13]. Moreover, Indonesia is currently adopting 3D Printing technology, also known

as Additive Layer Manufacturing, which means manufacturing objects in three dimensions or any form from digital models.

2.3 3D Concrete Printing Technology

3D Printing technology has been widely applied in many countries in the world, such as the United States, Britain, Russia, United Arab Emirates, as well as China [14]. The use of 3D printing technology in projects in the United Arab Emirates has reduced labour costs by 50%-80% and construction waste by 30%-60%. Also, in Russia, a residential house was successfully constructed in 24 hours in Moscow with a surface area of 400 ft^2 [15].

3 Research Methodology

The flow and method of this research are described in the following flowchart.

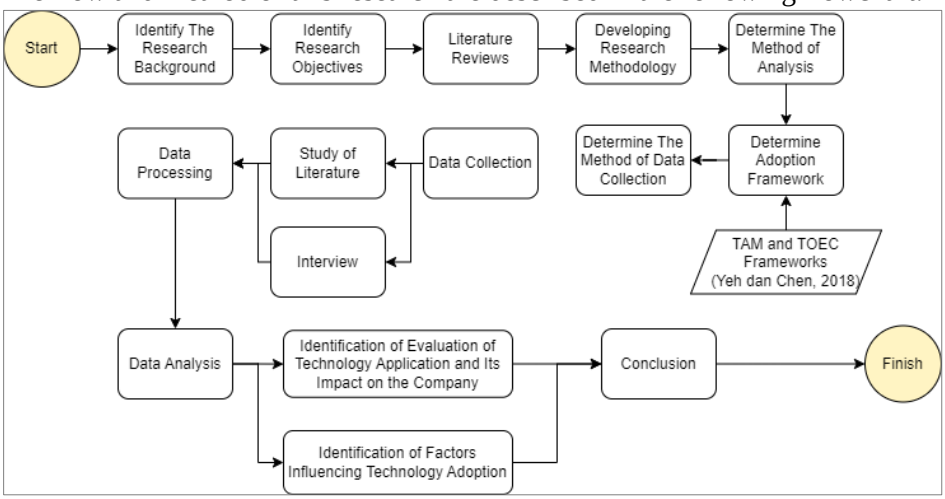

Figure 2 Research Flow

3.1 Adoption Framework

In adopting technology, various adoption models have been developed to understand the different dimensions that affect technology acceptance from a company [16], [17]. One is the Technology-Organization-Environment (TOE) framework, which was developed by Tornatzky and Fleischer (1990). This TOE framework has been widely used to explain steps in adopting technological innovation from an organisational perspective [17], [18]. The TOE Framework is carried out by identifying the factors that influence the implementation of technological innovations in the context of technology, organisation, and environment. In addition to these factors, another factor that is also important is the cost dimension factor for adopting 3D Printing technology from an organisational perspective. Thus, a review of technology adoption becomes TOEC [18]. In addition, another method that is also commonly used in analysing

the application of technology (especially user acceptance behaviour) is the Technology Acceptance Model (TAM) introduced by Davis et al. (1986) [19]. This model is based on social psychological theory and the Theory of Reasoned Action (TRA) [19]. TRA explains that users' beliefs influence the attitudes that lead to intentions and produce behaviour. Accordingly, Davis (1986) introduces the constructs in TAM in the following illustration [19].

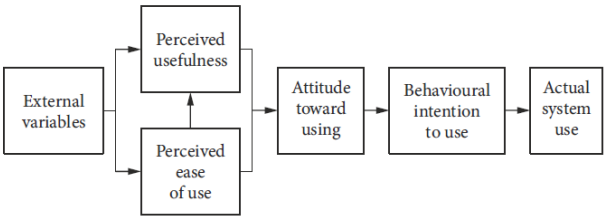

Figure 3 Illustration of Technology Acceptance Model (TAM) Framework

The factors observed in this method are Perceived Usefulness (PU), Perceived Ease of Use (PEOU), Attitude, and Behavioral Intention to Actual Use or how the technology is used/applied [19]. Another framework that can also use is the Diffusion of Innovation (DOI) [20]. Rogers (1983) defines diffusion as "the process by which an innovation is communicated through certain channels over time among the members of a social system" [21]. According to Rogers (1983), the speed of diffusion of an innovation is influenced by four elements, namely (1) the characteristics of the innovation; (2) The communication channel used to communicate the benefits of the innovation; (3) the time since the innovation was introduced; and (4) the social system where the innovation diffuses [20], [21].

3.2 Data Collecting and Analysis Method

This research is generally qualitative and based on the frameworks previously mentioned. This qualitative research was conducted based on the principle that qualitative data is emphasised on people's life experiences, basically very suitable to discover the meanings that people place on the events, processes, and structures of their lives and for relating these meanings to the social world around them [22]. The data collection method in this study is as follows:

1. Interviews aim to determine experts' opinions regarding the adoption factors of this 3d printing technology. The determination of sources (the experts) uses the principle of purposive sampling [23]. Purposive sampling is a technique widely used in qualitative research to identify and select information-rich cases for the most effective use of scarce resources [23], [24]. This technique involves the identification and selection of individuals or groups of individuals with specific knowledge or experience of a phenomenon [23], [25].

2. Document Analysis and Literature Study. Document analysis is carried out by collecting data, reviewing, dissecting, and coding content into research subjects.

Literature data analysis is done by the inductive approach, a systematic method of analysing qualitative data in which precise evaluation objectives can guide the analysis. In this research, inductive analysis refers to approaches that primarily use detailed readings of raw data to derive concepts, themes, or a model through interpretations made from the raw data by an evaluator or researcher [26]. In addition, for the interview data, Miles and Huberman's (1984) analysis method was also used, which included data reduction (condensation), data display, and conclusion drawing/verification [22], [26].

4 Discussion of The Research

4.1 Identification of Factors Influencing Technology Adoption

The factors that influence the application of this technology are obtained from several theories and frameworks taken from several references, including the Technology-Organization-Environment-Cost (TOEC) framework, Diffusion of Technology (DOI) theory, Technology Acceptance Model (TAM), as well as other influencing factors obtained from various references with the following details.

Table 1 Identification of Factors Influencing Technology Application Based on Several Theories and Thinking Frameworks

No	Teori/Framework	Faktor	Literatur
1	Diffusion of Technology (DOI)	Relative Advantage (Benefits of Technology for Companies), Compatibility (Compatibility with Company Needs), Complexity (Difficulty of Technology Implementation), Trialability (Easy to be Tried), Observability (Clarity of Appearance of Technology)	[20]
2	Technology Acceptance Model (TAM)	External Variable, Perceived Usefulness, Perceived Ease of Use, Attitude (Company's Attitude in Adopting), Behavioral Intention (Company's Intention to Implement Technology in Further Projects), Actual Use (Application of Technology)	[19]
3	Technology-Organisation-Environment-Cost (TOEC)	**Technology:** Can Improve the Quality of the Construction Process; **Organization:** Company Management System, Number of Experts or Research Conducted; **Environment:** Competition with Other Companies. Government Regulations; **Cost/Economic:** Investment Cost, Profit Prediction.	[19]

4	Other Technology Application Factors	Improving Construction Quality (Efficiency or Productivity Improvement), Software Requirements, Hardware Requirements for Software, Technology Implementation in the Field, Company Support, Government Support, Cost Investment, and Supporting Company Goals.	[27]
5	TOE Framework	**Technology:** Technology Competence, Relative Advantage (Benefits of Technology for Companies); **Organization:** Organisational Structure, Top Management Role, and Support, Company's Financial Readiness to Invest; **Environment:** Competitor in the Construction Industry, Government Regulations, Consumer Readiness.	[28]
6	Other Technology Application Factors	Advantages over Competitors, Improving Product and Process Quality, Increasing Productivity, Market Demand, Increasing Profitability, Expanding the Construction Market, and Reducing Production Costs.	[29]
7	Other Technology Application Factors	The linkage between Company Business Strategy and Adopted Technology.	[30]
8	Technology Acceptance Model (TAM)	External Variable: Conformity with Needs, Frequency of Use, Ease of Use; Internal Variables: Perceived Usefulness, Perceived Ease of Use, Attitude (Company's Attitude in Adopting), Behavioral Intention (Company's Intention to Implement Technology in Next Projects), Actual Use (Use/Application Technology)	[31]
9	Fishbone Diagram	Goals: Improvement Quality, Productivity; Project Characteristic: Complexity, Fit to Task, Compatibility; Vision/Mission: Tangible/Intangible Value, Company Policy; Strategic Finance Policy: RoI, Life Cycle Cost, Training Cost; Attributes of The Technology: Trialability, Specification, Ease of Use, Usefulness; Innovator: Technical Expertise, Reliability; Individual: Culture, Personal Motivation; Board: Network Effects, Socioeconomic Status.	[32]
10	Theoretical Framework	Culture: Organizational, National; Policy: National, Organizational; Cost: Direct, Indirect.	[33]

Factors developing from various references will be used in this study because the factors mentioned follow business conditions in Indonesia, especially for the construction business. From the various factors, the TAM-TOEC theoretical framework will be used to identify influencing factors. Factors that influence the application of technology from other literature will be grouped based on the categories of the TAM-TOEC framework, and the factors that have similarities will be combined. So, in simple terms, grouping results.

Table 2 Merging Factors Influencing Technology Application from Various Literature in the TAM-TOEC Framework

No	TAM-TOEC Framework		Factors	Resource
1	External Factors	Organisation	Company Purpose (Vision/Mission)	[20], [27], [32]
2			Company Business Plan and Strategy	[30]
3			Enterprise Management System	[19], [27], [28], [32], [33]
4			The Capacity of Experts and Number of Research	[19], [32]
5		Environment	Competitor in Construction Business	[19], [28], [29]
6			Construction Market	[28], [29], [32], [33]
7			Government Regulation	[19], [27], [28], [33]
8		Cost/Economic	Investment Cost	[19], [27], [28], [32], [33]
9			Profit and RoR	[19], [29], [32]
10		Technology	Supporting Software/Hardware Requirements	[27]
11			Work Efficiency and Productivity	[19], [27]–[29], [32]
12	Internal Factors	Perceived Ease of Use	Perceived Ease of Use and Complexity of Implementing 3D printing in the Field	[19], [20], [27], [31], [32]
13		Perceived Usefulness	Perceived Usefulness of 3D printing for Construction Companies	[19], [20], [28], [31], [32]
14		Behavioural Intention	The Construction Company's Behavioral Intention to Use 3D printing in Their Next Project	[19], [31]–[33]

The TAM-TOEC framework is used in this study because the chart model and categories used in this framework conform with the condition that 3D Printing technology has just been implemented in Indonesia in a residential project. Thus, these factors can be deepened to the acceptance of the newly used technology. The classification of each factor in each category in the TAM-TOEC framework is based on the literature, which identifies factors that influence technology adoption with the TAM and TOEC frameworks. Thus, similar factors from another theoretical framework are included following the factors that have already been included in the TAM-TOEC framework by these references. In simple terms, the TAM-TOEC model obtained for this study is depicted in the following chart.

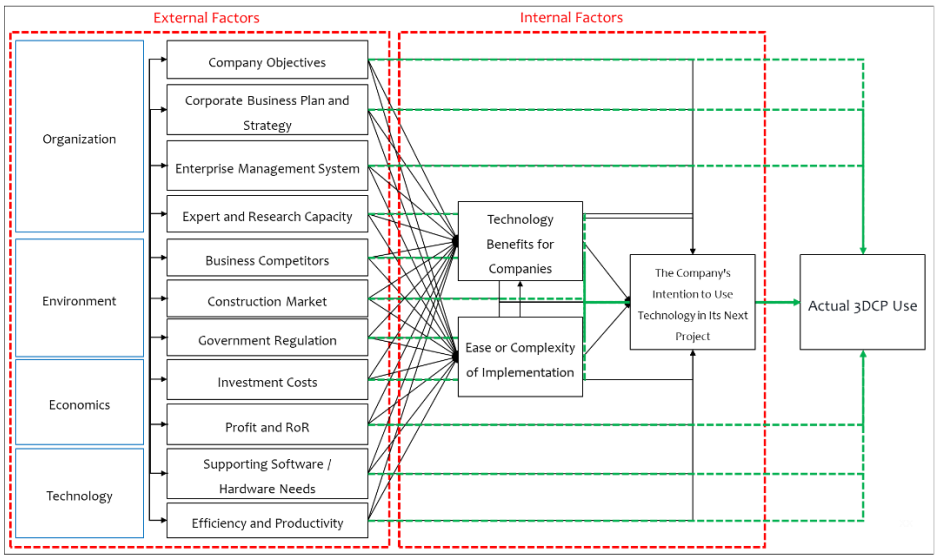

Figure 4 TAM-TOEC Model and Details Factors for This Study

The factors that have been previously identified are then asked by several experts who are directly involved in the application of this 3D printing technology. According to experts, the factors that most influence a company's decision to adopt 3D printing technology in their projects are the suitability of implementing this technology with business plans and company goals, the benefits of technology for companies, the resulting efficiency and increased productivity, the profitability of using technology, and the investment costs. The experts will assess whether the application of this technology can positively impact the company's business and how the applied technology will benefit the company after the project. In the TAM-TOEC model above, of course, it can also be calculated for the influence of one factor on other factors quantitatively, with the ANP method or SEM, but this is not done in this study, so what is produced is what Factors Affecting Technology Adoption, and which of these factors are the most influential according to the assessment of experts in a case study of the application of 3D Printing technology to the construction of this residential house.

4.2 Evaluation of Implementation of 3D Printing Technology in The Field

The implementation of 3D printing technology in residential construction is the first implementation of 3D printing technology for building scale in Indonesia. The implementation of technology in this project still has many shortcomings. Evaluation of the implementation of 3D printing technology is conducted to find out more about increasing performance and productivity from applying this technology. Performance is defined as the extent to which they successfully carry

out their duties and their ability to achieve their intended objective [34], [35]. Time, cost, and quality are the essential criteria for the project's success; almost all related papers mention these three and emphasise their importance in a construction project [36]. In this case, several evaluations of the essential criteria for the project's success are mentioned and explained as follows, with detailed calculations regarding efficiency and productivity improvements that cannot be shared by the company:

1. **Cost**. The company claims that this technology reduces the cost of wall materials for Type-36 houses by up to 10%-15%, assuming the average cost of wall materials in Indonesia is IDR 45,000,000.00. In addition, the need for labour for Type-36 houses in Indonesia with conventional methods is as many as seven people, and with 3D printing, only 4-5 people are needed. This reduction in labour requirements will affect productivity and overall construction costs.
2. **Quality**. The quality of the mortar material with this technology is better in terms of compressive strength, with the ratio of strength produced by 3D printing to red brick (3-5 MPa) or light brick (7-10 MPa), while 3D printing mortar has a strength of 25 MPa.
3. **Time**. In Indonesia, a Type-36 house is usually built within three months, whereas 3D printing can reduce it to 1.5-2 months. With notes, this duration is during project implementation in the field and does not include machine/equipment fabrication. This reduction in duration will undoubtedly affect the project's indirect costs, thereby increasing productivity.

In addition, construction project performance is also assessed by its quality, such as health and work safety, environmental impact, and its relation to sustainability. However, the work that can be done using 3D printing technology is still confined to non-structural elements, while the structural elements are still performed manually. The assessment of project performance is explained below:

1. Building Quality and Capacity/Strength. In general, as previously explained, the quality of mortar as a substitute for brick walls is better. However, this does not include shear tests and tests for the resulting intact structure. This building has also not been tested against earthquake loads. So, in this regard, it is necessary to carry out further tests related to Indonesia's location as an earthquake-prone country. Apart from that, it is also necessary to check whether the bond between the layers on the mortar wall is too rigid because this will, of course, be related to the response of the building to earthquake forces.
2. Occupational Health and Safety. In terms of OHS, this technology has fewer work accidents because most of the work is done by machines.

However, there has been no quantification of the reduction in the rate of work accidents resulting from the application of 3D printing technology.

3. Environmental Impact and Sustainable Construction. In general, all sources acknowledged that the use of this technology supports the concept of sustainability. The waste generated from this project is much less when compared to conventional methods. However, an evaluation regarding the emissions from the engine used has not been mentioned by the company or through sources. Of course, this needs to be studied more deeply because if engine emissions are high enough, the use of this technology is incompatible with the concept of sustainability.

However, apart from the advantages previously mentioned, all interviewees acknowledged that the overall production costs for the field process are still expensive, especially for architectural and operational costs. The cost of finishing the surface is quite a lot; wall work is done in two layers with a zigzag shape in between. Compared to the conventional wall method, the cladding may not be as expensive as a too-thick layer is not required. With this 3D printing, wall covering requires much mortar because the resulting surface is uneven and rough. However, if the wall is cast in situ, it may not be very costly to cover, but it will cost money to manufacture and install the formwork for the wall.

In addition, most sources felt that the residential project did not meet their expectations. The increase in cost efficiency, quality, and time mentioned is still considered not meeting expectations, mainly because production costs are still costly. So, the company has no plans to utilise/implement this 3D printing technology for future projects.

5 Conclusion

Factors influencing the application of 3D Printing technology in this case study were identified as 14 factors, with the enormous contribution being the connection between technology and company business plans and strategies, company goals, benefits of 3D printing for construction companies, work efficiency and productivity, profit and RoR predictions, and costs investment. Meanwhile, the most negligible contributions are government regulations, supporting software/hardware requirements, ease and complexity of implementing 3D printing in the field, and competitors in the construction business. After the project was implemented, most interviewees felt that this residential house project did not meet their expectations because the cost of producing a type 36 residential house was still too expensive. Thus, it is considered not to provide an increase in efficiency, and for now, the company still has no plans to utilise this 3D printing technology for future projects.

6 Acknowledgement

This research is supported by sources who are representatives of review companies that cannot be shared. The validity of the results of this study applies to one company, the company that is the object of this research. Meanwhile, for other companies, the influencing factors may be different. We are grateful to our lecturers at the Bandung Institute of Technology, who provided insights and expertise that greatly assisted this research.

7 References

[1] GSR, "Renewables 2022: Global Status Report," 2022.

[2] O. O. Fadiya, P. Georgakis, and E. Chinyio, "Quantitative Analysis of the Sources of Construction Waste," *Journal of Construction Engineering*, vol. 2014, pp. 1–9, Oct. 2014, doi: 10.1155/2014/651060.

[3] K. M. Patil and M. S. Patil, "Sustainable Construction Materials & Technology in Context with Sustainable Development," *International Journal of Engineering Research and Technology*, vol. 10, no. 1, pp. 112–117, 2017, [Online]. Available: http://www.irphouse.com

[4] R. Permatasari, I. Mahardika, and B. W. Soemardi, "Kajian Penerapan Teknologi Konstruksi Oleh Kontraktor Dalam Menghadapi Kondisi Pandemi Covid-19," in *Konferensi Nasional Teknik Sipil 15, Semarang 20 - 21 Oktober 2021*, 2021.

[5] S. El-Sayegh, L. Romdhane, and S. Manjikian, "A Critical Review of 3D Printing in Construction: Benefits, Challenges, and Risks," *Archives of Civil and Mechanical Engineering*, vol. 20, no. 34, Jun. 2020, doi: 10.1007/s43452-020-00038-w.

[6] J. R. (John R. Turner, *The Handbook of Project-Based Management: Leading Strategic Change in Organisations*, 3rd ed. McGraw-Hill, 2009.

[7] D. Baccarini, "The Concept of Project Complexity - A Review," *International Journal of Project Management*, vol. 14, no. 4, pp. 201–204, 1996, doi: 10.1016/0263-7863(95)00093-3.

[8] M. Nikolić and A. Cerić, "Classification of Key Elements of Construction Project Complexity From The Contractor Perspective," *MDPI Buildings*, vol. 12, no. 696, May 2022, doi: 10.3390/BUILDINGS12050696.

[9] M. A. El-Reedy, *Construction Management for Industrial Project*. Beverly: Scrivener Publishing, 2011.

[10] R. Badham, V. L. Cançado, and T. Darief, "An Introduction to The 5M Framework: Reframing Change Management Education," *BAR - Brazilian Administration Review*, vol. 12, no. 1, pp. 22–38, 2015, doi: 10.1590/1807-7692bar2015140033.

[11] A. Jayady, "Teknologi Konstruksi - Sebuah Analisis," *Jurnal Karkasa*, vol. 4, no. 1, 2018.

[12] R. G. K. Pradoto, B. W. Soemardi, A. Gazali, A. T. Putri, R. P. Purba, and I. Mahardika, "The Technology Landscape of Construction Material in The Indonesian Construction Industry," in *ICONCESS*, 2021.

[13] I. M. A. Megapathi, I. G. A. A. Putera, and N. M. Jaya, "Tingkat Implementasi dan Hambatan Adopsi Building Information Modeling Pada Pelaku Proyek

Konstruksi di Bali," *Jurnal Spektran*, vol. 9, no. 1, pp. 1–11, Jan. 2021, [Online]. Available: http://ojs.unud.ac.id/index.php/jsn/index

[14] F. Lyu, D. Zhao, X. Hou, L. Sun, and Q. Zhang, "Overview of The Development of 3D Printing Concrete: A Review," *Applied Sciences (Switzerland)*, vol. 11, Nov. 2021, doi: 10.3390/app11219822.

[15] M. Sakin and Y. C. Kiroglu, "3D Printing of Buildings: Construction of the Sustainable Houses of the Future by BIM," in *Energy Procedia, 9th International Conference on Sustainability in Energy and Buildings, SEB-17*, 2017, vol. 134, pp. 702–711. doi: 10.1016/j.egypro.2017.09.562.

[16] L. Muylle, "Technology Readiness and Adoption Of 3D Printing In The Construction Industry," Ghent University, Ghent, 2019.

[17] S. P. Sonwalkar, "Roadmap for Adopting 3D Concrete Printing Technology for Production of Affordable Houses," University of Twente, Enschede, 2020.

[18] C. C. Yeh and Y. F. Chen, "Critical Success Factors for Adoption of 3D Printing," *Technol Forecast Soc Change*, vol. 132, pp. 209–216, Jul. 2018, doi: 10.1016/j.techfore.2018.02.003.

[19] X. Qin, Y. Shi, K. Lyu, and Y. Mo, "Using a TAM-TOE Model To Explore Factors of Building Information Modelling (BIM) Adoption in The Construction Industry," *Journal of Civil Engineering and Management*, vol. 26, no. 3, pp. 259–277, Feb. 2020, doi: 10.3846/jcem.2020.12176.

[20] F. Wahid and L. Iswari, "Adopsi Teknologi Informasi Oleh Usaha Kecil dan Menengah di Indonesia," in *Seminar Nasional Aplikasi Teknologi Informasi*, Jun. 2007, pp. 75–79.

[21] E. M. Rogers, *Diffusion of Innovations*, 3rd ed. New York: The Free Press, 1983.

[22] M. B. Miles, A. M. Huberman, and J. Saldana, *Qualitative Data Analysis: A Methods Sourcebook*, 3rd ed. California: Sage Publications, Inc., 2014.

[23] L. A. Palinkas, S. M. Horwitz, C. A. Green, J. P. Wisdom, N. Duan, and K. Hoagwood, "Purposeful Sampling for Qualitative Data Collection and Analysis in Mixed Method Implementation Research," *Administration and Policy in Mental Health and Mental Health Services Research*, vol. 42, no. 5, pp. 533–544, Sep. 2015, doi: 10.1007/s10488-013-0528-y.

[24] M. Q. Patton, *Qualitative Research and Evaluation Methods*, 3rd ed. California: Sage Publications, Inc., 2002.

[25] J. W. Creswell and V. L. Plano Clark, *Designing and Conducting Mixed Methods Research*, 3rd ed. California: Sage Publications, Inc., 2018.

[26] D. R. Thomas, "A General Inductive Approach for Analysing Qualitative Evaluation Data," *American Journal of Evaluation*, vol. 27, no. 2, pp. 237–246, 2006, doi: 10.1177/1098214005283748.

[27] H. Fitriani and W. P. Br Bangun, "Kesiapan Adopsi Building Information Modeling (BIM) Pada Konsultan Perencana di Kota Palembang," *Teras Jurnal*, vol. 11, no. 2, pp. 437–450, Sep. 2021, doi: 10.29103/tj.v11i2.568.

[28] M. I. Effendi, D. Sugandini, Y. Istanto, R. Arundati, and T. Adisti, *The Technology-Organization-Environment Framework: Adopsi Teknologi Pada UKM*. Sleman: Zahir Publishing, 2020. [Online]. Available: https://www.researchgate.net/publication/345989050

[29] L. Ellitan, "Factors Influencing the Success Of Technology Adoption: A Case Study Of Indonesian Manufacturing Firms," *Jurnal Manajemen &*

Kewirausahaan, vol. 4, no. 1, pp. 1–14, Mar. 2002, [Online]. Available: http://puslit.petra.ac.id/journals/management/

[30] G. D. Pires and J. Aisbett, "The Relationship Between Technology Adoption and Strategy in Business-to-Business Markets: The Case of e-Commerce," *Industrial Marketing Management*, vol. 32, no. 4, pp. 291–300, 2003, doi: 10.1016/S0019-8501(02)00237-7.

[31] E. S. Park and M. S. Park, "Factors of The Technology Acceptance Model for Construction IT," *Applied Sciences (Switzerland)*, vol. 10, no. 22, pp. 1–15, Nov. 2020, doi: 10.3390/app10228299.

[32] S. M. E. Sepasgozar and S. Davis, "Construction Technology Adoption Cube: An investigation on Process, Factors, Barriers, Drivers and Decision Makers Using NVivo and AHP Analysis," *Buildings*, vol. 8, no. 6, May 2018, doi: 10.3390/buildings8060074.

[33] N. Usman and I. Said, "Key Factors that Affects Adoption of Technology in the Nigerian Construction Firms: A Theoretical Framework," *International Journal of Accounting and Business Management*, vol. 2, no. 2, 2014.

[34] J. L. Gibson, J. M. Ivancevich, H. H. Donnely Jr., and R. Konopaske, *Organizations Behavior, Structure, Processes, Fourteenth Edition*, 14th ed. California: McGraw-Hill, 2012.

[35] A. Prasetya, "Analysis of Factors That Influence Employee Performance: Study on Permanent Employees in Operational Section of PT WIMCycle Indonesia - Surabaya," *Jurnal Profit*, vol. 12, no. 1, 2018, [Online]. Available: https://profit.ub.ac.id

[36] A. P. Chan, "Framework for Measuring Success of Construction Projects," Brisbane, 2001.

Proceedings of the 3rd ITB Graduate School Conference ISSN: 2963-718X
Enhancing Creativity in Research Through Developing Innovative Capabilities
December 21, 2022

Comparison of Dissolved Gas Analysis Interpretation Methods for Power Transformer

Dhiastara Rahmanda* & Suwarno

School of Electrical Engineering and Informatics, Institut Teknologi Bandung, Bandung, Indonesia
*Email: 23221314@std.stei.itb.ac.id

Abstract. In this works, a comparison is made regarding the interpretation of Dissolved Gas Analysis for power transformer using IEEE C57.104-2019, IEEE C57.104-2008, and IEC 60599-2022. The purpose of this work is to know which typical value from those standards that more in line with the actual conditions of the power transformer. The database that is used to make this comparison is 125 DGA data mineral oil from 50 power transformers that are in operation. The DGA database has been confirmed by further testing to find out more about the actual condition of the power transformer. From the comparison results, the interpretation using IEC 60599-2022 has the highest accuracy, followed by IEEE C57.104-2008, then IEEE C57.104-2019. The reason for that result is because in IEEE C57.104-2019 there are typical values that are quite strict, especially on the value of Delta and Gas Rates.

Keywords: *Transformer; Dissolved Gas Analysis; Mineral Oil; IEEE C57.104-2019; IEC 60599-2022.*

1 Introduction

The power transformer is the most expensive asset in the transmission and distribution network [1]. To distribute electricity to other places, the power transformer is one of the most important things [2]. It can increase or decrease the voltage as needed. The important role of the power transformer suggests that we must regularly monitor the condition of the power transformer so that if there is a disturbance or problem with the power transformer, it can be detected earlier before the disturbance that occurs causes more severe problems.

One method for monitoring the condition of the power transformers, especially in oil-immersed transformers is Dissolved Gas Analysis. Dissolved Gas Analysis is a method that is widely used to detect the incipient fault in a power transformer [3]. The method is carried out by looking at the dissolved gas content in the transformer oil [4]. Each gas content produced in transformer oil can be predicting whether the condition of the power transformer is under normal

conditions or abnormal conditions. It can also predict the fault type that occurs in the power transformer.

There are several guidelines for interpreting the dissolved gas in transformer oil to distinguish gas content is a normal or abnormal condition. The most commonly used guidelines are IEEE C57.104 and IEC 60599. The New IEEE C57.104 just published in 2019 is the result from revised IEEE C57.104-2008, while the most recent IEC 60599 is IEC 60599-2022. Both standards provide information regarding the normal characteristics of the dissolved gas content in power transformer oil. IEEE C57.104 uses more than 1 million DGA data and IEC 60599 uses 20,000 DGA data which results in the typical value of dissolved gases in the power transformer.

However, in the application of these standards in the interpretation of DGA, there are still some possibilities of false negatives or false positives. From the literature study conducted there has been no research that has made comparisons of these standards in detecting gas abnormalities, most of the comparisons made are comparisons related to the identification of initial disturbances that occur.Therefore, in this study, the accuracy of some of these standards will be compared in detecting gas abnormalities, especially in DGA which has not been in Extreme conditions based on [5].

2 Materials and Methods

2.1 Database description

The DGA database used by the author in this paper is data from the PT Petrolab Service laboratory. The database is the sample oil from an energized power transformer. The gas content in the database is hydrogen, methane, ethane, ethylene, acetylene, oxygen, nitrogen, carbon monoxide, and carbon dioxide with units of parts per million (ppm).

The amount of DGA data used is 125 DGA data from 50 power transformers. The transformers are divided into 40 transformers with a nominal voltage of 20 kV, 2 transformers with a nominal voltage of 70 kV, 3 transformers with a nominal voltage of 150 kV, and 5 transformers with a nominal voltage of 500 kV. The DGA database is the data that has been confirmed by the condition of the power transformer in the field. The confirmations meant are electrical tests, internal inspections, gas monitoring after the transformer oil treatment, for example, purification and oil changes, or confirmation of other tests, such as furan testing, by also looking at the development of the gases produced.

2.2 Description of Anlyzed Criteria

The DGA database that has been collected is interpreted using several interpretation standards, namely, IEC 60599-2022 [6], IEEE C57.104-2008 [7], and IEEE C57.104-2019. After the interpretation is carried out using the three interpretation standards, then the results will be checked by the transformer conditions in the field. In this way, the accuracy or representative level of the typical values of each standard is obtained.

3 Result and Discussion

3.1 Database Analysis

The database consists of the gas content of the oil immersed-transformer mineral oil. The data is divided into two status conditions, normal and abnormal. Normal status is categorized if the information on the condition of the transformer has been obtained from checking by the transformer owner or monitoring of several samples has been carried out after an oil treatment activities such as purification or after being included by other tests, such as furan testing. An abnormal status is given when information on the condition of the transformer is found when an internal inspection or electrical test is carried out, or after monitoring the gas content after the purification process, the gas content continues to increase significantly or from other test confirmations indicating relevance to high gas content, for example, the relevance between gas content of Carbon monoxide and Carbon dioxide with furan content as in the study [8].

Electrical tests, such as Insulation resistance, Turn to Turn Ratio, DC Winding Resistance can confirm the DGA results interpreted using IEE C57.104 or IEC 60599, which indicates an initial fault in the transformer. So if the DGA interpretation results have the same result as the actual condition, the typical value that is used is representative enough, so it can be said that the interpretation is correct. However, if after the electrical test no findings, but the DGA interpretation give the result is abnormal status, it is necessary to monitor again for some DGA sample to determine the condition of the transformer because in some case the incipient fault can't be detected by the electrical test.

Purification of transformer oil can reduce significantly the gas content in transformer oil [9]. If the DGA interpretation result, used IEEE C57.104 or IEC 60599, is abnormal but after purification is carried out and resampling some sample DGA and resulting the gas rates are normal condition it can be concluded the transformer is in normal condition. So, the DGA interpretation doesn't have the same result as the actual condition.

Some data, especially if there is significant CO and CO2 content, is confirmed with furan content and also periodic monitoring after purification to confirm whether the CO2 or CO conditions, that interpreted according to IEC 60599 or IEE C57.104, are correct due to abnormal decomposition of the paper.

3.2 IEEE C57.104-2019

One of the widely used methods for interpreting DGA is IEEE C57.104-2019. The scope of this standard only differentiates power transformers based on their age and ratio of oxygen and nitrogen. wind turbine transformers or network transformers and only for mineral oil in main tanks. It provides clearer interpretation details than IEEE C57.104-2008, one of which is the typical value of the rate of gas development for each gas content. Generally, the flow chart of DGA interpretation using IEEE C57.104-2019 is shown in Figure 1. DGA status using this standard is divided into DGA status 1, DGA Status 2, DGA status 3. So in this work, the normal condition is if DGA interpretation results in DGA status 1. And abnormal conditions if the interpretation results in DGA status 2 or DGA status 3.

Accuracy of DGA status results from Interpretation using IEEE C57.104-2019 with actual transformer conditions can be seen in Table I. There are 32% of DGA status data from 50 transformers that have the same result as the actual condition. The reason for that may be caused by the strict limitations given by IEEE C57.104-2019, especially on the limits of the Gas Rates value and the Delta value at IEEE C57.104-2019 so that a lot of data are categorized as DGA status 2 or DGA status 3 because its value even with low gas content.

The gas rates value is calculated based on the value of the slope (gradient) of 3-6 samples in a period of 2 years, it also often makes the gas rates exceed the limit value in table 4 in IEEE C57.104-2019. Gas rates rule and value in IEEE C57.104-2019 has also been questioned in research [10]. Therefore, it may be necessary to make adjustments to the typical values of Delta and gas rates. It makes DGA interpretation less efficient in determining DGA status.

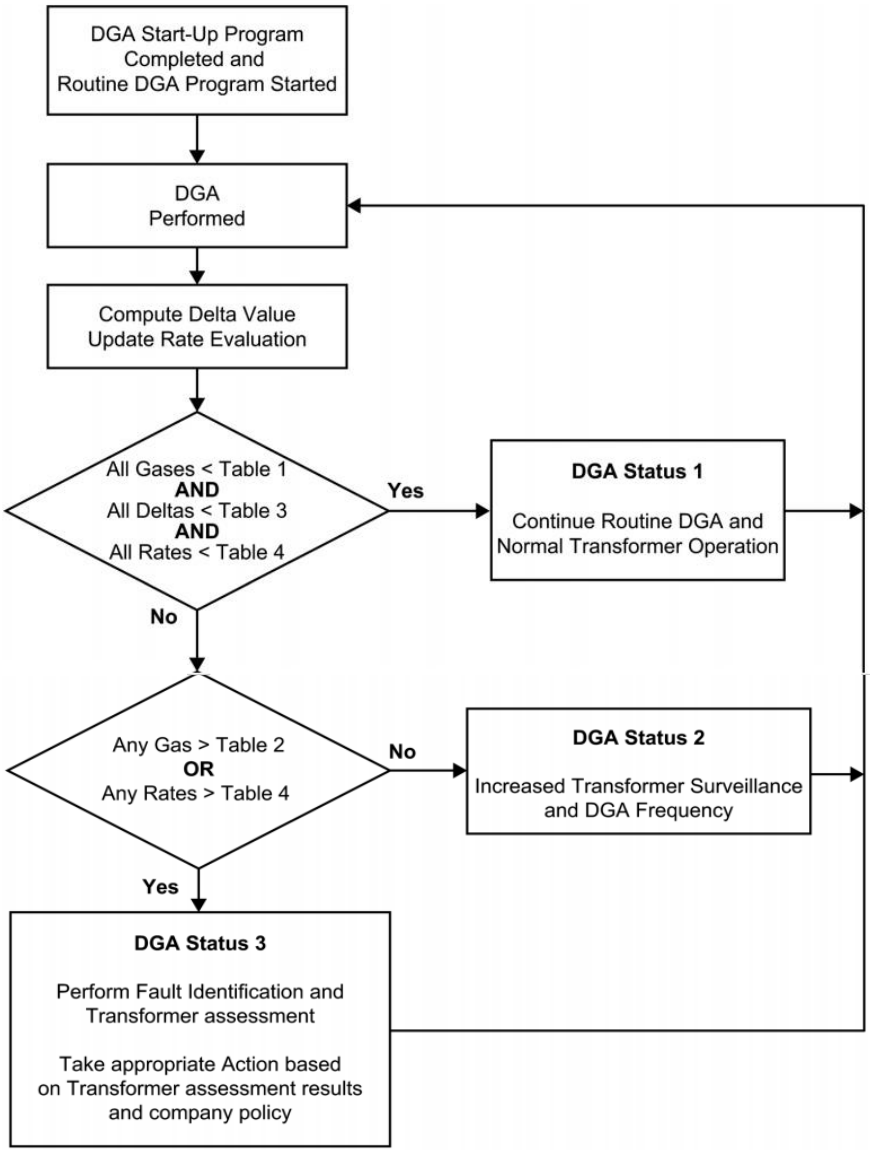

Figure 1 Flow chart IEEE C57.104-2019 Interpretation

3.3 IEEE C57.104-2008

IEEE C57.104-2008 can be applied to power transformers that use mineral oil, but there are notes in this standard, the numbers in this limitation are in parts of gas per million parts of oil [μL/L (ppm)] volumetrically and are based on a large power transformer with several thousand gallons of oil. With a smaller oil volume, the same volume of gas will give a higher gas concentration. Small distribution transformers and voltage regulators may contain combustible gases because of the operation of internal expulsion fuses or load break switches. The status codes in this limitation are also not applicable to other apparatus in which load break switches operate under oil. The accuracy of the DGA interpretation using the typical value of IEEE C57.104-2008 is higher than that of IEEE C57.104-2019. The accuracy is 68% from the actual condition of 50 power transformers as shown in Table I. One of the reasons for this is that the typical value of IEEE C57.104-2008 is not as strict as IEEE C58.104-2019.

Typical values for individual gas content in IEEE C57.104 2008 are divided into 4 conditions for each individual gas, namely H2, CH4, C2H6, C2H4, C2H2, CO, CO2. If there are one or more gases content is outside condition 1, the rate of development of the Total Dissolved Gas Analysis value will be checked. However, if all gases are in condition 1 then the DGA status is normal. This is what makes it different from IEEE C57.104-2019, where the latest IEEE will still give DGA an abnormal status even though the gas content is low, but with Gas rates that exceed the typical value in that standard.

However, this IEEE C57.104-2008 standard lacks in looking at the gas rate of individual gases. For example, if there is acetylene content outside condition 1 and increases significantly (other combustible gas is normal condition), then the DGA interpretation using this standard may not detect this. The flow chart of DGA interpretation using this standard can be seen in Figure 2.

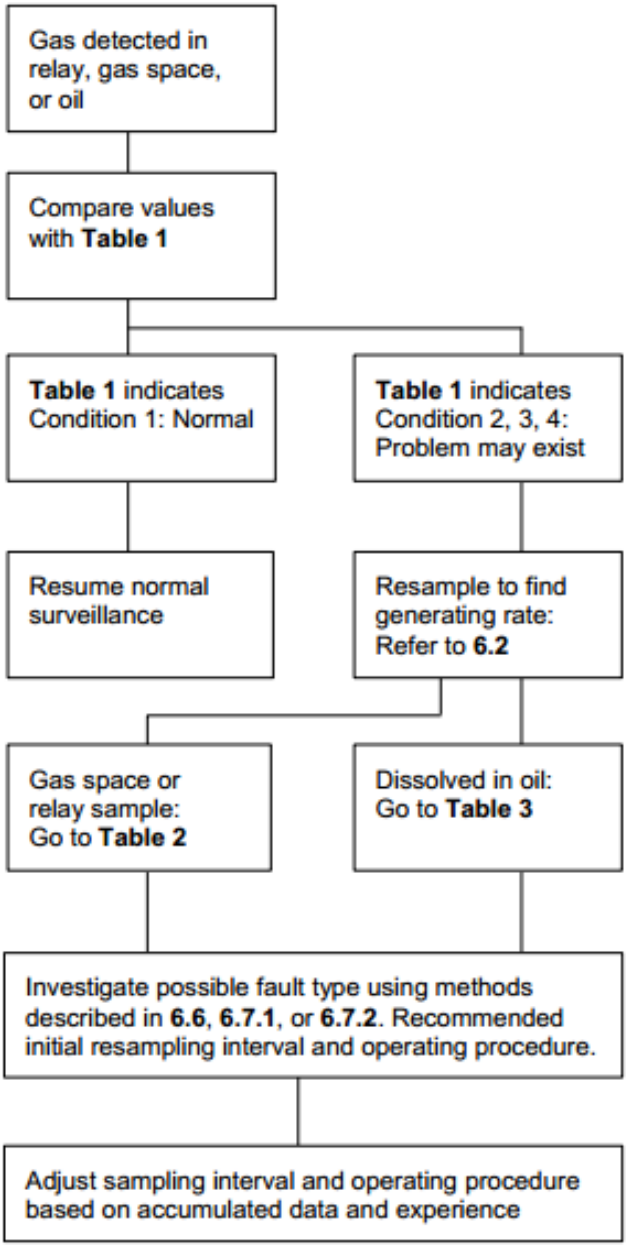

Figure 2 Flow chart IEEE C57.104-2008 Interpretation

3.4 IEC 60599-2022

One of the guidelines for the interpretation of DGA which is also widely used is IEC 60599-2022. Note in this standard is typical values in this standard recommended for large power transformers with an oil volume > 5 000 liters. Values in small transformers (< 5.000 l) are usually lower. The flow of interpretation using this standard can be seen in Figure 3.

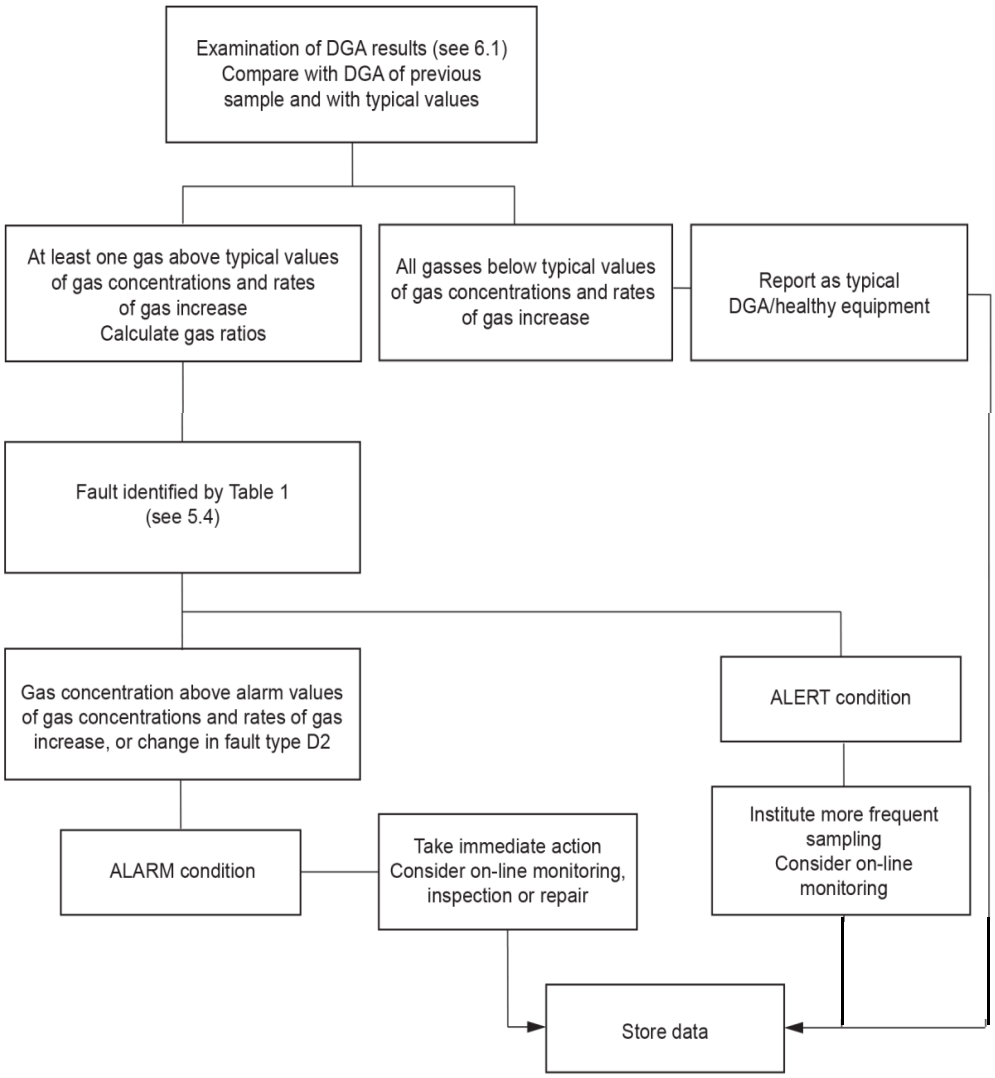

Figure 3 Flow Chart DGA Interpretation IEC 60599-2022

Interpretation using this standard is to compare the individual gas contents, namely H2, CH4, C2H6, C2H4, C2H2, CO, CO2 with a typical value. If there are one or more gas contents outside the typical value then check the rate increase of each gas. If there is an abnormal rate increase of gas, it is necessary to have further monitoring with a faster sampling frequency or other measures such as an electrical test.

The suitability of the DGA interpretation using IEC 60599-2022 with the actual condition of the power transformer is quite high, is 84%. This is because the typical value of IEC 60599-2022 is not too strict, but is also quite good at detecting any indication of abnormality in the power transformer because each individual gas has a typical value for its rates increase. In table 1 below, the accuracy value of each of these standards is written

Table 1 Accuracy of DGA Interpretation standar

IEEE C57.104-2019	CD	16/50
	WD	34/50
IEEE C57.104-2008	CD	34/50
	WD	16/50
IEC 60599-2022	CD	42/50
	WD	8/50

CD = Correct Diagnosis
WD = Wrong Diagnosis

3.5 Study Case

For example, we use data from the power transformer with manufacture years in 2013. It has a rating of 55 MVA and an operating voltage of 30/11 with an oil volume is 33000 kg. The data used is DGA data in 2017-2019. By using these data, interpretation will be made using typical values and interpretation flow based on IEEE C57.104-2019, IEEE C57.104 2008, and IEC 60599-2022. The DGA power transformer data is listed in Table 2. In table 1 below, the accuracy value of each of these standards is written

Table 2 DGA Data of Power transformer

Date	23 January 2017	05 June 2017	12 September 2017	28 August 2019
H2	<5	98	133	<4
CH4	1	10	14	<1
C2H6	<1	4	3	<1
C2H4	2	2	2	<1
C2H2	15	25	22	<1
CO	5	49	64	128
CO2	94	452	507	1214
TDCG	23	118	238	128
O2	5337	5112	5634	14074
N2	16678	11982	11369	5657
O2/N2	0.32	0.43	0.50	2.49

The DGA interpretation for the January 23, 2017 sample is as follows:

- IEEE C57.104-2019: DGA Status 3 due to acetylene gas exceeding the values in Typical Table 2 of IEEE C57.104-2019
- IEEE C57.104-2008: DGA status Abnormal because Acetylene is in condition 3.
- IEC 60599-2022: DGA status Normal because no gas content exceeds the typical value.

The DGA interpretation for the June 5, 2017 sample is as follows:

- IEEE C57.104-2019: DGA Status 3 because hydrogen gas and acetylene gas exceed the values in Table 2 of IEEE C57.104-2019 and the Delta value (difference of two consecutive samples) of hydrogen and acetylene gas exceeds the values in Table 3 of IEEE C57 .104-2019
- IEEE C57.104-2008: DGA status Normal due to value and development rate of TDCG is normal according to IEEE C57.104-2008
- IEC 60599-2022: DGA status Abnormal because Hydrogen gas rate increase exceeds the typical value of IEC 60599-2022.

The DGA interpretation for the September 12, 2017 sample is as follows:

- IEEE C57.104-2019: DGA Status 3 because hydrogen gas and acetylene gas exceed the values in Table 2 IEEE C57.104-2019 and the Delta value (difference of two consecutive samples) of hydrogen gas exceeds the values in Table 3 in IEEE C57.104 -2019 and the Gas rates for hydrogen, methane, and acetylene gases exceed the values in Table 4 IEEE C57.104-2019

- IEEE C57.104-2008: DGA status Normal due to value and development rate of TDCG is normal according to IEEE C57.104-2008 .

- IEC 60599-2022: DGA status is Normal because the individual gas content and gas rate increase do not exceed the typical values of IEC 60599-2022.

So, according to IEEE C57.104-2008 and IEC 60599-2022 active gassing has decreased which indicates an incipient fault does not exist, the owner of the transformer decided to carry out purification on November 15, 2018. One year later, the sample was taken again and gas content and gas rates are normal. It can be concluded that the gas content in the previous samples was not due to an active fault. Therefore the IEEE C57.104-2008 and IEC 60599-2022 interpretations have a better result because they more correlate with the actual condition of power transformer than IEEE C57.104-2019. It is may that IEEE C57.104-2019 can produce DGA status 1, but with several samples again, so it is less efficient.

4 Conclusion

In comparisons of interpretations based on IEEE C57.104-2019, IEEE C57.104-2008, and IEC 60599-2022, the highest percentage of conformity with actual power transformer conditions is the interpretation using IEC 60599-2022, IEEE C57.104-2008, then IEEE C57.104-2019.

This may be caused by the tightness of the typical values of IEEE C57.104-2019, especially in the value of Delta and Gas rates and also the rules for using gas rates which use 3-6 samples, making it difficult to obtain normal gas rates. Therefore there needs to be a slight adjustment to the IEEE C57.104-2019 standard.

Recommendation from author is to make typical data values that also consider the real conditions of the transformer. That is also future action from author.

Acknowledgement

Thanks to PT Petrolab Service for supporting this works

References

[1] Tang, S W. H. & Wu, Q. H., *Condition Monitoring and Assessment of Power Transformers Using Computational Intelligence*, London: Springer, 2011.

[2] C. Chattranont, W., Sakhon, W., Poonsri, R. & Nattachote, *Dissolved Gas Analysis of 115 kV Steel Industry Transformer using New IEEE Standar*, 18th International Conference on Electrical Engineering/Electronic, Computer, Telecommunications and Infirmation Technology (ECTI-CON), 2021.

[3] Demicri, M., Gozde, H. M. C. & Tappalamacioglu, *Comparative Dissolved Gas Analysis with Machine Learning and Traditional Methods*, 3rd International Congress on Human-Computer Interaction, Optimization and Robotic Applications (HORA), 2021.

[4] Fofana, I., *The Gassing of Insulating Fluids*, 3rd International Conference on Electrical Materials and Power Equipment, 2021.

[5] "IEEE Guide for the Interpretation of Gases Generated in Oil-Immersed Transformers," IEEE Standard C57.104-2019. 2019.

[6] *IEC Mineral Oil-Impregnated Electrical Equipment in Service - Guide to the Interpretation of Dissolved and Free Gases Analysis*, IEC 60599, 2022.

[7] *IEEE Guide for the Interpretation of Gases Generated in Oil-Immersed Transformers*, IEEE Standard C57.104, 2008.

[8] Miyagi, K., Oe E., Yamagata N., *Evaluation of Aging for Thermally Upgraded Paper in Mineral Oil*, Journal of International Council on Electrical Engineering Vol. 1, No. 2, pp. 181~187, 2011.

[9] *Mineral insulating oils in electrical equipment – Supervision and maintenance guidance*, IEC 60422, 2013.

[10] Hosseini M., Brian G., Stewart & Kearns M., *Construction of a Transformer DGA Health Index Based on DGA Screening Processes*, IEEE Conference on Electrical Insulation and Dielectric Phenomena, 2020.

Proceedings of the 3rd ITB Graduate School Conference ISSN: 2963-718X
Enhancing Creativity in Research Through Developing Innovative Capabilities
December 21, 2022

Synthesis of Silica Nanoparticle and Cd-Based Carboxyl Quantum Dots (SiNP@QDs) Conjugates as Biosensing Platform: A Pleriminary Study

Diaz Ayu Widyasari[1,2], Fauzan Aulia[3], Agustina Sus Andreani[3], Rizna Triana Dewi[4], Ni Luh Wulan Septiani[2, 5] Brian Yuliarto[2,6*] & Siti Nurul Aisyiyah Jenie[3,6]

[1]Master Program of Nanotechnology, Graduate School, Institut Teknologi Bandung (ITB), Jl. Ganesha 10, Bandung 40312, West Java, Indonesia
[2]Advanced Functional Materials Research Group, Faculty of Industrial Technology, Institut Teknologi Bandung, Bandung 40132, Indonesia
[3]Research Centre for Chemistry, National Research and Innovation Agency (BRIN), Kawasan PUSPIPTEK, Serpong, South Tangerang 15314, Banten, Indonesia
[4]Research Center for Pharmaceutical Ingredients and Traditional Medicine, National Research and Innovation Agency (BRIN), Cibinong Science Center (CSC), Bogor, West Java 16911, Indonesia
[5]Research Center for Advanced Materials, Research and Innovation Agency (BRIN), Kawasan PUSPIPTEK, Serpong, South Tangerang 15314, Banten, Indonesia
[6]BRIN and ITB Collaborative Research Center for Biosensors and Biodevices, Jl. Ganesha 10, Bandung, West Java, 40132 Indonesia.
*Email: brian@itb.ac.id

Abstract. Silica nanoparticles (SiNP) are one of the most promising materials for biosensors. The introduction of functional groups make silica nanoparticles highly versatile. In this work, the silica nanoparticle was synthesized using sol-gel method from natural based precursor, which is geothermal precipitate. Based on the characterization result of SiNP, the specific surface area is 138 m^2/g and nanoparticle size is 43.56 nm. The XRD result shows SiNP in amorphous phase. The surface of SiNP was modified using silanization method with 3-Aminopropyl triethoxysilane (APTES) as an amino silane to immobilize the quantum dot and *E coli* antibody. The FTIR analysis shows that amine group in SiNP@QDs surface reacted with carboxyl group of antibodies indicated by the presence of a peak at the wavelength of 1620 cm^{-1}. The detection of *E. coli* bacteria was carried out using fluorescence spectroscopy through the reduced of maximum intensity of SiNP@QDs-Ab before and after *E coli* addition at wavelength of 595 nm. The fluorescence intensity of SiNP@QDs-Ab is 633.10 a.u and the intensity is reduced to 281.86 a.u. in the presence of *E. coli* (1 x 10^7 CFU/mL).

Keywords: *Biosensors; E. coli, quantum dots; silica nanoparticles; silanization*

1 Introduction

Biosensors have been applied for clinical, environmental, forensic and food monitoring purposes and have shown some promise in detecting foodborne bacteria[1]. Biosensors technology has many advantage such as rapid, selective and sensitive[2]. Silica nanoparticles are one of the most promising materials for biosensors due to their remarkable properties comprising relative inertness in many conditions, stability over a wide range of pH (excluding alkaline), and transparency in the UV-vis spectrum [3].

Surface modification by various functional groups make silica nanoparticles highly versatile[4]. 3-Aminopropyl triethoxysilane (APTES), as source of amino silane group is a coupling agents that is frequently used for the silanization in silica nanoparticle surface[5]. The silane layer obtained from APTES produce amine functionality on the surface[6] making APTES is mainly attractive for biotechnology application as it acts like a glue layer[7]. Goftman et al (2016) used APTES to functionalize silica to create silica coated CdSe QDs, the silica nanoparticle encapsulating the quantum dot through a water in oil reverse microemulsion process[8].

Silica is commonly used to stabilize quantum dot in harsh condition. The advantage of silica is its ability to conjugate with various functional groups with excellent biocompatibility, stability and low toxicity. Lv et. al. conducted a research on silica encapsulated CdSe/ZnS quantum dots and biomolecule immobilization to create stable fluorescence immunoassay[9].

In this paper study on the effect of silica addition to quantum dot for *E coli* bacteria fluorescence sensing, was carried out. Natural based silica precursor was used to obtain silica nanoparticles (SiNP) through the sol-gel method. The SiNP surface was then modified using silanization method to support immobilization of quantum dot and *E. coli* antibody.

2 Materials and Method

2.1 Materials

The materials used in this study were geothermal precipitate, as the raw material, supplied from the Geodipa geothermal power plants at Dieng, Central Java, Indonesia. Sodium hydroxide (NaOH), Hydrochloric acid (HCl) 37%, Cetyltrimethylammonium Bromide (CTAB), Toluene, 1-Ethyl-3-(3-dimethylaminopropyl)carbodiimide (EDC), N- Hydroxysuccinimide (NHS), 3-Aminopropyl Triethoxysilane (APTES) Escherichia coli (*E.coli*) antibody, and Phospate Buffer Silane (PBS) were purchased from Sigma-Aldrich, Cd-based

Carboxyl Quantum Dots were purchased from Ocean Nanotech, and *E. coli* ATCC 25922 were obtained from National Food and Drug Agency Republic Indonesia.

2.2 Synthesis of Silica Nanoparticles (SiNP)

A total of 20 g of washed silica geothermal powder was mixed with 800 mL of 1.5 N NaOH in a beaker glass to form sodium silicate. The mixture was then stirred using a magnetic stirrer for 60 minutes and heated at 90 °C. The mixture was filtered through filter paper to separate the solution with solids. The sodium silicate solution, then titrated with 2 N HCl to form the gel until pH 5. The formed gel was added with 2% of CTAB (w/w). The formed gel was allowed to stand for 18 hours and washed with DI water until pH 7 and dried in an oven at 100 ºC, overnight. The dried samples were labelled as Silica Nanoparticles (SiNP)

2.3 Surface modification of silica nanoparticles through silanization method

1 g of SiNP was added to 5% (v/v) APTES in toluene solution and shaked at room temperature for 1 hour. The precipitate was rinsed with toluene 2 times, then dried at room temperature, overnight resulted SiNP-APT.

2.4 Preparation of silica nanoparticle encapsulated quantum dot (SiNP@QDs)

30 mg of SiNP-APT was added to the mixture of 200 µL of EDC (5 mg/mL), 100 µL of NHS (5 mg/mL) and 100 µL of Cd-based Carboxyl Quantum Dots in 600 µL of PBS. The mixture was shaked for 24 hours at room temperature. The mixture was then centrifuged for 3 minutes at 10,000 rpm, the resulting supernatant was discarded and then washed with PBS 2 times. Samples were dried at room temperature and labelled as SiNP@QDs

2.5 Preparation of conjugation SiNP@QDs with *E. coli* antibody

The SiNP@QDs was added with 1 mL of PBS and sonicated for 10 minutes. The solution was added into the mixture containing 10 mL of EDC (10 mg/mL) and 100 µL NHS (5 mg/mL), then was shaked at room temperature for 30 minutes. The SiNP@QDs were precipitated and separated using centrifuge for 20 minutes at 10,000 rpm, the precipitate was added to 250 µL of PBS and 2 µl of *E. coli* aliquot antibody (1 µg/µL). The samples were labelled as antibody modified silica nanoparticles, SiNP@QDs-Ab. The SiNP@QDs-Ab sample was shaked for 1 hour, then added with 2.5 µL BSA 1%, then shaked again for 60 minutes. The antibody modified SiNP@QDs-Ab was stored in refrigerator 4 °C prior to the application.

2.6 *E. coli* sensing experiments using SiNP@QDs-Ab

A total of 4500 µL of *E. coli* bacteria with concentration of 1 x 10^7 CFU/mL was added to 500 µL SiNP@QDs-Ab (1 mg/mL) and mixed for 15 minutes. The mixture was measured using a fluorescence spectrometer at an excitation wavelength of 360 nm and emission wavelength at 400-800 nm.

2.7 Characterization of nanoparticles

Nitrogen absorption-desorption isotherm was conducted in 77 K on Microtrimetritics Tristar II 3020, USA to obtain the Brunauer-Emmertt-Teller (BET) surface area. The samples were degassed at 300 °C and 10^{-4-} Torr preasure prior to the measurement.

X-ray diffraction (XRD) analysis was carried out for crystallographic phases identification of the silica nanoparticles using a Philip PW 1710 diffractometer, using Cu Kα radition at 40 kV and 30 mA, and a secondary graphite monochromator.

Fourier Transform Infrared (FTIR) spectra was recorded on a FTIR Prestige-21 in transmittance mode, at 16 cm^{-1} resolution, over the range of 300-400 cm^{-1} with an accumulating average of 10 scans. The software used to generate the spectra was IR solution (Shimadzu).

Fluorescence intensity was recorded with a fluorescence spectrophotometer (Agilent, Singapore) at an excitation wavelength of 360 nm and the emission was recorded in the wavelength range 400-800 nm.

3 Result and Discussion

In this study, the precursor of the nanoparticle was natural-based silica from geothermal precipitate. The synthesis was conducted using sol-gel method which produces very homogeneous composites with very high purity (99.99% purity)[10][11]. Silica nanoparticles are formed by hydrolysis and condensation reactions. Hydrolysis was conducted in acid conditions, hence the addition of HCl causes protonation of the siloxy group ($Si\text{-}O^-$) to become silanol (Si-OH). The silanol groupsare then further attacked by siloxy groups ($Si\text{-}O^-$) with the help of an acid catalyst to form siloxane bonds (Si-O-Si) [12]. The optimum of gelling time was chosen based on our previous works which is 18 h with NaOH concentration NaOH of 1.5 N[13][14].

The reaction in the synthesis of SiNP by sol-gel method can be formulated as follow:

SiO_2 (geothermal precipitate)$_{(s)}$ + 2 NaOH $_{(aq)}$ → Na_2SiO_3 $_{(aq)}$ + H_2O $_{(aq)}$

Na_2SiO_3 $_{(aq)}$ + 2HCl $_{(aq)}$ → SiO_2 (nanoparticles)$_{(s)}$ + 2NaCl $_{(aq)}$ + H_2O $_{(g)}$

The addition of CTAB as the surfactant resulted in a uniform particle size and dispersion[15]. Surface area was measured using BET method with a degassing temperature of 300 °C for 3 hours.

Table 1 Result of BET analysis

No	Specification	Value
1	Surface Area	138 m^2/g
2	Pore Size	21.34 nm
3	Pore Volume	0.72 m^2/g
4	Nanoparticle Size	43.5 nm

Figure 1 shows the XRD diffraction pattern of SiNP. Based on the results, the sample shows a widening peak in the range 2θ of 20-30°, referring to JCPDS 47-0715 which indicates that the SiNP is in its amorph phase[16].

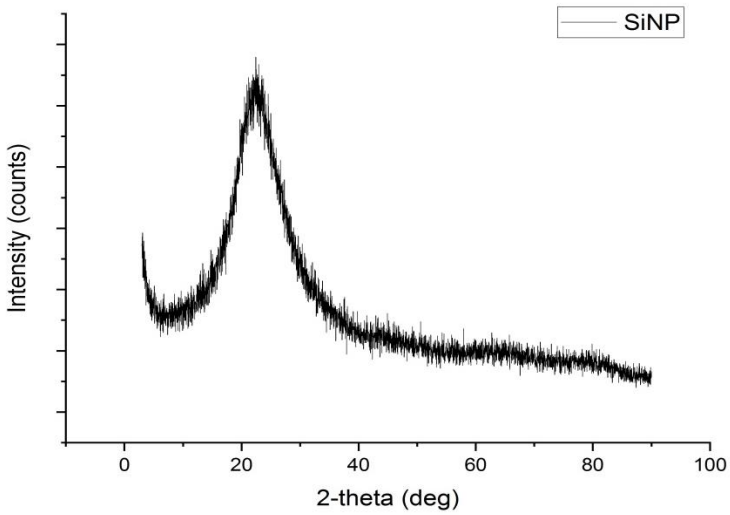

Figure 1. Crystallographic pattern of SiNP

The conjugation reaction between SiNP@QDs and biomolecule *E coli* antibody were observed using FTIR analysis. The FTIR result are shown in Figure 2. The functionalization of nanoparticles using APTES, replaced the –OH group of SiNP

by an amine group that is more reactive and has a charge on the surface[6]. The blue spectra (SiNP APT), shows bands in the region 1400–1700 cm^{-1} which corresponds to the absorption bands of amine group I at 1610-1690 cm^{-1} from the C=O stretching vibration, and amine II group around 1500-1600 from the N-H bending and C-N stretching [17]. Meanwhile the peaks at 2800–2980 cm^{-1} were assigned to N-CH_2 stretch indicating the presence of APTES on the surface [18] .

The amine in group in SiNP@QDs surface was reacted to the carboxyl group of antibody and created acylamide binding in the presence of EDC as the activator. The red spectra (SiNP@QDs-Ab) shows characteristic bands at 1620 cm^{-1} indicating carboxyl stretching vibration. The C=O stretching vibration was derived from carboxyl group on the *E coli* antibody[17].

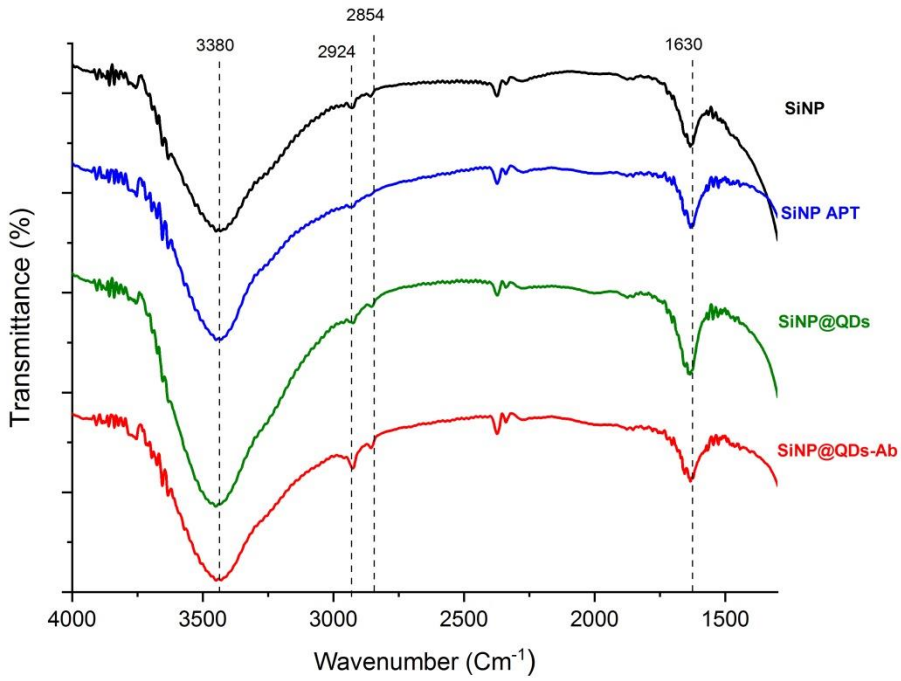

Figure 2. FTIR spectra of SiNP (black), SiNP-APTES (blue), SiNP@QDs (green), SiNP@QDs-Ab (red)

To measure the fluorescence intensity, 1 mg of SiNP@QDs-Ab were dispersed in 1 mL of PBS (Figure 3). The fluorescence intensity of SiNP@QDs-Ab were observed using fluorescence spectrophotometer and the maximum intensity was observed at wavelength of 595 nm is being 633.10 a.u.

The *E coli* detection was also observed using fluorescence spectrophotometer which resulted in maximum intensity of 281.86 a.u at the same wavelength of 595 nm. The decrease in fluorescence intensity indicated that the presence of *E. coli* (1 x 10^7 CFU/mL) caused fluorescence quenching of the SiNP@QDs-Ab. The maximum fluorescence intensity change was used as the indication of sensing due to its sensitivity[19].

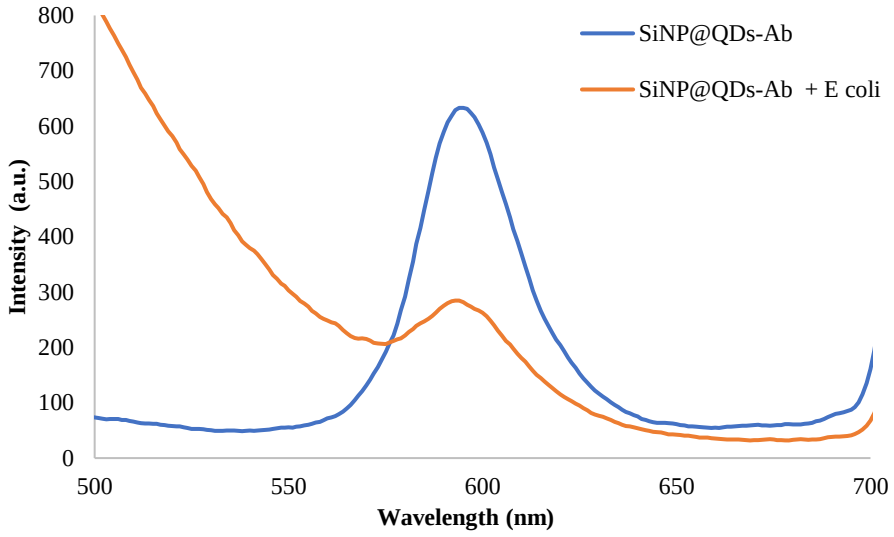

Figure 3. The fluorescence emission spectra of SiNP@QDs-Ab in PBS with concentration 1 mg/mL (blue) and SiNP@QDs-Ab in the presence of 1 x 10^7 CFU/mL of *E. coli* (red)

4 Conclusion

The synthesis of SiNP from natural based silica using sol-gel method was successfully carried out, with the specific surface area of 138 m^2/g and nanoparticle size of 43.5 nm. The XRD result shows the SiNP is in its amorphous phase. The surface of SiNP was modified using silanization method to immobilize the quantum dots and *E coli* antibody, the amide bonds between antibody and modified nanoparticles were confirmed by FTIR at wavenumber 1610-1690 cm^{-1} . The detection of *E coli* bacteria resulted in the decreaseingof the maximum intensity at 595 nm of SiNP@QDs-Ab before and after *E coli*, which are 633.10 a.u and 281.86 a.u, respectively. This preliminary study of the surface modification of SiNP using silanization method for SiNP@QDs as *E. coli*

detection opens up to the possibilities of employing such system in bacteria detection in the future.

Acknowledgement

This research was funded by the BRIN-ITB Collaboration Research Centre for Biosensors and Biodevices Grant No. 01/PKR/PPK-DFRI/2022; 220/1T1.B07/KS.00/2022 and the JFS SEA-EU/LPDP NAPARBA Project Grant No. SEAEUROPEJFS19ST-117. The authors acknowledge the facilities, scientific and technical support from Advanced Characterization Laboratories Serpong, National Research and Innovation Institute through E-Layanan Sains, Badan Riset dan Inovasi Nasional, and Characterization Laboratories of Research Centre for Nanoscience and Nanotechnology, Labotopia.Ltd. S.N.A.J is the main contributor of this manuscript.

Reference

[1] H. Du, Z. Li, Y. Wang, Q. Yang, & W. Wu, *Nanomaterial-based Optical Biosensors for the Detection of Foodborne Bacteria*, Food Rev. *Int.*, **38**(4), pp. 655–684, 2022. (Journal)

[2] H. Sharma & R. Mutharasan, Review of biosensors for foodborne pathogens and toxins *Sensors Actuators, B Chem.*, **183**, pp. 535–549, 2013. (Journal)

[3] E. Bagheri., Silica–Quantum Dot Nanomaterials as a Versatile Sensing Platform, *Crit. Rev. Anal. Chem.*, pp. 1–22, 2020. (Journal)

[4] D. Douroumis, I. Onyesom, M. Maniruzzaman, & J. Mitchell, "Mesoporous silica nanoparticles in nanotechnology," *Crit. Rev. Biotechnol.*, **48**, no. September 2011, pp. 1–17, 2012. (Journal)

[5] M. Mousavi and E. Fini, "Silanization Mechanism of Silica Nanoparticles in Bitumen Using 3-Aminopropyl Triethoxysilane (APTES) and 3-Glycidyloxypropyl Trimethoxysilane (GPTMS)," *ACS Sustainable Chemistry and Engineering*, **8**(8). pp. 3231–3240, 2020. (Journal)

[6] D. A. Widyasari *et al.*, "Conjugation of E.coli antibody with fluorescent natural silica-based nanoparticles: Preparation and characterization," *AIP Conf. Proc.*, **2382**, 2021. (Conference Proceeding)

[7] N. N. Alias, K. A. Yaacob, and C. K. Yew, "Effect of etchant on SOI wafer surface roughness for APTES silanization," *Mater. Today Proc.*, **17**, pp. 700–706, 2019. (Journal)

[8] V. V. Goftman *et al.*, "Synthesis, modification, bioconjugation of silica coated fluorescent quantum dots and their application for mycotoxin detection," *Biosens. Bioelectron.*, **79**, pp. 476–481, 2016. (Journal)

[9] Y. Lv *et al.*, "Silica-encapsulated quantum dots for highly efficient and stable fluorescence immunoassay of C-reactive protein," *Biochem. Eng. J.*, **137**, pp. 344–351, 2018. (Journal)

[10] K. Kajihara, "Recent advances in sol – gel synthesis of monolithic silica and silica-based glasses," *J. Asian Ceram. Soc.*, **1**(2), pp. 121–133, 2013. (Journal)

[11] M. C. Gonçalves, "Sol-gel silica nanoparticles in medicine: A natural choice. design, synthesis and products," *Molecules*, **23**(8), pp. 1–26, 2018. (Journal)

[12] P. A. Handayani, E. Nurjanah, & W. D. P. Rengga, "Pemanfaatan Limbah Sekam Padi Menjadi Silika Gel," *J. Bahan Alam Terbaruka*, **4**(2), pp. 55–59, 2015. (Journal)

[13] S. N. A. Jenie, A. Ghaisani, Y. P. Ningrum, & A. Kristiani, "Preparation of Silica Nanoparticles from Geothermal Sludge via Sol-Gel Method," *AIP Conf. Proc.*, vol. 020008, pp. 1–6, 2018. (Conference Proceeding)

[14] Y. Maulitiva Untoro, D. Ayu Widyasari, E. Supriadi, and S. Nurul Aisyiyah Jenie, "The Effect of Rhodamine B on The Properties of Fluorescent Nanoparticles Derived from Geothermal Silica," *J. Pure Appl. Chem. Res.*, **9**(3), pp. 171–176, 2020. (Conference Proceeding)

[15] V. H. Le, C. N. H. Thuc, and H. H. Thuc, "Synthesis of silica nanoparticles from Vietnamese rice husk by sol–gel method," *Nanoscale Res. Lett.*, **8**(1), pp. 58, 2013. (Journal)

[16] T. G. Kim, G. S. An, J. S. Han, J. U. Hur, B. G. Park, and S. C. Choi, "Synthesis of size controlled spherical silica nanoparticles via sol-gel process within hydrophilic solvent," *J. Korean Ceram. Soc.*, **54**(1), pp. 49–54, 2017. (Journal)

[17] Z. Qiu, J. Shu, and D. Tang, "Bioresponsive Release System for Visual Fluorescence Detection of Carcinoembryonic Antigen from Mesoporous Silica Nanocontainers Mediated Optical Color on Quantum Dot-Enzyme-Impregnated Paper," *Anal. Chem.*, **89**(9), pp. 5152–5160, 2017. (Journal)

[18] S. Mura *et al.*, "FTIR nanobiosensors for Escherichia coli detection," *Beilstein J. Nanotechnol.*, **3**(1), pp. 485–492, 2012. (Journal)

[19] Y. Che, Y. Xu, R. Wang, and L. Chen, "Rapid fluorescence detection of pathogenic bacteria using magnetic enrichment technique combined with magnetophoretic chromatography," *Anal. Bioanal. Chem.*, **409**(20), pp. 4709–4718, 2017. (Journal)

Proceedings of the 3rd ITB Graduate School Conference ISSN: 2963-718X
Enhancing Creativity in Research Through Developing Innovative Capabilities
December 21, 2022

Analysis of Achievements of Irrigators on Pillar Three of Irrigation Modernization in the Rentang Irrigation Area

Ernawati [1, *], Indratmo Soekarno[1], Joko Siswanto[2] & Yadi Suryadi[1]

[1]Faculty of Civil and Enviromental Engineering, Institut Teknologi Bandung, Indonesia
[2]Faculty of Industrial Technology, Institut Teknologi Bandung, Indonesia
[*]Email: erna_ernawati73@yahoo.co.id

Abstract. In irrigation modernization, there are five pillars namely the first pillar of water availability, the second pillar of irrigation infrastructure, the third pillar of irrigation management, the fourth pillar of irrigation institutions, and the fifth pillar of humans as actors in irrigation management. Each pillar of irrigation modernization is mutually supportive and interrelated. Humans are one of the most important elements as the main actors of Irrigation modernization. Irrigation modernization readiness is measured by IKMI, namely the irrigation modernization readiness index. The Rentang irrigation area is one of the irrigation areas whose IKMI value has been analyzed with an IKMI value of 66.9. This research will examine the achievements of the third pillar of irrigation modernization, namely irrigation management in the Rentang irrigation area. Achievements on the condition of the Rentang Irrigation Area related to the three pillars are majority sufficient. Periodic maintenance and repair, participation, financing system, and cropping pattern is quite good. related to IT-based IT-based OP information management facilities in a good category because indeed the advantages of spanning weirs in irrigation management using computer devices, and water management at the tertiary level are good. For the achievements of POB, POP, PPA, Mantri and interpreters towards Pillar 3 of Irrigation Modernization with a score range of 2.5 -3.5 from the achievement target of 5. A value of 3.5 on Completion of the OP form system and Distribution & distribution of water.

Keywords: *Three pillar; Rentang Irrigation Area; Irrigation Modernization.*

1 Introduction

Irrigation Modernization in Indonesia is basically Irrigation modernization in Indonesia an effort to realize a participatory irrigation management system oriented towards fulfilling irrigation service levels effectively, efficiently, and sustainably in the context of supporting food and water security, through increasing the reliability of water supply, infrastructure, irrigation management, management institutions, and human resources[1]. So far, 17 irrigation areas have

[1] Ministry of Public Work and Housing (MPWH) Pokok-pokok modernsasi irigasi Indonesia (The Principle of modernization of irrigation of Indonesia) 2014

had their IKMI values measured. IKMI (Irrigation Modernization Readiness Index) is a measurement tool developed by the Ministry of Public Works (PU) in since 2011. IKMI is used to measure irrigation modernization readiness in Indonesia. The Rentang Irrigation Area is one of 17 irrigation areas whose IKMI value has been analyzed with an adequate rating, in the range of 66.90[2]. The IKMI assessment cannot be separated from the evaluation of the five pillars of irrigation modernization which consist of the first pillar of water availability, the second pillar of irrigation infrastructure, the third pillar of irrigation management, the fourth pillar of irrigation institutions, the fifth pillar of humans as actors in irrigation management[3].

One pillar with the other pillars is interrelated. The most important factor for driving and realizing irrigation modernization is human resources, because the availability of irrigation facilities and infrastructure without the support of human resources will greatly influence the realization of the success of this irrigation modernization. Because even though it cannot be denied that the role of humans is the most important factor because humans will always be the main role[4]. All the pillars of irrigation modernization are directly related to the human role, especially the third, fourth and fifth pillars.
In this study, the third pillar of irrigation modernization will be studied, namely irrigation management. Irrigation management cannot be separated from irrigators. In this research, the irrigators that will be studied are POB, PPA and Matri in the Rentang irrigation area. By examining the extent to which the role of human resources, especially POB, POP. PPA and Mantri who will be correlated with the third pillar of irrigation modernization. The results of this study in outline are the achievements of POB, POP, PPA and Mantri/trainees towards Pillar 3 of Irrigation modernization in the Rentang Irrigation area.

2 Method

The method used in this study is a qualitative method with a phenomenological approach. This study analyzes and describes an individual phenomenon that occurs in this case the Weir Operation Guard (POB), Door Operation Guard (POP), Water Gate Guard (PPA) and Mantri/Executor. By gathering information through interviews with the Weir Operation Guard (POB), Door Operation Guard (POP), Water Gate Guard (PPA) and mantri in the Rentang Irrigation Area. In

---

[2] Ernawati Research and Proposal Human Resources Improvement Model That Are Competent In The Framework Of Irrigation Modernization Irrigation Areas Rentang And Irrigation Areas Jatiluhur Irrigation Area,Institut Teknology Bandung,2021

[3] Ministry of Public Work and Housing (MPWH), 2018, Draft Pedoman Teknis Modernisasi Irigasi

[4] Ernawati, E., Soekarno, I., Siswanto, J., & Suryadi, Y. (2021). Aspek Sumber Daya Manusia yang Kompeten Sebagai Pendukung Utama Urban Farming. *Jurnal Keteknikan Pertanian Tropis Dan Biosistem*

addition to the interviews, questionnaires were also distributed to several Water Gate Guards (PPA) and Mantri with questions related to the modernization of the three pillars of irrigation, namely the Irrigation Management System.

3 Analysis and Discussion

3.1 Irrigation Modernization

Irrigation modernization in Indonesia has indicators including increasing water productivity (kg GKG/m3 of water), increasing irrigation services (adequacy, reliability, fairness, and speed of service), increasing irrigation efficiency, reducing OP costs, increasing OP costs (OM cost recovery). Increased financial sustainability, reduced disputes and reduced environmental degradation1The implementation of Irrigation Modernization goes through a long process and is carried out in stages. Because modernization is a continuous and sustainable process, as well as realizing the goals of Irrigation Modernization, namely the fulfillment of irrigation service levels in an effective, efficient and sustainable manner in order to support food security.

The first stage is to measure the readiness of irrigation modernization using the IKMI (Irrigation Modernization Readiness Index). IKMI as a measuring tool developed by the Ministry of Public Works since 2011 to measure the readiness of irrigation modernization. Before going to IKMI there are several stages that must be passed including Irrigation Asset Management (PAI) and IKSI Study of Irrigation System Network Performance Index (IKSI)[5]

The value of the IKMI Irrigation Modernization Readiness Index can be used to formulate priorities and the next stages of irrigation modernization.

Table 1 Calculation results of IKMI values in Rentang

No	Indicator	IKMI Value
1	Water Availability	12,40
2	Irrigation Infrastructure	17,25
3	Management system	9,45
4	Management Institution	14,60
5	Human Resource	13,20
		66,90

Source: IKMI Reports in Rentang 2015

[5] Ernawati Research and Proposal Human Resources Improvement Model That Are Competent In The Framework Of Irrigation Modernization Irrigation Areas Rentang And Irrigation Areas Jatiluhur Irrigation Area,Institut Teknology Bandung, 2019

Based on the results of IKMI calculations for the DI Range management system, the value is lower, 9.45

3.2 Irrigation management

Irrigation management irrigation management will be oriented towards the rights and obligations of the community in order to be able to access local resources in an equitable manner to support food sovereignty policies as well as other agriculture, is open, participatory, accountable, efficient, effective, easy to operate, accurate, supports management towards real time, real allocation, real losses basis. To be able to guarantee its implementation, it must be supported by information and communication technology (Information Communication and Technology / ICT).

3.3 Rentang Irrigation Area

Rentang Irrigation Area is one of the national rice barns with a service area of 87,840 ha covering three regencies with the following areas: Majalengka Regency covering an area of 1,094 ha, Cirebon Regency covering an area of 20,571 ha and Indramayu Regency covering an area of 66,175 ha. The Rentang irrigation area has a Rentang weir which is located in Jatipuh District, Majalengka Regency. The weir divides water into two main canals, namely: through the Left Span tapping gate is SI Cipelang with a maximum discharge of 62.20 m3/second. Through the Right Span tapping door is SI Sinduparaja with a maximum discharge of 79.40 m3/second[6]. Rentang weir is one of the weirs in Indonesia where irrigation management uses a computer device

Figure 1 of Rentang Irrigation Area Map

[6] IKMI Report Rentang Irigation Area, 2015

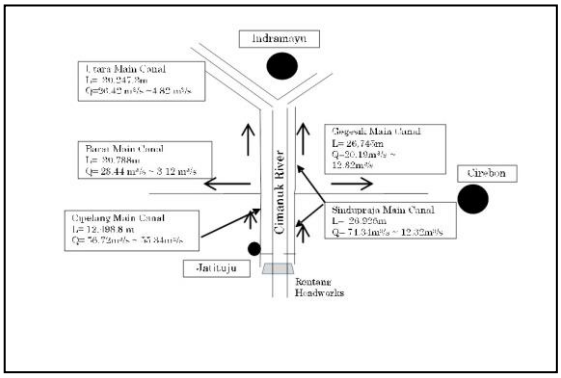

Figure 2 of Rentang Irrigation Area Map

3.4 Questionnaire and Interview

To gather information by distributing questionnaires and conducting interviews with 48 irrigators in the field (13 POB, 6 POP, 9 PPA and 20 paramedics/trainees) by gathering information through interviews and questionnaires related to the pillar irrigators. three. The following is a recapitulation of the results of the interviews and questionnaires to (POB, POP, PPA and Matri/Juru

Table 2 Achievement of Irrigation Area Conditions Rentang of pillar 3

No	Component Pillar three	POB, POP, PPA, Mantri /Juru
1	Water needs	Adequate
2	distribution of water	Adequate
3	Assessment period and door operation	Adequate
4	Calculation of water loss	Deficient
5	Completion of the blank system: 12 O blanks, and 10 P blanks	Adequate
6	Water Productivity	Adequate
7	Allotment of Irrigation Water	Adequate
8	Monitoring of water management: adequacy, reliability, fairness, flexibility, quality of water quality	
9	Water flow control system	Adequate
10	Water delivery system	Adequate
11	Periodic maintenance and repair	Pretty good
12	Emergency Response	Adequate
13	Participation	Pretty good
14	OP facilities - Transportation and communication tools - OP's fieldwork equipment - Uniform	Adequate
15	Equipment, means of IT-based OP information management system	Adequate
16	Water management at the tertiary level	Adequate
17	Financing System	Pretty good
18	Planting pattern	Pretty good

Source: Analysis Result

Table 3 Achievements of POB, POP, PPA paramedics and interpreters towards Pillar 3 of Irrigation Modernization

No	Substance Pillar 3 Agencies in Rentang	Target	Achievement
1	Water Needs	5	3
2	Distribution and distribution of water	5	3,5
3	Assessment period and door operation	5	3
4	Calculation of water loss	5	3
5	Completion of the OP blank system	5	3,5
6	Water productivity	5	2,5
7	Allotment of Irrigation Water	5	3
8	Monitoring Water management: adequacy etc	5	2,5
9	Water flow control system	5	2,5
10	Water delivery system	5	2,5
11	Periodic maintenance and repair	5	3
12	Emergency response	5	2,5
13	Participation	5	3
14	OPs facility	5	3
15	IT-based OP information management system equipment	5	2,9
16	water management at the tertiary level	5	3
17	Financing system	5	2,5
18	Planting pattern	5	3

Source: Analysis Result

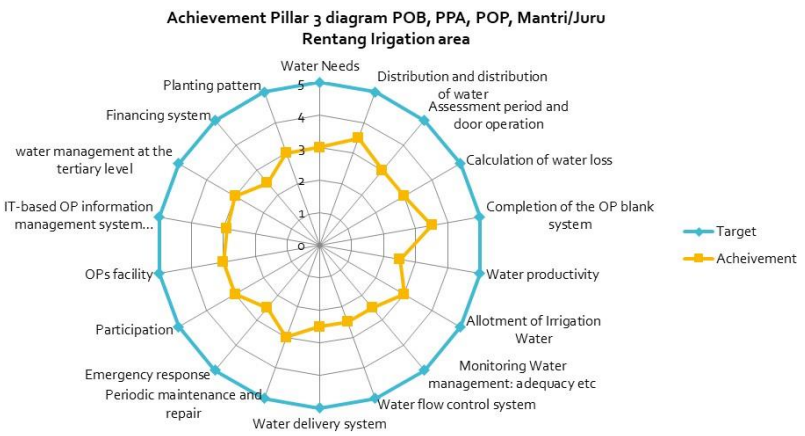

Figure 2 Achievement pilar 3 Diagram Rentang Irrigation Area

4 Conclusion

Achievements to The Condition of the Range Irrigation Area related to the three majorities are sufficient. Periodic maintenance and repair, participation, financing system, and planting pattern are quite good. related to the equipment of the OP information management system based on IT category is good because it is indeed the advantage of Bendung Rentang in irrigation management using computer devices, water management at the tertiary level is good. For the Achievement of POB, POP, PPA, Mantri and Interpreters towards Pillar 3 of Irrigation Modernization with a value range of 2.5 -3.5 of the achievement targets 5 Improvement of the OP blangko system improvement and division and provision of water. For maximum achievement, it is necessary to understand irrigation modernization as a whole for each irrigator so that it is properly planned and what priorities must be carried out. In managing irrigation, cooperation between fellow irrigators, both agency and officers in the field, is needed, even P3A, GP3A and IP3A.

Acknowledgement

Thank you, the authors say to Prof. Sigit Supadmo Arif Gajah Mada University for his input regarding irrigation modernization, RISTEK DIKTI simlitabmas for Doctoral Dissertation Research scholarship, Faculty of Civil and Environmental Engineering Institute Bandung Technology, PUPR Indonesia.

References

[1] Ministry of Public Work and Housing (MPWH) Pokok-pokok modernsasi irigasi Indonesia (The Principle of modernization of irrigation of Indonesia) 2014

[2] Ernawati Research and Proposal Human Resources Improvement Model That Are Competent In The Framework Of Irrigation Modernization Irrigation Areas Rentang And Irrigation Areas Jatiluhur Irrigation Area,Institut Teknology Bandung,2021

[3] Ministry of Public Work and Housing (MPWH), 2018, Draft Pedoman Teknis Modernisasi Irigasi

[4] Ernawati, E., Soekarno, I., Siswanto, J., & Suryadi, Y. (2021). Aspek Sumber Daya Manusia yang Kompeten Sebagai Pendukung Utama Urban Farming. *Jurnal Keteknikan Pertanian Tropis Dan Biosistem;*, **9**(1)(2021). https://doi.org/10.21776/ub.jkptb.2021.009.01.01

[5] Ernawati Research and Proposal Human Resources Improvement Model That Are Competent In The Framework Of Irrigation Modernization Irrigation Areas Rentang And Irrigation Areas Jatiluhur Irrigation Area,Institut Teknology Bandung, 2019

[6] IKMI Report Rentang Irigation Area, 2015

Proceedings of the 3rd ITB Graduate School Conference ISSN: 2963-718X
Enhancing Creativity in Research Through Developing Innovative Capabilities
December 21, 2022

Study of Pipe Selection Methods to Be Rehabilitated: A Case Study of Jakarta City

Ervin J. Mansyur[1, *], Biemo W. Soemardi[2] & Reini D. Wirahadikusumah[2]

[1] Students of Civil Engineering Doctoral Program, Bandung Institute of Technology
[2] Civil Engineering, Bandung Institute of Technology
[*]Email: ervinmth@engineer.com

Abstract. Some water distribution pipelines in Jakarta were built decades ago and are currently in a defective condition. Pipeline network managers must carry out a reactive maintenance strategy by repairing many leaks and rehabilitating defective pipes with limited budgets. The current method of selecting pipes to be rehabilitated does not consider economic aspects and is still subjective. Some of the latest methods from the existing literature have considered economic analysis but are not suitable for conditions of reactive maintenance strategies with limited budgets. For this reason, a new method is proposed by considering the reactive maintenance strategy that is currently implemented and considering budget constraints. The proposed new method is in the form of an optimization model for selecting pipes to be rehabilitated to provide maximum economic benefits with the existing budget constraints. Economic benefits consist of the benefits of reduced leak repair costs and the benefits of increased revenue due to eliminated leaks in rehabilitated pipelines. By applying the optimization model to the selection of pipes to be rehabilitated, it is expected that there will be economic benefits that can increase the rehabilitation budget in subsequent years which will speed up the replacement of defective pipes.

Keywords: *pipe rehabilitation; reactive maintenance; pipe rehabilitation benefits; pipe leak; pipe repair.*

1 Introduction

Water is an essential element for human life, and in 2010 the United Nations stated in [1] that the right to clean water and safe sanitation is a human right. In line with this, the Indonesian government has targeted that by 2030 all Indonesian citizens will have easy access to clean water. However, the fulfillment of clean water for all citizens is not easy and full of challenges. In 2019 the Agency for Increasing the Implementation of Drinking Water Supply Systems (BPPSPAM) in [2] reported that one of the main problems in meeting water needs in Indonesia is the high rate of leakage, which is reflected in the high Non-Revenue Water (NRW). NRW is water that is produced and distributed but does not generate income for the water service manager.

According to the International Water Association (2011) in [3], the NRW level is affected by several factors including physical leaks in pipelines, unpaid consumption, unaccounted consumption, and under-consumption water meter readings. One of the factors that determine the NRW level in a clean water distribution system is leakage in the piping network. Leakage rates in pipelines rank first as the cause of high NRW. The level of leakage in the pipeline network has been compiled by Kahn (2020) in [4], where the highest level of leakage is at the level of 1.2 leaks/km/year.

It is necessary to carry out a maintenance activity to maintain the condition of the pipeline network. Proper maintenance is carried out in a proactive way so that the pipeline does not experience a failure requiring corrective action. According to Van Zyl (2014) in [5], the dominant maintenance activities in the proactive maintenance type include monitoring the condition of pipeline components, corrosion control, protection of the surrounding environment, checking the condition of the inside of the pipe wall, recording maintenance activities, and other preventive maintenance activities.

The older the pipe, the more frequent leaks occur and the higher the need to rehabilitate the pipes. Therefore, part of the water pipe network system in an area with old pipelines requires rehabilitation. Pipeline rehabilitation is carried out to replace damaged old pipelines with new pipes that are in good condition.

An example of a high leakage rate is in old pipe networks that can be found in one area in the city of Jakarta. The average leak rate of pipelines in one of the areas in the city of Jakarta during the period from January 2017 to March 2020 was at a rate of 1.71 leaks/km/year. The leak rate is at a high level compared to the leak level criteria compiled by Khan (2020), which states that a leak rate above 1.2 leaks/km/year is at a high level.

Before carrying out the rehabilitation of a pipeline or pipeline network, it is necessary to carry out a process of selecting the pipeline to be rehabilitated. The method for selecting rehabilitated pipelines has been implemented by one of the managers of clean water pipelines in Jakarta.

2 Current Method For Selecting Pipes To Be Rehabilitated

Pipeline leaks affect NRW or revenue levels. To provide optimal revenue, it is necessary to consider economic aspects in the form of rehabilitation benefits obtained when selecting pipes to be rehabilitated. The relationship between the condition of the pipeline or the level of leakage in the pipeline to revenue is as shown in Figure 1.

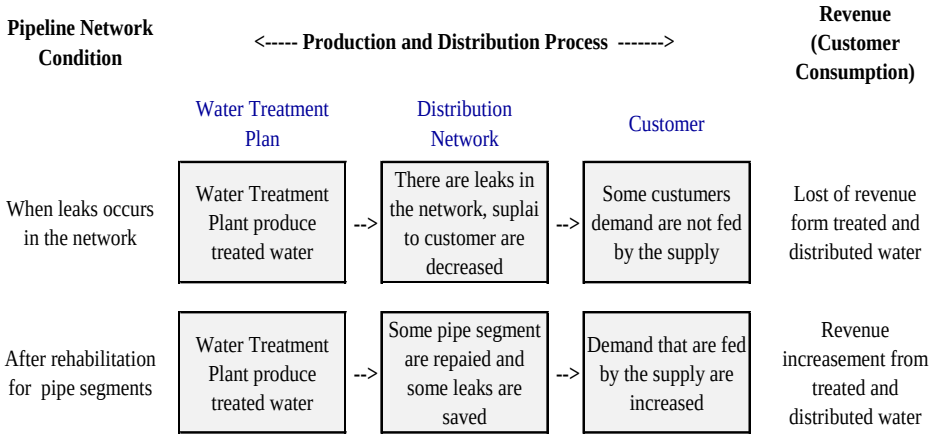

Figure 1 The correlation between pipeline network conditions and revenue

Water treated and produced at a Water Treatment Plant (WTP) is intended for consumption by customers. When leaks occur in the network (shown in the first process line in Figure 1), supply to the customers is reduced so that the customer's consumption becomes less. Loss of water in the pipe network results in loss of income for clean water service managers because some of the water produced is not consumed as expected. After several pipelines were repaired or rehabilitated, the leaks in the pipelines decreased and converted into customer consumption. In the condition after the pipe rehabilitation, the revenue of the clean water service manager increases.

In Jakarta, the selection of pipeline sections to be rehabilitated is based on the results of an assessment of each pipeline's reliability. The assessment of the reliability of the pipeline includes an assessment of several variables, namely pipe age, pipe material, pipe diameter, pipe roughness, and the number of leaks. The determination of these sections does not consider the economic aspect.

In the practice of selecting pipe segments based on the above method, each variable is weighted as follows; pipe material by 20%, pipe age by 25%, the number of leaks by 35%, and pipe roughness by 20%. Each of these variables is assessed qualitatively under certain conditions and ranges as shown in Table 1.

The result of the total assessment is the average score of the four variables considered. Pipe sections assessed are grouped based on the results of the assessment carried out. The grouping consists of 5 categories as follows.

1. Score above 80% = Well conserved, pipes in good condition
2. Score between 60% to 79% = Conserved enough, the pipe is in good condition but has started to decline

3. Score between 40% to 59% = Less conserved, pipe condition decreases with increasing leakage
4. Score between 20% to 39% = Degraded, the pipe condition is getting worse and needs to be rehabilitated
5. Score below 20% = Poorly conserved, critical pipe condition (worst), and rehabilitation priority

Table 1 Ratings on each of the criteria on the currently used method of selecting rehabilitated pipes

Criteria	Indicator	Score
Pipe age	Age = 0 year	1
	Age > 50 year	0
	0 < Age < 50 year	Interpolated
Pipe material	Cast Iron	0.9
	Asbestos Cement	0.6
	HDPE	0.5
	PVC	0.5
	Steel	0.1
	Ductile Cast Iron	0.1
	Galvanized Iron Pipe	0.05
	Others	0.5
Leak number per km	Leaks = 0	1
	Leaks = 0.015	0
	0 < Leaks< 0.015	Interpolated
Pipe friction	Friction > 120	1
	100 < Friction < 120	0.8
	80 < Friction < 100	0.6
	70 < Friction < 80	0.4
	Friction < 70	0

Selected pipes for rehabilitation are pipes with a score below 20% and fall into the poorly conserved condition category. Poorly conserved conditions are critical pipe conditions and are included in rehabilitation priority. Pipelines to be rehabilitated are selected from pipes that fall into this category. This assessment method classifies pipe reliability conditions with available quantitative data. The grouping of pipe assessment result categories is categorized subjectively with certain ranges of values. The selection of pipe sections to be rehabilitated is carried out subjectively from the group with poorly conserved categories.

3 Case Study, Selection of Pipeline to Be Rehabilitated in 2021

3.1 Pipeline Selection

The selection of primary pipelines to be rehabilitated in 2021 is described as follows. The primary pipe is the pipe that carries water from the Water Treatment Plant (WTP) to the distribution pipeline network. A primary pipe is a pipe with a minimum size of 400 mm in diameter. Primary pipes are generally not in an inlet of a District Meter Area (DMA). From the results of the assessment using the method currently used, 186 primary pipelines are categorized as being in a poorly conserved condition, critical pipeline condition, and already on rehabilitation priority. The selection of pipes in poorly conserved conditions to be followed up in the rehabilitation program is carried out by considering other matters which are generally outside the technical aspects. In 2021 a review will be carried out again on the number of leaks that have occurred in each pipeline segment. Of the primary pipes which were assessed as being in a poorly conserved condition, a total of 17 pipes had recorded leaks more than 10 times. The list of the 17 pipes is shown in Table 2.

Table 2 List of pipes that fall into the poorly conserved category with more than ten leaks

No	Segments	Material	Installation Date	Number of Leaks	Final Score
1	Pejagalan Raya	DCI	1985	43	0.17
2	Latuharhari	DCI	1975	38	0.12
3	Margono	DCI	1975	31	0.12
4	Hasyim Ashari	DCI	1985	28	0.17
5	Kali Besar Brt	DCI	1985	27	0.17
6	Kopi 1	DCI	1985	23	0.17
7	Martadinata	DCI	1985	23	0.17
8	Gatot Subroto 3	DCI	1985	21	0.17
9	P. Diponegoro	DCI	1975	21	0.12
10	Wahid Hasyim	DCI	1975	20	0.12
11	Cimahi	DCI	1975	19	0.12
12	Soepomo	DCI	1990	15	0.20
13	Gatot Subroto 2	DCI	1985	13	0.17
14	Gatot Subroto 1	DCI	1985	11	0.17
15	Hayam Wuruk	DCI	1985	10	0.17
16	Kopi 2	DCI	1985	10	0.17
17	Manggarai U. 2	DCI	1975	10	0.12

In 2021, the pipe being rehabilitated is the pipe in line no. 2, namely the pipe on the Latuharhari road with a diameter of 800 mm and a length of 110 meters. The rehabilitation was constructed from 24 June 2021 to 26 June 2021. The assessment was carried out using actual data but in the end, the selection of the

pipe to be rehabilitated was made based on certain aspects which were carried out subjectively. The pipe corrosion condition variable is considered important according to Van Zyl (2014) in [5], but in the current assessment, it is not considered.

3.2 Pipe Rehabilitation Results

The results of the rehabilitation can be seen from changes in the flow (amount of flow) flowing in the supply areas of the rehabilitated pipes and changes in pressure (pressure) in the downstream network of the rehabilitated pipelines. After rehabilitation, the pressure on the network in the downstream area of the rehabilitated pipeline increased from 0.2 m to 3.2 m with an average increase of 1.4 m from 5.4 m, and the increase in flow in areas supplied from the rehabilitated pipeline was 12.7 l/s. The changes are based on measurements of conditions before rehabilitation and after rehabilitation. The measurement results are shown in Figure 2.

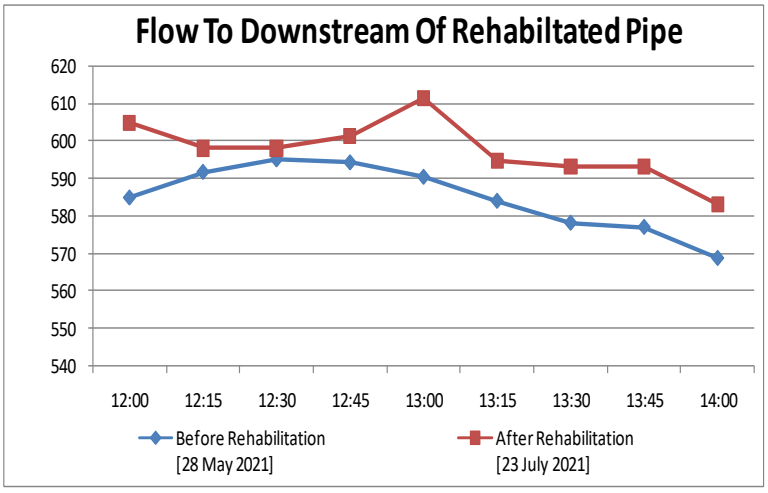

Figure 2 Changes in flow in the pipe before and after rehabilitation

The improvement from the rehabilitation can be seen from the results of flow and pressure measurements in the served area of the rehabilitated pipe. It is indicated that there was an improvement in supply to the areas served by the pipelines. However, it is not yet known how much the resulting increase in revenue will be from the increase in existing supply. The results of this increase have not shown any economic benefits related to NRW.

3.3 Weaknesses of the Selection Method Used

The currently applied pipeline rehabilitation selection method has some weaknesses or drawbacks when applied to the ongoing pipeline maintenance strategy. These weaknesses are as follows.

1. Budget limitations are not accommodated in the method used. Budget constraints generally occur in the reactive maintenance strategy that is currently implemented in pipelines in the city of Jakarta.

2. There is no economic analysis in the current method. Selection of pipes based purely on the physical condition of the pipeline. In reactive maintenance conditions where the rate of leakage is high and the budget for rehabilitation is limited, it is necessary to have a method for selecting rehabilitated pipelines that is more suitable for implementation.

3. The assessment is calculated considering the service life of each pipe material is the same. The determination of the score for pipe age is the same for each pipe material even though the service life for each pipe material is different. For example, the service life of pipes with PVC is shorter than pipes with HDPE material.

4. One of the assessment variables used is pipe roughness which is more closely correlated with the pipe operational capability than the pipe reliability based on physical condition. Pipes with high roughness do not necessarily have poor reliability nor do they necessarily have good reliability. Currently, no research correlates the relationship between pipes with high roughness and pipe damage conditions. In the assessment of this pipe condition variable, the actual results of the investigation on the inside of the pipe that map the corrosion rate of the pipe will more accurately assess the pipe condition constraints compared to the estimation of the pipe roughness.

4 Alternative Methods for Selecting Pipelines for Rehabilitation

Each pipe will suffer a decrease in reliability. Several factors affect the degradation of water pipes. The factors generally considered to have the greatest impact on pipe failure are pipe age, installation period, corrosion, diameter, length, material, seasonal variations, soil conditions, pressure, and nearby excavation as reported by Li (2013) in [6].

According to Li, maintenance is considered a key activity for water utilities to prevent water pipe failures and improve network performance. This

maintenance contributes to quality service and enriches all the company's experiences around the services provided. Pipeline managers repair and rehabilitate leaky pipes. Sutjahjo (2021) in [7] stated that pipeline maintenance can be conducted proactively to prevent leaks and reactively carried out after a leak by repairing leaking pipes.

Pipes with poor conditions need to be rehabilitated. Good pipe rehabilitation is carried out with a proactive maintenance strategy, which is to prevent and delay the pipes from being damaged. Some cities have resorted to reactive maintenance strategies. In the reactive maintenance strategy, there are too many leaky pipes so the cost to rehabilitate the leaky pipes is too much compared to the available budget.

Some literature has developed methods for selecting rehabilitated pipelines. Method developed is a model for determining the schedule for the rehabilitation of a pipeline in a proactive maintenance strategy with some literature accompanied by the ability to select the pipeline to be rehabilitated. Currently, a model is needed that can be applied to reactive maintenance strategies with limited budgets to rehabilitate damaged pipes. An overview of the capabilities of the current pipeline selection method, the latest developed models (since 2019), and the proposed model are as follows.

1. *Model of deterioration and optimal rehabilitation modelling for urban water distribution systems*

The model developed by Zhou (2019) in [8] is oriented towards proactive maintenance with the expected research results in the form of a long-term view for multi-objective decision-making by using many variables and disclosing in detail the effect of each of the variables in each module. Unfortunately, the results of this study, which are oriented towards proactive maintenance, cannot be widely used by most pipeline network managers whose maintenance is reactive. As is the case in most other proactive maintenance-oriented studies, the benefits of rehabilitation were not considered in more detail in the form of reduced repair costs and increased consumption from reduced leakage conversions in the rehabilitated pipelines.

2. *Model of economic-based approach for predicting optimal water pipe renewal period based on risk and failure rate*

Kim et al, (2019) in [9] proposed a model by considering the risk factors in the cost-benefit analysis of pipeline rehabilitation. Kim uses failure risk as a failure cost that is included in the cost analysis. The maintenance orientation used is reactive-proactive which brings cost estimates to the cost-benefit analysis which are still in the form of budgetary costs with several assumptions. The results of this study are difficult to implement for the type of proactive maintenance as a

whole because there is not much discussion about determining reactive rehabilitation that will affect benefits in the short term.

3. *Model of water pipe replacement scheduling based on life cycle cost assessment and optimization algorithm*

Meanwhile, Ghobadi (2021) in [10] uses the same variables as previous studies, namely data on pipe conditions and pipe leaks, which has considered aspects of the life cycle cost of each pipe segment.

4. *A risk-based approach in rehabilitation of water distribution networks model*

This model was developed by Raspati et al (2022) in [11] to prioritize the rehabilitation of pipelines based on pipeline data and leak rate data. The model is quite simple in that the prioritization of rehabilitated pipelines is risk-based using qualitative risk analysis. The economic aspect was not considered in the research he developed.

Several models for determining rehabilitated pipelines, including those currently in use, have different purposes and capabilities. The ability that is commonly used in general is to predict the future rehabilitation time which is generally required in a proactive maintenance strategy. The models in the proactive maintenance strategy have many incompatibilities when applied to pipeline conditions with reactive maintenance strategies, although some models can determine the priority of several alternative pipelines to be rehabilitated and have economic analysis capabilities. Differences in the capabilities of the current methods with the proposed method are arranged in Table 3.

Table 3 Capabilities on the latest models, the model currently used, and the proposed model

No	Author (Year)	Providing Rehab. Scheduling	Determining Priority For Rehab.	Analyzing The Economic Benefits	Accommodating Budget Limitation
1	Zhou (2019)	√		√	
2	Kim, et al. (2019)	√		√	
3	Ghobadi et al. (2021)	√		√	
4	Raspati et al. (2022)		√		
Current method			√		
Proposed method			√	√	√

Currently, there has not been a single model developed that can accommodate budget constraints on reactive maintenance strategies such as the condition of pipelines in Jakarta. The proposed model cannot predict future pipe rehabilitation schedules in the proactive maintenance strategy that has been developed. However, the new model can be applied to reactive maintenance strategies with a limited budget by considering technical and economic aspects.

5 Pipeline Selection Modeling in Reactive Maintenance Strategy

The methods developed in some of the literature and the methods used today are part of the method for determining rehabilitated pipes using different approaches. These models are not specialized to apply to a reactive maintenance strategy with a limited budget. So, for determining the rehabilitated pipelines on the reactive maintenance type with problems with already high leakage rates, there is an incompatibility in the models studied as follows.

1. All methods of determining rehabilitated pipes above did not consider the condition of a decrease in revenue due to high leakage rates in reactive maintenance types. High leakage causes the pressure to drop and causes the customer's consumption to decrease. In conditions where customer consumption is down and leakage rates are high, rehabilitation of a pipe will lead to an increase in consumption which cannot be ignored. For this reason, it is necessary to develop a model to calculate the benefits of rehabilitation on the increase in revenue due to reduced leakage after rehabilitation.

2. The leakage rate approach in all studied models is estimated for conditions in the distant future with the pipeline still in good condition. This approach cannot be applied to network maintenance with a reactive type when the leakage rate is already very high so the leakage rate is no longer necessary to estimate the condition of the pipes that are still good.

3. All the rehabilitated pipe determination methods in the literature reviewed did not include budget constraints as a direct limitation on the rehabilitated pipe determination model they developed. In the model for determining rehabilitated pipelines for the reactive maintenance type, the limited rehabilitation budget is one of the main influencing variables.

From this mismatch, it is necessary to develop a model that can be applied to reactive types of maintenance with high leakage rates. The conceptual framework of the model corresponding to these conditions can be described as follows.

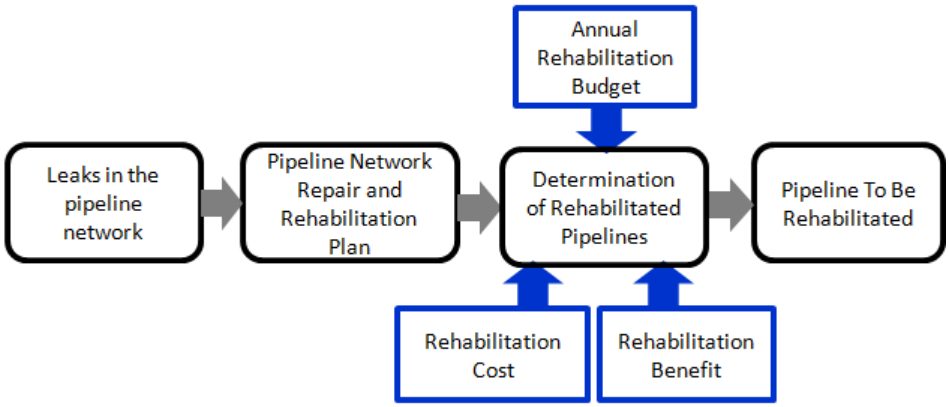

Figure 3 The proposed model conceptual framework

There is a series of processes starting from damage to the pipe, planning for repair and rehabilitation of the pipeline network, and determining the pipeline to be rehabilitated. In the process of determining the pipe to be rehabilitated, the variables that influence it are the rehabilitation budget, rehabilitation costs, and rehabilitation benefits. Some of the existing literature obtained the variables that influence it. The following table presents the influencing variables and how to get them.

Table 4 The calculated variables and their data sources

No	Variables	Sources For Obtaining Information
1	Rehabilitation cost	Annual budget plan
2	Pipe length	Network pipeline database (GIS)
3	Pipe diameter	Network pipeline database (GIS)
4	Rehabilitation unit price	Annual frame contract rate
5	Leaks rate	Network pipeline database (GIS)
6	Cycle time	Network pipeline database (GIS)
7	Repair unit price	Annual frame contract rate
8	Costumer consumption	Customer database
9	Water charge	Local government regulations
10	Leaks in the pipeline	Network pipeline database (GIS) or direct measurement form the field
11	Pipeline network data	Network pipeline database (GIS)

A schematic of the relationship between these variables is obtained in the rehabilitation program of a pipeline network. From the existing literature, the variables and the relationship scheme between these variables are shown in Figure 4.

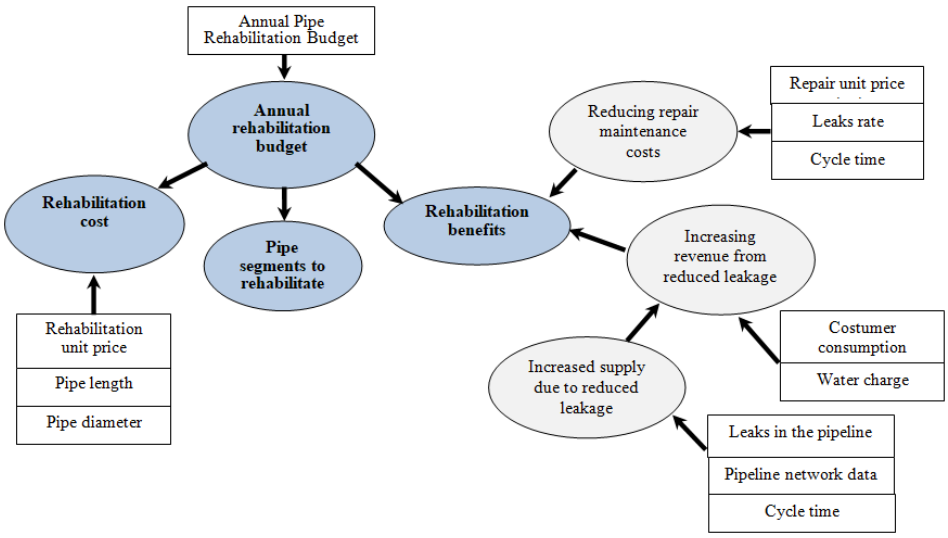

Figure 4 The relationship between variables in the optimization model for selecting pipelines to be rehabilitated

An optimization model for selecting the pipelines to be rehabilitated needs to be developed. The model is based on the relationship scheme between the variables above. The selection of pipe to be rehabilitated is determined by the rehabilitation budget, rehabilitation costs, and rehabilitation benefits.

The main variables considered in the optimization model are the rehabilitation budget, rehabilitation costs, and rehabilitation benefits. In the reactive maintenance type where the leakage rate is very high, a very large rehabilitation cost is required, so budget constraints affect the optimization model. Rehabilitation benefits consist of benefits from reduced repair costs and benefits from increased revenue due to reduced leakage in the rehabilitated pipelines. When the leakage rate is high, the pressure in the network drops and customer consumption decreases so that when the pipeline is rehabilitated, there will be benefits from increased revenue (customer consumption) due to increased pressure after reduced leakage. The development of this optimization model is needed to assist in optimizing the determination of rehabilitated pipelines for the reactive maintenance type.

The model for obtaining the main variables is obtained from the following references as shown in Table 5. Rehabilitation cost is modeled by Jayaram et al. (2008) in [12], Shin et al. (2016) in [13] and Ibrahim (2018) in [14]. Meanwhile, benefit from reduced repair costs is modeled by Jayaram et al. (2008) in [12], Shin et al. (2016) in [13], Mahmoodian et al. (2017) in [15],

Ibrahim (2018) in [14] and Kim et al. (2019) in [9]. Benefit of increasing revenue due to reducing leaks is modeled by Kim et al. (2018) in [9].

Table 5 References to the model for calculating the costs and benefits of rehabilitation

Variable	References
Rehabilitation cost	Jayaram et al. (2008), Li (2013), Shin et al. (2016), Ibrahim (2018)
Benefit from reduced repair cost	Jayaram et al. (2008), Li (2013), Shin et al. (2016), Mahmoodian et al. (2017), Ibrahim (2018), Kim et al. (2019)
Benefit from increasing revenue due to leaks reduction	Kim et al. (2019)

The optimization model that is carried out is a model to get the maximum benefit/cost ratio. The optimization equation can be described as follows.

$$Z = \frac{F(X2) + F(X3)}{F(X1)} \tag{1}$$

Where Z is optimization value, F(X1) is the rehabilitation cost, F(X2) is the benefit of reduced repair costs, and F(X3) is the benefit of increasing revenue from reduced leakage. In the optimization model, there are limitations to the rehabilitation budget.

6 Conclusion

The existing methods are basically built from a rehabilitation approach to a proactive maintenance strategy by assuming there are no budget constraints. While the problems faced by many water distribution providers in Indonesia are generally due to budget constraints.

Based on this, it is necessary to apply a method based on a reactive maintenance strategy to overcome the problem of selecting pipes to be rehabilitated in water distribution pipelines in Indonesia. The method based on a reactive maintenance strategy is apart from budget constraints and the leakage rate is already very high. Thus, the proposed method must consider the economic and technical aspects simultaneously in a cost-benefit consideration.

References

[1] United Nations, 64/292. The human right to water and sanitation, Resolution adopted by the General Assembly on 28 July 2010, United Nations, 2010. (Resolution Report)

[2] BPPSPAM, *Buku Kinerja BUMD Penyelenggara SPAM 2019*, Jakarta, Indonesia, 2019. (Book)
[3] Asian Development Bank, *The Issues and Challenges of Reducing Non-Revenue Water*, Metro Manila, Philipines, 2010. (Book)
[4] Kahn C., Damiani A., Ge S., *Validation of water main failure predictions: A 2-year case study*, AWWA Water Science. New Jersey, US, 2020. (Journal)
[5] Van Zyl J., *Introduction to Operation and Maintenance of Water Distribution Systems*, Republic of South Africa, 2014. (Book)
[6] Li, F., *Multi-Criteria Optimisation of Group Replacement Schedules For Distributed Water Pipeline Assets*, Queensland University Of Technology, 2013. (Thesis or Dissertation)
[7] Sutjahjo B., *Melaksanakan Manajemen Operasi Dan Pemeliharaan Sistem Penyediaan Air Minum*, Pelatihan Manajemen Air Minum Tingkat Mandya Berbasis Kompetensi, Yayasan PTD PAMSI, Jakarta, Indonesia, 2021. (Book)
[8] Zhou, Y., *Deterioration and Optimal Rehabilitation Modeling for Urban Water Distribution Systems*, Delft University of Technology, 2019. (Thesis or Dissertation)
[9] Kim, K., Seo, J., Hyung, J., Kim, T., Kim, J., Koo, J., *Economic-based approach for predicting optimal water pipe renewal period based on risk and failure rate*, Korean Society of Enviromental Engineering, 2020. (Journal)
[10] Ghobadi F., Jeong G., Kang D., *Water Pipe Replacement Scheduling Based on Life Cycle Cost Assessment and Optimization Algorithm*, 2021. (Journal)
[11] Raspati G. S., Bruaset S., Bosco C., Mushom L., Johannessen B., Ugarelli R., A *Risk-Based Approach in Rehabilitation of Water Distribution Networks*, International Journal of Environmental Research and Public Health, 2022. (Journal)
[12] Jayaram N., Srinivasan K., *Performance-based optimal design and rehabilitation of water distribution networks using life cycle costing*, Water Resources Research, 2008. (Journal)
[13] Shin, H., Joob, C., Kooa, J., *Optimal Rehabilitation Model for Water Pipeline Systems with Genetic Algorithm*, 12th International Conference on Hydroinformatics, 2016. (Journal)
[14] Ibrahim, S., *A Water Main Life Cycle Analysis Framework for the Economic Evaluation of OM&R (Operation, Maintenance, and Renovation) Strategies*, Waterloo, Canada, 2018. (Thesis or Dissertation)
[15] Mahmoodian, M., Phelan, J., Shahparvari, M., *Reliability-Based Maintenance Management Methodology to Minimise Life cycle Cost of Water Supply Networks*, International Journal of Civil and Environmental Engineering, Vol:11, No:11, 2017. (Journal)

Proceedings of the 3rd ITB Graduate School Conference ISSN: 2963-718X
Enhancing Creativity in Research Through Developing Innovative Capabilities
December 21, 2022

The Role of Agrotourism in Environmental Sustainability (Case Study: Batu City, East Java)

Fardiah Qonita Ummi Naila* & Djoko Santoso Abi Suroso

School of Architecture, Planning, and Policy Development, Institut Teknologi Bandung
*Email: Fardiahqonita123@gmail.com

Abstract. The change in tourism trends during the Covid-19 pandemic to rural tourism is the basis for considering the role of agro-tourism as a rural tourism option. Previous research has shown an increase in demand for the tourism market has a correlation with increased consumption of clean water, giving rise to issues of justice for access to rural air. Therefore, this study seeks to be able to give consideration to environmental potential in agro-tourism activities with the case study of Batu City. In this study, a comparative study was used in three different villages in Batu City with vegetation characteristics as an agro-tourism attraction offered by the Temperature Vegetation Dryness Index (TVDI) methodology. The results showed that there was a relationship between the area of the vegetation index as shown by the Normalized Difference Vegetation Index (NDVI) approach in each village and the degree of drought shown in the results of the Temperature Vegetation Dryness Index (TVDI). The results of the study show that agro-tourism plays a big role in maintaining air availability as indicated by the minimum level of drought in areas with high vegetation.

Keywords: *Agrotourism; Environmental Sustainability; Drought Level.*

1 Introduction

We have now entered the city century and the term urbanization will become a perspective that is more widely used in viewing social, economic and environmental characteristics in the future [1]. Scientists agree, we are currently living in a new urban era which is termed as 'Asticcene' which refers to the meaning of humans changing environmental functions globally [2]. The context of urbanization can also be brought into the context of tourism, where currently urban tourism tends to increase rapidly compared to other forms of tourism [3].

Besides being an important destination, cities have a significant role in the tourism as a whole system, by being a gateway for international and domestic tourists as well as being a node in the transportation system [4]. Furthermore, regarding the role of the city as a multifunctional entity and an attraction for tourists to be able to visit, it has the opportunity to shape the relationship between urbanity and various tourism activities. This is because there is an intersection

between the needs of residents and tourists so that cities face different demands in the provision of services and facilities. The tourist burden in a city can have an impact on reducing the quality of urban life.

The rapid development of the tourism industry is a real threat to the issue of climate change [5]. This is evidenced by data regarding a number of countries that are vulnerable to climate change which are both domestic and international tourist destinations [4], this condition will also cause drastic changes in the decline in tourist visits including in coastal, mountainous and polar regions. due to drought, heat waves and hurricanes. The amount of dependence on other sectors causes the tourism industry to be the first to receive the impact of a disaster. On the other hand, the tourism sector is one of the factors that perpetuate global warming and natural disasters. The tourism sector is a contributor of 8% of greenhouse gas (GHG) emissions as a result of aviation (40%), transportation (30%), and consumption of goods and services (30%) including accommodation needs [6]. This causes the tourism sector to be a bigger pollutant sector than the construction sector.

In the context of Southeast Asia, many countries make the tourism sector a driving force for the economy. According to data from Southeast Asia: Travel and Tourism GDP Contribution, 2021 the tourism sector in Southeast Asia as a whole made the highest contribution in 2019, namely 393.12 billion dollars, then in experienced a significant decrease to 180.21 billion dollars in 2020 and amounted to 143.25 billion dollars in 2020. 2021 due to the covid-19 pandemic.

Limited access to foreign tourists is the main factor in the decline in the contribution of the economic sector to GDP. Therefore, many countries in Southeast Asia have developed a strategy for recovering the tourism sector by promoting domestic tourism by implementing policies [7], [8]:

1) Identify new niches in the domestic tourism market
2) Re-orientation of tourism services
3) Support SMEs and startups
4) Develop tourism in rural areas

The demand for rural tourism increased during the covid-19 pandemic due to the need for psychological and physical recovery during the face of the covid-19 pandemic [9], [10]. This shift in tourism preferences is also supported by the need to implement health protocols. Rural tourism is defined as tourism that showcases artistic, cultural and heritage life in rural areas [11]. Rural tourism, specifically, is also defined as agro-tourism where tourism activities are integrated with agricultural activities of local communities [12].

In the context of tourism, as a specific activity for rural areas, concentrated in rural areas as a destination, offering functional accommodation structures and other special services. Rural tourism has been recognized as:

- An alternative to the declining agricultural sector, which is unable to sustain the subsistence needs of the rural population;
- As a possibility to stimulate entrepreneurial opportunities for rural farmers, ensuring stability through the new jobs created

Among the forms of rural tourism, agro-tourism is one of the potential areas of concern because it demands the maintenance of the original characteristics of rural areas under current development demands.

The same phenomenon also occurs in the study location, Batu City, East Java. The designation of Batu City as a National Tourism Destination (DPN) with a type of natural tourist attraction in the 2010-2025 National Tourism Development Master Plan as stipulated in the Government Regulation of the Republic of Indonesia Number 50 of 2011 has a direct impact on the development of infrastructure, infrastructure and public facilities, increasing empowerment community and investment development. Supporting this, the construction of a number of supporting infrastructure for the tourism sector in Batu City will encourage the growth and development rate of the city marked by an increase in population, increased economic and social interaction between interconnected areas that lead to spatial and a-spatial transformation in the Batu City area. In the transformation of the spatial aspect, it can be seen that Batu City has experienced an increase in residential land cover reaching 33% in the period 2013 – 2022. Meanwhile, in the a-spatial aspect, Batu City continues to experience urban growth and development, especially in the trade, agriculture, construction and accommodation provision sectors. in terms of GRDP data according to constant prices in 2013-2019 and population growth. GRDP as a measure of economic growth in Batu City has increased, but on the other hand, the development of tourism in Batu City continues to have an impact on the sustainability of agro-tourism activities in Batu City.

Meanwhile, the intent and purpose of this research is to see the role of agro-tourism in environmental sustainability. To be able to analyze the relationship between agro-tourism and environmental sustainability, it was carried out by comparing the environmental performance of agro-tourism in three different villages in Batu City with different vegetation characteristics, namely Sidomulyo Village with flower vegetation types, Sumbergondo Village with fruit (apple) plant vegetation types, and Tulungrejo Village with types of vegetable vegetation.

2 Methods

The research was conducted and placed in a rural area of Batu City, a region with high potential for agro-tourism which can offer a wide variety of agricultural-based tourism products including vegetables, flowers and fruit. Where these three agricultural products depend on meeting water needs, therefore, three areas are selected which are developed from a vegetation point of view as agro-tourism attractions selected, and compared using the Temperature Vegetation Dryness Index (TVDI) approach.

TVDI is a drought index based on the sensitivity spectrum of visible and near infrared light on vegetation behavior and vegetation stress conditions associated with water shortages. In general, NDVI, the Normalized Vegetation Index will increase along with a decrease in surface temperature (LST). This is related to the ability of vegetation to regulate temperature through latent heat transfer, namely heat transfer through evapotranspiration. Radiation absorbed and the amount of water available at the soil surface are the two main elements that regulate surface temperature. When the availability of water becomes minimal whether the land is vegetated or not, the surface temperature will increase. The consideration for using the TVDI approach in this study is because TVDI shows better linearity in vegetation density under existing conditions [13]. Following are the details of the equations used in the study:

$$\textbf{NDVI} = \frac{(\rho BOANIR - \rho BOARED)}{(\rho BOANIR + \rho BOARED)}, \quad \textbf{(1)}$$

$$\textbf{LST} = \frac{Tb}{1+(\lambda * \frac{Tb}{\rho} * ln\varepsilon)} \quad \textbf{(2)}$$

$$\textbf{TVDI} = \frac{(LST - LST\ min)}{(LSTmax - LSTmin)}, \quad \textbf{(3)}$$

Keterangan:

NDVI : Normalized Difference Vegetation Index
LSTmin : Minimum Surface Temperature
LSTmax : Maximum Surface Temperature
LST : The observed surface temperature at a Pixels
TVDI : Temperature Vegetation Dryness Index

Table 1 Dryness Index According to TVDI:

Dryness Index	TVID
Very Wet	0 < TVDI≤ 0.2
Wet	0.2 < TVDI≤ 0.4
Normal	0.4< TVDI≤ 0.6

Dryness Index	TVID
Dry	0.6 < TVDI≤ 0.8
Very Dry	0.8 < TVDI≤ 1.0

Source: [14]

3 Results

3.1 Representation of Agrotourism Areas in Sidomulyo Village, Batu City

Sidomulyo Village is one of the agro-tourism destinations in Bumiaji District, Batu City with superior ornamental plant products. According to the vegetation analysis, using the NDVI method it is known that Sidomulyo Village has the following plantation area:

Table 2 Normalized Difference Vegetation Index (NDVI) in Sidomulyo Village, Bumiaji, Batu City

Vegetation Index	Coverage (Ha)	Percentage
High Vegetation	1.74	0.17%
Medium Vegetation	758.88	74.28%
Very Low Vegetation	142.08	13.91%
Low Vegetation	102.38	10.02%
Non Vegetation	16.56	1.62%

Source: Analytical Resource, 2022

TVDI as an indicator used to measure the level of drought in one study area, in the context of the research The Role of Agro-tourism in Environmental Sustainability is used as a basis for measuring the role of tourist attraction in Sidomulyo Village on the basis of superior ornamental plant products seen from the level of drought

Table 3 Temperature Vegetation Dryness Index (TVDI) in Sidomulyo Village, Bumiaji, Batu City

Class	Dryness Index	TDVI	Coverage (Ha)	Pecentage
Class 1	Very Wet	0 - 0.2	100.43	41.40%
Class 2	Wet	0.2 - 0.4	108.16	44.60%
Class 3	Normal	0.4 - 0.6	33.03	13.60%
Class 4	Dry	0.6 - 0.8	0.68	0.30%
Class 5	Very Dry	0.8 - 1.0	0.00	-
	Total		242.31	100%

Sumber: Analytical Result, 2022

3.2 Agrotourism Area Representation in Sumbergondo Village, Batu City

Sumbergondo Village is one of the agro-tourism destinations in Bumiaji District, Batu City with superior apple products. According to the vegetation analysis, using the NDVI method, it is known that Sumbergondo Village has the following plantation areas:

Table 4 Normalized Difference Vegetation Index (NDVI) di Desa Sumbergondo, Bumiaji, Kota Batu

Vegetation Index	Coverage (Ha)	Percentage
High Vegetation	115.27	2.18%
Medium Vegetation	3972.54	74.98%
Very Low Vegetation	450.93	8.51%
Low Vegetation	748.27	14.12%
Non Vegetasi	10.95	0.21%

Source: Analytical Result, 2022

TVDI as an indicator of drought level measurement in a certain study area, in the context of The Role of Agrotourism on Environment Sustainibility study, it function as a fundamental on measuring the Tourism Attraction in Sumbergondo Village with apple product as its superior based product reviewed from the drought level.

Table 5 Temperature Vegetation Dryness Index (TVDI) in Sumbergondo Village, Bumiaji, Kota Batu

Class	Dryness Indeks	TDVI	Coverage (Ha)	Percentage
Class 1	Very Wet	0 - 0.2	519.88	28%
Class 2	Wet	0.2 - 0.4	663.73	36%
Class 3	Normal	0.4 - 0.6	489.80	27%
Class 4	Dry	0.6 - 0.8	156.02	8%
Class 5	Very Dry	0.8 - 1.0	10.67	1%
	Total		1840.10	100%

Source: Analytical Result, 2022

3.3 Agrotourism Area Representation in Tulungrejo Village, Batu City

Tulungrejo Village is one of several agrotourism destination on Bumiaji District, Batu City with apple as its superior product. Based on a vegatation analysis, using NDVI method, it is known that Tulungrejo Village has total land coverage as presented in the following table :

Table 6 Normalized Difference Vegetation Index (NDVI) di Desa Tulungrejo, Bumiaji, Kota Batu

Vegetation Index	Coverage (Ha)	Percentage
High Vegetation	672.55	10%
Medium Vegetation	5289.11	77%
Very Low Vegetation	364.37	5%
Low Vegetation	541.82	8%
Non Vegetation	42.15	1%

Source: Analytical Result, 2022

TVDI as an indicator of drought level measurement in a certain study area, in the context of The Role of Agrotourism on Environment Sustainibility study, it function as a fundamental on measuring the Tourism Attraction in Tulungrejo Village with apple product as its superior based product reviewed from the drought level.

Table 7 Temperature Vegetation Dryness Index (TVDI) di Desa Tulungrejo, Bumiaji, Kota Batu

Class	Dryness Index	TDVI	Coverage (Ha)	Percentage
Class 1	Very Wet	0 - 0.2	1333.49	48%
Class 2	Wet	0.2 - 0.4	924.75	33%
Class 3	Normal	0.4 - 0.6	447.06	16%
Class 4	Dry	0.6 - 0.8	88.80	3%
Class 5	Very Dry	0.8 - 1.0	0.00	-
	Total		2794.10	100%

Source: Analytical Result, 2022

4 Discussion

The result of the study shows that most of the research related with agrotourism in the last few years indicating a shift in consumer preference from conventional tourism to agrotourism. Besides, earlier study about agrotourism development are focused on qualitative method, resulting in the shortcoming of this paper on methodology contribution.

The result of the analysis in Batu City shows that agrotourism could be promoted as one of the alternative on environment sustainability. In this research 3 (three) village with agrotourism potential are chosen as a subject of case study in order to be given a rating towards agrotourism's role on environment sustainability. In general, environment continuity on the potential tourism site could be measured through dryness index which has an impact on water crisis for the locals where drought as a normal climate feature and recurring phenomena has a consequence

towards the decreasing of rainfall or temperature in a long period of time. On many cases, an escalation of drought phenomena are positively corelated on vegetation in most of the region [15], [16]. This study adds an understanding about vegetation ability on withhold drought and from this research findings give an evidence to support the response towards drought threat as a result of the increasing activity of tourism.

In this research, vegetation index are divided into 5 (Five) category, which is High Vegetation, Medium Vegetation, Very Low Vegetation, Low Vegetation, and Non Vegetation. The higher the vegetation indeks has a positive correlation towards the ability to minimize drought risks.

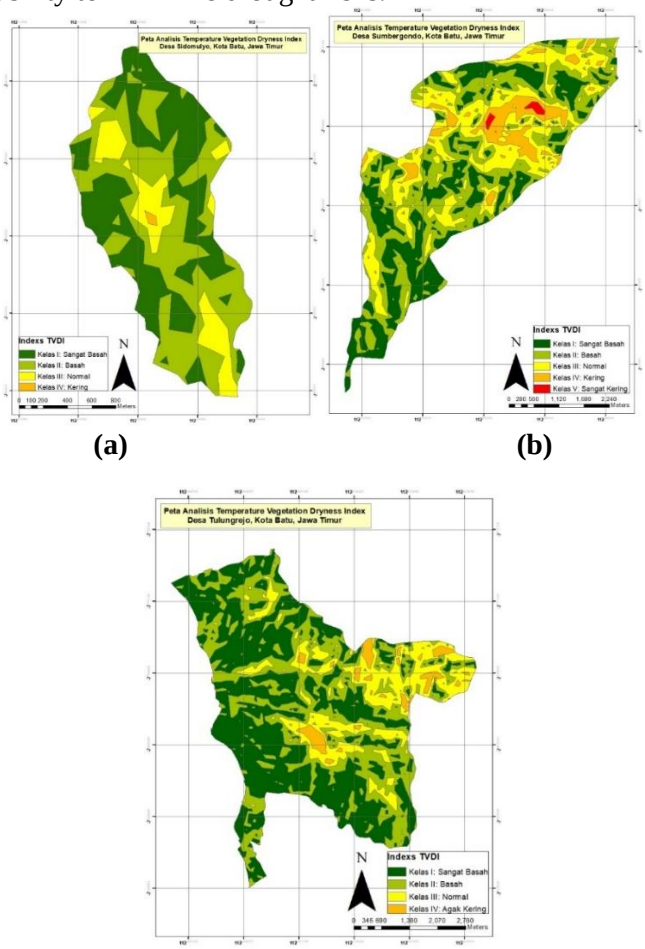

Figure 1 Map Analysis *Temperature Vegetation Dryness Index*
Batu City, East Java
Source: Analytical Result, 2022

NDVI and TVDI application on this research, shows that there is an evidence on correlated response between vegetation and drought that affected by an increasing tourism activity resulting in drought potential escalation which endanger a regional system ecology.

Picture 1 Map Analysis Temperature Vegetation Dryness Index shows a significant difference on drought level in each study location. Tulungrejo Village with the highest vegetation index compared to Sumbergondo Village and Sidomulyo Village with Vegetation Index of 10%, has a land coverage percentage with the lowest drought level on level 1 and 2. Meanwhile, in Sumebergondo Village with coverage percentation accumulation with *very low*, *low*, and *non-vegetation* Vegetation Indeks higher than the two other village on 22.84% has a relation towards drought response that shown by TVDI index normal classification (Level 3) with 27% percentage, dry (Level 4) with 8% percentage, and very dry (Level 5) with 1% percentage.

5 Conclusion

Analytical result on the 3 (three) village which is Sidomulyo Village, Sumbergondo Village, and Tulungrejo Village shows a correlation between coverage index that shown with *Normalized Difference Vegetation Index* (NDVI) approach on each village on drought level that are shown by *Temperature Vegetation Dryness Index*.

The changes in tourism tren are expected to increase the role of agrotourism in increasing environment sustainibility in emphasizing agricultural plantation as a tourism charm by taking care of water availibility that are shown by the low drought level on an area with high vegetation in Batu City.

Nevertheless, this study has some limitations that must be resolved in future research. First, how can agro-tourism be questioned more through ecosystem services. Second, how is the ecological risk assessment model of agro-tourism development. Third, a comparison of approaches in determining the results of an ecological risk assessment of the development of agro-tourism.

References

[1] K. C. Seto, R. Sánchez-Rodríguez, and M. Fragkias, “The New Geography of Contemporary Urbanization and the Environment,” *http://dx.doi.org/10.1146/annurev-environ-100809-125336*, vol. 35, pp. 167–194, Oct. 2010, doi: 10.1146/ANNUREV-ENVIRON-100809-125336.

[2] "What does astycene mean - Definition of astycene - Word finder." https://findwords.info/term/astycene (accessed Sep. 14, 2022).
[3] C. Aall and K. Koens, "The discourse on sustainable urban tourism: The need for discussing more than overtourism," *Sustain.*, vol. 11, no. 15, pp. 1–12, 2019, doi: 10.3390/su11154228.
[4] D. Edwards, T. Griffin, and B. Hayllar, "Urban Tourism Research. Developing an Agenda," *Ann. Tour. Res.*, vol. 35, no. 4, pp. 1032–1052, 2008, doi: 10.1016/j.annals.2008.09.002.
[5] "The Link Between Tourism and Climate Change — Sea Going Green," Mar. 03, 2020. https://www.seagoinggreen.org/blog/the-link-between-tourism-and-climate-change (accessed Sep. 14, 2022).
[6] M. Lenzen, Y. Y. Sun, F. Faturay, Y. P. Ting, A. Geschke, and A. Malik, "The carbon footprint of global tourism," *Nat. Clim. Chang. 2018 86*, vol. 8, no. 6, pp. 522–528, May 2018, doi: 10.1038/s41558-018-0141-x.
[7] M. Goretti *et al.*, *Tourism in the Post-Pandemic World*, no. 21. 2021.
[8] Asian Development Bank, "Domestic Tourism in Southeast Asia: Opportunities and Pathways - Matthias Helble and Jaeyeon Choe | Asian Development Bank." https://www.adb.org/news/op-ed/domestic-tourism-southeast-asia-opportunities-and-pathways-matthias-helble-and-jaeyeon (accessed Oct. 22, 2022).
[9] F. Nearchou and E. Douglas, "Traumatic Distress of COVID-19 and Depression in the General Population: Exploring the Role of Resilience, Anxiety, and Hope," *Int. J. Environ. Res. Public Health*, vol. 18, no. 16, Aug. 2021, doi: 10.3390/IJERPH18168485.
[10] S. Zach, J. Fernandez-Rio, A. Zeev, M. Ophir, and S. Eilat-Adar, "Correction to: Physical activity, resilience, emotions, moods, and weight control, during the COVID-19 global crisis," *Isr. J. Health Policy Res.*, vol. 10, no. 1, p. 55, Dec. 2021, doi: 10.1186/S13584-021-00489-3.
[11] "UNWTO Recommendations on Tourism and Rural Development – A Guide to Making Tourism an Effective Tool for Rural Development," *UNWTO Recomm. Tour. Rural Dev. – A Guid. to Mak. Tour. an Eff. Tool Rural Dev.*, Sep. 2020, doi: 10.18111/9789284422173.
[12] S. Rauniyar, M. K. Awasthi, S. Kapoor, and A. K. Mishra, "Agritourism: structured literature review and bibliometric analysis," *Tour. Recreat. Res.*, vol. 46, no. 1, pp. 52–70, 2021, doi: 10.1080/02508281.2020.1753913.
[13] A. Bannari, H. Asalhi, and P. M. Teillet, "Transformed difference vegetation index (TDVI) for vegetation cover mapping," *Int. Geosci. Remote Sens. Symp.*, vol. 5, no. March, pp. 3053–3055, 2002, doi: 10.1109/igarss.2002.1026867.
[14] I. Sandholt, K. Rasmussen, and J. Andersen, "A simple interpretation of the surface temperature/vegetation index space for assessment of surface moisture status," *Remote Sens. Environ.*, vol. 79, no. 2–3, pp. 213–224, Feb. 2002, doi: 10.1016/S0034-4257(01)00274-7.

[15] Z. Gao, W. Gao, and N. Bin Chang, "Integrating temperature vegetation dryness index (TVDI) and regional water stress index (RWSI) for drought assessment with the aid of LANDSAT TM/ETM+ images," *Int. J. Appl. Earth Obs. Geoinf.*, vol. 13, no. 3, pp. 495–503, Jun. 2011, doi: 10.1016/J.JAG.2010.10.005.

[16] X. Shi, F. Chen, H. Ding, M. Shi, and Y. Li, "Assessing Vegetation Ecosystem Resistance to Drought in the Middle Reaches of the Yellow River Basin, China," *Int. J. Environ. Res. Public Health*, vol. 19, no. 7, Apr. 2022, doi: 10.3390/IJERPH19074180.

Proceedings of the 3rd ITB Graduate School Conference ISSN: 2963-718X
Enhancing Creativity in Research Through Developing Innovative Capabilities
December 21, 2022

Cost-benefit Analysis Elements for Green Building Concepts in Architectural Projects

Furry Andini Wilis[1,2,*] & Dewi Larasati[2]

[1] Doctoral Student of Architecture, Bandung Institute of Technology
[2]Department of Architecture, Bandung Institute of Technology
[*]Email: furryandini@gmail.com

Abstract. Cost-benefit analysis is an approach used to determine a project's costs and benefits, including architectural projects that apply the green building concept. Through the application of cost-benefit analysis, it can be seen how much additional costs must be incurred as well as how many additional benefits from an architectural project if implementing the green building concept. This article aims to identify the cost and benefit elements when the green building concept is applied to an architectural project. The literature study results show that the cost elements are generally divided into soft costs and hard costs. As for the benefit elements, they can be grouped into environmental benefits, social benefits, and economic benefits related to energy savings.

Keywords: *cost-benefit analysis; green building; architectural projects; cost elements; benefit elements.*

1 Introduction

Cost-benefit analysis (CBA) is known as an analysis of the rate of return and the principles are the same as the procedures followed in the evaluation of investment projects ([1]). In addition, CBA is also known as a systematic and analytical process for comparing benefits and costs in evaluating a project or program which is often social in nature. CBA is the basis for government decision-making and is established as a formal technique for making informed decisions about the use of community resources [2]. CBA is often used to verify the economic viability of public projects because it is often difficult to ascertain the economic impact of public projects. CBA can also be said to be a framework that helps predict whether a project will improve social welfare in the future [3].

As we know that green building is a process of creating buildings and supporting infrastructure that can reduce the use of resources, a healthier environment for its inhabitants, and minimize negative impacts on ecosystems, both local, regional and global ecosystems [4]. In addition, the World Green Building Council [5] defines green buildings as buildings that, in their design, construction or

operation, reduce or eliminate negative impacts and can create positive impacts on the climate and environment.

Green building design and development have become part of the global response to climate change and the depletion of natural resources. Indonesia as one of the most populous countries in the world is an important part of the global movement toward a sustainable future. There are three main factors in green building requirements that make them very important, namely health, energy saving, and climate change [6].

If referring to PUPR Ministerial Regulation No. 21 of 2021 concerning Assessment of the Performance of Green Buildings, green buildings mean buildings that meet building technical standards and have significant measurable performance in saving energy, water, and other resources through the application of green building principles according to their functions and classifications in every maintenance [7].

2 Research Method

The methodology used in this paper consist of several stages, including:

1. Systemic literature review and collection of research examples related to the application of green building concepts and cost-benefit analysis.

2. Grouping literature into several sections, such as Application of Cost-Benefit Analysis in Architectural Projects with the Green Building Concept dan Elements of Cost-Benefit for the Application of the Green Building Concept in Architectural Projects.
3. Explanation of the results of the literature review.
4. Drawing conclusions.

3 Application of Cost-Benefit Analysis in Architectural Projects with the Green Building Concept

Discussion of the application of cost-benefit analysis in architectural projects with a green building concept is more related to housing which is carried out to be able to see the increased costs and benefits obtained, as in research conducted by [8]–[12]. However, research on office buildings has also been conducted by [13], [14].

Research by Bradshaw et al., 2005, looks at the cost-benefits of green affordable housing in the United States. The cost data used in this study consists of total development costs, costs from the LEED category along with other components

and systems, savings costs based on the LEED category, operational costs, material replacement/renovation costs, and NPV (net present value). The results of the study show that green affordable housing is financially feasible in the long run. Although indeed with the current system to assess the financial feasibility of green affordable housing is too burdensome for initial capital costs. 14 of the 16 case studies studied demonstrated project benefits exceeding project costs over the life of the building 30 years, with an average NPV of over $15,000 per unit [9].

Then Williams and Bourland, 2010, conducted research related to affordable green housing in the United States. The results show that the total development cost is around 9-18% above the cost for conventional affordable housing. The average cost increase as a result of green features was 2.4% (median 2.9%). Experience from the company and a growing number of affordable housing developers and homeowners increasingly demonstrates that certain green methods and materials have lower initial costs than conventional construction practices and can help offset any gradually higher costs associated with other green features in projects [12].

Furthermore, Deniz et al. in 2018 conducted a study on affordable homes with energy-efficient designs in Philadelphia, which has the highest poverty rate in the USA. It compares the estimated cost of the baseline design with the proposed good-performing design alternatives. Design alternatives with good performance have higher estimated costs. However, the payback duration of the improvements gained and reduced utility costs are also considered in the analysis to enable affordable prototyping. In the final stage of the analysis, the solar panels were reduced from 20 to just 11. The results show that the prototype investment has a payback period of more than 16 years with fewer ongoing operating costs than a typical house [10].

Research conducted by Vyas & Jha, 2018 in India, shows that green buildings have advantages, both for business and the environment. Investment in green building is economically profitable due to reduced CO2 emissions. Financial analyzes conducted to evaluate the economic viability of green buildings prove to be financially attractive over their life cycle. Cost analysis of government of India green building projects shows that although green building construction costs are higher than conventional costs, they are in the range of 2-5% for 3-star rated buildings, and 5-17% for 5-star rated buildings when environmental aspects are considered. Payback periods range from 2.04-7.56 years for 3-stars and 2.37-9.14 years for 5-stars. Furthermore, it is also known that the life cycle cost of green buildings is positive, which means that the savings generated from green buildings can cover the additional costs of green buildings [11].

Ade-Ojo & Ogunsemi, 2019, conducted a study related to the prediction of green affordable house financing in Nigeria from several aspects such as site design, water quality and conservation, energy and environment, indoor air quality, and materials. The results of the study show that these aspects make green buildings more expensive when compared to conventional buildings. However, this can be predicted and assessed through three approaches. The first approach sees that green building features are only considered as an additional 'task' compared to the decision-making process. The second approach is to examine existing cost predictions and budgets. the final approach is to compare the costs of similar projects as alternatives [8].

Research from Latief et al., 2017, discusses how to optimize the premium cost of 12 new office buildings that have been green building certified based on the GREENSHIP assessment system in Indonesia. The results of the study found that three main aspects affect the premium cost of new green buildings in Indonesia, namely energy efficiency and conservation, site management, and material sources and cycles. The platinum and gold levels have insignificant differences in energy and water savings when compared to the silver-to-gold levels. The silver level has the fastest return period among the existing levels. However, investors or developers prefer gold-level green buildings because of a medium premium cost with energy savings and medium to high water savings [13].

Furthermore, Ross et al., 2007, assessed the investment in green office buildings that are certified green buildings. The benefits are calculated based on energy consumption savings (electrical energy savings kWh x per unit tariff for the baseline and what is cost efficiency. The additional cost of implementing the green concept is $ 111,143.68 for a discount rate of 5.72% and a 10-year return scenario. Then calculate the NPV (net present value) seen from the cash flow of the resulting energy savings. The results obtained are that the NPV is 29,841.24. A positive NPV implies the financial feasibility of the project. For IRR (internal rate of return) seen from whether the IRR value is greater than the discount rate, if yes, then the decision is financially feasible. In the case studied by Ross et al., it can be seen that the IRR is 11.83% which is greater than the discount rate (5.72%). In general, it can be concluded that the application of the green building concept is financially feasible (NPV $\geq$ 0 and IRR $\geq$ 5.72%) [14].

4 Elements of Cost-Benefit for the Application of the Green Building Concept in Architectural Projects

The application of the green building concept from several works of literature is stated to have a high cost. This additional cost is referred to as an incremental cost, which is an additional investment cost, which can increase in green building projects compared to ordinary buildings [15]. In general, increased economic

benefits are considered as dominant benefits, meaning that economic benefits are directly brought to investors and consumers. Green building has great profit potential [16]. Wu and Ma, then divide the incremental cost components into indirect costs and direct costs, as shown in Figure 1.

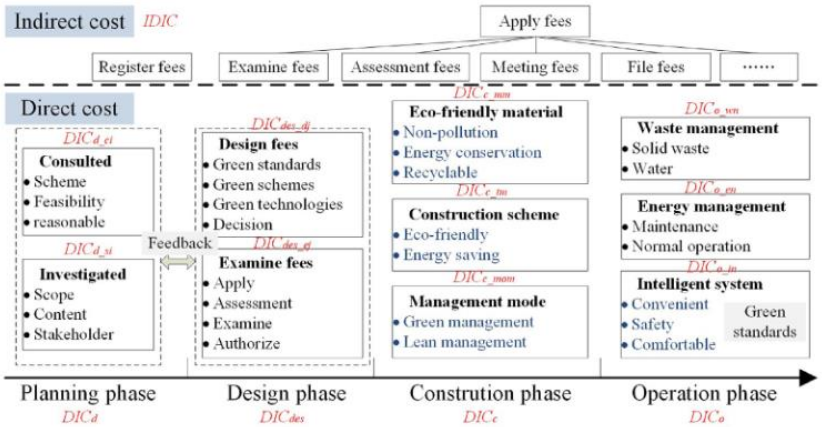

Figure 1 Indirect Cost and Direct Cost Element Components [12]

According to Northbridge Environmental Management Consultants, 2003, the costs of green building projects are divided into pre-construction and post-construction costs. Pre-construction costs include soft costs and hard costs. Soft costs are related to design, commissioning and documentation costs [17]. Meanwhile, hard costs are related to construction, materials, and building service costs [18]. Post-construction costs consist of operational costs from energy consumption, water use, maintenance, and management. Benefits accrue, including savings and financial benefits during construction and post-construction (such as higher property market values, higher rents, marketing opportunities resulting from social benefits, higher energy savings, less sick leave and higher productivity) [19].

Then Ross et al., 2007, looked at the costs of green building projects as seen from the construction costs (materials and labor wages), the design team (architects, HVAC engineers, energy commissioners, energy architects, light design, site planners, misc. fees), and LEED certification costs (LEED administration fees, fees from renewable energy credits) [14].

Fan et al., 2018, created a framework related to cost-benefit analysis in green building projects. from the interviews and literature review conducted, it was found that there are extra costs for green building projects which consist of actual costs and transaction costs. Actual costs consist of land costs, consulting fees, construction costs, and certification costs. Meanwhile,

information search costs, research/learning costs, negotiation/coordination costs, approval fees, monitoring costs, and verification costs are included in transaction costs. Apart from extra costs, there are also extra benefits which consist of actual benefits and hidden benefits. Allowance for gross floor area, increase in the value of green buildings, energy savings, and water savings are included in the actual benefits. Then what includes hidden benefits include reputation/branding from the private sector, private sector competitiveness, job opportunities for the environment, health/productivity (indoor), and environmental benefits (outdoor) [15].

Abidin & Azizi, 2021, focuses on soft costs research on green building projects. There are eight elements of soft costs which are referred to as project preparation costs, consultant fees, green certification, pre-development charges, contribution fees, marketing costs, project overhead costs, and security of the funding [20]. Meanwhile Ade & Rehm, 2021., divides the cost element into two parts, namely hard construction costs and soft construction costs. Hard costs relate to tangible objects that need to be purchased to complete a dwelling, such as insulation, glass, etc. Meanwhile, soft costs include administration and audit fees, appraiser fees and additional design costs [21].

Furthermore, Long et al., 2021, looked at the increased cost of green building projects from primary and secondary indicators, as shown in **Table 1**. He explained that the increased cost of implementing green buildings is an investment [22].

Table 1 Incremental Cost Indicator [18]

Primary Indicators	Secondary Indicators
Energy saving and utilization	Energy-saving maintenance structure (energy-saving doors and windows and building floor cost)
	Energy-saving lighting system (cost difference between natural lighting and green lighting)
	Renewable resource systems (cost solar energy, geothermal energy, and wind energy)
Land saving and outdoor environment	Site utilization (increased cost of abandoned sites and underground space)
	Outdoor environment (cost of noise control, ground landscape design, three-dimensional greening)
	Pervious ground (cost increase caused by permeable paving method and permeable floor tile)
Water saving and utilization of water resources	Water-saving system (water source collection, reasonable discharge, etc.)
	Water-saving equipment (cost difference of water-saving faucet and water-saving sanitary ware compared with ordinary equipment)
	Water recycling (increased cost of clearing roads, toilet cleaning, air conditioning cooling water)
Material savings and utilization	Green building materials (increased cost of construction materials with little environmental impact and no pollution)
	Material recycling (cost increase to improve the utilization of building materials)
	Waste recycling (increased cost of waste treatment)

From the literature described above, it can be concluded that the cost elements in green building projects are divided into hard costs (related to construction, material, service, and operational costs) and soft costs (related to as shown in Table 2.

Table 2 Mapping Cost Elements in Green Building Architectural Projects

Cost Elements	Factors studied in research	Source
Soft cost/ non-construction cost	• Consultant fee • Design fee • Certification fee • Certificate fee • Documentation fee • Research fee • Marketing fee • Commissioning fee • Supervision fee	[14]–[17], [20], [21], [23]
Hard cost/ construction cost	• Material cost • Construction cost • Waste management cost • Labor cost • Operational cost • Service cost • Land cost	[14], [16], [18], [19], [21]–[23]

Furthermore, the benefit element in the application of the green building concept is important because it can be used as a reference for calculating benefits in a cost-benefit analysis. Ross et al., 2007, saw the benefits of implementing the green building concept through empirical evidence of saving energy consumption [14].

Grouping the benefits of implementing the concept of green building/sustainability into three major groups, namely environmental benefits/environmental benefits, social benefits/social benefits, and economic benefits/economic benefits has been carried out by several researchers [16], [22], [24]–[26]. The grouping of benefits is carried out based on sustainable building and construction or sustainable (green) construction so the benefit elements tend to be very broad [24]–[26]. Meanwhile, other research has focused more on architectural projects [16], [22].

Research from Long et al., 2021, saw that there are incremental costs and benefits to green buildings. The existing benefits are still divided into three main groups, namely environmental benefits, social benefits, and economic benefits. Energy savings, government subsidies, and material savings go into the economic profit. Meanwhile, social benefits are related to improving welfare and increasing income. Then the environmental benefits consist of

reducing pollution, extending the life of the building, and reducing the occurrence of disease [22].

Wu and Ma, 2022, focus more on research on additional benefits that have an immediate impact when implementing the green building concept. Implicitly, there are benefits to society – society benefits (health, comfort, and waste reduction) and explicitly to water, energy, land, and materials which are included in the economic benefits. The results of the perceived benefits have an indirect impact on the environment (environmental benefits) such as reduced CO2 emissions and CO2 absorption as shown in Figure 2.

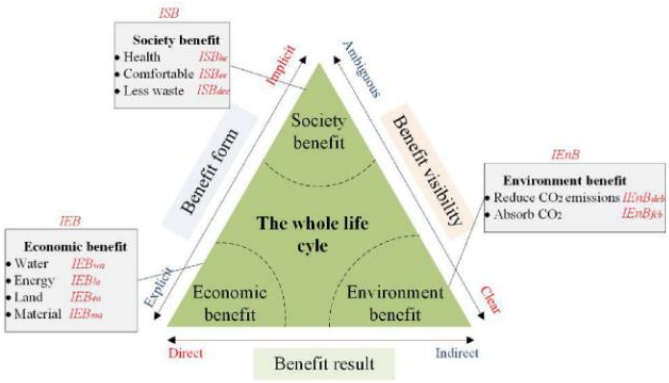

Figure 2 Benefits of Implementing Green Building [12]

Fan et al., 2018, divided benefits into 2, namely actual benefits and hidden benefits. Actual benefits relate to benefits that can be directly felt by the stakeholders involved, such as the GFA (gross floor area) concession, increasing the value of green buildings, saving energy, and saving water. While hidden benefits are benefits that are not directly felt but whose impact is still felt, some of them are reputation/image in the private sector, competition in the private sector, job opportunities for the community, health/productivity (indoors), and benefits for the environment (outdoors) [15].

Another benefit that is felt is the cost savings from reducing energy consumption in buildings. In addition, there are also indirect benefits that can improve health [27] The same thing was also mentioned by Assylbekov et al., 2021, who stated that green buildings can reduce negative impacts on the environment through water and energy efficiency. In addition, the application of the green building concept, especially water and energy efficiency, has the potential to reduce life cycle costs by around 40% [28].

Based on the literature related to the elements of benefit, it can be concluded that the benefits of implementing the green building concept are very broad. However, the majority of studies state that the perceived benefits are related to energy

efficiency. Derivative elements of benefits related to energy efficiency can be seen in Table 3.

Table 3 Mapping Benefit Elements in Green Building Architectural Projects

Benefit Elements	Factors studied in research	Source
Environmental benefits	• Energy efficiency • Water efficiency • Reduce CO_2 emissions	[16], [22], [25]–[28]
Economic benefits	• Saving on energy consumption cost • Saving on water consumption cost • Saving on operational and management cost	[16], [25], [26]
Social benefits	• Improved air quality • Comfort and health • Waste reduction	[16], [24]

5 Conclusion

Implementing green building concepts in architectural projects will increase the investment cost, called incremental cost. But there is also the incremental benefit that the stakeholder of the project can get. One of the approaches that can be used to determine the incremental cost and benefit in the green architectural project is cost-benefit analysis. As per the literature review, there are cost elements, including soft cost or non-construction cost and hard cost or construction cost related. While for benefit elements, it can conclude into three groups, environmental benefit, economic benefit, and social benefit.

Acknowledgment

This paper is part of Riset Inovatif-Produktif (RISPRO) with the title Implementation of Low Energy Affordable Apartment in The Hot-Humid Climate of Indonesia (Towards Nearly Zero Energy Building/ NEZB) funded by Lembaga Pengelola Dana Pendidikan (LPDP) Kementerian Keuangan Republik Indonesia.

References

[1] G. Psacharopoulos, “The Cost-Benefit Model,” 1987.
[2] E. J. Mishan and E. Quah, “Cost–Benefit Analysis, 5th Edition,” 2007.

[3] E. Shin and H. Kim, "Benefit-Cost analysis of Green Roof initiative projects: The case of Jung-gu, Seoul," *Sustainability (Switzerland)*, vol. 11, no. 12, 2019, doi: 10.3390/SU11123319.

[4] Global Green USA, *Blueprint for Greening Affordable Housing*. Washington DC: Island Press, 2007.

[5] WGBC, "What is green building?," 2022. https://www.worldgbc.org/what-green-building (accessed Oct. 19, 2022).

[6] B. Wiryomartono, "'Green building' and sustainable development policy in Indonesia since 2004," *International Journal of Sustainable Building Technology and Urban Development*, vol. 6, no. 2, pp. 82–89, Apr. 2015, doi: 10.1080/2093761X.2015.1025450.

[7] Kementerian PUPR, *Peraturan Menteri PUPR No. 21 Tahun 2021*. Indonesia: https://jdih.pu.go.id/detail-dokumen/2881/1#div_cari_detail, 2021.

[8] O. C. Ade-Ojo and D. R. Ogunsemi, "Cost Prediction for Green Affordable Housing in Nigeria," in *Greening Affordable Housing: an interactive approach*, CRC Press Taylor & Francis Group, 2019, pp. 265–281.

[9] W. Bradshaw *et al.*, "The Costs and Benefi ts of Green Affordable Housing What is Green Affordable Housing? Community Based Organizations as Vehicles for Green Affordable Housing Challenges to Building Green Affordable Housing Why Focus on Affordable Housing?," 2005.

[10] G. Ozcan-Deniz, R. Fryer, and A. de C. A. Ferreira, "The design of net-zero-energy affordable housing in Philadelphia," *Designs (Basel)*, vol. 2, no. 3, pp. 1–13, Sep. 2018, doi: 10.3390/designs2030026.

[11] G. S. Vyas and K. N. Jha, "What does it cost to convert a non-rated building into a green building?," *Sustain Cities Soc*, vol. 36, pp. 107–115, Jan. 2018, doi: 10.1016/j.scs.2017.09.023.

[12] S. Williams and D. Bourland, "Green Affordable Housing: Enterprise's Green Communities Initiative," in *Greening Our Built World*, Island Press, 2010, pp. 40–45.

[13] Y. Latief, M. A. Berawi, V. Basten, R. Budiman, and Riswanto, "Premium cost optimization of operational and maintenance of green building in Indonesia using life cycle assessment method," in *AIP Conference Proceedings*, Jun. 2017, vol. 1855. doi: 10.1063/1.4985452.

[14] B. Ross, M. López-Alcalá, and A. A. Small, "MODELING THE PRIVATE FINANCIAL RETURNS FROM GREEN BUILDING INVESTMENTS," pp. 97–105, 2007, [Online]. Available: http://meridian.allenpress.com/jgb/article-pdf/2/1/97/1770350/jgb_2_1_97.pdf

[15] K. Fan, E. H. W. Chan, and C. K. Chau, "Costs and benefits of implementing green building economic incentives: Case study of a Gross Floor Area Concession Scheme in Hong Kong," *Sustainability (Switzerland)*, vol. 10, no. 8, Aug. 2018, doi: 10.3390/su10082814.

[16] Z. Wu and G. Ma, "Incremental cost-benefit quantitative assessment of green building: A case study in China," *Energy Build*, vol. 269, Aug. 2022, doi: 10.1016/j.enbuild.2022.112251.

[17] Northbridge Environmental Management Consultants, "Analyzing the Cost of Obtaining LEED Certification," 2003.

[18] J. Yudelson and S. R. Fedrizzi, *The Green Building Revolution*. Washington, DC: Island Press, 2007.

[19] M. Khoshbakht, Z. Gou, and K. Dupre, "Cost-benefit Prediction of Green Buildings: SWOT Analysis of Research Methods and Recent Applications," in *Procedia Engineering*, 2017, vol. 180, pp. 167–178. doi: 10.1016/j.proeng.2017.04.176.

[20] N. Z. Abidin and N. Z. M. Azizi, "Soft cost elements: Exploring management components of project costs in green building projects," *Environ Impact Assess Rev*, vol. 87, p. 106545, Mar. 2021, doi: 10.1016/j.eiar.2020.106545.

[21] R. Ade and M. Rehm, "AT WHAT COST? AN ANALYSIS OF THE GREEN COST PREMIUM TO ACHIEVE 6-HOMESTAR IN NEW ZEALAND," *Journal of Green Building*, pp. 131–155, 2021, [Online]. Available: http://meridian.allenpress.com/jgb/article-pdf/15/2/131/2551371/i1943-4618-15-2-131.pdf

[22] G. Long, T. Xu, and C. Li, "Evaluation of green building incremental cost and benefit based on SD model," in *E3S Web of Conferences*, Feb. 2021, vol. 237. doi: 10.1051/e3sconf/202123703012.

[23] P. Miraj, M. A. Berawi, and S. R. Utami, "Economic feasibility of green office building: combining life cycle cost analysis and cost–benefit evaluation," *Building Research and Information*, vol. 49, no. 6, pp. 624–638, 2021, doi: 10.1080/09613218.2021.1896354.

[24] Y. H. Ahn, A. R. Pearce, Y. Wang, and G. Wang, "Drivers and barriers of sustainable design and construction: The perception of green building experience," *International Journal of Sustainable Building Technology and Urban Development*, vol. 4, no. 1. Taylor and Francis Ltd., pp. 35–45, 2013. doi: 10.1080/2093761X.2012.759887.

[25] S. Durdyev, E. K. Zavadskas, D. Thurnell, A. Banaitis, and A. Ihtiyar, "Sustainable construction industry in Cambodia: Awareness, drivers and barriers," *Sustainability (Switzerland)*, vol. 10, no. 2, Feb. 2018, doi: 10.3390/su10020392.

[26] S. W. Whang and S. Kim, "Balanced sustainable implementation in the construction industry: The perspective of Korean contractors," *Energy Build*, vol. 96, pp. 76–85, Jun. 2015, doi: 10.1016/j.enbuild.2015.03.019.

[27] O. Balaban and J. A. Puppim de Oliveira, "Sustainable buildings for healthier cities: assessing the co-benefits of green buildings in Japan," *J Clean Prod*, vol. 163, pp. S68–S78, Oct. 2017, doi: 10.1016/j.jclepro.2016.01.086.

[28] D. Assylbekov, A. Nadeem, M. A. Hossain, G. Akhanova, and M. Khalfan, "Factors influencing green building development in Kazakhstan," *Buildings*, vol. 11, no. 12, Dec. 2021, doi: 10.3390/buildings11120634.

Proceedings of the 3rd ITB Graduate School Conference ISSN: 2963-718X
Enhancing Creativity in Research Through Developing Innovative Capabilities
December 21, 2022

Analysis of Resonance in Sumatra 500 kV Extra High Voltage Transmission Line Energization Schemes

Ika Mayla Sari* & Nanang Hariyanto

School of Electrical Engineering and Informatics, Bandung Institute of Technology, Bandung, Indonesia
*Email: 23220016@std.stei.itb.ac.id

Abstract. Various analyzes are needed on the transmission line before energizing the extra-high-voltage transmission line. One of the analyzes that need to be carried out in lightly loaded double-circuit transmission lines equipped with shunt reactors is resonance analysis. Resonance causes a high increase in voltage on the line that has not been energized due to the interaction of shunt reactors with the remaining energized phase(s)/circuit(s) through capacitive coupling. This study focuses on resonance analysis which is carried out using electromagnetic transient analysis. As a result, there are several potential resonances in Sumatra 500 kV transmission line energization schemes.

Keywords: *Resonance; shunt reactor; energization; EHV transmission line.*

1. Introduction

RUPTL PLN 2021-2030 was prepared to provide information and an overview of plans for developing Indonesia's future electric power system, including the Sumatra system development plan [1]. It is stated that the construction of a 500 kV backbone transmission will be carried out in the eastern corridor connecting large-scale power plants and large load centers in Sumatra. Transmission lines aim to transfer electric power from power plants with many cheap primary energy sources (South Sumatra, Jambi, and Riau) to load center areas with limited primary energy sources (Sumbagut). Based on the RUPTL PLN 2021-2030, it is planned to build the 500 kV New Aurduri - Peranap transmission line for 210 km and the 500 kV Peranap - Perawang transmission line for 180 km, which is estimated to be Commercial Operation Date (COD) in 2021. However, there are several obstacles in the project, so the estimated COD time of the transmission section would be COD in 2022.

Figure 1 New Aurduri - Peranap - Perawang 500 kV Transmission Line

For safety and reliability of operation, it is necessary to control voltage and reactive power that meet voltage limit standards (Grid Code) [2]. The shunt reactor is used to compensate for the existing capacitance along the transmission line to limit overvoltage on the transmission line [5]. Installing shunt reactors in lightly loaded double-circuit transmission lines causes parallel resonance on the de-energized transmission line [7]. Resonance causes a high increase in voltage on the line that has not been energized due to the interaction of shunt reactors with the remaining energized phase(s)/circuit(s) through capacitive coupling. Shunt capacitances of double-circuit lines occur between conductor to ground, interphase, intercircuit-unlike phases, and intercircuit-like phases [3]. Resonance can also happen on a fully shunt-compensated transmission line. Several studies have conducted resonance analysis on extra high voltage transmission lines [3][5][6][7][8]. The results show that the transmission line is very vulnerable to resonance. Therefore it is necessary to analyze the resonance potential of Sumatra 500 kV transmission line to bring the proper energization process.

2. Methodology

Load flow analysis is carried out to analyze power flow in the network. It is the basis for further investigation, such as electromagnetic transient analysis. The Load flow analysis for the New Aurduri - Peranap - Perawang transmission line energization schemes carried out under off-peak load conditions (LWBP). The off-peak load condition was chosen as the basis for the simulation because the transmission line load is lower in this condition, which means the transmission line is more capacitive. The result of load flow simulations should meet the criteria set out in the grid code. In this case, the system voltage must be

maintained within limits according to the Sumatra Electric Power System Network Rules as stated in the Minister of Energy and Mineral Resources Regulation No. 20 of 2020. It is noted that the system voltage must be maintained within the voltage limits listed in Table 1 :

Table 1 Nominal Voltage Limits of Sumatra Transmission Line

No	Nominal Voltage	Limits
1	500 kV	+5%, -5%
2	275 kV	+5%, -5%
3	150 kV	+5%, -10%

The voltage difference for the voltage synchronization process of the transmission line should not be more than 0.03 p.u. In this research, the power system analysis was performed using DIgSILENT PowerFactory software to calculate load flow and electromagnetic transient analysis on transmission lines. Electromagnetic transient analysis is performed to calculate transient analysis in the form of resonance. The main objective of the study of electromagnetic transients is to review whether there is a potential for resonance in New Aurduri - Peranap - Perawang 500 kV line energization schemes.

The simulation of 500 kV New Aurduri - Peranap - Perawang transmission line energization schemes was carried out from the New Aurduri side with four main conditions:

- The energization of 500 kV New Aurduri - Peranap (2 circuits) and 500 kV Peranap - Perawang (2 circuits) transmission lines
- The energization of 500 kV New Aurduri - Peranap (2 circuits) and GITET 500 kV Peranap - Perawang (1 circuit) transmission lines
- The energization of 500 kV New Aurduri - Peranap (1 circuit) and 500 kV Peranap - Perawang (1 circuit) transmission lines
- The energization of 500 kV New Aurduri - Peranap (1 circuit) and 500 kV Peranap - Perawang (2 circuits) transmission lines

The simulation of 500 kV Perawang - Peranap - New Aurduri transmission line energization schemes was carried out from the Perawang side with three main conditions:

- The energization of 500 kV Perawang - Peranap (2 circuits) and 500 kV Peranap - New Aurduri (2 circuits) transmission lines
- The energization of 500 kV Perawang - Peranap (1 circuit) and 500 kV Peranap - New Aurduri (2 circuits) transmission lines
- The energization of 500 kV Perawang - Peranap (2 circuits) and 500 kV Peranap - New Aurduri (1 circuit) transmission lines

The simulation of 500 kV Perawang - Peranap transmission line energization schemes was carried out from the Perawang side with three main conditions:

- Energization of 500 kV Perawang – Peranap (Circuit/Line 1) transmission line
- Energization of 500 kV Perawang – Peranap (Circuit/Line 2) transmission line
- Energization of 500 kV Perawang – Peranap (Circuit/Line 1 or 2) transmission line

The line coupling modeling for 500 kV New Aurduri – Peranap – Perawang can be seen in Figure 2. There are two transposition points on the T180 and T352 transmission towers from the 500 kV New Aurduri - Peranap substation and two transposition points on the T168 and T264 transmission towers from the 500 kV Peranap – Perawang substation.

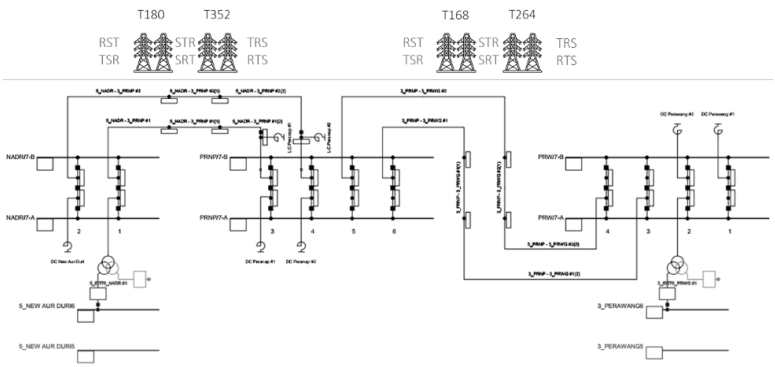

Figure 2 500 kV New Aurduri - Peranap - Perawang Transmission Line Coupling Model

The tower is a standard 500 kV (type AA) double-circuit transmission line shown in Figure 3.

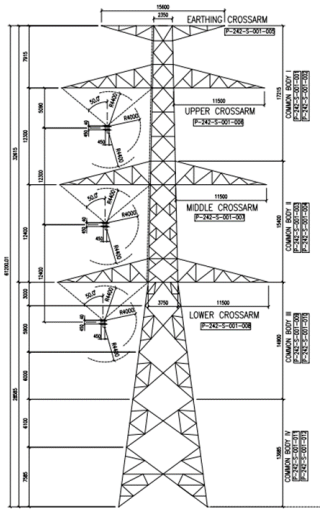

Figure 3 500 kV New Aurduri - Peranap - Perawang Transmission Tower

The shunt capacitances of the double-circuit transmission line can be seen in Figure 4.

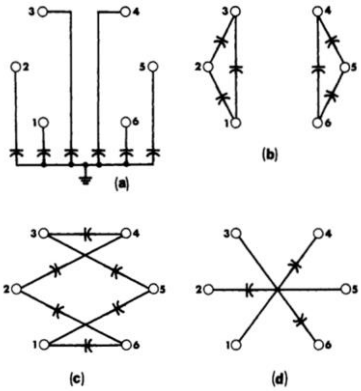

Figure 4 (a) conductor to ground, (b) interphase, (c) inter-circuit-unlike phases, and (d) inter-circuit-like phases

2.1 Transmission Line Charging

Line capacitance (network capacitance) and reactance (inductive reactance) are distributed along the transmission line. The charging MVar on extra high voltage transmission lines is calculated using the following relation.

$$r = 0.7788 \times r_a \quad (1)$$

$$C_N = \frac{2\pi k}{\ln\left(\frac{D_{eq}}{r}\right)} \quad (2)$$

$$X_C = \frac{1}{2\pi f \times C_N} \quad (3)$$

$$Q_c = \frac{U^2}{X_C} \quad (4)$$

Where r is the Geometric Mean Radius (cm), r_a is the conductor radius (cm), C_N is the capacitance to neutral (F/m), $k = 8.85 \times 10^{-12}\ F/m$, D_{eq} is the distance between the bundle centers (cm), X_C is the capacitance reactance ($\Omega.km$), f is the frequency (Hz), Q_c is the charging MVar (MVar/km), U is the line to neutral voltage (kV). Using an extra high voltage of 500 kV with 4 x ACSR Hawk bundle conductors will make the charging current (capacitive current) of the extra high voltage overhead lines significant, causing a relatively large line charging, around 1 MVar/km.

2.2 Resonance Analysis

Resonance causes a high increase in voltage on the line that has not been energized due to the interaction of shunt reactors with the remaining energized phase(s)/circuit(s) through capacitive coupling. Resonance can also occur on a fully shunt-compensated transmission line. Figure 5 explains how resonance occurs in a circuit that has not been energized.

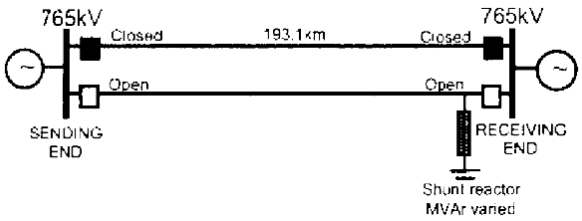

Figure 5 Resonance on the De-Energized Circuit

A reactor compensation of 70-80% (typical) should be used to avoid resonance. Several shunt reactors are on the 500 kV New Aurduri – Peranap – Perawang transmission line (diameter connected and line connected shunt reactors). The number and placement of shunt reactors in the actual conditions of the 500 kV New Aurduri – Peranap Perawang line are as follows:

- 500 kV New Aurduri substation: a shunt reactor (diameter connected, 100 MVar)
- 500 kV Peranap substation: two shunt reactors (diameter connected, each 100 MVar) and two shunt reactors (line connected, each 100 MVar) which are connected to 500 kV New Aurduri transmission lines
- 500 kV Perawang substation: two shunt reactors (diameter connected, each 100 MVar). The shunt reactors are under construction, but in this research, it is assumed that they also have been completed, so the resonance analysis in the energization schemes can be analyzed thoroughly

3. Result and Discussion

3.1 Resonance in 500 kV New Aurduri – Peranap – Perawang Transmission Line Energization Schemes

Figure 6 shows the resonance in the energization scheme for the 500 kV New Aurduri – Peranap – Perawang transmission line. Resonance occurs in line 2 of the 500 kV Perawang – Peranap transmission line when it is not energized yet.

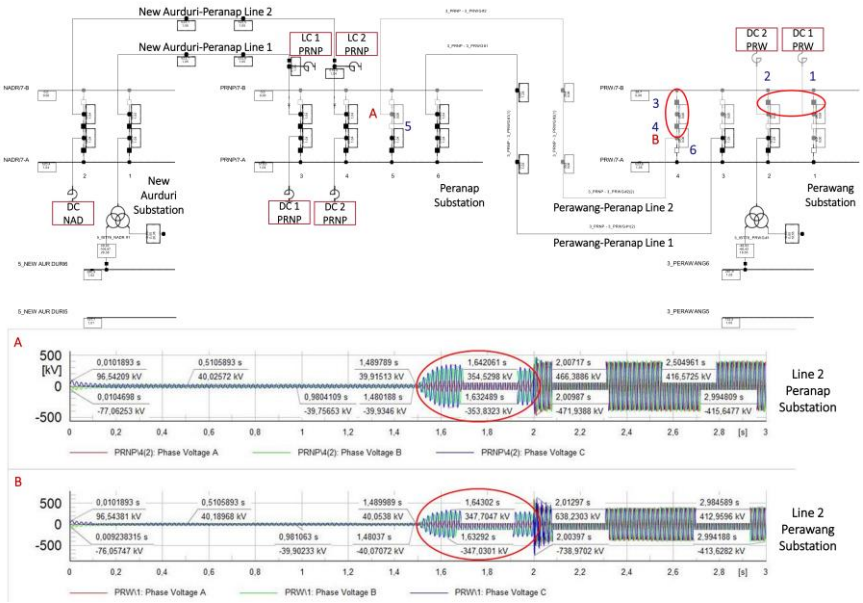

Figure 6 Resonance on the De-Energized Transmission Line (Diameter Connected Shunt Reactors)

Table 2 describes the closing steps of the circuit breaker. Closing the circuit breaker (PMT 7AB4 in Perawang substation) causes resonance and increases the voltage of line 2 up to 354.53 kVp.

Table 2 CB Closing Steps - Resonance on the De-Energized Transmission Line (Diameter Connected Shunt Reactors)

Step	CB	Transformer Tap	Time (s)	Description
1	7B1 PRW	-	0	Closing CB in Perawang Substation
2	7B2 PRW	-	0.5	
3	7B4 PRW	-	1	
4	7AB4 PRW	-	1.5	
5	7AB5 PRNP	-	2	Energizing Line 2 Perawang-Peranap
6	7A4 PRW	-	2.5	Synchronizing in Perawang Substation

Another scheme that causes resonance can be seen in Figure 7.

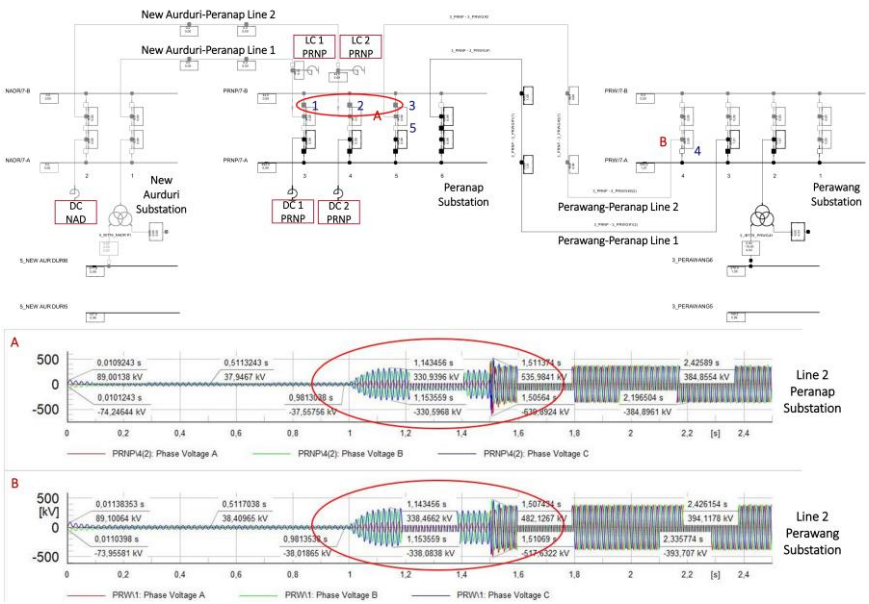

Figure 7 Resonance on the De-Energized Transmission Line (Line Connected Shunt Reactors)

Figure 7 shows the resonance in the energization scheme for the 500 kV Perawang – Peranap transmission line. Resonance occurs in line 2 of the 500 kV Perawang – Peranap transmission line when it is not energized yet. Table 3 describes the closing steps of the circuit breaker. Closing the circuit breaker (PMT

7B5 in Peranap substation) causes resonance and increases the voltage of line 2 up to 338.46 kVp.

Table 3 CB Closing Steps - Resonance on the De-Energized Transmission Line (Line Connected Shunt Reactors)

Step	CB	Transformer Tap	Time (s)	Description
1	7B3 PRNP	-	0	Closing CB of Line Connected Shunt Reactors in Peranap Substation
2	7B4 PRNP	-	0.5	
3	7B5 PRNP	-	1	
4	7A4 PRW	-	1.5	Energizing Line 2 Perawang-Peranap
5	7AB5 PRNP	-	2	Synchronizing in Peranap Substation

The schemes mentioned above cause resonance because the size of the shunt reactor's (diameter connected or line connected) compensation for line 2 has almost reached total compensation. The length of line 2 to be energized is ±180 km while the shunt reactor's capacity reaches 200 MVar. Therefore, it is necessary to change the steps of energization at this stage. From Figure 6 and 7, the energization scheme can be changed to a better one, so the resonance can be eliminated.

3.2 Changing the Energization Steps

Figure 8 shows the changing of the energization steps to avoid resonance in line 2 Perawang – Peranap (diameter connected shunt reactors).

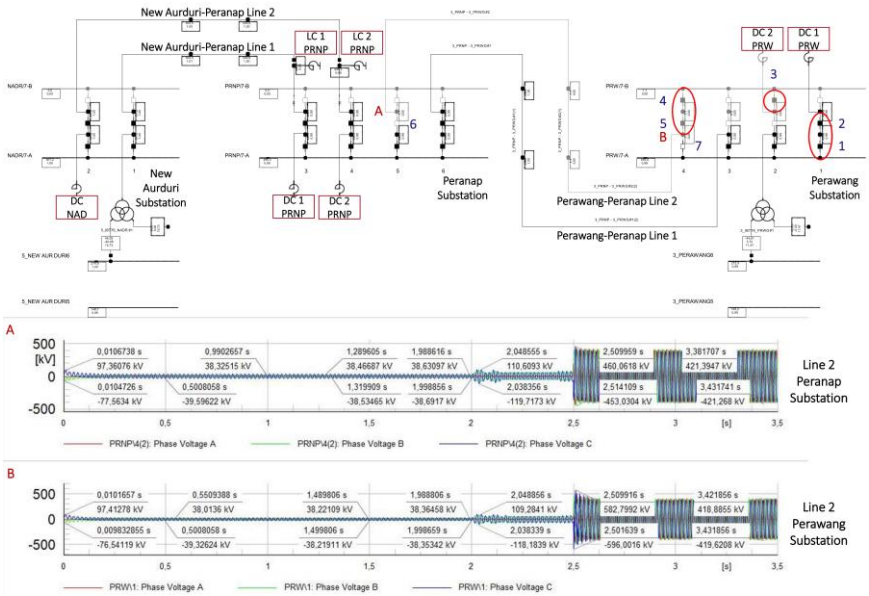

Figure 8 Changing of the Energization Scheme for Line 2 (Diameter Connected Shunt Reactors)

In Figure 8, it is found that the change in the energization steps is carried out by first energizing shunt reactor 1 in Perawang (diameter connected) before energizing line 2, which is connected to shunt reactor 2 in Perawang (diameter connected) so it does not cause resonance in line 2. Table 4 describes the changing of the energization scheme for Line 2 (diameter connected shunt reactors).

Table 4 CB Closing Steps - Changing of the Energization Scheme for Line 2 (Diameter Connected Shunt Reactors)

Step	CB	Transformer Tap	Time (s)	Description
1	7A1 PRW	-	0	Closing CB in Perawang Substation
2	7AB1 PRW	-	0.5	
3	7B2 PRW	-	1	
4	7B4 PRW	-	1.5	
5	7AB4 PRW	-	2	
6	7AB5 PRNP	-	2.5	Energizing Line 2 Perawang-Peranap
7	7A4 PRW	-	3	Synchronizing in Perawang Substation

The changing steps for the energization scheme 500 kV Perawang – Peranap (line connected shunt reactors) can be seen in Figure 9.

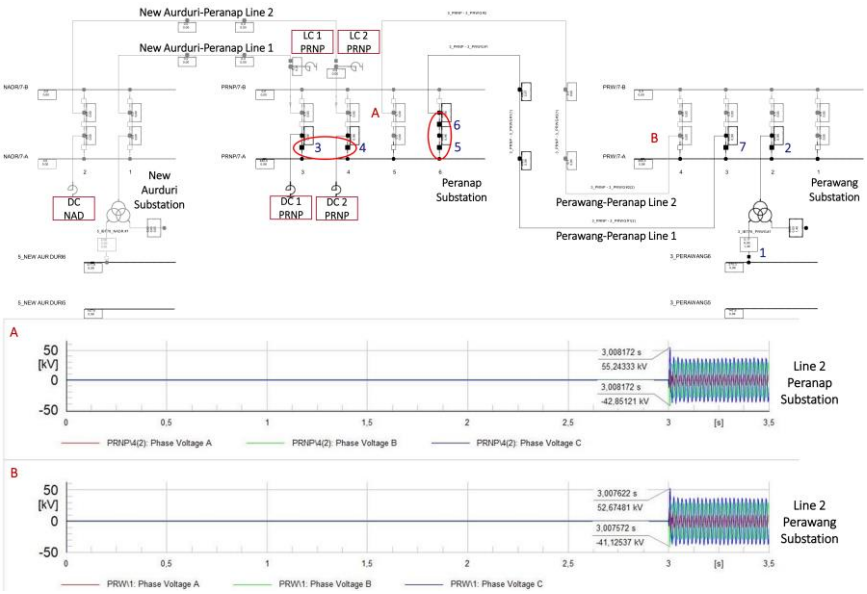

Figure 9 Changing of the Energization Scheme for Line 2 (Line Connected Shunt Reactors)

Some changes in the energizing steps of the Perawang – Peranap transmission line can only be carried out by energizing Line 1 or Line 2. Energization of 2 lines Perawang – Peranap transmission line is impossible because it causes resonance. Table 5 describes the changing of the energization scheme for Line 2 (line connected shunt reactors).

Table 5 CB Closing Steps - Changing of the Energization Schemes for Line 2 (Line Connected Shunt Reactors)

Step	CB	Transformer Tap	Time (s)	Description
1	275 kV PRW	-	0	Switching On the 500/275 kV Transformer
2	7A2 PRW	-	0.5	Energizing Busbar A in Perawang Substation
3	7A3 PRNP	-	1	Closing CB of Diameter Connected Shunt Reactors in Peranap Substation
4	7A4 PRNP	-	1.5	
5	7A6 PRNP	-	2	
6	7AB6 PRNP	-	2.5	
7	7A3 PRW	-	3	Energizing Line 1 Perawang-Peranap

4. Conclusion

From the results of resonance analysis in Sumatra 500 kV extra high voltage transmission line energization schemes, it is found that there is a potential for resonance to occur if the shunt reactor compensation for the line is almost at total compensation. Resonance causes the voltage of the de-energized transmission line to increase significantly (338.46 kVp & 354,53 kVp). Changing steps in the energization schemes could mitigate resonance.

References

[1] Rencana Usaha Penyediaan Tenaga Listrik (RUPTL) - PLN, Jakarta, 2021.

[2] Peraturan Menteri Energi Dan Sumber Daya Mineral Republik Indonesia Nomor 20 Tahun 2020 Tentang Aturan Jaringan Sistem Tenaga Listrik (*GRID CODE*), Jakarta, 2020.

[3] Edward W Kimbark, "Selective-Pole Switching of Long Double Circuit EHV Line", IEEE Transactions on Power Apparatus and Systems, Vol. Pas-95, No.1, January/February 1976.

[4] J. J. Grainger and W. Stevenson, "Power System Analysis", New York, 2008.

[5] Marta Val Escudero, Miles Redfern "Parametric Analysis of Parallel Resonance On Shunt Compensated Transmission Lines", 39th International Universities Power Engineering Conference (UPEC), 2004.

[6] E. E. Colapret and W.E. Reid, "Effects Of Faults And Shunt Reactor Parameters On Parallel Resonance", IEEE Transactions on Power Apparatus and Systems, Vol. PAS-l00, No. 2, February 1981.

[7] Marta Val Escudero, Miles Redfern, "Effects of Transmission Line Construction on Resonance in Shunt Compensated EHV Lines", International Conference on Power Systems Transients (IPST'05) in Montreal, Canada on June 19-23, 2005.

[8] Putu Agus Aditya Pramana, Buyung Sofiarto Munir, "Modeling and Simulation of Electrical Resonance in EHV Transmission Line Case Study in West Java Region 500 kV System", MATEC Web of Conferences 55, 05005 ACPEE, 2016.

Proceedings of the 3rd ITB Graduate School Conference ISSN: 2963-718X
Enhancing Creativity in Research Through Developing Innovative Capabilities
December 21, 2022

Branding Identity in Brochure as Media Branding of Destination On Purwakarta Tourism

Intan Kusuma Ayu[1, *] & Agung Eko Budiwaspada[2]

[1]Master of Design Postgraduate Student, FSRD ITB
[2]Visual Communication & Multimedia Research Group, FSRD ITB
[*]Email: intankusumayu@gmail.com

Abstract. Tourism is one of the main sectors being one of Indonesia's pride to develop the economic sector. It motivates local governments to take part in developing the tourism sector by developing their regional resources. Purwakarta tries to show its charm and identity to increase the interest of visitors to visit Purwakarta through branding by developing branding identity through communication media to achieve community significance in Purwakarta. This study aims to identify the use of branding identity in branding media through a trifold brochure using Norman Fairclough's critical discourse analysis by identifying the texts that are applied in branding discourse, production of media consumption, and the linkage on the spread of the text through the social culture. Data analysis was obtained through an interview process with the Tourism Office of Purwakarta and an interpretation process. Based on the results of the study, the identification of identity in the application branding media correlates with the spread of the text through the element of branding identity with the socio-cultural dimensions of Purwakarta. The results of the study aim to provide insight and reference for the Purwakarta Tourism Office as a reference in building potential in the tourism sector and the creative economy.

Keywords: *identity; tourism; visual branding; Purwakarta Regency.*

1 Introduction

The growth of an area is never apart from the character of the cities around it. Tourism is one of the main sectors making it the pride of Indonesia because of the abundant availability of resources in the tourism sector on various islands by utilizing its natural wealth. This provides potential for local and foreign tourists to try to visit various tourist attractions in Indonesia. As Permadi said in [1], the role of the tourism sector cannot be taken lightly because it is a major factor on building a better national and regional economy. In terms of earning foreign exchange and branding, the tourism sector in Indonesia is the main factor on implementing this matter. Supported by the ministry of tourism which issued destination branding from several tourist attractions in Indonesia, motivating local governments to take part in developing the tourism sector by developing

their respective regional resources. One of them is Purwakarta Regency which tries to show its charm and regional identity to the public to increase visitor interest in visiting Purwakarta Regency.

In this era of super-brands, a new notion has emerged that considers a city, state, region, or country as a brand. Destination branding is an interesting topic to academics and policy makers. As Dinnie said in [2], because cities tries to compete globally to attract tourism, investment and talent, as well as to achieve many other goals, the concept of brand strategy is increasingly being adopted from the commercial world and applied in pursuit of urban development, regeneration and quality of life. As stated by Pritchard and Morgan in Judisseno [3] that in the realm of tourism, a destination can be said to be a brand. And related brands are not only related to destinations, but also related to image or identity and relationships between visitors.

So far, outsiders' perception of Purwakarta Regency is as a small town that doesn't have any charm. In fact, Purwakarta has excellent tourism potential. Therefore, Purwakarta needs to communicate its tourism potential so that it could be recognized by the public. Through branding, Purwakarta Regency tries to build its regional identity, one of which is through the main graphic elements produced, one of which is through brochure printing media. The branding was carried out and implemented by the Youth Sports and Cultural Tourism Office of Purwakarta Regency, especially in the Tourism and Culture Sector, Tourism Product Promotion and Development Section led by Acep Yuli Mulya, S.Sos. The socio-cultural life of Purwakarta Regency is very close to Sundanese culture. Starting from various Sundanese cultural events, as well as several regional tourist attractions where community life is still attached to Sundanese culture. Tourism branding that has been implemented through brochures has a connection with the socio-cultural life of Purwakarta Regency. For this reason, city branding is an effort to create a city identity that is carried out through text, namely visual identity.

For this reason, researchers wants to trace back how Purwakarta Regency has established the media as a tool to promote its area and also how the media is used as a branding tool perceived by the public, especially its target audience, namely young families, both local and international. Because the media branding in the form of a brochure is intended to give identity to the tourism sector in Purwakarta Regency, it is also necessary to identify the culture and socio-cultural system in Purwakarta Regency. These three things will be explored in this research.

This research is considered important because branding is one of the marketing strategies in building the identity and image of a region. Brand identity is seen as one of the strategic business instruments and a capital in every opportunity to

form brand awareness, increasing recognition, and the quality of a brand. As well as the perceptions that arise in people's minds when visiting a place also contribute to forming the identity of a place. It is hoped that the results of this research can become a reference in developing tourism destination branding through its visual identity.

2 Literature Study

The American Marketing Association in Judisseno [3] argues that a brand is a name, term, design, symbol or any other feature that identifies the goods or services of a seller as a differentiator from the goods or services of other sellers. The legal term for a mark is a trademark. A brand can identify a single item, a family of items, or all items from that seller. when used for the company as a whole, the preferred term is trade name.

2.1 Branding

As Wheeler said in [4], branding is a disciplined process used to build awareness, attract new customers, and expand customer loyalty. Judisseno [3] argues that branding is an attempt by a product or service to show its identity. It is to convince consumers that a service or product has its own distinctive power and advantages that are beneficial to consumers (2019).

Baker in [5] suggests that there are several elements in branding, namely:
1. A name, sign, or symbol
2. Commitment
3. Distinctive added value
4. Personality and character
5. Customer thoughts and perceptions

A brand can add value, meaning, and an aura or spirit that is not visible to a product or entity - even generic products. Brand is not a physical entity. A true brand must implement a clear promise.

2.2 Destination Branding

According to Baker in [5], a destination brand is a totality of perceptions, thoughts, and feelings that customers have about a place. Meanwhile, destination branding is an organizing principle that involves the orchestration of messages and experiences associated with the place to ensure that the message is different, interesting, memorable and valuable. Successful destination branding is sure to be ingrained in the hearts and minds of customers, clearly distinguishing themselves, fulfilling valuable promises, and simplifying customer choices. The

value of a brand is built at every point of contact with the customer through an extraordinary experience with the relevant place, not by relying on the physical characteristics of the place alone.

Baker in [5] suggests that the image of a city can be considered as developing through three sequential stages:

a. Organic image.

Organic image is formed by the general awareness of the place itself through influences such as media coverage, books, films, and educational studies.

b. Marketing-induced image.

The image in this section is formed by marketing communications, such as advertising, public relations, websites and brochures. That is, this image is built through promotional messages in addition to an organic image or basic awareness of the place.

c. Experience phase.

Through the experiential phase, the image is enhanced by the person's direct encounter with the place he has visited.

2.3 Socio-Cultural

a. Social System

The social system can be described in several human activities related to the process of interaction, making contact, and associating with other humans based on certain patterns of customary behavior. And the nature adopted by the social system is concrete, observable, occurs in everyday life, and can be documented. Garna in Hisyam [6] argues that the social system is a device in social roles related to social groups that have the same values, norms, and goals. Therefore, social systems can be associated with systems of various actions.

b. Culture System

The cultural system is part of the culture that provides direction and encouragement to human behavior. And individual attitudes are generally determined based on their physical and psychological conditions. Not only that, the norms and concepts of cultural values he adheres to also play a big role.

c. Socio-Cultural System

The socio-cultural system can be said to be the whole of the elements of values, human behavior, and social systems that are related and mutually supportive to achieve the goals of human life in society.

3 Method

Through critical discourse analysis focusing on 3 dimensional levels. In the first dimension, each text simultaneously has three roles, namely identity, relation, and representation. Then at the second level, implementing discourse contains how media creators make productions in text. And at the third level, socio-cultural implementation is analyzed in three ways, namely politics which is connected to ideology and power, culture which has to do with identity and certain values, and the economy where all three can influence discourse and the media.

Through the first dimension, the analysis process of the text correlates with the Purwakarta District tourism media branding. Then through the second dimension the analysis process has a correlation with the text production process created. And in the third dimension, the analysis process has a correlation with its spread through the relevant communities. As previously explained, this research only focuses on text production to find out how the government implements tourism branding in Purwakarta Regency. The main assumption obtained through critical discourse analysis is knowing that language is used in various functions and has various impacts in it. According to Haryatmoko in [7], the resulting impact can aim to command, describe, appeal, influence, persuade, manipulate, to move a particular group. Through this, critical discourse analysis according to Fairclough can be divided into three dimensions, namely: text, discursive practice, and social praxis. When it is associated with the design object analyzed through this research, the text refers to speech, writing, or graphics related to the design elements, namely the Purwakarta tourism brochure. Then discursive practices related to everything related to the form of production and consumption of text through objects. As well as social praxis related to goals, networks, and social cultural praxis where this dimension has begun to enter into intertextual understanding. Through the three dimensions of critical discourse analysis that have been identified, it will direct and shape certain discourse systems which include the construction of genres and styles, dimensions of interpretation, and social structuring.

4 Result and Discussion

This study focuses on the branding media of Purwakarta Regency using the critical discourse analysis method of Norman Fairclough which is divided into three dimensions, namely the text dimension, the discourse practice dimension and the sociocultural dimension.

Text

a. Front Cover

Figure 1 Front Cover Trifold Brochure

Description

- At the top, there is the words "Place your story!! Only in Purwakarta"
- A writing of "Purwakarta Istimewa" with a relief background from the Wayang Gallery
- A picture of Tajug Gede Cilodong Mosque
- At the bottom it says Instagram, Twitter, Facebook and the website www.purwakarta-tourism.com

Analysis

The front page of the Purwakarta Regency Tourism Trifold brochure shows several iconic tourist attractions from Purwakarta. This brochure also invites readers to assemble stories in Purwakarta with various interesting tourist spots in Purwakarta

Interpretation

On the front page, the interpretation that appears is that Purwakarta has high cultural value seen from the existence of the Wayang Gallery tourist attraction, besides that Purwakarta is known for its religious city, it is shown that the Tajug Gede Cilodong Mosque has made it a religious icon in that place. Not only rich in culture, Purwakarta is also a place rich in religious values.

b. Back Cover

Figure 2 Back Cover Trifold Brochure

Description

- There is a photo of the Sribaduga Fountain Park at night with a photo of a colored fountain
- Logo DISPORAPARBUD Kab. Purwakarta and full address
- Purwakarta logo and Pesona Indonesia logo

Analysis

On the back page of the Purwakarta Regency Tourism Trifold brochure shows the tourist attractions of the Sri Baduga fountain at night and the logo of DISPORAPARBUD Kab. Purwakarta as well as the complete address and the Purwakarta Logo and the Pesona Indonesia Logo as the cover of the brochure section

Interpretation

On the back page, the interpretation that appears is the location of the Sri Baduga Fountain, especially when this photo was taken at night, giving the impression that you want to travel to Purwakarta by looking at the fountain at night so you can see the color of each fountain. Apart from that as the closing day or tour in Purwakarta.

c. Contents

1.

Figure 3 Content 1 Trifold Brochure

Description

- Detailed description of the location of the Sri Baduga Fountain Park
- On the right side there is a photo of a woman taking a photo with a forest in the background
- Explanation of the location of Pasin Langlang Panyawangan

Analysis

On page content 1, two tourist objects from Purwakarta are presented, namely the Sri Baduga fountain and Pasin Langlang Panyawangan as well as a detailed explanation of these places to provide information to the reader.

Interpretation

On the content page 1, the interpretation that appears is that there is a tourist attraction Pasir Langlang Panyawangan with an explanation of the green color as a background which gives a beautiful and calm impression, especially in that place, coupled with the presence of people taking pictures in that place with a beautiful forest background.

2.

Figure 4 Content 2 Trifold Brochure

Description

- Detailed description of the location of the Sri Baduga Fountain Park
- On the right side, there is an explanation of the location of the Bale Panyawangan Diorama Purwakarta with a dark gray background.

Analysis

On the content page 2, two tourist objects from Purwakarta are presented, namely the Sri Baduga fountain and Bale Panyawangan Diorama Purwakarta, at the bottom of the photo there is an explanation of the details of the place to provide information to the reader and there is information on the opening hours of the tourist attractions

Interpretation

On the contents page 2, the interpretation that appears is the existence of the Bale Panyawangan Diorama Purwakarta tourist attraction with a dark gray background, this color seems to give the impression that it is in accordance with the Bale Panyawangan Diorama because it has historical value, because it is a museum

3.

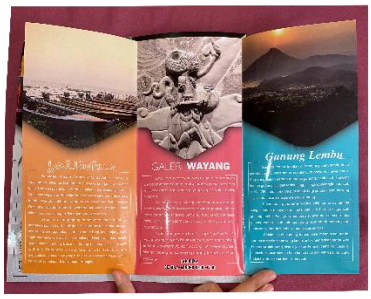

Figure 3 Content 3 Trifold Brochure

Description

- On the left side there is a photo of Jatiluhur Lake with an explanation of its location, as well as an explanation background in orange color
- In the center there is a photo of the Wayang Gallery along with the words "Puppet Gallery", and an explanation of the place with a pink/pink background
- On the right side there is a photo of Mount Lembu with the words "Mount Lembu" as well as a detailed description of the place with a blue background

Analysis

On page 3, three tourist objects from Purwakarta are presented, namely Jatiluhur Lake with an explanation of the place, as well as an explanation background in orange, the Puppet Gallery with the words "Puppet Gallery", and an explanation of the place with a pink/pink background, and On the right side there is a photo of Mount Lembu with the words "Mount Lembu" as well as a detailed explanation of the place with a blue background as well as each explanation regarding the details of the place to provide information to the reader as well as information on the opening hours of tourist attractions

Interpretation

On the contents page, 3 interpretations appear, namely Jatiluhur Lake with an explanatory background in orange, which gives a comfortable impression and is closely related to photos of the lake in the afternoon. Then there is the Puppet Gallery with a pink/pink background which gives a blabla impression, and finally there is a photo of Mount Lembu with a blue background in the description of the tourist attraction, this color gives a comfortable impression and gives a beautiful impression to the tourist attraction

Discourse Practice

In the text production section, it will relate to the editorial system that forms a context. Text production relates to discursive practice and is associated with interview results and supporting theory. In this section, the focus of the production process is on how the Tourism Office produces and represents brochure media through the visuals of the city. The production process was obtained through the results of interviews with the Head of Tourism Product Promotion and Development Section at the Purwakarta Tourism Office.

To build a brand, especially a destination brand, the Tourism Office needs to carry out in-depth preparation and planning to convey the message to be conveyed.

There are several things that apply to be explored deeper so that the message can be conveyed properly, namely:

a. Externalization

At this stage, a destination must be built so that it can be understood by the public, especially tourists. The social development of destinations in a brand is then externalized in the form of print media, namely brochure.

b. Internalization

In the next stage, the media that has been designed is socialized and its reality is seen in society. In other words, at this stage you will see the dissemination of information and one's opinion about a product. Based on this discourse, the product will be selected according to one's consideration.

The internalization stage of Purwakarta Regency branding looks at how the social system seen through public perceptions of Purwakarta branding which is implemented through the brochure media is built. So far, Purwakarta is only known for its culinary delights. However, the government does not only want Purwakarta to be known through its culinary delights, because its various tourist destinations have very good potential. Therefore, Purwakarta can become an attractive tourist destination. Through brochure media, the government tries to show that tourist destinations in Purwakarta also vary and have their own uniqueness.

The production of the text shown in the brochure refers to the existing reality. The designer text displays reality with the image of the Tajur Gede Mosque as the front cover of the brochure. Then displays a picture of the Sri Baduga Fountain show on the start page as the main show destination for Purwakarta and several other tourist destinations on the following pages. In this brochure, there are several activities and pictures of tourist destinations that want to show that Purwakarta has lots of interesting tourist destinations that can be visited.

Sociocultural Practice

Sociocultural practice is based on assumptions obtained through the interpretation of the social situation in society where it influences how discourse is formed in a media. This dimension attempts to identify how text is produced and displayed. There are several levels related to sociocultural which can be identified through Purwakarta branding where this will then influence branding discourse and ultimately have a broader meaning. These levels include:

a. Situational

Based on the results of the interview with the Tourism Office, there is the main thing they want to display through the brochure branding media about Purwakarta, namely having a variety of attractive tourist destinations. For this reason, the context in the brochure shows the diversity of Purwakarta tourist destinations. In presenting its city branding, Purwakarta took advantage of the conditions of the existing tourist destinations at that time. That way, this condition becomes the promotional branding.

b. Institutional

At this level, the social context is involved with organizational institutions in producing discourse. There is major involvement with the Department of Tourism in designing brochure media as Purwakarta branding. Not only that, the role of the brochure media has also become influential as an important media because it can be brought to the community, especially tourists as a guide for traveling.

c. Social

Through this level, the social context is formed through social factors that can have an impact on the emerging discourse. Purwakarta utilizes brochures as a media to construct imagery. Related imagery has its involvement with tourism, regional charm and is the construction of the image shown in the text. Through this image, a visual identity is designed so that it can attract the attention of tourists. Through the brochure, all positive images about tourist destinations are displayed. It aims to attract tourists to visit Purwakarta.

5 Conclusion

Critical Discourse Analysis Norman Fairclough has three dimensional stages, namely the text dimension which describes the graphic elements in the brochure media and the interpretation of how it is presented through the brochure media. Through the results of the first dimensional analysis, there are visual branding elements that present Purwakarta's character as a selling point. The dimension of discourse practice that was generated through interviews with the Tourism Office regarding text production is that there is a link between media branding and the potential tourist attraction of Purwakarta. As well as the sociocultural dimension which interprets the results of text analysis with text production where the role of the Tourism Office is seen in wanting to attract many tourists to improve the regional economy.

Acknowledgements

This research is part of the ongoing Master of Design FSRD ITB thesis entitled "Branding Destinasi Wisata Pesona Sunda Kabupaten Purwakarta". I would like to express my gratitude and appreciation for Dr. Agung Eko Budiwaspada, M.Sn as the first supervisor of the author whose guidance has been invaluable throughout this study.

References

[1] Permadi, Ricky Noor, *Wajah Pariwisata Indonesia Saat Ini*, Kumparan, https://kumparan.com/ricky-permadi/wajah-pariwisata-indonesia-hari-ini-1tfSJ24q0lz/full, (5 Mei 2020). (https://kumparan.com/ricky-permadi/wajah-pariwisata-indonesia-hari-ini-1tfSJ24q0lz/full)

[2] Dinnie, Keith., *City Branding, Theory and Cases*, Palgrave Macmillan. 2011.

[3] Judisseno, Rimsky. K., *Branding Destinasi dan Promosi Pariwisata*, PT Gramedia Pustaka Utama. 2019

[4] Wheeler, Alina., *Designing brand identity: an essential guide for the whole branding team*. John Wiley & Sons, 2017.

[5] Baker, Bill., *Destination Branding for Small Cities, The Essentials for Successful Place Branding*, Creative Leap Books. 2007.

[6] Hisyam, Ciek Julyati., *Sistem Sosial Budaya Indonesia*. Bumi Aksara, 2021.

[7] Haryatmoko D., *Critical Discourse Analysis*, PT Raja Grafindo Persada. 2019.

[8] Airey, David., *Identity Design the Definitive Guide to Visual Branding*, Rockport Publisher. 2019.

[9] Cudny, Waldemar., *City Branding and Promotion, The Strategic Approach*, Routledge. 2019.

[10] J. Phillips, Edward F. McQuarrie and Barbara., *Visual Branding, A Rhetorical and Historical Analysis*, Edward Elgar Publishing Limited. 2016.

[11] Prasetyo, Bambang D. & Nufian S. Febriani., *Strategi Branding; Teori dan Perspektif Komunikasi dalam Bisnis*, Universitas Brawijaya Press. 2020.

[12] Eringa, Klaes, and Shenghan Zhou., *A visual analysis of a cultural tourism destination*, Research in Hospitality Management, **5**(1), pp. 85-92, Jan. 2017.

Proceedings of the 3rd ITB Graduate School Conference ISSN: 2963-718X
Enhancing Creativity in Research Through Developing Innovative Capabilities
December 21, 2022

Even Mass Plutonium Effect On Plutonium Proliferation Evaluation For Delta Phase

Ismail Humolango[1], Muhamad Irfan[1], Imam Ghazali Yasmint[2], Sidik Permana[1,2,*], Sparisoma Viridi[1,2], Dwi Irwanto[1,2], & Abdul Waris[1,2]

[1]Graduate Program in Nuclear Engineering, Faculty of Mathematics and Natural Sciences, Bandung Institute of Technology Ganesha No. 10 Bandung, Indonesia
[2]Department of Physics, Faculty of Mathematics and Natural Sciences, Bandung Institute of Technology, Ganesha No. 10 Bandung, Indonesia
[*]Email: psidik@itb.ac.id

Abstract. Plutonium isotopes are one of the most popular sources used for making nuclear weapons. This is because the production of plutonium isotopes is quite a lot in nuclear reactors and has characteristics suitable for nuclear weapons. The resulting plutonium can exist in different phases depending on temperature. The delta phase is one of the phases most similar to metal, so it is easily forged and used as a nuclear weapon. The isotope of plutonium most often used as a nuclear weapon is the odd-numbered isotope because it has fissile capabilities, especially Pu-239, which is produced the most. One way to protect the isotope Pu-239 from being misused is to set up a plutonium isotope barrier. The regulation in question is adding (doping) and changing the composition of Pu-239 with an even-numbered isotope of plutonium. In this research, an analysis of the doping effect of even-numbered plutonium isotopes on Pu-239 will be carried out by focusing on the isotopic barrier parameters of plutonium, such as decay heat (DH), spontaneous fission neutron (SFN), bare critical mass (BCM) and Rossi-Alpha. These parameters were obtained by simulating a plutonium isotope fission event using a 4C MCNP with JENDL 3.3 library. Based on the simulation, the highest increase in decay heat was obtained by doping Pu-238. In the case of spontaneous fission of neutrons, it was found that Pu-238 doping gave high growth. Doping Pu-242 gives the highest increase in bare critical mass compared to other even-numbered isotopes. So for the decay heat and spontaneous fission neutron parameters, Pu-238 doping is the most effective doping. For bare critical mass and Rossi-alpha parameter, Pu-242 doping is the most effective.

Keywords: *Bare Critical Mass; Decay Heat; Isotopic Plutonium Barrier; Plutonium Doping, Rossi-Alpha; Spontaneous Fission Neutron.*

1 Introduction

Since the 1970s, plutonium conversion to explosive material has received significant interest. One of the most common sources used to create nuclear bombs is plutonium isotopes. Aside from the plutonium that already exists from

nuclear bombs, the growing amount of plutonium from spent fuel increases the need for its security. Nuclear reactors produce a sizable amount of plutonium isotopes, which have properties that make them appropriate for nuclear weapons. Depending on the temperature, the resultant plutonium can exist in a variety of phases. One of the phases that resembles metal the most is the delta phase, which makes it simple to create and utilize as a nuclear weapon.

The odd-numbered isotope of plutonium, in particular Pu-239, which is the most produced, has the ability to fission, making it the isotope most frequently utilized in nuclear weapons. Early in the 1980s, a good summary of the efforts to make plutonium less desirable for explosives was published [1]. Establishing a plutonium isotope barrier is one technique to stop the isotope Pu-239 from being abused. A further ineffective method involved mixing gamma emitter nuclides with plutonium [2] and even burning plutonium in the form of an inert matrix fuel [3]. The easiest method, however, is to add more Pu-238 to the total amount of plutonium, either through modified fuel cycles [4], prolonged irradiation [5], admixing Np-237 [6], or admixing all minor actinides into uranium fuel [7]. Other methods, such as adding (doping), involve replacing Pu-239 with an even-numbered isotope of plutonium. Pu-238 can significantly influence the features of plutonium due to its intrinsic properties, which include a relatively high DH of 567 W/kg and an SFN rate of 2660 n/g/s. Following IAEA criteria, plutonium that contains 80% Pu-238 is not a proliferation threat [8]. Pu-240 and Pu-242, which have SFN of 1030 and 1720 n/g/s, respectively, and Pu-238 both share comparatively excellent qualities in terms of proliferation deterrent. As a result, the interaction between these even-mass-number plutonium isotopes will influence the features of plutonium that make it resistant to propagation.

In this research, an analysis of the doping effect of even-numbered plutonium isotopes on Pu-239 will be carried out by focusing on the isotopic barrier parameters of plutonium, such as decay heat (DH), spontaneous fission neutron (SFN) and bare critical mass (BCM). These parameters were obtained by simulating a plutonium isotope fission event using a 4C MCNP with JENDL 3.3 library.

2 Analysis and Methods

Isotopes barrier parameters including Rossi-alpha, bare critical mass, spontaneous fission neutron, decay heat, and material attractiveness all made reference to the Figure of Merit (FOM) idea [9] and the ATTR, as well as Kessler's denaturing plutonium theory [10] and Plutonium content, which the IAEA examination [11] and [12] both exclude. One of the most crucial elements to becoming a material that may be utilized as a parameter to protect isotope Pu-239 from being exploited is the isotopic composition of plutonium with an even

mass. To get these characteristics, the 4C MCNP [13] and JENDL 3.3 library [14] were used to simulate a plutonium isotope fission event.

These features are used for determining proliferation resistance based explicitly on the plutonium composition since they are somewhat sensitive to the composition of plutonium isotopes. These crucial measurements include neutron spontaneous fission and decay heat. Even plutonium mass, such as Pu-238, Pu-240, and Pu-242, is utilized as a doping agent in the composition of Pu-239, a compound plutonium. Additionally, Based on the plutonium isotope composition as a function of time during reactor operation, these parameters were analyzed [15]. Equations (1) through (4) demonstrate those relationships between decay heat, spontaneous fission neutron, and elapsed time.

$$DH_i = DH_i^{ind} x r f Pu_i \quad (1)$$

$$DH_{comp} = \sum_{i=1}^{n} DH_i \quad (2)$$

$$SFN_i = SFN_i^{ind} x r f Pu_i \quad (3)$$

$$SFN_{comp} = \sum_{i=1}^{n} SFN \quad (4)$$

$$\alpha \equiv \frac{k_{eff}-1}{\tau_o} \quad (5)$$

Expression of DH_i defines a DH_i^{ind} is the decay heat value of each plutonium isotope for 100% pure isotopic plutonium, and $frPu_i$ is a fraction of the plutonium isotopic vector composition in the overall plutonium content as weight percentage. The DH comp parameter describes a plutonium compound's overall decay heat value, calculated using the contributions of all of its isotopes. The DH calculation also referred to in the Calculation of Spontaneous Fission Neutrons section, demonstrated that each SFN value of a specific plutonium isotope contributes to the SFN of the entire compound [15].

The ratio of super criticality (Keff-1), which essentially determines the energy yield of fissionable material to prompt neutron lifetime (τo), was demonstrated using the Rossi-alpha parameter as stated in equations (5) [16] and [9]. Based on the doping of Pu-239 with even-mass plutonium isotopes (Pu-238, Pu-240, and Pu-242), the Rossi-alpha value can be determined.

3 Results and Discussions

This section explains the relationship between doping addition and isotopic plutonium barrier parameters such as bare critical mass (BCM), Rossi-alpha, decay heat and spontaneous fission neutron (SFN). The discussion will be divided

into two parts, the first covering BCM and Rossi-alpha and the second covering heat decay and SFN. The discussion is limited to plutonium in the delta phase.

3.1 Effect of Even Mass Plutonium Doping to BCM and Rossi-alpha

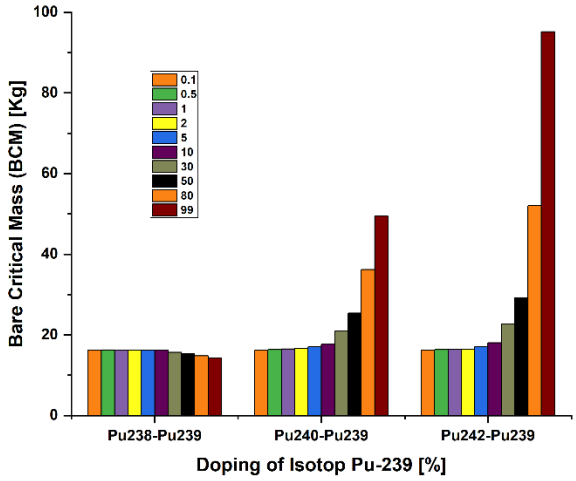

Figure 1 Bare Critical Mass (BCM) as a function of even mass plutonium doping composition.

Figure 1 shows the relationship between Bare Critical Mass (BCM) to the addition of doping. For the case of doping with Pu-238, the greater the addition of doping, the BCM will decrease. However, the decrease is not significant. This is because the BCM of Pu-238 is smaller than Pu-239, so a mixture of the two isotopes will give more or less the same BCM and decrease closer to BCM Pu-238 as the composition of Pu-238 increases. Meanwhile, for cases of doping with Pu-240 and Pu-242, the resulting BCM will be greater as the doping composition of Pu-240 and Pu-242 increases. This is also in line with the magnitude of the BCM of the isotopes Pu-240 and Pu-242.

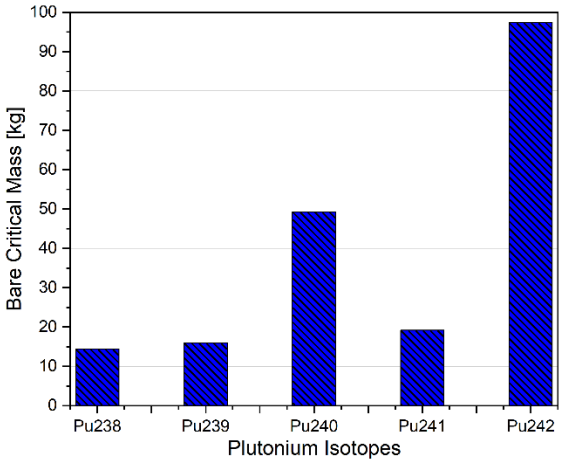

Figure 2 Bare Critical Mass (BCM) for each plutonium isotope.

The BCM for each plutonium isotope can be seen in Figure 2. Doping the isotope Pu-242 to Pu-239 will significantly increase BCM because it has the largest BCM value compared to other plutonium isotopes. The greater the BCM value, the more difficult it is for a material to be used as a nuclear weapon because it needs an enormous mass to become critical.

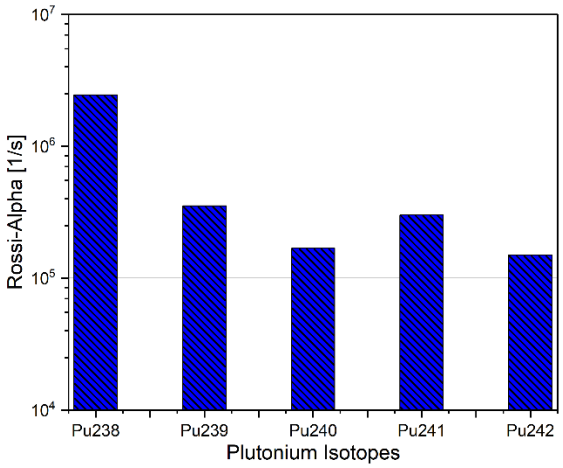

Figure 3 Rossi-alpha for each plutonium isotope.

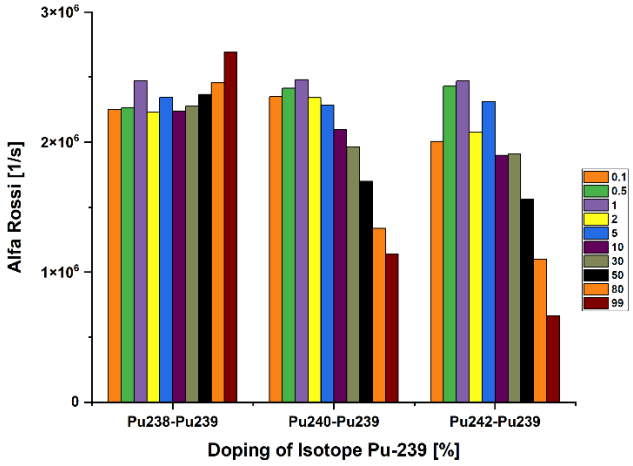

Figure 4 Rossi-alpha as a function of even mass plutonium doping composition.

Rossi-alpha is the ratio of super criticality to prompt neutron lifetime. Rossi-alpha value and BCM indicate the same thing for criticality. The difference is that criticality conditions will be more challenging to achieve with high BCM and low Rossi-alpha. The Rossi-alpha of each plutonium isotope follows Pu-238 > Pu-239 > Pu-241 > Pu-240 > Pu-242, as shown in Figure 3. This causes Rossi-alpha for doping Pu-238 to Pu-239 to increase following the increase in the composition of Pu-238. Likewise, Rossi-alpha mixed with Pu-240, or Pu-242 doping will decrease as the composition of Pu-240 or Pu-242 increases. The relationship between Rossi-alpha and the addition of doping can be seen in Figure 4. Thus, doping Pu-242 to Pu-239 will provide the most effective results for increasing the isotopic barrier parameters of BCM and Rossi-alpha.

3.2 Effect of Even Mass Plutonium Doping to Decay Heat and Spontaneous Fission Neutron (SFN)

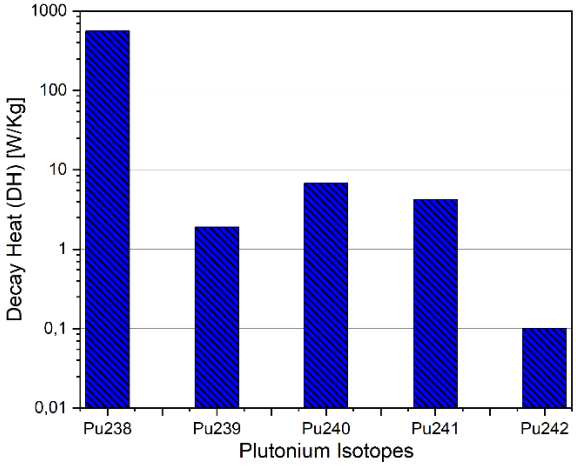

Figure 5 Decay heat for each plutonium isotope.

The results of the decay heat calculation from [17] are shown in Figure 5. The calculations found that the pure Pu-238 isotope had the highest decay heat compared to other plutonium isotopes in the order Pu-238 > Pu-240 > Pu-242 > Pu-239 > Pu-242. The higher the decay heat value, the higher the isotopic barrier parameter. This is because the high decay heat value requires a high heat-resistant handler/material, which will complicate its implementation in manufacturing nuclear weapons.

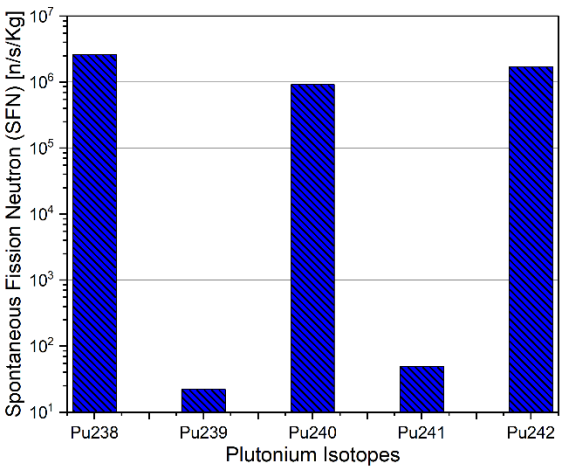

Figure 6 Spontaneous Fission Neutron (SFN) for each plutonium isotope.

Figure 6 shows the calculation results of spontaneous fission neutron (SFN) from [17], which is the intensity of spontaneous neutron production in the material. The higher the SFN value, the more neutrons are produced, which causes the material to become more unstable and challenging to control, so the isotopic barrier parameter is also higher. The SFN obtained are very large and quite similar for the even mass plutonium but very small for the odd mass plutonium.

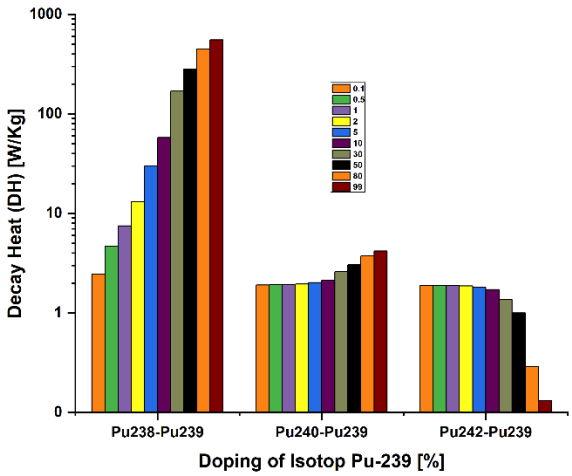

Figure 7 Decay heat as a function of even mass plutonium doping composition.

Figure 7 indicates the relationship of doping to the isotope Pu-239. The decay heat value of the Pu-239 isotope mixture increases with the Pu-238 or Pu-240 isotope composition but will decrease for the Pu-242 isotope. This is because the decay heat values of Pu-239 and Pu-240 are more significant than the decay heat values of Pu-239, and Pu-242 is the smallest among other plutonium isotopes.

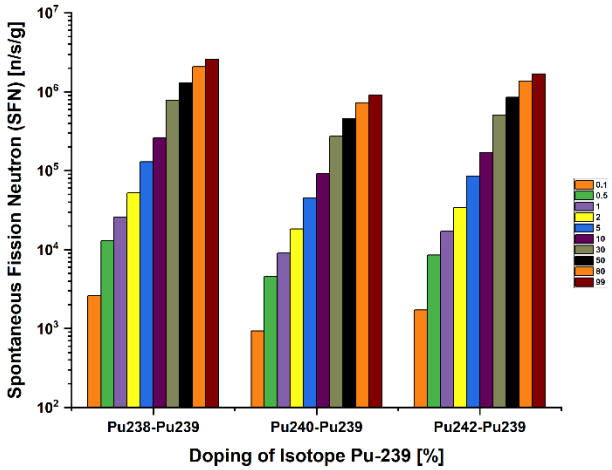

Figure 8 Spontaneous Fission Neutron (SFN) as a function of even mass plutonium doping composition.

Based on Figure 8, it was also found that the doping of the even-numbered isotope of plutonium against the isotope Pu-239 produced a somewhat similar SFN. The larger the isotope composition with an even number, the higher the SFN value in Pu-238-Pu-239 > Pu-242-Pu-239 > Pu-240-Pu-239. Thus, doping with the isotope Pu-238 to Pu-239 gives the most effective results for increasing the isotopic barrier parameter decay heat and is quite good (second position) for SFN.

4 Conclusion

The primary metrics for assessing proliferation survival based on plutonium composition are the barrier parameters for isotopic plutonium, such as decay heat, spontaneous fission neutrons, bare critical mass, and Rossi-alpha. To prevent the misuse of plutonium, especially for Pu-239, which has the highest fissile capacity, by adding or changing the composition of Pu-239 with even mass plutonium (Pu-238, Pu-240, and Pu-242).

The highest increase in decay heat was obtained by doping Pu-238. In the case of spontaneous fission of neutrons, it was found that Pu-238 doping gave high growth. Doping Pu-242 gives the highest increase in bare critical mass compared to other even-numbered isotopes. Pu-238 doping is therefore the most efficient doping for the neutron parameters of spontaneous fission and decay. For bare critical mass and Rossi-alpha parameter, Pu-242 doping is the most effective.

References

[1] DeVolpi A (1982), Denaturing Fissile Materials, Progress in Nucl. Energy, 10[2], 161.

[2] Selle J.E. et al. (1979), Technical Consideration of the Use of Nuclear Fuel Spikants for Proliferation Deterrence, Nuclear Technology, 45,269.

[3] Degueldre C. (2004), Zirconia Inert Matrix Fuel Deployment for Reducing Plutonium Stockpile in Reactors, the First International Science and Technology Forum on Protected Plutonium Utilization for Peace and Sustainable Prosperity, March 1 - 3, Tokyo, Japan.

[4] Massey J.V. and Schneider A. (1982), The Role of Plutonium-238 in Nuclear Fuel Cycles, Nuclear Technology, 56, 55.

[5] Peryoga Y. et al. (2002), Effect of Transplutonium Doping on Approach to Long-life Core in Uranium-fueled PWR, Journal of Nuclear Science and Technology, 39[8], 838.

[6] Nikitin K. et al., (1999), An Approach to Long-Life PWR Core with Advanced U-Np-Pu Fuel, Annals of Nuclear Energy, 26, 1021.

[7] Peryoga Y. et al., (2004), Inherent Protection of Plutonium by Doping Minor Actinide in Light Water

[8] Reactor Environment, submitted to Journal of Nuclear Science and Technology.

[9] International Atomic Energy Agency (1972), Information Circular, INFCIRC/153.

[10] Artisyuk, Vladirmir, Saito, Masaki, Ezoubtchenko, Alexey, 2008. Development of methodology to assess proliferation resistance of nuclear heavy metals. Proc. Nucl. Enery 50, 647-653.

[11] Kessler, G., 2007. Plutonium denaturing by Pu-238. Nuc. Sci. Eng. 155, 53-73.

[12] IAEA, Safeguards Glosary, International Nuclear Verification Series No.3, 2001.

[13] Wydler, P., Heer, W., Stiller, P., Wenger, H.U., 1980. Auranium-putonium-neptunium fuel cycle to produce isotopically denatured plutonium. Nuc. Tech. 49, 115-120.

[14] Briesmeister, J. (Ed), 2000. MCNP-A General Monte Carlo NParticle Transpotr Code Version 4C, LA-13709-M, LANL.

[15] Shibata, K., et al., 2002. Japanase evaluated nuclear data library version 3 revision-3: JENDL-3.3. J. Nucl. Sci. Technol. 39, 1125.

[16] Permana Sidik., 2020. Analysis on different material attractiveness concept based on plutonium composition of FBR blanked system. Nuc. Eng. 127, 2-3.

[17] Kimura, Y., Saito, M., Sagara, H., 2012. Improvent of evaluation methodology of plutonium for intrinsic feature of proliferation resistance based on its isotopic barrier. Ann. Nucl. Energy 40, 130-140.

[18] Saito, Masaki, Sagara, Hiroshi, Peryoga, Yoga, 2004. Development of innovative nuclear technologi to produce protected plutobium with high proliferation resistance (P^3-Project) – I. Trans. Am. Nucl. Soc 91 (1), 323-324.

Proceedings of the 3rd ITB Graduate School Conference ISSN: 2963-718X
Enhancing Creativity in Research Through Developing Innovative Capabilities
December 21, 2022

Sustainable Fashion: A Content Analysis of Indonesian Sustainable Lifestyle Instagram Influencer (Case Study: @dkwardhani)

Jennifer A Angwyn* & Hafiz Aziz Ahmad

Faculty of Art and Design, Bandung Institute of Technology, Jl. Ganesa 10 Bandung, Jawa Barat, Indonesia
*Email: jenniferangwyn.academics@gmail.com

Abstract. There has been an increasing call for slow or sustainable fashion, a type of fashion that prioritizes durability and long-lasting clothes instead of one-offs that are thrown away easily. This rise may be related to a boom in slow fashion social media influencers worldwide, as they have the capability of impacting their followers through their uploads, especially if learnt through the lens of influencers who specialize in sustainability. Unfortunately, slow fashion is still a niche concept in Indonesia as such this research aims to compile a portfolio and analyze the contents of an Influencer's Instagram account, one who specializes in sustainable lifestyle, based in Indonesia who have dabbled in sustainable fashion to find one of the many possible methods of spreading awareness and information regarding sustainable fashion through Instagram.

Keywords: *content analysis; sustainable lifestyle; sustainable fashion; instagram influencer; post structure*

1 Introduction

The concept and act of sustainability has recently been presented in every nook and cranny of the world, be it in the form of paper straws and cups replacing plastic ones, the invention of the solar panel, the 1980s anti-fur and various other movements in the fashion industry. Unfortunately, despite the growing trend of sustainable fashion, the fashion industry still continues to be one of the leading contributors of pollution. Nikita Shukla from EARTH.ORG, an organization focusing on the spread of sustainability awareness via online newsletters, reported the increase of textile production due high consumer demand. As a result, fast fashion brands produce two times the amount of clothes it did compared to the year of 2000 [1]. This can be attributed to how affordable fast fashion is, the boom of social media with influencers setting quickly changing trends and the negative perception that encompasses sustainable or slow fashion which discourages people from picking it up. However, social media, influencers especially, may also be able to aid in the spread of awareness and proper knowledge of sustainability by changing the perception people have of

sustainable fashion. As a platform that enables a person to build their own brand, social media can help with the spread of awareness and knowledge of sustainability by showcasing how it is possible to adopt a sustainable lifestyle in a day-to-day basis and connecting with people of similar interest thus allowing a community to be made which will, in turn, endear more people to the concept of sustainable fashion. A single person is usually the focus or 'lead' of the community and is called an influencer.

The purpose of this study is to analyze the ways Instagram influencers, specifically one who specializes in sustainable lifestyle, have spread the concept of sustainable fashion in a visual-based social media platform such as Instagram through content analysis. Instagram is chosen as the social media platform because it is one of the most used social media platforms in the world and in Indonesia. As reported by Andi Dwi Riyanto (2021) in Andi.link, Instagram is the third most used platform used by 86.6% from the total population with a split of 52,4% and 47,6% between women and men respectively. It is a visually inclined platform which makes it easier for people to take a photo and share said photo [2]. New mass communication technologies, such as Instagram, present a hereby unparalleled channel for the distribution of fashion information, providing sector and a rapid diffusion of fashion [4]. The higher in active engagement will lead to a more effective spread of awareness and it will help endear people in regards to a concept as niche as sustainable fashion.

Opinion leaders, first coined by Katz and Lazarsfield, are individuals in social networks on all levels of society who often hold some form of influence over one or several topics [2]. A social media influencer is someone who has built a reputation for their knowledge and expertise on a specific topic and usually has a following in a distinct niche, with whom they actively engage with [3]. Influencers can be categorized by different aspects: by their following size, by the type of content they engage in and by level of influence. Influencers are the opinion leaders in this newly established fashion communication [4]. Generally, it is easy to recognize and follow influencers with relevant fashion content but local citizen influencers, who are subjected to the same real-life environmental and cultural cues in a certain community, exert greater influence on local fashion [4]. It is for this reason that a local, Indonesian influencer will be analyzed to discern how sustainable fashion information may be spread from influencers with a background in sustainability.

2 Method

The study will use a qualitative approach in which an influencer with a sustainable background will be analyzed. First a portfolio consisting of the influencer's endeavors in sustainability and sustainable fashion, be it related or

unrelated to Instagram, will be compiled. Afterwards the influencer's feed will be checked through and posts that pertain to sustainable fashion. The parameter of sustainable fashion posts are posts that contain mentions of activities related to sustainable fashion such as thrifting, eco-friendly textiles, recycling and upcycling used clothing. Keywords taken into account are sustainable, sustainable fashion, upcycle, eco-friendly with the understanding that these keywords are used in relation to sustainable fashion.

The structures and components contained, such as the photo, caption and hashtags, in these posts will then be analyzed. Lastly, content pertaining to sustainable fashion will be analyzed to reach a theoretical conclusion of how exactly an Instagram influencer with a background of sustainable lifestyle may have done to spread the still niche concept of sustainable fashion in Indonesia. Overall respond from visitors of the analyzed sustainable fashion post will be taken and averaged from all sustainable fashion post found in the account.

3 Results and Discussion

This section will contain the full findings of this research. Starting with a compiled portfolio of the subject of this research, focusing on the start of their backgrounds in the influencer's topic of interest any reported contribution to sustainable fashion along with a brief summarization of the contents of their Instagram accounts as of the 27th of July 2022, the date the research was conducted.

3.1 Influencer Portofolio

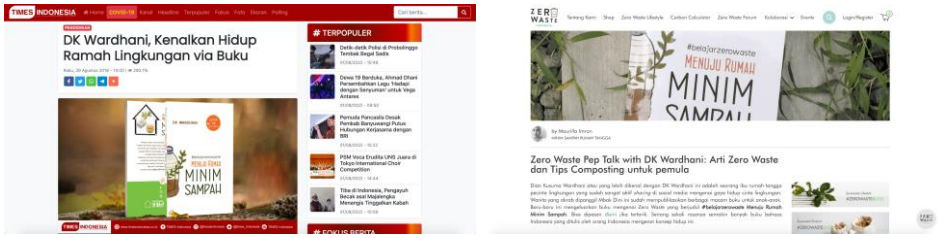

Figure 1 DK Wardhani's contributions to Sustainability

DK Wardhani (@dkwardhani) is an influencer focused on the topic of sustainability and sustainable lifestyle. DK Wardhani primarily studies and explores the concept of sustainability and sustainable lifestyle, sharing what she has learnt in her Instagram account. Several books regarding sustainable lifestyle have also been published by DK Wardhani. Some of her published books can be found in the Gramedia website as seen in **Figure 2** Besides being a published

author, DK Wardhani has also been featured in multiple websites, in articles for advocating of sustainable fashion, among which is *Times Indonesia* and *Zero Waste Indonesia*. She has also opened classes to teach the topic of zero waste living, promoting it frequently in her Instagram account with the hashtag of *#belajarzerowaste*, which is also the title of one of her most recent books *Menuju Rumah Minim Sampah*.

Figure 2 DK Wardhani's contributions to Sustainability

DK Wardhani's personal account has a total post of 1,410 posts, 58k followers and 1,865 following. Posts that pertain to direct sustainable lifestyle seems to have started picking up around the year of 2018, starting with various information and tips to reduce waste along with small experiments like the methods and making of environmentally friendly soap made from lemon oil, natural toners from rosewater and enzyme cleaners which later developed into lifestyle-affecting choices such as the making of compost bins and no-plastic shopping, a method that has recently started being implemented in general shopping activities by limiting plastic bags and charging carry-on bags. A brief summarization of DK Wardhani's overall content includes the following types 1) Published Books about Sustainable Lifestyle, 2) Tips on Composting, 3) Tips on Minimizing Waste among which includes household habits and groceries, 4) The effects of Pollution and Wasteful Habits, 5) Video Talks with Guests about Sustainability, 6) Examples of Stores and Accounts exploring Sustainability.

3.2 Categorization of the Influencer's Instagram Feed

Out of a total post of 1,410 as of the 27th of July 2022, 54.4% (768) of posts are categorized unrelated to fashion, sustainability and sustainable fashion while 45.6% (642) consist of post related to the three categories mentioned above as can be seen in **Figure 3**. In **Figure 4** among the three categories counted posts pertaining to sustainability take up 98.6% (635) followed by sustainable fashion at 1.1% (7) and lastly posts pertaining to fashion at 0.3% (2). The small number of posts pertaining to sustainable fashion is to be expected since sustainable

fashion is still a fairly niche concept in Indonesia and the focus of influencer DK Wardhani's account is not to fashion but to sustainable lifestyle that can be implemented to everyday life.

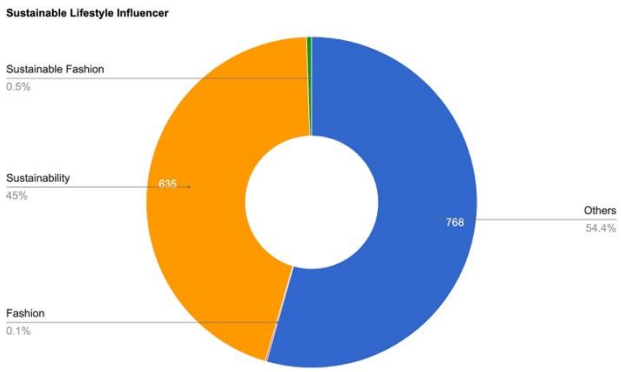

Figure 3 Types of posts separated into four categories

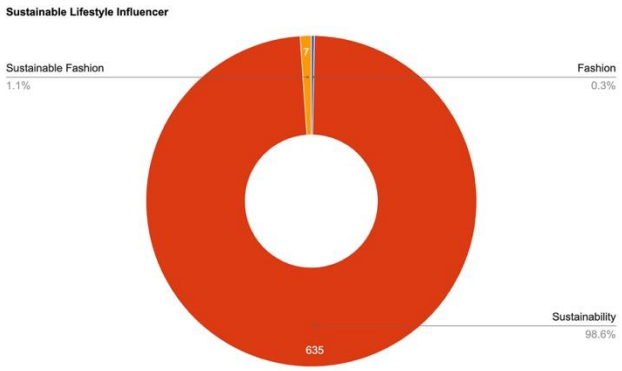

Figure 4 Types of post separated into three categories disregarding unrelated posts

3.3 Components of an Instagram Post

Instagram is a photo social application with functions of photo shooting, photo beautifying and sharing [6]. It can be seen as a new type of social media based on picture interaction because of its functions to assist people in building social networking based on pictures [7] and is also an important platform for bloggers to work [6]. Unlike other social medias Instagram puts as much focus on simple but effective strategy of picture production. It only retains basic functions such as capture, photo makeover, photo sharing and commenting [6].

As of today, key components of an Instagram post consist of can be seen broken down in **Figure 5**. 1) Photos, the main component, it may be personal or professionally taken depending on the owner of the account, which attracts other fellow Instagram users to explore the rest of the account. Several photos can be compiled into a series in a single post. 2) Captions, an explanation or story to accompany the Photo, written below or to the side depending on whether the post is being viewed on mobile or PC. 3) Hashtags, a feature that enables the post to be accessed through Instagram's Search function and is always prefixed by the symbol #. The function of hashtags can be classified into two types, to bookmark the contents of captions and to communicate within a community focusing on the same topic [7]. 4) Mentions, a method of including other Instagram users into the post by 'mentioning' or 'tagging them, it is usually prefixed with the symbol @. 5) Geotag, or more commonly known as Location, is a feature to include the location of the photo taken that, if clicked, will be directly linked to a map and an assortment of other photos that were taken in the same location. 6) Hearts/Likes and Comments, this is where user engagement can be seen and gauged by quantifying how much likes a post has received and the general tone of comments from users who have interacted with the post, the feature is similar to that of other social medias such as Twitter.

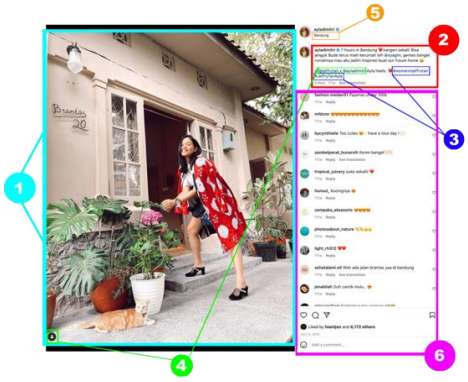

Figure 5. Instagram post components breakdown (picture taken from @ayladimitri)

3.4 Analysis of Sustainable Fashion Posts

As of the 27th of July, 2022, there are about 7 posts relating to sustainable fashion found in the influencer's Instagram feed. Posts with direct relation to sustainable clothing, promotion, manufacture or otherwise, will be separated and analyzed. Each post will be broken down into the components listed in sub-chapter **4 Components of an Instagram Post.** The research will refrain from theorizing any text not in English or Indonesian due to the possibility of misinterpretation. Post that will be analyzed can be seen in the following page in **Table 1. Posts**

Pertaining to Sustainable Fashion. The lowest and highest amount of accompanying secondary photos have been recorded to be one and nine pictures respectively. Only the first and second photo will be shown to prevent overflow but all photos were all taken into account during analyzing process.

Post 1

Figure 6 First photo of Post 1

Figure 7 Second photo of Post 1

Post 2

Figure 8 First photo of Post 2

Figure 9 Second photo of Post 2

Post 3

Figure 10 First photo of Post 3

Post 4

Figure 11 First photo of Post 4

Figure 12 Second photo of Post 4

Post 5	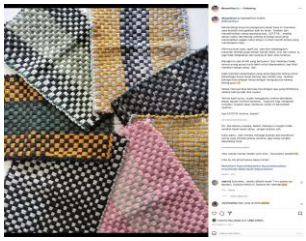	
	Figure 13 First photo of Post 5	**Figure 14 Second** photo of Post 5
Post 6		---
	Figure 15 First photo of Post 6	
Post 7		
	Figure 16 First photo of Post 7	**Figure 17 Second** photo of Post 7
	Primary Photo	Photo Series

Table 1. Posts pertaining to Sustainable Fashion

From the table it is observed that the types of sustainable fashion products focused on by the sustainable lifestyle influencer can be divided into three categories: one in the form of clothing as can be seen in post 1 and post 2, one the form of alternative materials which can then be turned into clothing as seen in post 3 and post 4 and lastly one in the form of home-life products made from used clothing as can be seen in post 5, post 6 and post 7.

Breaking down into the components mentioned in **4.1 Components of an Instagram Post** the photos of the post itself is observed to be simple, non-professional types of photography and is speculated to be used as a visual guide

for the anecdotes written out in the caption. The caption is where a majority of the post's information is located. A central theme related to sustainable fashion is always introduced first, sometimes with an accompanying question which will then be answered in the following paragraph. One such example is observed in post 3 with the central theme being eco-print and the process of eco-printing with the influencer writing four questions, translated from Indonesian to English, such as "What is eco-print?" and "What is the process?" with follow-up answers in the caption. Anecdotes of the influencer's experience relating to the theme brought up is also written in the caption as observed in a majority of the post. One example is post 2 anecdotes explaining the influencer's experience talking to the owner of an eco-gamis, a type of long-sleeved dress-like clothing, business regarding waste produced from clothes manufacturing. The business itself implements zero waste pattern cutting into the product as much as possible. Another example is seen in post 5 regarding the influencer's thought and experience in relation to the definition of Aesthetics and the upcycling of used shirts into useable clothing mats. In the same post the influencer also prompts visitors of the post regarding their own version of what Aesthetic is. In some posts it is observed that the influencer may give out alternative solutions to one problem, notably seen in post 6 about beanbags that can be filled with no longer useable cut-up old clothing instead of regular beanbag filling. In regards to used clothing two alternative solution besides being used as beanbag filling are provided: 1) can be cut up into strips and made into mats, rugs, or cat beds and 2) stated specifically only for clothing made of natural fiber like bamboo, it can be composted with a method called vermicomposting. In regards to the beanbag filling, eco-bricks can be used post visitors who are interested.

Instagram accounts, both business and personal related to sustainable fashion are also observed to be recommended through the *mention* feature, particularly post 1, post 2, post 4 and post 7 along with local non-social-media based business as seen in post 5. Hashtags are observed to be used not only to introduce the post to Instagram's Explore Feed and as a bookmark for the influencer. Currently it is observed that post traffic primarily comes from the influencer's social media community that is already built around the interest of ways to live a sustainable lifestyle, although further research will be needed to conclude the full scope of effects that come from the usage of hashtags.

3.5 Overall Responds from Post Visitors

Responds gathered from the seven sustainable fashion posts fall majorly in the Interested category at 44.8% (181), which consists of comments stating from post visitors stating that interest, willingness or participation and experience with the the topic of sustainable fashion in relation to the post. Replies from the influencer to comments posted by post visitors sit at 32.2% (130). Comments that consist of

positive support but does not state active interest in the topic of sustainable fashion relating to the theme of each respective post take up 21% (85) of total respond. Neutral responds consisting of unrelated or out of context comments in relation to the topics brought up in the posts take up a small number of 2% (8).

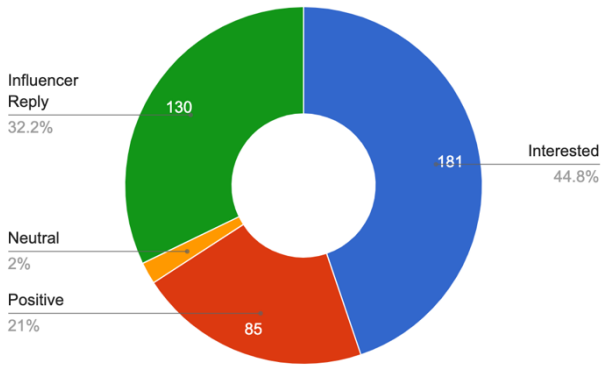

Figure 18 Overall responds split into four categories

The overall responds from post visitors regarding sustainable lifestyle influencer DK Wardhani's sustainable fashion posts consists of those interested in participating with the topic, often trading experience with the influencer or with others in the community. Comments from small business trying to adopt the principles and methods of sustainable fashion are also seen in the posts' comment section, some asking for resources or advice in regards to problems related to sustainable fashion that may arise.

4 Conclusion

Although sustainable fashion is yet to be explored much by social media Influencers in Indonesia, this does not mean it is entirely unexplored. An influencer specializing in sustainable lifestyle may explore parts of sustainable fashion since the clothing is also a major part of daily life.

According to the case study in the research, a sustainable lifestyle influencer may focus on the sustainability aspect of sustainable fashion, using a practical and experienced approach in spreading awareness of the topic along with providing information in a concise and in-depth manner, always with a primary theme, explanation, answer and often citing prior experiences the influencer has gone through as a basis; photos are used as a visual guide to anecdotes laid out in the caption. Local business and resources in relation to sustainable fashion have also

been observed to have been recommended as an alternative source of information for post visitors interested in a specific branch of sustainable fashion such as eco-friendly textile or a way to sustainably deal with waste resulting from clothes manufacturing. The overall responds to the introduction of sustainable fashion from the influencer in this case study is positive and actively interested in learning or participating in sustainable fashion.

References

[1] Nikita Shukla, *Fast Fashion Pollution and Climate Change*, EARTH. ORG, https://earth.org/fast-fashion-pollution-and-climate-change/, 21st February 2022

[2] Gulamali, Amber & Persson, Julia., *The Social Media Influencer and Brand Switching*, Thesis, Department of Business Administration., Lund University., Lund, 2017

[3] Werner Geyser, *what is an Influencer? - Social Media Influencers defined [Updated 2022]*, Influencer Marketing Hub, https://influencermarketinghub.com/what-is-an-influencer/, 4th April 2022

[4] Tomovska Elena, The Role of Instagram Influencers as a Source of Fashion Information, Tekstilna Industrija. 68. 58-64.

[5] Yang, Chen, *Research in Instagram Context: Approaches and Methods*, Journal of Social Sciences Research. 7. 15-21.

[6] Jin, Yea Jang., Han, Kyungsik., Shih, Patrick C. and Lee, Dongwoon, *Generation like: Comparative characteristics in Instagram*, In Acm Conference on Human Factors in Computing Systems.

[7] Zhan, M., Yu, Q., Wang, J. (2020): Effectively Organizing Hashtags on Instagram: a study of library-related captions. *Information Research*, 25(2), paper 858.

Proceedings of the 3rd ITB Graduate School Conference ISSN: 2963-718X
Enhancing Creativity in Research Through Developing Innovative Capabilities
December 21, 2022

Design and Analysis of 5 MW Kaplan Runner Wheel for Small Hydro Powerplant

Muhammad Febrilian Syah[1, *], Priyono Soetikno[1] & Isnain 'Aliman[2]

[1] Faculty of Mechanical and Aerospace Engineering, Institut Teknologi Bandung
[2]Department of Mechanical Engineering, The University of Melbourne
[*]Email: 23122003@mahasiswa.itb.ac.id

Abstract. In 2019 to 2028, Indonesia will build power plants by utilizing new and renewable energy with 9.5 GW comes from hydro power plants [5]. One of the realizations of the small hydro power plant in Indonesia is a power plant located on the Minahasa Peninsula, North Sulawesi, Indonesia that uses two runners with 5 MW generated from each runner. In this research, the suitable Kaplan runner will be designed complete with the spiral casing, guide vane, and draft tube with a desired capacity of 5 MW and flowrate of 39 m^3/s. The research was started by designing the runner geometry, draft tube, spiral casing, and guide vane and simulated using RANS Computational Fluid Dynamics at steady state in various variation. Variations used in this research are runner blade angle and guide vane angle. The results of the variation of the guide vane angle at each runner blade angle show the increase of hydraulic efficiency until it reaches a certain peak point before decrease. The configuration that produces the highest efficiency at 150 RPM operating rotational speed achieved at -2.5^o blade angle and 39.5^o guide vane angle with 6.49 MW hydraulic power and 84% efficiency.

Keywords: *computational fluid dynamics; draft tube; guide vane; hydroelectric power plant; kaplan runner; spiral casing.*

Nomenclature

n	=	runner rotational speed (RPM)
P	=	runner hydraulic power (kW)
H	=	head (m)
n_s	=	runner specific speed
N'_{sd}	=	runner power specific speed
D_{tip}	=	runner tip diameter (m)
D_{hub}	=	hub diameter (m)
N	=	hub dan tip diameter ratio
Q	=	flow rate (m^3/s)
ω	=	rotational speed (rad/s)
ε	=	runner glide angle (rad)
g	=	gravitational acceleration (m/s^2)
η_s	=	draft tube efficiency

η_{th}	=	runner theoretical efficiency
s''	=	chord length (m)
t''	=	distance between blades (m)
V_1	=	inlet water velocity (m/s)
C_{u1}	=	tangential absolute velocity (m/s)
V_{f1}	=	meridian absolute velocity (m/s)
U_1	=	blade velocity at leading edge (m/s)
U_2	=	blade velocity at trailing edge (m/s)
V_{r1}	=	relative velocity at blade inlet (m/s)
V_{ru1}	=	tangential relative velocity at blade inlet (m/s)
β_1	=	blade inlet angle (^{o})
β_2	=	blade outlet angle (^{o})
V_{r2}	=	relative velocity at blade outlet (m/s)
V_{ru2}	=	tangential relative velocity at blade outlet (m/s)

1 Introduction

Electrical energy is a basic human need, which continues to increase in direct proportion to the level of welfare. In 2030, Indonesia's population is predicted to reach 296 million people [1]. Population increase is followed by an increase in energy needs, including electrical energy. Indonesia's per capita electricity consumption in 2030 it is expected to reach 3,201 MWh/capita [2]. Therefore, it is necessary to add adequate power plants. Currently, the most widely used power plants are fossil fuel plants including in Indonesia which is dominated by steam power plants with 49.85% [3].

The usage of fossil-based power plant is less profitable considering the limited amount of fossil fuels and the resulting pollution is not good for the environment. For this reason, the community is required to find unlimited and environmentally friendly energy sources called renewable energy. There are several types of renewable energy that can be converted into electrical energy including hydro power [4]. In 2019 to 2028 power plants will be built by utilizing new and renewable energy with a total capacity of up to 16.7 GW. Among the total capacity, 9.5 GW of which comes from hydro and micro hydro power plants [5].

The essential part of converting hydro power into electricity is the runner. There are several types of runners such as Kaplan, Francis, and Pelton. Types of runners have different geometry and best operating conditions based on the net head, flow rate, and specific speed [6]. Table 1 shows the runner type and the suitable operating head range in meters. In addition to the runner, there are several other parts to support the energy conversion system of water flow into electrical energy including spiral casing, guide vane, and draft tube.

Table 1 Head range on each runner type [6]

Runner Type	Head (m)
Kaplan and *Propeller*	2 < H < 40
Francis	10 < H < 350
Pelton	50 < H < 1300
Michell-Banki	3 < H < 250
Turgo	50 < H < 250

Several studies already conducted in small hydropower system design including energy generation potential and component design. Leon *et al.* stated that water use can be optimized if the ratio of the net head does not exceed 15% gross head [7]. In draft tube design, Fulzele *et al.* stated that elbow draft tube type with circular inlet and rectangular outlet has efficiency range from 60% to 80% [8]. In the runner design, Zhang et al proposed series of equation for Kaplan runner. The equation proposed combined the geometric design with the dynamic operation to validate runner design and CFD simulations [9]. Abeykoon *et al.* developed the design and analysis of Kaplan runner wheel for 6 meters head and 5 m3/s flow rate and analyse the design using CFD analysis. According to CFD result, there is significant difference between the theoretical calculation efficiency and the simulation result efficiency where the theoretical efficiency is 94% and the efficiency of the simulation results is 50.98% [10]. Min also developed design for 50 kW Kaplan runner with the different flow condition from research conducted by Abeykoon *et al.* with the runner design result have different operating condition especially in guide vane opening angle and blade angel to achieve desired power shaft output [11]. The runner design may be varied due to the different flow characteristic between one region and another therefore runner design must be proposed for certain power output, head, and flowrate according to the potential that exists in the runner installation area.

One of the realizations of the small hydro power plant in Indonesia is a power plant located on the Minahasa Peninsula, North Sulawesi, Indonesia. The total power generated is 9.9 MW uses two runners with 5 MW generated from each runner. Water discharge for one runner is 39 m^3/s. The water reservoir used on the runner comes from dam located on the Bone River, North Sulawesi. The water level in the dam has a range of 94 to 96 meters above sea level with the runner installation system placed at a height of 78 meters above sea level and the minimum tail race water level is almost parallel to the runner installation height. According to the water level at the dam and tailrace, the head obtained is at a low head with the suitable runner type is the Kaplan runner.

In this study, a Kaplan runner was designed complete with a spiral casing and a draft tube with a capacity of 5 MW and a flow rate of 39 m^3/s with various variations, such as varying the angle of the guide vane and varying the angle of the runner. The variation intended to obtain the performance characteristic in the water runner in form of power and efficiency. The results of the design through analytical methods will be validated using Computational Fluid Dynamics (CFD)-based software, namely RANS Computational Fluid Dynamics.

2 Methods

The method used in this study begins by determining runner parameter from the given case study and continues with the design of the runner. The runner design process begins with developing the runner design continued with designing the guide vane, spiral casing, and draft tube. After all components have been designed, assembly is carried out using the design components to be simulated in RANS Computational Fluid Dynamics to obtain the characteristics and performance of the designed water turbine.

2.1 Runner Design

The operating conditions on the turbine are used to calculate runner specific speed. The operating parameter for runner is shown in Table 2. The value of the specific speed as a function of power (n_s) and power specific speed can be calculated using Eq. (1) and Eq. (2). With n is rotational speed, P is hydraulic power, and H is net head.

$$n_s = n\frac{\sqrt{P}}{H^{5/4}} \tag{1}$$

$$N'_{sd} = \frac{n\sqrt{1.341P}}{[3.28H]^{5/4}} \tag{2}$$

Table 2 Operating Parameter for Runner

Parameter	Value	Unit
Hydraulic power (P)	5	MW
Rotational speed design	200	RPM
Rotational speed operation	150	RPM
Net head (H)	14.5	Meters
Water Flowrate	39	m^3/s

The draft tube that will be used is elbow type with circular inlet and rectangular outlet. The efficiency of the draft tube with this type is in the range of 60% to 80% [8]. In this study, the draft tube is assumed to have an efficiency of 67.5%. The airfoil used is NACA 6409 with angle of attack 5°. The diameter of the runner will be determined using Eq. (3) and Eq. (4) [12]. N is the ratio of D_{tip} and D_{hub} with the value of 0.4 and number of blades 5 [12], Q is the flowrate, ω is rotational speed in rad/s, g is gravity acceleration, η_s is draft tube efficiency, and ε is the glide angle in rad.

$$D_{tip} = 1{,}155\left(\frac{1-\eta_s}{K_o\omega\varepsilon gH}\right)^{\frac{1}{7}}\left(\frac{Q}{1-N^2}\right)^{\frac{3}{7}} \tag{3}$$

$$K_o = \frac{2}{3} \times \frac{(1-N^2)}{(1-N^3)} \tag{4}$$

The velocity triangle will be used to determine the shape of the blade theoretically. A velocity triangle review is carried out on a cross section of the blades in five different radial distances measured from the centre of the hub. The five distances will be named R1, R2, R3, R4, and R5 with equation Eq. (5). The velocity triangle in the cross section of the blade can be seen in Figure 1. Further calculations for each parameter in velocity triangle will be carried out using Eq. (6) until Eq. (14) where i are 1,2,3,4, and 5 [14]. The relative velocity of the tangential direction, relative velocity, and angle to the horizontal at the centre of the blade will be determined using Eq. (15) until Eq. (17) [10]. From the equation, the subscript 1 is indicated the value of respective variable at the inlet and subscript 2 is at the outlet. V and U is water velocity and blade velocity due to rotation. C_u and V_f is tangential and meridian absolute velocity. V_r and V_{ru} is relative and tangential relative velocity. β is the blade angle and α is the angle between inlet water velocity and blade velocity due to rotation.

The ratio between the chord length and the distance between the blades will be set to 0.75 for the hub diameter section and 1.3 for the tip diameter section [10]. The distribution of the value of s”/t” and the value of t” is based on Eq. (18) and Eq. (19) with s” is the chord length and t” is the distance between blades. The value of β_1 must first be adjusted to the optimal blade angle that has been determined previously for the NACA 6409 airfoil, which is 5°. After adjusting to the 5° blade angle, then the $\beta_{rotation}$ will be defined which is the rotation value in the form of twist angle that must be given to the NACA 6409 airfoil profile. $\beta_{rotation}$ will be calculated based on Eq. (20).

$$R_i = \frac{D_{hub}}{2} + \frac{i-1}{4}\left(\frac{D_{tip}-D_{hub}}{2}\right) \tag{5}$$

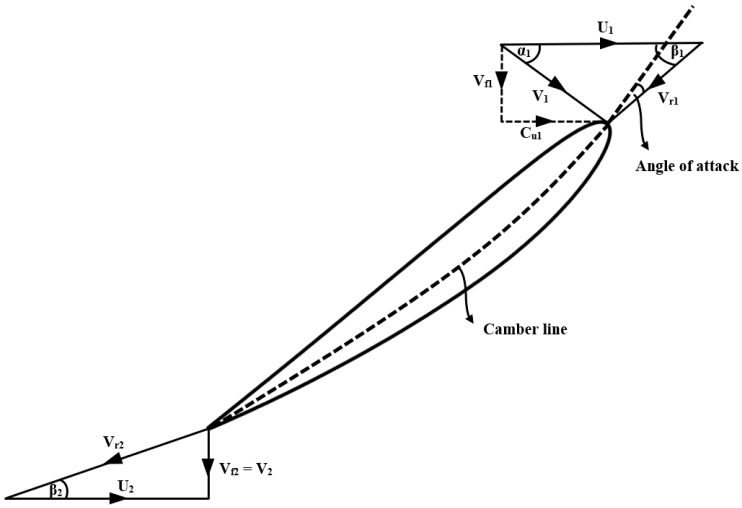

Figure 1 Cross section of blade and speed triangle [13]

$$v_{f1} = \frac{Q}{\frac{\pi}{4}({D_{tip}}^2 - D_{hub}^2)} \tag{6}$$

$$U_1(i) = U_2(i) = \frac{2\pi R_i n}{60} \tag{7}$$

$$C_{u1}(i) = \frac{\eta_{th} g H}{U_1(i)} \tag{8}$$

$$\tan\beta_1(i) = \frac{v_{f1}}{U_1(i) - C_{u1}(i)} \tag{9}$$

$$\tan\beta_2(i) = \frac{v_{f2}}{U_2(i)} = \frac{v_{f1}}{U_1(i)} \tag{10}$$

$$v_{r1}(i) = \sqrt{v_{f1}^2 + (U_1(i) - C_{u1}(i))^2} \tag{11}$$

$$v_{r2}(i) = \sqrt{v_{f2}^2 + (U_2(i))^2} \tag{12}$$

$$\alpha(i) = tan^{-1}\left(\frac{v_{f1}}{C_{u1}(i)}\right) \tag{13}$$

$$C_{u\infty}(i) = \frac{C_{u1}(i)}{2} \tag{14}$$

$$v_{ru\infty}(i) = U_1(i) - C_{u\infty}(i) \tag{15}$$

$$v_{r\infty}(i) = \sqrt{(v_{ru\infty}(i))^2 + {v_{f1}}^2} \tag{16}$$

$$\beta_\infty(i) = tan^{-1}\left(\frac{v_{f1}}{v_{ru\infty}}\right) \tag{17}$$

$$\left(\frac{s''}{t''}\right)_i = 0.75 + 0.55\left(\frac{i-1}{4}\right) \tag{18}$$

$$t''(i) = \frac{2R_i\pi}{Number\ of\ Blades} \tag{19}$$

$$\beta_{rotation}(i) = 180^0 - \beta_1(i) + 5^o \tag{20}$$

2.2 Guide vane, spiral casing, and draft tube design

NACA 2.5411 airfoil type is selected for guide vane profile. Several parameters will be assumed for the guide vane design including the chord length (L) 0.75 meters, guide vane height (H) 1 meter, the outer diameter (D_{gv}) of the guide vane circuit is 3.92 meters, and the number of guide vanes is 16.

Spiral casing is the component that provide uniform flow to the guide vane with cross-sectional area of the flow should decrease gradually along the circumference of the spiral casing [15]. The dimensions used in the design of the spiral casing are based on Figure 2. Furthermore, the cross-section of the flow area used is based on the places of runner is coincidence with the spiral casing according to Figure 2. The shape of the draft tube with elbow type can be seen in Figure 3 with the dimension for the draft tube are calculated using Eq. (21) until Eq. (30) with D_{tip} is the tip diameter and n_s is the specific speed.

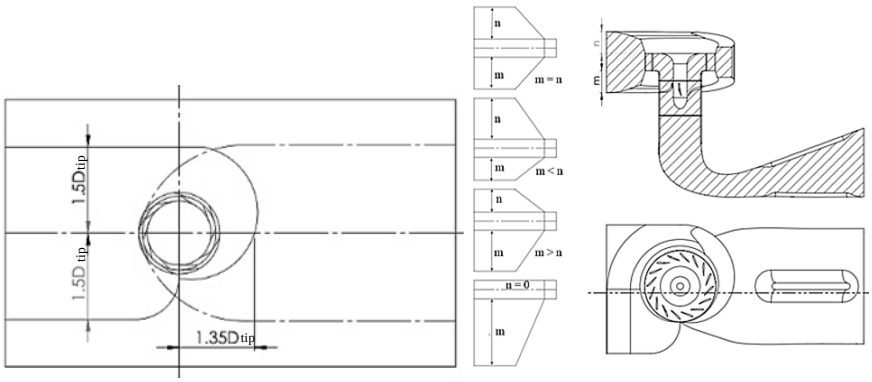

Figure 2 Spiral Casing Dimension (left) and Cross-sectional area of flow in Spiral casing (right) [15]

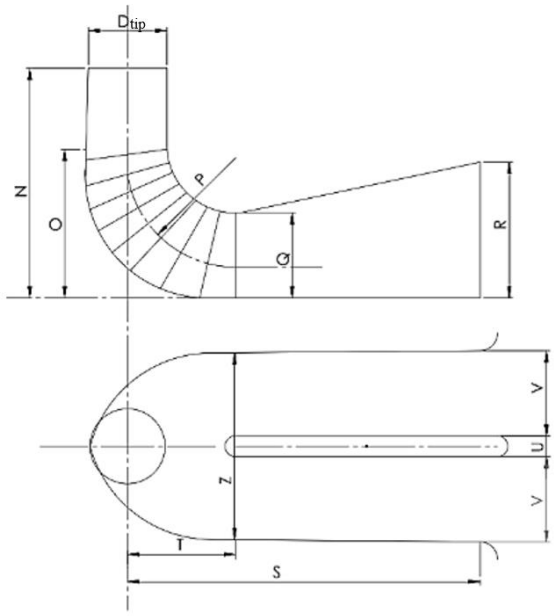

Figure 3 Elbow Type Draft Tube [15]

$$N = D_{tip}\left(1{,}54 + \frac{203{,}5}{n_s}\right) \tag{21}$$

$$O = D_{tip}\left(0{,}83 + \frac{140{,}7}{n_s}\right) \tag{22}$$

$$P = D_{tip}(1{,}37 - 0{,}00056n_s) \tag{23}$$

$$Q = D_{tip}\left(0{,}58 + \frac{22{,}6}{n_s}\right) \tag{24}$$

$$R = D_{tip}\left(1{,}6 - \frac{0{,}0013}{n_s}\right) \tag{25}$$

$$S = \frac{D_{tip}n_s}{(-9{,}2+0{,}25n_s)} \tag{26}$$

$$T = D_{tip}(1{,}5 + 0{,}00019n_s) \tag{27}$$

$$U = D_{tip}(0{,}51 - 0{,}0007n_s) \tag{28}$$

$$V = D_{tip}\left(1{,}1 + \frac{53{,}7}{n_s}\right) \tag{29}$$

$$Z = D_{tip}\left(2{,}63 + \frac{33{,}8}{n_s}\right) \tag{30}$$

2.3 Numerical Simulation

The numerical simulation process is carried out using the RANS Computational Fluid Dynamics software. The simulation used is steady state single phase simulation with k-ω SST turbulence model. k-ω SST has the advantage of predicting flow near the wall and away from the wall [16].

The spiral casing, guide vane, and draft tube components will be given a water-liquid type of fluid without any frame motion. The runner component will be given a water-liquid type of fluid with a frame motion in the form of rotation on the y-axis with a rotational speed of 150 RPM. Runner blade and runner hub wall condition converted into a moving wall in the form of rotation with a rotational speed of 0 RPM relative to the appropriate cell condition and the axis of rotation is on the y-axis.

At the outlet and inlet, the boundary conditions used are pressure outlet and inlet. The inlet pressure is determined by hydrostatic pressure according to net head. Turbo topology in RANS Computational Fluid Dynamics is defined to determine the topology of turbo engine applications so that the special post processing features of turbo topology can be used to see the performance of the designed runner.

2.4 Mesh independency test

Mesh independence test aims to determine the smallest number of meshes needed to ensure that the simulation shows results that are not much different when the number of meshes is varied. The parameter that will be seen in the mesh independence test is the average mass flow rate at the inlet and outlet with the error will be determined by (31). The smallest number of meshes that show mass flow rate errors less than 1% will be used in the simulation.

$$\%Error = \left| \frac{\dot{m}_{avg}^{previous} - \dot{m}_{avg}^{current}}{\dot{m}_{avg}^{current}} \right| \times 100\% \tag{31}$$

3 Results and Discussions

The result of design feature calculation according to the case study given in Table 2 are shown in Table 3. Data from Table 3 is used for calculation using Eq. (5) until Eq. (20) to obtain the theoretical calculation parameters of the blade. The calculation result for blade theoretical parameters is shown in Table 4. The data from Table 4 will be used to determine the runner airfoil coordinates in each segment. The result of the component assembly is shown in Figure 4.

Table 3 Design Feature Calculation

Parameter	Value	Unit
n_s design	500	-
n_s operation	375	
N'_{sd} design	130	-
N'_{sd} operation	98	
Efficiency [17]	95	%
Number of blades	6	-
N	0.45	-
Ko	0.58766	-
D	2.53	m

Table 4 Theoretical Calculation Parameters of Blade

Parameter	R1	R2	R3	R4	R5
D (m)	1,14	1,49	1,83	2,18	2,53
R (m)	0,57	0,74	0,92	1,09	1,26
V_{f1} (m/s)	12,08	12,08	12,08	12,08	12,08
U (m/s)	11,94	15,58	19,23	22,87	26,51
C_{u1} (m/s)	11,31	8,67	7,03	5,91	5,10
$C_{u\infty}$ (m/s)	5,66	4,33	3,51	2,95	2,55
α (°)	46,88	54,34	59,81	63,94	67,12
β_1 (°)	87,01	60,22	44,73	35,47	29,44
β_2 (°)	45,33	37,79	32,15	27,85	24,51
β_∞ (°)	62,51	47,05	37,56	31,25	26,76
s"/t"	1,30	1,16	1,02	0,89	0,75
t" (m)	0,59	0,78	0,96	1,14	1,32
s" (m)	0,78	0,90	0,98	1,01	0,99
$\beta_{rotation}$ (°)	97,98	124,78	140,27	149,53	155,56

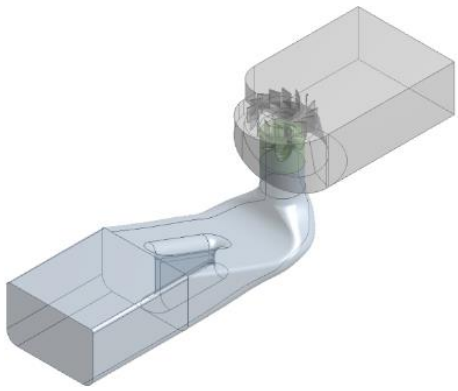

Figure 4 Components Assembly

The value of the mesh used for mesh independency test started from 700 thousand mesh to 2.9 million mesh. The results of the mesh independence test in Figure 5 shows that the number of meshes with the error value of the mass flow rate below 1% starts at 1.7 million meshes so that the number of meshes used as a reference for the simulation is 1.7 million.

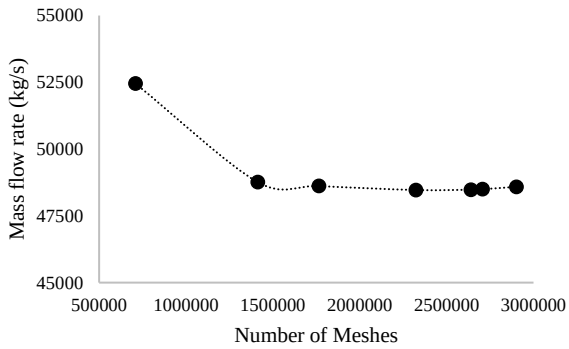

Figure 5 Mesh Independency Test

The variations of the guide vane angle show a tendency to decrease the mass flow rate when the guide vane angle is increased. The decreased mass flowrate is in accordance with the condition of the guide vane which shows that the larger the angle of the guide vane, the smaller the area around the guide vane that may pass the water, so that the mass flow rate will decrease as shown in Figure 6.

Runner hydraulic power at a certain guide vane angle in various variations of runner blade angle can be seen in Figure 7. For each variation of the blade angle, increasing the angle of the guide vane will cause the runner hydraulic power to

increase until it reaches a certain peak before finally decreasing. The simulation results show that the smaller the value of the runner blade angle, the greater the hydraulic power. This increasing hydraulic power is accompanied by a decrease in the operating range of the guide vane angle that can be given. In this study, the target output hydraulic power of 5 MW can be achieved for every blade angle variation.

At each varying blade angle, the value of efficiency will increase as the angle of the guide vane increases as shown in Figure 8. This increase in efficiency lasts until it reaches a certain peak before finally decreasing. The highest efficiency of 84% is obtained from the operating conditions of the guide vane angle of 39.5° and blade angle of -2.5°. The simulation conditions with the closest results to the runner design parameters with a flow rate of 39 m^3/s and a power of 5 MW were obtained with a blade angle configuration of 5° with a guide vane angle of 44.5°

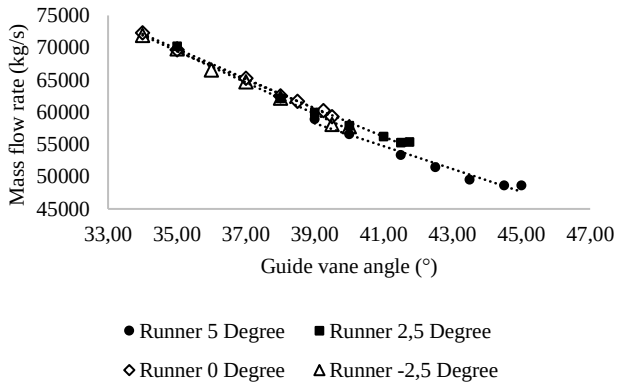

Figure 6 Mass flow rate calculated due to guide vane angle

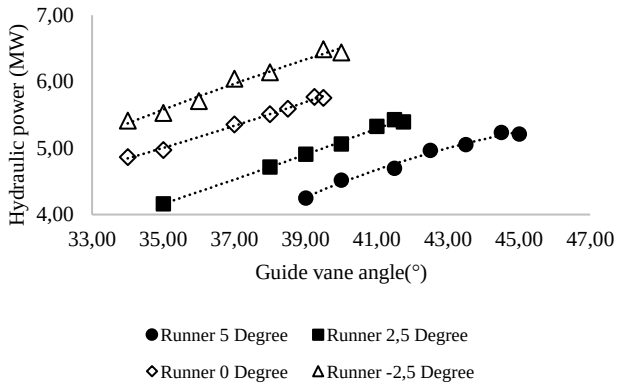

Figure 7 Runner hydraulic power

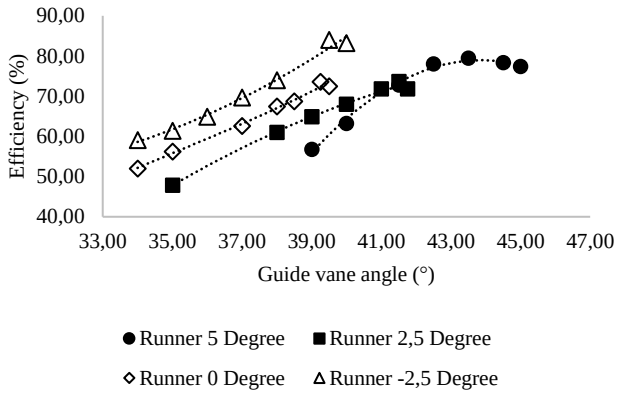

Figure 8 Efficiency versus guide vane angle

The pressure contour and wall shear contour on the blade is shown in Figure 9. Pressure contour indicates that there is cavitation that occurs in the area near the leading edge of the blade. The emergence of cavitation in the simulation results occurs because the conditions of the simulation settings at the outlet are assumed to be at atmospheric pressure while in operating conditions the Kaplan runner generally has an outlet channel below the tailrace water level. The wall shear contour shows that there are several region that have quite small wall shear values on the suction side of the blade. Evaluation of the velocity contour on the Figure 10 shows that in the area on the suction side of the blade, there are region where the velocity has decreased drastically while outside the area, the velocity value is relatively high indicated by the orange color on the contour. The velocity contour indicates that there is a flow separation caused by the non-adjusted thickness of the airfoil in the segment near the runner tip.

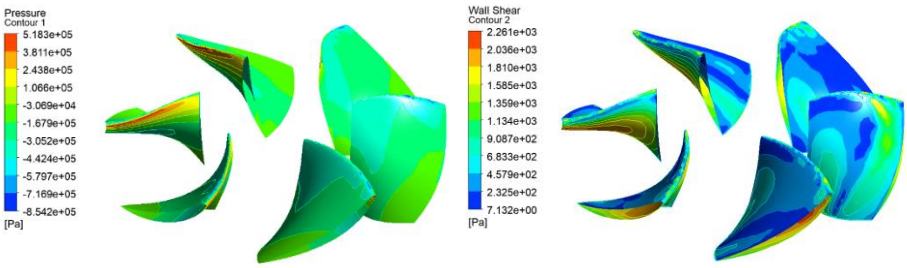

Figure 9 Pressure contour on the runner blade (left) and wall shear contour on the runner blade (right)

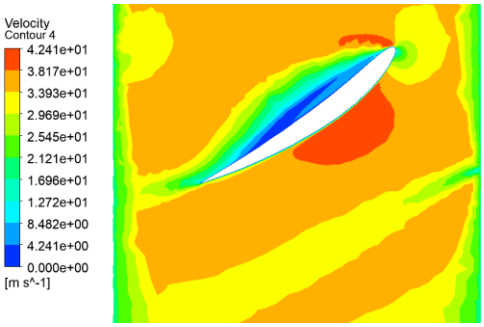

Figure 10 Velocity contour on the blade

4 Conclusions

The designed Kaplan runner has an outer diameter of 2.53 meters and a hub diameter of 1.14 meters with the number of runner blades used is 6 blades with the airfoil profile used is NACA 6409. The number of guide vane blades used is 16 blades with a chord length of 0.75 meters and a height of 1 meter and uses a NACA 2.5411 airfoil. The spiral casing design has a semi-spiral type and the type of draft tube used is elbow type. Target output hydraulic power of 5 MW can be achieved for every blade angle variation. The cavitation may occur at the suction side's leading edge of the blade due to flow separation therefore design optimization may conduct to minimalize the cavitation potential at the runner.

References

[1] Badan Pusat Statistik, "Berita Resmi Statistik No. 7/01/Th.XXIV," no. 27, pp. 1–52, 2021, [Online]. Available: https://papua.bps.go.id/pressrelease/2018/05/07/336/indeks-pembangunan-manusia-provinsi-papua-tahun-2017.html.

[2] Direktorat Jenderal Ketenagalistrikan, "Statistik Ketenagalistrikan 2019," vol. 33, no. 9, pp. 1689–1699, 2020.

[3] Direktorat Jenderal Keteragalistrikan, "Statistik Kelistrikan 2020," Kementrian Energi dan Sumber Daya Miner. Direktrat Jenderal Keteragalistrikan, vol. 13, no. April, p. 122, 2021.

[4] N. Alrikabi, "Renewable Energy Types," J. Clean Energy Technol., no. January 2014, pp. 61–64, 2014, doi: 10.7763/jocet.2014.v2.92.

[5] PT. PLN (Persero), "Electric Power Supply Business Plan (2019-2028)," pp. 2019–2028, 2019, [Online]. Available: http://gatrik.esdm.go.id/assets/uploads/download_index/files/5b16d-kepmen-esdm-no.-39-k-20-mem-2019-tentang-pengesahan-ruptl-pt-pln-2019-2028.pdf.

[6] European Small Hydropower Association, Layman's Guidebook on how to develop a small hydro site. Brussels: Directorate General for Energy, 1998.
[7] A. S. Leon, "A dimensional analysis for determining optimal discharge and penstock diameter in impulse and reaction water turbines," no. August, 2018, doi: 10.1016/j.renene.2014.06.024.
[8] C. D. Fulzele, "Introduction and Design of Elbow Type Draft Tube with Hexagonal Shape at Outlet," vol. 3, no. 1, pp. 1–3, 2020, doi: 10.5281/zenodo.3859299.
[9] Z. Zhang, "Master equation, design equations and runaway speed of the Kaplan turbine," J. Hydrodyn., vol. 33, no. 2, pp. 282–300, 2021, doi: 10.1007/s42241-021-0020-1.
[10] C. Abeykoon and T. Hantsch, "Design and analysis of a Kaplan turbine runner wheel," Proc. World Congr. Mech. Chem. Mater. Eng., vol. 2011, pp. 1–16, 2017, doi: 10.11159/htff17.151.
[11] M. M. Oo, "Design of 50 kW Kaplan Turbine for Micro hydro Power Plant," vol. 3, no. 2, pp. 264–270, 2019, [Online]. Available: http://www.irejournals.com/formatedpaper/1701517.pdf.
[12] J. Raabe, Hydro Power : The Design, Use, and Function of Hydromechanical, Hydraulic, and Electrical Equipment. Dusseldorf: VDI Verlag, 1985.
[13] Z. M. Chan and Z. N. Aung, "Design calculation of Kaplan Turbine Runner Blade for 15kw Micro Hydropower Plant," vol. 5, no. 4, pp. 14–16, 2020.
[14] S. Le Minn, H. H. Win, and M. Thien, "Design and Vibration Characteristic Analysis of 10kW Kaplan Turbine Runner Blade Profile," Int. J. Sci. Eng. Technol. Res., vol. 03, no. 06, pp. 1038–1044, 2014.
[15] R. S. Varshney, Hydro Power Structures (Including Canal Structures and Small Hydro). Roorkee: Nem Chand & Bros, 2001.
[16] D. Adanta, I. M. R. Fattah, and N. M. Muhammad, "COMPARISON OF STANDARD k-epsilon AND SST k-omega TURBULENCE MODEL FOR BREASTSHOT WATERWHEEL SIMULATION," J. Mech. Sci. Eng., vol. 7, no. 2, pp. 039–044, 2020, doi: 10.36706/jmse.v7i2.44.
[17] P. M. Gerhart, A. L. Gerhart, and J. I. Hochstein, Munson, Young, and Okiishi's Fundamentals of Fluid Mechanics, 8th ed. USA: John Wiley & Sons, Inc., 2016.

Proceedings of the 3rd ITB Graduate School Conference ISSN: 2963-718X
Enhancing Creativity in Research Through Developing Innovative Capabilities
December 21, 2022

On the Field Localization in a Thick Braneworld

Muhammad Taufiqur Rohman*, Triyanta & Agus Suroso

Theoretical High Energy Physics Division, Faculty of Mathematics and Natural Sciences, Institut Teknologi Bandung
*Email: mtrohman@students.itb.ac.id

Abstract. A braneworld theory is a higher dimension theory in which a 4D universe is assumed to be confined on a hypersurface embedded in the higher dimensional bulk. This theory is a good candidate that provides solution to the hierarchy problem in high-energy physics. In its development, the proof regarding complete field (such as massless and massive scalar, vector, and spinor) localization for several brane models has not been solved. In this article, we compared between thin and thick branes regarding the localization mechanism. We also analyzed the mechanism of field localization in two types of branes. The requirements for obtaining fields localization on thin branes are also examined.

Keywords: *braneworld; localization; weak field; Randall-Sundrum; thick brane.*

1 Introduction

The braneworld model, as one of the applications of the D-brane concept in string theory, provides a solution to the hierarchy problem in high-energy physics. The extra dimension is connected to the 4D universe by an exponential factor, called a warp factor. Any weak (TeV scale) fields or matter are assumed to be confined on a hypersurface, called a brane, embedded in a higher dimensional spacetime called a bulk. There are many models of brane that had been proposed. Some of the most popular are Randall-Sundrum (RS) [1]-[2], and its modified models [3].

Based on the characteristics of the warp factor, the brane models are classified into thin brane and thick brane. The thick brane model provides a more logical explanation regarding the minimal length scale in fundamental physics. The thick brane solutions are smooth. It can be applied in some higher-order derivative gravity theories. Meanwhile, the thin brane is described as a Dirac delta function in extra coordinates. Some of the thin brane models include Randall-Sundrum I and II, RS-like, and Modified Randall-Sundrum (MRS) by Jones, *et.al* in [3]. The idealistic thin brane model is still incomplete regarding field localization. The proposed MRS model provided better fields localization properties than RS model. Several studies in MRS have been conducted to examine the localization of scalar, vector, and spinor fields, each of them are massive and massless, by Wulandari, *et.al* in [5]-[8], and Rohman, *et.al* in [9].

In the case of thin branes, the localization mechanism follows Bajc *et.al* [4] and Jones *et.al* [3]. In this case, the separation of variables method is assumed and two conditions, namely the normalization and the mass term conditions, that enable ones to reduce the 5D into 4D action must be fulfilled.

In the case of thick brane, we consider a standard thick brane generated by scalar bulk, among them as in Liu, *et.al* [10]-[12]. In this case, the action is defined as 5D Einstein-scalar action with minimal coupling. By varying the action, the equations for the gravitational field and scalar field are obtained. From the field equations, the warp factor $A(y)$ and scalar field $\phi(y)$ maybe obtained after choosing and applying a mechanism such as a first-order formalism for the potential $V(\phi)$. In terms of localization, the warp factor plays an important role in field localization equation, called Schrödinger-like equation. The localization of the field $\phi(y)$ is defined as the following. If the energy of the field $\phi(y)$ is less than a critical energy the field is said to be localized. And vice versa, if its energy is greater than the critical energy it is said not localized. In the latter case the field propagates freely throughout the extra dimension. A paper by Dzhunushaliev *et.al* [14], as an example, discusses such a thing.

We assume the two scalar fields in thick and thin branes play two different roles. The scalar field that generates a thick brane is part of gravity, while the field in a thin brane is a matter or weak field that must be localized in the brane. So, the warp factor $A(y)$ obtained from the action of thick branes cannot be used in the normalization and mass equations in the case of the thin brane. This is because the general solution of the field cannot be obtained.

In Section 2, we will consider deriving the scalar and vector field localization equations in thin brane. In Section 3, we will discuss field localization in MRS-like, because we will determine the solution $A(y)$ of the scalar/vector field equations in extra dimension. Since we are looking for a localized field, the function $\chi(y)$ will be given specifically. In Section 4, we discuss field localization in thick branes. In addition, we also discuss the possibility of solution $A(y)$ in Section 3 when applied in this thick brane. In Section 5, discussion and conclusions.

2 Weak fields equations

Localization of several types of field is one of some important issues in braneworld. Here we consider a general metric of 5D braneworld system

$$ds^2 = p^2(x^5)\tilde{g}_{\mu\nu}dx^\mu dx^\nu - q^2(x^5)(dx^5)^2 \tag{1}$$

where $\bar{g}$ is the 4D brane metric and x^5 is the extra dimension coordinate. The factors $p(x^5)$ and $q(x^5)$ represent warp factors for brane and extra dimension coordinates, respectively. Several models of 5D braneworld have been developed. In RS model [2], it is recognized that $p(y) = e^{A(y)}$ and $q = 1$. In MRS model [3], the coordinate transformation for extra dimension $dz = e^{-A(y)}dy$ was applied, so that the metric has $p(z) = q(z) = e^{A(z)}$ for z-coordinate system. Based on this metric transformation, MRS model is better than RS model on localization properties of scalar, vector, and spinor weak fields, whether they are massless or massive. For the spinor field, its localization in the MRS model is possible when the gamma matrices in a curved space, rather than in a flat space, is taken into account [6]. In this section, we will review the localization requirements that must be met by scalar and vector fields.

2.1 Scalar field

An action of 5D scalar matter field $\phi(x^M)$ with mass m_s is given by

$$S_0 = \frac{1}{2}\int d^5x\sqrt{g}\left(g^{MN}\partial_M\phi\,\partial_N\phi - m_s^2\phi^2\right) \tag{2}$$

where M, N indices represent 5D coordinate system, g is a determinant of the metric tensor g_{MN} that is defined in equation (1). Following the localization mechanism used by Bajc, *et.al* [3] and Jones, *et.al* [4], the 5D scalar field action can be reduced to the 4D scalar field action by field decomposition.
The decomposition for the scalar field is

$$\phi(x^\mu, x^5) = \sum_n \varphi_n(x^\mu)\chi_n(x^5). \tag{3}$$

leads the action (2) into

$$S_0^{(5D)} = \frac{1}{2}\int d^4x\sqrt{\tilde{g}}\tilde{g}^{\mu\nu}\partial_\mu\varphi_m\partial_\nu\varphi_n\int_{-\infty}^{\infty} dx^5 p^2 q\,\chi_m\chi_n$$
$$-\frac{1}{2}\int d^4x\sqrt{\tilde{g}}\varphi_m\varphi_n\int_{-\infty}^{\infty} dx^5\left[p^4q^{-1}(\partial_5\chi_m)(\partial_5\chi_n) + p^4 q\, m_s^2\chi_m\chi_n\right].$$

This 5D action reduces to the 4D one, namely

$$S_0^{(4D)} = \frac{1}{2}\int d^4x\sqrt{\tilde{g}}\delta_{mn}\left(\tilde{g}^{\mu\nu}\partial_\mu\varphi_m\partial_\nu\varphi_n - m_m m_n\varphi_m\varphi_n\right). \tag{4}$$

The normalization equation

$$N_0 = \int_{-\infty}^{\infty} dx^5 p^2 q\,\chi_m(x^5)\chi_n(x^5) = \delta_{mn} \tag{5}$$

and 4D mass equation

$$m_0^2 = m_m m_n \delta_{mn} = \int_{-\infty}^{\infty} dx^5 \left[p^4 q^{-1}(\partial_5\chi_m)(\partial_5\chi_n) + p^4 q m_s^2 \chi_m \chi_n\right],$$
$$m_0^2 = \int_{-\infty}^{\infty} dx^5 \left[\frac{p^4}{q}(\partial_5\chi)^2 + p^4 q m_s^2 \chi^2\right]; \quad \text{for } m = n\,. \tag{6}$$

These two equations are called the properties or the conditions of localization. The equations (5) and (6) contain $\chi_n(x^5)$. This function should be in accordance with the scalar field equation, which is obtained by variation of the action S_0 with respect to the scalar field ϕ,

$$\frac{1}{\sqrt{g}}\left(\sqrt{g}g^{MN}\partial_N\phi\right) - m_s^2\phi = 0. \tag{7}$$

For a spacetime metric (1), the field equation can be derived as follows

$$\frac{1}{\sqrt{\tilde{g}}}\partial_\mu\left(\sqrt{\tilde{g}}\tilde{g}^{\mu\nu}\partial_\nu\phi\right) - \frac{p^2}{q^2}\left[\partial_5^2\phi + \left(4\frac{\partial_5 p}{p} - \frac{\partial_5 q}{q}\right)\partial_5\phi\right] - p^2 m_s^2\phi = 0. \tag{8}$$

Imposing the decomposition (4) and considering φ_n as 4D scalar field satisfying the massive 4D Klein-Gordon, $\frac{1}{\sqrt{\tilde{g}}}\left(\sqrt{\tilde{g}}\tilde{g}^{\mu\nu}\partial_\nu\varphi_n\right) = m_n^2\varphi_n$, then the field equation above reduces to equation for $\chi_n(x^5)$

$$\partial_5^2\chi_n + \left(4\frac{\partial_5 p}{p} - \frac{\partial_5 q}{q}\right)\partial_5\chi_n + q^2 m_s^2\chi_n - \frac{q^2}{p^2}m_n^2\chi_n = 0. \tag{9}$$

2.2 Vector field

Consider a 5D vector field

$$A_M(x^M) = \left(A_\mu(x^M), A_5\right) = \left(\sum_n a_\mu^{(n)}(x^\mu)\alpha_{(n)}(x^5), A_5\right) \tag{10}$$

where A_5 is chosen as a constant or zero [13]. The action of 5D vector field is given by

$$S_1 = -\frac{1}{4}\int d^5x\sqrt{-g}g^{MN}g^{RS}F_{MR}F_{NS}$$
$$= -\frac{1}{4}\int dx^5\sqrt{g}g^{\mu\nu}g^{\rho\sigma}\alpha_{(n)}^2\int d^4x f_{\mu\rho}^{(n)}f_{\nu\sigma}^{(n)} - \frac{1}{2}\int dx^5\sqrt{g}g^{55}g^{\rho\sigma}(\partial_5\alpha_{(n)})^2\int d^4x\, a_\rho^{(n)}a_\sigma^{(n)}.$$

with the field strength tensors $F_{MN} = \partial_M A_N - \partial_N A_M$, and $F_{\mu\nu} = \partial_\mu A_\nu - \partial_\nu A_\mu = \alpha_{(n)}(\partial_\mu a_\nu^{(n)} - \partial_\nu a_\mu^{(n)}) = \alpha f_{\mu\nu}^{(n)}$ is equivalent to

$$S_1^{(5D)} = -\frac{1}{4}\sum_n \left[\int dx^5 q\alpha_{(n)}^2 \int d^4x\sqrt{\tilde{g}}\tilde{g}^{\mu\nu}\tilde{g}^{\rho\sigma} f_{\mu\rho}^{(n)} f_{\nu\sigma}^{(n)} \right.$$
$$\left. +2\int dx^5 \frac{p^2}{q}(\partial_5\alpha_{(n)})^2 \int d^4x\sqrt{\tilde{g}}\tilde{g}^{\rho\sigma} a_\rho^{(n)} a_\sigma^{(n)} \right]$$

when the metric (1) is considered. This 5D action will reduce to the 4D one

$$S_1^{(4D)} = -\frac{1}{4}\sum_n \int d^4x\sqrt{\tilde{g}}\tilde{g}^{\mu\nu}\tilde{g}^{\rho\sigma} f_{\mu\rho}^{(n)} f_{\nu\sigma}^{(n)} - \frac{1}{2}\sum_n m_{1(n)}^2 \int d^4x\sqrt{\tilde{g}}\tilde{g}^{\rho\sigma} a_\rho^{(n)} a_\sigma^{(n)} \quad (11)$$

if the following normalization and mass equations

$$N_1 = \sum_n \int dx^5 q\alpha_{(n)}^2; \quad m_1^2 = \sum_n \int dx^5 \frac{p^2}{q}\left(\partial_5\alpha_{(n)}\right)^2 \quad (12)$$

are satisfied. It can be proven that the action S_1 and the metric (1) give rise to the field equations

$$\frac{1}{\sqrt{\tilde{g}}}\partial_\mu\left(\sqrt{\tilde{g}}\tilde{g}^{\mu\nu}\tilde{g}^{\rho\sigma} f_{\nu\sigma}^{(n)}\right) + \frac{a_{(n)}^\rho}{\alpha_{(n)}}\frac{1}{q}\partial_5\left(\frac{p^2}{q}\partial_5\alpha_{(n)}\right) = 0. \quad (13)$$

Consider two types of vector fields, a massive field and massless field. A 4D massive vector field $f_{\mu\nu}$ satisfying the Proca equation

$$\frac{1}{\sqrt{\tilde{g}}}\partial_\mu\left(\sqrt{\tilde{g}}\tilde{g}^{\mu\nu}\tilde{g}^{\rho\sigma} f_{\nu\sigma}^{(n)}\right) + m_{(n)}^2 a_{(n)}^\rho = 0 \quad (14)$$

leads to the equation for α_n

$$\frac{1}{q}\partial_5\left(\frac{p^2}{q}\partial_5\alpha_{(n)}\right) - m_{(n)}^2\alpha_{(n)} = 0. \quad (15)$$

For a 4D massless vector field, the Proca equation reduces to the Maxwell equation and the equation for α_n simplifies into

$$\frac{1}{q}\partial_5\left(\frac{p^2}{q}\partial_5\alpha_{(n)}\right) = 0. \quad (16)$$

3 Fields confinement on MRS-like

The MRS model, with z-coordinate system, has better properties of localization than the y-coordinate system in the RS model. In addition, the z-coordinate system has a proper distance for extra dimensions whose value is finite [3]. In the case of the MRS brane model with the warp factor $p(z) = q(z) = e^{A(z)}$, the normalization, mass, and field equations for scalar and vector fields are given as follows.

1. Scalar field

$$N_0 = \int_{-\infty}^{\infty} dz e^{3A(z)} \chi^2(z) = 1$$
$$m_0^2 = \int_{-\infty}^{\infty} dz \left[e^{3A(z)} (\partial_z \chi(z))^2 + e^{5A(z)} m_s^2 \chi^2(z) \right], \tag{18}$$

$$\partial_z^2 \chi(z) + 3\partial_z A(z) \partial_z \chi(z) - m^2 \chi(z) = 0; \quad (m_s = 0). \tag{19}$$

2. Vector field

$$N_1 = \int_{-\infty}^{\infty} dz e^{A(z)} \alpha^2(z); \quad m_1^2 = \int_{-\infty}^{\infty} dz e^{A(z)} \left(\partial_z \alpha(z) \right)^2 \tag{20}$$

$$\partial_z^2 \alpha(z) + \partial_z A(z) \partial_z \alpha(z) - m^2 \alpha(z) = 0. \tag{21}$$

We have a freedom to choose either $A(z)$ and $\chi(z)$ in (19) also $A(z)$ and $\alpha(z)$ in (21). In the following we will consider some simple choices.

The MRS model as a thin brane explicitly has the warp factor $A = -k|z|$, where k is a constant. This form of the warp factor is simple, so that it is easy to obtain general solution of $\chi(z)$ for all range of z. This model is better in terms of fields localization as compared to the RS model. However, it is worth to choose some forms of $A(z)$ explicitly that hopefully lead to a complete localization of the field. The given $A(z)$ must be used in the field equation (19) to find a solution $\chi(z)$. Then, the given $A(z)$ and the obtained $\chi(z)$ must satisfy the equation (18). From those equations, it is known that to obtain the finite value of the integral, the integrand must be convergent for the whole range of z.

Consider two functions F and G, for spin-0 and spin-1 fields

$$F_0(z) = e^{3A(z)} \chi^2(z), \quad G_0(z) = e^{3A(z)} (\partial_z \chi(z))^2$$
$$F_1(z) = e^{A(z)} \alpha^2(z), \quad G_1(z) = e^{A(z)} (\partial_z \alpha(z))^2 . \tag{22}$$

These functions are the integrands of the integrals (18) and (20). Choosing $A(z)$ must ensure that the general solutions of $\chi(z)$ and $\alpha(z)$ can be obtained. The functions F_s and G_s (for $s = 0,1$) must satisfy the following conditions

$$\int_{-\infty}^{\infty} F_s(z) dz < \infty, \quad \int_{-\infty}^{\infty} G_s(z) dz < \infty. \tag{23}$$

The integrals converge if the function F_s or G_s converges.

Choosing the function $\chi(z)$ is probably better than choosing the function $A(z)$. This is because we can choose the function $\chi(z)$ so that its values dominate around the brane, thus in accordance with the aim of finding a localized field. In

addition, to find solution $A(z)$, it is enough to solve the first-order differential equation (19), provided that at least the field function must be up to second-order differentiable.

A constant function of $\chi(z)$

Consider a constant $\chi(z)$. From the field equation (19), we get $m = 0$. It means that a constant field only valid for a massless scalar field. From equation (18), it also obtained that $m_s = 0$. Then, there is only an equation to determine the warp factor, that is

$$N_0 = \int_{-\infty}^{\infty} dz e^{3A(z)} = \chi^{-2} = \text{const.} \tag{24}$$

In this case, the warp factor $A(x^5)$ must satisfy equation (24).

A Gaussian function of $\chi(z)$

Consider a function $\chi(z) = e^{-az^2}$, where a is a constant. From the equation (19), a solution for the warp factor is

$$A(z) = \frac{1}{3}az^2 - \left(\frac{1}{3} + \frac{m^2}{6a}\right)\ln(z) + c\,. \tag{25}$$

For simplicity, we take $c = 0$ and $a = m = 1$. The normalization equation in (18) gives a convergent value. Meanwhile, from the mass equation in (18) gives a divergent value. So, the corresponding scalar field are not localized on the brane.

4 Thick brane generated by a scalar field

Consider a thick brane generated by a scalar bulk. The system is based on 5D Einstein-scalar gravity, where the action is given by

$$S_g = -\frac{1}{4}\int d^5x\sqrt{g}R + S_{\text{scalar}} = \int d^5x\sqrt{g}\left(-\frac{R}{4} + \frac{1}{2}g^{MN}\partial_M\phi\,\partial_N\phi - V(\phi)\right) \tag{26}$$

where R is Ricci scalar and $V(\phi)$ is a potential for scalar field $\phi(x^5)$. By varying the action (26) with respect to the metric g^{MN}, the Einstein field equation is obtained,

$$G_{MN} \equiv R_{MN} - \frac{1}{2}g_{MN}R = T_{MN} \tag{27}$$

where the energy-momentum tensor is

$$T_{MN} = \frac{-2}{\sqrt{g}} \frac{\delta S}{\delta g^{MN}}. \tag{28}$$

Consider a 5D spacetime with metric (1) and Minkowskian brane for simplicity. The components of Einstein tensor are

$$\begin{aligned} G_{\mu\nu} &= \eta_{\mu\nu} 3 \frac{p^2}{q^2} \left(\frac{p'q'}{pq} - \frac{p''}{p} - \frac{p'^2}{p^2} \right) \\ G_{55} &= 6 \frac{p'^2}{p^2} \end{aligned} \tag{29}$$

while non-zero components of the energy-momentum tensor are

$$\begin{aligned} T_{\mu\nu} &= \eta_{\mu\nu} \frac{p^2}{q^2} \left(\frac{1}{2} \phi'^2 + q^2 V \right) \\ T_{55} &= \frac{1}{2} \phi'^2 - q^2 V. \end{aligned} \tag{30}$$

Then, the components of Einstein equation are

$$\begin{aligned} (\mu, \nu): \quad & 3 \left(\frac{p'q'}{pq} - \frac{p''}{p} - \frac{p'^2}{p^2} \right) = \frac{1}{2} \phi'^2 + q^2 V \\ (5,5): \quad & 6 \frac{p'^2}{p^2} = \frac{1}{2} \phi'^2 - q^2 V. \end{aligned} \tag{31}$$

y**-coordinate system.** In y-coordinate system, $p(y) = e^{A(y)}$ and $q = 1$, the Einstein equations become

$$\begin{aligned} (\mu, \nu): \quad & -3 \left(A'' + 2A'^2 \right) = \frac{1}{2} \phi'^2 + V(\phi) \\ (y, y): \quad & 6A'^2 = \frac{1}{2} \phi'^2 - V(\phi). \end{aligned} \tag{32}$$

or they can be rewritten as

$$A'' = -\frac{1}{3} \phi'^2, \quad A'^2 = \frac{\phi'^2}{12} - \frac{V}{6}. \tag{33}$$

If the two equations are combined by eliminating the kinetic term, the potential is obtained

$$V = -\frac{3}{2} \left(A'' + 4A'^2 \right). \tag{34}$$

An appropriate warp factor can be inserted in this potential. In this coordinate system, we have to make the warp factor transformation from z to y-coordinate, $A(z) \to A(y)$, using

$$y = \int e^{A(z)} dz. \tag{35}$$

To get z as a function of y it is necessary to find the inverse of the function $y(z)$ in (35). Then, $z(y)$ is substituted into $A(z)$. If $A(z)$ considered gives the complete localization substituting into (34) will give an explicit form of potential that describes the braneworld gravitational system that localizes the weak fields.

z-coordinate system: In this coordinate, $p(z) = q(z) = e^{A(z)}$. The Einstein equations are

$$\begin{aligned} (\mu,\nu): \qquad -3\left(A'' + A'^2\right) &= \frac{1}{2}\phi'^2 + e^{2A}V \\ (z,z): \qquad 6A'^2 &= \frac{1}{2}\phi'^2 - e^{2A}V \end{aligned} \tag{36}$$

where

$$V = -\frac{3}{2}e^{-2A}\left(A'' + 3A'^2\right). \tag{37}$$

Without changing the coordinate system, solution $A(z)$ can be directly used in this equation.

4.1 Field localization mechanism in a thick brane

The warp factor solution is an important variable that determines the localization conditions of weak fields in the brane. In this section, the localization mechanism for a thick brane is given in case of the scalar field.

Consider a 5D real scalar field, $\phi(x^\mu, r)$,

$$S_0 = -\frac{1}{2}\int d^5x\sqrt{-g}\left(g^{MN}\partial_M\phi\partial_N\phi + m_{(5)}^2\phi^2\right) \tag{38}$$

where $m_{(5)}$ is a bulk scalar mass, g is a determinant of the metric tensor g_{MN}. By varying the action with respect to the scalar field, an equation of motion for a scalar field is obtained

$$\frac{1}{\sqrt{-g}}\partial_M\left(\sqrt{-g}g^{MN}\partial_N\phi\right) + m_{(5)}^2\phi = 0. \tag{39}$$

For a spacetime with metric

$$ds^2 = e^{2A}\left[\tilde{g}_{\mu\nu}dx^\mu dx^\nu - dz^2\right]. \tag{40}$$

The equation of motion for scalar field can be rewritten as

$$\frac{1}{\sqrt{-\tilde{g}}}\partial_\mu\left(\sqrt{-\tilde{g}}\tilde{g}^{\mu\nu}\partial_\nu\phi\right) + \phi'' + 3A'\phi' - m_{(5)}^2 e^{2A}\phi = 0. \tag{41}$$

Applying the Kaluza-Klein (KK) decomposition, $\phi(x^\mu, z) = \sum_n \varphi_n(x^\mu)\chi_n(z)$, and imposing that the 4D scalar field obeys 4D Klein-Gordon equation, then the field equation for scalar bulk ($m_{(5)} = 0$) is obtained

$$\chi_n'' + 3A'\chi_n' + m_n^2\chi_n = 0, \tag{42}$$

where m_n is KK mass spectrum. As described in the case of thin brane, the reduction of 5D action to 4D action requires normalization and mass conditions. In the articles discussing thick brane, these conditions were not tested further. In the case of thick branes, the field equations are transformed into Schrödinger-like equation, by defining a new scalar field

$$\tilde{\chi}_n(z) = e^{\frac{3}{2}A}\chi_n(z). \tag{43}$$

The equation for 5D scalar field is

$$\left[-\partial_z^2 + V_0(z)\right]\tilde{\chi}_n = m_n^2\tilde{\chi}_n; \qquad V_0(z) = \frac{3}{2}A'' + \frac{9}{4}A'^2, \tag{44}$$

where $V_0(z)$ is the effective potential of the scalar field. It depends on the warp factor only. The localization condition can be analyzed from the mass spectrum of the scalar field. A state related to the mass m_i must have an energy lower than the critical energy, to satisfy the field localization on the brane. A massless mode as an analogy to the ground state, and some massive modes as an analogy to the excited states.

5 Discussion and conclusions

By definition, a braneworld traps weak fields (TeV scale) in a brane as a hypersurface. As stated in previous studies, in RS brane model not all fields are well localized. For this reason, we tried to conduct a review regarding the localization of the fields. As is well known, there are two types of branes based on the characteristics of the warp factor, those are thick and thin branes. The two types of branes also describe a localization mechanism that is technically different, but fundamentally has the same mechanism. First, thin branes try to analyze localization which focuses on reducing 5D action to 4D action. Then, the normalization and mass equations are obtained. Weak scale fields must obey these equations to be said to be locally in the brane. Second, thick branes analyze

the localization of the field equations in the extra coordinates, which are called Schrödinger-like equations. The bound states (ground state and some excited states) in the system are analogous to a localized field with a certain mass mode.

Solution $A(x^5)$ obtained from the gravitational field equation for thick branes cannot be used for the normalization and mass equations for thin brane. If the solution $A(x^5)$ is applied in the field equation, then the general solution for the field cannot be obtained. Due to the impossibility of obtaining the general solution, we emphasize the review of the normalization and mass equations directly to obtain the solution conditions $A(x^5)$ or $\chi(x^5)$. As was done in Section 3, it would be better if explicit function of either $A(x^5)$ or $\chi(x^5)$ is given. Between the two, choosing the field function would be better, because we can choose a function that describes the presence of a field at a certain point or area. Physically, the Dirac delta function would be a good candidate, because it represents the field function in a thin brane. However, it becomes a problem when the Dirac delta function is applied to the field equations to obtain $A(x^5)$.

From the possibility that if we obtain $A(x^5)$ that meets the requirements in Section 3, then this $A(x^5)$ can be used to define braneworld metric. We have considered the bulk scalar brane system in Section 4 as the gravitational framework.

Acknowledgement

This research was supported by PPMI-ITB.

References

[1] Randall, L. & Sundrum, R., *Large mass hierarchy from a small extra dimension*, Physical Review Letters **83** (10) pp. 3370-3373, 1999.

[2] Randall, L., & Sundrum, R., *An Alternative to Compactification*, Physical Review Letters, **83**(23), pp. 4690-4693, 1999.

[3] Jones, P., Muñoz, G., Singleton, D., & Triyanta, *Field localization and the Nambu–Jona-Lasinio mass generation mechanism in an alternative five-dimensional brane model*, Physical Review D, **88**, 025048, 2013.

[4] Bajc, B. & Gabadadze, G., *Localization of matter and cosmological constant on a brane in Anti-de Sitter space*, Physics Letters B, 474 pp. 282-291, 2000.

[5] Wulandari, D., Triyanta, Kosasih, J. S. & Singleton, D., *Localization of a system of vector and scalar fields in a modified Randall-Sundrum model*, AIP Conference Proceedings, 040003, 2015.

[6] Wulandari, D., Triyanta, Kosasih, J. S., Singleton, D. & P. Jones, *Localization of interacting fields in five-dimensional braneworld models*, International Journal of Modern Physics A, 32, 2017.

[7] Wulandari, D. Triyanta, Kosasih, J. S. & Singleton, D., *Localization of matter fields that interact with gravity in a non-minimal derivative coupling in the Randall-Sundrum model*, Journal of Physics: Conference Series **1120** (11) 012040, 2018.

[8] Wulandari, D., Triyanta, Kosasih, J. S. & Singleton, D., *The Field Localization of Yukawa Interaction in a Modified Randall-Sundrum Model*, Journal of Physics: Conference Series, 2019.

[9] Rohman, M. T. & Triyanta, *Searching for a modification of a conformally flat metric in the five-dimensional braneworld model that localizes scalar and vector fields*, Journal of Physics: Conference Series, **1949** (6) 012004, 2021.

[10] Liu, Y., *Introduction to extra dimensions and thick braneworlds*, Memorial volume for Yi-shi Duan, pp. 211-275, 2018.

[11] Liu, Y., Guo, H., Fu, C., & Li, H., *Localization of gravity and bulk matters on a thick anti-de Sitter brane*, Physical Review D, **84**(4), 044033, 2011.

[12] Liu, Y., Zhang, L., Wei, S., & Duan, Y., *Localization and mass spectrum of matters on Weyl thick branes*, Journal of High Energy Physics, 2008 (08), 041, 2008.

[13] Guo, H., Herrera-Aguilar, A., Liu, Y., Malagón-Morejón, D., & Mora-Luna, R., *Localization of bulk matter fields, the hierarchy problem and corrections to Coulomb's law on a pure de Sitter thick braneworld*, Physical Review D, 87 (9), pp.1-21, 2013.

[14] Dzhunushaliev, V., Folomeev, V. & Minamitsuji, M., *Thick brane solutions*, Reports on Progress in Physics, **73** (2010) 066901.

Proceedings of the 3rd ITB Graduate School Conference ISSN: 2963-718X
Enhancing Creativity in Research Through Developing Innovative Capabilities
December 21, 2022

Development of Application Design to Support Mathematics Learning in the Subject of Three-Dimensional Geometry for Class XII High School Students

Nidya Putri[1] & Banung Grahita[2]

Magister Desain, Fakultas Seni Rupa dan Desain, Institut Teknologi Bandung
Jl. Ganesa No.10, Kota Bandung, 40132 (022) 2500935
Email: [1]nid.putri@gmail.com & [2]banung@itb.ac.id

Abstract. This study discusses the design of applications as a medium to help students solve three-dimensional geometry problems. Three-dimensional geometry is one of the abstract mathematics subjects. Students need good spatial abilities to understand and solve three-dimensional geometric problems well. However, in reality, many students find it difficult due to their lack of spatial abilities. This problem can happen because students work on a three-dimensional shape in a two-dimensional plane that they cannot interact with and explore. Therefore, an application will be designed through this research to overcome these two problems. This study uses a five-element user experience framework to find and understand the actual problems experienced by students and continue each stage of user-oriented design. This study's results expect to help students better understand and solve three-dimensional geometric problems.

Keyword*: application; user experience; user interface; three-dimensional geometry; high school students*

1 Introduction

Geometry is one of the subjects in mathematics that must be studied by elementary to high school students. Each level has a learning sequence starting from pure geometry, analytics, and transformation (Sholihah dan Afriansyah, 2017). As for the subject matter, the geometry studied at school consists of two-dimensional and three-dimensional geometry. Three-dimensional geometry is part of the geometry that discusses the relationship between points, lines, and planes (Novita et al.: 2018). Also, three essential competencies consist in geometry that XII high school students must learn. First, students are taught to solve problems related to distances between points, then about the distance from a point to a line, and the last distance from a point to a plane.

Learning three-dimensional geometry for class XII already involves distance measurement between shapes. According to essential competencies, students must be able to solve geometric problems not only from analytical problems but

also from visual objects (Kariadinata, 2010), which in class XII student material is the distance in space. The space distances can form if the questions are informed points, lines, and planes. However, these points, lines, and planes are not always parts that exist in shape but can come from the new one. With the lines and planes formed in these shapes, it is often difficult for students to imagine these shapes because they involve more than one object.

One factor that makes the spatial process difficult is the student's need for spatial ability, primarily when they work geometry in a two-dimensional plane. Capturing and rotating an element requires good visual-spatial skills when imagining objects from different perspectives to solve three-dimensional geometry problems (Febriana, 2015). According to Meier (1996), there are five indicators contained in spatial ability: 1) spatial perception: namely the ability related to how to see an object from a vertical and horizontal perspective 2) spatial visualization: the ability to show a change and locking of the constituents of an object either three-dimensional or two-dimensional 3) mental rotation: the ability to rotate objects in both three dimensions and two dimensions 4) spatial relations: the ability to understand the structure and parts of an object and also the relationships that these objects produce with others 5) spatial orientation: the ability to Observe an object from a different point of view.

Also known, a two-dimensional field such as paper or blackboard is a medium that cannot be interacted with. When students have difficulties in carrying out spatial processes, the choice they have to solve the problem is to draw again. According to Van Hiele, in phase-based learning theory, drawing is a skill that students must have when they want to understand geometry. Drawing becomes very important because at each level of learning geometry, according to Van Hiele, there is always a process of drawing. This drawing process also allows students to add information about the object they want to complete. However, research conducted by Rahmad et al. (2013) found that one of the indications that cause students to have difficulty understanding three-dimensional geometry is the lack of skills in drawing and using tools to draw three-dimensional and also because they tend to rely on formulas.

In addition to the ability to draw itself, the media also plays a role in students' success in solving three-dimensional geometry problems. Such as the use of blackboard and paper media will limit the process of exploring images by students, so media that can observe, manipulate, hear, and read is needed (Kadir & Yani, 2012). The teacher's ability is also crucial because some teachers need to start using assistive devices, so they do not help stimulate students' ability to understand the shapes. Students also tend to be afraid first, primarily if many plans form in one shape. Teaching media are also not diverse because most schools still use books and worksheets. In addition, students are also too used to

learnSing with visual shapes that are always the same, so when they face different visual objects, these students will experience confusion and need more time to understand and solve the problem. Based on this description, this research must produce a product that can facilitate students when studying and solving geometry problems.

2 Methodology

The method used in this study is qualitative, with a framework using the Five Elements of Users' Experience. This framework comprises five levels of designing a product, starting from the research process and data collection to produce a prototype. The five design levels consist of Strategy, Scope, Structure, Skeleton, and Surface, where each stage is interconnected from the bottom up. The data obtained at the strategy level will influence the following process in this framework. These results will also ascertain the difficulties students experience when working on three-dimensional geometry so that when they continue to design, the resulting product is needed and genuinely oriented to its users.

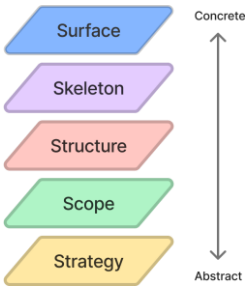

Figure 1 Five-elements of user experience

3 Results

Based on the background of the problem and the method proposed, the following results obtained.

3.1 Strategy

Data collection at this stage will help build product objectives, user needs, and persona. Data is collected by doing interviews and observations of 8 students of class XII in high school/equivalent who studied three-dimensional geometry. Students must answer five questions. Each of the questions represents basic competence in class XII three-dimensional geometry. This problem has different types to determine students' abilities in understanding the question, redrawing the pictures of questions, and understanding the pictures they draw again.

In working on the questions, it will observe six points from students. It starts with how students understand shapes. It can see how they commonly use the values and signs to identify images. Then the drawing activities were carried out by students. After that, the third point that will observe by students is how they separate the planes that formed in the shapes. Knowing what students are doing at this point will help to understand how students make decisions in solving problems, especially for images with a point of view that is difficult to understand.

Furthermore, the fourth point that will observe is their habit when drawing the object, whether they use specific tools to help them understand an image and draw again. The fifth point is to find out whether students can change the perspective of shapes because the planes formed in shape tend to be hard to understand, so for some students, apart from removing the plane, another way he can do this is to change the perspective of the shape. The last point is whether students have the habit of re-examining the pictures they make because their results influence the continuation of their problem-solving process.

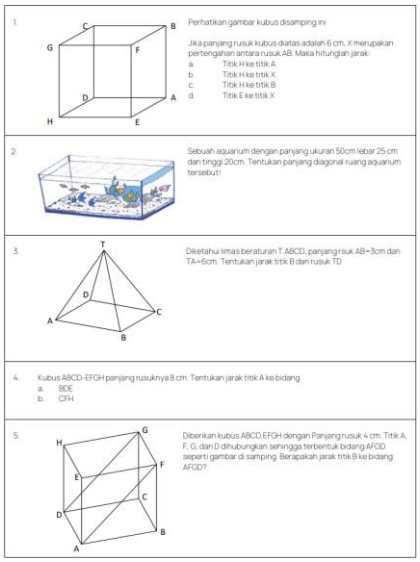

Figure 2 List of observation questions

In addition, there are also several considerations regarding the type of questions that students need to solve, such as 1) From the point of view, it is different from what the students usually do, 2) There are variations of the shape, 3) Some questions do not have an object, requiring students to draw pictures without examples in the questions.

After doing observation, the next step is to interview the student. This process will help to confirm the findings from the observations. It also obtains general information about students' habits and life to form a user persona. Apart from the user persona, the results obtained from these observations and interviews will help identify user needs and product objectives.

3.1.1 Observation Result

From observations and interviews conducted with students, several findings affect the process and results when students work on questions. There are several ways for students to determine the pictures that they will make. The student will immediately copy the object if there is an object in the question. It can see the different shapes from each edge on the front view of a shape. However, if there is no object, students usually use the information directly mentioned or derived from usually known measurements.

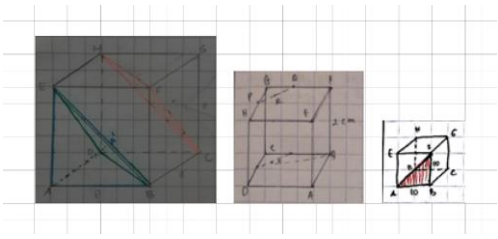

Figure 3 Student image size comparison

When students redraw their shapes, they also tend to use the number of boxes in their paper works books as a benchmark. Some students use many boxes, and some use a smaller number.

Of the eight students who observed and interviewed, all usually redraw the object in their paperwork which is usually a grid paper. When drawing, students often use some help. As in pictures 3 and 4, some use dash lines to show the spatial shape, and some use solid and colored lines.

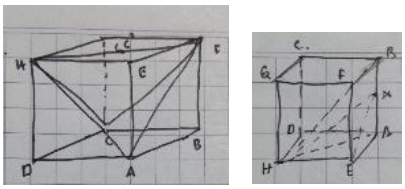

Figure 4 If there are many fields in a shape

When redrawing the shape, some students need to correct themselves in placing the point position. The point can place anywhere as long as it is the same as the

information given in the question. For example, there is a shape ABCD.EFGH, the order in placing these points must follow paths A, B, C, D, and E must be parallel to A, followed by F, G, and H. However, if the question is known, it is the shape of The ABDC.EFGH point placed must also follow A, B, D, C, E, F, G, H

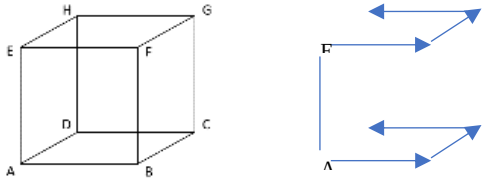

Figure 5 Build point sequence

When a new plane has formed on a shape, most students will take the plane out. However, there is also one student who works directly on the main shape. He will only move the plane if he finds it difficult to solve the problem.

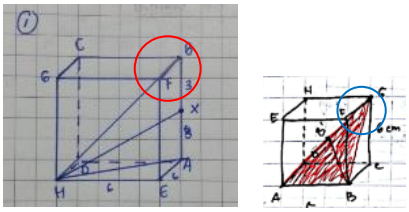

Figure 6 Student drawing results: effect of the position of the diagonal line in space

Students often lose the diagonal lines of space because of the orthogonal lines they make. It happens because students use the box grid in the paperwork as a benchmark for making tidal angles or angles formed between frontal and orthogonal lines.

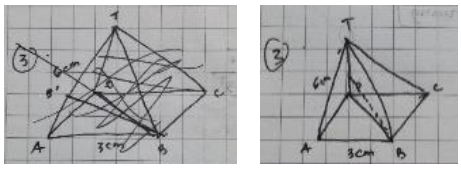

Figure 7 Prism image on the same problem (left)-(right)

Students also often lose lines when drawing prisms. In figure 7, the image on the left one gets crossed; the perpendicular line should be able to form towards the apex. Also, the oblique line TB is still visible, but this student is still determining if the shape produces the plane she needs. So she tries to change the shape, which

is missing the vertical line straight to the top of the T. This often happens when students draw a pyramid.

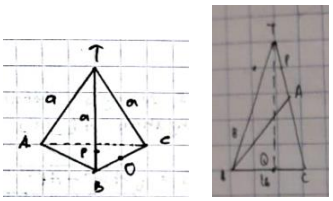

Figure 8 Triangular Pyramid

In addition to rectangular prisms, there are also triangular prisms. From this shape, we can see that the shape produced by students has no volume. The prism looks more like a plane.

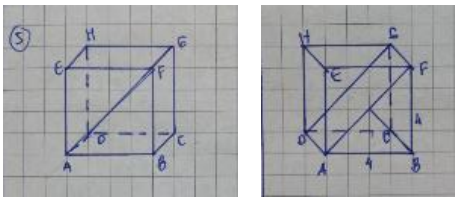

Figure 9 Changing Perspective

Because their drawing area is a math notebook which is a two-dimensional plane, there are two ways that most students do. It is to change the viewpoint and move the point on the shape. After that, they will draw the plane again.

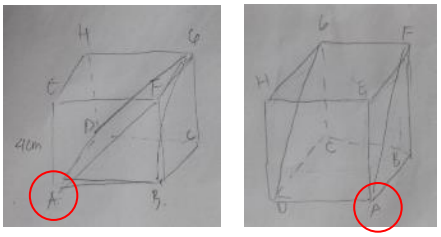

Figure 10 moving points

These two methods can replace the spatial rotation function that usually occurs in mind. It will help them to gain information.

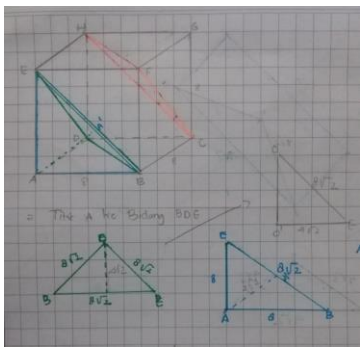

Figure 11 a picture of a student having difficulty moving the points

Even though changing perspective and rotating points is a solution, some students are afraid to do it. Because from their perspective, the image result is different from what they originally made. He feared that the difference would also affect the value of a side that was not even real. However, after changing the perspective and rotating the perspective, the resulting image is different, so they will have the perception that because visually if the shape is different, the size is also different.

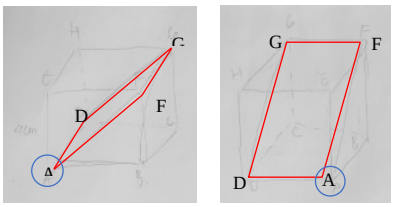

Figure 12 Visuals of different planes of the same

3.1.2 Interview Result

There are four parts to the interviews conducted with students.

Table 1 Table 1: interview results

First part: The experience of students learning three-dimensional geometry at school	> some teachers describe many planes in one form without removing these planes > Some teachers also do not use aids, visual aids, or anything that can distinguish a plane in terms of construction > The teaching materials used do not vary > The visual type of images that create are also always the same > When explaining space, some teachers associate the shape with the classroom. Some students thought it helped them, but some could not do it anymore According to the students, the things above were enough to influence their drawing habits and their ability to understand the plane and find ways to solve the geometric problems they were working on.

The second part: Student experience	> What is most difficult for students is if there are many planes in one shape > With so many planes, students often lose the plane they are looking for > Students agree that their ability to solve geometry can improve if they practice a lot
Third part: Students' experience with the visual images they are working on	> Visuals that are always the same can make them bored working on questions > If not familiar with the visuals, they will be afraid that they cannot solve the problem > While drawing, the student just tried to imitate the shape. It happens if they do not understand the shape and try to collect information about the shape > Some students need help such as rulers, colored writing instruments > Those who do not use assistive devices use techniques such as using dash lines or color blocks to help understand the objects > When drawing, students tend to draw on lined paper and use plain paper as a medium for them to make sketches > According to some students, cleanliness and tidiness are very important when drawing
Fourth part:	> One student who is an Olympiad is more focused on solving the mathematics aspect > Three students like mathematics but have difficulty learning mathematics in high school, and three do not like mathematics. They all fear being unable to solve problems and affecting their grades. Then there is one person who does not want to be too long associated with mathematics > Students stated that the teachers who taught in their classes did not make use of technology and that teachers preferred to use books as materials > Only a few subjects allow using technology, such as laptops and smartphones, for presentations and sharing teaching materials > Students who prefer using smartphones explained that devices are more concise and easy to be carried anywhere. Smartphones are also popular because of the applications they use to help students learn using the photo feature. > Also, some students use Chromebooks because they are taking an online course. Then some use laptops because they have many features > The information references needed by students tend to be text and audio-visual, but there are 3 out of 8 students who need features that can explain this information, like teachers in class > Students have many assignments, so they have a pretty hard time exploring things > Students use notebooks to keep good information obtained while studying at or outside school. Students use notes, so they do not have to look for the information in the original resource

	> Students' favorite social media are Instagram and TikTok. While using Instagram, students now rarely use the feed, more using the story feature > Some learning applications are familiar to the student, like Qanda, Ruangguru, RoboGuru, and also Quipper

Based on the results of the observations and interviews before, there are several recommendations obtained to help students learn and solve three-dimensional geometry problems, including:

1. It is easier for students to determine the shapes they want to find
2. Students can name the point correctly according to the position that informs in the question
3. Students do not lose the lines when drawing (especially for cubes and pyramids)
4. Students can distinguish the front and back of the shape so that they understand the spatial shape
5. Students can rotate the shapes without having to redraw them
6. Students can identify the image of the plane to be issued
7. When rotating the shape, Students can understand the shape and size of the object
8. More than one plane can be formed in shape, but students still have to see the differences easily
9. Students can save their work and still access it if they want to study it again

3.2 Scope

Recommendations obtained at the Scope stage will be developed to find the right features for users. These features are explained through user stories.

Table 2 User Story 1**:** As a user, I want to make it easier to define shapes

As a user, I want	> Have multiple build options > The builds I use frequently are the easiest-to-see/will be placed in first place > Change the perspective of the shape in perspective or isometric mode > There is a difference between shapes, especially cubes and blocks, other than the known size	> It does not take too long to draw from scratch > So that You do not have trouble looking for the shape > So that You can see the wake in various modes > So it does not mix up when choosing shapes (lines of the same length are the same color)

Feature: > Features for drawing: Solid, there is a choice of shapes. Shapes that frequently use are in the front position, > Changing view: o In order to be able to change the visual plane formed in shape to be perpendicular o See the whole shape in perspective and isometry

Table 3 User Story 2: As a user, I want to name the point correctly, so I understand the image (avoiding carelessness)

As a user, I want my	> Point positions are not to be swapped. > The Wrong point can be fixed. > My point is still visible even though behind the shape > Add a point inside a line > The selected point is different from the one that was not selected	> So that the image that I have made follows the question / is not wrong to continue the image > In order to be able to fix if it is wrong when typing a point or fix the point position > So that I can still see all the point > In order to make wake up > In order not to be mistaken when selecting the point being worked on
Feature: > The shape **moves automatically** in one way when it has finished naming a point. > (to prevent the student from unknowingly placing the points incorrectly. The feature will help order points same as the question) > **Delete:** can remove the wrong component/image by deleting or "holding and carrying" (erase/hold and drag) > **Undo:** for minor errors, there is no need to remove the component > The added point is not limited to the shape or space angle but can also be inside the line > **Opacity:** to help adjust the color density of shapes and planes > **Point:** to name the point > The currently selected point has a different color than the unselected point.		

Table 4 User Story 3: As a user, I want a rotatable shape so that it does not lose the diagonal and orthogonal lines

As a user, I want	> The perspective of the shape is changeable > Can add a line from a point > The plane that creates has a different color from the shape	> So it is not fixated on one perspective > In order to be able to draw new planes on the shape > So I know the point I took
Feature: > **Rotate button:** to rotate the shape (so as not to disturb the points or lines on the shape) > **Connect lines:** connect new or existing points > **Color:** it can change the color and also the planes according to what you want		

Table 5 User Story 4: As the user, I want it to be easier to see the shape so I do not get confused between the front and back that I am working on

As a user, I want	> There is a distinction between the front and back of the shape > The point on the back of the wake can still be seen clearly > There is an opacity option to adjust the density of the shape's color	> So that the spatial shape is apparent. Also, when rotated, the front and back are clearer > So that the position of the front and back points is not confused > So that it is clearer to see the plane position that formed in shape
Feature: > To help adjust the color opacity in shapes and planes, color density can be adjusted to bring out the point that is behind the shape		

Table 6 User Story 5: As a user, I want the shape to be visible from many sides, so I do not have to draw on each side like when using a two-dimensional drawing plane like paper

Sebagai pengguna, saya ingin	> Be able to rotate shapes	> So that I do not have to redraw from a different side
Feature: > **Rotate:** to rotate the shape without bothering the point or line		

Table 7 User Story 6: I want the plane that forms in shape still there, so there is no need to take out the plane, which often confuses me

As a user, I want	> No need to move the planes that formed in the shape > Rotate the plane on the horizontal and vertical planes	> So there is no need to redraw on a new plane > So that it is easier for me to see in a flat and straight plane so as not to get confused
Feature: > Just like perspective and isometrics, there is also a button that can activate the position of the selected plane to a vertical position so that it becomes flat and perpendicular, and a button to return to its initial position		

Table 8 User Story 7: I want to identify the planes that form in shape easily, even if there contains more than one plane. I do not want to be confused between one plane and another

Sebagai pengguna, saya ingin	> There is an option to give a different color to the selected plane	> So that one plane and another are not mixed
Feature : > **Color,** in order to change the color of the selected area > **Opacity,** to help set the thickness of the plane		

Table 9 User Story 8: I want to be able to save previous work so I can review it again if I need to

As a user, I want to	> Be able to save specific/previous work > There is history/recent wor	> So that it can be studied if necessary > So I can track the work I have done
Feature: > **Save,** if you want to save work and review specific work (requires login to the application) (students have a habit of studying the homework again, especially when going to exams)		

3.3 Structure

The structure is in the third stage of these five stages. This stage connects the strategy and scope to the next level in the skeleton stage. This stage will determine the end result of the product that the user will use. In the structure stage, it is made based on the stages for new users and also the stages when making a build. For new users, the process includes entering the application. Continuing to enter the canvas that can access with the create new, open, and recent buttons. The user can access open only if he has saved his previous work and logged in to the application. However, if they do not go through the login process, students can keep working but cannot save their work. Whereas through recent work can only access some previous work. If there are other jobs, the old ones can be lost.

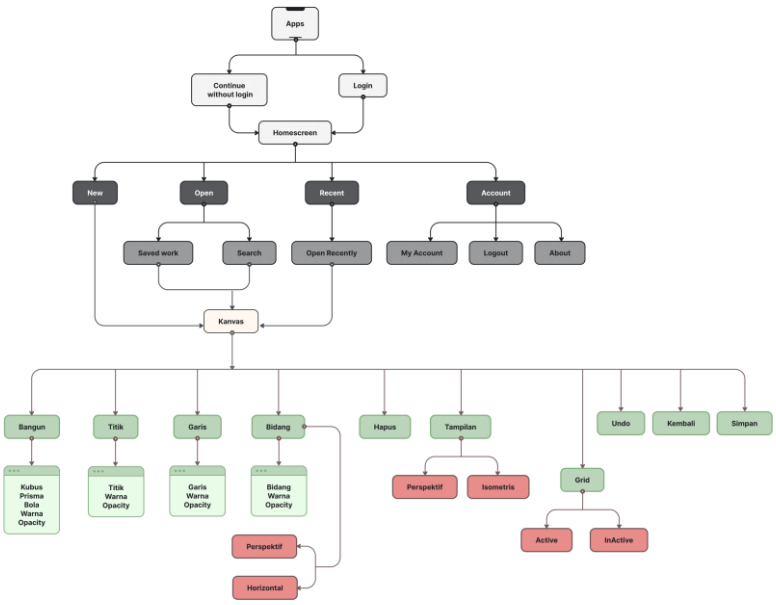

Figure 13 Information Architecture

Based on students' habits when working on problems, they always start by drawing, continue adding points, and connecting them with the line. For Olympiad students, he starts by knowingly analyzing the values in the questions to use or determine the best equation. Done with identifying and drawing the shapes, the students will recheck the question to find out what they need to solve the problem. The main features for drawing consist of shape, point, line, and plane options. Then there are also features such as activating the grid. That feature will help students who get used to using the squares on math paperwork to measure the shape size.

To prevent students from making mistakes, when adding a point, the shape will automatically rotate the shape so that students are confident in placing the point. Then there is also an undo feature that can use if the student misplaces the point. The automatic rotation of the shapes can prevent students from misplacing a point, but students can still misname it.

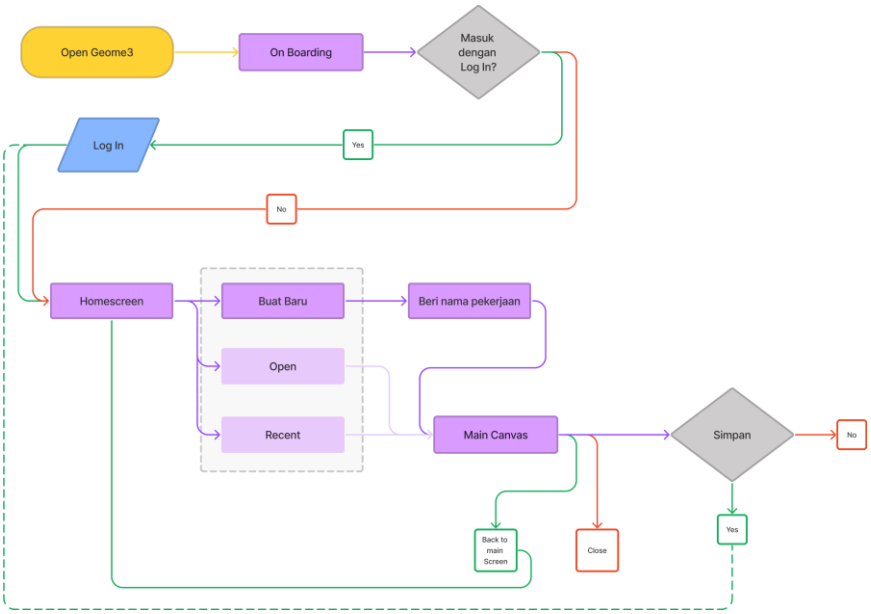

Figure 14 User flow

3.4 Skeleton

In the skeleton plane, three things must consider: interface design, navigation design, and information design. Interface design includes the design for components such as buttons, lists, and other interface components. Navigation design is a particular product from the interface that will adapt to the information. Meanwhile, information design presents communicative information.

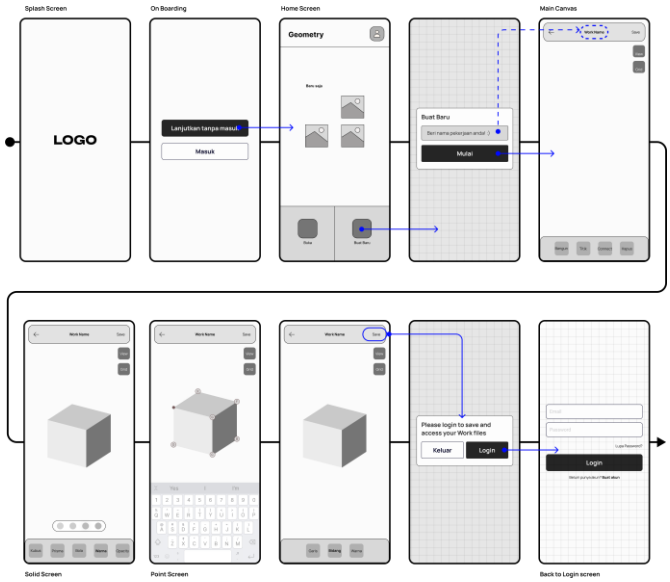

Figure 15 Wireframes

Next is made a wireframe, which is a place for interface design, Navigation design and information design to be put together. In the design, the screen starts from onboarding and continues to the home screen. While onboarding, the user can log into their account or continue without logging into the account. On the student home screen, there are also options for students to create new work, open work they have previously saved, or access what they have work. The recent work is different from the saved one. It will only show some of the last work and is not permanent. The one they just worked on also does not require access to the user account. Before entering the canvas, the user is asked to provide a name for the job. Entering the main canvas, users can access the main drawing tools: shape, point, line, area, and delete.

3.5 Surface

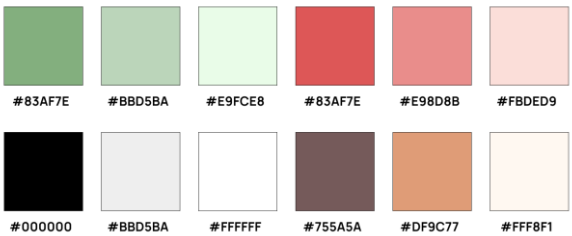

Figure 16 Colors

The surface has a focus on the user's sensory experience. One of them is vision. Vision is an area to develop the user experience from visuals, not only aesthetically but also how these visuals help the product run well.

It is the same with designing other visual designs. Color is needed to help lead users. Color can help impact users' perceptions when using a product. In addition, color also acts as a visual identity and can build a brand owned by a product.

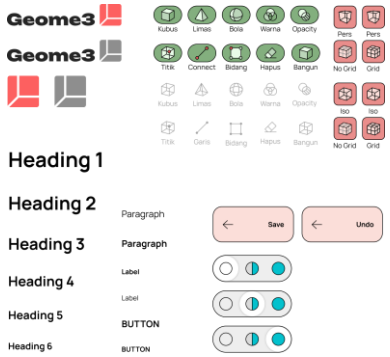

Figure 17 Typography and components

Based on the previous wireframes, the next step is combining that wireframes with colors, typography, and components. After that, make the interaction between each element and component so users can run and test this application to gain user experience.

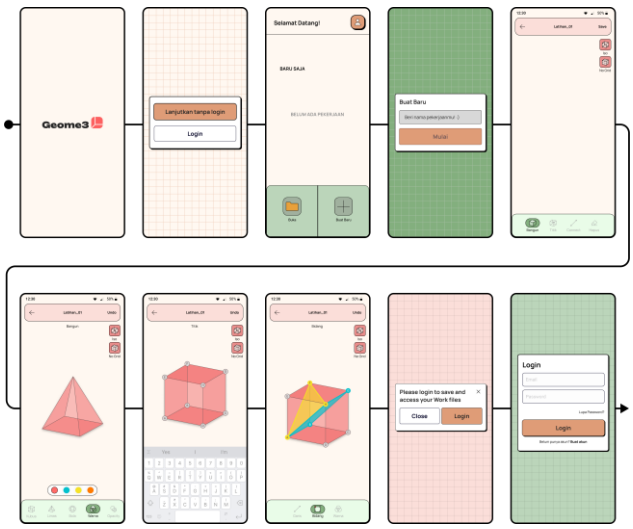

Figure 18 Interface

4 Conclusion

Something is needed to help students learn and solve three-dimensional geometry problems. Based on secondary data from previous research, they need a media that they can explore but does not confuse them. The media must be able to help students draw well and make them understand the shapes they draw. Research is continued on users using the Five Elements of Users Experience framework. The research conducted with this framework found the user needs. Some of the results in this study confirm previous secondary research, and other results serve as a reference for design recommendations to be implemented. The media that will use is an application. Because even though students have their favorite devices, such as laptops or chrome books, they all have smartphones and spend much of their time with them. This design is still a high-fidelity prototype with results starting from the user entering the application, using the drawing tool until finished using the application.

Reference

[1] Kadir, Yani. A. (2012) Pengaruh Alat Peraga Pembelajaran Dimensi-3 dan Dimensi-2 Terhadap Hasil Belajar Geometri Dimensi tiga Ditinjau dari Kemampuan Spasial Siswa MTS, ALGORITMA, 7, 121-140

[2] Kariadinata, R. (2010) Kemampuan visualisasi geometri spasial siswa madrasah aliyah negeri (man) kelas X melalui software pembelajaran mandiri, jurnal EDUMAT, 1, 1-13

[3] Febriana, E. (2015) Profil kemampuan spasial siswa menengah pertama (SMP) dalam menyelesaikan masalah geometri dimensi tiga ditinjau dari kemampuan matematika, Jurnal Elemen, 1, 13-23

[4] Maier P. H., (1996) Developments in Mathematics Education in Germany Selected Papers from the Annual Conference on Didactics of Mathematics, Regensburg. 69-81

[5] Novita, R., dkk (2018) penyebab kesulitan belajar geometri dimensi tiga, jurnal riset pendidikan matematika 5, 18-29

[6] Rahmad, Badi Hidayat; Sugiarto, Bambang; dan Pramesti, Getut. (2013). Analisis Kesalahan Siswa Dalam Menyelesaikan Soal Pada Materi Ruang Dimensi Tiga Ditinjau Dari Gaya Kognitif Siswa. Jurnal Pendidikan Matematika Solusi, 1 39 – 46

[7] Sholihah, S., Z. dan Afriansyah, E., A. (2017) Analisis kesulitan belajar dalam proses pemecahan masalah geometri berdasarkan tahapan berpikir van Viele, Masharafa, 6, 287-298

Proceedings of the 3rd ITB Graduate School Conference ISSN: 2963-718X
Enhancing Creativity in Research Through Developing Innovative Capabilities
December 21, 2022

Deformation Monitoring of Lava Dome Growth derived by Sentinel-1A images at Mt. Ibu, North Maluku, Indonesia

Nur Ayu Anas & Asep Saepuloh*

Geological Engineering, Faculty of Earth Sciences and Technology, Bandung Institute of Technology, Jl. Ganesha No. 10, bandung, Indonesia.
*Email: saepuloh@itb.ac.id

Abstract. Understanding the growth of lava domes in volcanoes is one of the most important tasks in volcanology because of the high threat to human life and infrastructure. One of the volcanoes with high lava dome growth is Mt. Ibu in North Maluku Province, Indonesia. Monitoring the growth of the lava dome on Mt. Ibu relied on the visual camera at the observation post. Therefore, the growth of the dome could only be observed from a few vantage points. To resolve this problem, the Sentinel-1A images have been used to monitor the area and volume lava dome regardless of cloud cover or ash plume from the eruption of Mt. Ibu. The current condition of the lava dome has expanded through the outer crater rim in the northern flank, which is about 5 km from urban areas. We used the pair-wise logic technique differential interferometric synthetic aperture radar (PLT D-InSAR) method to monitor the deformation of the lava dome growth from January 2020 to September 2022. The PLT D-InSAR deformation results show that the highest uplift and subsidence occurred in January 2022 about 0.667 m and in August 2020 about -0.48 m, respectively. The k-means clustering, median, and open filtering methods were also used to enhance the contrast of the deformation areas.

Keywords: *Deformation; PLT D-InSAR; K-Means clustering.*

1 Introduction

The existence of a lava dome on a volcano can cause a significant hazard when it becomes unstable and collapse [1]. Apart from instability, other things that can cause the collapse of a lava dome are related to the morphology and internal structure of the lava dome [2]. Examples of lava dome hazards have been occurred on Mt. Merapi and St. Helens. The 2010 Mt. Merapi eruptions occurred due to destructive pyroclastic density currents (PDCs) from the collapse of a lava dome with an area of more than15 km from the summit and caused the evacuation of one-third of one million people around Mt. Merapi [3]. Then on Mt. St. Helens, there was also lava dome eruptions that began with an explosive episode in 1980, which produced eruptive columns 13-15 km above sea level and pyroclastic flows down the northern flank of the volcano [4]. Examples of events on Mt. Merapi and St. Helens are the phenomenon to worry. One of Indonesia's volcanoes with a lava dome is Mt. Ibu, located in North Maluku Province, Indonesia (Figure 1).

Copyright © 2023 Published by ITB, ISSN: 2963-718X

Mt. Ibu is a stratovolcano where the growth of the lava dome needs to be monitored and worried because the lava dome has reached the outer crater rim on the north side. The differential interferometric synthetic aperture radar (D-InSAR) method is one way to monitor deformation. The method has been applied to observe the changes in the soil surface prior to the major eruption of Mt. Merapi in 2010 and to detect pre- and syn-eruptive signatures on Mt. Sinabung [5], [6]. Then the method developed into the pair-wise logic technique (PLT) D-InSAR, which has simple arithmetic to reduce the effect of the atmosphere on the image [7]. Based on this, the PLT D-InSAR method has been used to monitor the deformation of the Mt. Ibu. Deformation can be monitored by this method either in the form of subsidence or uplift. Then, the deformations obtained have been clustered using k-means and filtered using median open filtering. Accordingly, deformation monitoring at Mt. Ibu is necessary because the growth of the lava dome can be observed beyond the surface. We have used Sentinel-1A images to obtain deformation at the summit lava dome regardless of cloud cover or ash from the eruptions.

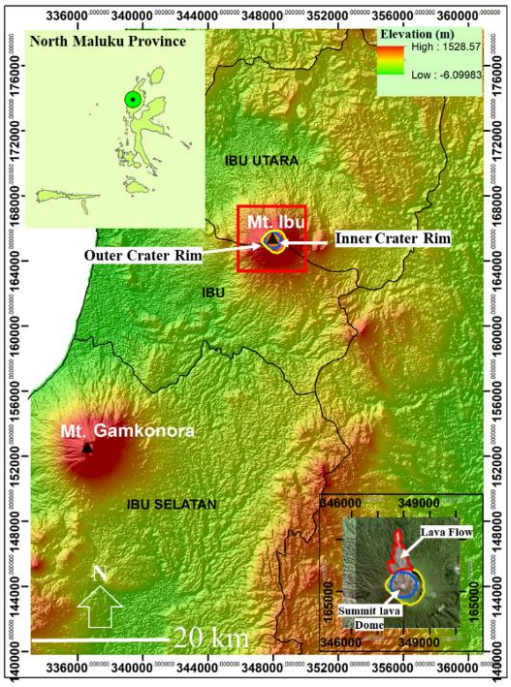

Figure 1 Location of Mt. Ibu given a red rectangle; at the top of Mt. Ibu has an inner crater rim (blue line) and an outer crater rim (yellow line). Then the below inset shows the summit of a lava dome and lava flow (red line).

2 Data used

This study used Sentinel-1A imagery with IW (interferometric wide-swath) beam mode acquisition, single look complex (SLC) file type, and C-band. We have used VV polarization because it can show up and down patterns on deformation correctly, as suggested by previous published study [8]. We have used three bursts from sub-swaths from 1 to 3 from January 2020 to August 2022 (**Table 1**). An example of Sentinel-1A images is shown in **Figure 2**.

Table 1. Sentinel 1A acquisition data.

Number	ID Scene	Acquisition	Polarization	Orbit	Abs Orbit
1	S1A_IW_SLC__1SDV_ 20200113 T21173620200113 T211803030787_0387F5_1019	13 January 2020	VV+VH	Descending	30787
2	S1A_IW_SLC__1SDV_202002 18T21173520200218T211802 031312_039A46_6113	18 February 2020	VV+VH	Descending	31312
3	S1A_IW_SLC__1SDV_202003 25T21173520200325T211802 _031837_03AC8B_4702	25 March 2020	VV+VH	Descending	31837
4	S1A_IW_SLC__1SDV_202004 18T211736_20200418T211803 _032187_03B8DA_D313	18 April 2020	VV+VH	Descending	32187
5	S1A_IW_SLC__1SDV_202005 24T21173820200524T211805 _032712_03CA0A_A7E6	24 May 2020	VV+VH	Descending	32712
6	S1A_IW_SLC__1SDV_202006 17T211739_20200617T211806 _033062_03D47A_D2CE	17 June 2020	VV+VH	Descending	33062
7	S1A_IW_SLC__1SDV_202007 11T211741_20200711T211808 _033412_03DF1B_82E1	11 July 2020	VV+VH	Descending	33412
8	S1A_IW_SLC__1SDV_202008 16T21174320200816T211810 _033937_03EFEA_1BA1	16 August 2020	VV+VH	Descending	33937
9	S1A_IW_SLC__1SDV_202009 21T211744_20200921T211811 _034462_04027B_CCA4	21 September 2020	VV+VH	Descending	34462
10	S1A_IW_SLC__1SDV_202010 15T211745_20201015T211812 _034812_040EB2_2D46	15 October 2020	VV+VH	Descending	34812
11	S1A_IW_SLC__1SDV_202011 20T211744_20201120T211811 _035337_0420DC_DE53	20 November 2020	VV+VH	Descending	35337
12	S1A_IW_SLC__1SDV_202012 26T211743_20201226T211810	26 December 2020	VV+VH	Descending	35862

	_035862_0432FF_FCEF				
13	S1A_IW_SLC__1SDV_20210119T211742_20210119T211809_036212_043F38_E99B	19 January 2021	VV+VH	Descending	36212
14	S1A_IW_SLC__1SDV_20210212T21174120210212T211808_036562_044B5A_5887	12 February 2021	VV+VH	Descending	36562
15	S1A_IW_SLC__1SDV_20210320T21174120210320T211808_037087_045DAB_F6D3	20 March 2021	VV+VH	Descending	37087
16	S1A_IW_SLC__1SDV_20210425T21174220210425T211809_037612_046FCA_12FA	25 April 2021	VV+VH	Descending	37612
17	S1A_IW_SLC__1SDV_20210519T21174320210519T211810_037962_047B09_05CC	19 May 2021	VV+VH	Descending	37962
18	S1A_IW_SLC__1SDV_20210624T21174620210624T211812_038487_048AB1_1D49	24 June 2021	VV+VH	Descending	38487
19	S1A_IW_SLC__1SDV_20210718T21174720210718T211814_038837_049537_E317	18 July 2021	VV+VH	Descending	38837
20	S1A_IW_SLC__1SDV_20210811T21174820210811T211815_039187_04A025_7E23	11 August 2021	VV+VH	Descending	39187
21	S1A_IW_SLC__1SDV_20210928T21175020210928T211817_039887_04B830_6CED	28 September 2021	VV+VH	Descending	39887
22	S1A_IW_SLC__1SDV_20211022T21175120211022T211818_040237_04C451_9F29	22 October 2021	VV+VH	Descending	40237
23	S1A_IW_SLC__1SDV_20211127T211750 20211127T211817_040762_04D686_C915	27 November 2021	VV+VH	Descending	40762
24	S1A_IW_SLC__1SDV_20211221T21174920211221T211816_041112_04E274_D059	21 December 2021	VV+VH	Descending	41112
25	S1A_IW_SLC__1SDV_20220126T211747 20220126T211814_041637_04F410_76A5	26 January 2021	VV+VH	Descending	41637
26	S1A_IW_SLC__1SDV_20220207T21174720220207T211814_041812_04FA14_0DFC	7 February 2022	VV+VH	Descending	41812
27	S1A_IW_SLC__1SDV_20220327T21174720220327T211814_042512_051208_5225	27 March 2022	VV+VH	Descending	42512

28	S1A_IW_SLC__1SDV_20220420T211748202204 20T211815_042862_051DCB_37D4	20 April 2022	VV+VH	Descending	42862
29	S1A_IW_SLC__1SDV_20220526T211750202205 26T211816_043387_052E61_2B31	26 May 2022	VV+VH	Descending	43387
30	S1A_IW_SLC__1SDV_20220619T211751202206 19T211818_043737_0538C5_5881	19 June 2022	VV+VH	Descending	43737
31	S1A_IW_SLC__1SDV_20220701T211752202207 01T211819_043912_053E00_BBBD	1 July 2022	VV+VH	Descending	43912
32	S1A_IW_SLC__1SDV_20220806T211755202208 06T211821_044437_054D8B_31B7	6 August 2022	VV+VH	Descending	44437
33	S1A_IW_SLC__1SDV_20220911T211756202209 11T211823044962_055F11_FA38	11 September 2022	VV+VH	Descending	44962

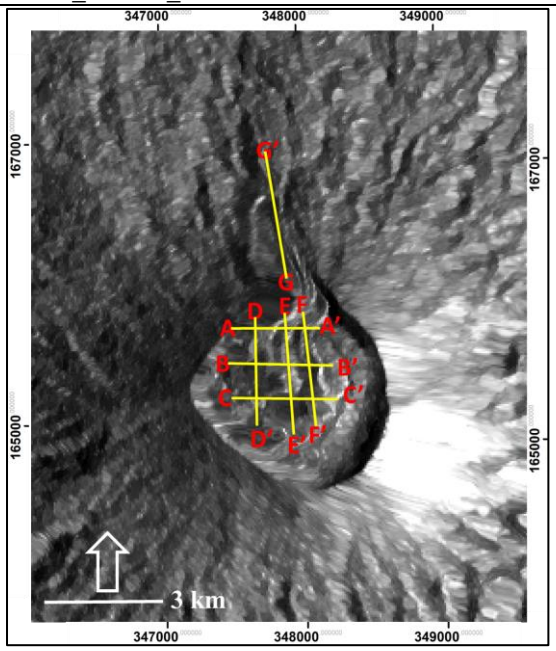

Figure 3 Sentinel-1A image on 26 May 2022 with seven cross sections (A-A', B-B', C-C', D-D', E-E', F-F', and G-G').

3 Pair-wise logic technique differential interferometric synthetic aperture radar (PLT D-InSAR) and k-means clustering

Deformation at lava dome of Mt. Ibu has been monitored using the PLT D-InSAR method. PLT D-InSAR is the development of the D-InSAR method. D-InSAR is

a phase reduction process in the deformation analysis, and atmospheric correction is necessary because the topographical components and atmospheric throttling must be removed, respectively [7]. Monitoring surface deformation using the D-InSAR method can provide spatial support for conventional vertical movement on the ground surface. The D-InSAR temporal method is an advanced synthetic aperture radar (InSAR) interferometry technique that processes several SAR images (to determine the separation of surface targets at different times as well as setting the wave delay from the atmosphere [7]. The D-InSAR method uses several pairs of interferograms at once to detect changes in surface topography with very high accuracy. D-InSAR aims to observe the movement or deformation of the ground surface using repeated-pass interferometry techniques because the changes observed are changes in the line of sight direction of the SAR sensor or line of sight (LOS). Then these changes can be measured based on wavelength units [7]. Sensor position factors and soil topography can influence the phase difference parameters as in the following equation:

$$\partial\varphi_P = -\frac{4\pi}{\lambda}\left(D_P - \frac{B\perp}{R_{1P}sin\theta_i}H_P + \in_{rr}\right) \quad (1)$$

where P is the object's surface point on the surface, λ is the wavelength used by the sensor, θ_i is the local angle of incidence, $B\perp$ is the sensor's perpendicular distance between two different times acquisition (perpendicular baseline), R_{1P} is the acquisition sensor distance at the point P, H_P are elevation heights of P above the earth's ellipsoid, and $\in_{rr}$ are wave propagation disturbances (noise) arising from atmospheric deceleration and faraday rotation [7]. Apart from D-InSAR, PLT D-InSAR was also done. In principle, the PLT D-InSAR technique attempts to overcome the waves slowing caused by the atmosphere by comparing interferograms covering different time intervals with the same data component. This method is reasonably practical for visually finding apparent deformation features caused by ionospheric disturbances [7]. Corrections made in PLT D-InSAR use simple arithmetic by sum up the two interferograms resulting from three SAR data with one SAR data used together (**Figure 3**). This approach is also called the linear combination method and is quite effective when the atmospheric anomaly is in the shared SAR data from two interferograms.

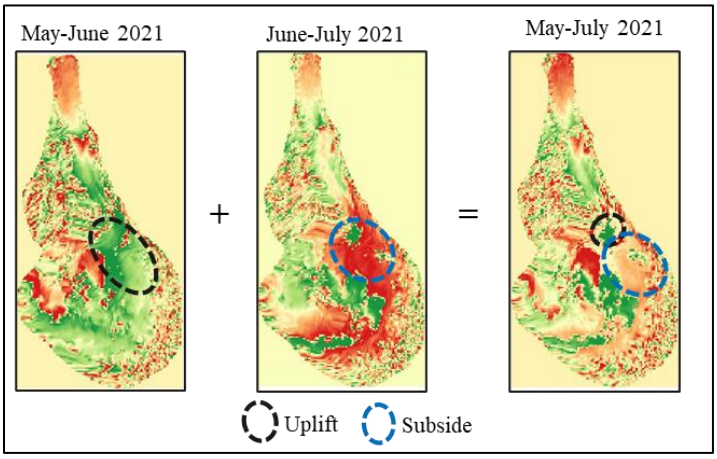

Figure 3 The sum of the two interferograms in May-June 2021 and June-July 2021 resulting an interferogram in May-July 2021. The areas in black circle (uplift) and blue circle (subside) are within one interferogram.

Apart from PLT D-InSAR, image clustering has been done based on the deformation results obtained. Deformation clustering has also been done from the previously published study by [9]. The type of clustering used is k-means clustering. The k-means clustering method is one of the clustering analysis algorithms with k being randomly selected objects as the initial clustering center [10]. The distance between each object and the initial clustering center is calculated and assigned to the nearest clustering center (centroid). This method groups the data based on the same characteristics. The k-means cluster approach is an unsupervised clustering algorithm that can group multidimensional samples into certain clusters (k) using the cost function. Suppose $C = \{C_i | \text{ i} = 1, .., n\}$ is the K-cluster of the data set, $Z = \{z_i | \text{ i} = 1, .., K\}$ is the center set of K [11]. This can be done by minimizing the squared error between randomly selected clusters and the samples contained in the clusters as follows [10]:

$$Cost = \sum_{i=1}^{n} dist(c_i, z_k) \tag{2}$$

where $dist(c_i, z_k)$ measures the Euclidean distance between pattern c_i and its cluster center z_k. The stages of k-means clustering are as follows [12]:

1. The centers of k initial $\{z_1, z_2, \dots, z_k\}$ must be selected randomly from n samples.
2. Sample x is assigned to cluster c if:
   $|x_i - z_j\| < \|x_i - z_p\|, p = 1,2,3, \dots, K and\ j \neq p, I = 1,2,3, \dots, n, and\ j\ \epsilon\{1,2,3, \dots, K\}$

3. Based on the equation (2), the other cluster centers $z_1 *, z_2 *, \dots, z_k *$z1$*$ should be calculated.

$$z_1 *= \frac{1}{n_i} \sum_{x_i \in C_i} x_j,\ i = 1,2,3, \dots, K$$

4. Terminate the process if centers $z_i *= z_i, I = 1,2,3, \dots, K$; if not, return to step 2.

After the clustering process, image processing has been done to the filtering stage, which aims to remove noise in the image by filtering it. In this study, we use median and open filtering. The median and opening filter removes noise in the image to get a better image contrast than the original image. In this process, noise intensity reduction is done. This process produces a smooth image and tends to eliminate noise. Then the results obtained from the deformation and k-means clustering are shown in (**Figure 4**).

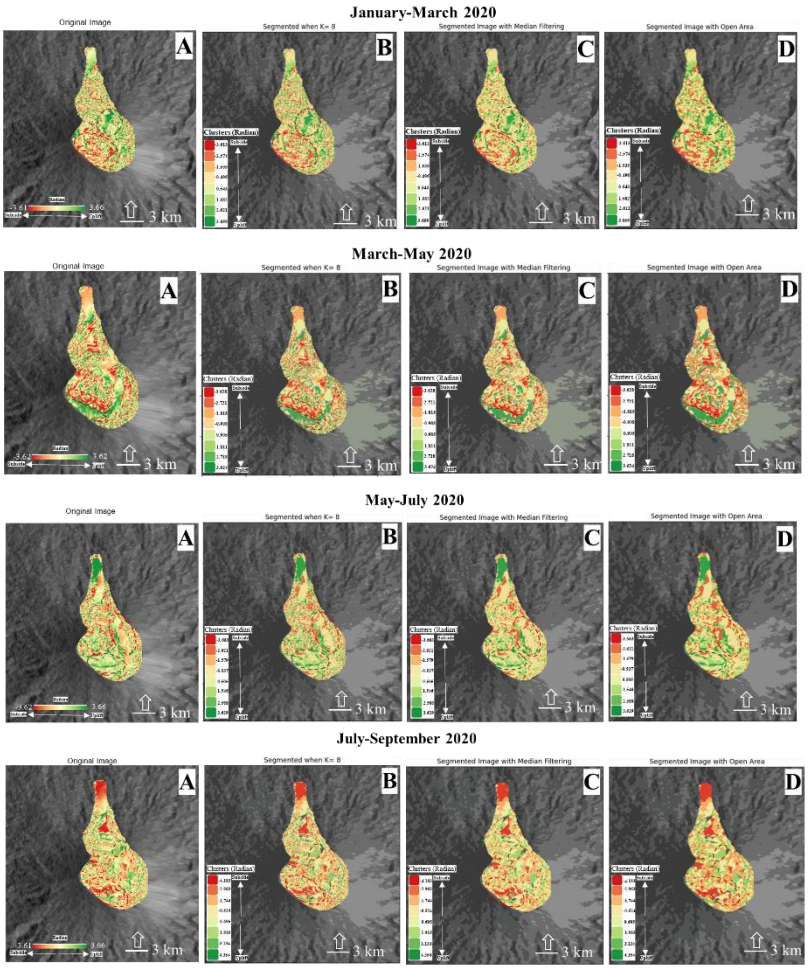

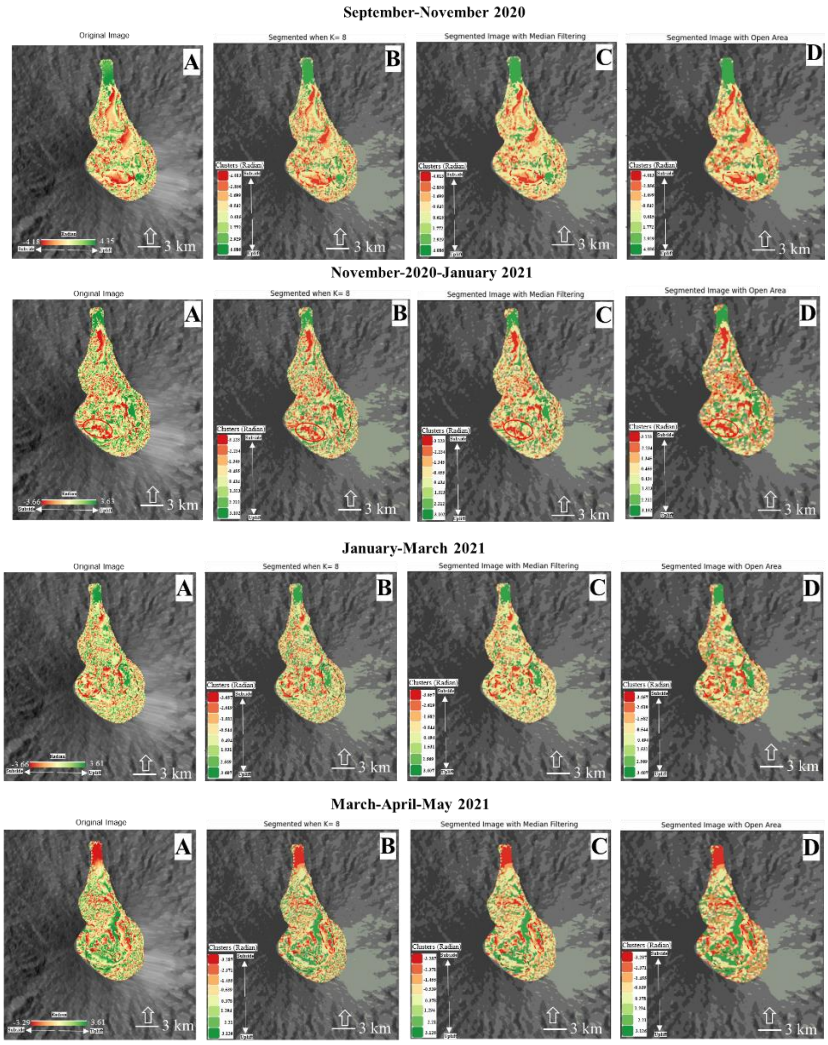
September-November 2020
Original Image
Segmented when K= 8
Segmented Image with Median Filtering
Segmented Image with Open Area
A
B
C
D
3 km
November-2020-January 2021
January-March 2021
March-April-May 2021

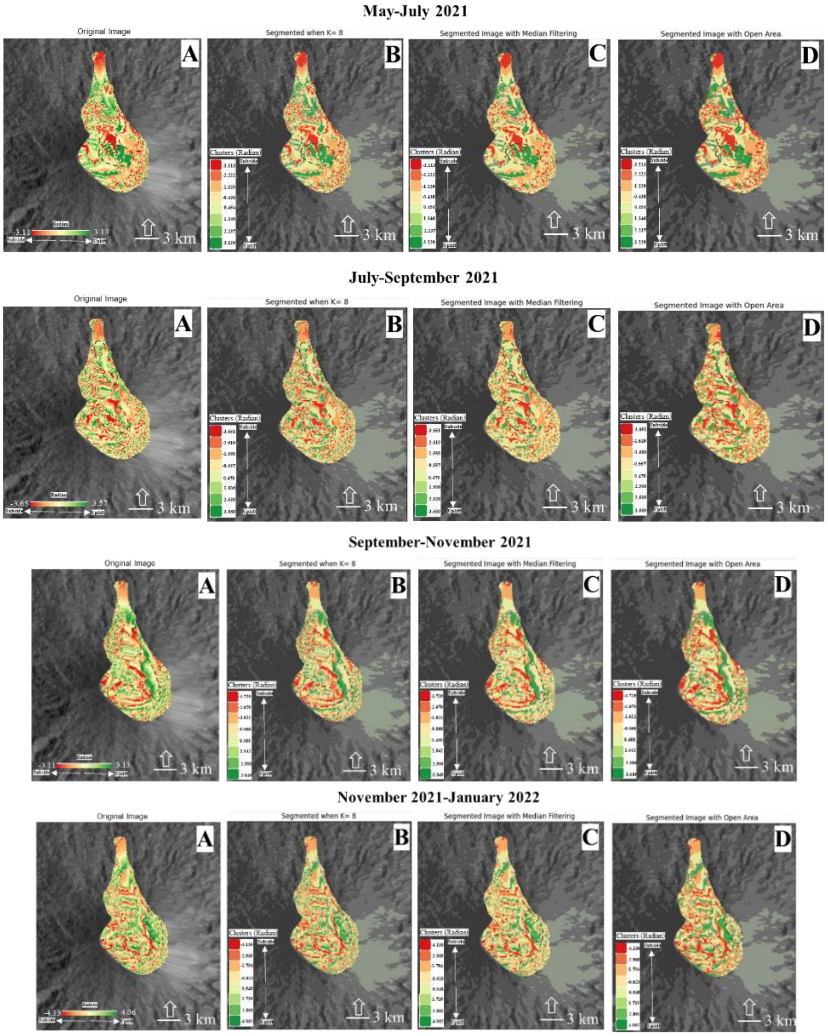
May-July 2021
Original Image
Segmented when K= 8
Segmented Image with Median Filtering
Segmented Image with Open Area
A
B
C
D
3 km
July-September 2021
September-November 2021
November 2021-January 2022

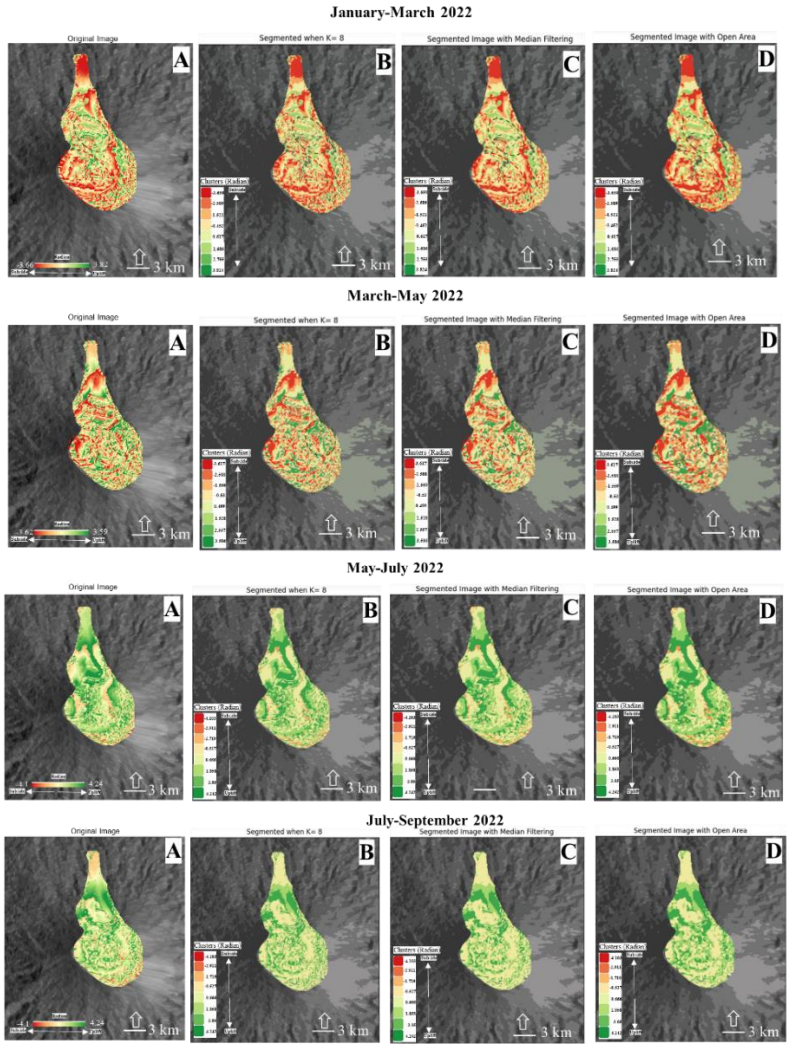

Figure 4 The interferogram generated by PLT D-InSAR method presented deformation vector of subsidence (red) and uplift (green) from January 2020 to September 2022. Original images of interferogram (A), segmented image using k-means clustering with k=8 (B), filtering image using median filtering (C), and filtering area using open filtering (D).

The PLT D-InSAR k-means clustering (k=8) image results are shown the uplift in 2020 (January, July, September, November and December), in 2021 (February, April, July and November), and in 2022 (January, March, April and August). Apart from uplift, subsidence phenomena has been occurred in 2020 (February, March, April, May, June, August and October), in 2021 (January, March, May, June, August, September, October and December), and in 2022 (February,

March, May, June, and July). Then the results of the k-means clustering (k=8) image and filtering show the noise in the segmented image is reduced, the image becomes sharpened, and values with the same characteristics as neighboring pixels are successfully grouped.

3 Discussion

Based on the results obtained from PLT D-InSAR, Mt. Ibu shows high deformation of the seven cross sections (A-A', B-B', C-C', D-D', E-E', F-F, and G-G'), which shows the highest uplift of about 0.667 m in January 2022, and the highest subsidence of about -0.48 m in August 2020 (**Figure 5**). The deformation value has been clustered using k = 6 to see its distribution on the lava dome based on time (**Figure 6**).

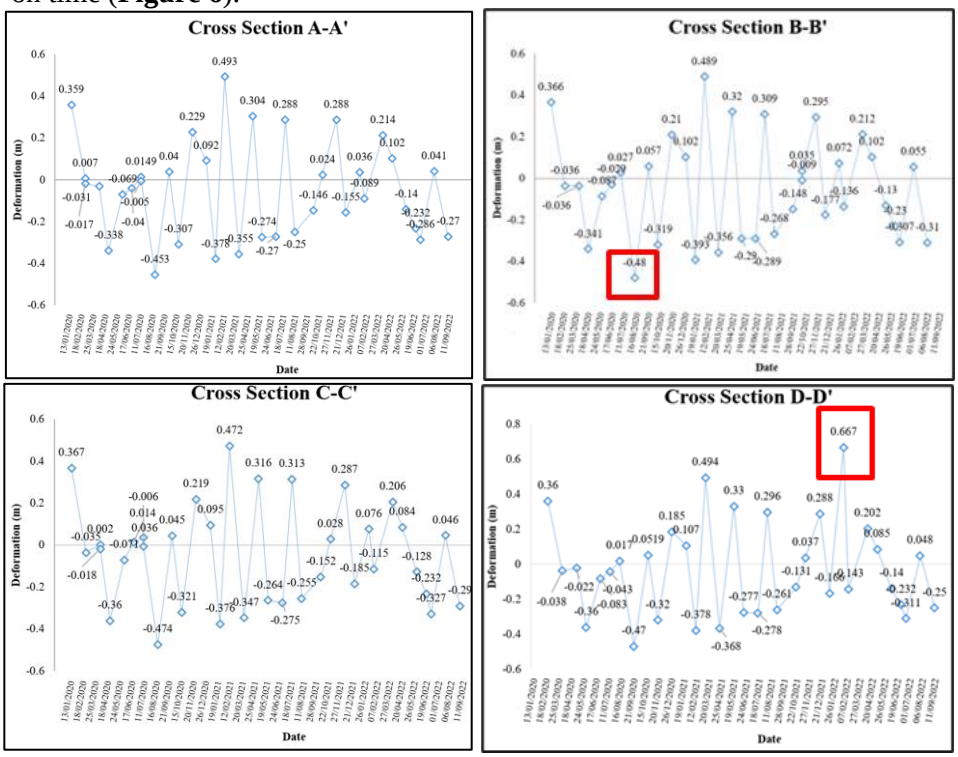

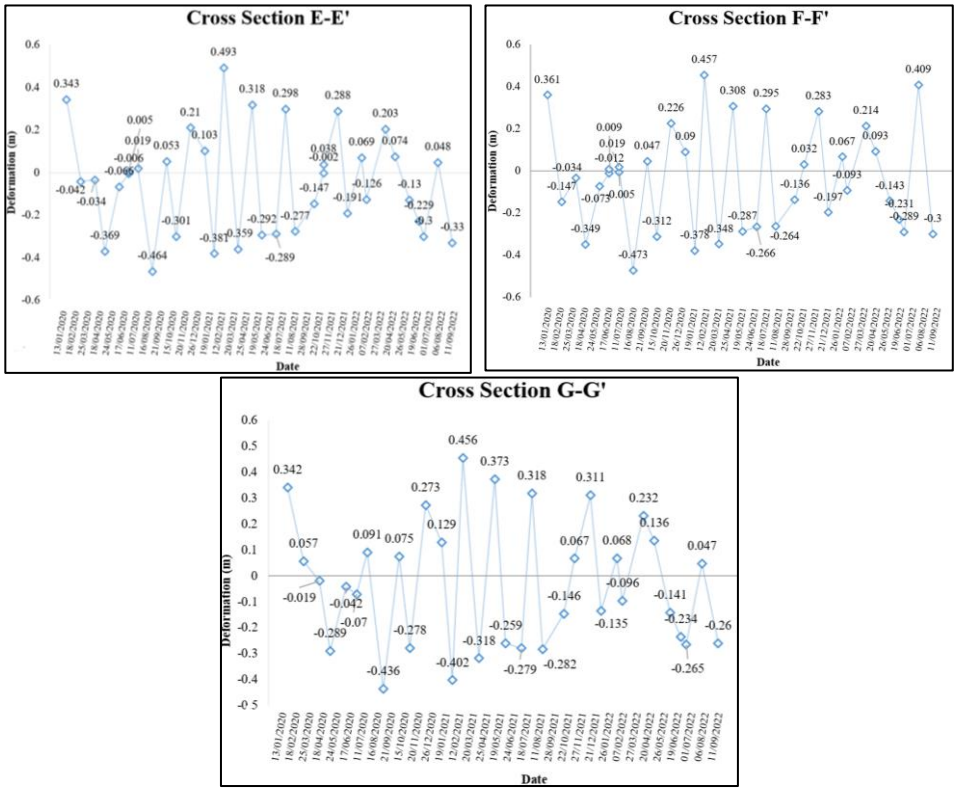

Figure 5 The deformation pattern of Mt. Ibu lava dome with subsidence deformation vector has been occurred 19 times and uplifted 14 times from January 2020 to August 2022.

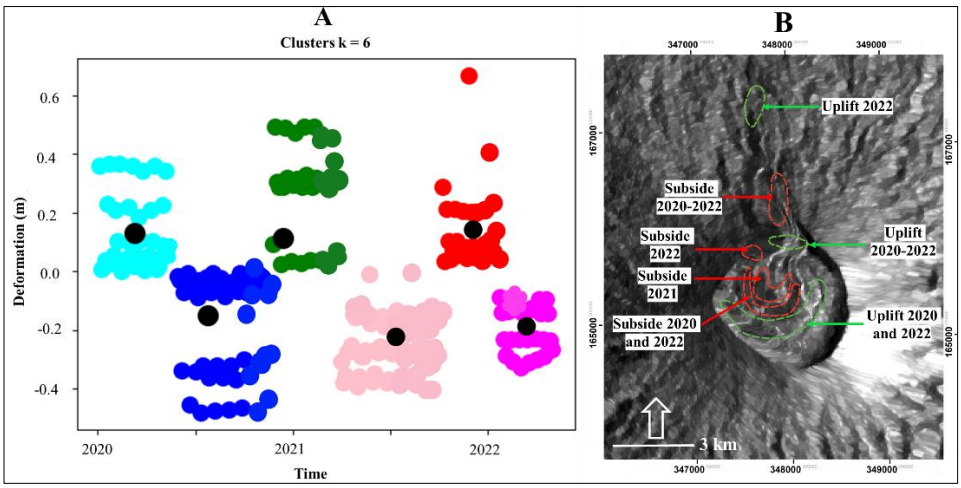

Figure 6 Clustering deformation values using cluster k=6 (A), and the distribution of deformation values based on clustering results overlaid with Sentinel-1A image (B).

Within 24 years of the first appearance of the 99-lava dome, the current Mt. Ibu is growing rapidly and has exceeded the inner crater and outer crater rim on the northern flank, thus further expanding the distribution of lava flows. Based on deformation clustering using k-means, subsidence generally occurs in the center of the lava dome, northwest, and towards the crater opening. Then the uplift generally occurs on the south of the lava dome, north on the crater opening, and north on the lava flow. Monitoring the deformation of Mt. Ibu from January 2020 to August 2022 shows that the high level of deformation is thought to have occurred due to the process of growing the lava dome which has continued to current today (September 2022). The growth of the lava dome and the direction of expansion occur due to pressure from the lava flow moving towards the crater opening, and the lava comes out through an active vent on the top of the lava dome. The deformation that occurred in the lava dome of Mt. Ibu occurs because when the growth process of the lava dome is underway, it can cause several effects such as pressure, growth cycles, lava dome decline, growth acceleration, and sudden explosive activity, as well as the disintegration of lava during the formation of pyroclastic flows, are some of the main phenomena that can occur. Causing deformation to the eruption of the lava dome [13].

4 Conclusion

In this study, the deformation at Mt. Ibu is clearly visible from PLT D-InSAR, and the k-means clustering algorithm. The results of the PLT D-InSAR deformation shows that subsidence has been occurred generally in the center of the lava dome, northwest, and towards the crater opening, and the uplift generally occurred on the south of the lava dome, north on the crater opening, and north on the lava flow. The highest uplift in January 2022 is about 0.667 m and subsidence in August 2020 about -0.48 m. Deformation analysis using PLT D-InSAR combined by k-means clustering produces clear deformation areas. This proposed method is advantage to obtain deformation at low coherence condition.

References

[1] E. S. Calder, R. Luckett, R. S. J. Sparks, and B. Voight, “Mechanisms of lava dome instability and generation of rockfalls and pyroclastic flows at Soufrière Hills Volcano, Montserrat,” *Geol. Soc. Mem.*, vol. 21, no. 1, pp. 173–190, 2002, doi: 10.1144/GSL.MEM.2002.021.01.08.

[2] C. E. Harnett and M. J. Heap, “Mechanical and topographic factors influencing lava dome growth and collapse,” *J. Volcanol. Geotherm. Res.*, vol. 420, 2021, doi: 10.1016/j.jvolgeores.2021.107398.

[3] Surono *et al.*, "The 2010 explosive eruption of Java's Merapi volcano-A '100-year' event," *J. Volcanol. Geotherm. Res.*, vol. 241–242, pp. 121–135, 2012, doi: 10.1016/j.jvolgeores.2012.06.018.

[4] USGS, "Explosions and Dome Growth, 1980-1986 and 1989-1991," 2022. https://www.usgs.gov/volcanoes/mount-st.-helens/explosions-and-dome-growth

[5] A. Saepuloh and K. Koike, "Discriminating Alteration of Pyroclastic Flow Deposits in an Active Volcano by SAR Image," in *Proceeding of the World Geothermal Congress*, 2010, no. April, pp. 25–29.

[6] A. Saepuloh, P. R. Mirelva, and K. Wikantika, "Advanced applications of Synthetic Aperture Radar (SAR) remote sensing for detecting pre- and syn-eruption signatures at Mount Sinabung, North Sumatra, Indonesia," *Indones. J. Geosci.*, vol. 6, no. 2, pp. 123–140, 2019, doi: 10.17014/ijog.6.2.123-140.

[7] A. Saepuloh, *Prinsip dan aplikasi penginderaan jauh geologi gunungapi*. Bandung: ITB Press, 2021.

[8] D. S. Vaka, S. Sharma, and Y. S. Rao, "Comparison of HH and VV Polarizations for Deformation Estimation using Persistent Scatterer Interferometry," *38th Asian Conf. Remote Sens. - Sp. Appl. Touching Hum. Lives, ACRS 2017*, vol. 2017-Octob, no. 2008, 2017.

[9] M. Cavur, J. Moraga, H. Sebnem Duzgun, H. Soydan, and G. Jin, "The DInSAR Analysis with Machine Learning for Delineating Geothermal Sites at the Brady Geothermal Field," *Proceedings*, vol. 46, no. Figure 1, pp. 1–11, 2021, [Online]. Available: https://scihub.copernicus.eu.

[10] G. Niu, Y. Ji, Z. Zhang, W. Wang, J. Chen, and P. Yu, "Clustering analysis of typical scenarios of island power supply system by using cohesive hierarchical clustering based K-Means clustering method," *Energy Reports*, vol. 7, pp. 250–256, 2021, doi: 10.1016/j.egyr.2021.08.049.

[11] R. Ghezelbash, A. Maghsoudi, and E. J. M. Carranza, "Mapping of single- and multi-element geochemical indicators based on catchment basin analysis: Application of fractal method and unsupervised clustering models," *J. Geochemical Explor.*, vol. 199, no. December 2018, pp. 90–104, 2019, doi: 10.1016/j.gexplo.2019.01.017.

[12] R. Ghezelbash, M. Daviran, A. Maghsoudi, and H. Ghaeminejad, "Applied Geochemistry Incorporating the genetic and firefly optimization algorithms into K-means clustering method for detection of porphyry and skarn Cu-related geochemical footprints in Baft district , Kerman , Iran," *Appl. Geochemistry*, vol. 148, no. November 2022, p. 105538, 2023, doi: 10.1016/j.apgeochem.2022.105538.

[13] R. S. J. Sparks, "Causes and consequences of pressurisation in lava dome eruptions," *Earth Planet. Sci. Lett.*, vol. 150, no. 3–4, pp. 177–189, 1997, doi: 10.1016/s0012-821x(97)00109-x.

Proceedings of the 3rd ITB Graduate School Conference ISSN: 2963-718X
Enhancing Creativity in Research Through Developing Innovative Capabilities
December 21, 2022

The Effect of Salt and Sulfuric Acid on the Resistivity Value of Bentonite Mixed with Calcium Carbonate Soil under DC Voltage

Pequinta Alnajua Wisyah*, Bambang Anggoro Soedjarno P & Pradita Octoviandiningrum Hadi

School of Electrical Engineering and Informatics, Bandung Institute of Technology, Bandung, Indonesia
*Email: 23220342@std.stei.itb.ac.id

Abstract. Mountainous areas are characterized by high soil resistivity, which may interfere with the grounding system and safety. Therefore, Ground Enhancement Material (GEM) is needed so that the resistivity value of the soil is following the grounding resistance standards regulated by General Electrical Installation Requirements or PUIL 2000. Bentonite as Ground Enhancement Materials (GEM) has been widely used, but studies on bentonite mixed with calcium carbonate using various stages of salts and acids for reducing soil resistivity are still few. This paper presents research conducted on bentonite mixed with calcium carbonate ($CaCO_3$) as a test soil, with salt (NaCl) and sulfuric acid (H_2SO_4) under DC voltage. In this research, laboratory experiments have been carried out. From the experiments, it was found that the average resistivity value of the soil in dry conditions was 57096.39 Ωm, then there was a decrease in resistivity of 99.96% with the lowest average resistivity value being 20.9 Ωm in the application of 18% NaCl solution. Whereas in the application of 18% H_2SO_4 the average resistivity value is 259.6 Ωm with a resistivity reduction percentage of 99.55%. The use of NaCl is more effective in reducing soil resistivity than H_2SO_4.

Keywords: *bentonite; calcium carbonate; ground enhancement materials; soil resistivity; salt variation; sulfuric acid variation.*

1 Introduction

The addition of space requirements for residence and infrastructure development causes land expansion to be unavoidable. This is also the case in the Bandung Regency area [1]. The total area of Bandung Regency is 176,238.67 Ha, and most of Bandung's area is between the hills and mountains that surround Bandung Regency [2]. Mountainous areas, for example, the northern slope of Mount Malabar, have soil characteristics with a resistivity value of up to 1438 Ωm according to the research conducted by Asep Harja, et.al in [3].

For residential buildings, a grounding system is one of the most important things to be considered. Electrical grounding must be installed to prevent fires, damage to electronic devices, or even fatalities due to lightning strikes to building structures. For the grounding system, the resistivity value of the soil in the mountainous area does not meet the requirements. The standard value of earthing resistance following the General Electrical Installation Requirements or PUIL 2000 is less than 5 Ω [4]. Conditioning of the soil, where the ground rod must be installed, should be done by adding Ground Enhancement Materials (GEM) to reduce soil resistivity [5]. Bentonite soil and calcium carbonate ($CaCO_3$) can be used as GEM materials by treating the soil with a chemical solution [6].

Research on the characteristics of bentonite and $CaCO_3$ soils to be used as GEM, respectively, has been carried out in [5], [7]. However, studies on the characteristics of bentonite mixed with $CaCO_3$ soil are still few. This paper reports a study on how to reduce resistivity values in a mixture of bentonite soil and $CaCO_3$ soil, which was treated with salt solution (NaCl) and sulfuric acid solution (H_2SO_4) under DC voltage. This study uses DC voltage variations to see the ground impedance value determined from pure resistance at zero frequency (dc).

2 Ionization Propagation Model

When a sufficiently high electric field is applied to the ground, the air voids are ionized. The ionization zone will increase in the form of several paths that propagate away from the energized electrode, as illustrated in Figure 1 [8]. Soil texture can affect variations in soil resistivity values. The finer the texture of the soil, the higher conductivity of the soil with a lower resistivity value, and vice versa when the grain of the soil is coarser [9].

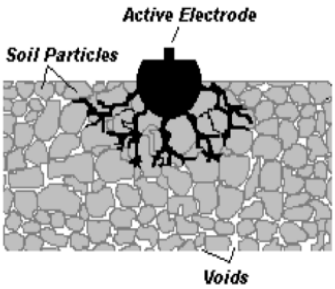

Figure 1 Ionization propagation model [8].

3 Methodology

3.1 Tested Soil

Mineralogically, bentonite is composed of smectite with the chemical formula ((Na, Ca)(Al, Mg)$_6$(Si4O10)$_3$(OH)$_6$-nH$_2$O) [10]. It has a layered structure with the swelling ability and has movable cations. The bentonite used in this study comes from the village of Sarimanggu, Karangnunggal, Tasikmalaya, Indonesia, and the type is Ca-bentonite. The $CaCO_3$ rock was obtained from a mining company located at PT Batu Wangi, Padalarang, West Java. Rocks need to be processed to get a smooth texture. The soil texture for this study can be seen in Figure 2. Bentonite soil has a coarser texture than $CaCO_3$ soil.

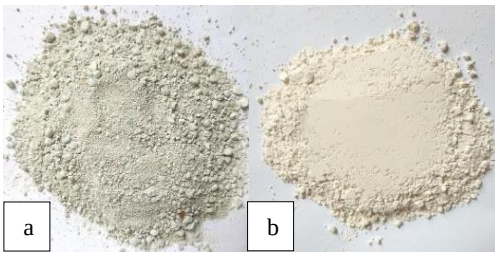

Figure 2. Soil texture of (a) bentonite and (b) $CaCO_3$

3.2 Test-Set Up`

Test-set up used in our experiment is illustrated in Figure 3. DC power supply was generated using a GW Instek SPS-1230 DC power supply with an input of 220 VAC 50 Hz, which produces an output voltage range between 0-11.5 VDC. The voltage from the DC supply flows to the tested ground through a ball-shaped aluminum electrode with a diameter of 10 cm. The soils tested were bentonite and $CaCO_3$ stored in an iron hemispherical test cell with a diameter of 46 cm. Measurements were made using a Micsig TO1102 tablet oscilloscope. Channel 1 (Ch1) probe is used to measure the voltage injected into the electrode while the resulting potential difference is measured with a channel 2 (Ch2) probe. A shunt resistor Rs of 500 Ω was used as a link between the test cell and the negative pole of the circuit, whose main function is to create a smaller resistance path for the flow of current.

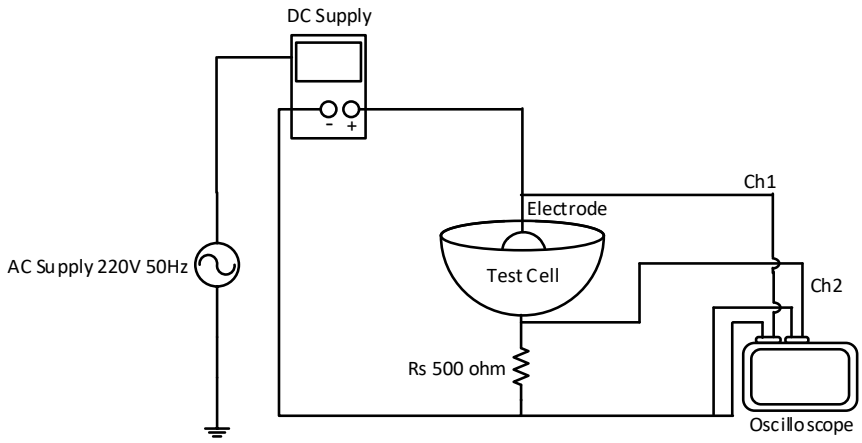

(a) Schematic diagram

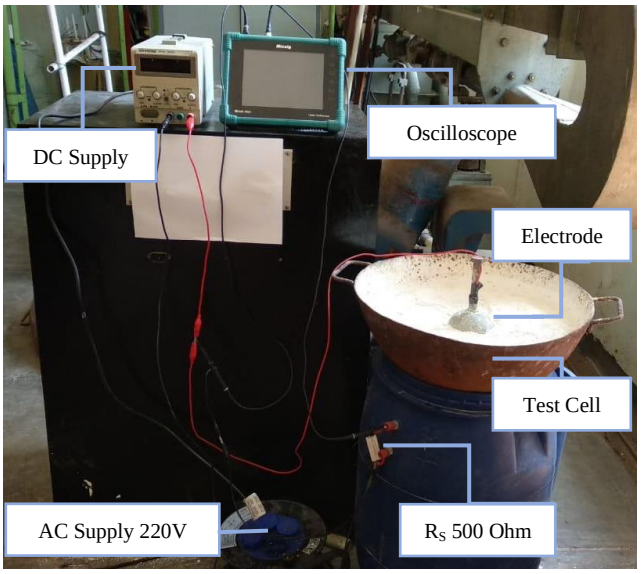

(b) Laboratory setting

Figure 3 Test set-up (a) schematic diagram and (b) laboratory setting

3.3 Experiment

A mixture of 5 kg of bentonite and 5 kg of $CaCO_3$ was used in this experiment, so the total soil used was 10 kg for each chemical treatment. The soil in the test cell was compacted to get a better measurement.

The salt used in this experiment used crystalline salt dissolved in tap water with a concentration of 35% or 0.6 M while the H_2SO_4 solution used was a concentration of 24.5% or 4.4 M. Considering the proportion of the solution stages given to the soil to be 0%, 6%, 12%, and 18%. The percentage of a solution is calculated for 10 kg of soil mass. The percentage of 0% solution is the soil in dry conditions and the percentage of solution used is 6%, which means that as much as 600 ml of solution is given to the soil being tested, and so on. The process of administering NaCl and H_2SO_4 solutions was carried out in a short time to minimize the effects of water settling and drying. To calculate the percentage solution in ml use equation (1).

$$Solution\ (ml) = \frac{6}{100}(10\ kg) = 600\ ml \qquad (1)$$

The NaCl solution was sprayed using a sprayer and stirred to get an even distribution of the solution throughout the soil. While the H_2SO_4 solution was not sprayed for safety considerations, so the acid solution was poured carefully from the bottle container on the soil surface and mixed manually. For experiments with acids, it is required to wear protective equipment, i.e. masks, gloves, safety shoes, and safety glasses.

Variations in the DC voltage applied to the soil for each percentage of solution are as many as 22 voltage variations in the range of 1-11.5 VDC, with a voltage difference of 0.5 VDC. The measured output voltage is then calculated by *Ohm's* law equation (2) to get the resistance value *R*:

$$R = \frac{Vin - Vout}{I} \qquad (2)$$

Where *Vin* is the voltage injected into the electrodes, *Vout* is the output voltage measured by the oscilloscope, and the current *I* calculated from equation (3):

$$I = \frac{Vout}{Rs} \qquad (3)$$

Rs is a shunt resistor. The resistivity value ρ is calculated using the formula in equation (4) from similar research that has been conducted in reference[10]:

$$\rho = \frac{2\pi R}{\left(\frac{1}{r_1} - \frac{1}{r_2}\right)} \qquad (4)$$

Where ρ is the soil resistivity, r_1 and r_2 are the radii of the electrode and test cell in meters.

4 Result and Discussion

4.1 Effect of NaCl Solution Percentages Variation to the Magnitude of Soil Resistivity

Table 1 shows the injected voltage and the measured voltage by the oscilloscope. The 0% condition is when the soil condition has not been given a NaCl solution, with an initial voltage of 1-1.5 VDC, causing the distribution of ionization in the soil to be not wide enough and the measured voltage is also very small, with an average voltage of 0.03 VDC, as tabulated on Table 1. The greater percentage of NaCl solution given to the soil, the measured voltage is closer to the initial injected voltage. The best maximum measured voltage value was obtained when the NaCl solution percentage of 18% was added to the soil. For instance, when the injected voltage is 11.5 VDC, then the measured voltage is 10.86 V indicating that 94% of the energized voltage is discharged to the ground.

Table 1 Voltage measured at each voltage variation using various NaCl solution percentages

Voltage (VDC)	Measured Voltage (VDC)			
	NaCl 0%	NaCl 6%	NaCl 12%	NaCl 18%
1.05	0.001	0.22	0.72	0.81
1.50	0.002	0.51	1.16	1.26
2.00	0.01	0.67	1.60	1.78
2.50	0.01	0.90	2.01	2.22
3.00	0.01	1.12	2.39	2.70
3.50	0.02	1.28	2.81	3.18
4.00	0.02	1.52	3.16	3.62
4.50	0.02	1.71	3.61	4.07
5.00	0.03	1.88	4.14	4.54
5.50	0.03	2.13	4.50	5.02
6.00	0.04	2.33	4.98	5.44
6.50	0.04	2.54	5.31	5.97
7.00	0.04	2.76	5.90	6.46
7.50	0.04	2.98	6.33	6.93
8.00	0.04	3.20	6.86	7.38
8.50	0.05	3.42	7.27	7.88
9.00	0.05	3.63	7.70	8.31
9.50	0.05	3.86	8.10	8.82
10.00	0.06	4.06	8.64	9.31
10.50	0.06	4.26	9.07	9.77
11.00	0.06	4.49	9.50	10.39
11.50	0.07	4.66	9.90	10.86
Avg.	0.03	2.46	5.26	5.76

Table 2 shows the results of soil resistivity using the NaCl solution. The average resistivity at 0% soil conditions is 57096.39 Ωm. When the value of the input voltage increases, the resistivity value will decrease correspondingly. At the addition of 6% solution, the soil began to react with the NaCl solution to reduce the resistivity value significantly with a decrease of 99.40% from the initial condition. Then, the solution was added twice (from 6% to 12%), and the average resistivity decreased to 43.59 Ωm or decreased by 99.92%. Likewise, from 6% to 18% (the solution becomes 3 times) there is a decrease of 99.96%. For all test voltages used in this measurement when the NaCl solution was 18%, the average resistivity is 20.9 Ωm, which is the lowest average soil resistivity acquired compared to other NaCl solution percentages used.

Table 2 Magnitude of soil resistivity versus voltage variation in with various NaCl solution percentages

Input Voltage (VDC)	**Resistivity (Ωm)**			
	NaCl 0%	**NaCl 6%**	**NaCl 12%**	**NaCl 18%**
1.05	347701.60	739.56	88.00	57.31
1.50	158256.80	394.29	59.50	37.85
2.00	57976.93	374.54	49.71	25.32
2.50	45004.89	355.59	48.81	25.01
3.00	42504.15	337.87	51.33	22.14
3.50	36579.13	348.97	49.02	20.41
4.00	38584.38	328.87	53.11	21.07
4.50	37276.79	327.48	49.48	21.21
5.00	34645.27	332.25	41.69	20.34
5.50	34296.81	318.05	44.60	19.19
6.00	34109.18	315.70	41.11	20.66
6.50	35251.29	312.11	44.98	17.82
7.00	35640.87	307.97	37.42	16.78
7.50	36248.35	305.12	37.10	16.51
8.00	36292.54	301.85	33.35	16.86
8.50	35342.19	298.87	33.96	15.79
9.00	35219.20	296.92	33.89	16.67
9.50	35307.15	293.27	34.69	15.47
10.00	34888.95	293.65	31.59	14.88
10.50	35219.20	294.00	31.64	15.00
11.00	35524.88	291.01	31.69	11.78
11.50	34250.00	294.61	32.44	11.83
Avg.	57096.39	340.25	43.59	20.90

Figure 4 depicts the curve of the injected voltage versus the soil resistivity value using different NaCl solution percentages. It is seen that with 0% NaCl the resistivity curve is quite steep when a voltage in the range of 1-1.5 VDC is

injected into the soil. This indicates that the soil used in this test was not dry enough, in other words, the soil still contains moisture. In this measurement, the propagation of the voltage injected to the electrode is affected by soil moisture causing a decrease in the resistivity value at each applied voltage.

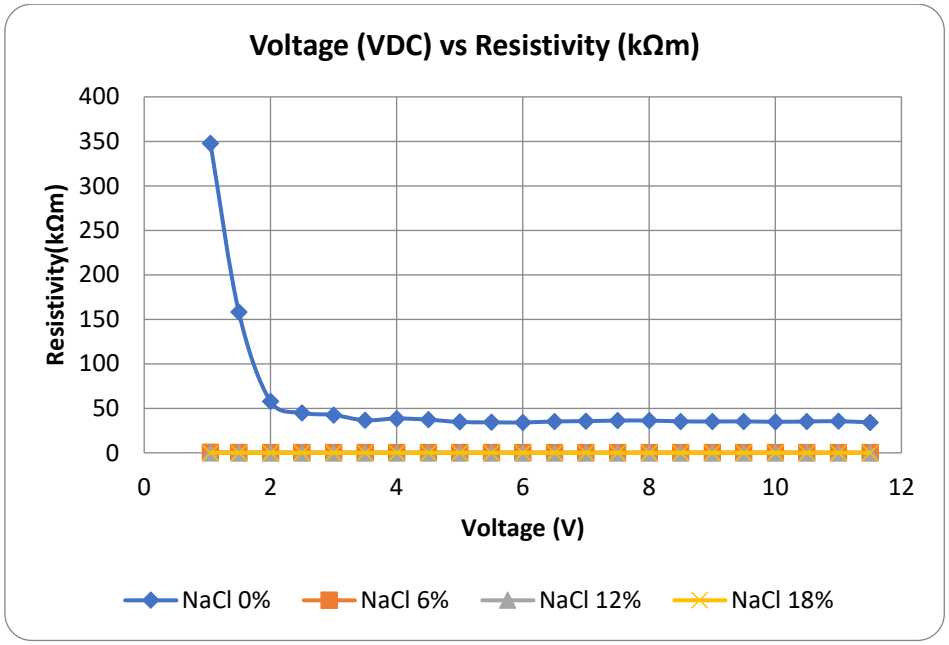

Figure 4 Graph of input voltage versus soil resistivity magnitudes with all various NaCl solution percentages

The ionization zone will spread out and is assumed to be like a current path that propagates away from the electrode that is being applied to the voltage. The speed of current propagation is very dependent on the applied voltage and the soil conductivity [8].

To clarify the graph of the decrease in resistivity in the application of 6%, 12%, and 18% NaCl can be seen in Figure 5. Figure 5 shows that any increase in the NaCl solution percentage level will cause a decrease in soil resistivity. This phenomenon might result in a change in the chemical composition of the soil. Moisture in the soil has an initially small conductivity, but when it reacts with a NaCl solution, the conductivity value becomes higher and the resistivity value decreases. With an 18% NaCl solution added to the soil, the soil tested and the ionization is more uniform compared to the other percentage stages used in this experiment. Therefore, the use of chemical compounds, such as NaCl, added to the bentonite and $CaCO_3$ soil can greatly help to reduce the soil resistivity value.

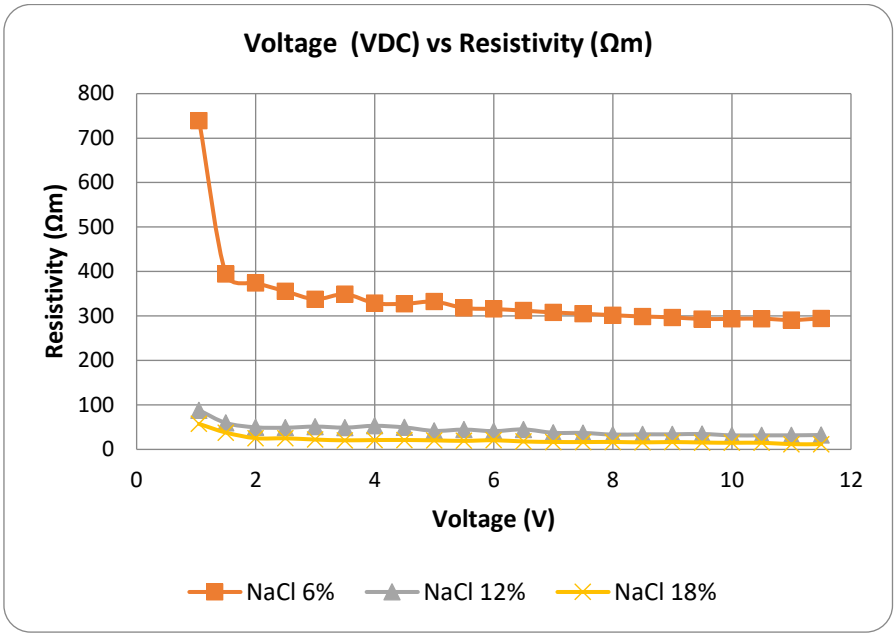

Figure 5 Graph of input voltage versus resistivity value with 6%, 12%, and 18% NaCl solution percentages

4.2 Effect of H_2SO_4 Percentages Variation to the Magnitude of Soil Resistivity

From Table 3, the maximum voltage value is obtained in the soil when the 18% H_2SO_4 solution is added to the soil under test. For instance, when the injected voltage to the ground electrode is 11.5 VDC, then the measured voltage is 5.59 VDC indicating that 49% of the injected voltage (11.5 VDC) at the ground electrode is discharged to the ground.

However, the ratio between the energized voltage to the measured voltage in the test using H_2SO_4 solution is still relatively small, for example when the soil is given a voltage of 10 VDC through the electrodes, the voltage measured at each addition of 6%, 12% and 18% H_2SO_4 respectively are 0.22 VDC, 2.30 VDC, 4.73 VDC. This means bentonite mixed with $CaCO_3$, using 4.4 M H_2SO_4 solution to conduct electric current is still not effective.

In addition, the soil resistivity value can be affected by the concentration of the chemical solution. In a concentrated solution, the movement of ions is more difficult so the conductivity becomes lower. And conversely, in a dilute solution, the ions in the solution move easily so that the conductivity is greater.

Table 3 Voltage measured at each voltage variation using various percentages of H_2SO_4 solution

Voltage (VDC)	Voltage Measured (VDC)			
	H_2SO_4 0%	H_2SO_4 6%	H_2SO_4 12%	H_2SO_4 18%
1.05	0.001	0.003	0.11	0.31
1.50	0.002	0.01	0.21	0.56
2.00	0.01	0.01	0.33	0.77
2.50	0.01	0.01	0.43	1.05
3.00	0.01	0.02	0.55	1.28
3.50	0.02	0.03	0.65	1.50
4.00	0.02	0.04	0.78	1.93
4.50	0.02	0.04	0.91	1.98
5.00	0.03	0.05	1.01	2.20
5.50	0.03	0.07	1.14	2.45
6.00	0.04	0.08	1.26	2.68
6.50	0.04	0.10	1.38	2.94
7.00	0.04	0.11	1.51	3.18
7.50	0.04	0.13	1.64	3.44
8.00	0.04	0.15	1.77	3.67
8.50	0.05	0.16	1.89	3.96
9.00	0.05	0.18	2.02	4.17
9.50	0.05	0.20	2.16	4.45
10.00	0.06	0.22	2.30	4.73
10.50	0.06	0.24	2.42	4.98
11.00	0.06	0.27	2.59	5.26
11.50	0.07	0.27	2.74	5.59
Avg.	0.03	0.11	1.36	2.87

From Table 4, when added 6% H_2SO_4 solution, the average resistivity decreased by 63%. Then, the solution was added twice (from 6% to 12%), and there was a decrease in resistivity of 98.55%. Likewise the addition of 6% to 18% (the solution becomes 3 times) there is a decrease of 99.55%. It is seen that the lowest average resistivity value was achieved when the percentage for the H_2SO_4 used is 18%. The average resistivity, in this case, is 259.6 Ωm, which is the lowest average resistivity, obtained compared to other H_2SO_4 solution percentages used in this experiment.

Table 4 Magnitude of soil resistivity versus voltage variation in with various H_2SO_4 solution percentages

Voltage (VDC)	Resistivity (Ωm)			
	H_2SO_4 0%	H_2SO_4 6%	H_2SO_4 12%	H_2SO_4 18%
1.05	347701.58	77110.91	1696.94	483.69
1.50	158256.81	49977.50	1212.76	339.81
2.00	57976.93	36292.54	1015.73	318.60
2.50	45004.89	35640.87	966.22	279.46
3.00	42504.15	31490.79	886.18	270.44
3.50	36579.13	24888.40	880.05	267.62
4.00	38584.38	22737.90	824.64	266.14
4.50	37276.79	21304.24	794.01	256.14
5.00	34645.27	18383.81	791.93	256.08
5.50	34296.81	16033.42	765.94	249.13
6.00	34109.18	14852.75	752.04	249.32
6.50	35251.29	13111.88	747.42	242.44
7.00	35640.87	12808.45	731.60	240.69
7.50	36248.35	11203.43	719.99	237.40
8.00	36292.54	10797.25	704.42	236.81
8.50	35342.19	10330.52	700.53	230.11
9.00	35219.20	9670.41	692.67	232.48
9.50	35307.15	9381.06	683.69	227.78
10.00	34888.95	9091.55	673.09	223.63
10.50	35219.20	8654.27	669.07	222.48
11.00	35524.88	7976.48	650.42	219.03
11.50	34250.00	8223.37	641.39	212.20
Avg.	57096.39	20907.35	827.31	259.61

As depicted in Figure 6, the 0% H_2SO_4 curve means that the soil is still dry and has not been yet mixed with the H_2SO_4 solution. It is the same with the results obtained using the 0% NaCl solution, indicating that the soil is not yet contaminated with chemical solutions from external factors. So, the percentage of adding a solution below 12% using H_2SO_4 does not significantly affect the decrease in soil resistivity values compared to adding a solution above 12%. To clarify the graph of the decrease in resistivity in the application of 12% and 18% H_2SO_4 can be seen in Figure 7. As shown in Figure 7, the use of H_2SO_4 can reduce soil resistivity but the effect is not too significant, because the soil's capacity to exchange ion become lower. The use of chemical compounds to activate bentonite and $CaCO_3$ that are used as a grounding medium certainly affects the soil pH and chemical reactions in the soil, which triggers the corrosion reactions.

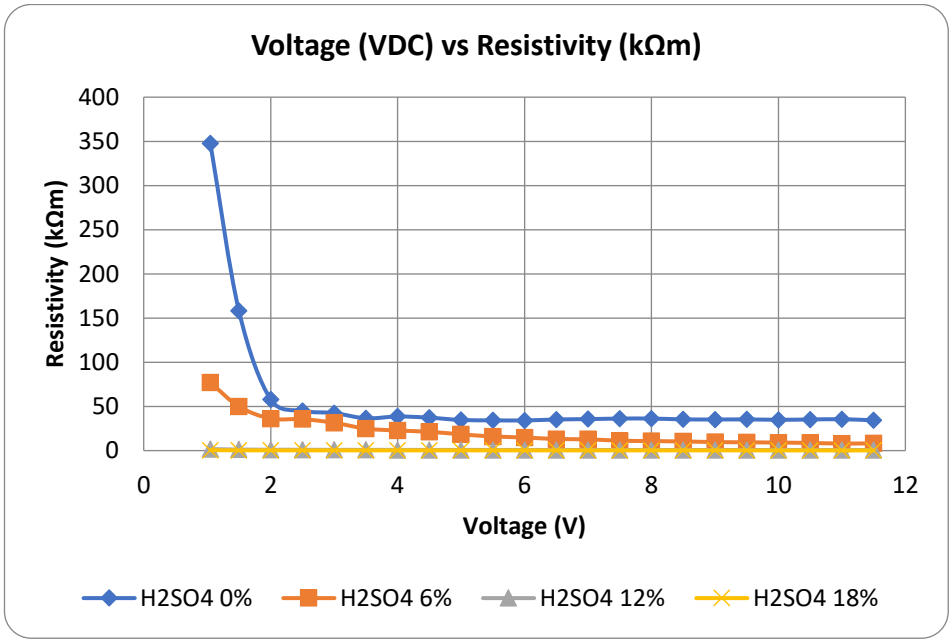

Figure 6 Graph of input voltage versus soil resistivity magnitudes with all various H_2SO_4 solution percentages

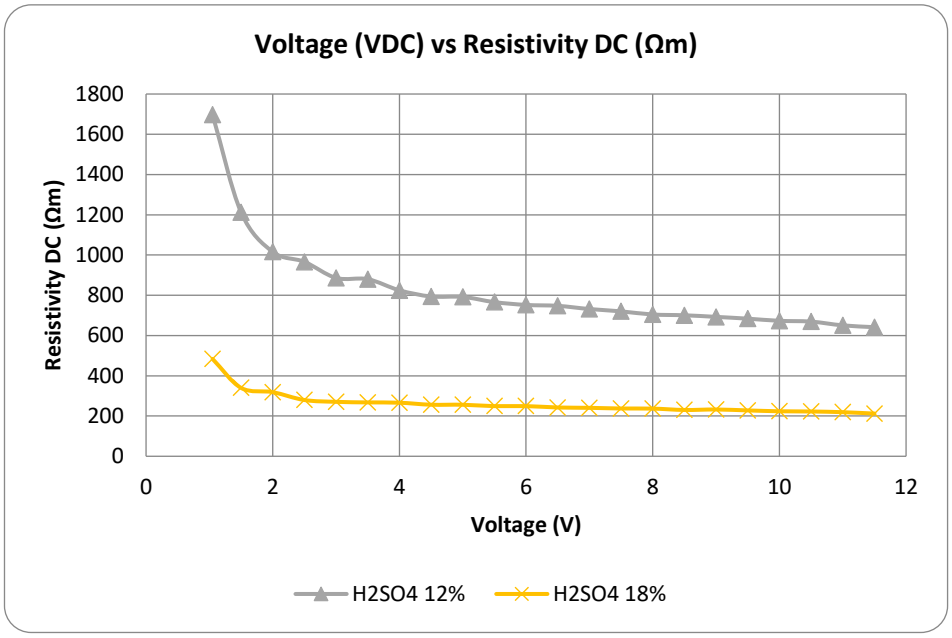

Figure 7 Graph of input voltage versus resistivity value with 12% and 18% H_2SO_4 solution percentages

Soils with high resistivity will reduce corrosion reactions. Thus, when only 6% H_2SO_4 is added, the corrosion reaction that occurs is small because the bentonite and $CaCO_3$ soils have high resistivity values. When the bentonite and $CaCO_3$ soils are mixed with 18% H_2SO_4, more soil particles are exposed to H_2SO_4, and the higher the corrosivity level will, in turn, make the resistivity gets smaller. The higher corrosivity of the soil, the greater the current flowing in the soil due to the low resistivity value, resulting in high conductivity. Therefore, the decrease in the soil resistivity using the H_2SO_4 is influenced by the corrosivity reaction and the change chemical properties of the soil [9] [11].

5 Conclusion

Laboratory experiments using a DC power supply to determine the resistivity value of the soil by adding chemical compounds in the form of H_2SO_4 and NaCl to the bentonite and $CaCO_3$ soil have been carried out in this research. In conclusion, the use of bentonite mixed with $CaCO_3$ can be used as ground enhancement materials (GEM), this material can reduce the resistivity value of the soil using an additional percentage of chemical solution. When the soil is dry (0%) without chemical solutions, the measured resistivity was 57096.39 Ωm. In the soil experiment tested with NaCl solution, the highest percentage level was 18%, and the average resistivity value decreased to 20.9 Ωm or decreased by 99.96%. With 18% H_2SO_4, the soil resistivity value is 259.6 Ωm or there is a 99.55% decrease. In a NaCl solution with a percentage of 6%, the average resistivity is 340.25 Ωm, whereas to achieve a resistivity value that is the same or close to that produced by 6% NaCl, it is necessary to add a solution of H_2SO_4 with a percentage of 18%. This shows that the percentage addition of the solution using NaCl solution to the soil has a 3-fold greater effect on reducing the resistivity than the H2SO4 solution. Based on the experimental results obtained in our study, when comparing the effectiveness of NaCl and H_2SO_4 in reducing grounding resistance, NaCl is more effective in reducing soil resistivity than H_2SO_4.

References

6

[1] Siti & Pambudi Handoyo Latifah, "Surround City Development (Effect of Conversion of Agricultural Land Functions into Elite Housing)," *Paradigma*, vol. 02, p. 1, 2014.

[2] "Rencana Aksi Daerah Penerapan Standar Pelayanan Minimal di Kabupaten Bandung Tahun 2021 - 2026," Bupati Bandung Barat, Kabupaten Bandung Barat, Lampiran Peraturan Bupati No. 93 tahun 2021, 2021.

[3] Asep Harja, et.al, "Hydrogeophysical Study of Malabar as the Highest Mountain on the Bandung," *Journal of Geology and Mineral Resources*, vol. 22, pp. 223-230, November 2021.

[4] "Persyaratan Umum Instalasi Listrik 2000 (PUIL 2000)," ANSI/IEEE, SNI 04-0225-2000, 2000.

[5] Nazra Anandu, "Analysis Of The Electrical Response Of Padalarang Limestone To Current Variation Under Water Content And Chemical Content Variation For Grounding Applications," School of Electrical and Informatics Engineering, Bandung Institute of Technology, Bandung, Thesis 2022.

[6] R.Z. Sabry, et.al, "Experimental investigation on breakdown characteristics of sand, bentonite and their mixes," *J. Electrostat*, vol. 93, pp. 79-84, April 2018.

[7] Aizat Azmi, et.al, "The use of enhancement material in grounding system: a review," *Indonesian Journal of Electrical Engineering and Computer Science*, vol. 13, no. 2, pp. 453-460, February 2019.

[8] Norazman Mohamad Nor, et.al, "Characterization of Ionization Phenomena in Soils Under Fast Impulses," *IEEE Transactions on Power Delivery*, vol. 353 - 361, pp. 353 - 361, February 2006.

[9] Yanwar Yusup Rukmana, et. al, "Potential corrosivity of the Citarum river floodplain sediment in Karawang, West Java," *Dinamika Lingkungan Indonesia*, vol. 7, no. 2, pp. 62-69, Juli 2020.

[10] Zakka Izzatur Rahman Noor, "Analysis Of The Electrical Response Of Karangnunggal Bentonite To Current Variation Under Water Content And Chemical Content Variation For Grounding Applications," School of Electrical and Informatics Engineering, Bandung Institute of Technology, Bandung, Thesis 2021.

[11] Omar Faruk Murad, "Obtaining Chemical Properties through Soil Electrical Resistivity," *Journal of Civil Engineering Research*, vol. 2(6), pp. 120-128, 2012.

Proceedings of the 3rd ITB Graduate School Conference ISSN: 2963-718X
Enhancing Creativity in Research Through Developing Innovative Capabilities
December 21, 2022

Effect of Water Level Elevation in Madiun River on Flooding in Jeroan River

Rif'atul Ummah [1,2,*], Arno Adi Kuntoro [2] & Hendrianto Alamsyah [1,2]

[1] Ministry of Public Works and Housing, Jalan Pattimura 20, Jakarta, Indonesia
[2] Water Resources Management, Faculty of Civil and Environmental Engineering, ITB, Jalan Ganesha 10, Bandung, Indonesia
*Email: rifatulummah@pu.go.id

Abstract. Jeroan River is one of sub-basin of Madiun River which located in Madiun Regency. Every year, the area around the Jeroan river experiences flooding caused by heavy rainfall, influence of full bank capacity, changes in land use and the presence of backwater from Madiun River. The study examines one of the causes of flooding, namely backwater from Madiun River. The effect of the Madiun River water level elevation on the flooded area that occurred around Jeroan River was analyzed by using the hydrological and hydraulics approach of the HEC-HMS 6.1 and HEC-RAS 4.1 programs. The area of Jeroan basin is ± 620 km2 with a length of ± 36 km of the main river. The Jeroan basin modeling is divided into 5 sub-basins, namely Upstream Jeroan sub-basin, Mejayan sub-basin, Klitik sub-basin, Piring-Sono sub-basin and Muneng sub-basin. The modeling uses unsteady flow modeling, with the upstream boundary is the return period discharge of each sub-basin and the downstream boundary is the highest water level and the average water level in the Madiun River. The results of the study show that the highest water level in the Madiun River causes a rise in the water level in the Jeroan River in the conditions of Q2, Q5, Q10 and Q25. The rise in the river water level ranges from 0.3-1.6 meters on the cross section with the worst conditions. Length of affected by backwater (until change in elevation of 5 cm) in various discharge around 15 km. Meanwhile, the average water level of Madiun River does not affect the flooding of Jeroan River.

Keywords: *jeroan river; flood; backwater madiun river; HEC-HMS; HEC-RAS.*

1 Introduction

Flood occur several times in the Madiun Basin (DAS) caused by the overflow of the Madiun River. Madiun River overflows caused by heavy rainfall and land use change in basin area that causes the flood discharge that occurs bigger from Madiun River capacity. Madiun Watershed is part of the Bengawan Solo River [1].

Jeroan River is one of the tributary streams of Madiun River located in Madiun Regency, East Java. Problems in the Jeroan River is flood occurs several times

that affect facilities and infrastructure area, affect land agriculture, and submerge settlement population especially in downstream area of Jeroan River. Flood caused by land use change and *backwater* effect from Madiun River [2].

Herlina (2011) analyzes the Factors of Jeroan River flood on 26 December 2007 are highest rainfall or high outliers, insufficient fullbank capacity, and land use change [3].

Recorded in last decades, The largest flood in Jeroan River happened in 2019 until inundated Ngawi-Kertosono Toll Road section throughout 400 meters on sections +603,600 to +604,000 and inundated National Road for 100 meters in the Garon Village, 500 meters in the Babadan Lor Village, inundated settlement as many as 4,317 households, and innundated thousand hectares of fields [4].

Based on problem above, then it will be analyzed one of the causes flooding in Jeroan River that is affected by Madiun River backwater based on Kali Jeroan discharge conditions with return periods of 2 years, 5 years, 10 years and 25 years.

In this study, simulation using the HEC-HMS software. The HEC-HMS model was designed for simulate the process of rainfall becomes runoff on a watershed system. HEC-HMS or *The Hydrologic Engineering Center's Hydrologic Modeling system* was developed by USACE-HEC. For imitate behavior flow inside watershed system, the HEC-HMS model requires adjustment of the so-called model parameters with calibration. The calibration conducted to the model parameters with evaluate similarity results simulation with observational data [5]. Whereas for simulation backwater effect to Jeroan River flood, carried out modeling using *unsteady flow* in HEC-RAS 4.1 software.

2 Materials and Methods

2.1 Study Area

Study area is located in the Jeroan Basin in Madiun Regency with a basin area of ± 620 km^2 consisting of of 5 Subbasin that is Jeroan Upstream Subbasin, Mejayan Subbasin, Klitik Subbasin, Piring-Sono Subbasin and Muneng Subbasin. Jeroan River through from Caruban area (Mejayan District) through Balerejo Subdistrict, Madiun Regency. The Upstream Jeroan is in the area of the slopes of Mount Wilis and Mount Pandan and the downstream is Madiun River.

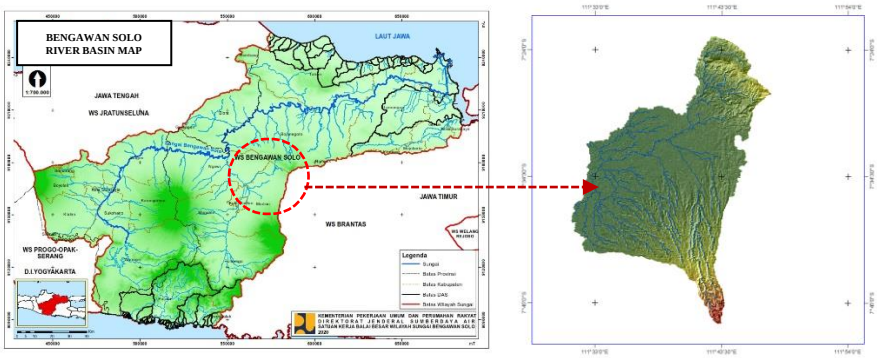

Figure 1 Location of the Jeroan Basin

2.2 Data Collection

Collection of necessary data in this study is secondary data. Required data is rainfall data, observation discharge data, water level elevation, land use map, geometric data and topography maps.

10 years rainfall data supprorted from the BBWS Bengawan Solo and the PUSDA East Java Government. Rainfall data originated from Sta Cermo, Sta Gemarang, Sta Pilangkenceng, Sta Saradan, Sta Kuwu, Sta Muneng, Sta Notopuro, Sta Jiwan, Sta Sooko, Sta Telaga Ngebel, Sta Tawang Mangu and Sta Pondok.

Observation discharge data, water level elevation data, and geometry data river suppoted from BBWS Bengawan Solo. Discharge data from Ketonggo control point and Madiun River elevation sourced from A. Yani control point.

Land use map from webgis Indonesia-geospatial.com sourced from the Ministry of the Environment and Forestry. Topographic map sourced from DEMNAS.

2.3 Data Analysis

On this styudy will be calculated data analysis on systematic includes:

2.3.1 Rainfall Analysis

Maximum daily rainfall from each rainfall sta will processed becomes rainfall area. The Formulation of rainfall area use method polygon *Thiessen* according to Eq. (1) [6].

$$d = \frac{A_1 d_1 + A_2 d_2 + A_3 d_3 \ldots + A_n d_n}{A} = \frac{\sum A_n d_n}{A} \quad (1)$$

Where:

A	=	area (km ^{2})
D	=	average rainfall data (mm)
$d_1, d_2, .. dn$	=	Rainfall in each sta (mm)
$A_1, A_2, .. An$	=	Effected Area of sta 1,2,… n

Rainfall distribution analysis in this study use *Generalized Extreme Value* (GEV) method by using *hydrognomon software* 4. GEV distribution probability is distribution probability continuously developed based on theory score extremes that include the Gumbel, Frechet, and Weibull distributions. The GEV distribution is the only one normalizing distribution score maximum on a distributed set of identical and independent data in a manner random [7].

Hydrognomon is application device for analysis and processing of hydrological data especially in form *time series*. This program also supports application hydrology special, includes evapotranspiration models, stages *discharge* and analysis of sediment discharges, tests homogeneity, method water balance, and hydrometry [8].

2.3.2 Flood Discharge Analysis

On this research, flood discharge is analyzed by using HEC-HMS. The runoff calculation is modelling by using *Soil Conservation Service* (SCS) *Curve Number* (CN) method. The SCS CN method is considered the easiest applied in calculation for estimate precipitation excess as cumulative function from rainfall, cover land, land use, and humidity (antecedent moisture) using Eq. (2) and Eq.(3) [9].

$$Pe = \frac{(p-Ia)^2}{P-Ia+S} \tag{2}$$

$$Ia = 0.2\ x\ S \tag{3}$$

Where:

Pe	=	Rainfall cumulative at time t
P	=	Depth of rainfall cumulative at time t
He	=	Initial abstraction
S	=	Storage maximum capacity

Initial abstraction is all lose water before happening rainfall started. The initial abstraction value is variable depending on land use. Empirical formula S in Eq. (4) [9].

$$S = \frac{25400 - 254\,CN}{CN} \text{ (SI units)} \quad (4)$$

Where

S	=	Maximun retention value
CN	=	Curve Number

CN (Curve Number) values vary from 100 (for waterlogged surface up to around 30 for impermeable surface with high infiltration rate. The CN value represents function of land use, type land, plant cover and humidity. For the land consists of some type land and land use accordingly the CN value is $CN_{composite}$ in accordance Eq. (5) [9].

$$CN_{\text{composite}} = \frac{\sum A_i CN_i}{\sum A_i} \quad (5)$$

Where

$CN_{composite}$	=	Land use composite value
Ai	=	Subbasin Area

On this research will use Snyder's hydrograph method. F.F. Snyder from the United States in 1938 made use of basin parameters for obtain hydrograph unit synthetic. A number of the watersheds studied by Snyder are on plains Appalachian height with watershed area ranges between 30 and 30,000 km ^{2} [10].

Snyder developed the model with connecting empirical coefficients elements hydrograph unit with basin characteristics. It is based on thought that conversion rainfall becomes runoff influenced by the basin system [11].

Hydrograph unit determined with element among Qp (m^3/sec), T_b (hours), and t_b (hours) and t_r (hours). The hydrograph element connected with basin area (km^2), main river length (km), and length river main be measured from the place measurement up to the point in the main river with basin weight point (km). With those elements, Snyder created a hydrograph unit synthetic model with Eq (6) – Eq (7) [10].

$$t_{\text{p}} = 0.75\,.\,Ct\,(L.Lc)^{0.3} \quad (6)$$

$$\text{Qp} = 2.75\,\frac{Cp.A}{tp} \quad (7)$$

where:

t_p	=	Time lag (hours)
Q_p	=	Peak Discharge (m^3/sec)

Ct and Cp are coefficients that depend on the unit and features of the basin [12]. The Ct and Cp coefficients should be determined empirically, because magnitude capricious among one area _ with the others. In the metric system, Ct ranges between 0.75 to 3.00, while Cp ranges between 0.9 to 1.4 [13].

3 Results and Discussion

3.1 Basin and Subbasin Delineation

The watershed delineation was carried out in the Madiun Basin for necessity calibration and Jeroan Basin as study location. Madiun Basin have watershed area of ± 3,828 km^2 and Jeroan Basin have watershed area of ± 620 $km^{2,}$ and with using the HEC-HMS program, the mapping process is carried out for determine the subbasin of Jeroan Basin so that 5 subbasin were obtained, namely the Upstream Jeroan subbasin with area of 111.95 km^2, Mejayan subbasin with area of 182.25 km 2, Klitik subbasin with area of 67.20 km^2, Piring-Sono with area of 198.46 $km^{2,}$ Muneng subbasin with area of 60.17 $km^{2.}$ The Delineation of Madiun Basin dan Jeroan Basin can be seen on Figure 2.

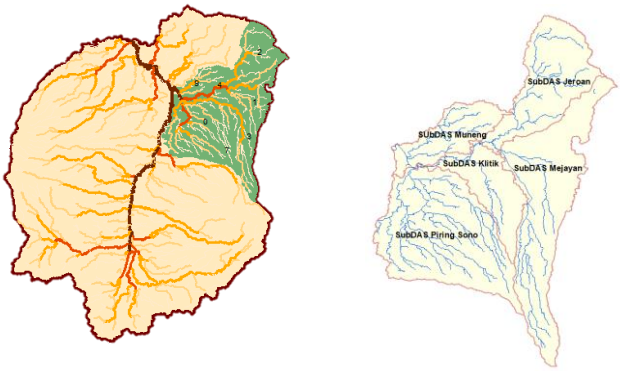

Figure 2 The Delineation results of Madiun Basin, Jeroan Basin and Subbasin's

3.2 Land Use Analysis

Land use of Madiun Basin consists of some classes that is shrubbery, dry land secondary forest, forest crops, settlements, plantations, mining, agriculture dry land, mix agriculture land, rice fields, open field and waters. From the land use map determined type soil from each cover land based on grouping criteria of Hydrological Soil Group (HSG) ie class B and class D so that obtained $CN_{composite}$ of 76.79. The $CN_{composite}$ values of the Upstream Jeroan Subbasin was 80.58, the Mejayan Subbasin of 76.96, Klitik Subbasin of 64.51, Piring-Sono Subbasin of 70.78, and the Muneng SUbbasin of 84.83.

3.3 Hydrology Analysis

3.3.1 Rainfall Analysis

Annually Maximum Rainfall (HHMT) analyzed to regional rainfall in each Subbasin using Polygon Thiessen method. Then it analyzed to return period rainfall by using GEV method then multiplied with ARF. The Rainfall Anlyasis shown on Table 1.

Table 1 Rainfall Frequency Analysis

Return Period	Rain Plan X ARF (mm)				
	Upstream Jeroan Subbasin	Mejanyan Subbasin	Klitik Subbasin	Piring-Sono Subbasin	Muneng Subbasin
2	116	100	104	97	178
5	139	113	115	105	201
10	151	121	121	110	213
25	163	130	128	114	225
50	171	136	132	117	232

3.3.2 Calibration

calibration conducted with comparing 3 events of flood discharge maximum events recorded on Ketonggo control point. The results of discharge from the rainfall on the same day of the 3 events using the HEC-HMS 4.10 program. Ct and Cp values were obtained with *trial-and-error* method so that obtained less than 10% error between calculation discharge and observed data on Ketonggo control point in 3 different years (Figure 3). Simulation use *SCS CN* loss method and *transform HSS Snyder*.

Duration used 12 hours rainfall distribution considering the Jeroan Basin including large Basin with time base hydrograph estimated less than 12 hours so that recommended for use 12 hours rain duration as base calculation. hourly rainfall distribution conducted using PSA-007 based Technical Instructions for Calculation of Flood Discharge at Dams 2017 [9]. Ct and Cp values obtained of the calibration process is 1.15 and 0.7 closest to observed data in 2014, 2017 and 2018.

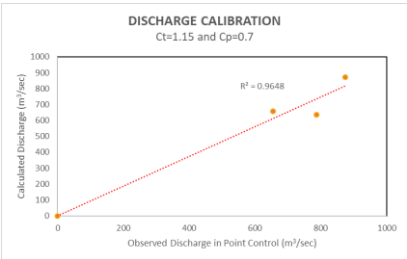

Figure 3 Discharge Calibration Results

The calibration parameters can be applied for discharge calculation in each subbasin in the location study with data input as in Table 2.

Table 2 Loss and Transform Parameters in HEC-HMS

No	Subbasin	CN	Initial Abstraction	Ct	Peaking Coefficient (Cp)	River Length(L)	Lc	Time Lag	Impervious
						(km)	(km)	(o'clock)	(%)
1	Upstream Jeroan	80.58	12.2	1.15	0.7	34.16	17.70	7.86	2.19
2	Majayan	76.96	15.2	1.15	0.7	40.28	13.03	7.53	2.00
3	Klitik	64.51	27.9	1.15	0.7	32.69	16.73	7.62	5.00
4	Piring-Sono	70.78	21.0	1.15	0.7	36.18	22.3	8.57	4.49
5	Muneng	84.83	9.1	1.15	0.7	24.98	14.43	6.73	5.23

3.3.3 Flood Discharge Analysis

Flood discharge analysis on this study use *Snyder* 's Hydrograph method with the HEC-HMS 4.10 program. Based on simulation results using HEC-HMS was obtained flood discharge hydrograph return period for each subbasin as shown in Figure 4. Peak discharge Flood could be seen in Table 3.

Table 3 Return Period Discharge

Return Period	Peak Discharge (m^3/sec)				
	Upstream Jeroan	Mejayan	Klitik	Piring-Sono	Muneng
2	161.7	199.1	47.2	153	213.1
5	221.8	242.1	57.2	165.2	247.7
10	253.7	269.1	63.9	177.6	265
25	275.5	302.8	73.8	293.2	285.2
50	292.1	329.3	79.4	213.9	296

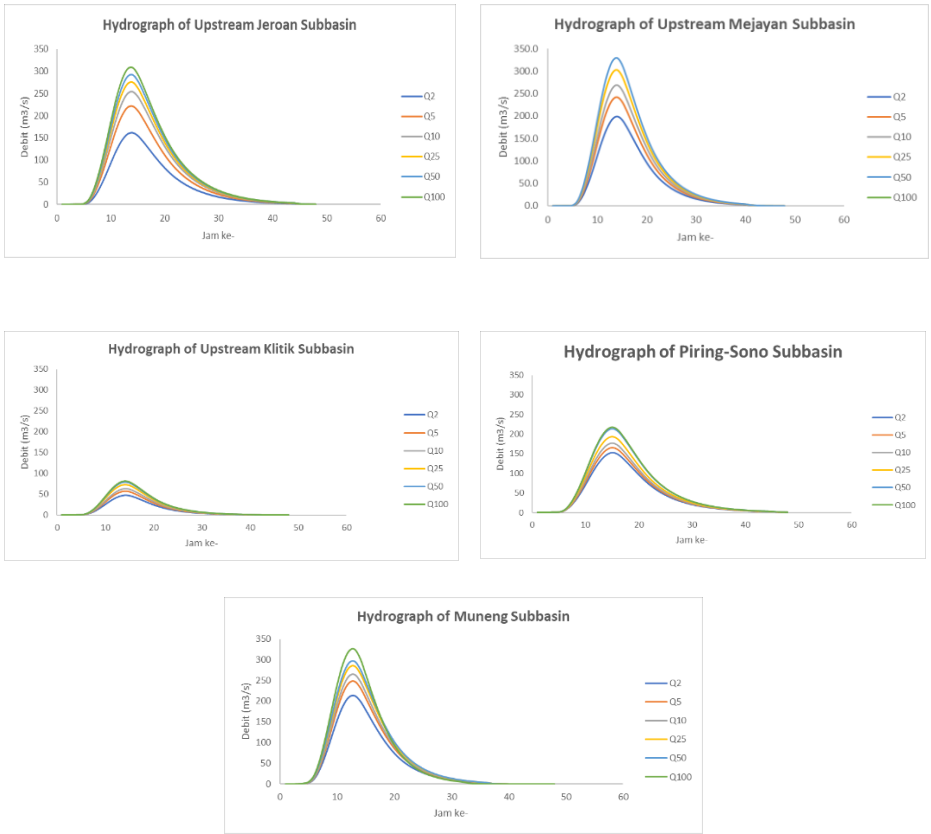

Figure 4 Hydrograph of Each Subbasin

3.3.4 The Water Level Elevation of Madiun River

The water level Elevation of the Madiun River at the junction between Jeroan River and Madiun River in Q25 was obtained from A. Yani control point. A. Yani control point was ± 8 km away from downstream of Jeroan River. So Q25 calculation based on comparison between basin area with A.Yani control point as an outlet (± 2202.42 km ^{2}) with basin area of Madiun River and Jeroan River meeting point as an outlet. The water level elevation is analyzed using rating curve graph on the segment of cross section in junction of two river. *Rating curves* obtained from cross-sectional in measurement 2009 that simulated using HEC-RAS. Water level elevation used in this simulation could be seen in Table 4.

Table 4 The Water Level Elevation of Madiun River at the Downstream of the Jeroan River

Outlets	Basin area (km^2)	Discharge (m^3/sec)		Elevation (mdpl)	
		Q25	Qaverage	Q25	average
Junction of Madiun and Jeroan River	2837	1029.25	168.22	56.43	49.34

3.1 Model Simulation

Modeling in this study is running on HEC-RAS 6.1.0 by implementing unsteady flow with the modeling scheme in Figure 5 and modeling scenario can be seen in Table 5.

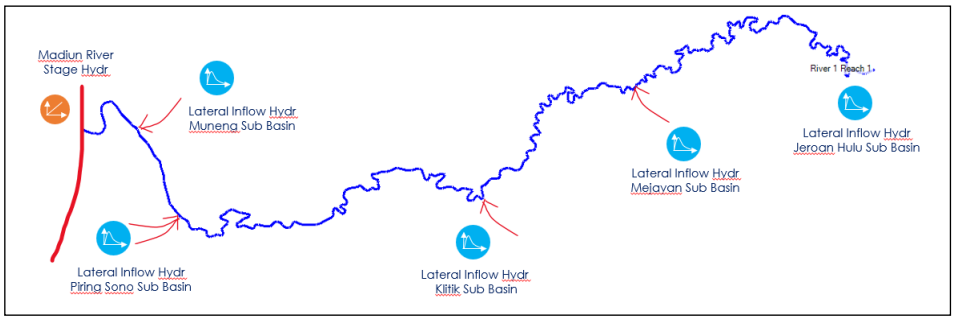

Figure 5 modeling scheme

Table 5 modeling scenario on HEC-RAS

Skenario	Upstream (Jeroan Basin)	Downstream (Madiun Basin)
1	Q2, Q5, Q10, Q25, Q50	Normal depth (slope 0.00077)
2	Q2, Q5, Q10, Q25, Q50	The highest water level elevation
3	Q2 dan Q25	The average water level elevation

In the upstream boundary scenario, Q2 hydrograph discharge is calculated from upstream toward Mejayan River (sta 327) as large as 161.7 m3/sec, section (sta 328–sta 212) along Mejayan River until Klitik River as large as 347.35 m3/sec, section (sta 213–sta 49) after Klitik River till Plate-Sono River as large as 383.33 m3/sec, section (sta 50-sta 27) along Plate-Sono River until Muneng River as large as 511.73 m3/sec, and section (sta 28–sta 0) after Muneng River confluence calculated discharge as large as 643.94 m3/sec. On the normal depth as a downstream boundary, the Jeroan River has experienced overflow along sta 300 – sta 490. This shows that the bankful capacity of the Jeroan River is no longer able to accommodate discharge that occurs without the influence of the backwater from the Madiun River.

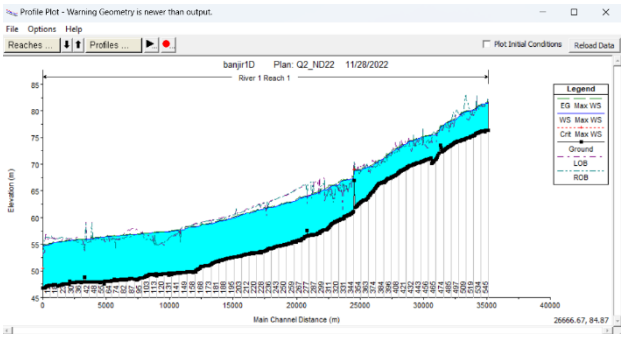

Figure 6 Simulation Result of Q2 (Upstream Boundary) and Normal Depth (Downstream Boundary)

In the simulation scenarios Q2, Q5, Q10, and Q25 as the upstream boundary and the highest TMA Madiun River as the downstream boundary, it is found that increasing water elevation in Jeroan River. This shows that there is backwater from Madiun River which has an effect on flooding in Jeroan River. The rise in Jeroan River water level can be seen in Figure 7 until Figure 9.

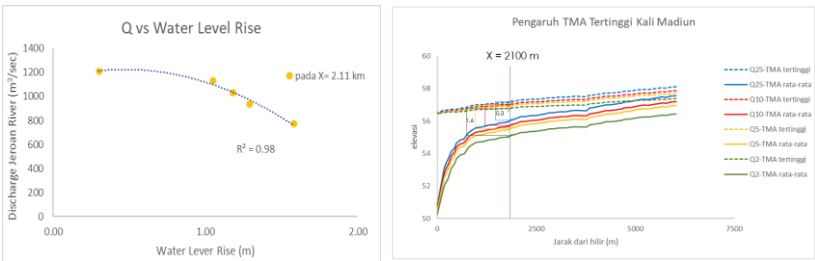

Figure 7 Elevation Changing of Jeroan River affected of Backwater from the Madiun River.

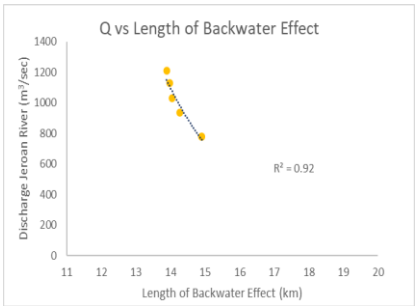

Figure 8 The Length Effect of Backwater

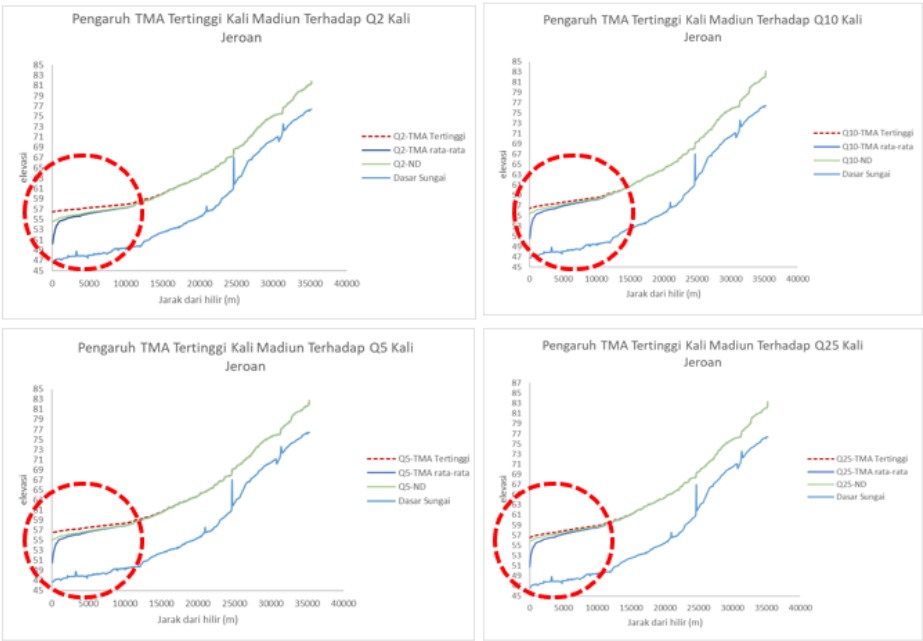

Figure 9 Elevation Changing of Jeroan River affected of Backwater from the Madiun River in Each Discharge Return Period

Based on scenario using average TMA Madiun River as the downstream boundary, it is found that Average TMA Madiun River does not affect water level of the Jeroan River. This shows that the condition of the Madiun River with an average water level does not cause backwater into Jeroan River. So, it can be concluded that the flooding that occurs is influenced by the amount of discharge from the sub-basin of Jeroan River.

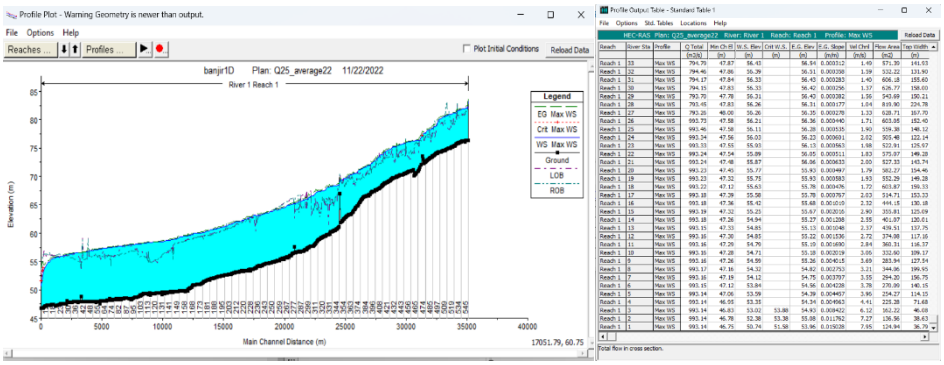

Figure 10 The Simulation Result of Q2 as Upstream Boundary and Average Water Level of Madiun River as Downstream Boundary

However, based on scenario Q25 as the upstream boundary and average water level of Madiun River as the downstream boundary, there is increasing velocity as much as 12% and critical flow occurs at downstream Jeroan River. This increasing velocity of water can be related to natural conditions of the Jeroan River which tend to experience degradation and frequent cliff slides, especially on the cliffs on the outer bend.

4 Conclusion

Based on the analysis result and discussion, it can be concluded as follows:

1. The Calibration result on Ketonggo point control, obtained the parameters Ct = 1.15 and Cp = 0.7 which can be used to calculate flood discharge design in each Jeroan sub-basin.

2. Based on hydrological analysis, the peak discharge during Q25 period in Upstream Jeroan sub-basin is 275.5 m3/sec, in the Mejayan sub-basin is 302.8 m3/sec, in the Klithik sub-basin is 73.8 m3/sec, in the Piring-Sono sub-basin is 293.2 m3/sec, and in the Muneng sub-basin is 285.2 m3/sec.

3. In the simulation uses Q2, Jeroan River has overflowed at several points along sta 300 to sta 490. This shows that the bankful capacity of the Jeroan River is no longer able to accommodate flow-discharge that occurs even without impact of backwater from Madiun River.

4. In the highest water level elevation conditions exists in Madiun River, it was found that highest conditions effects of rising water level from normal conditions, ranged from 0.3 to 1.6 meters with affected length around 15 km. This explains that Kali Madiun affects increasing of flood volume into Kali Jeroan.

5. In the average water level conditions occurs in Madiun River, it is found that there was no effect on rising of the water level to Jeroan River. It can be concluded that in this condition the Jeroan River flooding is caused by flow-discharge from its sub-basins that come from high rainfall or land use change in subbasin.

References

[1] K. PUPR, Rencana Pengelolaan Sumber Daya Air Wilayah Sungai Bengawan Solo, 2015. (Book)

[2] Devianto, V.B., Donny H. & Runi A., *Pengendalian Banjir di Sub DAS Jeroan Kabupaten Madiun*, Jurnal Aplikasi Teknik Pengairan, 8(2), pp 181-193, Nov. 2017. (Journal)

[3] Herlina, Pipit D., Kajian Alternatif Pengendalian Banjir Sungai Jerohan Kabupaten Ngawi, Masters in Natural Disaster Management Department, Gajah Mada University, Yogyakarta, 2011. (Thesis)

[4] Harianto, S., Detiknews, https://news.detik.com/berita-jawa-timur/d-4835991/geger-banjir-tol-di-madiun-yang-terjadi-jelang-pilpres-2019/2, (Dec 26, 2019). (URL Link)

[5] Fadhilla, I.N. & Umboro, L., *Pemodelan Hujan Discharge DAS Kali Madiun Menggunakan HEC-HMS*, Jurnal Aplikasi Teknik Sipil, 19(3), pp. 361-368, August. 2021. (Journal)

[6] Ningsih, D. H. U., *Metode Thiessen Polygon untuk Ramalan Curah Hujan Periode Tertentu pada Wilayah yang Tidak Memiliki Data Curah Hujan*, Jurnal Teknologi Informasi dan Pendidikan, 17(2), pp. 154-163. 2012. (Journal)

[7] K. PUPR, Modul 1 Analisis Curah Hujan Bimbingan Teknis Analisis Discharge Banjir Desain Dengan Menggunakan Data Hujan Satelit, Balai Teknik Bendungan, 2022. (Book)

[8] Kozanis, S., A. Christofides, N. Mamassis, A. Efstratiadis & D. Koutsoyiannis, *Hydrognomon: A hydrological data management and processing software tool*, European Geosciences Union General Assembly, 7(1), 2005. (Conference Proceedings)

[9] Feldman, A., *Hydrological Modeling System Technical Reference Manual*, Hydrological Model HEC-HMS Tech. Ref. Man, p.148, March, 2000. (Journal)

[10] Chow, V.T., Maidment, D.R., & Mays, L.W., *Applied Hydrology*. Mc Graw-Hill, 1988. (Book)

[11] Harto, Sri, *Analisis Hidrology*. PT. Gramedia Pustaka Utama, 1993. (Book)

[12] Wilson, E.M., *Hidrologi Teknik*. Institut Teknologi Bandung. 1993. (Book)

[13] Soemarto, C.D., *Hidrologi Teknik*. Erlangga, ed. 2, 1995. (Book)

Proceedings of the 3rd ITB Graduate School Conference ISSN: 2963-718X
Enhancing Creativity in Research Through Developing Innovative Capabilities
December 21, 2022

The Color Map of Death in the Scene of the Bridge Connecting the Land of the Living and the Land of the Dead in Coco Film

Satria Budiana Tresna[1], Chandra Tresnadi[2] & Pindi Setiawan[3]

[1]Master of Design Postgraduate Student, FSRD ITB
[2]Research Group of Design Sciences & Visual, FSRD ITB
[3]Research Group of Visual Communication and Multimedia, FSRD ITB
[*]Email: satriabudianatresna@gmail.com

Abstract. Death is something that cannot be avoided. Every culture in this world has a celebration or ceremony to honor people who have passed away. Dia de Los Muertos is one of the most famous Days of the Dead celebrations. The celebration was made magnificently and filled with very colorful decorations like a festival. The colors on the occasion play a very important role in death ceremonies in Mexico. The festival became a culture that was later adapted into an animated film Coco. It is necessary to study how the color of death is constructed in the animation, as well as how the color palette is generated. The application of this color plays a role in representing death in Coco's animation, this animation has various colors of death. The method for determining the color map of death in the animated film scene uses a qualitative research method using a color approach. The results of the colors are in the form of a color map, namely orange, yellow, dark blue, and pink. The research results can be used as a reference in an animation's visual depiction of the color of death.

Keywords: *color map; death; the land of the dead.*

1 Introduction

The many cultures in this world make various aspects of a celebration become many kinds. Celebrations certainly exist in every culture, one of which is the celebration of death. Celebrations of death in the form of ceremonies always involve many people and communities, these rituals generally have characteristics such as praying, eating, or gathering with family Aufa in [2]. As in a celebration, especially in the celebration of death in Mexico which is usually called The Day of The Dead. The Day of the Dead or called Dia de Los Muertos is a ceremony held by the people of Mexico where at the event people spend time in cemeteries, making shrines for people who have died, and displaying various decorations that decorating all places artistically by using colored skulls or called Calacas, flowers, as well as other ornaments. This celebration is believed to be a big family reunion between the two worlds, life, and death. Dia de Los Muertos

is not a moment of mourning, but of remembering family members and those who have passed away, keeping them close to our hearts Sadewa, 2018 [13].

In this celebration, many are decorated with various colors. The color commonly used to symbolize this celebration is the orange color of a *marigold flower*. The color is commonly depicted in funeral symbols in Mexico and as the color of mourning Amelinda & Franzia in [1]. Not just an aspect of color itself, color can have a visual perception. According to Darmaprawira [7], the general thing is that colors can affect the human soul and also affect emotions, and colors can also describe moods. Not only that but color perception can also be motivated by culture and beliefs. Color has a symbolic meaning that cannot be separated from mystical interpretation, where it appears at the peak of humanity (humanism) which can be specific and varies from social situation to another social situation. Colors can be classified based on their symbolic meaning, such as red which is often associated with the sun, blood, fire, or evil with both positive and negative connotations.

Coco animated film is an animation that elevates Mexican culture in celebrating the day of the dead. The film tells the story of a boy named Miguel who was born into a family that has a bad experience with music. Because music is the cursed thing in his family, Miguel's desire to become a musician like his idol Ernesto de la Cruz seems to be hindered. Until one day Miguel had to go through his journey into *The Land of the Dead* to seek help so he could return home with Hector's help and return to his family to start a new story with his family.

Color is an important visual element in an animated film Wang [14]. The role of color in animated films varies, not only to reflect the character but also to accompany the audience in the story in it. Brown (2013) [4] in Berens (2014) [4] argue that color is a spectacle that is as important as narration, where everything has an important role in every frame. The colors presented in the animation are many and varied. According to Blazer in [5] Color has extraordinary storytelling power, so that color can express emotions, clarify motivations, and even be able to dictate all meaning in a story, especially in animated films. The use of color in animation can present visual enjoyment which can enhance the visuals and aesthetics of a visual in an animated film Wang, 2017 [14].

In this research, the color of the Coco animation film is analyzed. Analysis was carried out to find out and understand how color is applied to each scene. As well as how the color of death appears as a color in Coco's animated depiction. Apart from the coloring that may be inspired by the culture in Mexico. This research aimed to understand in depth how this color works and how the coloring results of this film can be used as a reference for other animated films in conveying stories and visualizations with the theme of the world of death or the like. To

further investigate this film, an understanding of color theory, color related to culture, and the psychology of color is needed to provide an overview of the meaning or significance of color.

2 Study Literature

Color is one of the most important elements in making visual works or works of art. Where a color can stimulate the brain and eyes with what we see which can make the soul sway and cause emotions and can make an object look light and heavy, near or far, expensive and cheap where all of this depends on how the color is applied Bleicher in [6]. Everything arises from an influence on what we see which then influences our psychology so that we can conclude something.

2.1 Color in Design and Animation

The application of color in a visual form is very broad, one of the highlights of applying color in a visual form is from an animation. Animation is a film that is formed from a series of images that are processed in such a way as to be able to display moving images and tell stories, Gunawan in [11]. Not only that, the animated film is a medium that combines audio and visuals with stories that are packaged into animation, Fathurohman et al., [9]. It can be said that animation is a very complex medium because of the combination of stories, moving visuals, and also audio. Not only that, the colors in animation can form a mood and atmosphere in a visual. Mood and atmosphere are formed in a clear sequence, and in depictions such as describing fear, romance, sadness, emotion, or joy, it is done using a color so that it can appear in an image, Fowler [10].

All forms of application of color in animation can occur in various ways, whether building an atmosphere, impression, or perception. The most fundamental thing about applying this color is not far from the color system itself. Color is said to have the power to convey extraordinary stories, so that it can clarify a character's motivation in animation, express emotions, and even dictate all messages and meanings in the entire work, Blazer [5]. Three important things build a color system, including Hue, Saturation, and Value. Hue is a name for a color that makes it easier to identify it. by knowing the name of the color we can distinguish red, yellow, green, blue, and so on. Saturation or saturation is the intensity of color; how many colors contain gray in one color, Eiseman [8]. And Value is a level or color derivative from light to dark which will distinguish the quality of the color brightness level from color with a mixture of white to black, Darmaprawira WA [7].

2.2 Color in Culture

For centuries, color has been an important part of human life. Certain cultural, historical, and traditional aspects of color are capable of forming a perception that is then passed down from generation to generation, Eiseman [8]. For example, in Chinese culture, the application of Feng Shui considers red to be a symbol of prosperity. The Greeks and many others considered blue to be a protective color. Many cultures in the world understand and play the role of color, but one culture that tends to be strong in terms of color, especially in its application in animation, is Western culture.

Color is very important in human life. Culture is one that greatly influences every understanding of color symbolism. Colors can evoke various emotions and beliefs, as well as positive and negative connotations in culture, especially western culture. Here are some colors and symbolism in western or western culture.

1. Red is a very bright color like caffeine in visuals. This color is symbolized as an aggressive, anxious, and compulsive color. Red can be symbolized by speed like a fast car, and others, Bellantoni [3]

2. Yellow is the color of opposites, one of the reasons why it is a color of caution is because it is a visually aggressive color. Dr. Harry Hepner, Professor of Advertising Psychology at Syracuse University, claims, "Yellow is the color that is both the longest remembered and the most hated", Bellantoni [3].

3. Blue is a positive color and is considered the world's safest color choice. Blue represents authority, security, and trust in Europe and North America. Blue is arguably the most popular color worldwide, and some brands the world use blue in their logos/branding, Eiseman [8].

4. Orange is categorized as an arousing color, which stimulates conversation as well as appetite. Its physical nature encourages spontaneity and some degree of impulsivity. And this color is considered to be the hottest of all the colors because orange is never described as cool or cool. This color relationship is usually sunset, heat, or considered a color with high optimism, enthusiasm, cheerfulness, and energy, Eiseman [8].

5. Green. In history, the color green is associated with the meaning of the environment and life. The green color is also interpreted as a dichotomous color, where there are colors of fresh vegetables and rotting

meat, life, and danger, Bellantoni [3]. In addition, green is often used to depict strange creatures originating from legends or folklore, one of which is fairies, sprites, pixies, dragons, etc. Eiseman [8].

6. Purple is the color of nobility, spirituality, faith, piety, wealth and royalty are some of the terms associated with purple. In the past, purple dye was very rare and hard to come by because it was extracted from a certain species of sea slug, namely banded dye-murex. It was expensive to produce purple cloth, and it became a symbol of monarchy. The US military awards the Purple Heart award to military personnel who suffer injuries or are killed while on active duty (medium.com). In use in settings, purple is capable of establishing an air of majesty, but in church symbolism, it has a high position in representations of healing, contrition, and humility, and in the Middle Ages it was considered mystical, incomprehensible, and mysterious, Eiseman [8].

3 Method

This research uses quantitative research methods. By getting deep data in looking for a color map in an animation. This method is taken by researchers through color dissection to find a color map in a study conducted by Kahdar et al. 2018 [12], in search of Color Mapping of Natural Dyes in Coastal Batik of Batang Batik from Batang Regency. In this study, researchers only applied quantitative research as a research method because in this study they only collected colors from a series of images in animation and searched for color maps using a web-based application. This research focuses on the visuals obtained from the animated film Coco as a research object. The object research was carried out by taking samples from scenes in the Coco animation film. Sampling is based on keywords that have previously been made. These keywords make it easier to find scenes from the entire duration of the film that has appropriate visual elements, colors, and other elements that support these keywords.

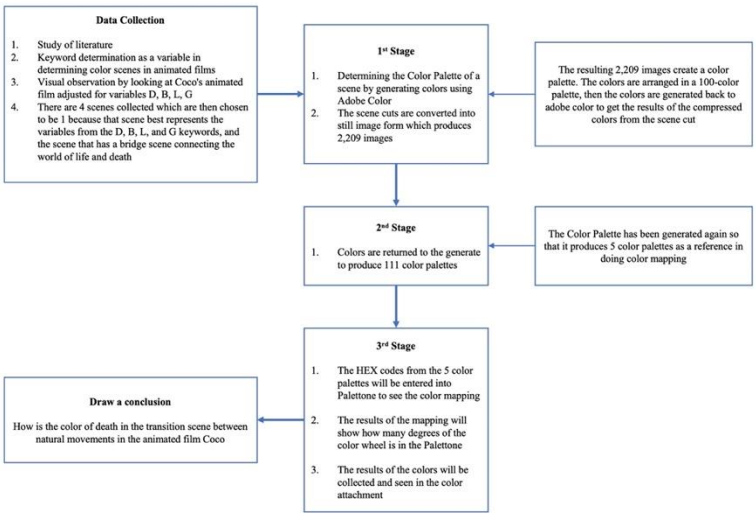

Figure 1 The Research Stage

The purpose of this study is to identify the colors in the animation scene so that a *color palette appears* which is then searched for color mapping so that it can be a reference in forming visuals with color mapping, especially the color of death in an animation. The steps taken by the author in conducting research can be seen in Figure 1.

1. From this series of processes, data collection was carried out by taking a series of shots from the Coco animated film. The initial stage in taking this shot is done by first determining the appropriate keywords from the Coco film. From several times seen, reviewed, and watched repeatedly, this Coco film has at least 25 important scenes in the series of films. Of the 25 scenes, they are purified based on keywords that correspond to the Coco film. These keywords are *The Land of the Dead* (D), Flowers (B), Ancestors (L), and *Gloomy* (G). The sample is then determined from these keywords which can visually represent the film.

2. The results of the scene are cut according to the scene. The cutting of the film is done using the *Adobe Premiere Pro application*. The use of this application facilitates the process of cutting shots according to the desired duration and timeline

3. Furthermore, the results of the scene will be analyzed by looking for the *color palette* first with various stages until it is formed into 5 *color palettes*. Then this *color palette* will later be used to find a color map

using a *palette*, how are the colors related, as well as the derivatives and proximity between each *color palette*.

4 Result and Discussion

Creating a color palette from the selected scene using Adobe Color. Adobe Color is a web-based application that is used to generate colors from images into a color palette. The results of the researcher's color palette will fully leave it to the system Adobe Color in generating colors from each converted image from the video that has been made.

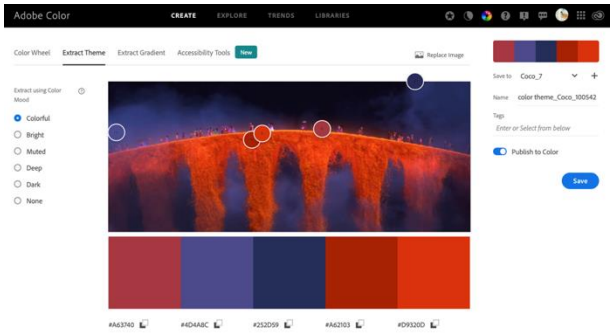

Figure 2 The process of generating color in Adobe Color

After the color generation process is carried out by extracting the image in Adobe Color, the color palette results are then collected and put together to carry out the 2nd color generation process. The results of this first color palette have a very large number, the second color generation process is carried out to simplify the colors of each scene. This process is carried out by collecting a color palette of 100 color palettes in one complete image which will be color generated again.

The results of this color generator are then generated back to the 3rd process to simplify again and extract the colors into one color palette in each scene. The result of each scene has 5 color palettes from each of each scene. The color palette is considered to be able to represent the colors of the scenes in each scene with different durations. The final color palette results from the scene can be seen in Figure 3.

Figure 3 The final Color Pallet of Coco's animated movie scene in Adobe Color

Results The color palette is then searched for its association with other colors using the Palettone. Use this web-based application to see the mapping on the color wheel. This color mapping is done by entering the HEX color code that has been obtained in one of the scenes. Then the code will change the color wheel and show a series of mappings for each color which will then be screen captured to see if any of the colors intersect and are related. The results of the color wheel can be seen in Figure 4 below.

Figure 4 Color Mapping

In the color wheel in Figure 4, there are colors that overlap in the value section of the color wheel, the areas where these intersecting colors are searched are then related to each other and become derivatives of the colors on the outermost circle called Hue. Determining intersecting parts is done by shifting the circle parts by paying attention to the circles in the area and lines to reference the location of the next circle that intersects. The color wheel in that scene has slices and color degrees. In detail, the slices and color degrees can be seen in Table 1.

Tabel 1 Scene color slices of the Bridge Connecting the Land of the Living and the Land of the Dead

HEX Code (Hue)	Position	Slice	Sliced Result
#1D2043	252°	#1D2043 (252°) x 3F51A7	#3D4FA4
#3F51A7	247°	(247°) = (249.5°)	#3F47A7
#D63765	346°	#3F51A7 (247°) x D63764	#D93D69
#EFD644	95°	(346°)	#F1D843
#F05F28	14°	#EFD644 (95’) x 3F51A7	#F17243
		(247°)	
		#EFD644 (95°) x D63764	#F2D947
		(346°)	#4249A8
		#F05E28 (14°) x D63764	#3F51A5
		(346°)	#DA406C
			#F27547
			#D93D69
			#3F47A7
			#3D4FA4
			#F1D843
			#F17243
			#EF6634
			#363EA5
			#3347A3
			#D72F5F
			#EFD334

The color of the sliced results will be seen by the HEX code, which then at every degree of the Hue will be changed to see the color on each slice will produce a color with what code. The color of the slices can be seen in Figure 6 below.

Figure 5 Color results from the Palettone color wheel and its derivatives

The mapping results have been completed by entering the HEX code results for each result from the color wheel. Then the results are arranged into a form as shown in Figure 5. The making of the color palette is to make it easier to see the colors and the derivatives of the resulting colors from the previous color generator. The final color generated result is *Space Cadet color* with code HEX #1D2043, *Violet Blue color with code HEX #3F51A7, Cherry* color with code HEX #D63765, *Sandstorm Yellow color* with code HEX #EFD644, *Neon Orange color* with code HEX # F05F28.

When viewed from a visual with a duration of 1:32 with the color results from the *color generator*. The overall visuals of the scene can produce the final *color palette* that can represent the color series from start to finish in the film cut. In achieving the final color, the animation sequence is converted into a still image with the fps that corresponds to the animation at 24fps. The resulting color results have a different tendency from each series of images to images, from dark to bright colors. However, after all these colors have been collected, you can then look at the next *color palette* by doing the *color generation* again, the resulting colors are only 5 colors. If you look at the final color with this visual, at least there is a connection where in this scene the color of the *Space Cadet* with code HEX #1D2043 represents the color of the sky, the color *Violet Blue* with code HEX #3F51A7 represents some of the colors of the sky which has a lighter

saturation, and the nuances of mist when entering the world death, *Cherry color* with code HEX #D63765 representing the clothes worn by Tia Rosita, as well as some colors representing the spirit of Alebrijes, and color reflections on the city environment in the world of death, *Sandstorm Yellow color* with code HEX #EFD644 representing candlelight, and the light coming out of the marigold petals that Miguel is stepping on and holding, the color *Neon Orange* with code HEX #F05F28 represents the color of the marigold flowers with various saturations, as well as the overall color of the bridge made of flowers, which in this scene is part of the bridge visually appealing enough.

5 Conclusion

Color palette search through various stages in finding out the color map, especially in the natural movement scene in the Coco animation film, the author can conclude that the final color of this study shows quite appropriate results, where the final color represents each of the keywords that have been determined in a variable in determining the color of death in determining the scene before generating the color. Each color generated represents a part of the visual elements contained in each scene, including flowers, candlelight, the blue color that appears in the night sky, as well as other colors that represent other lights in the sky during the celebration of the day of the dead in the film scene.

In these cut scenes, the story in the scene represents how important visuals and colors are presented, especially in the transition of nature from the world to death. The colors that are presented are no different from the colors in the world, the colors that are present are characterized by other parts of the character having an orange outer glow that makes it look like they are in another part of the real world, as well as the transition of light that comes out with orange from flowers showing the transition and sign as the main character begins to enter the world of death. The results of this study are expected to be a reference in building visuals, especially in depicting the color of death in an animation. Although the colors applied will differ depending on the culture of a place in celebrating or commemorating the day of the dead. For this reason, this finding can be tried to be applied in the visual depiction of animation in Indonesia to enrich the colors in animation, especially in presenting horror things with more colorful coloring.

Acknowledge

This research is part of the ongoing Master of Design FSRD ITB thesis entitled “Peta Warna Selebrasi Hari Kematian Dalam Film Animasi Coco”. Thanks to Dr. Pindi Setiawan, M.Sc. (Alm) as the first supervisor of the author.

References

[1] Amelinda, F. M., & Franzia, E. (2020, Maret). Analisis Elemen Visualisasi Budaya Kematian dalam Film Animasi "Coco". *DESKOMVIS: Jurnal Ilmiah Desain Komunikasi Visual, Seni Rupa dan Media*, *1*(1), 14-27. http://dx.doi.org/10.38010/dkv.v1i1.2

[2] Aufa, A. A. (2017). Memaknai Kematian dalam Upacara Kematian di Jawa. AN-NAS: Jurnal Humaniora, 1(1).

[3] Bellantoni, P. (2005). *If it's purple, someone's gonna die : the power of color in visual storytelling*. Elsevier/Focal Press.

[4] Berens, D. J. (2014, Mei). THE ROLE OF COLOUR IN FILMS: INFLUENCING THE AUDIENCE'S MOOD. *BA (Hons) Film & Moving Image Production Leeds Metropolitan University*.

[5] Blazer, L. (2016). *Animated Storytelling: Simple Steps for Creating Animation & Motion Graphics*. Peachpit Press.

[6] Bleicher, S. (2012). *Contemporary Color: Theory and Use*. Cengage Learning.

[7] Darmaprawira W. A., S. (2002). *Warna: teori dan kreativitas penggunaannya* (2nd ed.). Penerbit ITB.

[8] Eiseman, L. (2017). *The Complete Color Harmony, Pantone Edition: Expert Color Information for Professional Results*. Rockport Publishers.

[9] Fathurohman, I., Nurcahyo, A. D., & Rondli, W. S. (2014). FILM ANIMASI SEBAGAI MEDIA PEMBELAJARAN TERPADU UNTUK MEMACU KEAKSARAAN MULTIBAHASA PADA SISWA SEKOLAH DASAR. *REFLEKSI EDUKATIKA : Jurnal Ilmiah Kependidikan*, *4*(1). https://doi.org/10.24176/re.v5i1.430

[10] Fowler, M. S. (2002). *Animation Background Layout: From Student to Professional*. Fowler Cartooning Arts.

[11] Gunawan, B. B. (2013). *Nganimasi bersama Mas Be*. Elex Media Komputindo.

[12] Kahdar, K., Tresnadi, C., & Ratuannisa, T. (2018, April). Colour Mapping of Natural Dyes in Batik Pesisiran of Batik Batang from Batang Regency. *JURNAL SOSIOTEKNOLOGI*, *17*(1), 132-143. https://doi.org/10.5614/sostek.itbj.2018.17.1.13

[13] Sadewa, G. P. (2018, Juli). Coco: Relasi Keluarga Hingga Tradisi Budaya. NIRMANA, 18(2), 43-50.

[14] Wang, L. (2017, September). Application of Color Language and Aesthetic Value in Artistic Blending and Animation Color Design. *International Conference on Social Science, Management and Economics*, 203-208. 10.12783/dtssehs/ssme2017/12957

Proceedings of the 3rd ITB Graduate School Conference ISSN: 2963-718X
Enhancing Creativity in Research Through Developing Innovative Capabilities
December 21, 2022

The Associations of Children Characteristics, Sociodemographic, and Sanitation Factors and The Risk of Stunting in Bandung Regency (Case Study: Rancaekek and Majalaya District)

Sharnella Janet Yapfrine*, Katharina Oginawati, Nurul Fahimah, Indah Rachmatiah Siti Salami, & Septian Hadi Suseno

Environmental Engineering Study Program, Faculty of Civil and Engineering, Institut Teknologi Bandung, Jl Ganesha 10 Bandung 40132
*Email: sharnellajy24@gmail.com

Abstract. Stunting is a condition of failure in children-under-five's growth as a result of chronic malnutrition. Thus, children become too short for their age. In Indonesia, the stunting rate has decreased from the previous year. However, the prevalence still exceeds the maximum stunting rate target set by WHO. Bandung regency is one of the priority areas for stunting prevention in Indonesia. The causes of stunting are quite complex. This study aims to analyze the relationship among children characteristics', sociodemographic, sanitations factors and the incidence of stunting in the Bandung regency. The method used is a case-control study (retrospective), using a questionnaire and interviews to the parents, and observational method. The research subjects are children under five in Rancaekek and Majalaya District that is divided into 26 respondents for the case group and 25 respondents for the control group. The Chi-square Test analysis (bivariate) and the binary logistic regression (multivariate) are used to determine the significance of children's characteristic, sociodemographic, and sanitation factors on the risk of stunting. The results show that the significance factors to the risk of stunting is the sociodemographic factors, such as mothers' lower education (p-value = 0.017), fathers' lower education (p-value = 0.003), and lower household income (p-value = 0.005). The sociodemographic factor that contributed the most is the household income (OR = 10.063; 95% CI = 1.079 – 93.898).

Keywords: *children characteristics; sanitation; sociodemographic; statistic; stunting.*

1 Introduction

Globally, stunting affects approximately 162 million children under 5. In Indonesia, although in 2019 there was a decrease in the number of stunting cases, the number still exceeded the limit set by WHO. Therefore, The Government had determined 100 regencies to be the main priority for stunting intervention and management, and Bandung Regency is one of them. There are several factors that can trigger stinting in children under 5 years old, such as low birth weight, low

parental education, middle to lower economic status, and poor environmental sanitation. This indicates that nutritional and health conditions during pregnancy, the quality of consumed by children, and the sociodemographic factors must be considered in preventing stunting (Andini & Hardiansyah in [1]).

According to World Health Organization in [2], some factors that cause delays of growth (stunting) generally are the poor health and nutritional conditions before, during, and after the pregnancy period affecting the children's growth and development, the practice of feeding including non-exclusive breastfeeding and limited complementary food in the terms of quantity, quality, and variety, as well as the subclinical infection due to the exposure of contaminated environment and poor hygiene. Indirectly, stunting incidence is also influenced by social factors in the terms of politics and economics, public health, education, social culture, and environmental sanitation. Almatsier in [3] stated that there are several conditions affecting stunting. Those conditions are nutritional intake, gender, birth weight, number of household members, parent's education and occupation, and family economical status.

Based on Bandung Regency Health Profile in 2020, the number of stunting cases in Rancaekek District was the highest in Bandung Regency which reached 1585 cases. In Majalaya District, the number of stunting cases reached 915 cases (Dinas Kesehatan Kabupaten Bandung in [4]). Based on the background described, this study aims to determine the significance of the association between each of the children characteristics factors, the sociodemographic factors, and the sanitation factors and the risk of stunting and to determine the most influencing factors to the risk of stunting in Bandung Regency specifically in Rancaekek and Majalaya District.

2 Materials and Methods

This study was conducted using a quantitative approach with a retrospective epidemiological study model to observe the association among children's characteristics, sociodemographic, and sanitation factors with the incidence of stunting in children under 5. The field study was conducted in Bandung Regency, based on the health and nutrition data obtained from the local healthcare centre. The research was conducted in Majalaya and Rancaekek District. The sampling was done using the purposive sampling technique. Purposive sampling was a technique that considered certain considerations (Sugiyono in [5]). The total sample in this research was 51 respondents, with 26 respondents as the case group and 25 as the control group. The respondents for the case group were children under five years old who suffer from stunting. Meanwhile, the respondents for the control group were normal children under five years old. The respondents

were taken based on the inclusion criteria, such as aged 1-5 years old and domiciled in Rancaekek and Majalaya District.

2.1 Data Collection Method

The primary data in this study were obtained through interviews and observation. The data collection points from the 51 respondents in Bandung Regency are shown in **Figure 1**. The interview is conducted to obtain the children's characteristics and sociodemographic data and the observation is conducted to obtain the children's housing and sanitation condition. The respondents were given code based on the location of the data collection point. The respondents code used namely MJ code for the respondents form Majalaya District and RC code for the respondents from Rancaekek District. There are 26 respondents from Majalaya District with the code MJ and 25 respondents from Rancaekek District with the code RC.

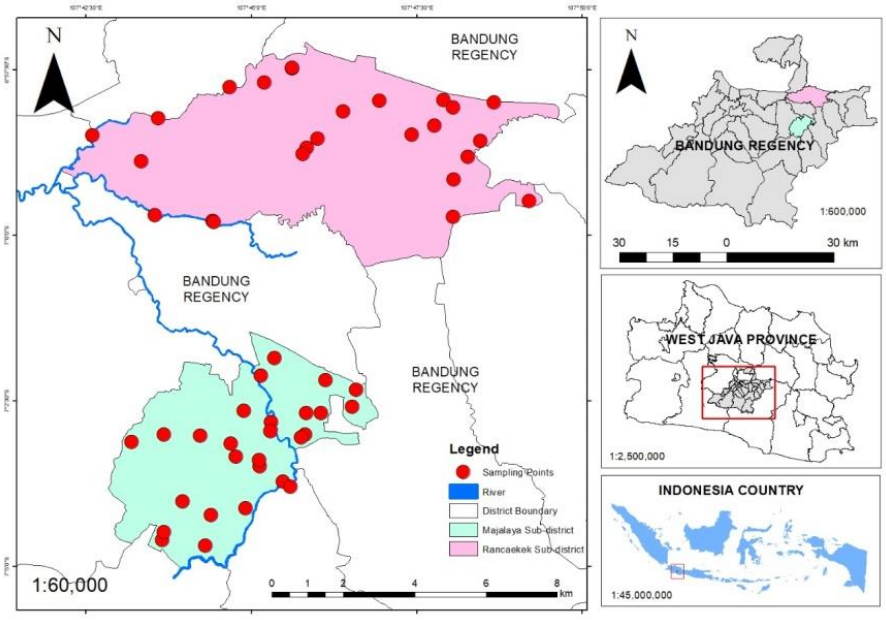

Figure 1 The location of the data collection points

2.2 Data Processing

The data obtained was processed and statistically analysed. The statistical analysis was carried out through bivariate and multivariate analysis. In the bivariate analysis, the Chi-square test was used to determine the significance of children's characteristic, sociodemographic, and sanitation on stunting incidence.

Then, the multivariate analysis using binary logistic regression is done to determine the most influential independent variables to the incidence of stunting. The statistical analysis was done with the help of Software Statistical Product and Service Solutions 22.0 (SPSS 22.0).

3 Result and Discussion

3.1 Stunting Incidence

Stunting is a condition of failure in children's growth as a result of chronic malnutrition so that the children become too short for their age or when a person is shorter than the average height of other people (of the same age) in general (Rahayu, *et al*. in [6]). HAZ (height to age z-score) is an anthropometry measurement to determine the stunting status. Based on the WHO classification, children are said to be stunted if the HAZ ≤ -2SD and severely stunted if the HAZ ≤ - 3 SD (World Health Organization in [7]. **Figure 2** shows the distribution of stunting cases based on the WHO classification.

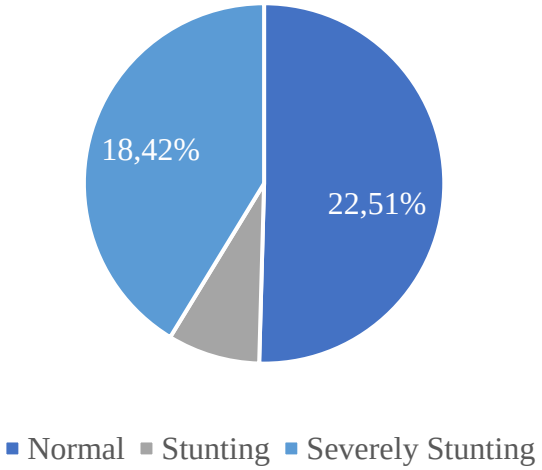

Figure 2 The distribution of the stunting cases in the study area

Stunting mostly occurs in children aged between 25 – 60 months as shown in **Figure 3**. The majority of stunting occurs in children aged 25 to 60 months, which shows that external factors such as environmental, economic, and social factors play a major role in the incidence of stunting.

This research shows that there are more female stunting children rather than the male children. In addition, there are more female children who experience stunting than who do not. The incidence of stunting among the children under five who become a respondent in the study based on the gender can be seen in Error! Reference source not found..

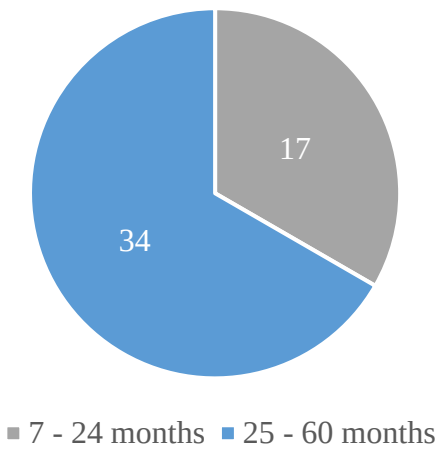

Figure 3 The distribution of stunting cases based on the age

Error! Reference source not found. is the distribution by gender of the i ncidence of stunting among children under five who become a respondent in the study.

Table 1 The stunting incidents distribution based on the genders in the study area

Gender	Case N = 26 (%)	Control N = 25 (%)
Male	12 (46.15%)	14 (53.85%)
Female	14 (56%)	11 (44%)

3.2 The Association of Children Characteristics, Sociodemographic, and Sanitation with The Risk of Stunting

The bivariate analysis to test the significance of each factor on the incidence of stunting is carried out using the chi-square test with the help of SPSS 22 software. Based on Error! Reference source not found., the independent variables t

hat were significantly associated with the risk of stunting in this study are the mother's education less than senior high school (p-value = 0.017), father's education less than senior high school (p-value = 0.003), and household income under the minimum wage (p-value = 0.005). There are three relationships linking the parental education with the children's health. The first is the mother's formal education directly transfer the health knowledge to the prospective mothers. Secondly, the literacy and numeracy skills that girls acquire from school will improve mothers' ability to recognize the children's illnesses and seek for the treatment, and to be able to read medical instructions better for treating the illness and applying them. The third one is the longer duration of formal education makes women become more receptive to modern medication (Glewwe in [8]). There had not been many studies that specifically explain the reasons why father's higher formal education can reduce the risk of stunting. However, the higher formal education of father is correlated with the better employment and leads to the better household income. The families with low household income will limit their spending on groceries. Although the staple foods can be fulfilled daily, the quality and quantity are not given much attention, thus low-income levels can indirectly trigger stunting in children under five (Gustina, *et al.* in [9]).

Table 2 The bivariate analysis of the association among the independent variables and the risk of stunting results

No	Factors	Case	Control	*p-value*	OR	95% CI
1	Low birth weight	7	2	0.16	4.237	0.786 – 22.843
2	Incomplete basic immunization status	13	7	0.186	2.571	0.803 – 8.230
3	Not receiving exclusive breastfeeding	6	6	1	0.950	0.260 – 3.465
4	Mother's last education less than senior high school	20	10	0.017	5	1.486 – 16.826
5	Father's last education less than senior high school	20	8	0.003	7.083	2.049 – 24.486
6	Household income below the minimum wage	25	15	0.005	16.667	1.936 – 143.509
7	Risky maternal age	5	5	1	0.952	0.239 – 3.795
8	Frequency of ANC visits less then 4	4	2	0.701	2.091	0.347 – 12.589
9	Number of family members more than 4	12	14	0.672	0.672	0.223 – 2.031
10	Exposure to cigarette smoke	22	19	0.673	1.737	0.426 – 7.087
11	No proper sanitation access	10	6	0.417	1.979	0.590 – 6.644
12	No habit of washing hand with soap	20	15	0.317	2.222	0.660 – 7.478

3.3 The Most Determining Factors of The Stunting Incidence

To determine the most determining factor of stunting, the multivariate analysis with binary logistic regression model will be used. The variables that have p-value < 0.25 in bivariate analysis will be input into the multivariate model and then re-selected by maintaining the variables that have p value ≤ α (0.05) and removing the variables that have p-value > α (0.05) gradually from the variable with the largest p-value (Hastono in [10]). Low birth weight, incomplete basic immunization status, mother's education less than senior high school, father's education less than senior high school, and household income below the minimum wage have a p-value < 0.25, thus these factors will be input into the multivariate model. The results of the multivariate analysis are shown in **Error! R eference source not found.**.

Error! Reference source not found. shows the results of the multivariate analysis o f the independent variables and the risk of stunting. Based on the table, it is known that among the 12 factors analyzed, there are factors which significantly associated with the risk of stunting (p-value ≤ 0.05). Those factors are father's education less than senior high school (p-value = 0.022) and household income below the minimum wage (p-value = 0.043). The most contributing factor to the risk of stunting in this study is the sociodemographic factor which is the household income below the minimum wage (OR = 10.063; 95% CI = 1.079 – 93.898).

Table 3 The multivariate analysis results

Stages	Factors	B	p-value	OR Exp(B)	95% CI Lower	95% CI Upper
Stage 1	Low birth weight	1.454	0.136	4.281	0.633	28.931
	Incomplete basic immunization status	0.711	0.343	2.035	0.468	8.852
	Mother's last education less than senior high school	0.685	0.442	1.983	0.346	11.352
	Father's last education less than senior high school	1.224	0.146	3.402	0.654	17.695
	Household income below the minimum wage	2.277	0.066	9.744	0.858	110.620
	Constant	-9.185	0.001			
Stage 2	Low birth weight	1.358	0.159	3.889	0.587	25.772
	Incomplete basic immunization status	0.847	0.242	2.333	0.585	9.641
	Father's last education less than senior high school	1.585	0.027	4.848	1.196	19.643
	Household income below the minimum wage	2.279	0.058	9.766	0.926	103.026

Stages	Factors	B	p-value	OR Exp(B)	95% CI Lower	95% CI Upper
	Constant	-8.809	0.002			
Stage 3	Low birth weight	1.406	0.141	4.081	0.627	26.579
	Father's last education less than senior high school	1.586	0.023	4.883	1.243	19.188
	Household income below the minimum wage	2.446	0.046	11.542	1.040	128.049
	Constant	-7.722	0.003			
Stage 4	Low birth weight	1.406	0.141	4.081	0.627	26.579
	Father's last education less than senior high school	1.586	0.023	4.883	1.243	19.188
	Household income below the minimum wage	2.446	0.046	11.542	1.040	128.049
	Constant	-7.722	0.003			
Stage 5	Father's last education less than senior high school	1.553	0.022	4.726	1.255	17.800
	Household income below the minimum wage	2.309	0.043	10.063	1.079	93.898
	Constant	-4.968	0.001	0.007		

4 Conclusion

Based on the previous results and discussion, it can be concluded that the independent variables which are significantly related to the risk of stunting in Majalaya and Rancaekek District of Bandung Regency are the sociodemographic factors and family history, such as mother's lower educational level (p-value = 0.017), father's lower educational levels (p-value = 0.003), and lower household income (p-value = 0.005). The largest contributing factor to the risk of stunting is the household income below the minimum wage (OR = 10.063; 95% CI = 1.089 – 93.898).

5 Acknowledgment

The author would like to express the gratitude towards Institut Teknologi Bandung as this research is the part of Community Service and Innovation (P2MI) FTSL ITB in 2022 funded by Institut Teknologi Bandung and also towards the research group of The Environmental Management Technology, Department of Environmental Engineering, Institut Teknologi Bandung.

Reference

[1] Andiani, & Hardiansyah. (2013). Determinants Factors of Stunting among Children 0-59 Months in Indonesia. Bogor: IPB University.

[2] WHO. (2014). Global Nutrition Targets 2025: Stunting Policy Brief. Geneva: World Health Organization.
[3] Almatsier, S. (2001). Prinsip Dasar Ilmu Gizi. Jakarta: PT Gramedia Pustaka Utama.
[4] Dinas Kesehatan Kabupaten Bandung. (2021). Profil Kesehatan Tahun 2020. Kabupaten Bandung: Kementerian Kesehatan Republik Indonesia.
[5] Sugiyono. (2019). Statistika untuk Penelitian. Bandung: Alfabeta.
[6] Rahayu, A., Yulidasari, F., Octaviana, A., & Anggraini, L. (2018). Study Guide – Stunting dan Upaya Pencegahannya. Bantul: CV Mine.
[7] WHO. (2017). Guideline: Assessming and Managing Children at Primary Health-care Facilities to Prevent Overweight and Obesity in The Context of The Double Burden of Malnutrition: Updates for The Integrated Management of Childhood Illness (IMCI). Geneva: World Health Organization.
[8] Glewwe, P. (1999). Why Does Mother's Schooling Raise Child Health in Developing Countries? Evidence from Morocco. The Journal of Human Resources, **34**(1), pp. 124-159. doi:https://doi.org/10.2307/146305.
[9] Gustina, E., et al. (2020). Good Parental Feeding Style Reduces The Risk of Stunting among Under-five Children in Yogyakarta, Indonesia. Public Health and Preventive Medicine Archive, **8**(2), 120-125.
[10] Hastono, S. P. (2006). Analisis Data. Depok: Fakultas Kesehatan Masyarakat, Universitas Indonesia.

Proceedings of the 3rd ITB Graduate School Conference ISSN: 2963-718X
Enhancing Creativity in Research Through Developing Innovative Capabilities
December 21, 2022

Flood Hazard Assessment in Kalinyamatan District Generated by Dam Break of Bakalan Dam in Jepara Regency

Tania Sinayangsih[1,2,*], Eka Oktariyanto Nugroho [1] & Agung Wiyono Hadi Soeharno[2]

[1] Magister Study Program of Water Resources Management, Civil Engineering Study Program, Faculty of Civil and Environmental Engineering, Bandung Institute of Technology, Bandung 40135, Indonesia
[2]Water Resources Engineering Research Group, Civil Engineering Study Program, Faculty of Civil Engineering and Environmental, Bandung Institute of Technology, Bandung 40135, Indonesia
*Email: nayangg97@gmail.com

Bakalan Dam is one of the dams planned to be built on the Bakalan River, Jepara Regency. This dam is designed to meet the needs of raw water, irrigation needs also flood control. Bakalan Dam not only has great benefits in controlling floods, and meeting raw water and irrigation needs, but also harbors potential hazards. With a height of up to 87 meters due to being built between extreme slopes, if the dam collapses, it can cause large losses of life and material loss. The collapse of this dam can be caused by overtopping, where water with a large discharge can no longer be flowed by the spillway, and flows over the top of the dam. The analysis was carried out using HEC RAS 2D and GIS, it is shown that Kalinyamatan District will be the one heavily affected by the collapse of Bakalan Dam. Through HEC RAS 2D, author can also determine the risk of flood inundation, speed of arrival of water, and arrival time of water in the affected area. Therefore, to avoid casualties, a map of the potential risk for dam collapse due to overtopping is planned. It is hoped with risk mapping, it can increase awareness of affected areas by estimating material losses and affected people.

Keywords: *Dam Break Analysis; Dam; Risk Map; Overtopping; HEC-RAS; Hazard Map; Vulnerability Map; Capacity Map; Jepara.*

1 Introduction

The Bakalan Dam is one of the dams planned to be built over the Bakalan River, Mount Muria, Jepara Regency. The Bakalan Dam is designed to meet the needs of raw water, irrigation water, and flood control. It is recorded that Jepara Regency does not yet have optimal coverage of drinking water and sanitation, until 2016 the percentage of households with access to proper raw water reached 80.73% and the percentage for IPLT services was 0.0056%. This is still far from the Ministry of Public Works and Public Housing 100-0-100 Program in 2019 where the target is 100% access to drinking water, 0% slum areas, and 100%

access to proper sanitation given by Regional Regulation of Jepara Regency in [1]. It was also noted that the condition of the irrigation network was not yet optimal. It is marked by the ratio of irrigation networks in good condition to new cultivation areas reaching 9.82 m/ha. The percentage of irrigation canals in good condition only reached 25.57% in 2016. The things above show that the availability and access to raw water and irrigation networks are still limited and far from the program target of the Ministry of Public Works and Public Housing given by Regional Regulation of Jepara Regency in [1]. Therefore, the Bakalan Dam is planned to be built where the benefits of the Dam are to meet the needs for raw water, irrigation needs, and flood control.

In general, dams not only save enormous potential benefits for humans but also carry risks, a namely sudden collapse which can cause many casualties and material losses downstream given by Che Ros F, et.al in [2]. The types of collapse scenarios that are often associated with dam failure cases are overtopping and piping. The actual number of cases of runoff and pipeline failure is dominant at 70.9% and 14.3%, respectively, usually this runoff water has a large discharge and high water velocity given by Sammen, S.S, et.al in [3]. Overtopping occurs when the uncontrolled flow of water goes beyond the top of the dam. The flow is the same as the flow that passes through the top of the dam body, where erosion occurs downstream of the dam and widens to the top of the dam which causes the dam to collapse given by Shahrim, M. F, et.al in [4]. Therefore, dam failure due to overtopping is unavoidable.

In calculating dam failure, several models and calculations can be found in related literature given by Cannata, M, et.al [5], Gogoaşe Nistoran, D. E, et.al in [6], Álvarez, M., et.al., in [7], Nabilah, R.A., et.al. in [8] and Pratiwi V., et.al., in [21]. Apart from that, this dam modeling also uses some software which is increasingly diverse in form and approach as well as what can be displayed in certain software, one of which is the famous HEC-RAS software given by HEC-RAS Manual in [9], where this software can also be found in several works of literature given by Torimtubun A.T, et.al I [10], Pramono A, et.al in [11], Muammar, A. Z, et.al., in [12], Palar, R.T, et al, in [13] and Balogun, O.S, et. al in [14] and Sandi, C., et. al [15]. In this study, the supporting software for modeling and calculating dam failure is HEC-RAS.

Therefore in this case, not only the calculation of the dam collapse, but preventive studies related to the risk of dam collapse caused by malfunctions and lack of management procedures during an emergency are very important given by De Moel, H et.al in [16] and Pu, J.H., et.al in [17]. Thus, the creation of disaster maps for affected areas is very important and a part of dam break calculations to better understand, mitigate and manage these risks given by Albano, R., et al., in [18].

2 Study Area

The Bakalan Dam was built on the Bakalan River and according to HEC RAS 2D, the Bakalan Dam collapse had the most severe impact on the Kalinyamatan District, Jepara Regency, Central Java Province, Indonesia. Figure 1 showed Jepara Regency area with each District.

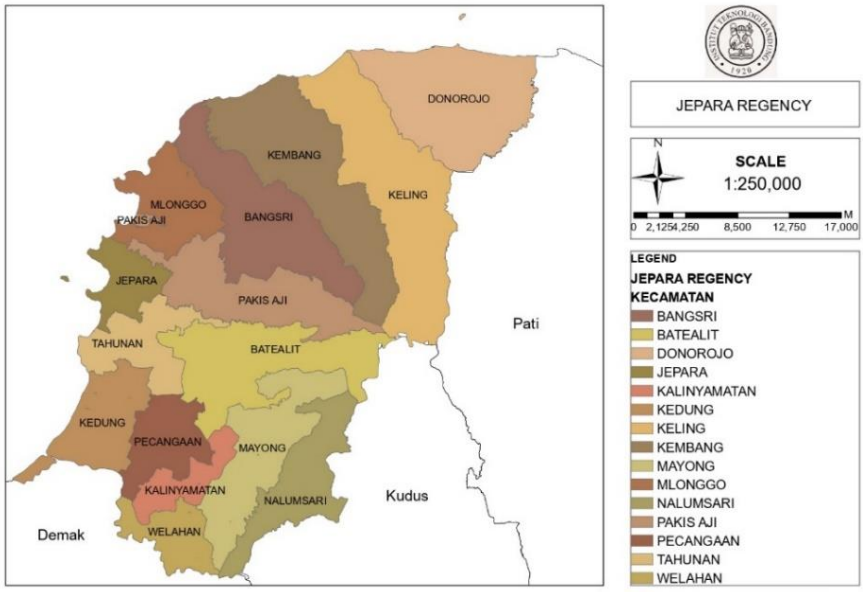

Figure 1 Study area, kalimanyatan district

Kalinyamatan district is located at 6º 43' 42" latitude, 110º 42' 48" east longitude is one of the districts in Jepara regency, Central Java province, Indonesia. There are 12 villages in the district which has an area of 24.2 km^2. Kalinyamatan district itself has a population of ± 62,550 people, with the majority of the population working as farmers and laborers shown in Figure 2. [19]

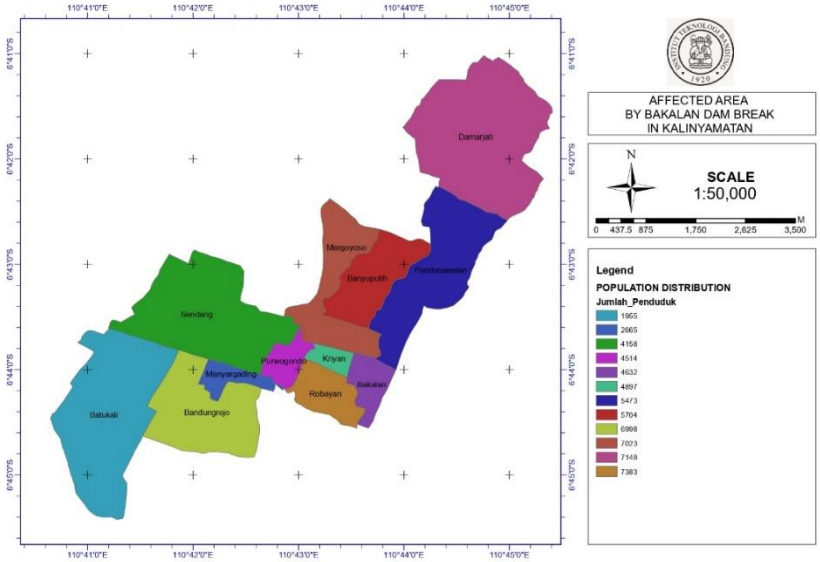

Figure 2 Population distribution in kalimanyatan district

Kalinyamatan district is mostly residential, agricultural, and rice fields. Several industries and factories are also developing in Kalinyamatan District including the Cigarette Factory, Brown Sugar Industry, and others shown in Figure 3. [19]

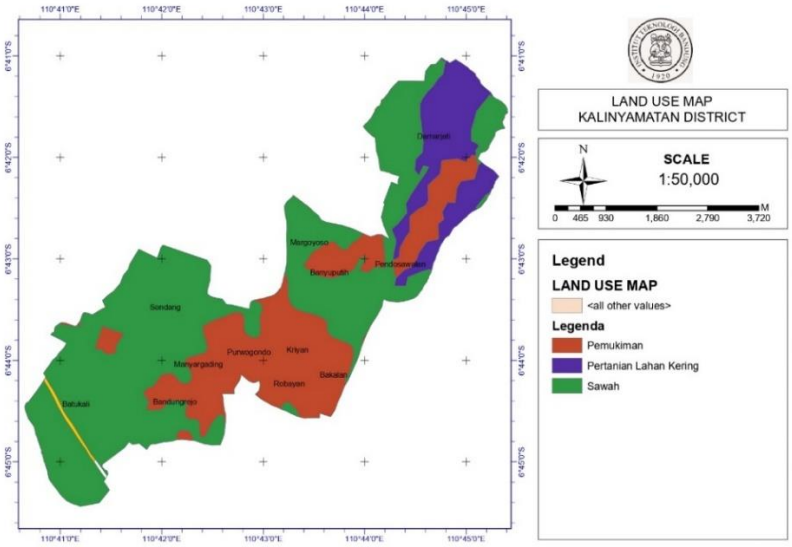

Figure 3 Land use in kalimanyatan district

Therefore, if Bakalan dam break disaster occurs, the Kalinyamatan district could potentially be inundated by flooding caused by the collapse of the Bakalan Dam.

3 Methodology

There are three steps in this study to decide the risk map in result of Dam Break Analysis.

1. Dam Break Analysis
2. Risk Mapping Area
   a. Hazard map
   b. Vulnerability map
   c. Capacity map

3.1 Dam Break Analysis

Dam Break analysis using HEC RAS 2D program. HEC-RAS is an integrated system of software, designed for interactive use in a multi-tasking, multi-user network environment. The HEC-RAS system contains four one-dimensional hydraulic analysis components for: (1) steady flow water surface profile computations; (2) unsteady flow simulation; (3) movable boundary sediment transport computations; and (4) temperature and water quality constituent transport modeling. A key element is that all four components use a common geometric data representation and common geometric and hydraulic computation routines. In addition to the four hydraulic analysis components, the system contains several hydraulic design features that can be invoked once the basic water surface profiles are computed. [9]

3.2 Risk Mapping Area

The risk mapping was taken from the 2D HEC RAS results and will be plot in Arc GIS. Using the Arc GIS program, the affected area will be shown. From that, we can plot the area onto Arc GIS program to get risk map which consist hazard map, vulnerability map, and capacity map.

Using Regulation of the Head of the National Disaster Management Agency No. 02 of 2012 concerning General Guidelines for Disaster Risk Assessment to determined the Indicator for Risk Mapping. [20]

4 Result and Discussion

4.1 Dam Break

In calculating the dam break process, some data has been processed beforehand, such as planned flood discharge data, QPMF data, reservoir data, river flow data, dam hydraulics data, and others. The following are the results of processing the initial data before calculating the Dam Break by HEC RAS 2D.

4.1.1 Dam Break Analysis

In dam break analysis, the first thing to do is to create Layers and Contour Maps using Arc GIS. After the contour and layer maps have been obtained, the Dam Break process can be continued on HEC RAS 2D. After getting the appropriate contour map, continue the dam break process using HEC RAS 2D. The following are the results of the Bakalan Dam running dam break from HEC RAS 2D shown on Figure 4.

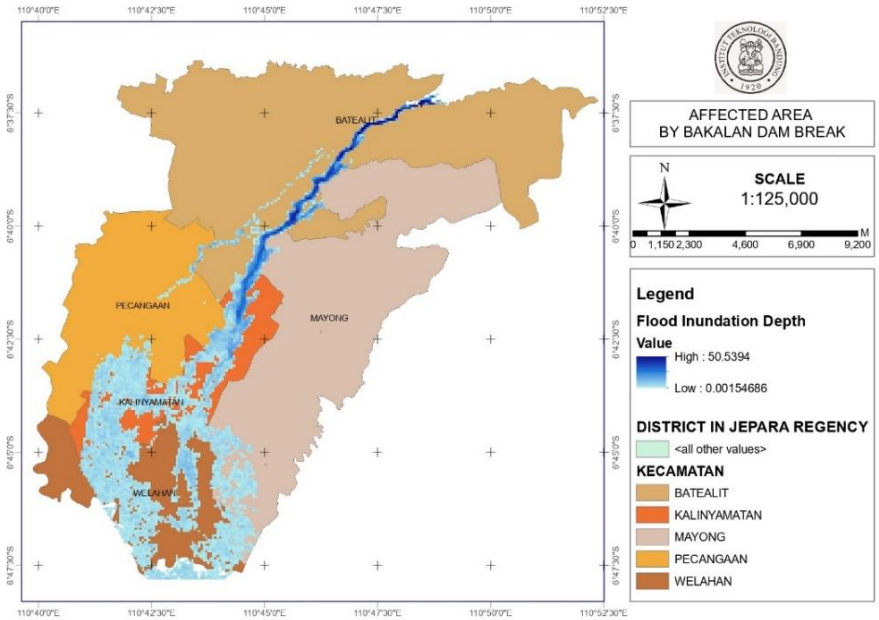

Figure 4 Affected area by bakalan dam break

4.2 Risk Mapping Area

Based on Regulation of the Head of the National Disaster Management Agency No. 02 of 2012 concerning General Guidelines for Disaster Risk Assessment, risk

mapping area consists of hazard map, vulnerability map and capacity map, which combined to get risk mapping area.

4.2.1 Hazard mapping area

Hazard map is calculated based on Meteorology, Climatology, and Geophysical Agency and Ministry of Public Works and Public Housing. Hazard level for flood risk shown on Table 1.

Table 8 Disaster threat index component.

No	Disaster	Index	Index Level			Total
			Low	Moderate	High	
1	Flood Risk	Zoning Map of Flood Areas	< 1m	(1-3m)	> 3m	100 %

From HEC RAS 2D analysis, depth of the flood in Kalinyamatan district can be seen through Figure 5. It can be seen through hazard map that flood inundation depth varies from 1-4 meters. Therefore, hazard score can be calculated shown in Table 2.

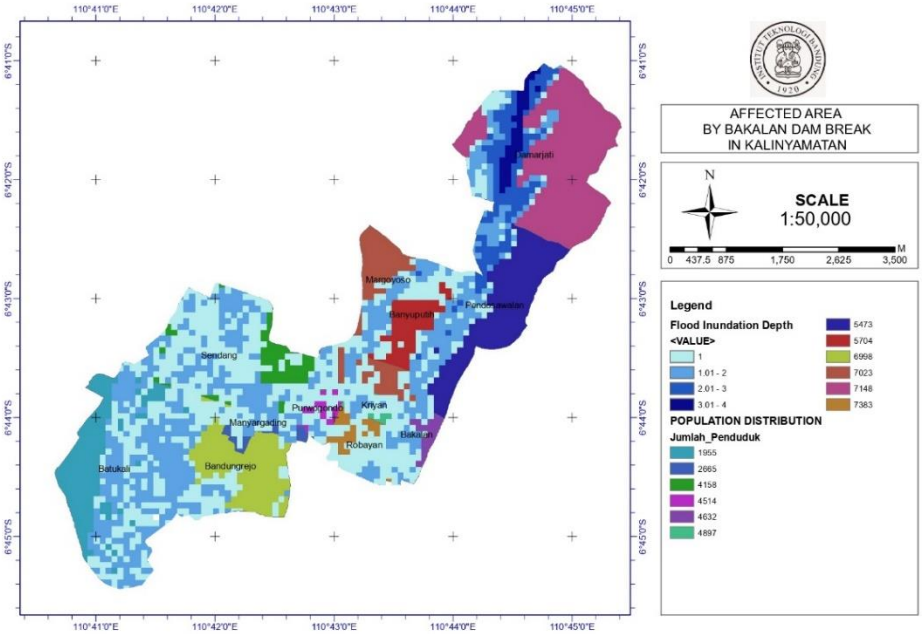

Figure 5 Affected area by bakalan dam break in Kalinyamatan.

It can be seen through hazard map that flood inundation depth varies from 1-4 meter. Therefore, hazard score can be calculated shown in Table 2.

Table 9 Hazard score per sub-district in Kalinyamatan District.

No	Sub-District	Depth Max (meters)	Level	Score
1	Kriyan	2	Moderate	0.6667
2	Bandungrejo	2	Moderate	0.6667
3	Pendosawalan	4	High	1
4	Margoyoso	2	Moderate	0.6667
5	Batukali	2	Moderate	0.6667
6	Robayan	2	Moderate	0.6667
7	Purwogondo	2	Moderate	0.6667
8	Banyuputih	3	Moderate	0.6667
9	Manyargading	2	Moderate	0.6667
10	Darmajati	4	High	1
11	Sendang	2	Moderate	0.6667
12	Bakalan	2	Moderate	0.6667

4.2.2 Vulnerability Map

Vulnerability map is calculated based on social vulnerability, economic vulnerability, physical vulnerability, and environmental/ecological vulnerability.

The calculation of the vulnerability score of an affected area is based on the Social Vulnerability Indicator (Regulation of the Head of the National Disaster Management Agency No. 02 of 2012 concerning General Guidelines for Disaster Risk Assessment). The following vulnerability scores are divided into social, economic, physical, and environmental vulnerabilities as follows:

Economic Vulnerability: using the indicators of Productive Land and Gross Regional Domestic Product [20] for the Kalimanyatan district as follows are shown in Table 3.

Table 10 Economic vulnerability.

Parameter	Weight	Value		Class	Score	Total Score
		Numbers	Percentage			
Productive Land	60%	Rp25,865,317	13%	High	0.22	0.13
Gross Regional Domestic Product	40%	Rp21,944,232	7%	Low	0.18	0.11
Economic Vulnerability						0.24

Physical Vulnerability: using indicators of housing, public facilities and critical facilities [20] for the district of Kalimanatan as follows are shown in Table 4.

Table 11 Physical vulnerability.

Parameter	Weight	Value		Class	Score	Total Score
		Numbers	Percentage			
Housing	40%	Rp. 575,000,000	72%	High	0.56	0.22
Public facilities	30%	Rp. 750,000,000	75%	Moderate	0.40	0.12
Critical Facilities	30%	Rp. 750,000,000	75%	Moderate	0.40	0.12
Physical Vulnerability						0.46

Environmental Vulnerability: using the indicators of Protected Forests, Natural Forests, Mangroves, Shrubs and Swamps [20] for the Kalimanyatan district as follows are shown in Table 5.

Table 12 Environmental vulnerability.

Parameter	Weight	Value		Class	Score	Total Score
		Numbers	Percentage			
Protected forest	30%	0	0%	Low	0.00	0
Natural Forest	30%	0	0%	Low	0.00	0
Mangrove forest	10%	0	0%	Low	0.00	0
Shrubs	10%	0	0%	Low	0	0
Swamp	20%	0	0%	Low	0	0
Environmental Vulnerability						0

Social Vulnerability: using the indicators of Population Density, Sex Ratio, Poverty Ratio, Ratio of People with Disabilities, and Age Group Ratio [20] for the district of Kalimanyatan as follows are shown in Table 6.

Table 13 Social vulnerability.

Parameter	Weight	Value		Class	Score	Total Score
		Numbers	Percentage			
Population Density	60%	2399	60%	High	1.00	0.60
Gender Ratio	10%	9.80%			0.98	0.10
Poverty Ratio	10%	7.44%			0.74	0.07
Disabled Person Ratio	10%	0.32%	24%	Moderate	0.03	0.00
Age Group Ratio	10%	6.25%			0.63	0.06
Social Vulnerability						0.84

Therefore, the value of the vulnerability score of the Kalinyamatan area in the face of flood disasters due to the dam break will be as follows:

Flood Vulnerability: (0.4 * Social Vulnerability Score + 0.25 * Economic Vulnerability Score + 0.25 * Physical Vulnerability Score + 0.1 * Environmental Vulnerability Score) [20]

The result of flood vulnerability for Kalimanyatan district is 0.51

After getting the results of the flood vulnerability score, the results were then plotted into a GIS arc and succeeded in getting a vulnerability map of the Kalimanyatan district consisting of 12 villages are shown in Figure 6.

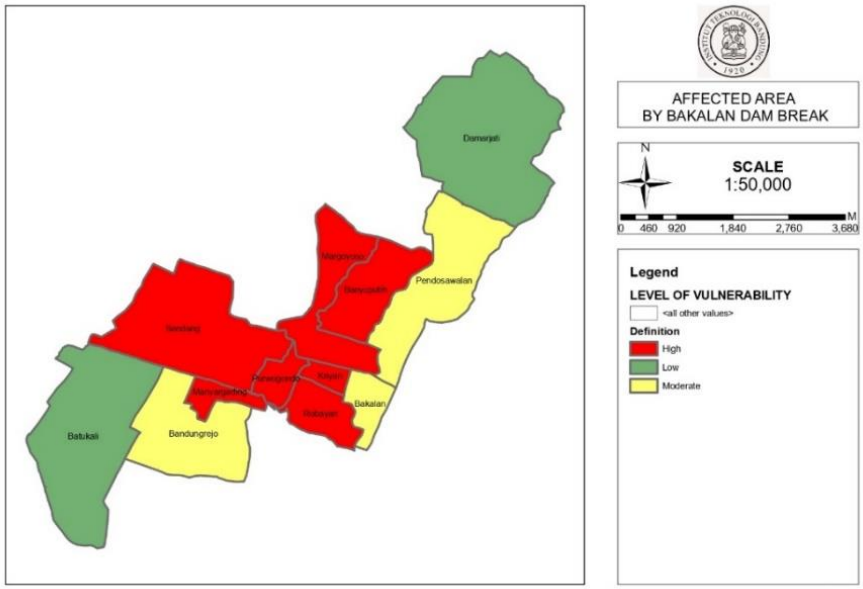

Figure 6 Vulnerability map in kalimanyatan district.

It can be seen on the map, 3 villages have moderate vulnerability, while 2 villages have low vulnerability, but 7 villages have high vulnerability when the flood disaster due to the dam collapse occurred.

4.2.3 Capacity Map

The calculation of the capacity map is based on the ability of the region and the community to take actions to reduce threats and potential losses due to disasters in a structured, planned, and integrated manner. In the case of the affected area, namely Kalinyamatan District, Jepara Regency, according to several articles, an annual disaster mitigation socialization has been held in several sub-districts in Jepara, but not yet in its entirety. Therefore, according to Regulation of the Head of the National Disaster Management Agency No. 02 of 2012 concerning General Guidelines for Disaster Risk Assessment [20], capacity map calculates the capacity available at the area to recover from certain disasters, where some of the components of the capacity index are shown on Table 7. [15]

Table 7 Capacity Index

No	Parameter	Max Value (%)	Existing Value	Score
1	Disaster Management Rules and Institutions	15	15%	0.15
2	Early Warning and Disaster Risk Assessment	15	15%	0.15
3	Disaster Education	20	10%	0.10
4	Basic Risk Factor Reduction	25	10%	0.10
5	Preparation Development at All Lines	25	15%	0.15
	Total Score			0.65

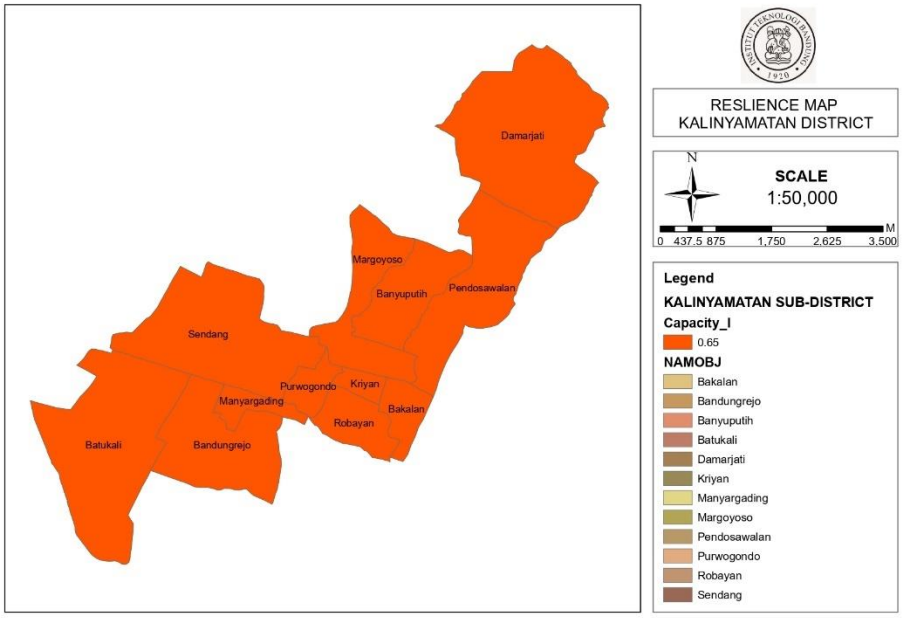

Figure 7 map in kalinyamatan district.

4.2.4 Risk Map

After calculated hazard map, vulnerability map and capacity map, with using formula from Regulation of the Head of the National Disaster Management Agency No. 02 of 2012 concerning General Guidelines for Disaster Risk Assessment [20] it showed from Table 8, the total risk calculated for risk map.

Table 8 Total risk.

No	Sub-District	Hazard	Vulnerability	Capacity	TOTAL
1	Kriyan	0.6667	0.2953	0.65	0.4100
2	Bandungrejo	0.6667	0.2840	0.65	0.4047
3	Pendosawalan	1	0.2830	0.65	0.4627
4	Margoyoso	0.6667	0.2983	0.65	0.4113
5	Batukali	0.6667	0.2742	0.65	0.4000
6	Robayan	0.6667	0.3017	0.65	0.4129
7	Purwogondo	0.6667	0.3084	0.65	0.4160
8	Banyuputih	0.6667	0.2952	0.65	0.4099
9	Manyargading	0.6667	0.2901	0.65	0.4075
10	Darmajati	1	0.2794	0.65	0.4607
11	Sendang	0.6667	0.2944	0.65	0.4096
12	Bakalan	0.6667	0.2839	0.65	0.4046

After getting the total risk, it can be seen from Figure 8 the Risk map for Flood Hazard generated by Dam Break in Kalinyamatan District.

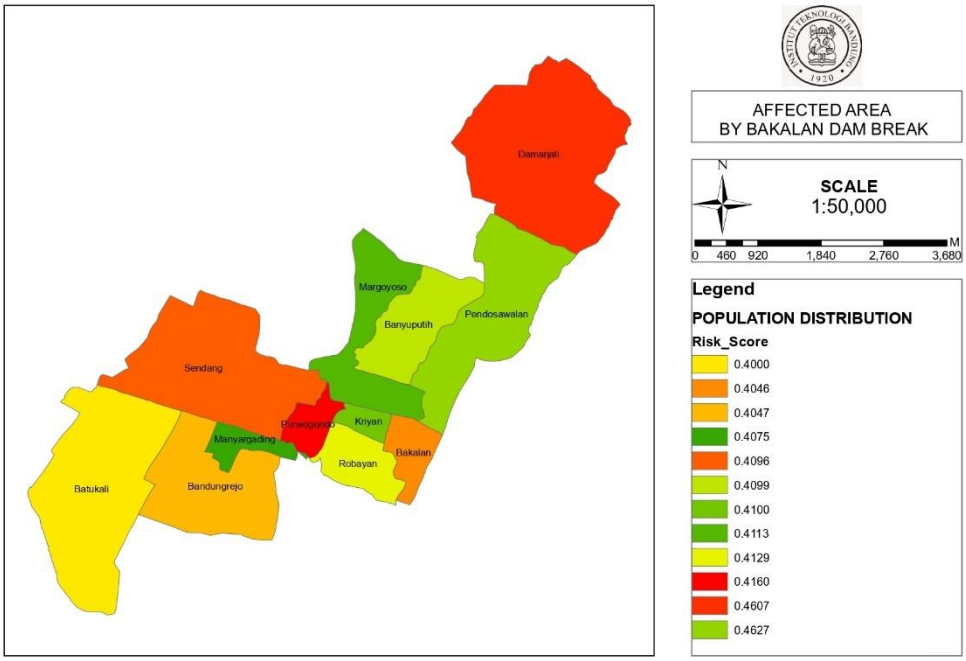

Figure 8 Risk map in kalinyamatan district.

5 Conclusion

The Bakalan Dam which was built in the Bakalan River, Jepara Regency has many useful functions, including meeting the needs of raw water, irrigation water and flood control. However, the dam will also have the potential to cause disaster, if the dam collapses. In this study, the dam collapse was analyzed using HEC RAS 2D and a hazard map was obtained in the Kalinyamatan area, Jepara Regency. Then the results are plotted in Arc GIS and the risk score index value is calculated based on the Regulation of the Head of the National Disaster Management Agency No. 02 of 2012 concerning General Guidelines for Disaster Risk Assessment, obtaining a score of hazard map, vulnerability map and capacity map. Some of the 12 villages in the Kalinyamatan area that were affected by flooding due to the dam collapse have mostly low and moderate level, but there are also 7 villages in the Kalinyamatan area that have moderate to high risk.

References

[1] Regional Regulation of Jepara Regency concerning Regional Medium-Term Development Plans, 2017.

[2] Che Ros F, Sidek L M, A Razad A Z, Nik Ibrahim N N, Ahmad M N, Dam Break Analysis For Hydroelectric Dam: Case Study Of Kenyir Dam, Terengganu, Malaysia Proceeding of International Seminar on Advances in Renewable Energy Technology (ISARET), 2009.

[3] Sammen, S.S, Mohamed, T.A, Ghazali, A.H, Sidek, L.M, El-Shafie, A., An Evaluation of Existent Methods for Estimation of Embankment Dam Breach Parameters, Natural Hazards, 87 (1), 545-566, 2017.

[4] Shahrim, M. F., F C Ros, Dam Break Analysis of Temenggor Dam Using HEC-RAS, The 7th AUN/SEED-Net Regional Conference on Natural Disaster (RCND), 2019.

[5] Cannata, M., & Marzocchi, R, Two-dimensional dam break flooding simulation: a GIS-embedded approach, Natural Hazards, 61(3), 1143–1159, 2011.

[6] Gogoaşe Nistoran, D. E., Gheorghe Popovici, D. A., Savin, B. A. C., & Armaş, I., GIS for Dam-Break Flooding Study Area: Bicaz-Izvorul Muntelui (Romania), Space and Time Visualisation, 253–280, 2016.

[7] Álvarez, M., Puertas, J., Peña, E., & Bermúdez, M., Two-Dimensional Dam-Break Flood Analysis in Data-Scarce Regions: The Case Study of Chipembe Dam, Mozambique, Water, 9(6), 432, 2017.

[8] Nabilah, R.A., et. al., Dam Break Analysis of Situ Gintung Dam Collapse Reconstruction, IOP Conf. Series: Earth and Environmental Science, 599, 2020.

[9] HEC-RAS. River Analysis System Hydraulic Reference Manual; Hydrologic Engineering Center US Army Corps of Engineer: Davis, CA, USA, 2016.
[10] Torimtubun A.T, Asmaranto R, Flood Analysis Due to the Collapse of the Banyukuwung Dam Using HEC-RAS, 2018.
[11] Pramono A, Juwono P.T, Asmaranto R, Flood analysis due to Wonorejo dam collapse using HEC-RAS, 2019.
[12] Muammar, A. Z. et al., Journal of Water Resources Technology and Engineering Vol. 1 No. 1, Analysis of the Malahayu Dam Collapse, Brebes Regency with the HEC-RAS Application and Calculation of Losses with the InaSAFE Application, p. 29-39, 2021.
[13] Palar, R.T, et al., Journal of Scientific Media Engineering Vol.11 No.2, Analysis of the Collapse of the Kuwil – Kawangkoan Reservoir Using the Assistance of the HEC-RAS Program, p. 113-122, 2021.
[14] Balogun, O.S, et. al., Nigerian Journal of Technology (NIJOTECH) Vol. 36, No. 1, Study and Analysis of Asa River Hypothetical Dam Break Using Hec-Ras, pp. 315 – 321, 2017.
[15] Sandi, C.; Nugroho, E. O.; Cahyono, M., Civil Engineering, Environmental, Disaster and Risk Management Symposium 2022, Analisis Risiko Dambreak Bendungan Jenelata dan Upaya Penanggulangannya, 2022.
[16] De Moel, H.; Bouwer, L.M.; Aerts, J.C.J.H. Uncertainty and sensitivity of flood risk calculations for a dikering in the south of the Netherlands. Sci. Total Environ, pp. 473–474, 224–234, 2014.
[17] Pu, J.H., Shao, S., Huang, Y., Hussain, K., Evaluations of SWEs and SPH numerical modelling techniques for dam break flows. Eng. Appl. Comput. Fluid Mech, pp. 544–563, 2013.
[18] Albano, R., et al., ISPRS Int. J. Geo-Inf, A GIS Tool for Mapping Dam-Break Flood Hazards in Italy, pp. 250, 2019.
[19] Jepara Regency Central Statistical Agency, Kalimatan sub-district in figures for 2022, 2022.
[20] Regulation of the Head of the National Disaster Management Agency, Regulation No. 02 of 2012 General Guidelines for Disaster Risk Assessment, 2012.
[21] Pratiwi, V.; Kusuma, M. S.B.; Kardhana, H.; Farid, M., International Journal Of GEOMATE, Nov., 2020, Vol.19, Issue 75, Experimental Study of Dam Break Flow Generated by The Flap Gate In Horizontal Channel, pp.19-26, 2020.

Proceedings of the 3rd ITB Graduate School Conference ISSN: 2963-718X
Enhancing Creativity in Research Through Developing Innovative Capabilities
December 21, 2022

Identifying Collapse of Topography Using Temporal Pansharpened Optical Images at Active Volcano: Case Study of Mt. Semeru Eruptions in 2021

Vismaia Isanjarini & Asep Saepuloh*

Geological Engineering Study Program, Faculty of Earth Sciences and Technology, Bandung Institute of Technology, Indonesia.
*Email: saepuloh@itb.ac.id

Mt. Semeru is one of active volcanoes in Java. The eruption material released by Mt. Semeru is in the form of unconsolidated volcanic material. The nature of the material is very easy to erode and collapse. The eruption that occurred in 2021 caused disruption to critical infrastructure, ranging from power cuts and the collapse of the main bridge. The collapsed topography was assumed to have caused the massive eruption in 2021 but was not detected by monitoring equipment at the time. To observe the phenomenon, the Landsat-8 and PlanetScope images were used. The Gram-Schmidt transformation was conducted to increase the spatial resolution of Landsat-8 image 30 m to Planetscope image 3 m. This method was applied to the images before and after the 2021 eruption for determining the possibility of a collapse topography. According to the visual pansharpened images, we could identify the collapse topography in the eastern sector following the eruption. The collapse sector formed landslide with quite deep incision about 650 m. The collapsed materials accumulated in the SE-flank of Kobokan drainage and sent down the pyroclastic flows about 700 m to the valley.

Keywords: *Collapse, Gram-Schmidt, Pan-Sharpening, Mt. Semeru.*

1. Introduction

Mt. Semeru is in Lumajang and Malang Regencies, East Java. Mt. Semeru is one of the most active volcanoes in Java. Hundreds of eruptive events in Mt Semeru occurred during the 19th and 20th centuries, it has been persistent since 1967. An eruption and dome collapse occurred near the summit on 4 December 2021, which produced a notable ash plume and pyroclastic flows, the latter of which generated major lahars [1]. Eruption material released by Mt. Semeru is in the form of unconsolidated volcanic material. The nature of the material is very easy to erode and collapse. As a result, several communities were partially buried, causing fatalities, disruption to critical infrastructure, ranging from power cuts and the collapse of the main bridge. The collapsed topography was assumed to have caused the massive eruption in 2021 but was not detected by monitoring equipment at the time. So, the aim of this research is to observe the topographical collapse that occurs because of the eruption.

Remote sensing techniques provide the opportunity to study active and dangerous volcanoes, allowing us to safely observe topography details over a large area. This is particularly true for Mt Semeru, as one of active volcano in Indonesia. Standard remote sensing techniques using high-spatial resolution images from PlanetScope offer a fruitful means with which to characterize the volcano's topography and to recognize the extent and effects of the eruptive processes.

To observe topography collapse, both Landsat-8 and PlanetScope were used. Gram schmidt transformation was conducted to pansharp Landsat-8 and PlanetScope data. In this method the statistical values of the high-resolution bands are adjusted to the values of the first transformation bands to produce a new set of transformation bands resulting in sharpened multispectral data. Gram-Schmidt has become one of the most popular algorithms for pan-sharpen multispectral images [2]. This method outperforms most other pan-sharpen methods in maximizing image sharpness, minimizing color distortion, and the most optimal method for collapse detection [5]. Gram-Schmidt is generally more accurate because it uses the spectral response function of a given sensor to approximate the appearance of the panchromatic data. This method was used on the images before and after the 2021 eruption to determine the possibility of collapse.

The Semeru-Tengger volcanic massif with an area of about 900 km^2 comprises a cluster of calderas and strato-cones aligned from north to south over 25 km, including: the Bromo-Tengger, Jambangan and Ajek-Ajek calderas; the Mt. Kepolo lava cone; and the composite cone of Mt. Mahameru-Semeru **(Figure 1)**. The recent composite cone of about 60 km^3 [9] has not been dated, but maybe Late Pleistocene to Holocene in age. The twofold edifice (Mahameru and Young Semeru) has been superimposed on, and but tressed to the N, by the Jambangan complex. To the S and SE Semeru overlies weathered volcaniclastic sediments and lava flows of the Oligocene–Miocene ‘Tuff and Old Andesite formation [8]. The equatorial monsoon climate produces as much as 2000 to 3700 mm per year on the E and SE flanks of Semeru while 200 mm of rain can fall in 24 h every 5 years on average [6].

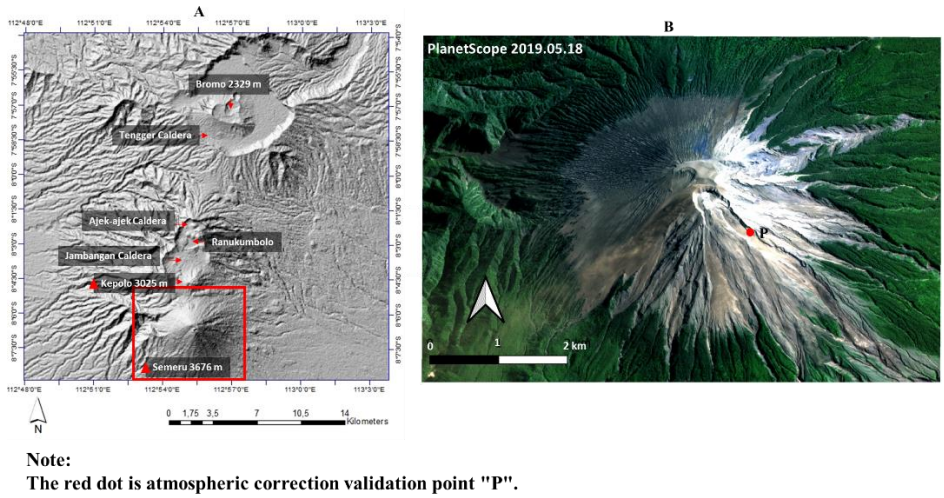

Figure 1 Digital Elevation Model (DEM) Mt. Semeru and its surrounding (A) and the natural color composite of Planetscope image with acquisition time May 18th, 2019, shows the morphology of Mt. Semeru (B).

2. Data used and selection

In this study we have selected Landsat-8 and PlanetScope. Landsat 8 imagery has 11 bands where there are different spatial resolution values for each band. In bands 1,2,3,4,5,6,7,9 it has a spatial resolution of 30 meters. Bands 10 and 11 have a spatial resolution of 100 meters. And band 8 has a spatial resolution of 15 meters. With the Pan-Sharpening technique, it can increase the spatial resolution of the composite bands by adding band 4,3,2 (natural color) from 30 m to 3m. Previously done pre-processing radiometric calibration and atmospheric correction. But for the images during the eruption and after the eruption which is landsat-8 collection 2 level 2 no pre-processing is required, because this data is already atmospherically corrected. To validate it, a spectral check was carried out (**Figure 2**). 10 scenes have been used under acquisition mode from January 28 th, 2019 to August 22th, 2022 (**Table 2**).

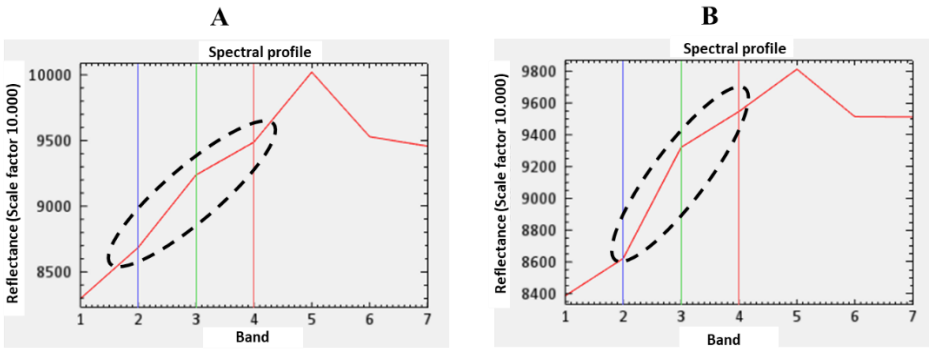

Figure 2 Spectral bands on the image during the eruption and after the eruption at SE trending scar on February 3, 2022 (A) and August 22, 2022 (B).

The following is a spectral validation where the blue band is lower than the red band and green band. In theory the blue band has a lower spectral value compared to the green band because it has a shorter wavelength. This indicates that this image has been corrected.

Planetscope images have used because of high resolution image about 3 m capable to observe topography. The data is available freely under proposed academic term and condition. The PlanetScope provides the image data for analytic basic, visual ortho, analytic ortho, visual ortho tile, and analytic ortho tile scenes. Orto tile image have been used because it provided 4-band multispectral image in blue (band 1), green (band 2), red (band 3), near-infrared (band 4). All of its bands have a resolution of 3 m. The detail specifications of PlanetScope wavebands are listed in **Table 1**.

Table 1 Bands description of the selected 4-band multispectral of PlanetScope images [3].

Number	Name	Description	Wavelength (nm)
1	B1	Blue	465-515
2	B2	Green	547-585
3	B3	Red	650-680
4	B4	Near Infrared	845-885

The 4-band multispectral of PlanetScope images has been processed at level 3B which is corrected geometrically and atmospherically. Comparisons were made among bands 1, 2, 3 and 4 for pansharpening method with landsat 8 (**Figure 2**). Based on this comparison, panhsarpening with band 4 (NIR) produces a clearer collapse topography and minimal distortion, because the wavelength of the Near

Infrared (NIR) is sensitive to collapse and on the histogram it can be seen that band 4 is normally distributed. So, in this pansharpening method we use the combination of landsat-8 multispectral data with planetary NIR band.

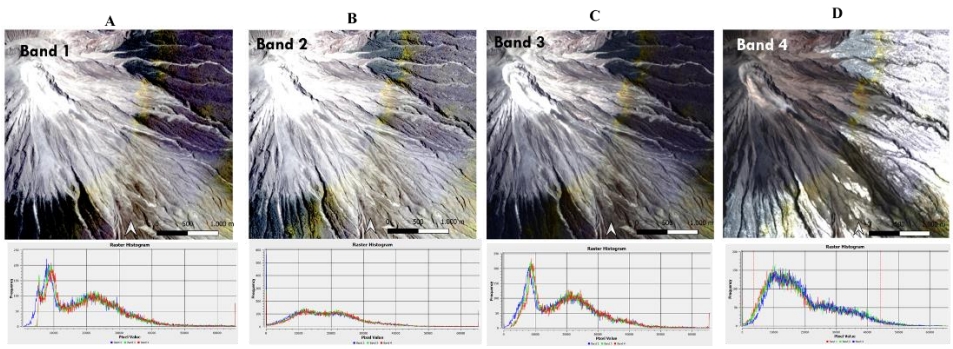

Figure 3 Visual of pansharpened images using PlanestScope image bands-1 (A), band-2 (B), band-3 (C), and band-4 (D) and their histograms.

The following is the available data with a minimum cloud (<10%) that can be used in this method **(Table 2)**. The years before (2019, 2020, 2021) and after (2022) the eruption is used to see the impact caused by the eruption. This pansharpening method is used when there are only Landsat images so that sharpening is needed, thus it is as if you have many planetScope images.

Table 2 The available data with a minimum cloud (<10%).

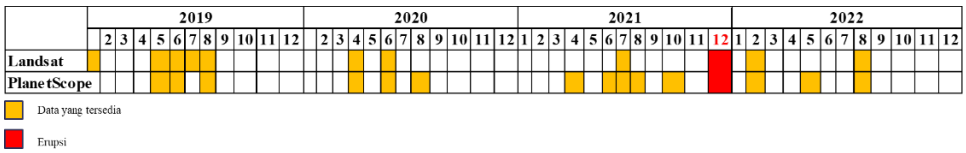

Table 3 The selected PlanetScope and Landsat-8 image used in this study with cloud cover less than 10% for each frame.

Image	Acquisition Date	Cloud Coverage	Event
PlanetScope	May 18th, 2019	3%	Before eruption
	June, 18th 2019	1%	
	August, 16th 2019	5%	
	April, 10th 2020	4%	
	April, 21st 2020	3%	
	June, 13th 2020	7%	
	August, 22nd 2020	3%	

	April, 19th 2021	1%	
	June 30th, 2021	8%	
	July, 2nd 2021	4%	
	August 26th, 2021	6%	
	Oktober, 17th 2021	0%	
	Desember, 13th 2021	3%	After eruption
	Febuary, 3rd 2022	3%	
	May 15th, 2022	9%	
	August 1st, 2022	2%	
Landsat-8	Januari 28th, 2019	2%	Before eruption
	May 18th, 2019	3%	
	Juni, 11st 2019	2%	
	Juni, 18th 2019	4%	
	July, 13th 2019	1%	
	August, 16th 2019	3%	
	April, 10th 2020	6%	
	June 13th, 2020	7%	
	July 2nd , 2021	2%	
	Febuari, 3rd, 2022	5%	After eruption
	August 22th, 2022	3%	

3. Method

The combination of panchromatic and multispectral images is known as pansharpening. Pansharpening is generally a method for combining high-resolution spatial values from panchromatic images with low-resolution multispectral images. In general, two or more images are integrated into one image by maintaining the important features. The resulting quality of the stitched images is related to many factors such as spatial, spectral, radiometric accuracy and distortion. Therefore, different pansharpening methods have been developed with different objectives.

Since its publication in 1998, the Gram-Schmidt pan-sharpen method has become one of the most popular algorithms for pan-sharpen multispectral images [2]. This method outperforms most other pan-sharpen methods in maximizing image sharpness, minimizing color distortion, and is the most optimal method for landslide detection [5]. Gram-Schmidt is generally more accurate because it uses the spectral response function of a given sensor to approximate the appearance of the panchromatic data.

Orthogonalization is the process of discovering two vectors that are at 90 degrees to each other. When two vectors are orthogonalized, they will become

orthonormal to each other. The gram-scmidt process is the process of converting a set of vectors into an orthonormal basis. The projection operator can be defined as followed:

$$Proj_u\ (v) = \langle \frac{u,v}{v,v} \rangle\ u \tag{1}$$

u and *v* are two vectors. <*u*, *v*> is the inner product of the two vectors, showing the component of *u* in the direction of *v*. When <*u*, *v*> = 0, the two vectors are orthogonal (at right angles with each other). This operation causes a projection transformation of the vector *v* in the line on which *u* is situated.

The Gram-Schmidt process uses this operator to compute two sequences, $u_1 \ldots u_i$ and $n_1 \ldots n_i$:

$$U_1 = v_1\ , n_1 = \frac{U_1}{||U_1\ ||} \tag{2}$$

$$U_2 = v_2 - Proj_{u1}\ (v_2\ ), n_2 = \frac{U_2}{||U_2\ ||} \tag{3}$$

$$U_3 = v_3 - Proj_{u1}\ (v_2\ ) - Proj_{u1}(v_3\ ), n_3 = \frac{U_3}{||U_3\ ||} \tag{4}$$

$$U_k = v_3 - (x+a)^n = \sum_{i=1}^{k-1} Proj_{u1}\ \ (v_k\ ), n_k = \frac{U_k}{||U_k\ ||} \tag{5}$$

The sequence $u_1 \ldots u_i$ is the set of orthogonal vectors. To calculate u_i, this process essentially transforms vi using the projection transformation onto the linear subspace created by $u_1 \ldots u_i$. u_i is therefore the difference between vi and this subspace. Calculating the sequence $u_1 \ldots u_i$ is Gram-Schmidt orthogonalization, giving us the required set of orthogonal vectors while calculating the vector set $n_1 \ldots n_i$ is Gram-Schmidt orthonormalization.

The first step in pansharpening using the Gram-Schmidt method is to create a high-resolution NIR band that matches the resolution of the multispectral bands. Next, the multispectral bands are decorrelated. Each one is treated as one multi-dimensional vector, with each pixel being one dimension. The greater the number of pixels, the greater the number of dimensions. This decorrelation is done using the Gram-Schmidt process. The high-resolution NIR band which we computed is taken as the first vector, u1. The multispectral bands are correlated and orthogonalized to this band. Next, the low-resolution band is replaced by the high-resolution one. The multi-spectral bands transform in the same way as the high-resolution NIR band. This produces high-resolution versions of themself.

The following is the result of pansharpening gram schmidt which is a combination of Landsat images with a resolution of 30 m multispectral band with

NIR planetscope images with a resolution of 3 m so that the resolution becomes 3 m (**Figure 3**). In the initial image (multispectral), object observed is not very clear, whereas in the pansharpening image can be seen much more detail. The panhsarpening image has information details such as NIR. Whereas for the color elements follow the multispectral. But, in some appearances, does not match the natural color, this is due a difference in the acquisition time of the two types data.

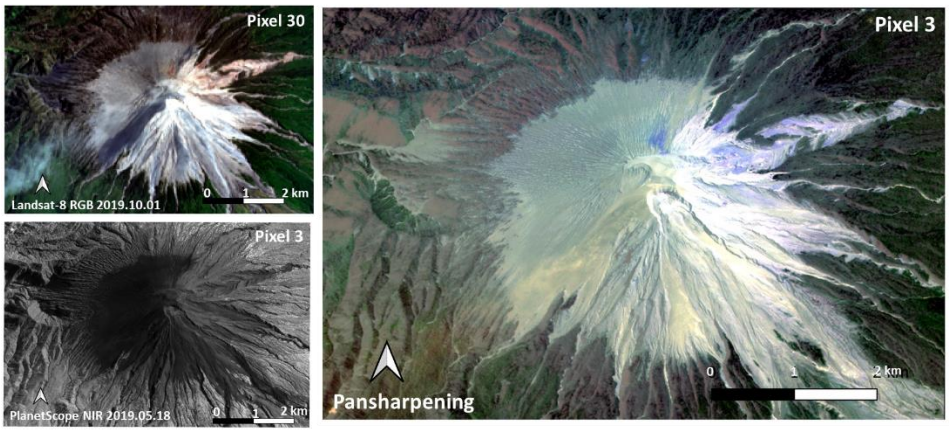

Figure 4 Pansharpening method scheme

4. Result and Discussion

The Gram-Schmidt transformation was conducted to pan-sharpening landsat-8 and planetscope image. This method was used on the images before (2019, 2020, 2021) and after eruption (2022) to determine the possibility of a collapse topography. Pansharpening results were evaluated using a qualitative approach which involves a visual comparison of the colors among the multispectral image, the NIR image and the pansharpening image [10]. To observe the visual appearance of the results pan-sharpening, this research takes a few samples for differences in visual appearance between landsat-8, planetscope and pansharpening images using the GramSchimdt method. The results of observations are as follows:

4.1 Before Eruption

There are 16 scenes taken from 2019-2021 to observe the appearance before the eruption. Based on the results of pansharpening before the eruption, it can be seen there is no volcanic activity, and there is no collapse detected. The upper northeastern flank of the summit cone appears more weathered, comprising

reddish brown, and unconsolidated deposits. For this reason, an image observation was carried out during and after the eruption to see if there was a collapse in Semeru on December 2021.

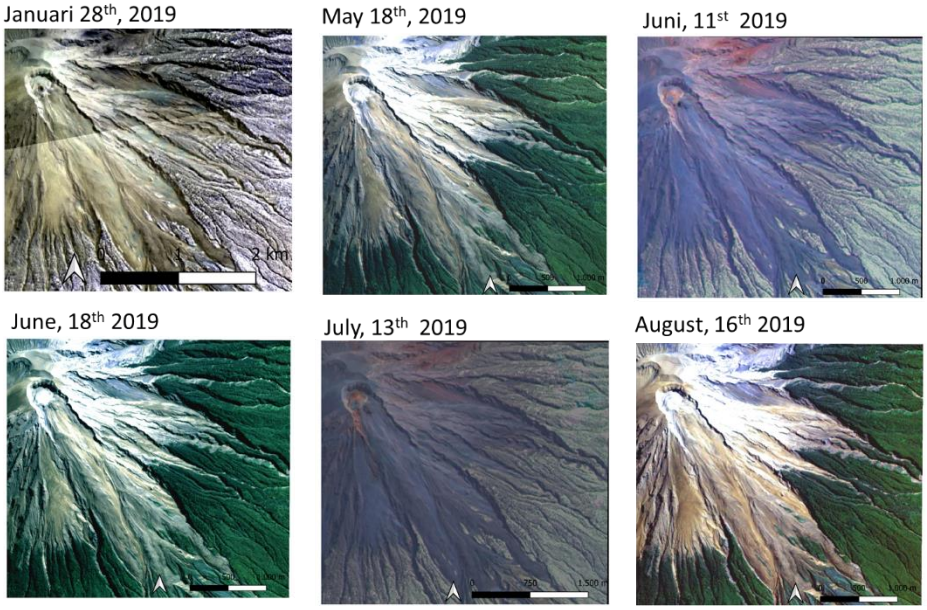

Figure 5 Observation through PlanetScope image in 2020 composite band 4 3 2 to see the appearance before collapse topography

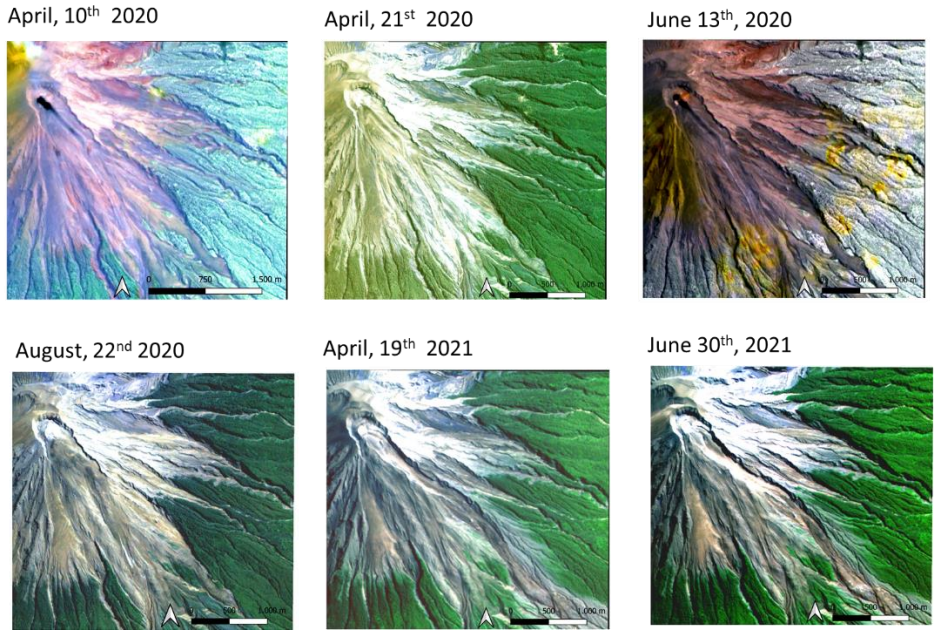

Figure 6 Observation through PlanetScope image in 2020 composite band 4 3 2 to see the appearance before collapse topography

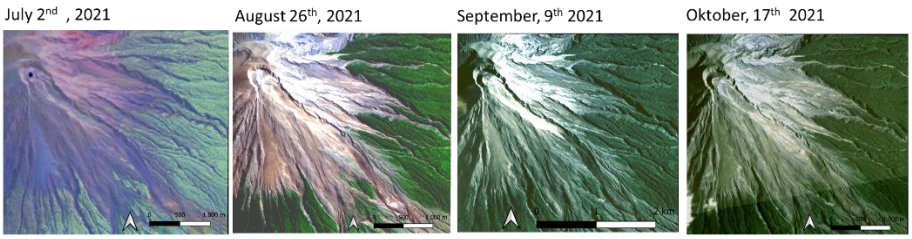

Figure 7 Observation through PlanetScope image in 2021 composite band 4 3 2 to see the appearance before collapse topography

4.2 After Eruption

In the analysis after the eruption used landsat data on August 22rd 2022 while the planet on June 29th 2022 because at that time it was very clear (not covered by clouds) so observations were easier. Collapse suspected like a pressure release valve that allowed magma to spew forth rapidly, escaping the volcano before crystals had had a chance to grow. Based on the results of pansharpening after the eruption, it can be seen collapses trace in the eastern part of Mt. Semeru.

Collapse dome also happened in Semeru's Jonggring Seloko Crater and SE-flank flow. It is also proven by almost all of the houses in the Curah Kobokan area had been destroyed, mainly by pyroclastic flows, though some residents reported roof collapses from ashfall [4]. Lava flows have filled the Kobokan head valley from the Jonggring-Seloko crater. As a result, the valley channel will become an area of aggradation produced by lava front collapses, which will be remobilized by rain-triggered lahars during the next rainy seasons.

Figure 8 Observation through PlanetScope image in 2022 composite band 4 3 2 to see the appearance after collapse topography

4.3 Pansharpening Evaluation

Pan-sharpening techniques can result in spectral distortions when pan sharpening satellite images as a result of the nature of the NIR band. The planetscope NIR band for example is not sensitive to blue light. As a result, the spectral characteristics of the raw NIR color image may not exactly match those of the corresponding low-resolution RGB image, resulting in altered color tones (**Figure 9**). This has resulted in the development of many algorithms that attempt to reduce this spectral distortion and to produce visually pleasing images. The following is an image before and after the eruption resulting from pansharpening which shows a collapse in the eastern part of Mount Semeru (**Figure 9**). This collapse material is transported up to 650m to the SE-flank Kobokan drainage. The results of these visual observations were then validated with existing secondary data which indicated that a collapse would occur in 2021. Based on PVMBG 2021, the seismic network recorded avalanche signals. Avalanches of incandescent material from the summit dome and SE-flank lava flows descended 500-800 m. Evidence of this collapse can be seen in the pansharpening images where there is an accumulation of collapsed material. Then these results were analyzed quantitatively

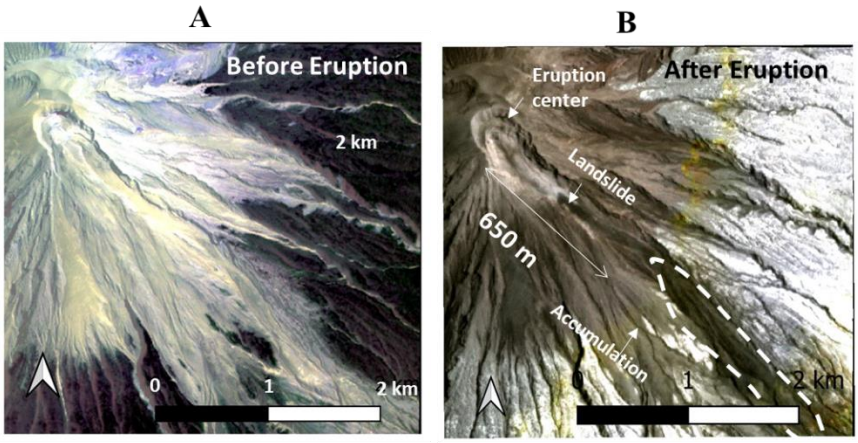

Figure 9 Pansharpening before (A) and after eruption (B)

Before pansharpening the pixel value is 30 m (x=125, y=114), then after pansharpening the pixel value changes to 3 m (x=1239, y=1134). Based on data, it was found that there was a change in the number of columns and rows in the image as well as the value of the digital image which indicated a change in image quality due to pansharpening. For this reason, image quality measurements are taken in the form of min, max, mean, and standard deviation (**Table 3 and 4**).

Table 4 Pansharpening quality measurement before eruption

Parameter	**Multispectral Landsat-8 (May 18th, 2019)**		
	Band 4 (red)	**Band 3 (green)**	**Band 2 (blue)**
Min	44	117	283
Max	4500	4076	3797
Mean	1157.8613905857	1183.5982977003	1078.7027263744
Standard deviation	682.58750780715	542.74476831045	552.91122531322
Parameter	**Planetcope (October 1st, 2019)**		
	Band 4 (NIR)		
Min	287		
Max	5099		
Mean	1710.718360039		
Standard deviation	802.61895315428		

Parameter	Pansharpening		
	Band 1 (red)	**Band 2 (green)**	**Band 3 (blue)**
Min	0	0	0
Max	981	938	1286
Mean	265.56345064744	408.22645916561	410.18563867751
Standard deviation	158.39913626069	141.96910617941	237.60461611649

Table 5 Pansharpening quality measurement after eruption

Parameter	Multispectral Landsat-8 (June 29th, 2022)		
	Band 4 (red)	**Band 3 (green)**	**Band 2 (blue)**
Min	4665	4922	373
Max	41279	40551	41996
Mean	14336.107146065	14097.481876572	13557.467984278
Standard deviation	9379.4475299996	9191.0299996829	9583.7508428908
Parameter	**Planetcope (August 22th, 2022)**		
	Band 4 (NIR)		
Min	531		
Max	5545		
Mean	1364.1652752376		
Standard deviation	653.88059427796		
Parameter	**Pansharpening**		
	Band red	**Band green**	**Band blue**
Min	0	0	0
Max	65535	65535	65535
Mean	13896.135166337	13659.617535142	13150.007287068
Standard deviation	9153.6296325029	9070.5203865447	9319.9147597041

Based on this table:

1. Min and max between the previous images are greater than the sharpened images, but the number of pixels in the pansharpening image is greater.

2. The mean value of the image before it is sharpened is much larger than the image after it is sharpened. This is because the density of the sharpened image increases and automatically the value of M (row) and N (column) as the divider of the number of pixel values is greater than the image before sharpening. So that the image analysis of the mean value shows that the sharpened image has a smaller mean because it has more row and column sizes. Based on the results of the Mean value, the image before sharpening has a larger value compared to the image that has been sharpened as well as the Standard Deviation value, so it can be concluded that after sharpening the pixel density increases and makes the image clearer.
3. Standard deviation (SD) before it is sharpened has a greater value than the image after it is sharpened. Standard Deviation is a reflection of the average deviation of the data from the mean. The Standard Deviation can describe how far the data varies. If the SD value is much greater than the mean value, the mean value is a bad representation of the entire data. Based on these data, the standard deviation value before pansharpening can be used as a representation of the entire data.

5. Conclusion

The results of the processing are in the form of suspected collapse topography which are characterized by the morphology in the eastern sector which appears in pan-sharpening images after the eruption. In the eastern part of Mount Semeru, it was seen that there was a landslide which was quite deep. Material collapsed from the unstable distal end of a 650m in the SE-flank Kobokan drainage, sending a pyroclastic flow 700 m down the valley. The results of this pansharpening were evaluated using quantitative analysis (min, max, mean, and standar deviation), which shows that pansharpening image can be used as a representation of the entire data.

Reference

[1] Bennis, K.L., and Andrews, B., eds. *Report on Semeru (Indonesia): Semeru (Indonesia) Pyroclastic flows, gas-and-ash emissions, and crater incandescence during January-June 2022.* Bulletin of the Global Volcanism Network, **47**:7. Smithsonian Institution.2022.

[2] Laben CA, Bernard V., Brower W. *Process for Enhancing the Spatial Resolution of Multispectral Imagery Using Pan-Sharpening*, US Patent. 2000.

[3] Planet. *Planet Imagery Product Spesification PlanetScope and RapidEye*. 2016

[4] Pusat Vulkanologi dan Mitigasi Bencana Geologi (PVMBG, also known as CVGHM). *Semeru Eruption on Desember 2021*. 2021.

[5] Santurri, L., Carlà, R., Fiorucci, F., Aiazzi, B., Baronti, S., Cardinali, M., dan Mondini, A. C. *Assessment of very high resolution satellite data fusion techniques for landslide recognition*, ISPRS Technical Commission VII Symposium, 100 Years ISPRS {\textendash} Advancing Remote Sensing Science, **38**, 1–6. 2010.

[6] Siswowidjoyo, S., Sudarsono, U., & Wirakusumah, A.D. *The threat of hazards in the Semeru volcano region in East Java, Indonesia*. Journal of Asian Earth Sciences, **15**, 185- 194.1997.

[7] Solikhin, A. *Geology , tectonics and post-2001 eruptive activity interpreted from high-spatial resolution satellite imagery : the case study of Merapi and Seremu volcanoes , Indonesia*, Doctoral School of Funfamental Sciences Universite Blaise Pascal.2015.

[8] Sutawijaya, I.S., Wahyudin, D., dan Kusdinar, E. *Peta geologi Gunung Api Semeru, Jawa Timur*, Direktorat Vulkanologi, Bandung.1996

[9] Thouret, J.-C., Lavigne, F., Suwa, H., Sukatja, B., Surono. *Volcanic hazard at MountSemeru, East Java (Indonesia), with emphasis on lahars*. Bulletin of Volcanology. **70**, 221–244. 2007

[10] Zhang, Yun. *Methods for Image Fusion Quality Assessment – A Review, Comparison and Analysis*. The International Archives of the Photogrammetry. Remote Sensing and Spatial Information Sciences. **38**. 2008.

Proceedings of the 3rd ITB Graduate School Conference ISSN: 2963-718X
Enhancing Creativity in Research Through Developing Innovative Capabilities
December 21, 2022

The Potential of Clay Material as CO_2 Capture Sorbent in the Pressure Temperature Swing Adsorption (PTSA) Process

Wahid Ahmadi[1, *] & Deni Shidqi Khaerudini[1,2]

1Postgraduate Master of Mechanical Engineering, Mercu Buana University, Jl. Meruya Selatan No. 1 Kembangan West Jakarta 11650
2Research Center for Advanced Materials, National Research and Innovation Agency (BRIN), Gd. 440 Puspitek Serpong Area, South Tangerang 15314, Banten
*Email: wahidfoundry@gmail.com

Abstract. The current state of increasing CO_2 emissions is become challenging due to reduce emissions targeting policy. One of the processes of catching CO_2 is pressure temperature swing adsorption (PTSA) with sorbent clay as an adsorbent material. The consideration of clay material is due to large availability in Indonesia and its CO_2 adsorption potential capacity as good as the Zeolite 13X of 0.7 mol/kg. Pretreatment is required for bentonite to change its structure so that it increases its CO_2 adsorption capacity. After going through the initial treatment process, the capacity adsorption CO_2 of bentonite increases from 6 to 47 x 10^{-6} mol/kg due the changing of surface area and pore volume.

Keywords: *CO_2; capture; sorbent; emissions.*

1 Introduction

The earth's surface temperature has increased recently, this is due to the Greenhouse Gases (GHGs) accumulation from human and industries activities. GHG heat is retained in the atmosphere and contributes significantly to temperature rise and global warming [1, 2, 3]. GHGs dominated by CO_2 gas by 83.83% and last a very long time in the atmosphere, only 50% can be absorbed by plants and oceans [4]. The rapid growth of global CO_2 concentrations will also lead to the potential for an irregular climate and rising sea level levels that could threaten life at sea and most importantly the activity and survival of humanity [5]. CO_2 emissions are generated from many sources such as the energy sector in power plants that use fossil-based fuels [6] as well as industries that produce exhaust gases such as the steel processing industry. Figure 1 taken from the 2018 Greenhouse Gas and MPV Inventory Report Ministry of Environment and Forestry of the Republic of Indonesia [10]. Shows a trend of increasing GHG emissions in Indonesia, every year it increases, especially in the energy sector in 2017 reaching 558,890 thousand tCO_2e and in the industrial process and product uses (IPPU) sector reaching 55,395 thousand tCO_2e. To overcome the increase of

GHG emission, many approach already proposed, included Carbon Capture and Storage (CCS), Carbon Capture and Utilization (CCU), lower use burn fossil material and enforcement of clean and renewable energy [7, 8, 9].

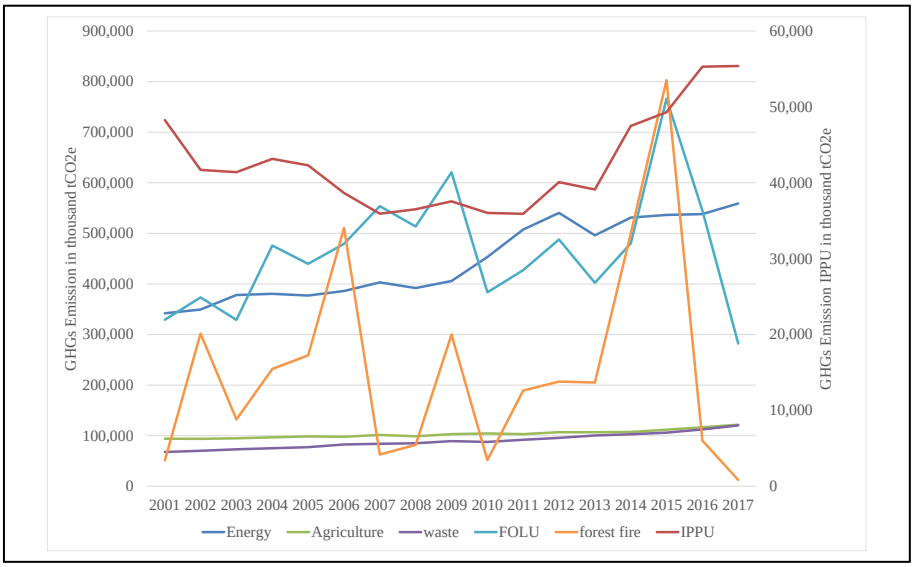

Figure 1 Greenhouse gas emissions by sector type [10]

Therefore, CO_2 capture technology has a very important role for the GHG gas reduction and climate change mitigation programs of the world. CO_2 capture technology has various methods such as absorption, membrane, adsorption, and chemical looping as shown in Figure 2 [11].

CO_2 capture technology is divided into three categories, namely pre-combustion, post combustion and Oxyfuel combustion [4]. Pre-combustion carbon capturing is most widely used in the production of mixed gases or called syngas, which contains mainly carbon monoxide and hydrogen. Carbon monoxide is separated from the mixture and converted into carbon dioxide, then obtained syngas raw materials used in chemical production and as thermal energy store. Oxyfuel combustion uses O_2 gas which is purer than free air, with the aim of burning fuel that will produce exhaust gases containing CO_2 and water vapor, then the exhaust gas is dehydrated to get CO_2 gas. Post combustion carbon capture (PCC) focus on CO_2 capture after the fossil fuel combustion process, usually in industry and power plants [4].

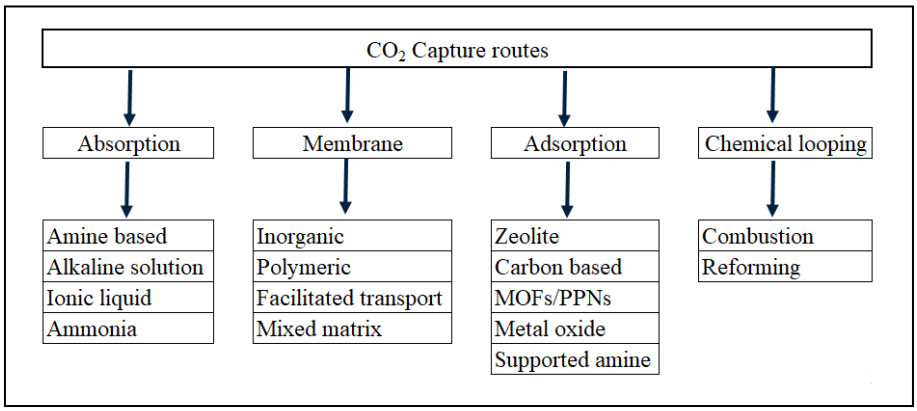

Figure 2 CO_2 capture methods [11]

The capture and separation of liquid CO_2 in an oxidant environment from the exhaust gases of a combustion system is called post combustion [12], one of the methods in post combustion is the adsorption method that is, the process by which molecules contained in a liquid or gas mixture stick to a solid surface, adsorbents. These molecules, even in small concentrations of flow, can be captured by this selective material. Properties of adsorbed particles (molecular size, molecular weight, and polarity) and adsorbent surface (polarity, pore size and distance) determine the quality of adsorption. The adsorption process is an exothermic process, the regeneration of adsorbents through desorption can be carried out by increasing temperature. However, when compared to the absorption method, the adsorption method uses lower energy. In the post combustion process, an adsorption method can be applied to capture CO_2 from exhaust gases. Process of CO_2 capture by adsorption method has been known to have advantages in terms of low investment costs and simple automation operations [13]. The best benefit of CO_2 adsorption capture is the material regeneration facility by applying heat and/or vacuum. Generally, the power consumption of the Vacuum Temperature Swing Adsorption (VTSA) process for the capture of CO_2 is lower than the absorption of chemicals such as MonoEthanolamine (MEA) solution [14]. Studies on the capture of CO_2 adsorption are generally investigated from new adsorbents, simulations and experiments [15]. New adsorbent materials have been synthesized and tested experimentally, and the measurement indicators consist of: working capacity, breakthrough curves and adsorption isotherms [16, 17].

The CO_2 capture process that uses the adsorption method is pressure temperature swing adsorption (PTSA), there are many sorbent materials that can be used such as activated carbon, zeolites, and metal organic frameworks (MOFs). In this study, we will review the characteristics of one type of clay material, namely

zeolite as sorbent and other alternative clay materials in the proses of CO_2 capture PTSA.

2 Research Methodology

The method used in this study is the observation of literature from various sources, both journals and credible government report data. The literature data obtained from these various sources are then compiled for review on:

- Pressure temperature swing adsorption (PTSA) process flow.
- Characteristics of zeolite material in the PTSA process.
- Alternative clay material in the PTSA process.

3 CO_2 Capturing Process

3.1 Pressure temperature swing adsorption (PTSA)

The PSA process is based on the adsorption of the desired gas (e.g., CO_2) on porous adsorbents at high pressure, and gas recovery at low pressure. TSA is based on the adsorption of the desired gas at low temperatures and desorption at high temperatures. Thus, porous sorbents can be reused for subsequent adsorption. PSA technology is considered due to low energy requirements and low capital investment costs [18, 19]. The application of the PSA process to separate and capture CO_2 is also being studied [20, 21, 22, 23]. The low recovery rate of CO_2 is one of the problems reported on the PSA process. For the PSA process to be successful, the removable sorbent must have high selectivity, high adsorption capacity, and the adsorption and desorption rates for CO_2 capture must be increased.

PTSA cycle steps are classified into two main groups: pressurization and feed are combined into the "adsorption" group, while depressurization, heating and cooling are grouped into the "desorption" group [13]. In Figure 3 shown you for the "adsorption" step, the treated exhaust gas is: it is taken to the compressor where the exhaust gas is compressed at high pressure. Then the compressed gas is fed to the adsorption column and the zeolite-like adsorbent reacts physically with carbon dioxide. The residual exhaust gases eventually radiate into the atmosphere. For the "desorption" step, CO_2 is deposited in the heating column to increase the temperature and CO_2 is then brought to the product line with a vacuum pump, it means that the column is maintained under atmospheric pressure. After heating and evacuation, the chamber is cooled to 303 ^{o}K, which is suitable for the adsorption of CO_2 in subsequent cycles, with cooling water circulation. For all adsorption columns, the cycle steps are carried out alternately.

Finally, the final gaseous product is compressed and transferred to the storage or usage location [13].

At room adsorption where happen process of adsorption gas exist sorbent material with purpose adsorb the gas that contained on gases then throw away to next process to release with pump vacuum thus generated product of CO_2 [13].

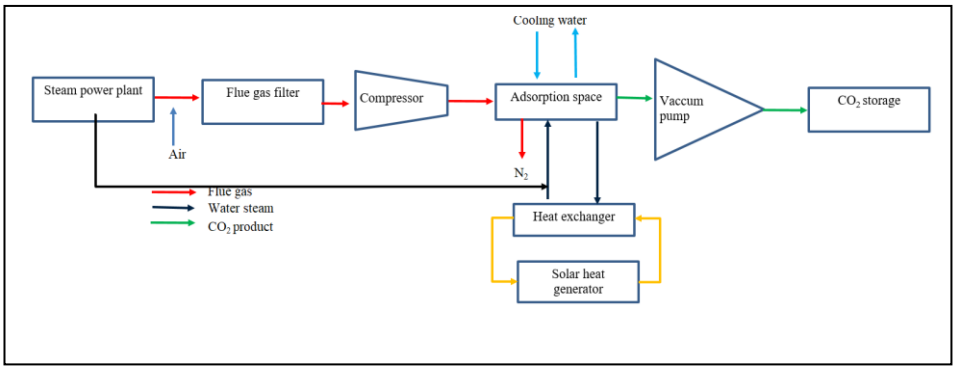

Figure 3 Integrated PTSA system with Coal Burning Power Plant

Figure 4 shows the stages of the process that occurs in the adsorption space:

Stages 1 – 2: the filling process with pressure so that the exhaust gases entering the room will increase. The sorbent material will draw CO_2 and release N_2.

Stage 2-3-4: evacuation and heating process where CO_2 will be absorbed continuously by the vacuum pump and provide thermal energy up to a temperature of T_{des} and P_{eva} are balanced. Increase of temperature and decrease of pressure cause the desorption of the absorbed gas in the sorbent material.

Phase 4-1: cooling process by water, on this phase are not exist again gas left and cycle will recurring back to moment temperature room adsorption same with T_{ads}[13].

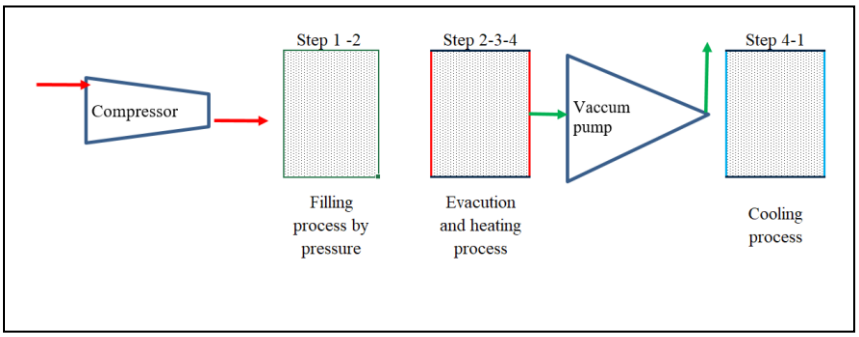

Figure 4 Stages in the PTSA cycle

3.2 Characteristics of material sorbent zeolite

One of the sorbent materials that belongs to the clay group is zeolite. This material is a highly porous and highly economical mineral alumina silicate [24]. Based on zeolite-forming units, the zeolite skeleton can be divided into three. First, the primary forming units that are the tetrahedral units of SiO_4 and AlO_4. Secondly, a secondary unit that is a combination of primary forming units that bind to each other through a ring-shaped oxygen atom. Third, polyhedral building units are composed of several secondary forming units that form pores. The electric charge contained in the zeolite skeleton both on the surface and in the pore causes zeolite to act as a cation exchanger, adsorption, and catalyst. The water molecules in zeolite are molecules that are easily released by heating above 100 ^{o}C which results in the pores of the zeolite getting bigger. This state allows zeolite to adsorb molecules smaller than the midline of zeolite molecules [24]. Zeolite in a common shaped powder and usually to sorbent material used deep shape granule or Monolithic like in Figure 5.

Figure 5 Granule zeolite 13X [25]

The basic properties of zeolite carried by cations allow for the strong capitation of acid molecules by increasing the density of the oxygen skeleton electron [26, 27]. This base strength increases by electro positives from the cation exchange [28]. More specifically, certain studies have shown that the basic strength of cationic zeolite containing Group 1A cations increases as follows: $Li^+ < Na^+ < K^+ < Rb^+ < Cs^+$ [29, 30]

Another consideration in the selection of zeolite material is a strong CO_2 adsorption affinity compared to N_2, zeolite 13X has high adsorption capacity at low partial pressure for exhaust gases PCC. In addition, 13X zeolite is among the most widely used as physical adsorbents for capturing CO_2 due to its low cost and profuse availability [31]. Zeolite shows promising results for the separation of CO_2 from gas mixtures and can potentially be used in PSA processes. [20, 21, 22, 23, 32, 3 3,3 4]. According to the Energy Agency's (IEA) coal research report, the PSA/TSA system will be more energy efficient if the sorbent operates at moderate temperatures (125°C) or higher temperatures (325°C).

Based on studies that have been carried out, the characteristics that determine the ability of adsorption capacity are large pore diameter and large Na/Si ratio as well [35].

Table 1 Physical properties of zeolite materials

Properties	**Zeolite type**					**Reference**
	13X	5A	4A	WE-G 592	APG-II	[35]
Pore diameter (Å)	10	5	4	10	10	
Composition (weight %)						
Na	11,7	3,8	10,8	13,7	8,8	
Si	18,2	16,7	16,1	16,5	14,3	
Na/Si	0,64	0,23	0,67	0,83	0,62	
Adsorption capacity CO_2 (mol/kg)	0,7	0,38	0,52	0,60	0,38	

Table 1 shows the properties of some zeolite materials where the results of the study show that the highest adsorption capacity can be achieved under the conditions of pore diameter and highest Na/Si ratio, namely in Zeolite 13X with pore diameter = 10 Å, Na/Si = 0,64 and adsorption capacity CO2 = 0,7 mol/kg and Zeolite WE-G 592 with pore diameter = 10 Å , Na/Si = 0,83 and adsorption capacity CO2 = 0,6 mol/kg [35].

With large pore diameter will make change process of cation Na^+ easier happen, with the presence of cation Na^+ will strengthen bond structure zeolite then make more endure on high temperature and absorb CO_2 higher. While with smaller pore diameter exchange process of cation Na^+ will more difficult thus make bond structure of zeolite will easy broken once applied higher temperature [35]. Shown in Figure 6 structure of zeolite A get change become structure B with the presence of change cation Na^+ and next structure of zeolite become structure C then make better properties [35].

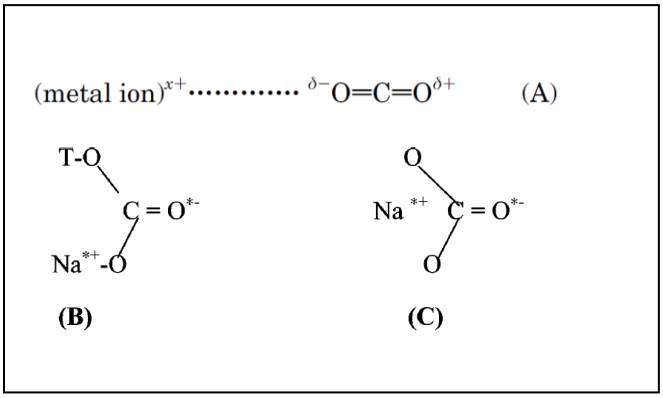

Figure 6 Zeolite structure in the changing process of Na^+ cations [35]

3.3 Alternative clay material in the PTSA process

Another type of clay material that has the potential to be used as sorbent material in the CO_2 capture process is bentonite. Bentonite is a type of soft rock resulting from sedimentation from volcanic ash of volcanic eruptions and reacts naturally with minerals in the earth and its deposited millions of years. Due to its porous nature, bentonite can combine functions to form composite materials for adsorption, catalysis, and separation. One study reported adsorption and catalytic properties of bentonite layers with iron (Fe), chrome (Cr) and iron/chromium coatings with different Fe/Cr molar ratios [36]. This very soft rock consists of montmorillonite, a mineral clay type of phyllosilicate family formed from fine particles. Montmorillonite consists of two tetrahedral layers (SiO_4) separated by an octahedral layer (Al $(OH)_6$), its chemical formula is (Al, $M^{2+})_2$ Si_4O_{10} $(OH)_2$, n H_2O with M^{2+} = Mg, Fe (Figure 8) [37].

Bentonite also have shape basis powder with size mesh 200 or 75 microns but to Sorbent material usually deep shape granule like at picture 7.

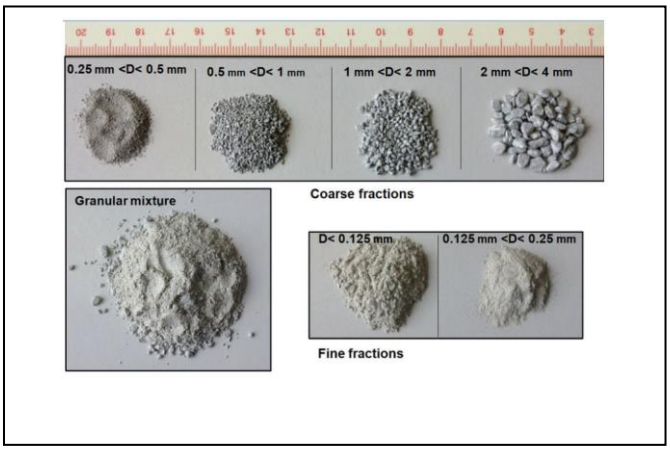

Figure 7 Bentonite granule [38]

Bentonite has a special place in water purification [39,40]. High specific surface area, chemical and mechanical stability, layered structure, high cation exchange capacity (CEC), tendency to retain water in its interlayer parts, and the presence of Brønsted and Lewis acidity have made clay an excellent adsorbent material [41, 42]. The chemical properties and pore structure of bentonite generally determine its adsorption ability [43, 44].

The adsorption properties of natural bentonite can be improved by several means such as the intercalation of organic, inorganic, or organometallic molecules in the interlamellar space, and by heat treatment or acidic [45, 46]. The applied method of increasing the adsorption capacity of bentonite consists of: the reaction of bentonite with a solution of strong acid, usually hydrochloric acid (HCl) or sulfuric acid (H_2SO_4). Acid activation leads to montmorillonite modifications with better properties such as increasing surface area, pore diameter, acid level, and catalytic activity. Natural treatment and montmorillonite treatment with hot mineral acids can replace cations with H^+ ions. Gradual washing of Al^{3+} on both tetrahedral and octahedral parts, however the silicate group remains largely intact [47, 48].

The natural physical properties of bentonite are similar with zeolite only differ in pore diameter and CO_2 adsorption capacity as shown in table 2 where bentonite has an adsorption capacity that smaller but along with the treatment of polyethyleneimine (PEI) material the adsorption capacity of CO_2 increases [49].

Table 1 properties of natural bentonite and after PEI treatment

Sample	V_{pore} (cm^3/g)	Adsorption capacity CO_2 (mol/kg)	Reference
Bentonite	0,28	6×10^{-6}	[49]
10% PEI	0,17	16×10^{-6}	
20% PEI	0,07	36×10^{-6}	
30% PEI	0,01	47×10^{-6}	

According to the study above, it shows that natural bentonite has the lowest adsorption capacity compared to bentonite which has undergone a treatment process by PEI, the treatment process it changes the structure of bentonite thus changing the pore volume and producing a different adsorption capacity of CO2 [49].

Bentonite in addition to having natural pores, for the Calcium based type can be modified chemically to expand the cross-sectional area as to increase the adsorption ability of the gas. The chemical modification process is called the acid activation process, using a high concentration of sulfuric acid can change and open the bentonite layer so that the cross-sectional area is larger. Table 3 shows the influence of the activation results of H2SO4 acid which can open the pores of bentonite to be larger due to the dissolution of impurities in bentonite so that the area its specific cross section increases [50]. As in Figure 8 the structure of bentonite consists of impurities Al, Mg, Fe, OH and others, with the acid activation process then the impurities are dissolved and wasted [50].

Table 2 Acid activation result data

Sample	Spesific surface area (m^2/g)	V_{pore} (cc/g)	Reference
Bentonite	78,6	0,073	[50]
Bentonite activated by H_2SO_4	157,6	0,132	

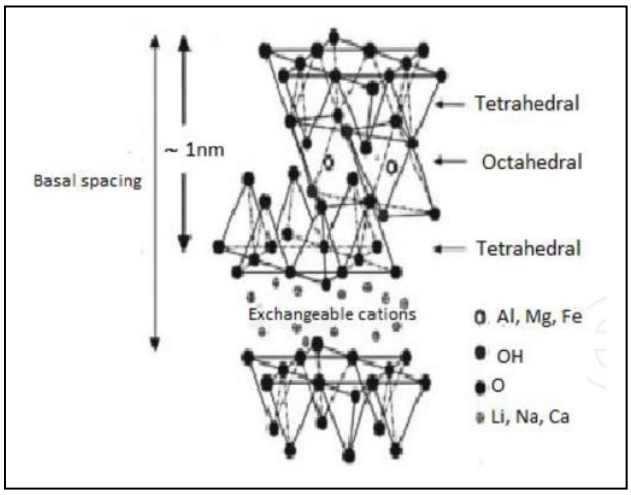

Figure 8 Bentonite structure [51]

4 Conclusion

Based on the review information above then it can be taken that clay material is chosen as sorbent material in the PTSA process because of its good CO2 adsorption capacity as 6 to 47 x 10-6 mol/kg. CO2 adsorption capacity of bentonite will increase after going through pretreatment process to change its structure such as specific area and pore volume. Large pore diameter will give easier Na+ cation exchange process thus better thermal resistance and higher CO2 adsorption capacity.

References

[1] M, Mokhta, Z., Ong, MY., Salman, B., Nomanbhay, S., Salleh, SF., Chew, KW. Simulation Studies on Microwave-assisted Pyrolysis of Biomass for Bioenergy Production with Special Attention on Waveguide Number and Location. Energy. 190: 116474. 2020.

[2] Antolini, D., Ail, SS., Patuzzi, F., Grigiante, M., Baratieri, M. Experimental Investigations of Air-CO_2 Biomass Gasification in Reversed Downdraft Gasifier. Fuel. 253 :1473: 81. 2019.

[3] Ma, Z., Liu, W., which, W., Li, W., Han, B. Temperature Effects on Redox Potentials and Implications to Semiconductor Photocatalysis. Fuel. 286(P2) :119490. 2021.

[4] Zachary, L., Zhao, S., Matthew, A., Sam, T. Carbon Capture Materials and Technologies: A Review. Current Research in Materials Chemistry. 3(1): 108. 2021.

[5] Qin, Y., Niu, G., Wang, X., Luo, D., Duan, Y. Status of CO_2 Conversion Using Microwave Plasma. J CO_2 Util. 28: 283–91. 2018.
[6] Ideris, F., Shamsuddin, AH., Nomanbhay, S., Kusumo, F., Silitonga, USA. , Ong, MY. Optimization of Ultrasound-assisted O il Extraction from Canarium Odontophyllum Kernel as a Novel Biodiesel Feedstock. J Cleaner Prod. 288: 125563. 2021.
[7] D, S, Alqarni. Ru-zirconia Catalyst Derived from MIL140C for Carbon Dioxide Conversion to Methane. Catalysis Today. 2020.
[8] M, Biset-Peiŕo., J, Guilera., T, Zhang., J, Arbiol., T, Andreu. On the Role of Ceria in Ni-Al_2O_3 Catalyst for CO_2 Plasma Methanation. Applied Catalysis A: General. 575: 223–229. 2018.
[9] Hussin, F., Aroua, MK. Recent Trends in the Development of Adsorption Technologies for Carbon Dioxide Capture: A Brief Literature and Patent Reviews (2014–2018). J Cleaner Prod. 253: 119707. 2020.
[10] Central Bureau of Statistics. "Greenhouse Gas and MPV Inventory Report, Ministry of Environment and Forestry of the Republic of Indonesia". (July 24, 2022). https://www.bps.go.id/statictable/2019/09/24/2072/emisi-gas-rumah-kaca-menurut-jenis-sektor-ribu-ton-CO_2e-2001-2017.html
[11] Ahmed, A. M., Anirudh, K., Ali, A. R., Fateme, R. Carbon Capture and Utilization Update. Energy Technology. 5: 1 – 17. 2017.
[12] Ahmed, I. O., Mahmoud, H., Abdel, M., Ahmed, M. E., David, W. R. Recent Advances in Carbon Capture Storage and Utilisation Technologies: a Review. Environmental Chemistry Letters. 19: 797–849. 2021.
[13] Ruikai, Z., Longcheng, L., Li, Z., Shuai, D., Shuangjun, L., Yue, Z., Hailong, L. Techno-Economic Analysis of Carbon Capture from a Coal-Fired Power Plant Integrating Solar-Assisted Pressure-Temperature Swing Adsorption (PTSA). Journal of Cleaner Production. 214: 440-451. 2019.
[14] Wang, L., Liu, Z., Li, P., Yu, J., Rodrigues, A.E., Experimental and modeling investigation on post-combustion carbon dioxide capture using zeolite 13XAPG by hybrid VTSA process. Chem. Eng. J. 197: 151-161. 2012.
[15] Chaffee, AL., Knowles, GP., Liang, Z., Zhang, J., Xiao, P., Webley, PA. CO_2 Capture by Adsorption: Materials and Process Development. International Journal of Greenhouse Gas Control. 1:11-18. 2007. (Journal)
[16] Lee, SY., Park, SJ. A Rreview on Solid Adsorbents for Carbon Dioxide Capture. J. Ind. Eng. Chem. 23:1-11. 2015.
[17] Wu, B., Zhang, X., Xu, Y., Bao, D., Zhang, S. Assessment of the Energy Consumption of the Biogas Upgrading Process with Pressure Swing Adsorption Using Novel Adsorbents. J. Clean. Prod. 101: 251-261. 2015.
[18] Skarstrom, CW. US Patent. No. 2,944,627. 1960.
[19] Guerrin de Montgareuil, P., Domine, D. U.S. Patent. No. 3,155,468. 1964.
[20] Cheu, K., Jong-Nam, K., Yun-Jong, Y., Soon-Haeng, C. Fundamentals of Adsorption: Proceedings of the Fifth International Conference on

Fundamentals of Adsorption. Le Van, M. D., Ed., Kluwer Academic Publishers: Boston. 203-210. 1996.
[21] Dong, F., Lou, H., Goto, M., Hirose, M. Purif Technol. 15:31-40. 1990.
[22] Sircar, S., Golden, T. C. Ind. Eng. Chem. Res. 34: 2881- 2888. 1995.
[23] Daeho, K., Siriwardane, RV., Biegler, LT. Ind. Eng. Chem. Res. 42:39-348. 2003.
[24] DLHK banten province. "Zeolite Sa Adsorbent Logam Bclosely". (July 24,2022) https://dlhk.bantenprov.go.id/read/article/24/zeolit_sebagai_adsorben_logam_berat.html.
[25] Jiangxi OIM Chemical Co., Ltd AL. "Product Adsorbents-MS Series". (July 24,2022) https://www.oimchem.com/adsorbents-ms-series/13x-apg-III-molecular-sieve.html.
[26] Martra, G., Ocule, R., Marchese, L. Centi G and Coluccia S. Catal Today. 73:83. 2002.
[27] Barthomeuf, D., Mallmann, A. Innovation in Zeolite Materials Science. Studies in Surface Science and Catalysis. 37. 1988.
[28] Doskocil, E, J., Davis, R, J. J. Catal. 188: 353. 1999.
[29] Huang, M., Kaliaguine, S. J. Chem. Soc. Faraday Trans. 88:751. 1992.
[30] Tsuji, H., Yagi, F., Hattori, H. Chem. Lett.; 1881. 1991.
[31] Chen, C., Park, DW., Ahn, WS. CO_2 Capture Using Zeolite 13X Prepared from Bentonite. Appl. Surf. Sci. 292: 63-67. 2014.
[32] Siriwardane, RV., Shen, M., Fisher, EP., Poston, JP. Energy Fuels. 15: 279-284. 2001.
[33] Inui, T., Okugawa, Y., Yasuda, M. Ind. Eng. Chem. Res. 27: 1103- 109. 1988.
[34] Akten, ED., Siriwardane, R., Sholl, DS. Energy Fuels. 17:977-983. 2003.
[35] Ranjani, V. S., Ming-Shing, S., Edward, P. F. Adsorption of CO_2 on Zeolites at Moderate Temperatures, Energy & Fuels. 19: 1153-1159. 2005.
[36] F. Tomul. Adsorption and Catalytic Properties of Fe/Cr-Pillared Bentonites. Chemical Engineering Journal. 185 –186 (185): 380–390. 2012.
[37] Suquet, H., de la Calle, C., Pezerate, H. Swelling and Structural Organization of Saponite. Clay Clay Miner. 23: 1-9. 1975.
[38] Ali, S. Thermo-hydro-mechanical Characterisation and Modelling of Wyoming Granular Bentonite. Techinical report. 15-05: 35. 2015.
[39] Arfaoui, S., Frini-Srasra, N., Srasra, E. Application of Clays to Treatment of Tannery S ewages. Desalination. 185: 419-426. 2005.
[40] Hamdi, N., Srasra, E. Remove of Fluoride from Acidic wastewater by Clay Mineral Effect of Solid–liquid Ratios. Desalination. 206: 238-244. 2007.
[41] Al-Asheh, S., Banat, F., Abu-Aitah, L. Adsorption of Phenol Using Different Types of Activated Bentonites. Sep. Purif. Technol. 33: 1-10. 2003.

[42] Fu-Chuang, H., Jiunn-Fwu, L., Chung-Kung, L., Huang-Ping, C. Effects of Cation Exchange on the Pore and Surface Structure and Adsorption Characteristics of Montmorillonite. Colloid Surf. A: Physicochem. Eng. Aspects. 239: 41-47. 2004.
[43] Min-Yu, T., Su-Hsia, L., Removal of Basic Dye from Water onto Pristine and HCl Activated Montmorillonite in fixed beds. Desalination. 194: 156-165. 2006.
[44] Okada, K., Arimitsu, N., Kameshima, Y., Akira, N., Kenneth, MacKenzie, JD. Solid A cidity of 2:1 Type Clay Minerals Activated by Selective Leaching. Appl. Clay Sci. 31: 185-193. 2006.
[45] Pinnavaia, T.J. Intercalated Clay Catalysts. Science. 220: 365-371. 1983.
[46] Carrado, K, A. Synthetic Organoand Polymer-clays: preparation, characterization, and materials applications. Appl. Clay Sci. 17: 1-23. 2000.
[47] Falaras, P., Kovanis, I., Lezou, F., Seiragakis, G. Cottonseed Oil Bleaching by Acid Activated Montmorillonite. Clays Clay Miner. 34: 221-232. 1999.
[48] Hussin, F., Aroua, MK., David, WMAW. Textural Characteristics, Surface Chemistry and Activation of Bleaching Earth: a Review. Chem. Eng. J. 170: 90-106. 2011.
[49] Chao, C., Dong, WP., Wha, SA. Surface Modification of a LowCost Bentonite for Post-Combustion CO_2 Capture. Applied Surface Science. 283: 699– 704. 2013.
[50] Khoirina, D. N., Dian, M. W., Daryani, Y. H. Kajian A activation H_2SO_4 Terhadap Proses Pemilaran Al_2O_3 Pada Lempung Alam Pacitan, ALCHEMY Journal of Chemical Research. 12 (2): 190 – 203. 2016.
[51] Reda, M., Nacer, D., Nadia, B., Fatima, O., Faiza, Z. Study of Adsorption Properties of Bentonite Clay. Intech Open. 978-1-83968-604-7: 2. 2021.

ISSN 2963-718X